A STUDY ON STRENGTH AND DEFORMATION OF GRADED GLASS FIBER REINFORCED CONCRETE UNDER UNIAXIAL STRESS

Submitted in partial fulfilment of the requirements
for the award of the degree of

DOCTOR OF PHILOSOPHY
in
CIVIL ENGINEERING

by

Hanuma Kasagani

(Roll No: 714104)

Supervisor

Dr. C.B. Kameswara Rao

Professor

STRUCTURES DIVISION

DEPARTMENT OF CIVIL ENGINEERING

NATIONAL INSTITUTE OF TECHNOLOGY

WARANGAL- 506 004 (T.S.) INDIA

FEBRUARY 2019

NATIONAL INSTITUTE OF TECHNOLOGY

WARANGAL

CERTIFICATE

This is to certify that the thesis entitled "**A STUDY ON STRENGTH AND DEFORMATION OF GRADED GLASS FIBER REINFORCED CONCRETE UNDER UNIAXIAL STRESS"** being submitted by **Mr. HANUMA KASAGANI** for the award of the degree of **DOCTOR OF PHILOSOPHY** to the Faculty of **Civil Engineering** of **NATIONAL INSTITUTE OF TECHNOLOGY, WARANGAL** is a record of bonafide research work carried out by him under my supervision and it has not been submitted elsewhere for award of any degree.

Dr. C.B. KAMESWARA RAO
Thesis Supervisor
Professor
Department of Civil Engineering
National Institute of Technology, Warangal
Warangal (T.S.) – INDIA

APPROVAL SHEET

This Thesis entitled "**A STUDY ON STRENGTH AND DEFORMATION OF GRADED GLASS FIBER REINFORCED CONCRETE UNDER UNIAXIAL STRESS**" by **Mr. HANUMA KASAGANI** is approved for the degree of Doctor of Philosophy.

Examiners

_____

_____

_____

Supervisor

_____

Chairman

_____

Date: _____

DECLARATION

This is to certify that the work presented in the thesis entitled **"A STUDY ON STRENGTH AND DEFORMATION OF GRADED GLASS FIBER REINFORCED CONCRETE UNDER UNIAXIAL STRESS"** is a bonafide work done by me under the supervision of **Prof. C.B. KAMESWARA RAO** and was not submitted elsewhere for the award of any degree. I declare that this written submission represents my ideas in my own words and where others ideas or words have been included, I have adequately cited and referenced the original sources. I also declare that I have adhered to all principles of academic honesty and integrity and have not misrepresented or fabricated or falsified any idea / data / fact /source in my submission. I understand that any violation of the above will be a cause for disciplinary action by the Institute and can also evoke penal action from the sources which have thus not been properly cited or from whom proper permission has not been taken when needed.

_____

(**HANUMA KASAGANI**)

(Roll No: **714104**)

Date: _____

Dedicated To

My Beloved Family

ACKNOWLEDGEMENTS

With great pleasure and proud privilege, I manifest my heartier thankfulness to my research supervisor, Prof. C.B. Kameswara Rao**,** Department of Civil Engineering, for his invaluable suggestions, sagacious guidance, scholarly advice and comprehensive critical remarks in bringing out this research work with artistry.

I am perspicuous to divulge my sincere gratefulness to Prof. M. Chandrasekhar**,** Head, Department of Civil Engineering and Chairman, Doctoral Scrutiny Committee for his enlightening guidance and immense help rendered in bringing out this work.

I am grateful to Prof. D. Ramaseshu, Department of Civil Engineering, Prof. M. Sydulu, Department of Electrical and Electronic Engineering, Dr. T.P Tezeswi, Assistant Professor in Department of Civil Engineering members of Doctoral Scrutiny Committee, for their guidance and help during the investigation.

I am also thankful to Prof. T.D. Guneswara Rao, Prof. G. Rajesh Kumar, Prof. P.Ratish Kumar, Sri M. Sudhakar, Dr. S Venkateswara Rao, Dr. K. Gopi Krishna, Dr. M.V.N. Siva Kumar and Dr. Ravi Prasad, the faculty members of Structures Division, NITW for the moral support given during the period of research work.

I am also thankful to Dr. R. Arockia Kumar, Assistant Professor, Metallurgical and Materials Engineering department, for his support and guidance while performing experimentation in material characterization technique laboratory.

I thank my friends and fellow research scholars Mr. B. Murali Krishna, Mr. P S Ravi Teja, Mr. Oggu Praveen, Mr. T.Chaitnaya Krishna, Mr. Srikanth. K, Mr. M Venu, Mr. D. Karthik for their direct or indirect suggestions throughout the period of my research work.

I am thankful to Sri A. Chandranarayana, and Sri A. Laxman Mechanics in Structural Engineering Laboratories, Sri P. Ashok Kumar, Sri P. Rajendra Prasad, Sri Y. Mahesh Kumar, Sri Md. Hussain and Administrative staff for the help done during the research period.

Finally I thank everyone, who contributed either directly or indirectly in successful completion of this work.

- ***Hanuma Kasagani***

ABSTRACT

Concrete is a brittle material, with low tensile strength and strain capacity. However, the tensile behaviour of concrete can be significantly improved by addition of fibers. Glass fibers are fundamentally different and their strength in tension is significantly higher than that of the host matrix. The fine size of the fibers also allows large volume fractions to be easily mixed and uniformly dispersed in the matrix. Closely spaced fibers can then provide effective reinforcing at the micro-cracking level, prevent the coalescence of micro-cracks into unstable macro-cracks, and increase the strength.

In most cases, fiber reinforced concrete (FRC) contains only one type of fiber. A given type of fiber can be effective only in a limited range of strength gain, ductility and toughness. FRC mainly dependent on the fiber properties and dimensions of the fibers. The combination of one type of fiber with another type of fiber or one length of fiber with another length of fiber, is commonly known as hybrid fiber reinforced concrete (HFRC). In hybrid fiber reinforced concrete, different fibers such as steel, glass and polypropylene etc. are combinedly used as fibers and it improves pre peak strength and post peak toughness by properly dispersing fibers.

Hybrid fiber reinforced concrete is a research area in which different types of fibers are combined where the best qualities of each contribute to improve strength and deformation of concrete. Short length and long length fibers are also combined to achieve the same benefits of hybrid reinforced concrete. Combining short length and long length fibers in concrete is named as Graded fiber reinforced concrete. Earlier research shows that short length fibres primarily control the propagation of micro cracks, and improve the ultimate strength whereas, long length fibers arrest the macro cracks and improve the post peak deformation of concrete. Thus different combinations of short and long length fibers would help in arresting the micro as well as macro cracks to improve both pre and post peak performances of concrete. Synergy between Short fiber-long fiber hybridization is realised but not investigated at length.

The present research work is carried out in two phases and are explained briefly. The first phase of investigation is aimed to understand the behaviour of Mono Glass Fiber Reinforced Concrete (MGFRC). The main variables of this study are length of fiber

and volume fraction. Four different fiber lengths 3mm, 6mm, 12mm and 20mm and five different volume fractions 0.1%, 0.2%, 0.3%, 0.4% and 0.5% are used to study. This work is carried out with the two grades of concrete (M30 and M50).

The second phase of study is aimed to understand the behaviour of Graded Glass Fiber Reinforced Concrete (GGFRC). Two or more length of fibers are mixed to form Graded Fibers. When the mixture consists of 3mm and 6mm is named as Short Graded Fiber (SGF), mixture consists of 12mm and 20mm is named as Long Graded Fiber (LGF) and mixture of all the four lengths 3mm, 6mm, 12mm and 20mm is named as Combined Graded Fiber (CGF). The main variables of this study is short graded fibers (3mm+6mm), long graded fibers (12mm+20mm), combined graded fibers (3mm+6mm+12mm+20mm) and total volume fraction (0.3%, 0.4% and 0.5%). In this study mixing of fibers is done in proportion of 20%+80%, 40%+60%, 50%+50%, 60%+40% and 80%+20% to obtain graded fibers. This work is carried out with the two grades of concrete (M30 and M50).

Phase-I: Study on Mono Glass Fiber Reinforced Concrete (MGFRC)

In this investigation, the experimental work was carried out under uniaxial tension and uniaxial compression for M30 and M50 grade of concrete with the 0.1%, 0.2%, 0.3%, 0.4% and 0.50% fiber volume of Mono Glass Fibers (3mm, 6 mm, 12 mm and 20 mm length fiber). In order to understand the workability of Mono Glass Fiber Reinforced Concrete (MGFRC) the slump test was conducted. As volume of fiber and length of fiber increased from 0.1% to 0.5% the slump decreased. However, 0.4% and 0.5% volume of fibers led to bundling, balling and hence significant reduction in workability is observed in composite. Hence, Workability of MGFRC decreased with increase in fiber length and volume fraction. The specimens with 0.3% fiber volume content has shown the maximum improvement in compressive strength.

The tensile and compressive stress strain curves are analysed to obtain the initial slope, strengthening factor, ductility factor, strain hardening slope and Strain softening slope of the composite. Specimens with long length fibers (12mm and 20mm) exhibited higher ductility factor, energy absorption capacity than that of short length fibers (3mm and 6mm). Specimens with short length fibers showed higher strengthening and initial slope compared to the long length fibers.

Specimens with Short length fibers (3mm and 6mm) have given higher tensile strength than the specimens with Long length fibers (12mm and 20mm). Specimens with long length fibers (12mm and 20mm) have contributed more post crack deformation capacity than the specimens with short length fibers (3mm and 6 mm) in tension. Specimens with Short length fibers (3mm and 6mm) have given higher peak strength than the specimens with long length fibers (12mm and 20mm). Specimens with long length fibers (12mm and 20mm) have contributed more post peak deformation capacity than the specimens with short length fibers (3mm and 6 mm) in compression. Hence, the short fibers are more effective in improving the strength by delaying the formation of micro cracks and long fibers are more effective in increasing the deformations by bridging the macro cracks in both tension and compression.

Tensile properties of fibre concrete are governed mainly by the number, dispersion and orientation of fibres in the cracking area, as well as dispersion characteristics of fibres. Several techniques (Yang Y, 2002; Yilmaz Akkaya et al, 2001 and Bang Yeon Lee, 2009) including image analysis, transmission X-ray photography, and Advanced CCD Imaging Spectrometer (ACIS) are available for evaluating the fibre distribution in a composite made of cement matrix and steel, carbon, glass, or organic fibres; i.e., these techniques can be employed to determine the degree of fibre dispersion and orientation in the composite. Among these techniques, image analysis is the most applicable and trusted method to evaluate the distribution characteristics of fibres in a composite.

Fiber dispersion and fiber orientation at fracture plane of specimens is examined through optical microscope. The strength of the fiber reinforced composite is influenced by the fiber length coefficient (η_l), fiber orientation coefficient (η_θ) and fiber dispersion coefficient (η_d). Higher the fiber dispersion coefficient and fiber orientation coefficient higher the strength of composite due to homogeneity of fiber dispersion and fibers performs efficiently across the fracture plane.

Normal compressive stress generates transverse tensile strain. As the compressive stress reaches peak stress, dilation of concrete initiates and lateral deformation increases. Presence of fibers restrain the lateral deformation. Degree of resistance offered to lateral deformation is proportional to volume of fibers and the fibers come into action after cracking in concrete in compression which is similar to the action of

fibers in concrete after the onset of cracking in tension. The fibers present in concrete will participate by resisting dilation of concrete only after sufficient mobilization of dilation of concrete. That is why there is a remarkable improvement in strain softening of concrete in compression with the increase in fiber content

Strain softening in compression and strain hardening in tension is noticed. Irrespective of length of fiber, specimens with 0.3%, 0.4% and 0.5% have exhibited strain hardening in tension and corresponding strain softening is noticed in compression. It is noted that strain hardening in tension is not observed for specimens with 0.1% and 0.2% and corresponding strain softening in compression is not significantly present. The amount of deformation and slope in the strain hardening and strain softening region are directly influenced by the volume of fiber and length of fiber. In order to understand the complementary behaviour of strain hardening behaviour in tension and strain softening behaviour in compression, the normalised stress and normalised strain at the onset of strain hardening and at the inflection point of strain softening is taken for a given fiber length (L_f) and volume of the fiber (V_f).

Reinforcing index (RI_{MF}) is defined as product of volume fraction (V_f) and aspect ratio of fiber (L_f/D_f). Tensile and compressive stress strain behaviour is predicted for different reinforcing indexes. In order to correlate tensile and compression data for various Reinforcing Index ($RI_{MF} = V_f (L_f/D_f)$) of MGFRC, a relationship between Reinforcing Index and strain hardening in tension, strain softening in compression is proposed. Specimens with Short fibers i.e. RI_{MF} of 0.64 and 1.29 producing low strain hardening in tension and strain softening behaviour in compression, where as in specimens with long fibers i.e., RI_{MF} of 2.57 and 4.29 exhibited significant strain hardening in tension and strain softening behaviour in compression. As the reinforcing index (RI_{MF}) of mono fibers increases the strain hardening in tension complements strain softening in compression.

A model is developed for predicting stress–strain curves of MFRC in tension and compression. All properties required for the generation of compressive stress-strain curves are estimated using the reinforcing index (RI_{MF}). A material parameter β is developed for predicting stress–strain curves of MGFRC. The analytical curves show good correlation with experimental test results of MGFRC in both tension and compression.

Phase-II: Study on Graded Glass Fiber Reinforced Concrete (GGFRC)

In this investigation combination of different lengths of mono fibers are considered and named as Graded fiber reinforced concrete to distinguish from Hybrid fiber reinforced concrete. Inspiration is obtained from concrete mix proportioning where in different sizes of aggregates are combined to obtain well graded aggregates. Similar synergy with well Graded fibers of different lengths may improve strength and deformation of concrete. In the present work four lengths of AR glass fibers 3mm, 6mm, 12mm and 20mm are combined in different proportions to form Graded Glass Fibers.

MGFRC results shows that the given length of fiber can be effective only in a limited range of strength gain, ductility and energy absorption. To further improve the properties (strength and ductility) of the composite simultaneously different lengths of fibers are mixed together with different fiber volume combinations and named as Graded Fibers. In this investigation, two or more length of fibers are mixed to form Graded Fibers. When the mixture consists of 3mm and 6mm is named as Short Graded Fiber (SGF), mixture consists of 12mm and 20mm is named as Long Graded Fiber (LGF) and mixture of all the four lengths 3mm, 6mm, 12mm and 20mm is named as Combined Graded Fiber (CGF). In this present work, an attempt has been made to study the effect of addition of Graded Glass Fibers with different fiber length and volume fraction in Glass Fiber Reinforced Concrete. The experimental work was carried out under uniaxial tension and uniaxial compression for M30 and M50 grade of concrete with the 0.3%, 0.4% and 0.50% total fiber volume of SGF, LGF and CGF.

In order to understand the workability of graded fibers, slump test was conducted for M30-GGFRC and M50-GGFRC with 0.3%, 0.4% and 0.5% volume fraction. It can be concluded that, there is significant difference existed in the loss of the slump for mono glass fibers. The slump loss was small in the concrete with graded fibers. Hence, graded fibers improves workability.

Compression test was conducted on cube specimens of M30-GGFRC and M50-GGFRC with 0.3%, 0.4% and 0.5% volume fraction. Results shows that different fiber volume combinations of SGF mixes showed that cube compressive strength of SGF with 40%3mm+60%6mm is greater than all other short graded fibers whereas in LGF mixes showed LGF with 40%12mm+60%20mm is greater than all other long graded fibers and in case of CGF mixes showed that cube compressive strength of CGF with

40%SGF+60%LGF is greater than all other combined graded fibers. In any given volume fraction (0.3%, 0.4% and 0.5%), among all the mixes shows that CGF have given the best improvement in terms of cube compressive strength compared to MGF, SGF and LGF. It can be concluded that the combined graded fibers (CGF) improves the cube compressive strength of concrete.

In order to understand the tensile and compressive stress strain behaviour of Graded fibers (SGF, LGF and CGF). Uniaxial tensile and uniaxial compression test was conducted on dog-bone and prism specimens of M30-GGFRC and M50-GGFRC with volume fractions of 0.3%, 0.4% and 0.5%. Irrespective of volume of fibers i.e., 0.3%, 0.4% or 0.5%, the specimens containing the 40%3mm + 60%6mm of SGF has given the best benefit of improvement in both strength and deformation compared to all other short graded fibers and specimens containing the 40% 12mm + 60% 20mm of LGF has given the best benefit of improvement in both strength and deformation compared to all other long graded fibers. Specimens containing the 40% SGF + 60% LGF of CGF has given the best benefit of improvement in both strength and deformation compared to all other combined graded fibers.

Short graded fibers are more effective in improving the ultimate strength by delaying the formation of micro cracks and long graded fibers are more effective in increasing the deformations by bridging the macro cracks. The combination of short graded and long graded fibers forms the combined graded fibers. It can be concluded that the combined graded fibers (CGF) has given the best benefit performance in terms of strength and deformation compared to SGF and LGF. Irrespective of volume of fibers i.e., 0.3%, 0.4% or 0.5%, different lengths of fibers have controlled the different levels of cracking thus contributing to increases in strength and deformation of Graded Glass Fiber Reinforced Concrete.

In all, irrespective of volume of the fiber (0.3%, 0.4% and 0.5%) and grade of concrete (M30 and M50), long graded fibers (LGF) exhibited higher ductility factor, energy absorption capacity than that of short graded fibers (SGF). Short graded fibers showed higher strengthening and initial slope compared to the long length fibers. Hence, the combination of SGF and LGF i.e., CGF have exhibited the higher strengthening factor, ductility factor and energy absorption capacity than that of SGF, LGF and MGF in both tension and compression.

Fiber dispersion and orientation are the two important parameters to understand the tensile behaviour of the composite. These parameters are examined on fracture plane of M30-GGFRC and M50-GGFRC specimens with 0.3%, 0.4% and 0.5% volume fraction. It shows that the composite with SGF has more the fiber density at the center and less at the edges and corners. Where as in long graded fibers, the fiber density is more at the edges and corners and less at the center. Composite with CGF (containing SGF + LGF) showed the almost uniform distribution. The results of image analysis shows that graded fibers with different fiber volume combinations disperse homogeneously avoiding clumping or balling. Graded fibers showed the higher fiber dispersion coefficient and higher fiber orientation coefficient when compared to the mono fibers.

An equation is proposed to arrive at RI_{GF} for graded fibers. This is developed on observing of stress strain behaviour and fiber density variations of GGFRC with different fiber volume combinations. The composite tensile strength and corresponding composite tensile strain of GGFRC is calculated based on the RI_{GF}. The predicted composite tensile strength and composite tensile strain values are closer to the experimental values. A model is proposed to predict the tensile and compressive stress strain behaviour. All properties required for the generation of stress–strain curves are estimated using the reinforcing index (RI_{GF}). A model is developed for predicting compressive stress–strain curves of MGFRC and GGFRC. The analytical curves show good correlation with experimental test results.

The strain hardening in tension and strain softening in compression phenomena is noticed in the stress strain behaviour of GGFRC which is similar to that of MGFRC. Degree of resistance offered to lateral deformation is proportional to grading of fibers (SGF, LGF and CGF) and volume of fibers (0.3%, 0.4% and 0.5%), and the fibers come into action after cracking in concrete in compression which is similar to the action of fibers in concrete after the onset of cracking in tension. With well grading of fibers, the strain hardening in tension complements strain softening in compression.

In order to understand the strain hardening behaviour in tension and strain softening behaviour in compression for M30-GGFRC and M50-GGFRC, a relationship between Reinforcing Index (RI_{GF}) and strain hardening in tension, strain softening in compression is proposed.

The gradient of increase of strain hardening in tension is similar to the gradient of strain softening in compression for the specimen with the same RI_{GF} and it is influenced by RI_{GF}. It was observed as the value of RI_{GF} decreased, the strain softening in compression increased and also increase in strain hardening in tension.

Contents

List of Tables

This page is intentionally left blank

List of Figures

This page is intentionally left blank

Notations

Latin Capital Characters

A_0	Original area of the fiber
A_m	Measured area of the fiber
C*	Cube Specimens
D*	Dog-bone specimens
D_f	Diameter of the fiber
DF^C	Ductility Factor in Compression, $\varepsilon^c{}_{IP} / \varepsilon^B{}_u$
DF^t	Ductility Factor in Tension, $\varepsilon^Q{}_{t\,/}\,\varepsilon^P{}_t$
$E^C{}_i$	Initial Slope in Compression, $f^A /\ \varepsilon^A$
$E^t{}_i$	Initial Slope in Tension, $\sigma^P{}_{t\ /}\,\varepsilon^P{}_t$
EA_{SHR}	Energy Absorption in Strain Hardening Region
EA_{SSR}	Energy Absorption in Strain Softening Region
EA_{MF}^{SHR}	Energy Absorption in Strain Hardening Region for Mono Fibers
EA_{MF}^{SSR}	Energy Absorption in Strain Softening Region for Mono Fibers
$EA^0{}_{SSR}$	Energy Absorption in Strain Softening Region for plain concrete
E_{SH}	Strain Hardening Slope, $(\sigma^Q t - \sigma^P t) / (\varepsilon^Q t - \varepsilon^P t)$
E_{SS}	Strain Softening Slope, $(f^B{}_u - f^C{}_u) / (\varepsilon^c{}_{IP} - \varepsilon^B{}_u)$
F_{max}	Peak pull-out loads, Newton
Lc	Fiber critical transfer length, mm
Le	Fiber embedded length, mm
L_f	Length of fiber
N_f	Number of fibers when aligned uniformly distributed
P*	Prism Specimens
RI''_{GF}	Reinforcing index of graded fibers from Linear combination method
RI'_{GF}	M A Rasheed et, al 2018 Method for Reinforcing index of graded fibers
RI_{GF}	Reinforcing Index of Graded Fibers
RI_L	Reinforcing Index of Long Fibers
RI_{MF}	Reinforcing Index of Mono Fibers
RI_s	Reinforcing Index of Short Fibers
STF^C	Strengthening Factor in Compression, $f^B{}_u /\ f_0$
STF^t	Strengthening Factor in Tension, $\sigma^Q{}_{t\,/}\,\sigma_t$

V_f	Volume Fraction, %

Latin Small Characters

f_0	Compressive strength of plain concrete, MPa
f^A	Stress at point A, MPa
$f^B{}_u$	Peak Stress at point B, MPa
f_c	Stress values on the curve
$f^C{}_{IP}$	Stress at inflection point C, MPa
f_d	Fiber Density Factor, n_e / N_f
f_{dL}	Fiber Density Factor for Long Fibers
f_{dS}	Fiber Density Factor for Short Fibers
f_u	Peak strength of fiber is reinforced concrete
n_e	Estimated Maximum number of fibers
r	Correlation coefficient
Sy/x	Standard error estimate

Greek Characters

β	Material Parameter
$\varepsilon^A{}_u$	Strain at point A
$\varepsilon^B{}_u$	Strain at peak point B
ε_c	Strain values on the curve
ε_{ct}	Tensile strain at ultimate tensile strength of composite
$\varepsilon^C{}_{IP}$	Strain at inflection point C
ε_{mt}	Strain at ultimate tensile strength of plain concrete
$\varepsilon^P{}_t$	Strain at point P
$\varepsilon^Q{}_t$	Strain at point Q
ε_u	Strain at Peak Strength
σ_b	Bond Strength of fiber
σ_{ct}	Tensile strength of composite
σ_{fu}	Tensile strength of the fiber
$\sigma^{GF}{}_{tu}$	Experimental ultimate tensile strength of GGFRC, MPa
$\sigma^{GF}{}_{ct}$	Calculated ultimate tensile strength of GGFRC from equation (10), MPa

σ_{mt}	Tensile strength of plain concrete, MPa
σ^{MFt}_{u}	Experimental ultimate tensile strength of MGFRC, Mpa
σ^{MF1}_{u}	Calculated ultimate tensile strength of MGFRC from equation (9), MPa
σ^{MF2}_{u}	Calculated ultimate tensile strength of MGFRC from equation (10),MPa
σ^{P}_{t}	Stress at point P, MPa
σ^{Q}_{t}	Stress at point Q, MPa
η	Fiber efficiency (η_d η_θ η_l)
η_d	Fiber dispersion coefficient
η_d'	Predicted fiber dispersion coefficient
η_l	Fiber length coefficient
η_l'	Predicted fiber length coefficient
η_θ	Fiber orientation coefficient
η_θ'	Predicted fiber orientation coefficient

Abbreviations

CGF	Combined Graded Fibers
FRC	Fiber Reinforced Concrete
GGFRC	Graded Glass Fiber Reinforced Concrete
GF	Graded Fibers
GFRC	Glass Fiber Reinforced Concrete
HFRC	Hybrid Fiber Reinforced Concrete
LGF	Long Graded Fibers
MGF	Mono Glass Fibers
MF	Mono Fibers
MGFRC	Mono Glass Fiber Reinforced Concrete
SD	Specimen Designation
SGF	Short Graded Fibers
SHR	Strain Hardening Region
SSR	Strain Softening Region

Chapter-1
Introduction

1.1 General

Concrete is a brittle material, with low tensile strength and strain capacity. However, the tensile behaviour of concrete can be significantly improved by addition of fibers. Historically, Joseph Lambot's idea of using continuous fibers in mesh form to create new building materials led to the development of Ferro-cement and reinforced concrete. Romualdi et al (1963) used short randomly oriented fibers in order to improve tensile strength of concrete. Nowadays, several types of reinforcing fibers, in various shapes and sizes, such as steel, polymer, glass, carbon, or natural fiber, are produced and used widely. Based on type of fibers, different fiber reinforced concretes (FRCs) were developed, namely steel fiber reinforced concrete (SFRC), carbon fiber reinforced concrete (CFRC) and glass fiber reinforced concrete (GFRC) etc.

In most cases, fiber reinforced concrete (FRC) contains only one type of fiber. A given type of fiber can be effective only in a limited range of strength gain, ductility and toughness. FRC mainly dependent on the fiber properties and dimensions of the fibers. The combination of one type of fiber with another type of fiber or one length of fiber with another length of fiber, is commonly known as hybrid fiber reinforced concrete (HFRC). In hybrid fiber reinforced concrete, different fibers such as steel, glass and polypropylene etc. are combinedly used as fibers and it improves pre peak strength and post peak toughness by properly dispersing fibers.

The advantage of using discontinuous fibers in brittle matrices, such as a cementitious matrix, is usually realized only after the matrix cracks. The fibers can prevent a sudden loss in load-carrying capacity of the cracked composite by providing a load transfer mechanism across the crack, resulting in a pseudo-ductile response. In conventional concrete, micro-cracks exist even before the structure is loaded because of drying shrinkage and other causes of volume change. Use of short fibers in concrete matrix reduces the drying shrinkage cracks and increases the flexural toughness of concrete structure. When the structure is loaded, the micro cracks open up and propagate which may lead to inelastic deformation in concrete. Micro or short randomly dispersed fibers in concrete help to resist the opening of marco cracks by arresting the micro cracks

and enhancing the pre crack strength. Moreover, the small fibers dispersed and distributed randomly in concrete help to bridge the internal micro cracks thus improve concrete properties in all directions (L.R. Betterman et al 1995). However addition of higher volume of fibers leads to practical problems such as bundling, balling, reduction in workability, strength and toughness.

In a given volume, shorter the length of fiber, number of fiber will be more, closer will be the spacing of fibers and will be as near as possible to the micro cracks. These fibers may initially contribute to delay the formation of cracks but may be pulled out after micro cracks transformed into macro cracks (Fig.1.1). Thus long length fibers bridge the macro crack and improves the post peak deformations of concrete. As the length of fiber increases, resistance to post peak deformations increases. Hence, Combination of short length and long length fibers forms the synergy, improvement in both the pre peak stress and post peak toughening can be expected (Amon Bentur et al. 1990; Banthia et al. 1990).

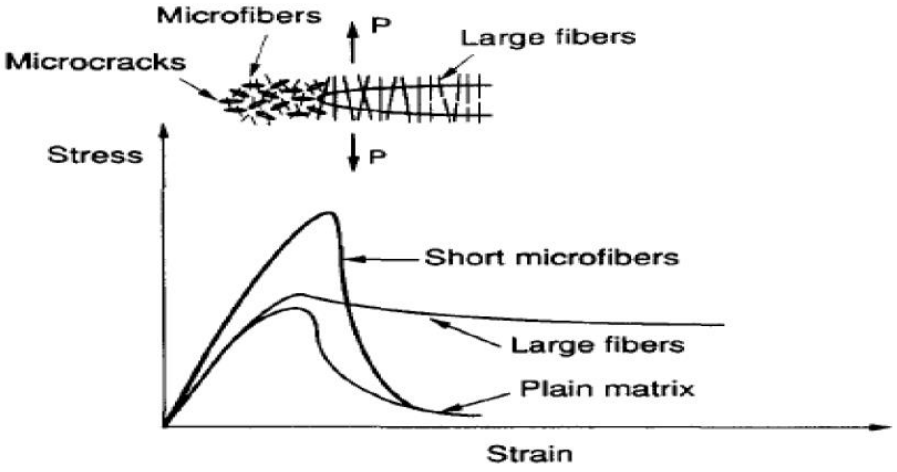

Fig.1.1 Illustration of different sizes of fibers on crack bridging (L.R. Betterman, 1995)

The improvement of such mechanical properties can be achieved through the addition of a moderate amount of properly distributed and orientated fibres. This improvement can be maximized by controlling the alignment and dispersion of fibres in the matrix. Short fibers are dispersed randomly in all directions so as to exhibit isotropic behaviour. However, the real fibre distribution is strongly influenced by various factors such as fiber characteristics (diameter, length, and volume fraction), the fluidity of the

matrix, placing method, and shape of the form (Bang Yeon Lee et al, 2009; Yilmaz Akkaya et al, 2000).

Su-Tae Kang et al. 2011 and Burcu Akcay et al 2012 have focused on the systematic approach with special interest in the fiber orientation and distribution. Their approaches were limited to analytical studies with the assumption of an idealized fiber distribution and did not consider the actual fiber distribution, which is affected by diverse factors such as placing method, form shape, and fiber geometry. In order to quantify the fiber characteristics, a systematic approach is followed from microscopic to macroscopic view, that is, from the bond behaviour of individual fiber distributed in the composites to the tensile behaviour of a fiber reinforced composite and its structural performance.

1.2 Background of Glass fibers

The Use of glass fibers in concrete was first attempted in the USSR in the late 1950s .It was established that ordinary E-glass fibers to an alkaline environment leads to rapid deterioration process which involves strength and weight losses, and reduction in the filament diameter. This process can be attributed to breaking of the Si−O−Si bonds in the glass network, by the OH− ions which are highly concentrated in the alkaline pore solution is shown in Fig.1.2.

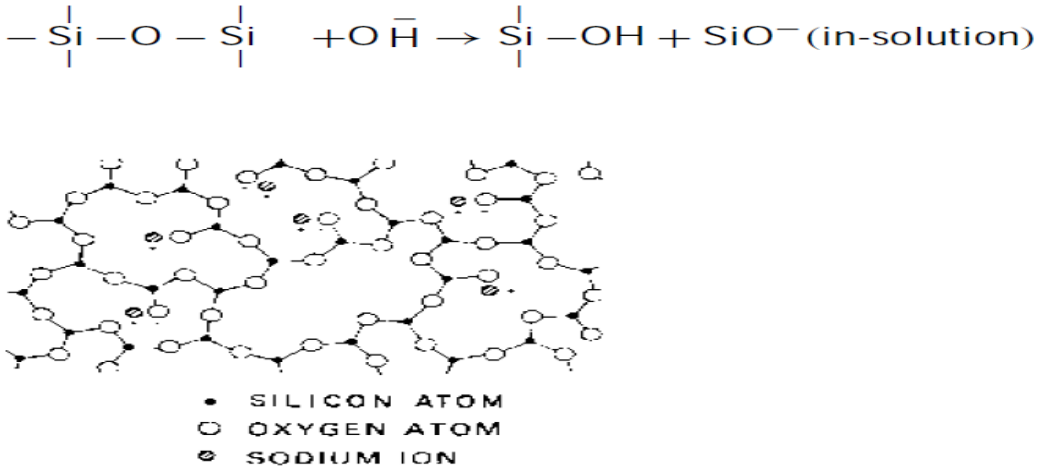

Fig.1.2 Schematic structure of glass (Bentur et al. 1990).

To overcome this problem, special alkali-resistant glass formulations (AR glass fibers) was developed and properties of E-glass and AR-glass are given in Table 1.1 and 1.2. In this AR glass fibers, Zirconium content is about 16% due to which it prevents the deterioration of glass fibers by controlling the alkali silica reaction between cement

paste and glass. Due to the presence of ZrO2 in AR glass fibers it imparts stability to the glass structure by serving as a diffusion barrier to reduce the rate of further attack in the alkaline environment. This led to a considerable number of commercialized products nylon and polypropylene fiber are contemporary to glass or steel fibers (ACI 549.3R-09, 2009 and ACI 544.1R-96).

Table 1.1 Mechanical properties of E and AR glass (Amon Bentur et al. 1990).

Property	E glass	AR glass
Density (Kg/m3)	2540	2780
Tensile strength (MPa)	3500	2500
Modulus of elasticity (GPa)	72.5	70.0
Elongation at break (%)	4.8	3.6

Table 1.2 Chemical composition of E and AR glass (Amon Bentur et al. 1990).

Composition	E glass	AR glass
SiO2	52.4%	71%
K2O + Na2O	0.8	11
B_2O_3	10.4	--
Al_2O_3	14.4	18
MgO	5.2	--
CaO	16.6	--
ZrO_2	--	16

1.3 Manufacturing of Glass Fibers

Manufacturing of glass fibers is shown in Fig.1.3 and it contains mainly three processing units. The raw materials are mixed in a required proportions by weigh batch and these materials are transferred into the batch charging at a temperature of about 1700 °C. The molten glass flows directly to the furnace and then transported into a remelting chamber. Bottom of the remelting chamber contains series of electrically heated platinum bushings each of which has large number of holes. The bushing allows a molten glass pass through holes under gravitational force and drawn filaments of 8 to 15μm diameter mechanically downwards at a speed of 1000 meter/minute or more. The molten glass is rapidly cooled by sprayed water at the bushing to prevent crystallization and formed into glass fibers by a process known as fiberization. The diameter of the glass fiber depends upon the molten glass viscosity, gravity, length and diameter of the nozzle and the speed of the winding.

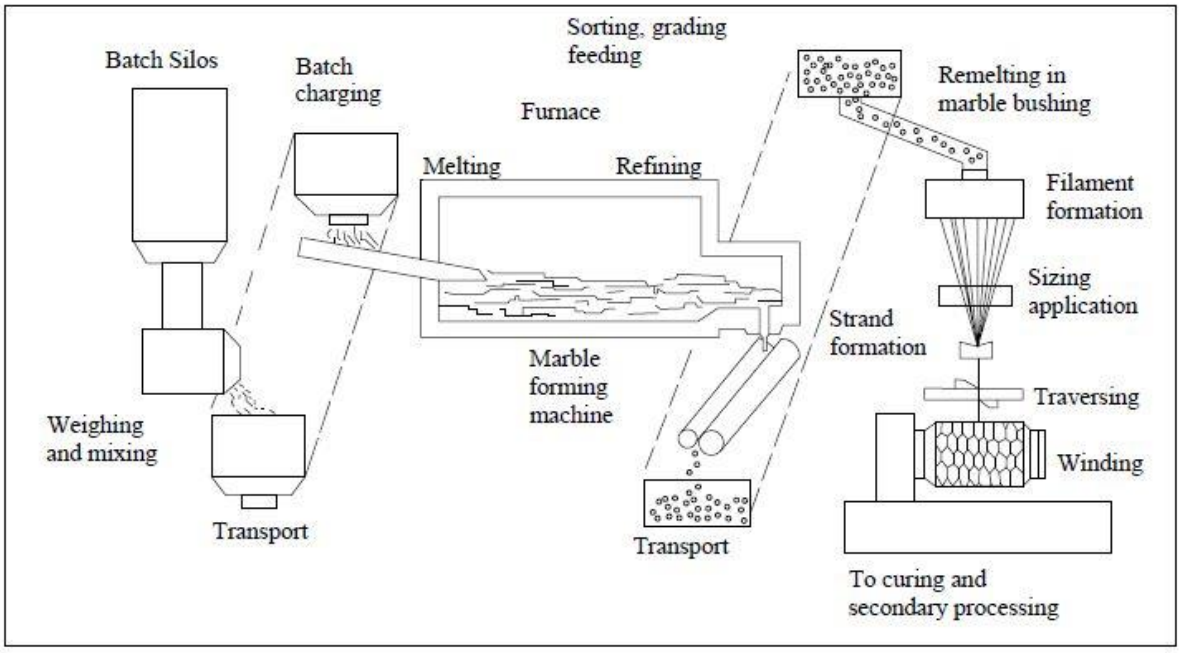

Fig.1.3 Flow chart of Glass Fiber Manufacturing Process

1.4 Role of Glass Fibers in Concrete

Use of Alkali Resistant (AR) glass fibers in concrete presents an area of opportunity to utilize the strength and stiffness of fibers in reinforcing the brittle matrix. Concrete materials produced with short randomly distributed AR Glass fibers would be superior to other FRC (Fiber Reinforced Concrete) materials for several reasons. In comparison to steel fibers, the small diameter of the individual glass fibers ensures a better and

more uniform dispersion. In addition, the high surface area and relatively small size of glass fibers offer significant distribution capability and crack bridging potential as compared to steel fibers. The glass fibers are randomly distributed offering efficiency in load transfer. Furthermore, the bond strength of the glass fiber is far superior to the polypropylene fibers, thus increasing the efficiency of fiber length so that there is limited de-bonding and fiber pull-out (Tejal Desai et al. 2003). Length and Orientation of fibers in the matrix plays a major role in arresting the crack propagation .Glass fibers can be incorporated into a matrix either in continuous lengths or in discontinuous (chopped) lengths (Amon Bentur et Al.1990).

1.5 Methods of Mixing

It is very important that the fibers are dispersed uniformly throughout the mixture. This must be done during the batching and mixing phase. Several mixing sequences have been used (ACI 544.1R-96 and ACI 549.3R-09), some of them are presented below.

In normal method, all required fine and coarse aggregates are mixed in the truck mixer, with water. Then fibers are added in a clump free state to the mixer hopper at the rate of about 45 kg/minute and mixture rotating with a full speed for 40 to 50 revolations. Fibers can be added manually by emptying the containers into the truck hopper or via a blower or conveyor belt

In another method, In order to prevent the fiber clumping, fibers are added manually on top of the aggregates on the charging conveyor belt. The aggregate stream in the batching plant before the aggregate is added to the mixer.

1.6 Applications of GFRC

Glass fiber reinforced concrete (GFRC) was first introduced to the building industry in the early 1970's in the United Kingdom. Today, it is one of the most popular and innovative building materials used throughout the United States, Europe, Middle East and Asia. The single largest application of GFRC has been in the manufacture of exterior building facade panels. This application makes up to at least 80 percent of all GFRC architectural and structural components manufactured in the U.S. Since the introduction of AR-glass in the 1970s, growth in applications has been appreciable. According to the Precast Concrete Institute, over 60 million square feet of GFRC architectural cladding panels have been erected from 1977 to 1993. Initial problems in

controlling panel warpage were solved using steel-stud frames, which also facilitated efficient attachment to building structures.

Another application for GFRC is as a plasticized or sprayed coating in surface bond masonry, where masonry blocks dry stacked, with mortar used only to minimize the necessary to keep them plumb, are coated on both vertical faces with a hand plastered or sprayed layer of GFRC.

At present, GFRC is predominantly used in small units including roof tiles, cable trays, drainage channels, decorative façade units and cladding panels. GFRC is also finding applications in the building and bridge construction industries for the production of permanent formwork systems since it is easy to prefabricate, allows for the creation of complex shapes, and has superior durability, aesthetic appearance and low self-weight (G B Kim 2010).

GFRC products are easy to transfer and can be produced in desired shapes and are good noise and sound barriers. They are widely used in urban areas and roads to reduce noise pollution.

GFRC is very light in weight than steel reinforced concrete and also have high tensile strength. Hence they are used in structural purposes to reduce building weight and consequently lateral loads of earthquake and structural drift.

1.7 Advantages of GFRC

The main advantages of GFRC in comparison to concrete are as follows:

- Higher flexural strength, tensile strength and Impact Strength than plain concrete due to the presence of the glass fibres.
- No cover requirement to be provided thus resulting in thinner sections.
- Fibres are lightweight that minimizes the load added to existing structures.
- Improved Chemical Resistance, for example GFRC exhibits better chloride penetration resistance than steel.
- It does not rust or corrode.
- Good acoustic properties
- Low permeability that increases water or air pollution resistance
- It is Recyclable and environment friendly.

1.8 Thesis organization

The present thesis is organised in the following way

Chapter-1: An introduction to development of fiber reinforced concrete (FRC), hybrid fiber reinforced concrete (HFRC), role of AR- glass fibers, factors effecting properties of glass fiber reinforced concrete (GFRC) and applications in various fields of construction industry is presented in this chapter.

Chapter-2: The second chapter consists of collection of literature on the mechanical and stress strain behaviour of FRC, HFRC and GFRC in tension and compression. Pull-out behaviour of different types of fibers are presented. Mechanism for the maximum pre crack strength and post crack deformation of FRC and HFRC, and the influence of randomly dispersed and orientation of fibers on tensile behaviour of composite are presented. Different stress strain models of FRC are described.

Chapter-3: The third chapter is the scope and objectives of investigation is stated.

Chapter-4: The fourth chapter describes the experimental program for behaviour of Mono Glass Fiber Reinforced Concrete (MGFRC) and Graded Glass Fiber Reinforced Concrete (GGFRC) under uni-axial tensile and compression test. Specimen preparation (cubes, prisms and dog-bone), testing procedure, equipment setup and parameters of investigation are given.

Chapter-5: This chapter is focused on behaviour of Mono Glass Fiber Reinforced Concrete (MGFRC) with varying volume fractions of different lengths of glass fibers. In this investigation uni-axial tension and compression tests are performed on dog-bone specimens and prismatic specimens respectively. This study is aimed at understanding the effect of volume fraction and fiber length on the properties in fresh and hardened state of MGFRC. Results of stress strain behaviour of MGFRC in tension and compression are presented.

Chapter-6: This chapter is focused on behaviour Graded Glass Fiber Reinforced Concrete (GGFRC) with varying volume fractions of different grading of glass fiber lengths. In this investigation uni-axial tension and compression tests are performed on dog-bone specimens and prismatic specimens respectively. This study is aimed at understanding the effect of grading of fibers and different percentage of fiber volume

combinations on the properties in fresh and hardened state composite. Results of stress strain behaviour of GGFRC in tension and compression are presented.

Chapter-7: Finally, in the seventh chapter consist of conclusions, along with a discussion on the limitations of the present study are presented. The scope for further research and references are also presented.

This page is intentionally left blank

Chapter-2

Literature Review

There is a wide range of research is going on in the field of fiber reinforced Concrete. In the present study, many of the important publications were reviewed to get an overview on fiber reinforced concrete. This section presents a state of art report on the development of FRC, Factors affecting the properties of FRC, modelling of Stress Strain behaviour of FRC. A brief report of the literature study is presented below.

2.1 Literature review on Glass Fiber Reinforced Concrete (GFRC)

Zollo (1982), Proposed the E-glass fibers can be used as reinforcement for cement matrix. The combination of cement paste with E-glass fibers helps in producing flat sheet material. Over a period of time, these E-glass fibers are chemically attacked by the strong alkaline environment of cement paste and it contributed to loss of strength in GFRC. Glass fibers are chemically coated with zirconium content (alkali resistant glass fibers) and it reduced the exposure of GFRC to high humidity of environment. Hence, the loss of strength can be eliminated by using alkali resistant (AR) glass fibers.

Marsh and Clarke (1985), investigated, the influence of AR-glass fibers on the mechanical properties of glass fiber reinforced concrete (GFRC). Addition of AR-glass fibers has improved the flexural strength of GFRC by 4.8 times and compressive strength increased from 20 to 25% compared to the plain concrete flexural and compressive strength.

Tejal Desai et. al, (2003), studied the effect of different lengths of AR-glass fibers on strength and ductility of concrete. Results have shown that concrete with 12mm fiber length exhibits higher flexural strength and toughness compared to other lengths. The ductility of concrete with 12mm length fiber showed 140% higher than the concrete with 40mm length fiber and the control samples. This may be due to a better dispersion of the 12mm fiber length compared to the 40mm length fiber in the composite. As the volume of the fiber increased the strength and ductility also increased, due to ability of the fibers to maintain the cracked specimen together.

Barluenga et. al, (2007), studied the controlling of cracks in concrete by using randomly distributed AR-glass fibers of 12mm length with normal strength concrete

(NSC) and Self-Compacting Concrete (SCC). Both NSC and SCC are prepared with addition of fiber volumes 600g/m^3, 900g/m^3 and 1000g/m^3 of high dispersion AR glass fibers (dry in paper bags) and W70 glass fibers (supplied wet in plastic bags). Concrete shrinks at an early age and drying shrinkage cracks are developed. In order to control crack growth, a little amounts of the AR-glass fibers are added in concrete. Fibers can control the drying shrinkage cracks and acted as a local reinforcement. At a 600g/m^3 of volume fraction, high dispersion glass fibers reduced 95% of crack area whereas W70 glass fibers produced a reduction of crack area of around 55% in both the NSC and SSC. The less efficiency of crack reduction is observed at 900g/m^3 and 1000g/m^3 of fiber content irrespective of type of fiber and type of concrete. Composition with high dispersion AR glass fibers have shown maximum reduction in crack length than the W70 glass fiber composition and exhibited less crack area and maximum controlling on growth of crack.

Tassew et al, (2014), studied the influence of glass fibers on the rheological and mechanical properties of ceramic concrete. Workability decreased with increased in fiber content and fiber length. The flexural strength, shear strength of ceramic concrete increased with increases in the fiber content and fiber length. The flexural strengths of glass fiber reinforced ceramic concrete were 13 to 30% of the corresponding compressive strength. The flexure, shear and compressive test results showed that the fiber failure mode was predominantly by fracture rather than pull-out.

2.2 Literature review on workability and mechanical behaviour of Fiber Reinforced Concrete (FRC)

Hughes et al, (1976), conducted the slump test to assess the workability of various fibre-reinforced concrete mixes. Slump decreased with increasing volume fraction, length, aspect ratio and decreased fibre diameter. Concrete mixes reinforced with crimped steel fibres resulted in a larger slump than mixes reinforced with deformed or round steel fibres. That is because of their shape, over-all length and diameter of fibre.

Bing Chen et al. (2005), Studied the influence of steel, carbon and polypropylene (PP) fiber on workability and mechanical properties of lightweight concrete (LWC). PP fiber showed the less reduction in slump i.e., 20.8% and steel fiber showed the highest reduction in slump i.e., 54.2% when compared to the plain concrete slump. Hence the

PP and carbon fibers produced good workability than steel fibers. LWC with carbon and steel fibers provide increase in split tensile strength and compressive strength compared to PP fibers. Compared to all other combinations, the mixture of carbon and steel fibers gave the best increase in compressive strength and split tensile strength of 27.64% and 54.2% respectively.

Mustafa Sahmaran et al. (2005), Investigated the influence of different types of steel fiber on fresh and hardened state of concrete. The hybridization of steel fibers in the concrete showed increased workability and toughness when compared to the individual fiber addition in the concrete. In order to achieve maximum workability with FRC, the quantity of cement paste in the mix must be increased to provide better fiber dispersion in the composite.

Chaohua Jiang et al. (2014), observed that adding Basalt Fibers into the concrete significantly improved the flexural strength, tensile strength and toughness index compared to the polypropylene fiber reinforced concrete, but there is not much improvement in compressive strength. Moreover, the Basalt fiber (BF) length showed the beneficial influence on the mechanical properties of concrete. Compared with the host matrix, the flexural and tensile strength of concrete with 12mm length of Basalt fiber increased from 6.30% to 9.58% and 14.06 to 24.35 reactively. As the BF length increased 12mm to 22mm, the corresponding tensile and flexural strength increased from 7.34 to 10.36% and 14.95 to 25.52%. The preferable quantity of BF in concrete is 0.3% volume fraction.

Amin Noushini et al. (2014), studied the addition of polyvinyl alcohol (PVA) fibres of 6mm and 12 mm length in concrete. To evaluate the influence of PVA fibers on fresh and hardened properties of FRC, four different volume fractions 0.12%, 0.25%, 0.375% and 0.5% were considered. It was concluded that the workability of concrete decreased with increased in fiber content and fiber length. The maximum improvement in compressive strength was noticed at 0.25% volume fraction. Concrete reinforced with 6mm PVA fiber length showed 6.5% improvement in compressive strength than that of 12mm PVA fiber length.

Soylev et al. (2014), investigated the influence of polypropylene, glass and Steel fiber addition in concrete at low volume fractions on the mechanical, physical properties of

concrete under two different water–cement ratios (w/c=0.45, w/c=0.65) and two curing (air and moist curing) conditions. Moist curing was found to be more effective in FRC. In this study, all types of FRC were tested under compression, split tensile and flexure. Glass fibers of 12mm length and 0.1% of volume of concrete are added and its mechanical properties and physical properties are tested. A slight increase of flexural tensile strength, split tensile strength is observed for both the w/c ratios whereas compressive strength slightly increased for w/c=0.65 and decreased for w/c=0.45. Moreover SFRC has the lowest entrapped air content and GFRC has the highest. The difference of entrapped air content between GFRC and control concrete are 72% and 46% for 0.45-w/c and 0.65-w/c concretes, respectively. Concrete permeability increased with increased air content and it strongly effected the mechanical properties of the FRC.

2.3 Literature review on stress strain behaviour of FRC and HFRC

(a) FRC

Banthia et al. (1995), studied the stress strain behaviour of micro fibre reinforced composite with carbon (diameter: length, 0.018mm: 3mm), steel (0.025mm: 3mm), and polypropylene (0.004mm: 6mm) fibers under uniaxial tension. The cement matrix with steel fibers showed higher improvement in ultimate tensile strength compared to carbon and polypropylene (PP) fibers. Composite with carbon fibers provided better ductility than that of other fibers and on other hand, PP fibers exhibited better toughening at large crack openings. Hybridization of carbon and steel fibers provided considerable increase in both pre peak tensile strength and post peak ductility compared to other combinations.

Neves et al. (2005), studied the effect of steel fiber diameter i.e., 0.38mm and 0.55mm and fiber content i.e., 0.38%, 0.75%, 1.13% and 1.50% on compressive stress stain behaviour of SFRC. In this investigation, compressive strength of concrete 35Mpa and 60MPa were considered. Addition of small diameter fibers enhanced the pre peak strength of concrete whereas large diameter fibers exhibited post peak deformation of concrete. As the volume of the fiber increased to 0.38% to 1.50%, the strain at peak stress and toughness of the concrete significantly increased.

Benjamin A. Graybeal (2007), conducted experiments to investigate the stress strain response of ultra-high performance fiber-reinforced concrete (UPHFRC). Cylinders

were tested under uni axial compression and the results were analysed to note the peak stress, young's modulus, strain at failure, and complete stress strain response of UHPFRC. It was concluded that this concrete exhibited an exponential improvement in compressive strength and significant increase in stiffness compared to plain concrete. Equations are established for pre peak stress strain behaviour of UHPFRC and post peak stress strain response.

Wen-Cheng Liao et al. (2015), compared stress strain behaviour of steel fiber reinforced concrete (SFRC) to the existing FRC stress strain models. Effect of addition of steel fibers in concrete improved the strain at peak stress slightly but increased the post deformation capacity more. Effect of bond strength between fiber and matrix along with fiber volume fraction and aspect ratio are introduced in the development of stress strain curve. The proposed stress strain model was applied to predict stress-strain relationship of SFRC with compressive strength ranging from 70 to 115 MPa. The post peak response of SFRC was well defined by taking into account of bond strength. Restraint of steel fibers for lateral deformations is treated as similar to the lateral confinement.

Tehmina Ayub et al. (2015), studied the effect of basalt fibers on stress strain behaviour of high strength fiber reinforced concrete (HSFRC) in compression. The strength of the concrete ranging from 70 to 85MPa with volume fraction from 1 to 3%. The addition of basalt fibers showed the less improvement in compressive strength. The advantage of basalt fibers in concrete mainly increased the strain at peak stress from 4.85 to 12.24% and it enhanced the toughness index from 3.8 to 47.15% for all HSFRC with different fiber volume combinations. Reinforcing Index (RI) is the combination of volume fraction and aspect ratio of the fiber (length/diameter) and it influenced the stress strain behaviour of HSFRC. An equation is proposed considering the RI and compressive strength of the concrete. The predicted stress strain values are in good correlation with the experimental values.

(b) HFRC

Betterman et al. (1995), investigated the effect of fiber-matrix interaction in microfiber-reinforced mortar. Mortar reinforced with PVA fiber lengths of 4mm and 12mm were tested under uniaxial tension. Pull-out test is conducted for different embedded lengths. The results showed that 12mm length fiber exhibited better peak load than 6mm fiber length. Composite with 4mm length fiber increased the pre crack strength and 12mm length fiber improved the post cracking strength. The combination of 4mm and 12mm length fiber exhibited higher pre crack, post crack strength and strain capacity compared to that of composite with single fiber length.

CK. YI, et al. (2001), the cracking process and crack fiber interactions that lead to the quasi-brittle behaviour of composites were investigated. The strength and toughness enhancement is associated with crack wake mechanisms. Aggregate bridging and pull-out and secondary crack formations associated with microfiber bridging sites are predominant during the strain hardening regime. Multiple secondary micro cracks perpendicular to the fiber-matrix interface is the dominant failure mode beyond peak load in the strain softening regime.

Banthia et al. (2003), Studied the effect of hybrid fibers on resistance against the crack growth in the cement composite. Two types of each steel (continuously crimped fiber and flattened ends with round shafts fiber) and PP fibers (monofilament and fibrillated fiber) were investigated. Based on the single fiber pull-out test and flexural test, the crimped fibers showed the better pulling capacity and toughness compared to the other steel fiber. It is clearly observed that the monofilament pp fibers exhibited better performance compared to the fibrillated pp fibers. Composite with steel fibers addressed the larger cracks and micro PP fibers controlled the propagation of the micro cracks. Addition of small amount of micro PP fibers showed maximum effectiveness in increasing the efficiency of steel fibers in composite. It was concluded that the composite with steel and PP fibers enhanced the resistance against crack growth compared to single fiber alone.

Banthia and Gupta (2004), investigated the fiber hybridization. In this study, concrete compressive strength of 85 MPa was considered. Companion, single fiber, two fiber and three fiber hybrid composites were cast with micro and macro fibers of polypropylene (PP), carbon and steel. At any volume fraction, composite with steel

fibers exhibited better flexural toughness than any other single fiber. The composite with crimped PP macro-fiber with micro-fibers of carbon and PP showed higher synergy compared to all other combinations. The combination of two micro-PP fibers clearly showed more synergy when compared to single micro-PP fibers alone. The effectiveness of the composite with two micro-PP fiber is further increased when carbon fiber is added as a third fiber.

Banthia et al. (2007), Studied the hybridization of different diameter of crimped steel fibers on strength and toughness of concrete. Smaller diameter of fibers are dispersed easily and closer together in the composite than that of long length fibers. Composite containing smaller diameter fibers, delay the formation of macro cracks by arresting the micro cracks thus provided the strength of the composite. Whereas, large diameter fibers bridged the propagation of macro cracks and improved the toughness of the concrete. The hybridization of smaller diameter fiber with larger diameter forms the synergy and therefore substantial amount of improvement in strength and toughness of the composite was noticed.

Vandewalle (2007), studied post cracking behaviour of hybrid steel fiber reinforced concrete. In this investigation two short steel fibers of 6mm and 13mm length with diameter 0.16mm, one long hooked end steel fiber of length 35mm with 0.55mm diameter were used. Concrete with short fibers able to control the formation of cracks efficiently and then lead to a higher peak strength because they are in very fine size, more number present at the crack section and less spacing between them. However, concrete with large fibers restrains the propagation of large cracks and it provides the ductility. The combination of short and long steel fibers significantly improved strength and ductility of concrete.

Sivakumar et al. (2007), studied the influence of steel–polyester, steel–polypropylene, and steel–glass fibers in the concrete on bending strength. Addition of lower stiffness fibers (polyester, polypropylene, glass fibers) into concrete enhance the pre peak region of load deflection curve whereas higher stiffness fibers (steel fibers) contributed to improve the post peak region of load deflection curve. Polyester, polypropylene, glass fibers, controlled the smaller cracks lead to a higher peak strength but once crack width increased, these fibers were not able to resist the propagation of large crack width and produced poor deflection. The concrete

containing steel–polypropylene significantly improved the pre peak and post peak performance of the concrete compare to the other combinations of steel- polyester and steel-glass fibers.

Machine Hsie et al. (2008), studied mechanical properties of polypropylene hybrid fiber-reinforced concrete. In this study, coarse monofilament polypropylene fibers of fiber content of 3 kg/m^3, 6 kg/m^3, and 9 kg/m^3, are used respectively and staple polypropylene fibers of 0.6 kg/m^3 fiber content was allowed. The coarse monofilament fibers have high young's modulus and it restrains the lateral deformations and increases the strain capacity. However, the fine size staple fibers dispersed easily thought the composite and provided the strength of the composite. The combination of two-fibers in the composite complementing the both the benefits better than the composite containing single fiber alone. Hybridization of polypropylene fibers dispersed uniformly throughout the composites and it decreased the drying shrinkage strains. Compared to the plain concrete properties, polypropylene HFRC improved the modulus of rupture and splitting tensile strength by 24.60% and 13.35% respectively.

Banthia et, al. (2013), studied the Synergy Performance in Hybrid fiber Reinforced Concrete. Hooked end steel fiber, double deformed steel fiber and cellulose fiber are used in this study. There is a clear indication of positive improvement between steel and cellulose fibers in all combinations. Interestingly, cellulose fiber, which by itself does not add much to the toughness of plain concrete, is an effective contributor to toughness in the presence of a steel fiber. Improvement is more pronounced at smaller crack openings and at smaller dosage rates of steel fiber. Both hooked end and double deformed steel fibers are effective for hybridization with cellulose fiber.

Yin Chi et al. (2014), Studied the effect of steel and polypropylene fibers on mechanical properties of hybrid fiber reinforced concrete under direct compression. Addition of steel fibers in the concrete improved the post peak deformation and addition of polypropylene fibers increased the pre peak behaviour of the concrete. As the volume of the fiber increased peak strength, corresponding peak strain and toughness of the concrete improved compare to the plain concrete. The combination of polypropylene and steel fibers formed the hybrid fiber reinforced concrete and enhanced the pre peak and post peak ductility of the concrete compared to the fiber reinforced concrete with single type fiber. Analytical equations are developed with

aspect ratio and fiber volume fraction as influencing parameters, to predict the stress strain relationship of HFRC.

2.4 Literature review on effect of fiber dispersion and orientation on FRC

Shao-Yun Fu et al. (1996), developed an analytical method considering the effect of fiber orientation and fiber length for predicting the composite tensile strength. The fiber length distribution and orientation distribution is modelled by using probability density function. The composite strength is dependent on fiber inclination angle about the loading direction and critical length of fiber. The tensile strength of composite is derived as a function of fiber length and fiber orientation. This model is useful to compute composite strength for a given fiber length, orientation and fiber-matrix interaction properties

Akkaya et al. (2000), studied the influence of fiber length on flexural and tensile behaviour of PVA fiber reinforced cement composite. Composite made up of 0.3% volume fraction by considering the three different fiber lengths of 2mm, 4mm and 6mm. Composite with 2mm length fibers exhibited higher tensile stress compared to any other lengths of composite. The results indicated that the composite containing 2mm short length fibers failed with an enhanced the post cracking tensile stress with multiple crack, whereas composite containing 4mm and 6mm long length fibers have not exhibited multiple cracking behaviour. It was conclude that the short length fibers dispersed better than long length fibers after microstructural examination, and this is the reason for increased the tensile strength of the composite. Short fibers were easier to handle during mixing and they dispersed easily in the composite.

Yilmaz Akkaya et al. (2001), investigated the effect of fiber dispersion on the multiple cracking behaviour of fiber reinforced composites. Microstructural parameters such as the fiber dispersion and the size of the fiber-free areas plays a key role in the initiation and order of the composite cracking. Fiber dispersion affects the strength of the composites by its role in transfer the load to the other parts of the composite. An effective crack bridging and increase in the toughness of the composite can be achieved if the fiber dispersion is better at the first crack location. Fiber-free areas is directly proportional to the cracking strength of the composite. A series of sequential cracks form depending on the size of the fiber-free areas in the composite. As fiber to

fiber spacing reduced, the toughness of the composite significantly increased. The results indicated that the fiber dispersion can also play a great role in the first crack strength and multiple cracking behaviour of the composites.

Torigoe et al. (2003), given the evaluation method for polyvinyl alcohol (PVA) fiber dispersion in engineered cementitious composites (ECC). Estimating the fiber dispersion in ECC was a conundrum because of the lower contrast of the PVA fiber in the composite. To surmount this quandary, an incipient evaluation technique was developed for the dispersion of PVA fibers in ECC. Fluorescence technique is used to detect PVA fibers as green to yellow spots in the composite cross section. After capturing the fluorescence image with a CCD camera through a microscope, the image was divided into minuscule units of the congruous pixel size. The degree of dispersion was computed with the deviation from the average fiber numbers in one unit. Authors proposed a relationship between the degree of dispersion and the ultimate tensile strength of the composite.

Bang Yeon Lee (2008), proposed a method to estimate the fiber distribution by using digital image processing technique and its influence on the tensile performance of fiber reinforced composites. The distribution characteristics of fiber were quantitatively estimated by calculating coefficients predicated on the coordinates of fibers and the shape of the fibers on a plane. A high-resolution camera was used to obtain the images on fracture plane. Images were uploaded in the image J software for processing. The shinning objects were first selected and the images were made binary based on a set threshold object detection method. Binary image was divided into equal square units which is equal to the number of fibers present on the image. The number of fibers were counted in each unit. An expression is proposed and degree of fiber dispersion is quantitatively calculated.

Su-Tae Kang et al. (2011), studied the influence of the fiber distribution and orientation on the pre cracking and post cracking tensile behaviour of the composite. Experimental results showed that the as fiber orientation coefficient increased, the first cracking strength increased whereas post cracking strength increased effectively. Fiber dispersion effects the toughness of the composite by transferring the loads to the other parts of the composite. It was observed that higher the fiber dispersion in the composite higher the first cracking strength. Analytical method is proposed to predict

the tensile strength of the composite by considering the fiber orientation and length distribution in the composite. The predicted tensile strength results are verified with the experimental results, and it showed the satisfactory results

Burcu Akcay et al. (2012), investigated the effect of fiber dispersion on mechanical behaviour of self-compacting concrete with hybrid steel fibers. In this study, three different types of steel fibers i.e., high strength straight steel fiber (length: diameter, 6mm: 0.15mm), normal and strength hoked steel fibers (30mm: 0.55mm), and two different volume fractions (0.75% and 1.5%) are considered. Hybrid combination of high strength short steel fibers with long steel fibers contributed to improve the toughness of composite compared to the hybrid combination of high strength short steel fibers with normal strength long steel fibers. Based on the microstructural studies it was formed that the hybrid fibers are more vertically oriented and homogeneously dispersed in the composite than that of composite containing single fiber. It was concluded that the homogeneous dispersion and uniformly oriented fibres have effects on the mechanical properties of the composite.

Irem Sanal et al. (2013), investigated the effect of fiber orientation. It was found that fiber orientation strongly effects the mechanical behaviour of high performance self-compacting fiber reinforced concrete. The fibers of 6mm length are more effectively aligned in the direction of flow compared to the fibers of 13mm length. Short fibers showed higher fiber orientation, good flow ability compared to long length fibers. It is reported that this is due to the short fibers are mixed and movement easily compared to long length fibers. Composite with short fibers significantly improved the load carrying capacity and long length fibers exhibited deflection hardening.

Kamile Tosun-Felekoglu et al. (2014), studied the effect of fiber dispersion on tensile strength and ductility of PVA-engineered cementitious composites (PVA-ECC) using image analysis. Results showed that the homogeneous fiber dispersion lead to enhance the tensile strength and corresponding strain capacity of the composite. In this investigation two approaches (Torigoe and Lee) are used to estimate the fiber dispersion on fracture plane of PVA-ECC and compared the two methods. Of the two methods, Lee approach is found to be a better presentation of fiber dispersion compared to Torigoe approach. The lake of sensitivity in Torigoe approach is observed while computing the fiber dispersion.

Irem Sanal et al. (2016), studied the influence of fiber dispersion and orientation on SFRC using advanced digital image analysis. Results showed that the SFRC with 6mm and 13mm length fibers exhibited better fiber orientation and density than that of 35mm and 50mm length fibers. It was observed that the short steel fibers (6mm and 13mm) controlled the propagation of micro cracks thus lead to improve the first cracking strength whereas long length fiber bridged the macro cracks and it increased the post cracking ductility. Moreover, the number of cracks increased with an increase in length of fiber. It showed greater multiple cracking capacity and accordingly strain hardening behaviour. Long length steel fibers produced higher energy absorption capacity than the short steel fibers.

2.5 Literature review on pull-out behaviour of fibers

Wang et al. (1987), studied the pull-out tests on polypropylene and nylon fibers emended in cement composites. Experimental results indicated that the Pull-out load increased with increase in embedded length. During the pull-out experiments, scanning electron microscope revealed the increased shear resistance between the fiber-matrix exhibiting the fiber surface abrasion. The fiber surface abrasion was increased with increase in fiber slippage in the matrix. For establishing the possible relationship between the pull-out load and displacement a theoretical model was developed based on the fiber-matrix interaction as a function of slippage distance. The model showed the good correlation with the experimental results.

Shah and Jenq (1987), studied the interfacial bond behaviour between fibers and matrix by conducting the pull-out test. The bonding between fiber and matrix was assumed to be perfect before the pull-out load is applied. It was observed that the major contribution of energy absorption due to the addition of fibers is mainly provided by interfacial frictional forces during fiber pull-out. Results indicated, for achieving the high-energy absorption capacity, fiber fracture in fiber reinforced composite should be avoided.

Gopalaratnam and Cheng (1987), investigated the stability of the de-bonding process by varying the basic properties of the fiber-matrix interface, the fiber diameter and fiber embedment length. Later strain restraint due to fiber matrix interface stress is treated as confining stress. Change in volume restrained under multiaxial stress has a similar effect. Lateral stress effects the resistance to frictional slippage. Hence, the

load transfer (matrix to the fiber) problem is occurred due to the all anteriorly mentioned effects i.e., Poisson's effect, de-bonding, frictional slip and elastic shear transfer.

Youjiang Wang et al. (1988), reported the theoretical analysis of fibre pull-out from a cement matrix. Fiber pull-out is often modelled by considering elastic bond strength and a frictional bond strength for the fibre-matrix interface. However, the frictional bond strength generally varies with the fibre slippage distance relative to the matrix. In this investigation, a theoretical model for the pull-out test has been developed which takes into account the variation of bond strength during fiber pull-out. Good predictions of the experimental load vs crack separation relations are reported for pull-out test with polypropylene, nylon and steel fibres.

Naaman et al. (1991), investigated the bond-stress-slip relationship between smooth fibers and cement composites. Relationship between the bond strength and local slippage at the fiber-matrix interface is developed. Moreover, it is very difficult to measure the stains in short randomly distributed fibers and made unmanageable to develop the experimental bond strength versus slip curves for short randomly distributed fiber reinforced composite. To overcome this problem, a complete pull-out model is developed and predicted by assumed bond-slip relationship.

Jamal Shannag et al. (1997), studied comprehensive experimental program on pull-out tests of steel fiber embedded with different lengths (i.e., 6mm, 12mm and 18mm) in cement matrix. Increase in embedment length of fiber from 6 to 18 mm, resulted in a remarkable increase in the peak pull-out strength. This is due to the increase in the fiber de-bond surface area. Hence, the maximum pull-out load has not appeared to be directly proportional to embedded length of fiber. The frictional bond strength values are reported to be more stable for 12 and 18 mm embedment lengths.

Sehaj Singh et al. (2004), experiments were conducted to understand the pull-out behaviour of polypropylene fiber with embedded lengths (i.e., 19mm, 25mm and 38mm) from a cementitious matrix. It was concluded that the peak pull-out load increased with increased embedded fiber length in the cement matrix. This gain can be impute to the increase in friction between the fiber and matrix due to the fiber abrasion as it slips out of the matrix. The abrasion effect tends to increase with the increase in embedded fiber length. Fiber pull-out properties changed with increase in

the embedded fiber length in the cement matrix. A new method for improving the interfacial bond between polypropylene fibers and cement mortar matrix is developed. In this investigation, mechanical depression were created on the fiber surface by pressing the fibers between two hardened steel surfaces having projections with a pressure of 200, 500 and 700 kPa. Depression at 700 kPa gave the best performance.

Di Maida et al. (2015), studied the effects of nano-silica treatment on the bonding characteristics of polypropylene (PP) fibers with embedded lengths (20mm and 30mm) in a cement matrix. It was concluded that the peak pull-out load increased with increase in embedded length. Sol–gel technique was used to coat the nano silica on the surface of PP fibers. Surface morphology of PP fibers was observed before and after the pull-out test. Peak pull-out load and interfacial stress increased for treated fibers than that of untreated fibers.

Doo-Yeol Yoo et al. (2017), studied the influence of fiber type and concrete strength on the fiber pull-out behaviour of high performance fiber-reinforced cementitious composites (HPFRCC). Three different concrete strengths and two different steel fibers, i.e., hooked and straight steel fibers were used. Fiber pull-out capacity increased with increase in strength of the concrete. At lower slippage, the hooked end steel fibers exhibiting the higher bond strength and peak pull-out load than that of straight steel fibers. Straight steel fibers were more efficient in improving the pull-out performance with increasing matrix strength, compared to that of hooked steel fibers. The shorter straight steel fibers were most efficiently improved in average bond strength and long straight steel fibers significantly increased the peak pull-out load.

2.6 Literature review on stress strain models of FRC

Fanella et al. (1985), proposed an analytical model to predict the compressive stress-strain curve of fiber-reinforced composite by considering the fiber geometry and volume fraction. Different parameters are used to define the ascending and descending portions of the stress strain curve. Four constants were used to represent the ascending region and four more to determine the descending region. These constants were obtained from empirical relationships obtained from the experimental curves.

Ezeldin et al. (1992), studied the normal and high strength fiber-reinforced concrete under compression. Compressive strength ranging from 35 to 85 MPa, three fiber volume contents (Vf) of 30, 45, and 60 kg/m3 and aspect ratios (L/D) of 60, 75 and 100 are considered. Effect of reinforcing index parameter (Vf. L/D) on the peak stress, strain at peak stress, modulus of elasticity, energy absorption of concrete and the shape of the curve are reported. Previously developed empirical equation is modified and proposed a simplified equation to predict the complete stress strain curve.

Nataraja et al. (1999), Proposed the model to predict the compressive stress strain curve for the compressive strength ranging from 30 to 50MPa. Two crimped steel fibers of aspect ratios of 55 and 82 with three different volume fractions of 0.5%, 0.75% and 1.0% were considered. Addition of fibers to the concrete improved the main parameters of the stress strain curve i.e., peak stress, corresponding strain, energy absorption capacity. A simple stress strain analytical model is proposed to predict the pre peak and post peak region of the stress strain curve. Predicted stress strain curves have good correlation with the experimental stress strain curves. Equations are also proposed to quantify the influence of fibers on peak strength, strain at peak strength and energy absorption capacity of FRC with respect to the fiber reinforcing index.

Barros et al. (1999), investigated the flexural stress strain behaviour of SFRC. Compressive strength of plain concrete varied from 32 to 56 MPa. The aspect ratios of hooked end steel fibers with reinforcing index (RI) varied from 0.23 to 0.57 were considered. As the reinforcing index increased the peak stress, strain at peak stress and energy absorptions increased. An analytical stress strain model is developed to formulate both the ascending and descending parts. These analytical results showed the good agreement with the experimental results. Equations are also proposed with respect to the fiber reinforcing index for computing the peak strength, strain at peak strength and energy absorption capacity of FRC.

Ou et al. (2012), investigated the effect of high reinforcing index on stress-strain behaviour of steel fiber-reinforced concrete (SFRC) under uniaxial compression. Hooked-end steel fibers of various lengths and aspect ratios i.e., 50 and 60 were considered. The fiber reinforcing index for short and long hooked end streel fibers varied from 0.4 to 1.7. It was reported that addition of hooked steel fibers exhibited a little influence on the compressive strength and modulus of elasticity of SFRC. Long

hooked end steel fibers and fibers having a lower aspect ratio showed a significant improvement of the toughness of SFRC. Based on this observation, a models of the stress-strain curve in compression and toughness of SFRC with respect to a fiber reinforcing index up to 1.7 are proposed.

Aref Abadel et al. (2016), studied the mechanical behaviour of hybrid fibre-reinforced concrete (HFRC). HFRC was made up of different proportions of plain Kevlar, crimped polypropylene and hooked-ended steel fibres with a total fibre volume fraction of 1·2% and 1·4%. Experimental results indicated that the concrete with hybrid fibers slightly improved the compressive strength and significantly increased the energy absorption capacity. A model is proposed for predicting the stress strain curves of HFRC. Major parameters required for generating the stress strain curve are computed by using fiber reinforcing index. The predicted stress strain curves showed good coincidence with experimental results and considerable improvement over the existing FRC models.

2.7 Literature review on Strain Hardening and Strain Softening behaviour of FRC

Tetsushi Kanda et al. (2000), studied a new theoretical approach for predicting the tensile stress-strain relation of random short-fiber-reinforced cement composites showing pseudo strain hardening. This approach is based on micromechanics theory, considering pseudo strain hardening phenomenon in terms of constitutive properties of the fiber, matrix, and fiber/matrix interface. The proposed model requires theoretical treatment of an inelastic strain due to multiple cracking, and it is achieved by employing a probabilistic description of initial flaw size distribution, which should be known for predicting the stress-strain relation. A comparison with the test data indicates that the proposed model is capable of reasonably reproducing the stress strain relation of ‘‘similar’’ composites.

Fantilli et al. (2009), Investigated the strain hardening behaviour of High Performance Fiber-Reinforced Cementitious Composite (HPFRCC). Strain hardening initiated after composite cracking. Multiple cracks are developed and it formed single unstable tensile crack in the post cracking region before complete failure. These cracks are restrained by the fibers present in the composite and improved the post cracking strength. Strain hardening of HPFRC increased with increased in fiber length and

volume fraction. A model is proposed to predict the spacing of the cracks and design of FRC.

Ahmed et al. (2008), Studied the multiple cracking behaviour and strain hardening performance of hybrid fiber reinforced concrete with different fiber volume fractions of polyethylene and steel fibers of 12mm and 18mm lengths. The peak tensile strength and corresponding strain capacity of the composite is found to increase with increased in length (18mm) and content of polyethylene fiber, however higher fiber content showed decrement in tensile strength. Composite with steel fibers improved the post cracking strength and ductility of the composite. The hybrid combination of 1% steel fibers with 0.25% of polyethylene fibers (18mm length) improved the strain hardening behaviour compared to the composite containing 1% steel and 0.2% polyethylene fibers (12mm length). Higher volume fraction and increase in length of polyethylene fiber resulted in multiple cracking, 1.5 times increase in strain capacity and enhanced the strain hardening behaviour of composite.

Faiz Uddin Ahmed et al. (2011), investigated the effect of hybrid PVA fibers on strain hardening behaviour of PVA- FRC under bending. The composite with 6mm length fibers improved the pre crack strength by arresting the micro cracks and composite with 12mm and 24mm length fibers contributed to increase in post peak ductility. A matrix of 2% -24mm and 1% - 6mm fiber showed better performance in terms of pre crack strength and post peak ductility compared to the combination of 2% - 12mm and 1% - 6mm fiber. Improved performance is due to different lengths of fibers controlling the different scales of cracking in composite.

2.8 Summary of literature review:

- Workability decreased with an increase in fiber content and fiber length
- Fracture in the concrete is a gradual and multi-scale process
- Hybridization of fibers is an effective solution for concrete brittleness and early age shrinkage cracks
- Blending of Short and long length of fibers enhances the properties of concrete at peak strength and post peak deformation of composite
- The peak pull-out load increases with the increase in embedded length
- Effective fiber orientation increases the first cracking strength slightly and more efficiently increases the post cracking strength
- Fiber dispersion affects the toughness of the composites by its role in transferring the load to the other parts of the specimen. An effective crack bridging and increase in the toughness of the composite can be achieved if the fiber dispersion is better at the first crack location

Chapter-3

Scope and objectives of the Work

3.1 General

Earlier research shows that short length fibres primarily control the propagation of micro cracks, and improve the pre crack strength, whereas long length fibers arrest the macro cracks and improve the post crack deformation of concrete. Thus different combinations of short and long length fibers would help in arresting the micro as well as macro cracks to improve both pre and post crack performances of concrete; a synergistic combination of different fiber properties that cannot be achieved with either of the fiber type acting alone.

Hybrid fiber reinforced concrete (HFRC) is a research area where the best qualities of different types of fibers contribute to improve strength and deformation of concrete. To achieve the similar benefits of HFRC, one type of short length and long length fibers are combined in concrete and is named as Graded fiber reinforced concrete. Therefore, an attempt has been made to study the effect of addition of Graded Glass Fibers with different fiber length and volume fraction in Glass Fiber Reinforced Concrete.

3.2 Need for the investigation

- Most of the studies were conducted on HFRC using with two different kind of fibers.
- Synergy between Short fiber-long fiber hybridization is realised but not investigated at length.
- Need to study the strength and strain in uniaxial state of Glass Fiber Reinforced concrete by considering the effects of different influencing parameters i.e., fiber length, Fiber orientation and fiber dispersion.
- Necessity to establish the relationship between the Reinforcing Index (i.e., for mono and graded fibers) and mechanical properties of Mono Glass Fiber Reinforced Concrete and Graded Glass Fiber Reinforced concrete in both Tension and Compression.

- Need to study the relationship between the strain hardening in tension and strain softening in compression for Mono Glass Fiber Reinforced Concrete and Graded Glass Fiber Reinforced concrete.

3.3 Scope of the present investigation:

- Scope of present research is limited to four lengths of AR Glass Fibers 3mm, 6mm, 12mm and 20mm lengths are combined in different proportions to form Graded glass fibers with normal strength concrete of M30 and M50 Grade.

3.4 Research Significance:

In this investigation combination of different lengths of mono fibers are considered and named as Graded fiber reinforced concrete to distinguish from Hybrid fiber reinforced concrete. Inspiration is obtained from concrete mix proportioning where in different sizes of aggregates are combined to obtain well graded aggregates. Similar synergy with well Graded fibers of different lengths may improve strength and deformation of concrete. In the present work four lengths of AR glass fibers 3mm, 6mm, 12mm and 20mm are combined in different proportions to form Graded Glass Fibers. This study systematically correlate the tensile and compressive properties of Mono and Graded Glass Fiber Reinforced concrete by considering the Reinforcing Index of mono and graded fibers.

3.5 Objectives:

- To investigate the influence of Mono-Fibres on the tensile and compressive properties.
- To study the effect of Graded-Fibres on the tensile and compressive properties.
- To Examine the Fiber distribution, Fiber-orientation & Fiber pull out behaviour of GFRC with Mono and Graded Fibers.
- To model the tensile and compressive behaviour of Mono-GFRC & Graded-GFRC with different Fiber length and Fiber volume combinations.

To achieve the above objectives, the investigation is devoted in two phases of work. The objectives of different phases of work are presented here.

3.6 Research Methodology

To achieve the above objectives and keeping in view the scope of the research work, a detailed experimental program is planned and the work is divided into two phases.

3.6.1 Phase-I: Study on Mono Glass Fiber Reinforced Concrete (MGFRC)

The first phase of investigation is aimed to understand the behaviour of Mono Glass Fiber Reinforced Concrete (MGFRC). The main variables of this study are length of fiber and volume fraction. Four different fiber lengths 3mm, 6mm, 12mm and 20mm and five different volume fractions 0.1%, 0.2%, 0.3%, 0.4% and 0.5% are used to study. This work is carried out with the two grades of concrete (M30 and M50). This Phase of investigation is divided into four parts and given below.

Part-A: Studies on slump and compressive strength of MGFRC

To assess the workability of the concrete, slump cone test is to be conducted on fresh MGFRC mixes. Different volume of fibers and different lengths of fiber will have different effects on the slump. Cube specimens are prepared for the MGFRC and it will be tested under compression. The variation of compressive strength of MGRC specimens will be compared with the plain concrete strength.

Part-B: Investigation of strain hardening behaviour (SHB) in Tension

In order to understand the stress strain behaviour of MGFRC in tension, dog-bone specimens will be cast and it will be tested under uniaxial tension. Initial slope, strain hardening slope, strengthening factor and ductility factor will be estimated based on the experimental stress-strain results. Fiber dispersion and orientation can be quantified for different fiber length and volume fraction of MGFRC.

Part-C: Investigation of strain softening behaviour (SSB) in Compression

In order to understand the stress strain behaviour of MGFRC in compression. Prism specimens will be cast and it will be tested under uniaxial compression. Initial slope, strain softening slope, strengthening factor and ductility factor will be estimated based on the experimental compressive stress-strain results.

Part-D: Relationship between SHB in Tension and SSB in Compression

After analysing the experimental results of stress strain behaviour of MGFRC in tension and compression, relationship between Strain hardening in tension and strain softening in compression will be studied.

3.6.2 Phase-II: Study on Graded Glass Fiber Reinforced Concrete (GGFRC)

The second phase of study is aimed to understand the behaviour of Graded Glass Fiber Reinforced Concrete (GGFRC). Two or more length of fibers are mixed to form Graded Fibers. When the mixture consists of 3mm and 6mm is named as Short Graded Fiber (SGF), mixture consists of 12mm and 20mm is named as Long Graded Fiber (LGF) and mixture of all the four lengths 3mm, 6mm, 12mm and 20mm is named as Combined Graded Fiber (CGF). The main variables of this study is short graded fibers (3mm+6mm), long graded fibers (12mm+20mm), combined graded fibers (3mm+6mm+12mm+20mm) and total volume fraction (0.3%, 0.4% and 0.5%). In this study mixing of fibers is done in proportion of 20%+80%, 40%+60%, 50%+50%, 60%+40% and 80%+20% to obtain graded fibers. This work is carried out with the two grades of concrete (M30 and M50). This Phase of investigation is divided into four parts and given below.

Part-A: Studies on slump and compressive strength of GGFRC

Slump cone test is to be conducted on freshly prepared SGFRC, LGFRC and CGFRC mixes to assess the workability. Grading of fibers with different fiber volume combinations will have different effects on the slump. Cube specimens will be prepared for the SGFRC, LGFRC and CGFRC, then these specimens will be tested under compression. The variation of compressive strength of SGFRC, LGFRC and CGFRC specimens will be compared with the compressive strength of MGFRC and control specimens.

Part-B: Investigation of strain hardening behaviour (SHB) in Tension

In order to understand the stress strain behaviour of SGFRC, LGFRC and CGFRC in tension, dog-bone specimens will be cast and tested under uniaxial tension. Initial slope, strain hardening slope, strengthening factor and ductility factor will be estimated based on the experimental stress strain results. The mechanical behaviour of SGF, LGF and CGF will be compared with the MGFRC. Fiber dispersion and orientation can

be quantified for different fiber grading and different fiber volume combinations of GGFRC.

Part-C: Investigation of strain softening behaviour (SSB) in Compression

In order to understand the stress strain behaviour of SGFRC, LGFRC and CGFRC in compression, prism specimens will be cast and tested under uniaxial compression. Initial slope, strain softening slope, strengthening factor and ductility factor will be estimated based on the experimental stress strain results. The mechanical behaviour of SGF, LGF and CGF will be compared with the MGFRC. Fiber dispersion and orientation can be quantified for different fiber grading and different fiber volume combinations of GGFRC.

Part-D: Relationship between SHB in Tension and SSB in Compression

After analysing the experimental results of stress strain behaviour of GGFRC in tension and compression, relationship between Strain hardening in tension and strain softening in compression will be studied.

The parameters of investigation consist of

- Strength of concrete - 36.01MPa (M30 grade), 57.02MPa (M50 grade)
- Volume fraction - 0.1%, 0.2%, 0.3%, 0.4% and 0.5%
- Mono glass fibers - AR-Glass fibers of length 3mm, 6mm, 12mm and 20mm
- Graded glass fibers - Short graded fibers (3mm+6mm)
  Long graded fibers (12mm+20mm)
  Combined graded fibers (3mm+6mm+12mm+20mm)

A schematic diagram of the research methodology adopted along with the variables considered in each phase is shown in Fig 3.1.

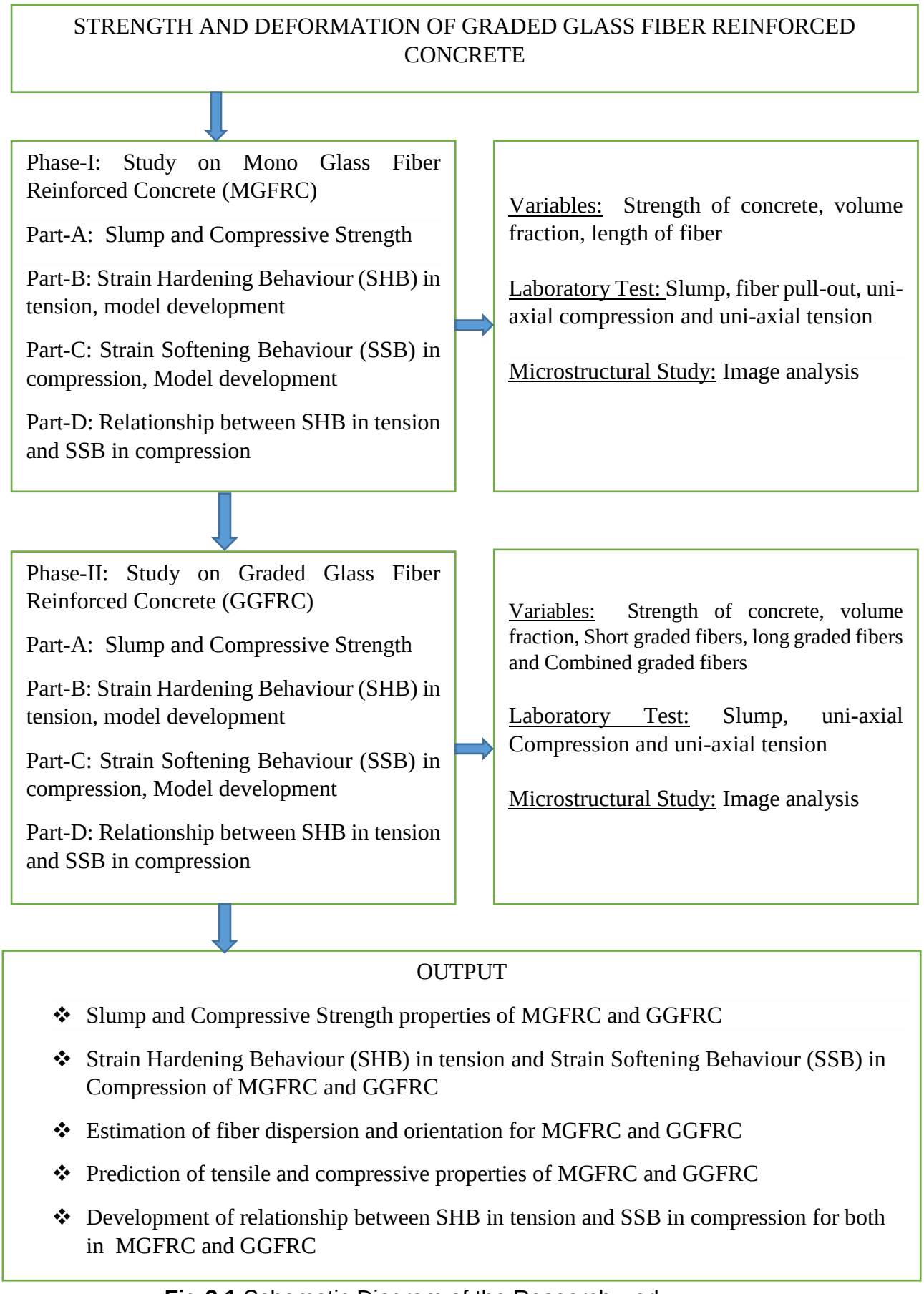

Fig.3.1 Schematic Diagram of the Research work

Chapter-4

Experimental Program

4.1 Introduction

Experimental programme is designed to fulfil the objectives stated in the chapter-3. Two grades of concrete, M30 and M50, are taken to study the effect of variation of matrix. AR-glass fibers of 14μm diameter are obtained from Chemzest Enterprises in a single lot. Varying the volume of fiber for a fiber length is considered as one type and combining different lengths in a volume is considered as another type. Above fundamental variation will focus on addressing the objectives of this research. In the present work uni-axial tension and compression tests were performed on dog-bone specimens and prismatic specimens. Scheme of experimental programme is given in Fig.4.1.

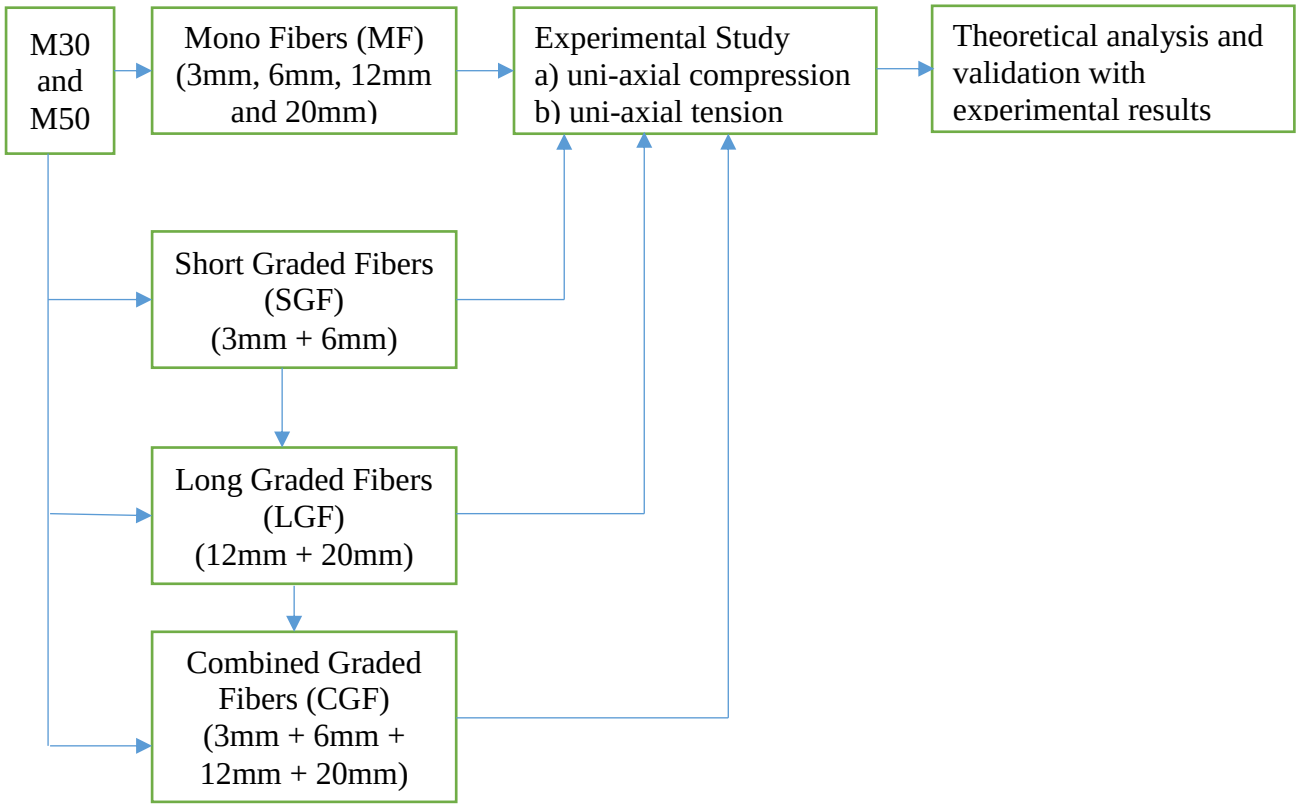

Fig.4.1 Scheme of experimental program

4.1.1 Experimental Program with mono fibers (MF)

Specimen containing only one length type of fiber is called Mono Fiber (MF). This part of investigation is focused on Mono glass fiber reinforced concrete (MGFRC) with varying volume fractions of different length Glass Fibers. Variables in MF specimens are volume of fiber 0.1%, 0.2%, 0.3%, 0.4% and 0.5% and length of AR-glass fibers 3mm, 6mm, 12mm and 20mm. There are 21 mixes in total which includes 1 mix of plain concrete and 20 mixes (four lengths and five volume fractions) of MGFRC. For each mix, three cubes, three prisms and three dog-bone specimens are cast for M30 and M50 grade of concrete. Details of experimental program is given in Table 4.1. Alphabet a, b, c, d, e stands for volume of fiber, the numbers 3, 6, 12, 20 stands for length of fiber.

Table 4.1 Details of experimental program for MGFRC

S. No.	Specimen Designation	V_f (%)	Glass Fiber Length				No. of Specimens		
			3mm (F3)	6mm (F6)	12mm (F12)	20mm (F20)	C*	P*	D*
1	MF0-0	0	-	-	-	-	3	3	3
2	MF3-a	0.1 (a)	100%	-	-	-	3	3	3
3	MF6-a		-	100%	-	-	3	3	3
4	MF12-a		-	-	100%	-	3	3	3
5	MF20-a		-	-	-	100%	3	3	3
6	MF3-b	0.2 (b)	100%	-	-	-	3	3	3
7	MF6-b		-	100%	-	-	3	3	3
8	MF12-b		-	-	100%	-	3	3	3
9	MF20-b		-	-	-	100%	3	3	3
10	MF3-c	0.3 (c)	100%	-	-	-	3	3	3
11	MF6-c		-	100%	-	-	3	3	3
12	MF12-c		-	-	100%	-	3	3	3
13	MF20-c		-	-	-	100%	3	3	3
14	MF3-d	0.4 (d)	100%	-	-	-	3	3	3
15	MF6-d		-	100%	-	-	3	3	3
16	MF12-d		-	-	100%	-	3	3	3
17	MF20-d		-	-	-	100%	3	3	3
18	MF3-e	0.5 (e)	100%	-	-	-	3	3	3
19	MF6-e		-	100%	-	-	3	3	3
20	MF12-e		-	-	100%	-	3	3	3
21	MF20-e		-	-	-	100%	3	3	3
Total							**63**	**63**	**63**
Grand Total							**189**		
C* = Cubes, P* = Prisms, D* = Dog-bone									

4.1.2. Experimental Program with Graded Fibers (GF)

Specimens containing two or more length of fibers are mixed to form Graded Fibers. This part of investigation is focused on graded glass fiber reinforced concrete (GGFRC) with varying volume fraction and mixture of different length glass fibers. When the mixture consists of 3mm and 6mm is named as Short Graded Fiber (SGF), mixture consists of 12mm and 20mm is named as Long Graded Fiber (LGF) and mixture of all the four lengths 3mm, 6mm, 12mm and 20mm is named as Combined Graded Fiber (CGF).

There are 45 mixes of GGFRC in total which includes 15 mixes (three volume fractions i.e., 0.3%, 0.4% and 0.5% with five different grading of fibers) of SGF, LGF and CGF each. For each mix, three cubes, three prisms and three dog-bone specimens are cast for M30 and M50 grade of concrete.

Alphabet #c, #d, and #e stands for volume of fiber 0.3%, 0.4% and 0.5% respectively, the numbers 3, 6, 12, 20 stands for length of fiber. The mixture of different lengths of fibers are designated by roman numbers I to V, where I stands for 20% + 80%, II stands for 40% + 60%, III stands for 50% + 50%, IV stands for 60% + 40%, and V stands for 80% + 20%. Of the percentage of fibers in the mixture of different length, normally the first percentage refers to shorter and second percentage refers to longer of two. Details of experimental program is given in Table 4.2.

Table 4.2 Details of experimental program for GGFRC

S. No.	Specimen Designation	Vf (%)	Glass Fiber Length				No. of Specimens		
			3mm	6mm	12mm	20mm	C*	P*	D*
1	SGF-I#c	0.3	20%	80%	-	-	3	3	3
2	SGF-II#c		40%	60%	-	-	3	3	3
3	SGF-III#c		50%	50%	-	-	3	3	3
4	SGF-IV#c		60%	40%	-	-	3	3	3
5	SGF-V#c		80%	20%	-	-	3	3	3
6	LGF-I#c	0.3	-	-	20%	80%	3	3	3
7	LGF-II#c		-	-	40%	60%	3	3	3
8	LGF-III#c		-	-	50%	50%	3	3	3
9	LGF-IV#c		-	-	60%	40%	3	3	3
10	LGF-V#c		-	-	80%	20%	3	3	3
11	CGF-I#c = 20%SGF- +80%LGF	0.3	8%	12%	32%	48%	3	3	3
12	CGF-II#c= 40%SGF- +60%LGF		16%	24%	24%	36%	3	3	3
13	CGF-III#c= 50%SGF- +50%LGF		20%	30%	20%	30%	3	3	3
14	CGF-IV#c= 60%SGF- +40%LGF		24%	36%	16%	24%	3	3	3
15	CGF-V#c= 80%SGF +20%LGF		32%	48%	8%	12%	3	3	3
16	SGF-I#d	0.4	20%	80%	-	-	3	3	3

17	SGF-II#d		40%	60%	-	-	3	3	3
18	SGF-III#d		50%	50%	-	-	3	3	3
19	SGF-IV#d		60%	40%	-	-	3	3	3
20	SGF-V#d		80%	20%	-	-	3	3	3
21	LGF-I#d		-	-	20%	80%	3	3	3
22	LGF-II#d		-	-	40%	60%	3	3	3
23	LGF-III#d	0.4	-	-	50%	50%	3	3	3
24	LGF-IV#d		-	-	60%	40%	3	3	3
25	LGF-V#d		-	-	80%	20%	3	3	3
26	CGF-I#d = 20%SGF- +80%LGF		8%	12%	32%	48%	3	3	3
27	CGF-II#d= 40%SGF- +60%LGF		16%	24%	24%	36%	3	3	3
28	CGF-III#d= 50%SGF- +50%LGF	0.4	20%	30%	20%	30%	3	3	3
29	CGF-IV#d= 60%SGF- +40%LGF		24%	36%	16%	24%	3	3	3
30	CGF-V#d= 80%SGF +20%LGF		32%	48%	8%	12%	3	3	3
31	SGF-I#e		20%	80%	-	-	3	3	3
32	SGF-II#e		40%	60%	-	-	3	3	3
33	SGF-III#e	0.5	50%	50%	-	-	3	3	3
34	SGF-IV#e		60%	40%	-	-	3	3	3
35	SGF-V#e		80%	20%	-	-	3	3	3
36	LGF-I#e		-	-	20%	80%	3	3	3
37	LGF-II#e		-	-	40%	60%	3	3	3
38	LGF-III#e	0.5	-	-	50%	50%	3	3	3
39	LGF-IV#e		-	-	60%	40%	3	3	3
40	LGF-V#e		-	-	80%	20%	3	3	3
41	CGF-I#e = 20%SGF- +80%LGF		8%	12%	32%	48%	3	3	3
42	CGF-II#e= 40%SGF- +60%LGF		16%	24%	24%	36%	3	3	3
43	CGF-III#e= 50%SGF- +50%LGF	0.5	20%	30%	20%	30%	3	3	3
44	CGF-IV#e= 60%SGF- +40%LGF		24%	36%	16%	24%	3	3	3
45	CGF-V#e= 80%SGF +20%LGF		32%	48%	8%	12%	3	3	3
Total							**135**	**135**	**135**
Grand Total							**405**		
C* = Cubes, P* = Prisms, D* = Dog-bone Short Graded Fiber (3mm+6mm) & Long Graded Fiber (12mm+20mm) Combined Graded Fiber **(SGF(40%3mm+60%6mm)+LGF (40%12mm+60%20mm))**									

4.2 Materials

The materials used in this investigation are Ordinary Portland cement (53 Grade), Fly ash, Fine Aggregate, Coarse Aggregate, Water, Super plasticizer SP430 and AR-Glass Fibers.

4.2.1 Cement

Ordinary Portland cement confirming to IS12269 of 53 grade (compressive strength of 53MPa) were used in this entire experimental study. Procured cement was stored properly. Specific gravity of cement varies from 3.12 to 3.14 for the consignment obtained.

4.2.2 Fly Ash

Fly ash was brought from Ramagundam Thermal Power Plant, India and it was stored properly. The specific gravity of fly ash is 2.17. The chemical composition of Fly ash (% by mass) was SiO_2 = 60.11%, Al_2O_3 = 26.53, Fe_2O_3 = 4.25, SO_3 = 0.35, CaO = 4.00, MgO = 1.25, Na_2O = 0.22, LOI = 3.25.

4.2.3 Fine Aggregate

Fine aggregate conforming to Zone-II according to IS 383-2016 was used. The Fine aggregate used was obtained from a nearby river source. The sand obtained was sieved as per IS sieves (i.e. 2.36, 1.18, 0.6, 0.3, and 0.15mm). Sand retained on each sieve was filled in different bags and stacked separately for use. To obtain required fineness modulus of sand consistently, sand retained on each sieve is mixed in appropriate proportion. The bulk density, specific gravity, and fineness modulus of the sand used were 1.41 g/cc, 2.68, and 3.25 respectively. Fineness Modulus of fine aggregate is used in this entire experimental study and given in Table 4.3.

Table 4.3 Fineness Modulus of fine aggregate

Sieve size (mm)	Mass retained (gm)	% Retained	Cumulative % passing	Cumulative % retained
10	0	0	100	0
4.75	0	0	100	0
2.36	125	25	75	25
1.18	95	19	56	44
600µm	100	20	36	64
300µm	140	28	8	92
150µm	40	8	0	100
Total	500		Total	325
Fineness Modulus = 325/100 = 3.25				

4.2.4 Coarse Aggregate

Crushed granite was used as coarse aggregate. The coarse aggregate was obtained from a local crushing unit having 16mm nominal size. 16mm well graded aggregate according to IS 383-2016 was used in this investigation. The coarse aggregate consists of 40% passing through 16 mm and retained on 12.5 mm sieve, 30% passing through 12.5 mm and retained on 10 mm sieve, and 30% passing through 10 mm and retained on 4.75 mm sieve. The material retained on each sieve was filled in bags and stacked separately. The bulk density, specific gravity, and fineness modulus of coarse

aggregate used were 1.41 g/cc, 2.68, and 7.1 respectively. Fineness Modulus of coarse aggregate is used in this entire experimental study.

4.2.5 Water

Potable water was used in the experimental work for both mixing and curing as per IS 456 2000.

4.2.6 Super Plasticizer

Conplast SP430 of FOSROC chemicals was used for all mixes.

4.2.7 Glass fibers

AR-glass fibers obtained from Chemzest Enterprises, Channai, India is shown in Fig.4.2. Glass fibers used in the present study have tensile strength-1700 MPa, Modulus of elasticity-73 GPa, Specific gravity 2.6.

(a) 3mm

(b) 6mm

(c) 12mm

(d) 20mm

Fig.4.2 Different lengths of Glass Fibers

4.3 Mix Design proportions

M30 and M50 mixes were designed as per IS 10262-2009 and the proportions are given in the Table 4.4 per cubic meter of concrete.

Table 4.4 Mix Proportions for M30 and M50 Grade of Concrete.

Mix	Coarse aggregate kg/m^3	Fine aggregate kg/m^3	Cement kg/m^3	Fly-ash kg/m^3	SP430 (lit/m^3)	W/B
M30	1145	764	300	100	1.0	0.43
M50	1004	669	430	100	2.0	0.37

4.4 Moulds and Equipment

4.4.1 Cube moulds

Standard moulds of 100mm X 100mm X 100mm made of cast iron were used to cast as controlled cube specimens for M30 and M50 grades of concrete for obtaining compressive strength of concrete.

4.4.2 Prism Moulds

Cast iron moulds of size 100mm x 100mm x 200mm were used for casting of the concrete prisms and testing the specimens for M30 and M50 grades of concrete developing the compressive stress strain curves.

4.4.3 Dog-bone Moulds

The geometry of dog-bone specimens for uniaxial tension test is shown in Fig.4.3 and the section of tensile specimens used is 80mm X 40mm and the gauge length of the specimens is 150mm. The sample has a shoulder at each end and a gauge section in between. The shoulders are wider than the gauge section. Dog bone sample is designed to ensure the highest probability that the sample will fail in the gauge section. The dog-bone specimens were used for casting of the concrete prisms and testing the specimens for M30 and M50 grades of concrete developing the tensile stress strain curves.

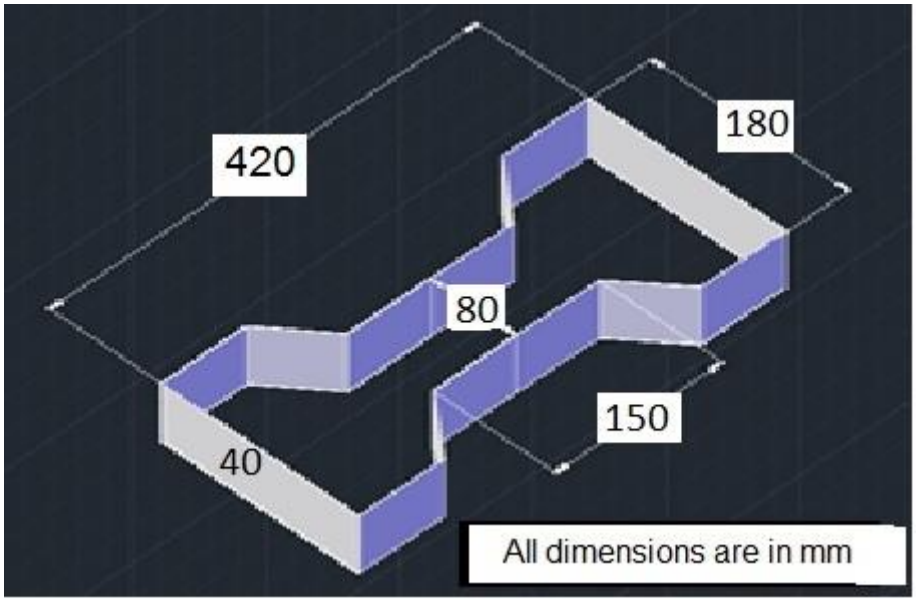

Fig.4.3 Geometry of dog-bone specimen

4.5 Mixing, Casting and Curing

Coarse and fine aggregates were mixed together into a homogeneous mix. Cement and fly ash were separately mixed and then glass fibers were dispersed into the cement-fly ash mixture. The contents were then added into the pan mixer capacity of 100kg mixture. Finally, water was added with super plasticizer and then the contents were thoroughly mixed. Proper homogenous mixing was ensured by continuous mixing for 5 to 7 minute. Slump test was conducted to ensure workability of plain concrete mix and each GFRC mix before casting. The concrete batch was then poured into each mould and compacted on a vibrating table. All the test specimens were removed from mould after setting, and then cured for 28 days under water. Fig.4.4 shows the steps of preparation of test specimens.


(a) Mixing


(b) Casting


(c) After curing

Fig.4.4 Stages of preparation of test specimen

4.6 Testing Procedures for Fresh and Hardened State of GFRC

4.6.1 Slump Cone Test

Freshly prepared plain concrete and GFRC mixes are tested for workability using standard slump cone apparatus (Fig.4.5). Slump test is conducted strictly as per IS 7320-1974.

Fig.4.5 Slump cone test of GFRC

4.6.2 Compressive Strength Test

The cube specimens are tested on compression testing machine of capacity 2000 kN is shown in Fig.4.6. The specimen is placed on the machine in such a manner that the load is applied on the faces orthogonal to the direction of casting the cube. The axis of the specimen is carefully aligned to the centre of the loading frame. The load is increased continuously at a constant rate until the resistance of the specimen to the increasing load breaks down and no longer can be sustained. The maximum load applied on the specimen is recorded. The rate of loading is adopted as per IS 516-1959.

Fig.4.6 Testing of cube under compression

4.6.3 Uniaxial Compression Test

The prism Specimen was arranged in the Tinus-Olsen Testing Machine of 2000 KN capacity. Load Cell of 2 MN was used to measure the load acting on the prism, while 2 LVDTs are placed at the opposite corners to obtain the corresponding displacement over a gauge length of 100mm. Load cell and LVDTs are connected to the DAC as shown in Fig.4.7. The axis of the specimen was carefully aligned at the center of the loading frame and specimen is subjected to gradual increase of load and deformations are recorded till failure. Three Specimens were tested shown in Fig.4.8 and for each parameter to obtain average stress-strain behaviour.

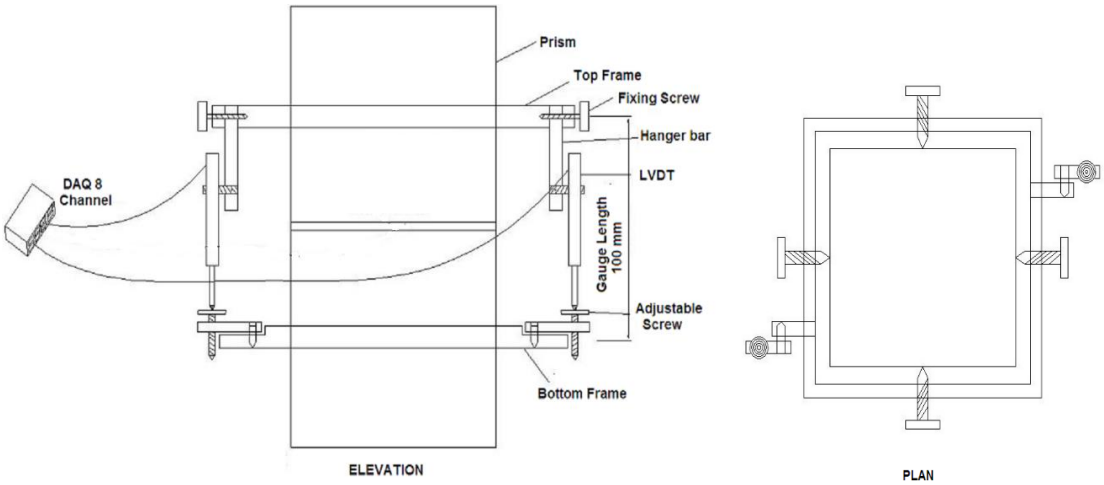

Fig.4.7. Schematic diagram of compression test setup

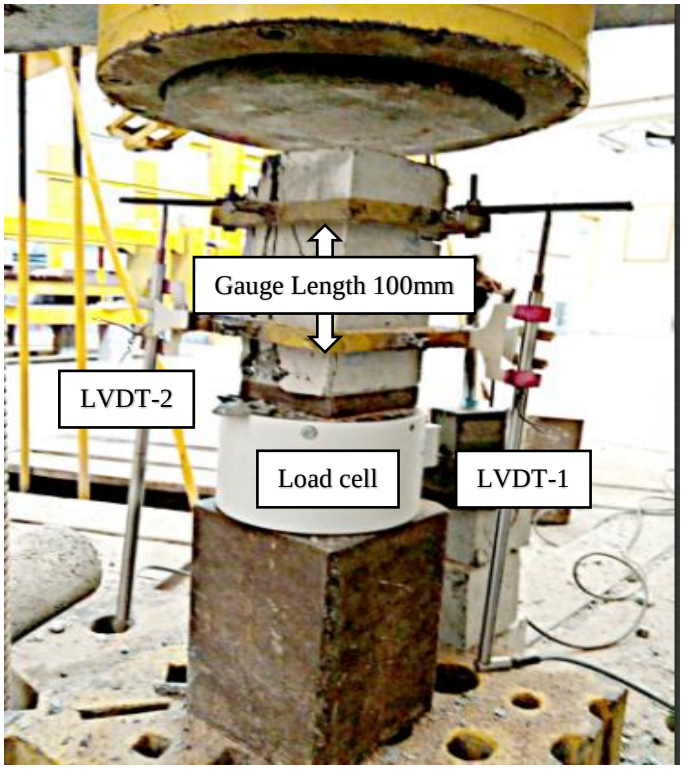

Fig.4.8 Testing of Prisms under uniaxial compression

4.6.4 Uniaxial Tension Test

Dog bone specimens are used in tensile test. Dog bone specimen is designed to ensure the highest probability that the specimen will fail in the gauge section. Nuts and double ring arrangement of test setup ensures to avoid eccentricity (Fig.4.9). Steel plates and steel grips to hold the specimen will enable self-alignment of specimen under load. Uniaxial tensile tests were performed with a servo hydraulic testing frame of 50 KN capacity (Fig.4.10), under displacement control (0.2 mm/sec). Data acquisition system is used to record the load and displacement continuously.

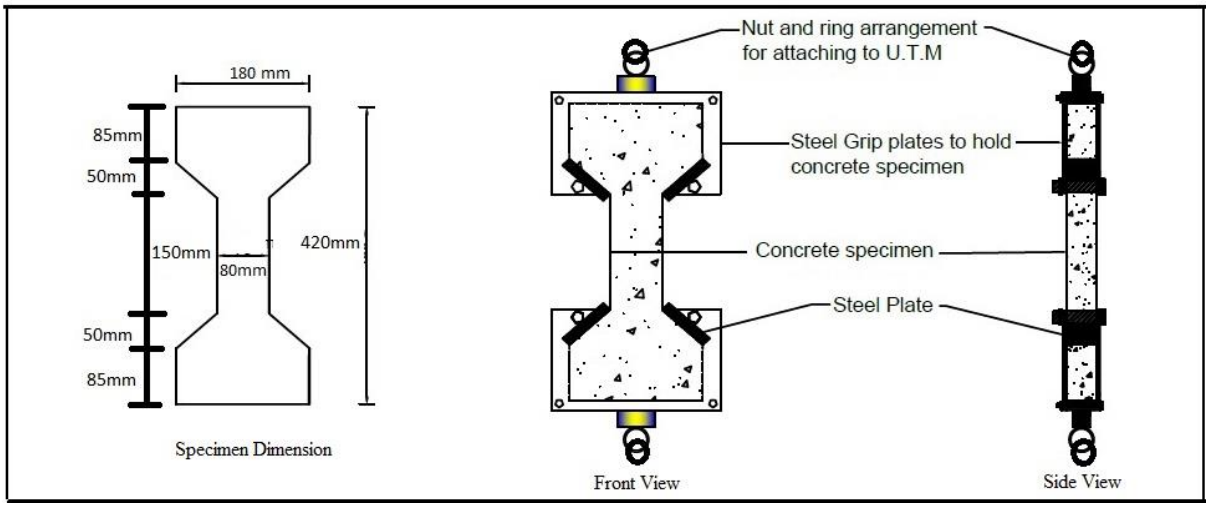

Fig.4.9. Schematic diagram of tension test setup

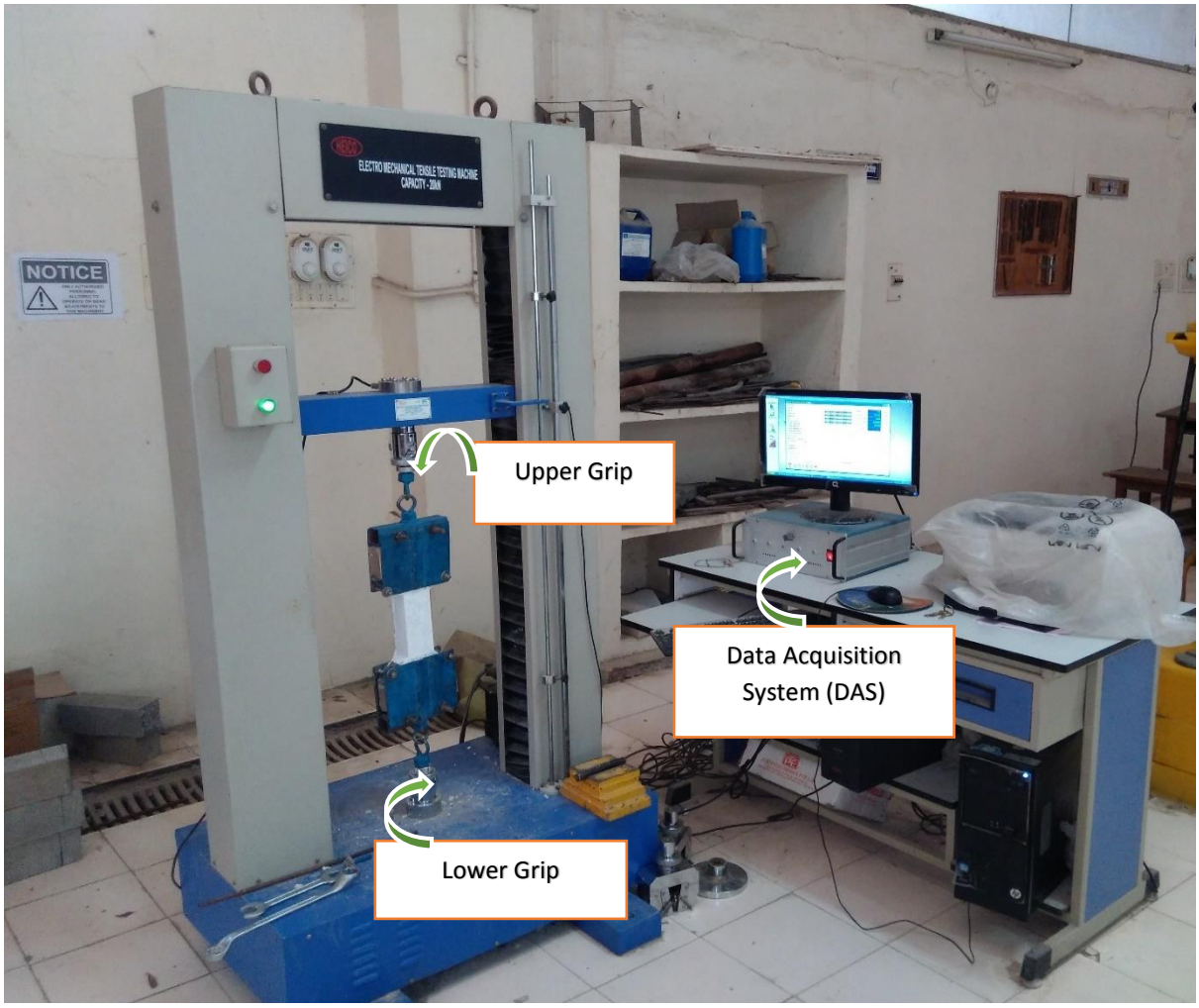

Fig.4.10 Electro Mechanical Tension Testing Machine

4.6.5 Fiber pull-out Test

Fiber pull-out from a concrete matrix was used to characterize the interfacial bond between the matrix and the fiber. These samples were cast in 70mm X 70mm X 70mm iron moulds. Fresh state concrete was poured in the mould, with embedded length of fiber Le (3mm, 6mm, 12mm or 20mm). The samples were allowed to harden in air for 24 hrs and then placed in a wet bath for a period of 28 days is shown in Fig.4.11, after which, the pull-out tests were carried out. A schematic of the pull-out sample used in this study is shown in Fig.4.12.The sample was held on the Electro Mechanical Tension Testing Machine capacity of 50 kN, and the fiber was loaded in tension until the fiber failure (slip or snap). The rate of pull-out used in this study was 0.02 mm/s. The pull-out load and the end displacement of the fiber were continuously recorded. The results were used to develop pull-out load versus end displacement curves. These curves were used to obtain the peak pull-out loads.

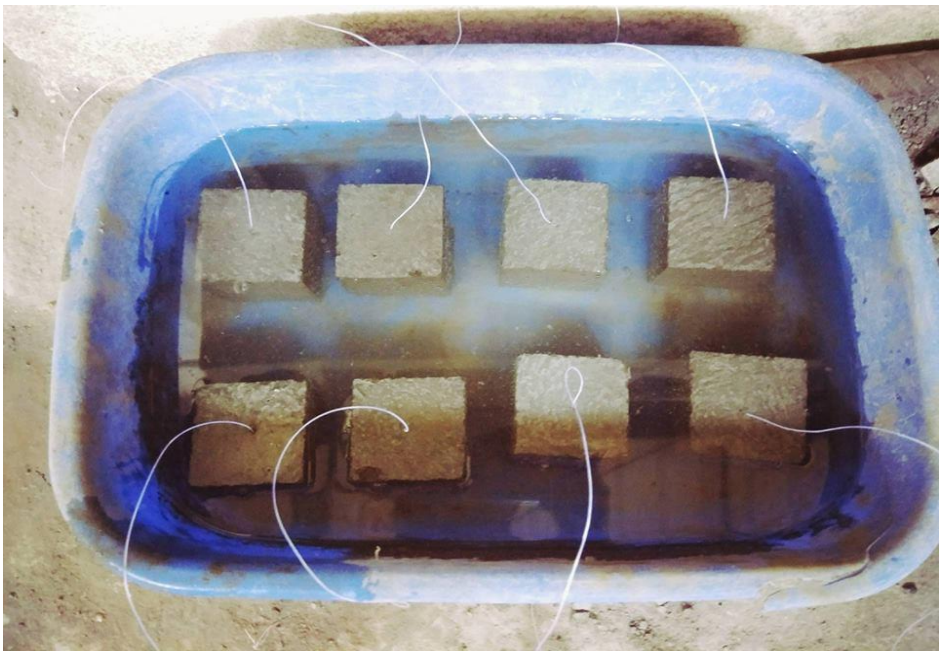

Fig.4.11 Fiber Pull-out Specimens

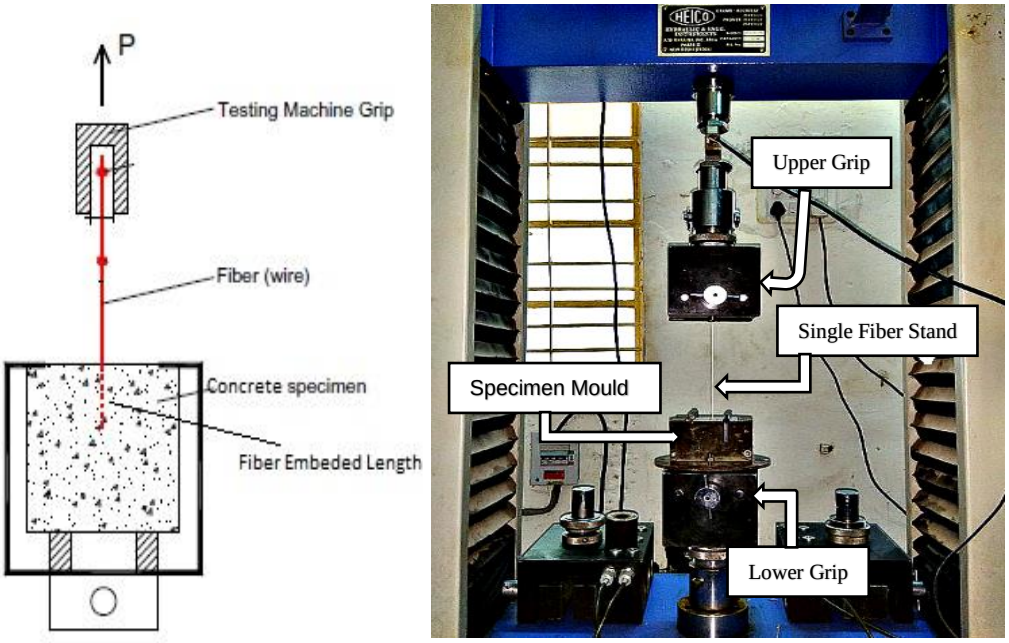

Fig.4.12. Schematic test setup and pull-out test

Chapter-5

Study on Mono Glass Fiber Reinforced Concrete

5.1 Introduction

This investigation is focused on Mono fiber reinforced concrete with varying volume fractions of different lengths of glass fibers. In the present work uniaxial tension and compression tests are performed on dog-bone specimens and prismatic specimens respectively. The study is aimed at understanding the effect of volume fraction and fiber length on the properties in fresh and hardened state composite.

In order to understand the workability of Mono Glass Fiber Reinforced Concrete (MGFRC) slump test was conducted and the results are presented. Tensile stress strain curves and compressive stress strain curves are drawn for each specimen and average curve of three MGFRC specimens for each parameter are considered. The parameters that characterize the behaviour of concrete in tension and compression are peak stress, strain at peak stress, initial slope, energy absorption, strengthening factor, ductility factor, strain hardening slope and strain softening slope. Values of these are taken from the stress strain diagram and results will be discussed.

Pull-out test is conducted on different embedded lengths of fibers. The main goal of the fibre pull-out tests is to understand the fiber matrix interfacial bond strength and the utilisation of tensile capacity of fibres during their pull-out. The fibre distribution and orientation is determined from an optical microscope images. The results of the fibre pull-out tests, fiber dispersion and orientation analysis are used in the analysis of tensile behaviour of GFRC. A material parameter is developed based on the experimental results to predict the compressive stress strain behaviour. A relation between strain softening and strain hardening is proposed.

5.2 Slump of MGFRC

The values of slump for MGFRC of M30 grade concrete is shown in Fig.5.1. It can be seen that different volume of fibers and different lengths of fiber have different effects on the slump. For the plain concrete, the slump is 160mm. After adding Glass fibers, as volume content increased from 0.1% to 0.5% the slump decreased from 126mm to 39 mm. However, at 0.4% and 0.5% volume of fibers led to bundling, balling and hence reduction in workability is observed in composite. As the length of fiber increased from

3mm to 20mm the slump decreased from 126mm to 106mm in case of 0.1% volume fibers and similar decrease is observed in other volume fraction. Moreover, it can be seen that the addition of short fibers (3mm, 6mm) showed higher slump than that of long fibers (12mm, 20mm).

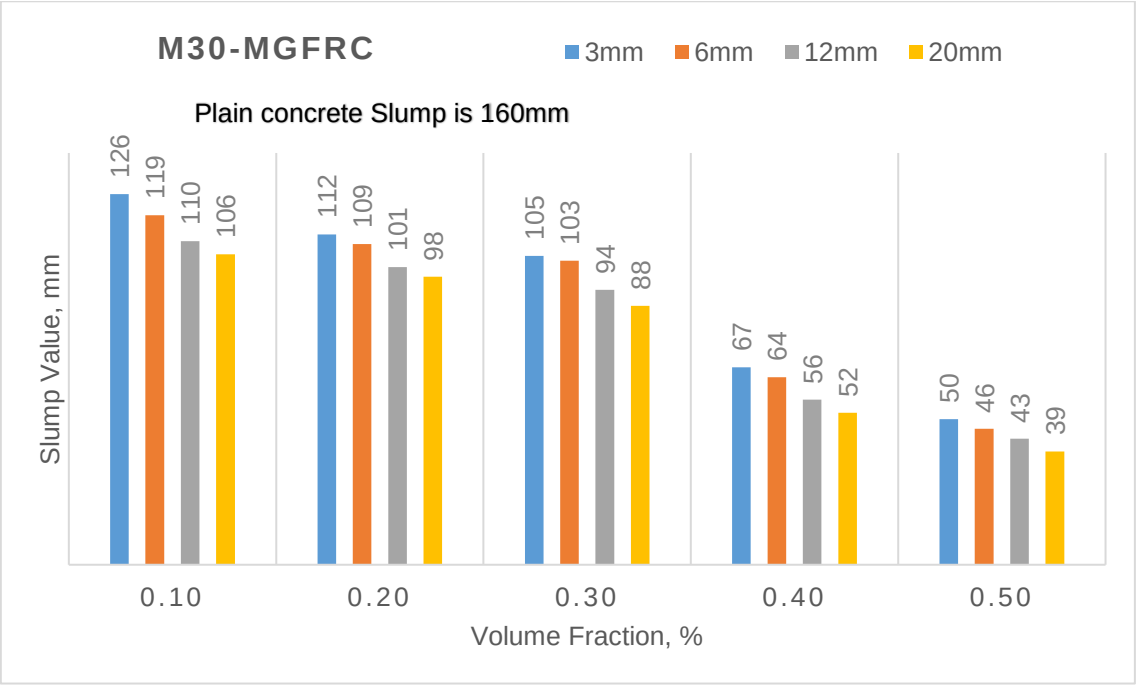

Fig.5.1 Slump as a function of Volume fraction for M30-MGFRC

The values of slump for MGFRC of M50 grade concrete is shown in Fig.5.2 and workability is similar to M30-MGFRC. It can be seen that different volume of fibers and different lengths of fiber have different effects on the slump. For the plain concrete, the slump is 160mm. After adding Glass fibers, as volume fiber increase from 0.1% to 0.5% the slump decreased from 134mm to 41mm. However, at 0.4% and 0.5% volume of fibers led to bundling, balling and hence reduction in workability is observed in composite. As the length of fiber increased from 3mm to 20mm the slump decreased from 134mm to 112mm in case of 0.1% volume fibers and similar decrease is observed in other volume fraction. Moreover, it can be seen that the addition of short fibers (3mm, 6mm) showed higher slump than that of long fibers (12mm, 20mm). The reason may be that the long fibres might have resisted free flow of concrete matrix which might have resulted in the reduction of the slump of the concrete for both M30 and M50.

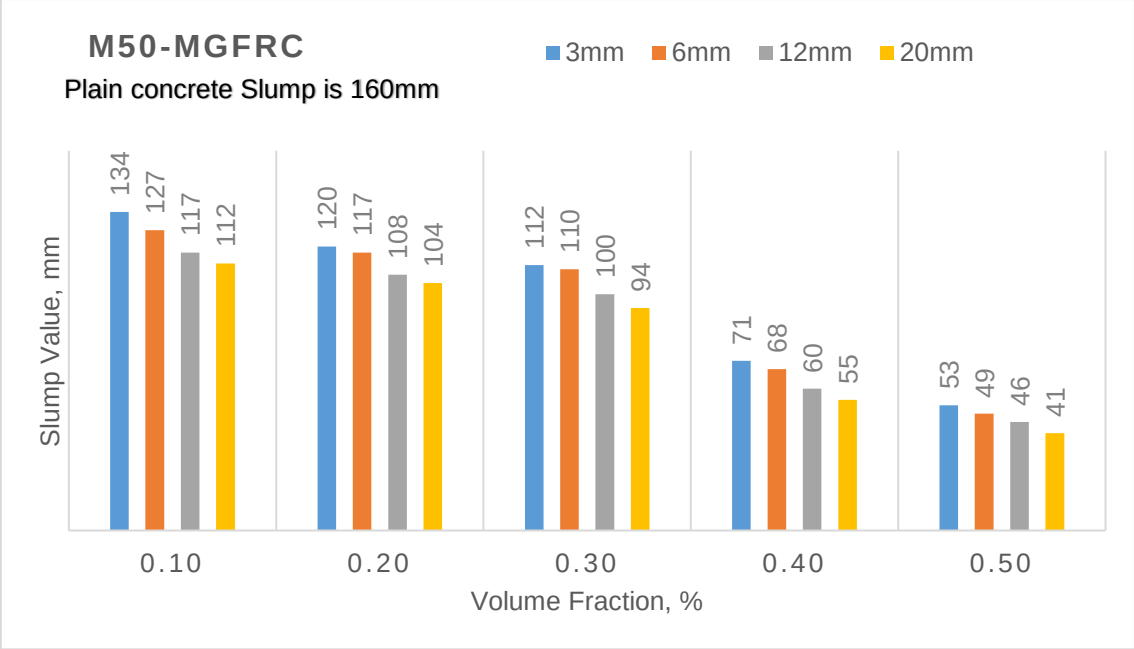

Fig.5.2 Slump as a function of Volume fraction for M50-MGFRC

Different grades of concrete have different effects on the slump. In M50 grade of concrete with MF (3mm,6mm,12mm and 20mm) showed lowest effect, when the slump decreased from 19% to 290%, while in M30 grade of concrete with MF (3mm,6mm,12mm and 20mm) showed highest effect, which is reduced from 27% to 316%. The reduction of workability is higher for all the GFRC mixes with M30 grade of concrete when compared M50 grade of concrete. In overall, the slump of MGFRC with M50 grade concrete is more by 7% than that of MGFRC with M30 grade of concrete. It was observed that, M50 grade of concrete contained large volume of cement paste compared to M30 grade of concrete and hence M50 grade might have shown higher slump compared to M30 grade. Thus it is possible to examine relation between workability and paste to achieve desired flow with minimum cement content.

At higher volume fraction of 0.4% and 0.5%, the fibers act as a barrier to coarse aggregates movement reducing the materials mobility (Fig.5.3). So, increasing the fiber aspect ratio the flow-ability of the material will be reduced. It may be due to the tendency of fiber to wrap around of aggregate, to reduce the mixture from seggregation and flow. Fibers present in the matrix restrains the cement paste reducing the flowability of concrete.

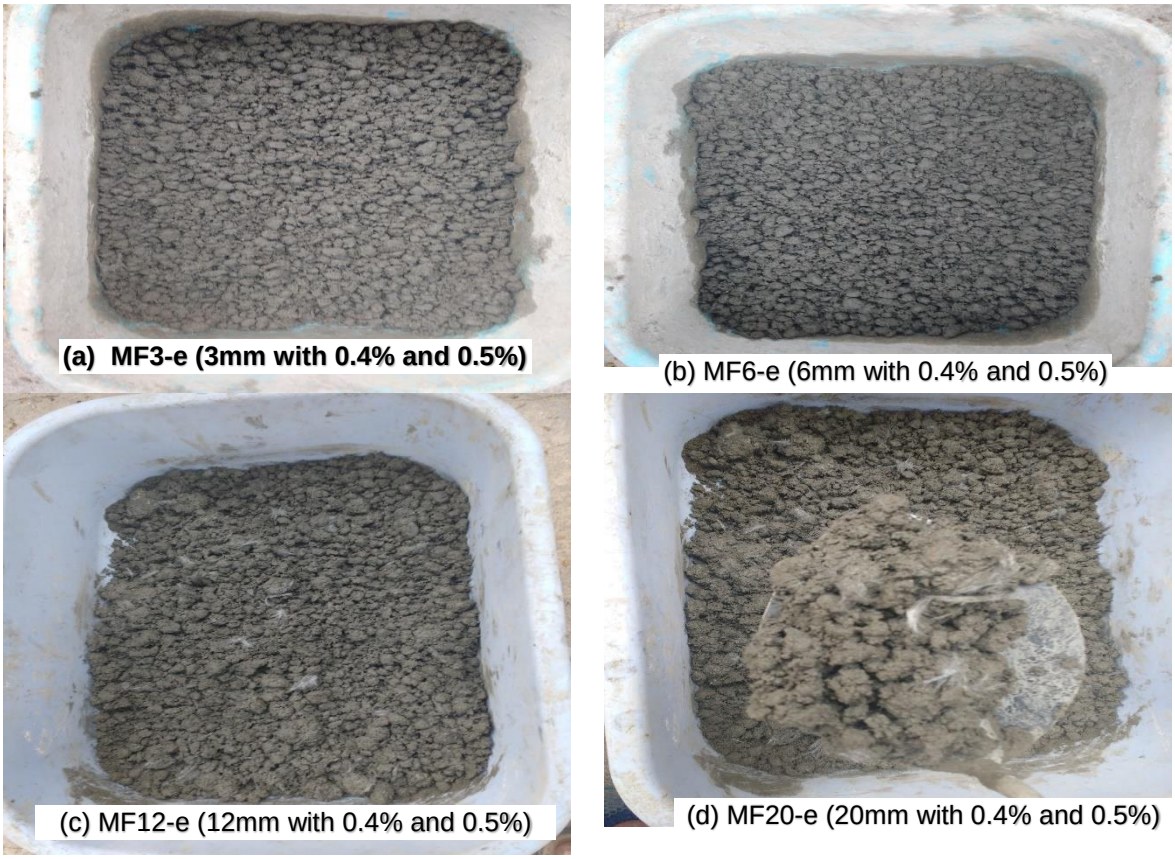

Fig.5.3 Effect of fiber balling in the concrete (a) to (d)

5.3 Cube Compressive strength of MGFRC

The compressive strength results of M30-MGFRC is shown in Fig.5.4. The compressive strength of plain concrete for M30 is 36.10 MPa. Compressive strength of specimens with fiber volume fractions of 0.1%, 0.2%, 0.3%, 0.4% and 0.5% varied from 37.76 MPa to 40.43 MPa. As the volume of the fiber increased from 0.1% to 0.3%, the compressive strength increased from 38.27 MPa to 40.43 MPa and it decreased from 38.63 MPa to 37.76 MPa for 0.4% and 0.5% fiber volume content. Thus specimens with 0.3% fiber volume content has shown the maximum improvement in compressive strength. As the length of the fiber increased from 3mm to 20mm for 0.1% volume fiber, compressive strength varied from 38.27 MPa to 37.40 MPa. Similar observation can be noticed with other volume fraction.

The compressive strength results of M50-MGFRC is shown in Fig.5.5. The compressive strength of plain concrete for M50 is 57.02 MPa. Compressive strength of specimens with fiber volume fractions of 0.1%, 0.2%, 0.3%, 0.4% and 0.5% varied from 60.13 MPa to 62.22 MPa. As the volume of the fiber increased 0.1% to 0.3%, the compressive strength is increased from 60.13 MPa to 62.22 MPa and it decreased

from 60.66 MPa to 58.85 MPa for 0.4% and 0.5% fiber volume content. Thus specimens with 0.3% fiber volume content has shown the maximum improvement in compressive strength. As the length of the fiber increased from 3mm to 20mm for 0.1% volume fiber, compressive strength varied from 60.13 MPa to 58.29 MPa. Similar observation can be noticed with other volume fraction.

All MGFRC specimens have shown an increase in compressive strength compared to the companion plain concrete strength. The compressive strength change of M30-MGFRC and M50-MGFRC ranges from 4% to 12% and 5% to 9% respectively. The specimens with 0.3% volume fraction showed the maximum improvement in compressive strength. In M30-MFRC, specimens with same volume fraction, as the length of the fiber increased from 3mm to 20mm the compressive strength decreased from 12% to 8% whereas in case of M50-MGFRC the compressive strength reduced form 9% to 7%. Use of 3mm fibers in concrete showed a larger increase of compressive strength than that of 20mm fibers. It can be found from the above results that higher length of fibre may not give beneficial effect on compressive strength. It may be due to that it is more difficult for fibre to distribute uniformly in cementitious composites, which adversely effects the development of strength.

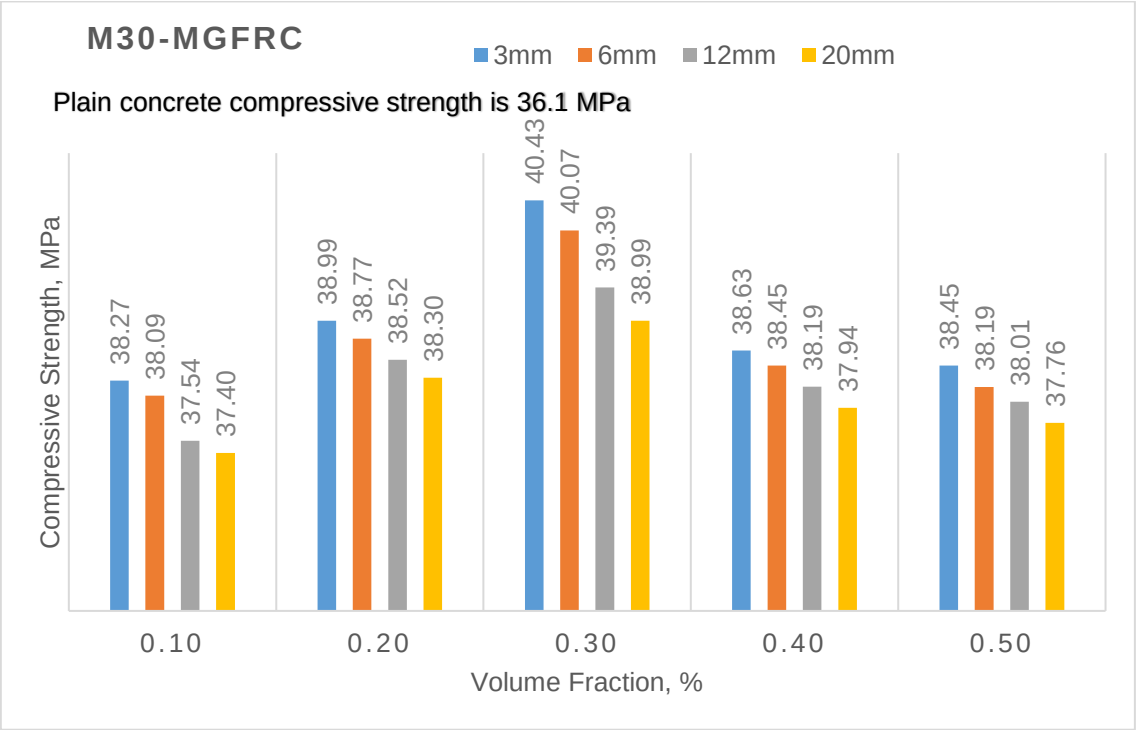

Fig.5.4 Compressive strength as a function of Volume fraction for M30-MGFRC

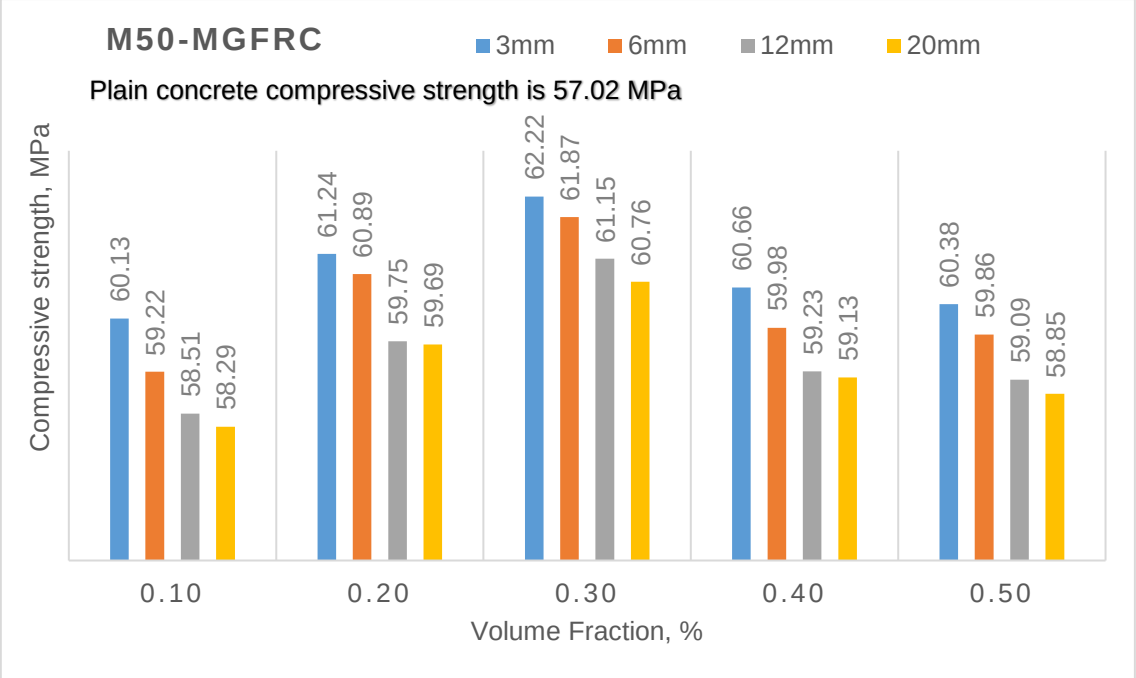

Fig.5.5 Compressive strength as a function of Volume fraction for M50-MGFRC

Based on slump and cube compressive strength results, it can be concluded that the addition of fibers in concrete changes its mobility. The loss of mobility occurs primarily by the fibers blocking the relative movement of the aggregates and this effect increases with increase in length of fiber and it may further lead to strength reduction of hardened MGFRC.

5.4 Tensile stress strain behaviour of MGFRC

Tensile Stress-Strain curves are drawn for each specimen and average curve of three dog bone specimens for each parameter is shown in Fig.5.6 to 5.10 for M30-MGFRC. Tensile stress increased with the increase in strain linearly for plain concrete specimen right up to peak stress and failed suddenly. Specimens with 0.1% and 0.2% volume of fiber exhibited similar linear increase in stress with the increase in strain right up to peak stress. There is a little improvement in load carrying capacity and deformation with reference to the plain concrete as shown in Fig.5.6 and 5.7. Specimen with 0.3% volume fraction (Fig.5.8) is similar to 0.2% for 3mm and 6mm fiber length specimen but 12mm and 20mm fiber length specimen showed more deformation capacity.

Higher percentage volume of fiber in the specimen has not contributed to increase in load carrying capacity but it has improved deformations as can be seen in Fig.5.9 and 5.10 for all 3mm to 20mm length fibers. For any given percentage volume of fibers, long length fibers of 12mm and 20mm has not contributed to increase in load carrying

capacity compared to short length fibers of 3mm and 6mm. Similarly short length fibers has not contributed to increase in deformation capacity compared to long length fibers. There is definite gradual and progressive improvement in deformation capacity with increase in length of fiber and volume of fibers.

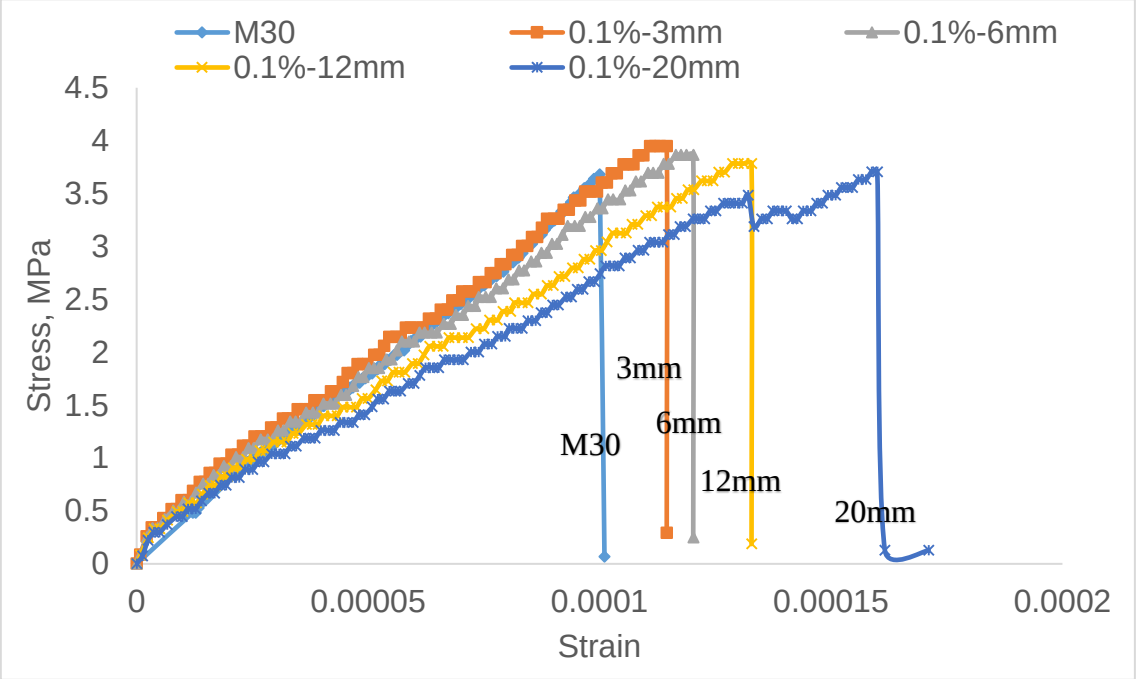

Fig.5.6 Tensile Stress-Strain behaviour of M30-MGFRC with V_f = 0.1%

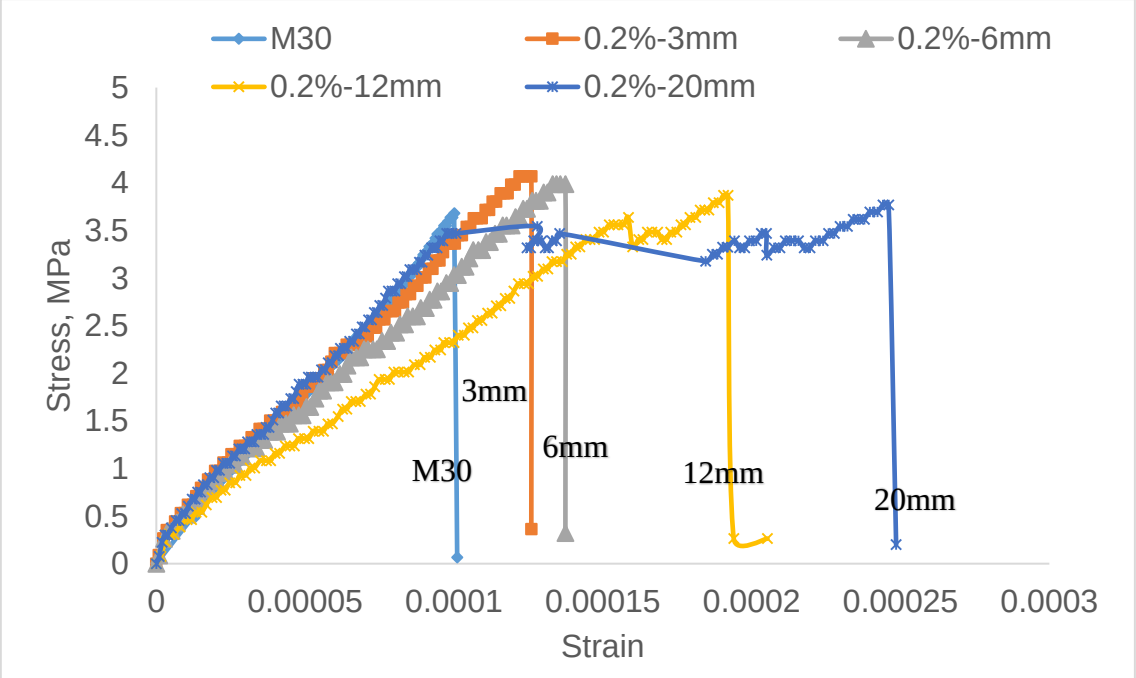

Fig.5.7 Tensile Stress-Strain behaviour of M30-MGFRC with V_f = 0.2%

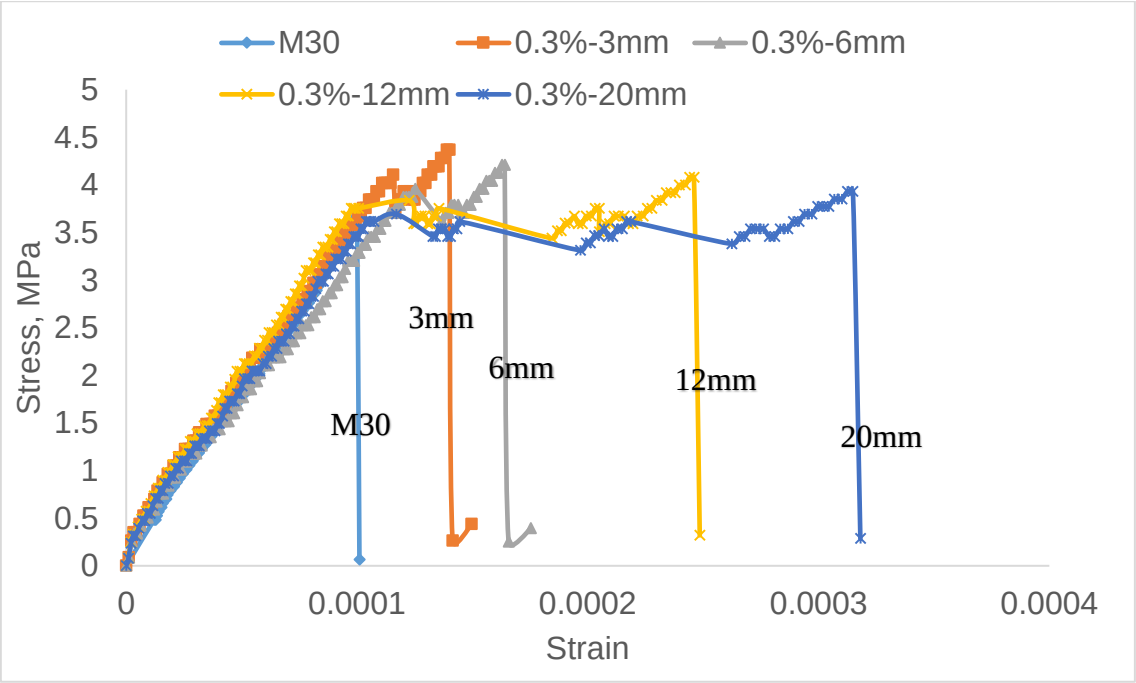

Fig.5.8 Tensile Stress-Strain behaviour of M30-MGFRC with V_f = 0.3%

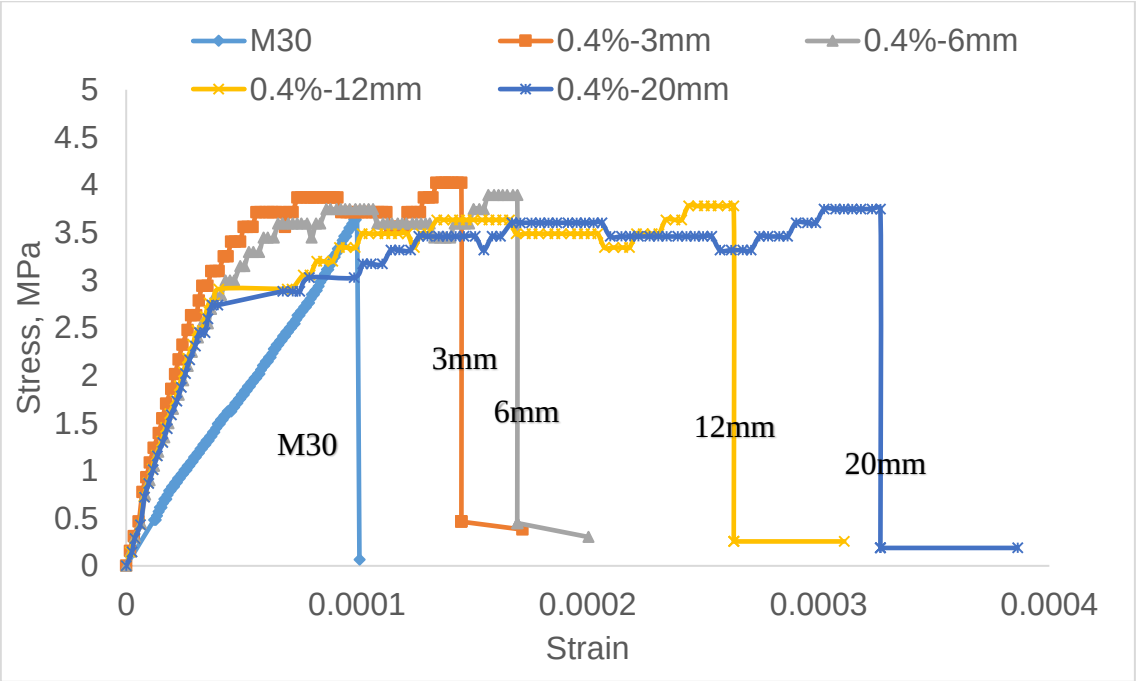

Fig.5.9 Tensile Stress-Strain behaviour of M30-MGFRC with V_f = 0.4%

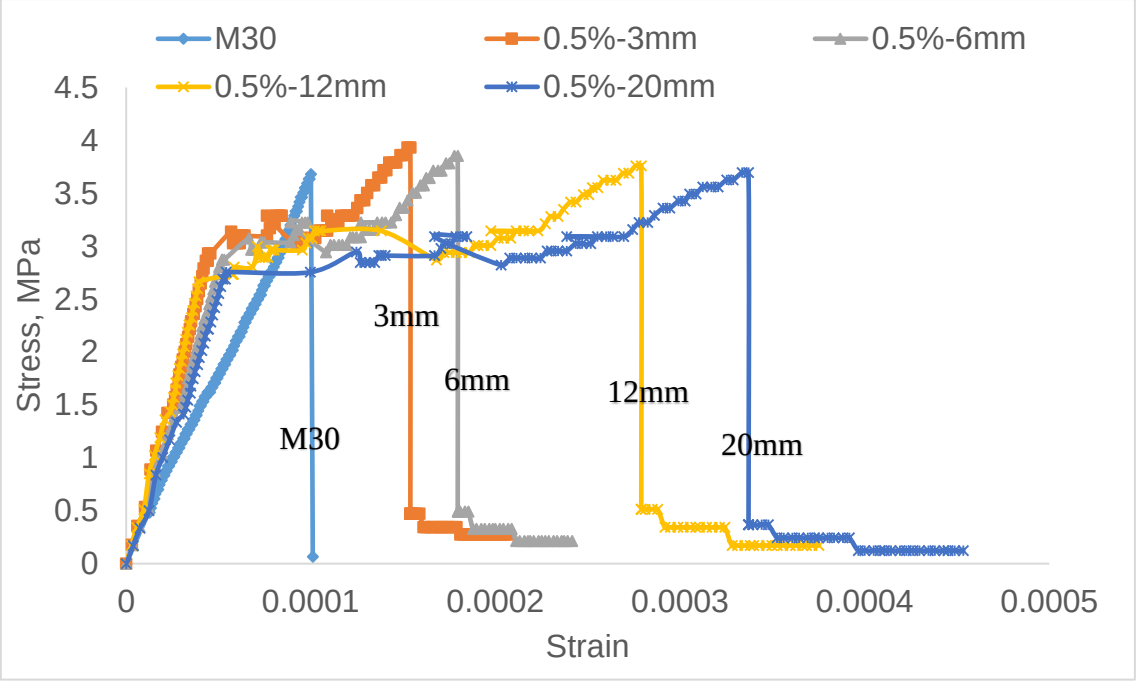

Fig.5.10 Tensile Stress-Strain behaviour of M30-MGFRC with V_f = 0.5%

Tensile Stress-Strain curves are shown in Fig.5.11 to 5.15 for M50-MGFRC. Tensile stress increased with the increase in strain linearly for plain concrete specimen right up to peak stress and failed suddenly. Specimens with 0.1% and 0.2% volume of fiber exhibited similar linear increase in stress with the increase in strain right up to peak stress. There is a little improvement in load carrying capacity and deformation with reference to the plain concrete as shown in Fig.5.11 and 5.12. Specimen with 0.3% volume fraction (Fig.5.13) is similar to 0.2% for 3mm and 6mm fiber length specimen but 12mm and 20mm fiber length specimen showed more deformation capacity.

Higher percentage volume of fiber in the specimen has not contributed to increase in load carrying capacity but it has improved deformations as can be seen in Fig.5.14 and 5.15 for all 3mm to 20mm length fibers. For any given percentage volume of fibers, long length fibers of 12mm and 20mm has not contributed to increase in load carrying capacity compared to short length fibers of 3mm and 6mm. Similarly short length fibers has not contributed to increase in deformation capacity compared to long length fibers. There is definite gradual and progressive improvement in deformation capacity with increase in length of fiber and volume of fibers. Behaviour of M30 grade and M50 grade of MGFRC are similar.

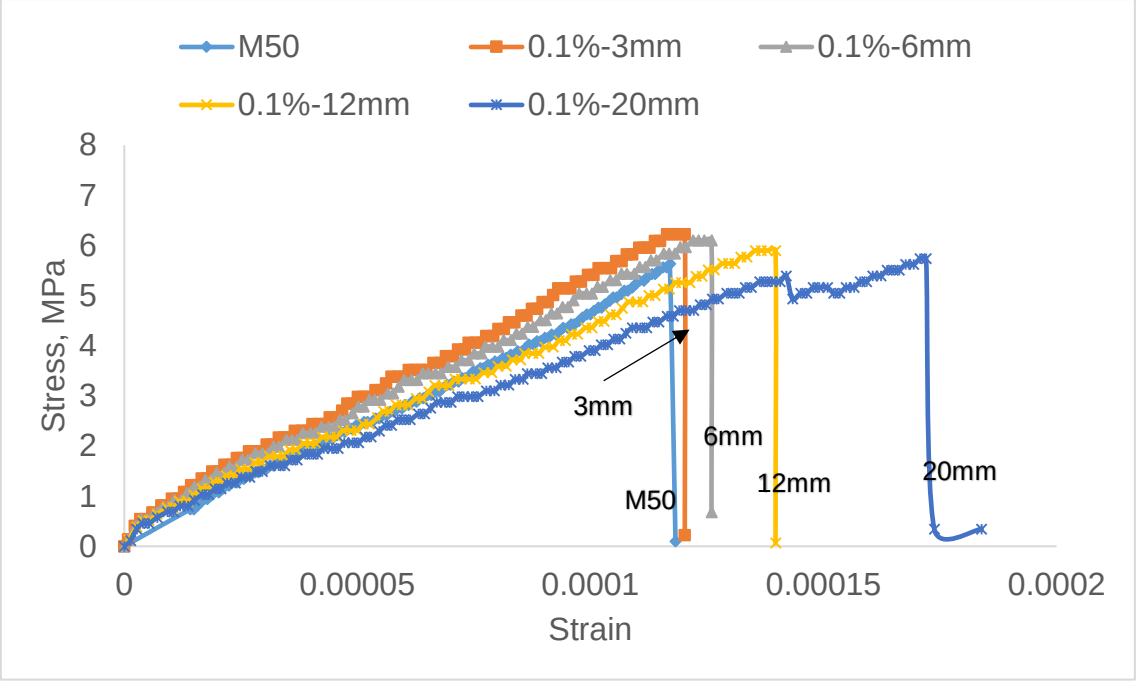

Fig.5.11 Tensile Stress-Strain behaviour of M50-MGFRC with V_f = 0.1%

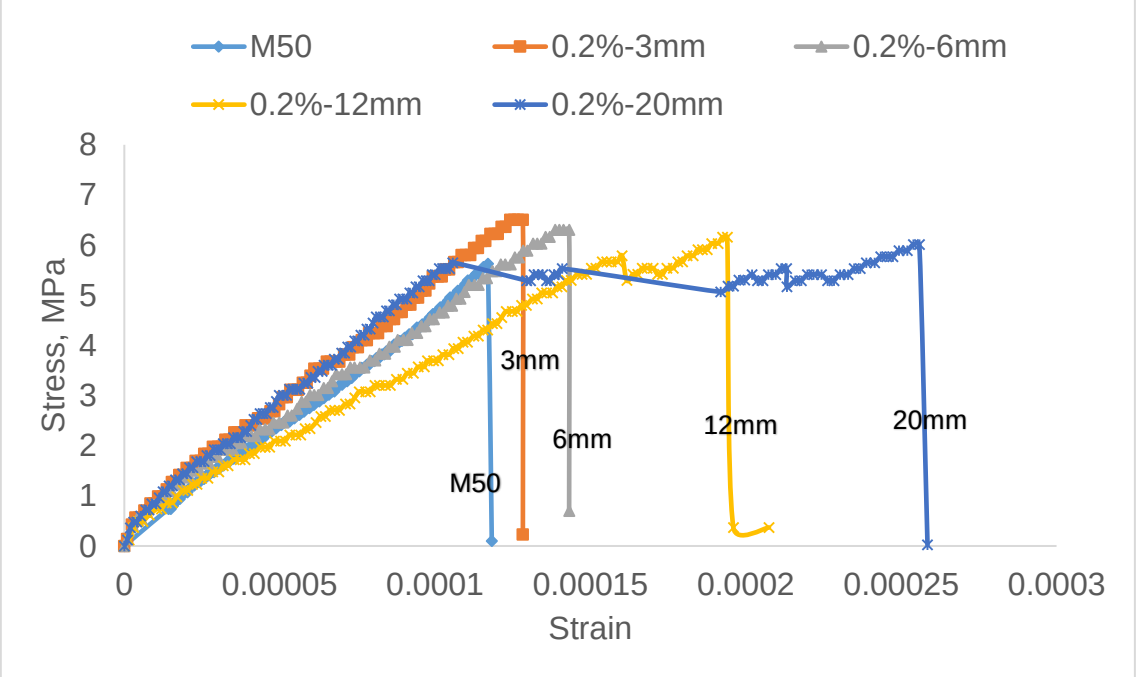

Fig.5.12 Tensile Stress-Strain behaviour of M50-MGFRC with V_f = 0.2%

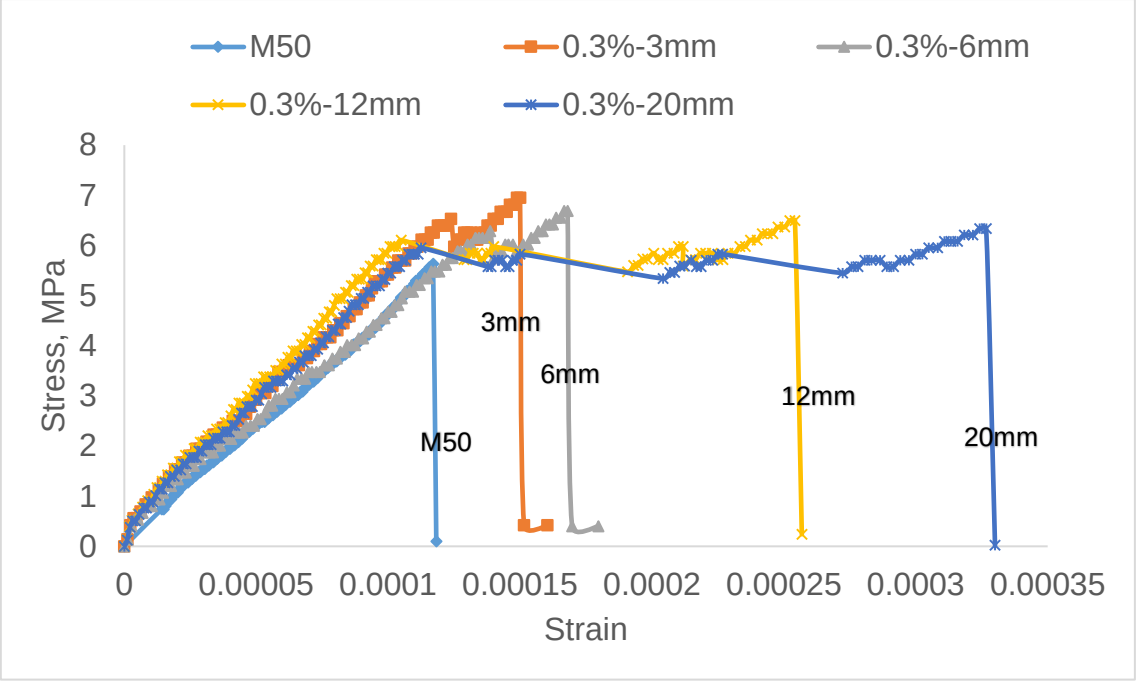

Fig.5.13 Tensile Stress-Strain behaviour of M50-MGFRC with V_f = 0.3%

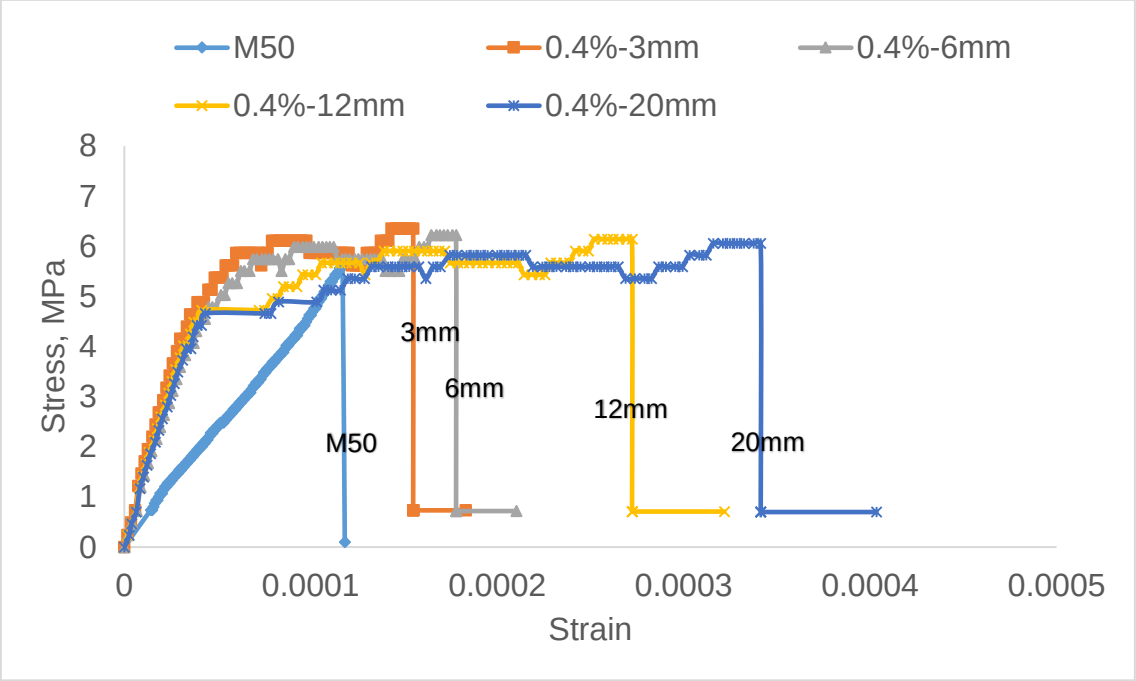

Fig.5.14 Tensile Stress-Strain behaviour of M50-MGFRC with V_f = 0.4%

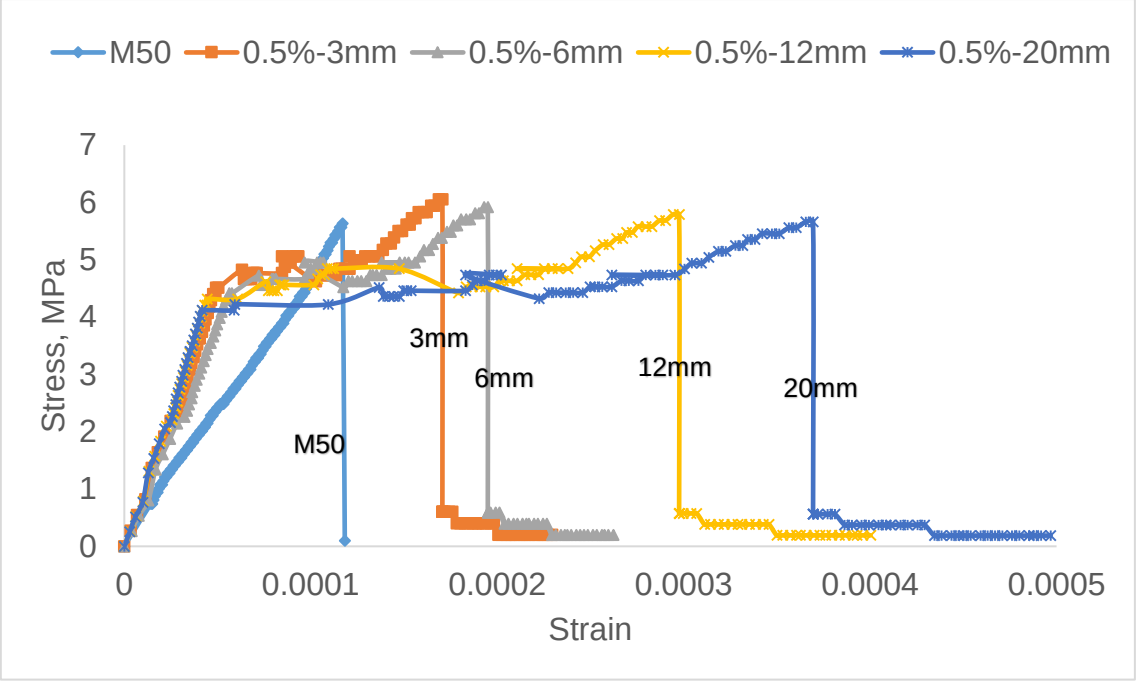

Fig.5.15 Tensile Stress-Strain behaviour of M50-MGFRC with V_f = 0.5%

Plain concrete specimen broke into two parts once a tensile crack occurred. But for the GFRC, the addition of fibre effectively slowed down the propagation of crack, and thus improved the mechanical behaviour in both M30 and M50 grade of concrete.

It is also observed that the improvement of deformations becomes more prominent with the increase in volume of fibers in both M30-MGFRC and M50-MGFRC. However, when the fibre volume fraction increases from 0.4% to 0.5%, a slight drop in peak stress is noted compared to specimens with fibre volume fraction of 0.3%. It can be concluded that the volume fraction of 0.3% shows maximum improvement in peak stress in both M30-MGFRC and M50-MGFRC.

In addition, it can be seen that GFRC with short fibers of 3mm and 6mm shows a better peak stress than that with 20mm fiber length and it is also observed GFRC with long fibers of 12mm and 20mm length fibers shows a significant improvement in deformation compared to short length fibers of 3mm and 6mm. It is to say that, with in the same volume fraction, there are more number of short fibers at any section to control formation of cracks and thus helped to improve peak stress capacity. Whereas Long fibres have shown a stronger anchorage and bridging effect, besides, the bonding between fibre and concrete matrix, which would contribute to the improvement of deformation capacity.

5.5 Mechanical properties of MGFRC in Tension

The properties that characterize the stress strain behaviour of M30-MGFRC and M50-MGFRC in uni-axial tension are peak stress, strain at peak stress, initial slope, strengthening factor, and ductility factor and energy absorption capacity. Values of these are taken from the stress strain diagram and are given in Table 5.1 to 5.2.

An examination of stress strain behaviour of MGFRC with different lengths and volume fractions for M30 and M50 grade concrete given in Fig.5.6 to 5.15 shows that load increased with deformation linearly up to a certain point and there is a deviation in the slope thereafter wherein the increase of load is slow with increase of deformation. This general behaviour in the initial linear region and deviation thereafter may be attributed to the onset of cracking in the specimens. In general cracking initiates as the stress at point in the specimen at any section reaches the tensile strength of concrete. Thus the deviation in the stress strain diagram at the end of initial linear portion may be treated as the onset of cracking. This stress at this point of the stress strain diagram may normally be taken as around the tensile stress of concrete. Comparison of tensile stress of plain concrete with the onset of cracking shows that for the specimens having higher fiber content or long length have stress at the onset lower than the tensile strength of concrete and specimens with shorter length or lower fiber content have shown stress at the end of initial linear region higher stress than cracking tensile strength of concrete. In all, the end of initial linear region can be treated as the onset of cracking in the specimen under tensile loading. This point is noted as P in the Fig.5.16. Further deformation in the specimen from the point P resulted in a little increase in load. This amount of increase in deformation and load is directly influenced by the length of fiber and volume of fiber. Short length and low volume of fiber have shown less improvement in deformation compared to long length fiber or higher volume fiber content. The ultimate stress of the specimen is designated as Q as shown in Fig.5.16 thus the stress strain diagram of MGFRC has two distinct regions normally the initial linear region OP i.e., pre-cracking and cracking region PQ. After reaching ultimate stress most of the specimens failed suddenly and specimens with long length or higher volume content have shown resistance even after the sudden drop in stress. These points are designated as R and S as shown in Fig.5.16.

Point P is the onset of cracking, point Q is ultimate stress and strain, point R is sudden drop in stress after peak stress and point S is breaking stress. It may be noticed that

there is a slow increase in stress after reaching a stress corresponding to point P and then the specimens have undergone large deformation beyond the point P and up to point Q. Hence, the P to Q region can be called as strain hardening region. Based on the above observation, the stress strain curves are analysed to obtain the initial slope (ratio of peak tensile strength (σ^{P}_{t}) to the corresponding strain (ε^{P}_{t})), strengthening factor (ratio of composite ultimate tensile strength (σ^{Q}_{t}) to the plain concrete peak tensile strength (σ_{mt})), ductility factor (ratio of strain at ultimate tensile strength (ε^{Q}_{t}) to the strain at onset of cracking (ε^{P}_{t})), strain hardening slope (ratio of change in stress (σ^{Q}_{t}- σ^{P}_{t}) to the change in strain (ε^{Q}_{t}-ε^{P}_{t}) in the strain hardening region) of the composite. The corresponding stress strain values are reported in Table 5.1 and 5.2.

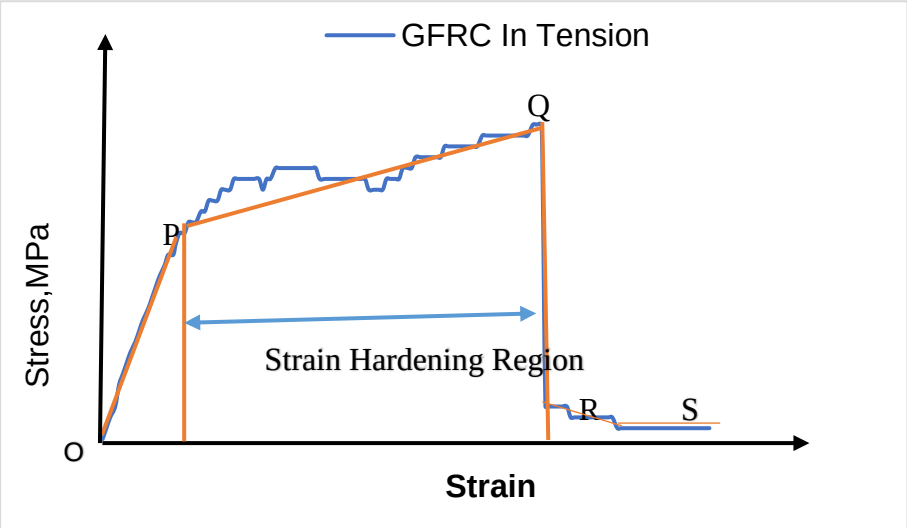

Fig. 5.16 Salient features of GFRC Specimen in Tension

Initial slope (E^{t}_{i}) is computed for M30-MGFRC and M50-MGFRC and given in column 7 of Table 5.1 and 5.2. As the length of fiber increased the initial slope decreased for percentage volume of fiber (Fig.5.17). As the volume of fiber increased thus initial slope increased. Hence, as the length of fiber increased the initial stiffness decreased and as the volume of fiber increases thus initial stiffness increased. Strain hardening slope (E_{SH}) is calculated for M30-MGFRC and M50-MGFRC and reported in column 10 of Table 5.1 and 5.2. Strain hardening is not noticed for specimens with 0.1% and 0.2% fiber volume for 3mm and 6mm length fibers and it is noticed for 12mm and 20mm length fibers. Specimen with 0.3%, 0.4% and 0.5% for 3mm, 6mm, 12mm and 20mm fiber lengths have exhibited strain hardening behaviour out of which the specimen with the 0.4% and 0.5% is very noticeable (Fig.5.18). Strengthening factors (STF^{t}) and ductility factors (DF^{t}) for M30-MGFRC and M50-MGFRC (Fig.5.19 and

5.20) are computed and values are reported in column 8 and 9 of Table 5.1 and 5.2. Strengthening factor increased up to 0.3% volume fraction, thereafter it decreased for 0.4% and 0.5% volume fractions for any length of fiber. However, ductility factor increased with both increase in volume fractions and increase in fiber length is shown in Fig.5.20. Energy absorption is computed by tacking area under stress-strain diagram and given in column 11 of Table 5.1 and 5.2. The variations with respect to volume fraction is shown in Fig.5.21. As the volume of fiber or length of fiber increased Energy absorption capacity increased.

Table 5.1 Summary of test results for M30-MGFRC in Tension

SD (1)	V_f (%) (2)	Strain Hardening Region				E^t_i ($X10^4$) MPa (7)	STF^t (8)	DF^t (9)	E_{SH} ($X10^4$) MPa (10)	EA_{SHR} ($X10^{-2}$) N/mm (11)
		σ^P_t, MPa (3)	ε^P_t ($X10^{-4}$) (4)	σ^Q_t, MPa (5)	ε^Q_t ($X10^{-4}$) (6)					
MF0	0.0	3.68	1.00	3.68	1.00	3.68	1	1	0.00	0.02
Tensile strength of plain concrete (σ_{mt}) = 3.68 MPa										
MF3-a	0.1 (a)	3.95	1.15	3.95	1.15	3.45	1.07	1	0.00	0.025
MF6-a		3.86	1.20	3.86	1.20	3.21	1.05	1	0.00	0.025
MF12-a		3.78	1.30	3.78	1.30	2.85	1.03	1	0.00	0.027
MF20-a		3.48	1.32	3.71	1.60	2.64	1.01	1.21	0.82	0.035
MF3-b	0.2 (b)	4.07	1.26	4.07	1.26	3.23	1.10	1	0.00	0.028
MF6-b		3.99	1.37	3.99	1.37	2.90	1.08	1	0.00	0.030
MF12-b		3.64	1.59	3.87	1.92	2.29	1.05	1.21	0.70	0.044
MF20-b		3.54	1.28	3.77	2.46	2.77	1.02	1.92	0.19	0.069
MF3-c	0.3 (c)	4.02	1.11	4.37	1.40	3.62	1.19	1.26	1.21	0.036
MF6-c		3.96	1.25	4.21	1.64	3.17	1.14	1.31	0.64	0.041
MF12-c		3.84	1.23	4.08	2.46	3.13	1.11	2.00	0.20	0.075
MF20-c		3.69	1.17	3.93	3.15	3.17	1.07	2.70	0.12	0.095
MF3-d	0.4 (d)	3.87	0.99	4.02	1.45	3.90	1.09	1.46	0.33	0.048
MF6-d		3.75	1.07	3.90	1.69	3.50	1.06	1.58	0.24	0.054
MF12-d		3.29	0.98	3.78	2.63	3.36	1.03	2.66	0.30	0.084
MF20-d		2.89	0.85	3.75	3.27	3.40	1.02	3.81	0.36	0.104
MF3-e	0.5 (e)	3.14	0.56	3.93	1.54	5.60	1.07	2.75	0.81	0.049
MF6-e		3.07	0.62	3.85	1.80	4.95	1.05	2.91	0.66	0.055
MF12-e		2.73	0.72	3.76	2.79	3.79	1.02	3.89	0.50	0.086
MF20-e		2.75	0.71	3.69	3.37	3.87	1.00	4.74	0.35	0.106

Note:Initial Slope (E^t_i) = σ^P_t, / ε^P_t , Strengthening Factor (STF^t)= σ^Q_t / σ_{mt} ,
Ductility Factor (DF^t) = ε^Q_t / ε^P_t , Strain Hardening slope (E_{SH}) = (σ^Q_t - σ^P_t) / (ε^Q_t -ε^P_t), Energy Absorption (EA_{SHR}) = Area under the stress strain curve in Strain Hardening Region,
SD = Specimen Designation

Table 5.2 Summary of test results for M50-MGFRC in Tension

SD (1)	V_f (%) (2)	Strain Hardening Region				E^t_i ($X10^4$) MPa (7)	STF^t (8)	DF^t (9)	E_{SH} ($X10^4$) MPa (10)	EA_{SHR} ($X10^{-2}$) N/mm (11)
		σ^P_t, MPa (3)	ε^P_t ($X10^{-4}$) (4)	σ^Q_t, MPa (5)	ε^Q_t ($X10^{-4}$) (6)					
MF0	0.0	5.63	1.17	5.63	1.17	4.81	1.00	1.00	0.0	0.033
Tensile strength of plain concrete (σ_{mt}) = 5.63 MPa										
MF3-a	0.1 (a)	6.22	1.20	6.22	1.20	5.18	1.10	1.00	0.00	0.041
MF6-a		6.10	1.23	6.10	1.23	4.98	1.08	1.00	0.00	0.041
MF12-a		5.98	1.40	5.98	1.40	4.28	1.06	1.00	0.00	0.046
MF20-a		5.44	1.42	5.79	1.72	3.83	1.03	1.21	1.17	0.058
MF3-b	0.2 (b)	6.63	1.28	6.63	1.28	5.17	1.18	1.00	0.00	0.046
MF6-b		6.51	1.40	6.51	1.40	4.66	1.16	1.00	0.00	0.050
MF12-b		6.01	1.60	6.32	1.94	3.75	1.12	1.21	0.91	0.072
MF20-b		5.05	1.18	6.17	2.56	3.25	1.10	2.16	0.81	0.117
MF3-c	0.3 (c)	6.25	1.13	6.95	1.44	5.53	1.23	1.27	2.26	0.059
MF6-c		6.38	1.18	6.79	1.68	5.40	1.21	1.42	0.82	0.067
MF12-c		6.07	1.22	6.60	2.54	4.97	1.17	2.08	0.40	0.125
MF20-c		6.05	1.59	6.44	3.27	3.80	1.14	2.82	0.23	0.162
MF3-d	0.4 (d)	5.80	1.02	6.35	1.51	5.68	1.13	1.48	1.12	0.078
MF6-d		5.74	1.06	6.22	1.78	5.41	1.11	1.67	0.67	0.090
MF12-d		4.69	0.99	6.10	2.72	4.73	1.08	2.73	0.82	0.141
MF20-d		4.53	0.96	5.97	3.41	4.71	1.06	3.53	0.59	0.176
MF3-e	0.5 (e)	4.82	0.59	6.05	1.67	8.16	1.07	2.79	1.14	0.079
MF6-e		4.55	0.66	5.92	1.95	6.89	1.05	2.95	1.06	0.092
MF12-e		4.31	0.73	5.79	2.98	5.90	1.03	4.08	0.66	0.144
MF20-e		4.11	0.77	5.66	3.69	5.33	1.01	4.79	0.53	0.178

Note:Initial Slope (E^t_i) = σ^P_t, / ε^P_t , Strengthening Factor (STF^t)= σ^Q_t / σ_{mt} ,
Ductility Factor (DF^t) = ε^Q_t / ε^P_t , Strain Hardening slope (E_{SH}) = (σ^Q_t - σ^P_t) / (ε^Q_t -ε^P_t), Energy Absorption (EA_{SHR}) = Area under the stress strain curve in Strain Hardening Region, SD = Specimen Designation

Finally, It can be noted that the strength enhancement for short length fibers (3mm and 6mm) varied from 1·07 to 1.23 and for long length fibers (12mm and 20mm) from1.03 to 1.17. The shows that there was a significant improvement in strength for specimens with short length fibers when compared to the specimens with long length fibers. A significant enhancement in ductility occurred in the case of the long length fibers (12mm and 20mm) between 1.21 and 4.79 compared to short length fibers (3mm and 6mm) between 1.0 and 2.95. Hence the short fibers are more effective in

improving the peak strength by delaying the formation of micro cracks and long fibers are more effective in increasing the deformations by bridging the macro cracks.

In overall, long length fibers (12mm and 20mm) exhibited higher ductility factor, energy absorption capacity than that of short length fibers (3mm and 6mm). Short length fibers showed higher strengthening and initial slope compared to the long length fibers. Hence, the short length fibers contributed to improve the strength of the composite where as long length fibers contributed to improve the deformations of the composite.

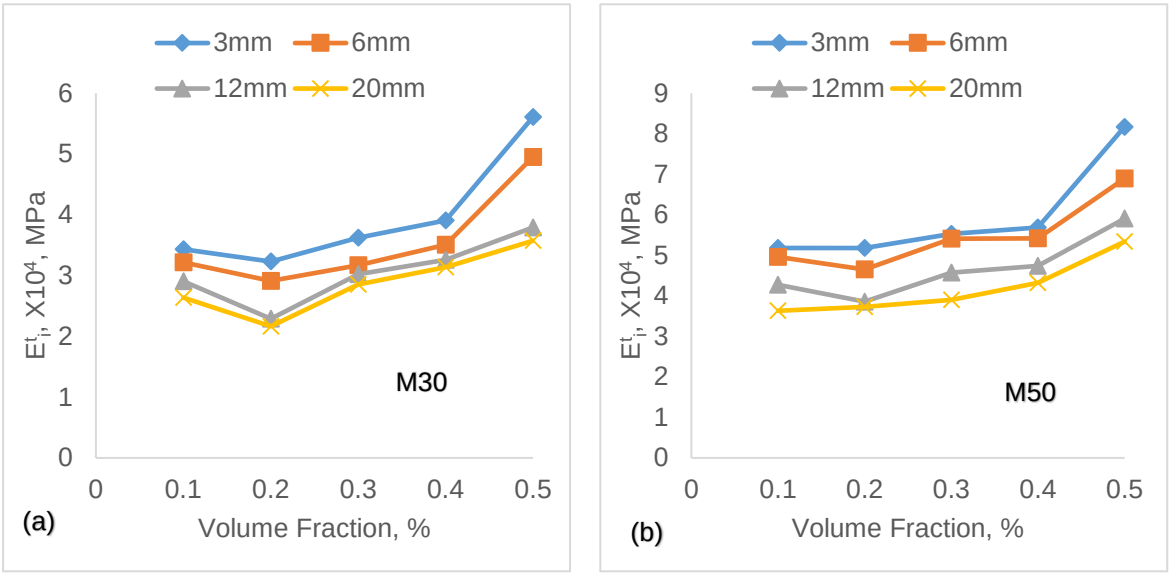

Fig.5.17 Initial slope(E_i^t) as a function of volume fraction for MGFRC in Tension

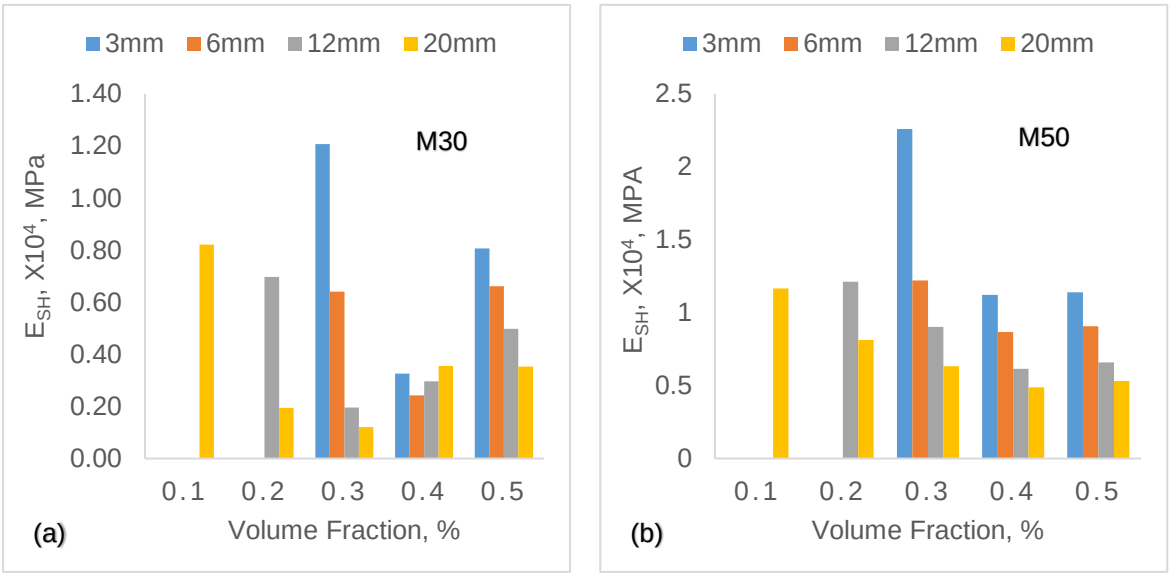

Fig.5.18 Strain Hardening slope (E_{SH}) as a function of volume fraction for MGFRC in Tension.

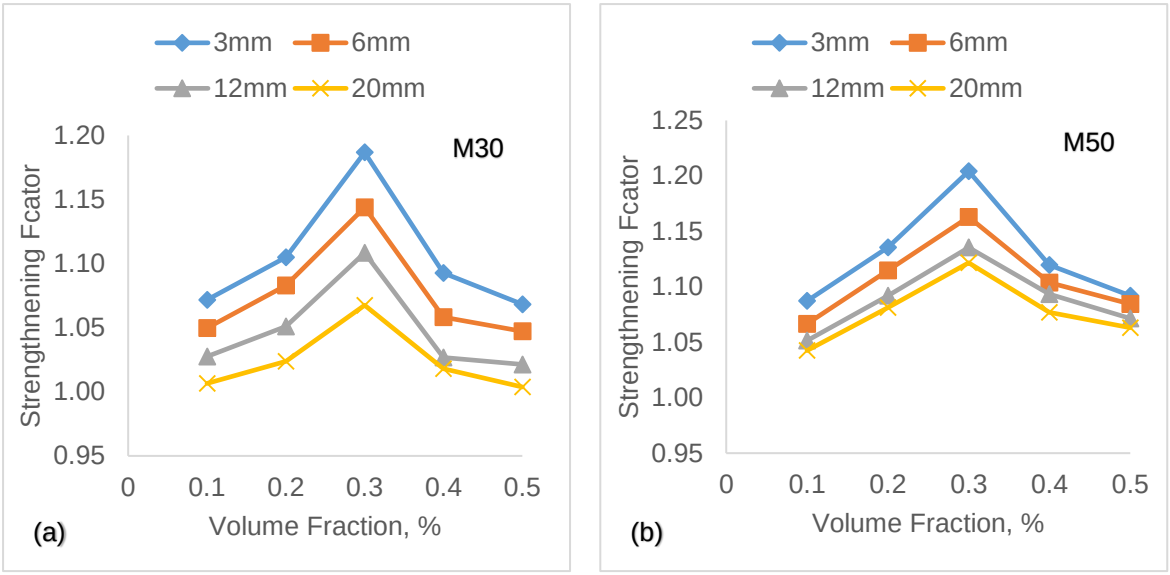

Fig.5.19 Strengthening Factor as a function of volume fraction for MGFRC in Tension

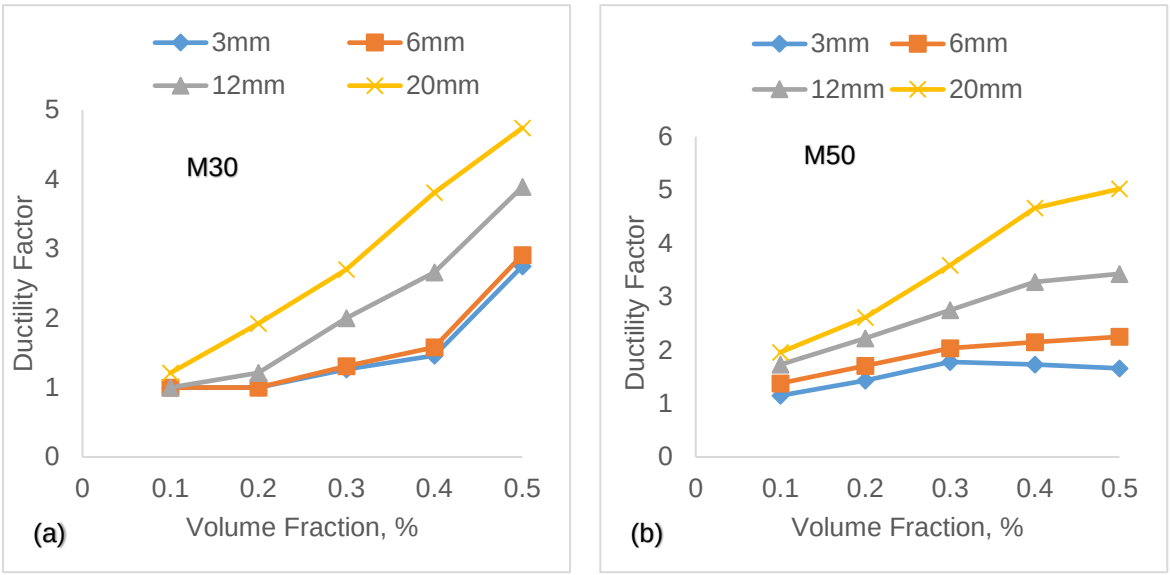

Fig.5.20 Ductility Factor as a function of volume fraction for MGFRC in Tension

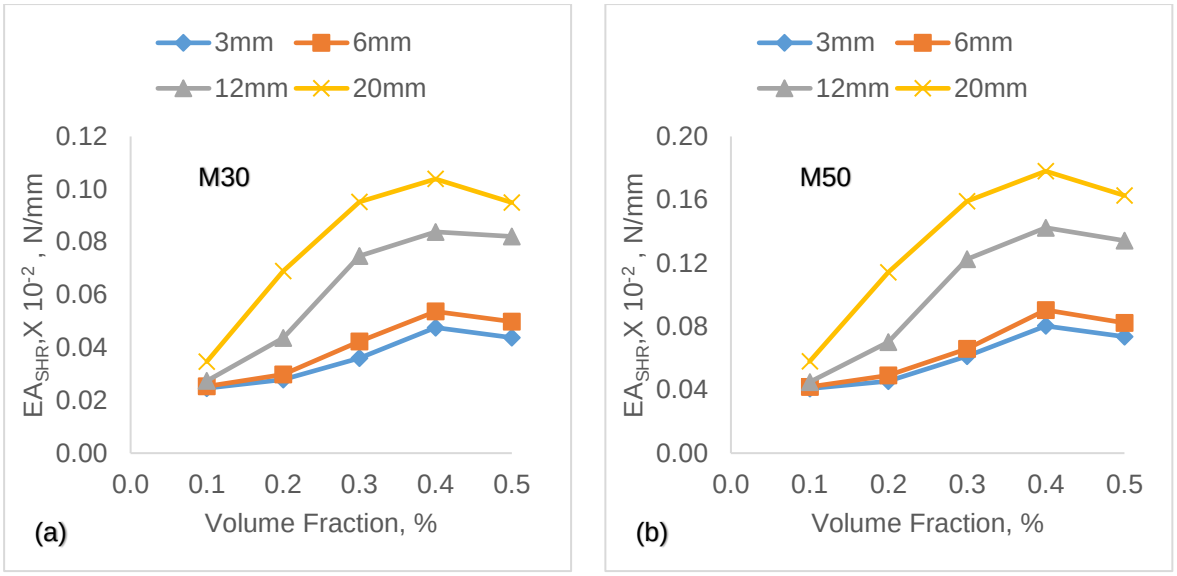

Fig.5.21 Energy Absorption in strain hardening region (EA_{SHR}) as a function of Volume Fraction for MGFRC in Tension

5.6 Image Analysis

Tensile strength of composite can be estimated using law of mixtures. Contribution of fiber in composite strength depends on fiber orientation and distribution. Hence, tensile properties of fibre concrete are governed mainly by the number, dispersion and orientation of fibres in the cracking area, as well as dispersion characteristics of fibres. Several techniques (Guild FJ et al, 1993; Yang Y, 2002; Yilmaz Akkaya et al, 2001 and Bang Yeon Lee, 2009) including image analysis, transmission X-ray photography, and Advanced CCD Imaging Spectrometer (ACIS) are available for evaluating the fibre distribution in a composite made of cement matrix and steel, carbon, glass, or organic fibres; i.e., these techniques can be employed to determine the degree of fibre dispersion and orientation in the composite. Among these techniques, image analysis is the most applicable and trusted method to evaluate the distribution characteristics of fibres in a composite.

5.6.1 Specimen preparation and Image Acquisition

In this study, fiber number, dispersion and orientation was estimated on the fracture plane of the specimen (Fig.5.22 (b)). Three specimens from each of the designation were selected for the image analysis and care was taken to choose specimens with fracture surface almost perpendicular to the tensile loading direction. Failed specimens (Fig.5.22 (a)) were cut close to the fractured surface. The cut cross sectional surfaces were then polished and cleaned. For each cross-section (80mm X

40mm), 64 images were captured, as illustrated in Fig.5.23. Polarised optical microscope (Fig.5.24) is used for capturing images. Images at each grid was taken at the fractured plane by optical microscope. Image at location 1 is shown in Fig.5.25.

Fig.5.22 (a) Failed specimens

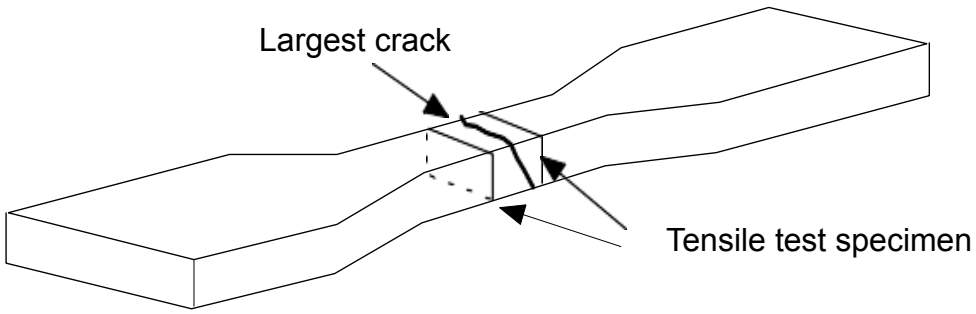

Fig. 5.22 (b) Fracture plane of the specimen

Fig.5.22 Failed specimens and fracture plane of the specimen

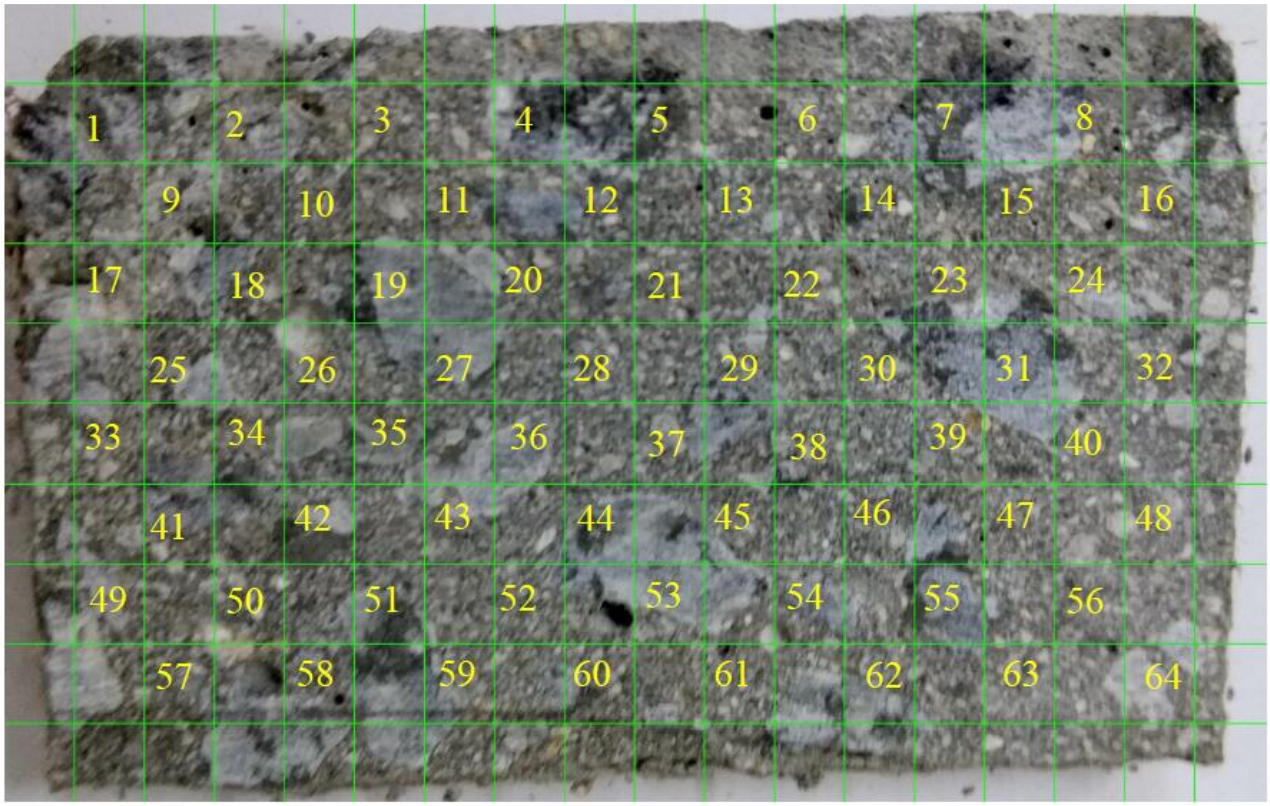

Fig.5.23 Grid notation of the cutting plane and area of each captured image in comparison with whole cross-section (Small squares represents the area captured by microscope camera).

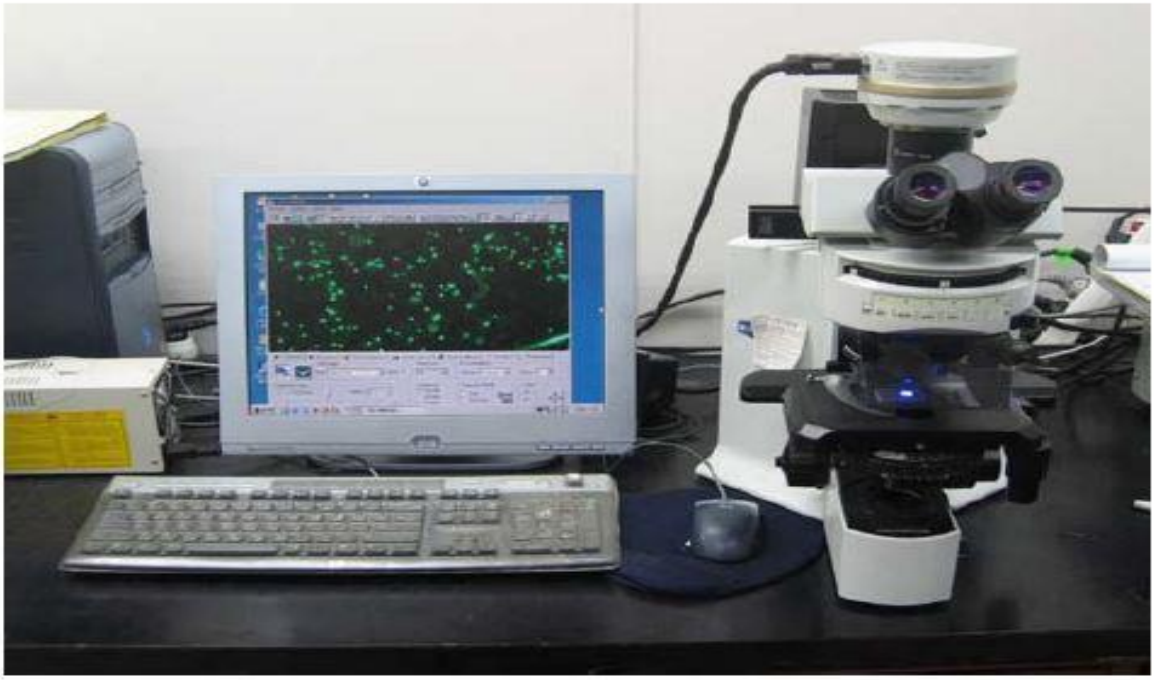

Fig.5.24 Polarised optical microscope (Olympus BX Series)

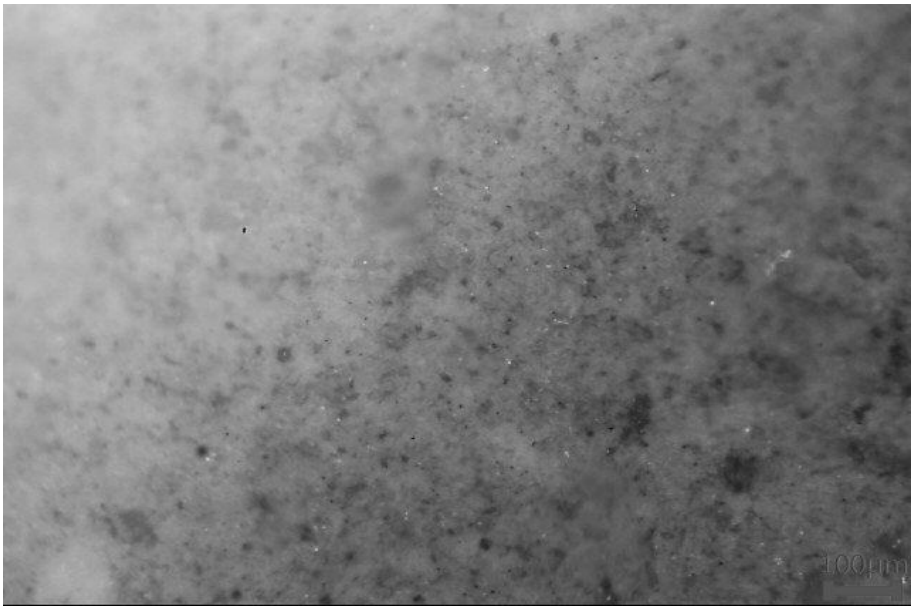

Fig.5.25 Optical microscopic image about fiber dispersion of specimen with V_f = 0.1% (for representative element 1 in Fig.5.23)

5.6.2 Detection of fibers

Images were uploaded in Image J software for processing. The shinning objects were first selected and the images were made binary based on a set threshold object detection method. Since some aggregates in concrete were also selected by the program as shining objects, these were extracted manually from the image as shown in Fig.5.26.

The above method is applied for the binary images of failed specimens with 0.1%, 0.2%, 0.3%, 0.4% and 0.5% volume fractions for mono fibers (3mm, 6mm, 12mm and 20mm). Total number of fibers present at the failed cross section are examined and the number of fibers present in each location is counted. As stated earlier there are sixty four locations (Fig.5.23) and the fiber present in corresponding location is given in Table 5.3. Sum of fibers present in sixty four locations is taken as estimated number of fibers at fracture plain. The number is doubled to get the total number of fibers (n_e) in the cross-section. In an ideal situation, assuming that all the fibers are aligned and distributed uniformly over entire volume, number of fibers (N_f) at a cross-section is estimated for the specimen with a volume fraction. The number (N_f) depends on V_f only but not length of fiber. Values of N_f is given in Table 5.4. At a section fiber density factor (f_d = Estimated number of fibers (n_e) / Number of fibers when aligned uniformly distributed (N_f)) is calculated and is given in Table 5.4.

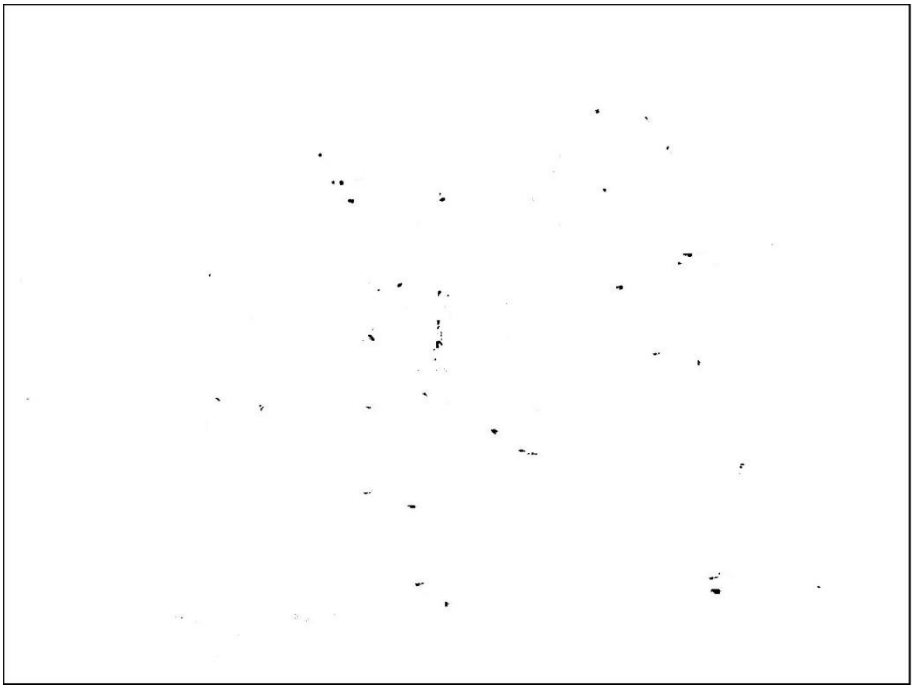

Fig.5.26 Binary image at location 1

Table 5.3 fiber number at each location for 0.1%-3mm For M30-MGFRC

36		56		58		52		55		53		46		56	
	64		75		75		77		72		65		64		35
46		70		77		72		77		75		65		56	
	65		85		85		85		80		65		65		46
58		70		80		89		86		72		63		64	
	65		75		77		85		77		68		65		52
52		65		75		68		74		71		72		55	
	46		49		58		46		46		58		46		50
Estimated number of fibers (n_e) = 2 X 4310 = 8620															

Table 5.4 Number of fibers and Fiber density factor For M30-MGFRC

Vf,%	Number of Fibers when aligned uniformly distributed (N_f)	Estimated Maximum number of fibers (n_e)				Fiber Density Factor ($f_d=n_e/N_f$)			
		3mm	6mm	12mm	20mm	3mm	6mm	12mm	20mm
0.1	20798	8260	5926	2346	1522	0.40	0.28	0.11	0.07
0.2	41596	11166	6944	3942	2546	0.27	0.17	0.09	0.06
0.3	62394	13718	9800	6278	3696	0.22	0.16	0.10	0.06
0.4	83193	10308	5964	3310	2294	0.12	0.07	0.04	0.03
0.5	103991	9200	4802	2718	2058	0.09	0.05	0.03	0.02

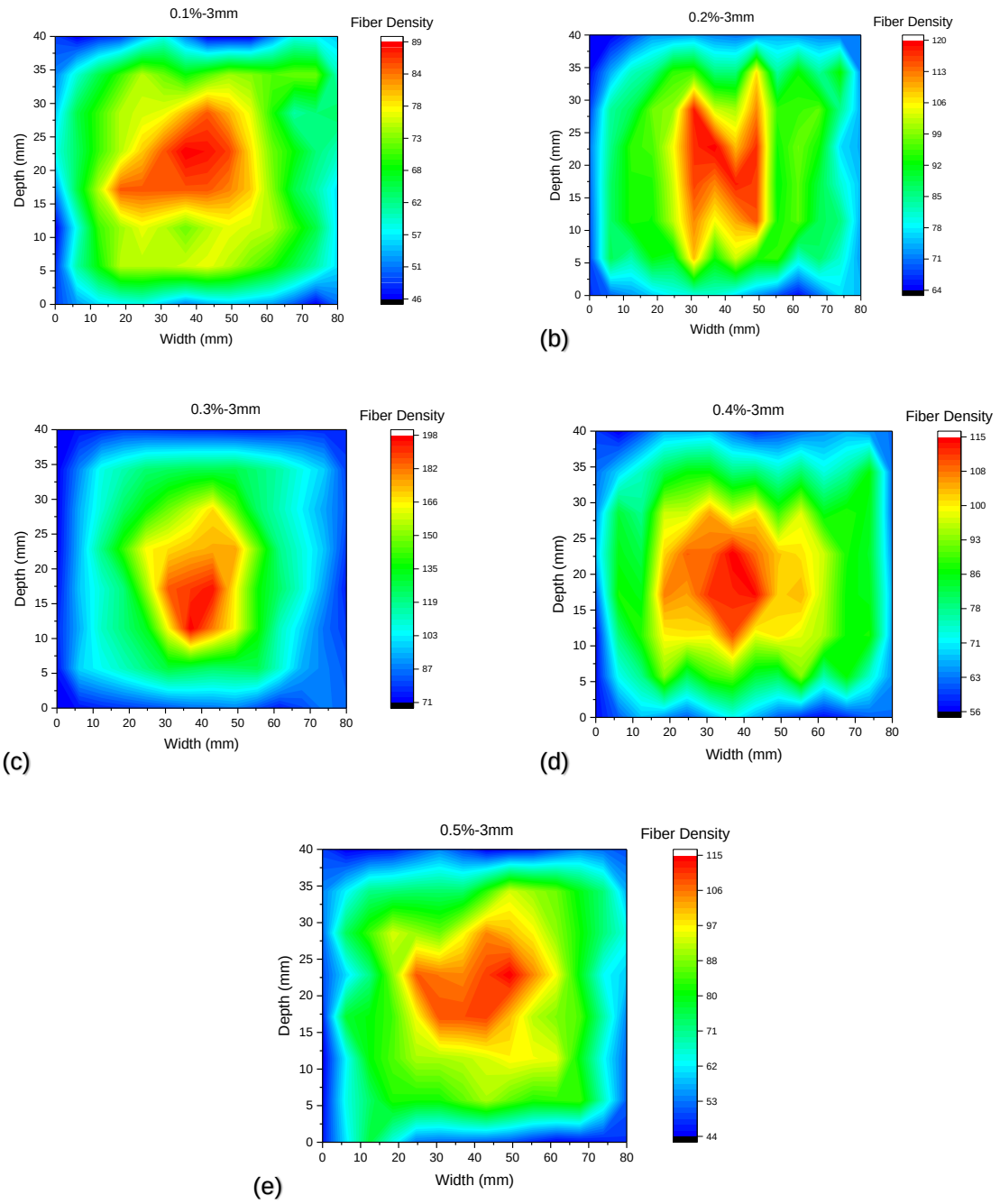

Fig.5.27 Variation of fibers present along the thickness and width direction for 3mm length fiber. (a) 0.1%-3mm, (b) 0.2%-3mm, (c) 0.3%-3mm, (d) 0.4%-3mm and (e) 0.5%-3mm

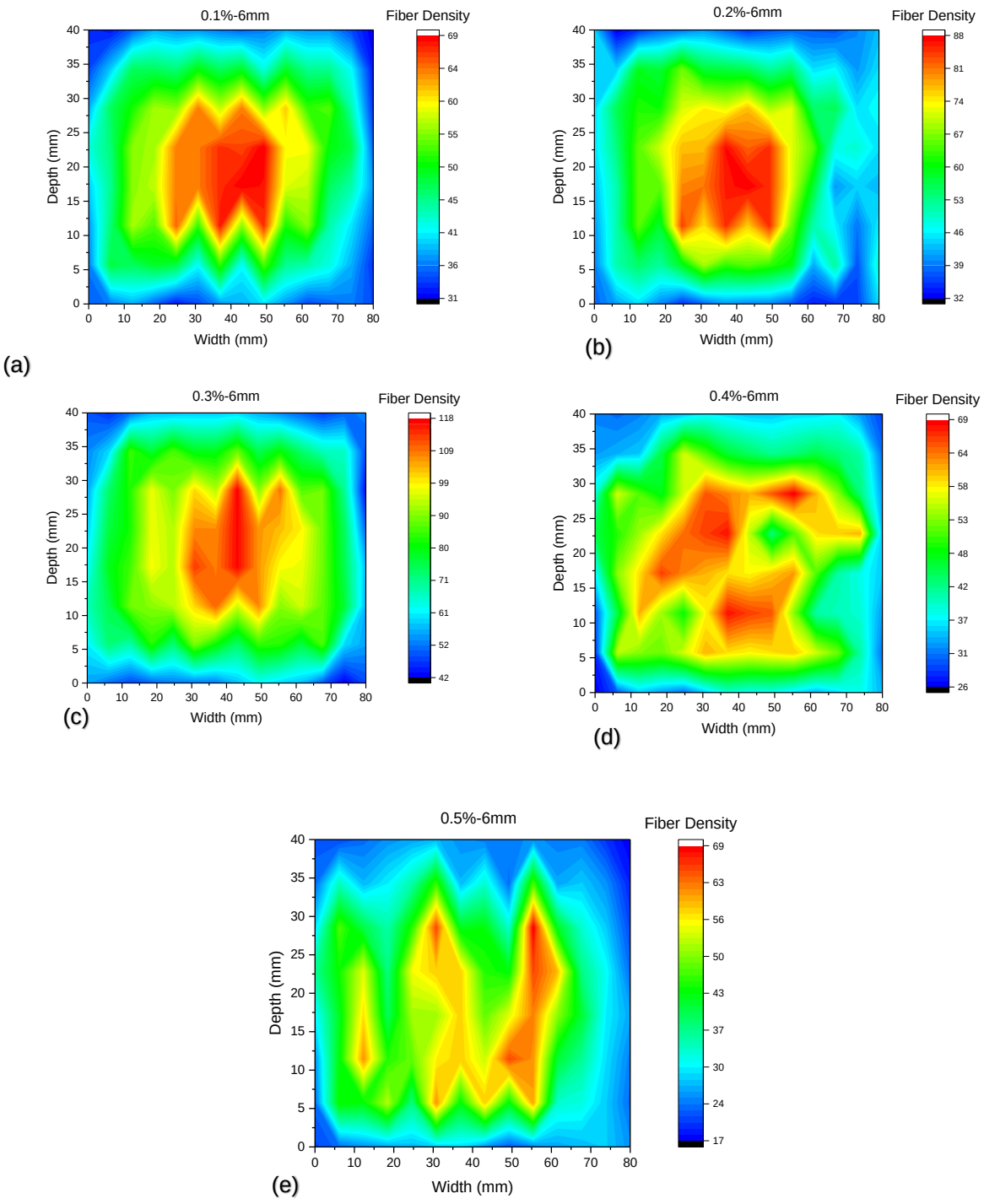

Fig.5.28 Variation of fibers present along the thickness and width direction for 6mm length fiber. (a) 0.1%-6mm, (b) 0.2%-6mm, (c) 0.3%-6mm, (d) 0.4%-6mm and (e) 0.5%-6mm.

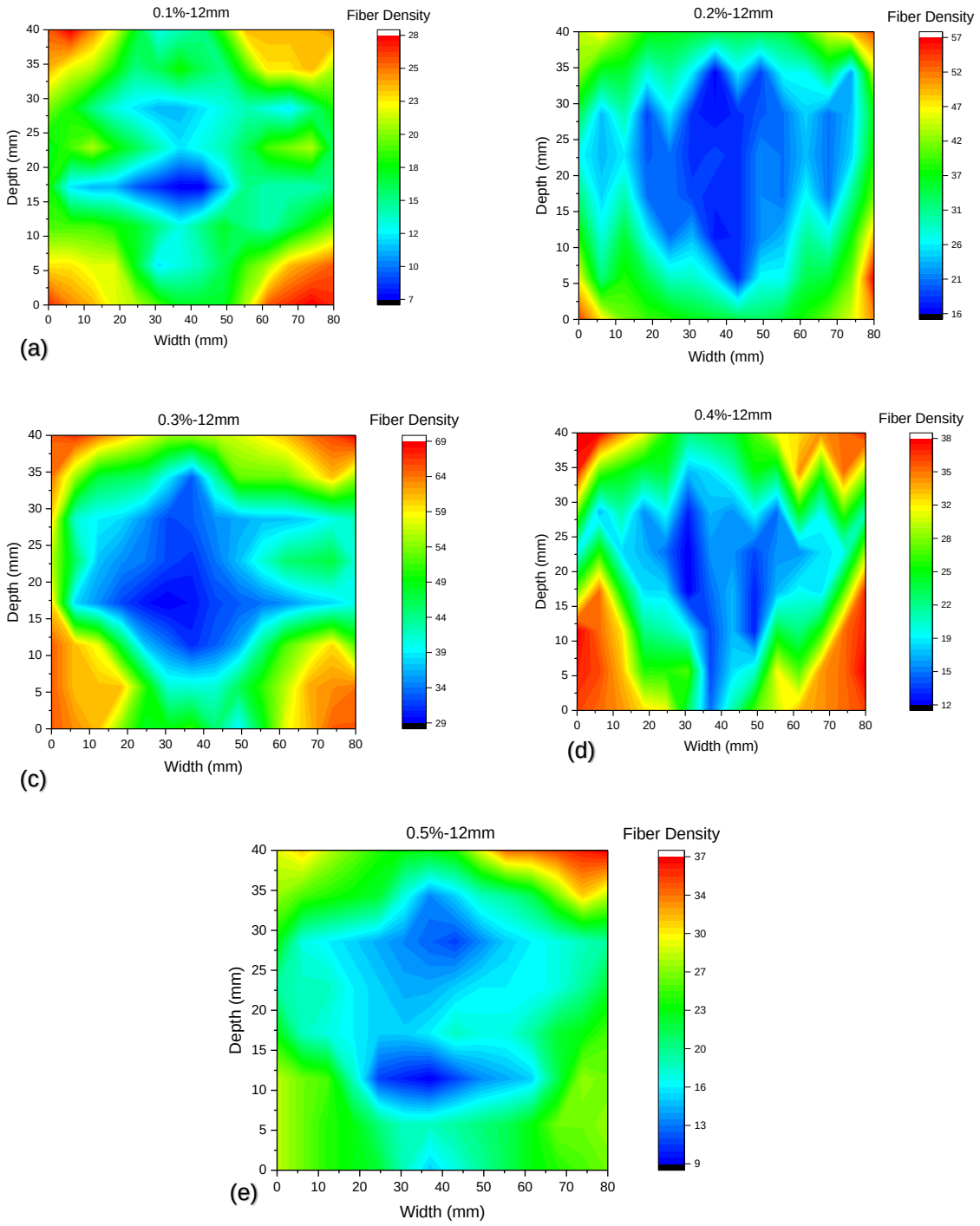

Fig.5.29 Variation of fibers present along the thickness and width direction for 12mm fiber. (a) 0.1%-12mm, (b) 0.2%-12mm, (c) 0.3%-6mm, (d) 0.4%-12mm and (e) 0.5%-12mm

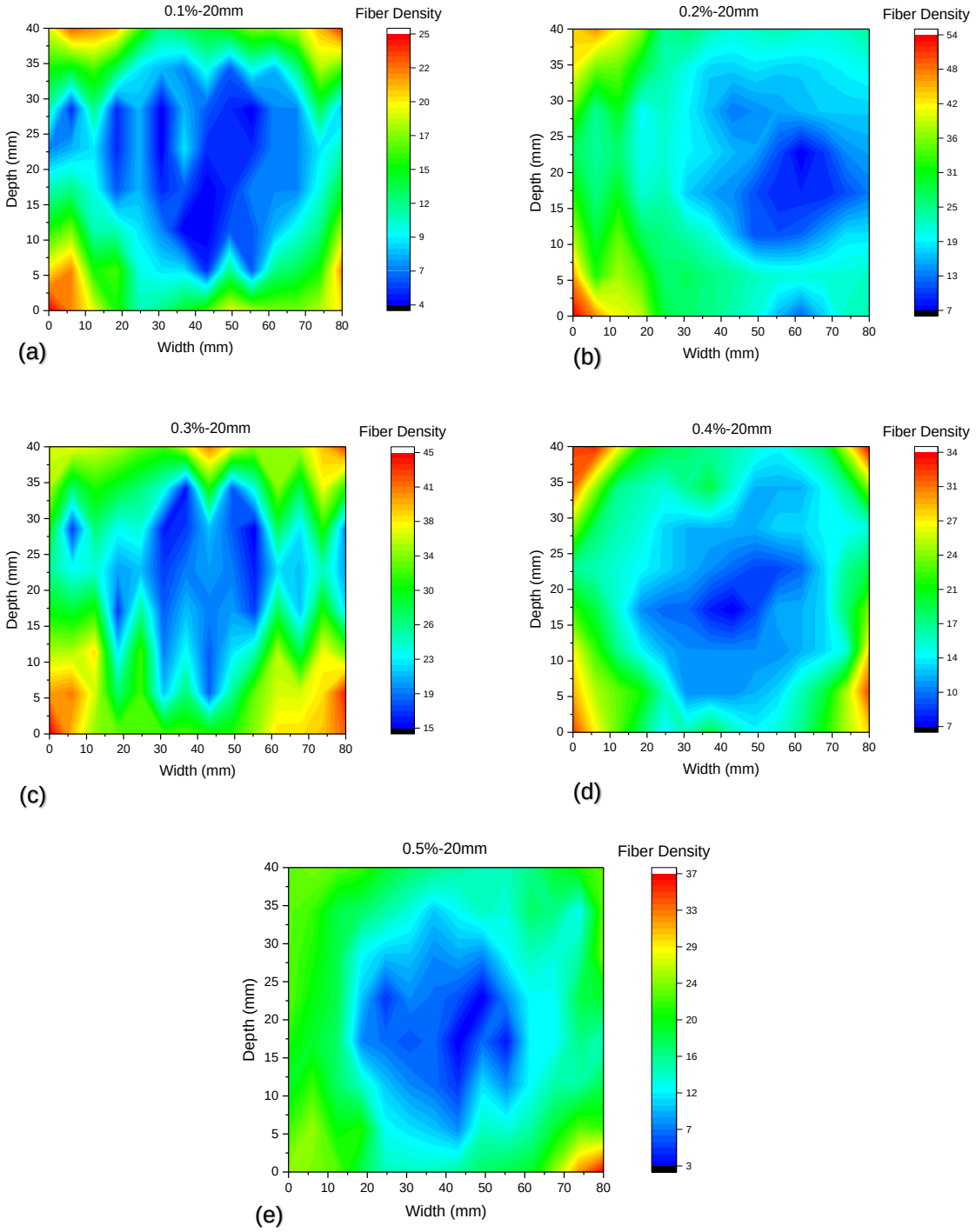

Fig.5.30 Variation of fibers present along the thickness and width direction for 20mm fiber. (a) 0.1%-20mm, (b) 0.2%-20mm, (c) 0.3%-20mm, (d) 0.4%-20mm and (e) 0.5%-20mm.

Fibers are not distributed uniformly across the section. Variation of fibers present in the concrete is shown in Fig 5.27 to 5.30 for different volume fractions and different fiber length. Less fibers are present at the corners and edges compared to the center of cross-section in case of 3mm and 6mm length of fibers (Fig 5.27 and 5.28). Where

as in case of 12mm and 20mm length fibers, less fibers are present at the center of cross-section compared to corners and edges (Fig.5.29 and 5.30). However, the specimens with 0.3% volume of the fibers has maximum number of fibers on fractured plane. That is why, irrespective of fiber length specimen with 0.3% volume fraction had maximum slump and maximum strength in fresh and hardened state compared to any other volume fraction.

5.6.3 Calculation of Fiber Dispersion coefficient (η_d)

Bang Yeon Lee et al, 2009, proposed an expression to represent the fiber dispersion and is given in equation (1). It is used and named as fiber dispersion coefficient (η_d).

$$\eta_d = exp\left[\sqrt{\frac{\Sigma\,(x_i-1)^2}{n}}\right] \text{---------- (1)}$$

Where n is the total number of fibers on the image and x_i denotes the number of fibers in the i^{th} unit, which is a square portion allocated to the i^{th} fiber on the assumption that the fiber dispersion is perfectly homogeneous.

Divide the binary image Fig.5.26 into squares as shown in Fig.5.31. The number of squares equals to the number of fibers (n). Count the number of fibers in each square area (x_i). Fiber dispersion coefficient (η_d) can be obtained from equation (1) for each location. Values η_d in 64 locations is shown in Table 5.5. Then, average of 64 η_d is calculated and taken as average η_d for the specimen, which is taken as for the specimen η_d herein after. The η_d values calculated for each specimen as stated above.

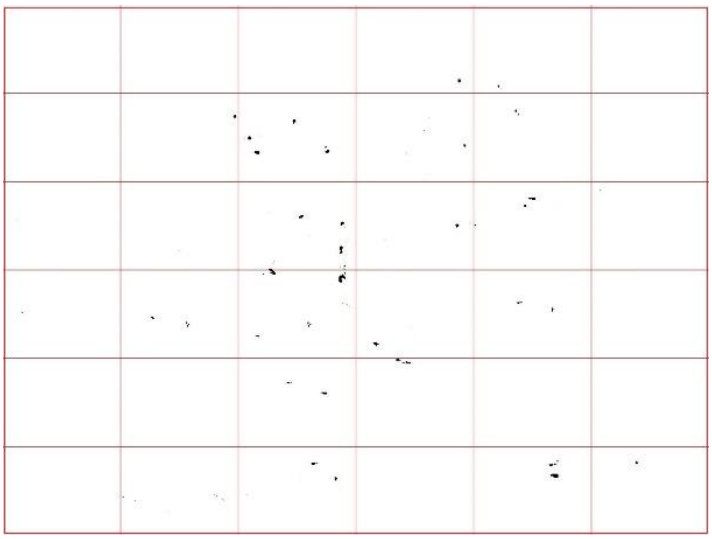

Fig. 5.31 Binary image dividing the equal square units

Table 5.5 Summary of the η_d at each location for 0.1%-3mm for M30-MGFRC

0.31		0.30		0.32		0.31		0.32		0.31		0.29		0.31	
	0.32		0.33		0.32		0.32		0.33		0.3		0.32		0.29
0.30		0.33		0.38		0.36		0.34		0.39		0.32		0.30	
	0.32		0.35		0.35		0.38		0.37		0.32		0.32		0.30
0.32		0.32		0.33		0.38		0.38		0.32		0.30		0.32	
	0.34		0.36		0.36		0.37		0.35		0.34		0.34		0.30
0.30		0.31		0.32		0.32		0.32		0.33		0.31		0.30	
	0.29		0.30		0.31		0.33		0.31		0.31		0.29		0.30
Avg η_d = 0.33															

The above method is applied for the binary images of failed specimens with 0.1%, 0.2%, 0.3%, 0.4% and 0.5% volume fractions for mono fibers (3mm, 6mm, 12mm and 20mm). Specimens with 0.1%, 0.2%, 0.3%, 0.4% and 0.5% volume fractions having the fiber dispersion coefficients for mono fiber specimen 3mm, 6mm, 12mm and 20mm fiber lengths respectively is given in column 2, 3, 4 and 5 of Table.5.6. If the value of η_d is '1' then fiber dispersion is homogeneous, whereas if the η_d values tends to '0' then the fiber dispersion is non- homogeneous. Hence higher the fiber dispersion coefficient higher the homogeneity of fiber dispersion.

Table 5.6 Fiber dispersion coefficient (η_d) for M30-MGFRC

V_f, % (1)	η_d			
	3mm (2)	6mm (3)	12mm (4)	20mm (5)
0.1	0.33	0.29	0.26	0.24
0.2	0.39	0.35	0.31	0.28
0.3	0.43	0.38	0.34	0.30
0.4	0.36	0.32	0.29	0.27
0.5	0.31	0.28	0.25	0.23

5.6.4 Fiber orientation coefficient (η_θ)

Each fiber particle in the binary image Fig.5.26 is estimated for its shape and area. The cross section of a fiber inclined to the loading direction will be ellipse and the area of such fiber is less than circular cross sectional area of fiber. Hence, the fiber particles whose area is less than or equal to circular cross sectional area of fiber are consider and also other are neglected. The orientation coefficient (η_θ is given in equation (2)) was determined by the ratio of measured area of the fiber (A_m) to the original area of fiber (A_0) on fracture plane and given in Table 5.7. Values given in Table 5.8 is the average η_θ of all the fibers taken on the fracture plane.

$$\eta_\theta = A_m / A_0 \text{ ---------- (2)}$$

Table 5.7 Summary of the η_θ at each location for 0.1%-3mm of M30-MGFRC

0.59		0.51		0.51		0.51		0.59		0.59		0.62		0.59	
	0.52		0.51		0.58		0.54		0.57		0.59		0.52		0.58
0.55		0.57		0.53		0.46		0.58		0.45		0.56		0.55	
	0.58		0.55		0.45		0.46		0.45		0.53		0.58		0.53
0.53		0.55		0.53		0.45		0.52		0.55		0.55		0.53	
	0.52		0.52		0.48		0.51		0.53		0.51		0.52		0.54
0.52		0.52		0.59		0.6		0.54		0.58		0.54		0.52	
	0.55		0.51		0.52		0.55		0.54		0.57		0.55		0.53
Avg. η_θ = 0.53															

If the orientation coefficient is '1' fibers are aligned perpendicularly to the cracking plane, which means that fibers can most effectively perform in fracture plane. Specimens with 0.1%, 0.2%, 0.3%, 0.4% and 0.5% volume fractions having the fiber orientation coefficients for 3mm, 6mm, 12mm and 20mm fiber lengths respectively is given in column 2, 3, 4 and 5 of Table 5.8.

Table 5.8 Fiber orientation coefficient (η_θ) for M30-MGFRC

V_f, % (1)	η_θ			
	3mm (2)	6mm (3)	12mm (4)	20mm (5)
0.1	0.53	0.50	0.36	0.31
0.2	0.60	0.56	0.41	0.37
0.3	0.66	0.60	0.45	0.42
0.4	0.56	0.53	0.40	0.38
0.5	0.51	0.50	0.37	0.33

5.7 Summary of the Image analysis for M50-MGFRC

The above method is applied for the M50-MGFRC-images of failed specimens with 0.1%, 0.2%, 0.3%, 0.4% and 0.5% volume fractions for mono fibers (3mm, 6mm, 12mm and 20mm). Number of fibers, fiber dispersion coefficient (η_d), fiber orientation coefficient (η_θ) at a cross section on a fracture plane is given in Table 5.9, 5.10 and 5.11 respectively.

Table 5.9 Number of fibers and Fiber density factor For M50-MGFRC

V_f, % (1)	Number of Fibers when aligned uniformly distributed (N_f) (2)	Estimated Maximum number of fibers (n_e)				Fiber Density Factor ($f_d = n_e / N_f$)			
		3mm (3)	6mm (4)	12mm (5)	20mm (6)	3mm (7)	6mm (8)	12mm (9)	20mm (10)
0.1	20798	8698	6100	2414	1580	0.42	0.29	0.12	0.08
0.2	41596	11696	7192	4170	2624	0.28	0.17	0.10	0.06
0.3	62394	14808	10174	6700	3886	0.24	0.16	0.11	0.06
0.4	83193	10838	8832	3450	2374	0.13	0.11	0.04	0.03
0.5	103991	9580	5080	2814	2134	0.09	0.05	0.03	0.02

Table 5.10 Fiber dispersion coefficient (η_d) for M50-MGFRC

V_f, % (1)	η_d			
	3mm (2)	6mm (3)	12mm (4)	20mm (5)
0.1	0.35	0.31	0.28	0.25
0.2	0.41	0.36	0.33	0.30
0.3	0.45	0.40	0.36	0.32
0.4	0.38	0.34	0.31	0.28
0.5	0.33	0.29	0.26	0.24

Table 5.11 Fiber orientation coefficient (η_θ) for M50-MGFRC

V_f, % (1)	η_θ			
	3mm (2)	6mm (3)	12mm (4)	20mm (5)
0.1	0.55	0.52	0.37	0.32
0.2	0.62	0.58	0.42	0.38
0.3	0.68	0.62	0.46	0.43
0.4	0.58	0.54	0.41	0.39
0.5	0.53	0.52	0.38	0.34

5.8 Calculation of Fiber Length coefficient (η_l)

η_l is a function of fiber length. If a uniform interfacial shear stress transfer is assumed, η_l is given by equation (3) to (6) (C. R. Chiang 1993).

$$\text{For } L_f < L_c \quad \eta_l = L_f / 2L_c \qquad \text{---------- (3)}$$

$$\text{For } L_f \geq L_c \quad \eta_l = 1 - (L_c / 2L_f) \qquad \text{---------- (4)}$$

Where L_f is the fiber length and Lc is the fiber critical transfer length.

The fiber critical transfer length (Lc) = $(\sigma_{fu} . D_f) / (2 \sigma_{fb})$ ---------- (5)

The bond strength of the fiber $(\sigma_b) = F_{max} / (\pi . D_f . L_e)$ ---------- (6)

Where σ_{fu} is tensile strength of fiber, F_{max} is fiber pull-out load and L_e is embedded length of fiber.

Different embedded lengths result in a distribution in the resistance of the fiber to pull-out in a cement based matrix. Pull-out tests were carried out for four different embedded lengths of 3, 6, 12 and 20mm fibers in a concrete matrix. The rate of pull-out used in this study was 0.02 mm/s. The pull-out load and the end displacement of the fiber were continuously recorded. The peak pull-out loads (F_{max}) values for different embedded lengths is given in column 2 of Table 5.12. Fiber length coefficient (η_l) is computed from equation (3) to equation (6) and reported in column 5 of Table 5.12. In similar manner, the fiber length coefficient was calculated for M50-MGFRC with different embedded lengths of 3mm, 6mm, 12mm and 20mm respectively and is given in Table 5.13.

Table 5.12 Fiber length coefficient (η_l) calculations for M30-MGFRC

L_e (1)	F_{max} (Newton) (2)	σ_b (MPa) (3)	Lc (mm) (4)	η_l (5)
3mm	0.41	3.12	3.81	0.39
6mm	0.45	1.72	6.92	0.43
12mm	0.54	1.02	11.67	0.51
20mm	0.63	0.712	16.71	0.58
Diameter of the fiber (D_f) = 0.014mm, Tensile strength of the fiber (σ_{fu})= 1700 MPa, L_e = Embedded length of fiber				

Table 5.13 Fiber length coefficient (η_l) calculations for M50-MGFRC

L_e (1)	F_{max} (Newton) (2)	σ_b (MPa) (3)	Lc (mm) (4)	η_l (5)
3mm	0.47	3.59	3.32	0.45
6mm	0.52	1.98	6.02	0.50
12mm	0.62	1.17	10.14	0.58
20mm	0.72	0.82	14.53	0.64
Diameter of the fiber (D_f) = 0.014mm, Tensile strength of the fiber (σ_{fu})= 1700 MPa, L_e = Embedded length of fiber				

5.9 Variation of η_d and η_θ with reinforcing index (RI_{MF})

Reinforcing index (RI_{MF}) is defined as product of volume fraction (V_f) and aspect ratio of fiber (L_f / D_f). This is well established parameter (Ezeldin A.S 1992; M.C. Nataraja et al 1999 and Aref Abadel et al 2015). Relationship between Reinforcing Index (RI_{MF}) and the coefficients of fiber composite, viz., fiber dispersion coefficient (η_d) and fiber orientation coefficient (η_θ) and of concrete is presented in the fallowing paras.

5.9.1 Reinforcing Index (RI_{MF}) Vs Fiber dispersion coefficient (η_d)

Different fiber lengths and volume fractions influences on fiber dispersion coefficient. The reinforcing index of each mix was calculated and is given in column 4 of Table 5.14. In order to understand the variation of η_d with RI_{MF}, points are plotted as shown in Fig.5.32 (a). An examination of the plot and various trails to arrive at the best fit, led to understand that η_d varies as power function of RI_{MF} in the form of $\eta_d = k / (RI_{MF})^n$. The power function is modified by multiplying both sides by RI_{MF}. The modified relation is $(RI_{MF})\ \eta_d = k\ (RI_{MF})^{(1-n)}$. Now points are plotted with RI_{MF} as abscissa and $RI_{MF}.\ \eta_d$ as ordinate as shown in Fig.5.32 (b). The regression expression obtained is $(RI_{MF})\ \eta_d = 0.3656\ (RI_{MF})^{0.8956}$ with regression coefficient $R^2 = 0.9741$. Then the relation between RI_{MF} and η_d can be expressed as

$$\eta_d = 0.3656.(RI_{MF})^{-0.1044} \text{--------- (7)}$$

A plot of reinforcing index vs fiber dispersion coefficient for M30 and M50 is shown in Fig.5.32.

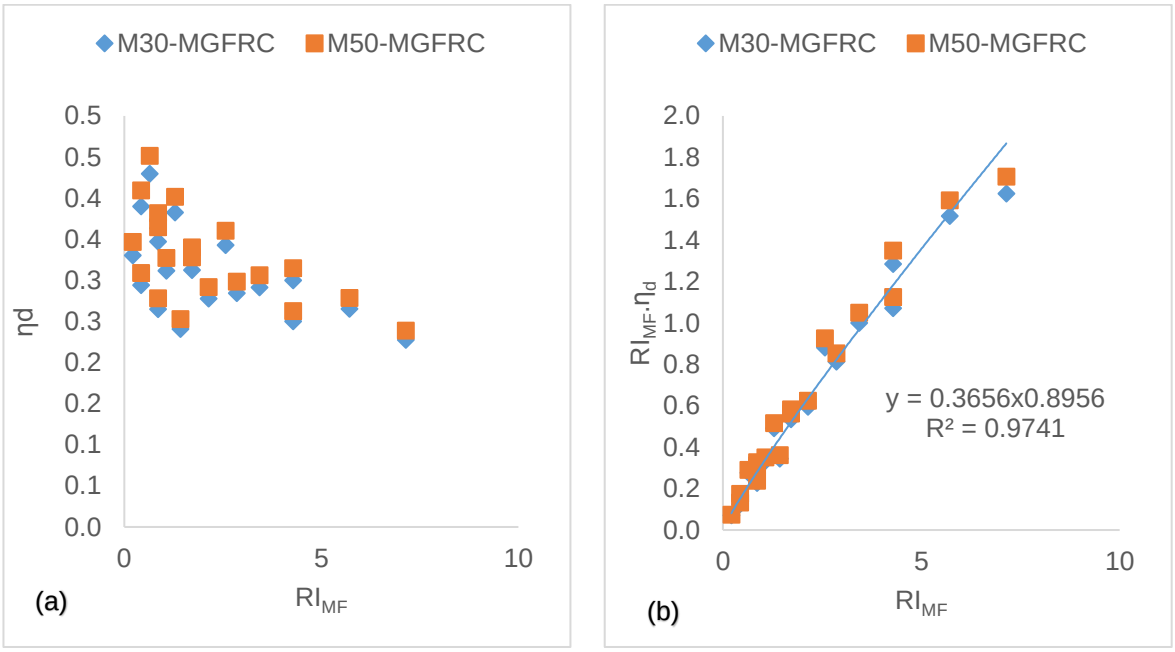

Fig. 5.32 Reinforcing Index (RI_{MF}) Vs Fiber dispersion coefficient (η_d)

Table 5.14 η_d and η_θ for MGFRC

L_f, mm (1)	D_f, mm (2)	V_f, % (3)	RI_{MF} (4)	M30-MGFRC		M50-MGFRC	
				η_d (5)	η_θ (6)	η_d (7)	η_θ (8)
3	0.014	0.1	0.21	0.33	0.53	0.35	0.55
		0.2	0.43	0.39	0.60	0.41	0.62
		0.3	0.64	0.43	0.66	0.45	0.68
		0.4	0.86	0.36	0.56	0.38	0.58
		0.5	1.07	0.31	0.51	0.33	0.53
6		0.1	0.43	0.29	0.50	0.31	0.52
		0.2	0.86	0.35	0.56	0.36	0.58
		0.3	1.29	0.38	0.60	0.40	0.62
		0.4	1.71	0.32	0.53	0.34	0.54
		0.5	2.14	0.28	0.50	0.29	0.52
12		0.1	0.86	0.26	0.36	0.28	0.37
		0.2	1.71	0.31	0.41	0.33	0.42
		0.3	2.57	0.34	0.45	0.36	0.46
		0.4	3.43	0.29	0.40	0.31	0.41
		0.5	4.29	0.25	0.37	0.26	0.38
20		0.1	1.43	0.24	0.31	0.25	0.32
		0.2	2.86	0.28	0.37	0.30	0.38
		0.3	4.29	0.30	0.42	0.32	0.43
		0.4	5.71	0.27	0.38	0.28	0.39
		0.5	7.14	0.23	0.33	0.24	0.34
Reinforcing Index of mono fibers (RI_{MF})= $V_f.(L_f / D_f)$,							

5.9.2 Reinforcing Index (RI_{MF}) Vs Fiber orientation coefficient (η_θ)

Different fiber lengths and volume fractions influences on fiber orientation coefficient. The reinforcing index of each mix was calculated and is given in column 4 of Table 5.14. In order to understand the variation of η_θ with RI_{MF}, points are plotted as shown in Fig.5.33 (a). An examination of the plot and various trails to arrive at the best fit, led to understand that η_θ varies as power function of RI_{MF} in the form of $\eta_\theta = k / (RI_{MF})^n$. The power function is modified by multiplying both sides by RI_{MF}. The modified relation is $(RI_{MF})\ \eta_\theta = k\ (RI_{MF})^{(1-n)}$. Now points are plotted with RI_{MF} as abscissa and $RI_{MF}.\eta_\theta$ as ordinate as shown in Fig.5.33 (b). The regression expression obtained is $(RI_{MF})\ \eta_\theta = 0.4686\ (RI_{MF})^{0.8481}$ with regression coefficient $R^2 = 0.9577$. Then the relation between RI_{MF} and η_θ can be expressed as

$$\eta_\theta = 0.4686.(RI_{MF})^{-0.1519} \text{--------- (8)}$$

A plot of reinforcing index vs fiber orientation coefficient for M30 and M50 is shown in Fig.5.32.

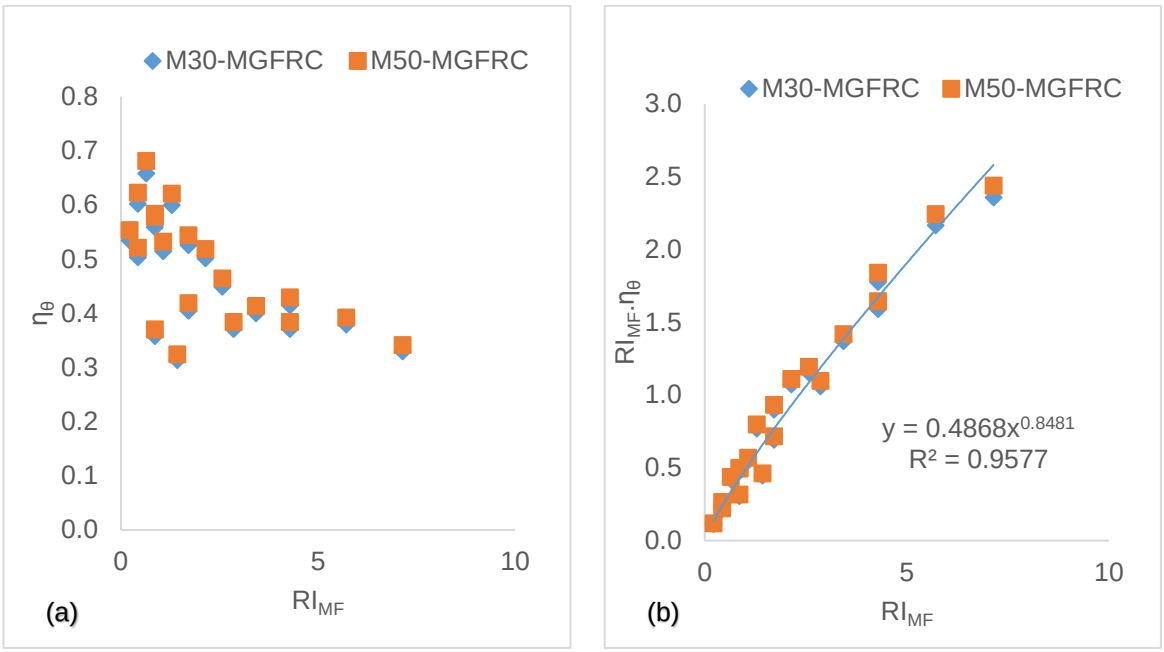

Fig.5.33 Reinforcing Index (RI_{MF}) Vs Fiber orientation coefficient (η_θ)

5.10 Theoretical analysis for predicting the tensile stress strain behaviour

5.10.1 General Theory

General behaviour of stress strain relation in uni axial tension for MGFRC is observed to be bilinear as depicted in Fig.5.16. Initial linear region in pre crack region and next linear region is strain hardening region which is due to resistant to crack propagation. It is noted from the test that as load increased gradually deformation increased up to cracking. During this period the resistance to load is offered is only by concrete and fibers present in the matrix are passive to applied load. Once the stress in concrete is nearing the cracking stress the fibers present in the matrix become active. The deviation point from the idealized that deviation point from initial linearity is assumed to occur at a stress equal to cracking stress of concrete and this deviation point (σ_{mt}, ε_{mt}) is marked as shown in Fig.5.34. After the initial linear region stress in concrete at several points increases to more than cracking stress. In all, such situations and at all such points the fibers present resist the formation of crack and also propagation of crack. This situation continuous till the internal cracks are well connected at a critical

section leading to ultimate resistance. During this region the slope of stress strain diagram falls drastically. The amount of deformation and slope in this region are directly influenced by the volume of fiber (V_f) and length of fiber (L_f). This is the characteristic region of FRC is treated as strain hardening region. The culmination of this region is marked as ultimate state (σ_{ct}, ε_{ct}) as shown in Fig.5.34.

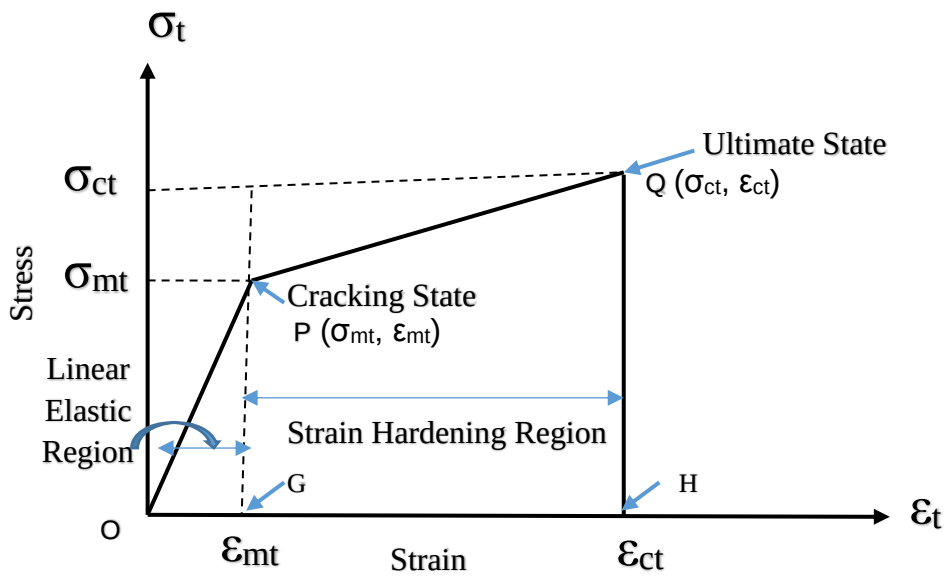

Fig.5.34 Idealized Stress Strain Curve in Tension

In order to predict the tensile stress strain behaviour of M30-MGFRC and M50-MGFRC, the points P (σ_{mt}, ε_{mt}) and Q (σ_{ct}, ε_{ct}) are needed to be determined. σ_{mt} can be obtained from direct tensile test on different grades of concrete whereas in case of ε_{mt} not much variation in strain values are observed with variation of concrete strength (Ivan Markovic 2006 and Supat W. Suwannakarn 2009). From the experimental tensile test results, in this investigation σ_{mt} for M30 and M50 grade of concrete is 3.68 MPa and 5.63 MPa respectively and ε_{mt} can be taken as 1.18 X 10^{-4} for both M30 and M50 grade of concrete. The strength of the composite (σ_{ct}) is the combination of matrix contribution (V_m. σ_{mt}) and fiber contribution (V_f. σ_{fu}). However, the fiber contribution mainly depends up on the fiber dispersion, fiber orientation and length of the fiber, this is explained in article 5.10.2. Finally, the composite tensile strain (ε_{ct}) is calculated by considering the area of strain hardening region as shown in Fig.5.34 and it is given in article 5.10.3.

5.10.2 Tensile strength of composite (σ_{ct})

Rule of Mixture is often used to predict the strength of fibre reinforced composite by equation (9) and fiber-matrix constant interfacial shear stress is assumed (Su Tae Kang et al 2011).

$$\sigma_{ct} = \eta_\theta \eta_l V_f \sigma_{fu} + V_m \sigma_{mt} \text{ ----------(9)}$$

η_θ, η_l are the fiber orientation coefficient and fiber length coefficient. σ_{ct}, σ_{fu} and σ_{mt}, are the composite tensile strength, ultimate tensile strength of the fibre and the matrix tensile strength respectively. V_f is the fibre volume fraction and V_m is the matrix volume fraction (1 -V_f).

Fiber dispersion is an important property that controls the mechanical properties of composite. Uniformly dispersed short fibers will be reinforcing micro cracks effectively in the volume thus improves the strength of composite. Fiber dispersion coefficient (η_d) is introduced in to equation (9) to take account of fiber spacing in the fracture plane. The modified equation is given in equation (10)

$$\sigma_{ct} = \eta_d \eta_\theta \eta_l V_f \sigma_{fu} + V_m \sigma_{mt} \text{ ----------(10)}$$

η_d, η_θ and η_l are computed from equation 7, 8 and 3 or 4. These values are given in column 4, 5 and 6 of Table 5.15. The strength of fiber reinforced composite (M30-MGFRC) is calculated based on equation (9) and (10) and the values are reported in column 8 and 9 of Table.5.15 and these values are compared with the experimental values given in column 7 of Table 5.15. The ratio of the calculated strength of fiber composite to that of experimental strength are also shown in column 10 and 11 of Table 5.15. It can be noted that the composite strength values obtained from equation (10) are close to the experimental composite strength values compared to the equation (9).

Similarly for M50-MGFRC, η_d, η_θ and η_l are computed from equation 7, 8 and 4. These values are given in column 4, 5 and 6 of Table 5.16. The strength of fiber reinforced composite (M50-MGFRC) is calculated based on equation (9) and (10) and the values are reported in column 8 and 9 of Table.5.16 and these values are compared with the experimental values are given in column 7 of Table 5.16. The ratio of the calculated strength of fiber composite to that of experimental strength are also shown in column 10 and 11 of Table 5.16. It can be noted that the composite strength values obtained

from equation (10) are close to the experimental composite strength values compared to the equation (9).

From the studies of M30-MGFRC and M50-MGFRC on tensile strength, the equation (10) predicted close to the experimental tensile strength. Hence, it can be concluded that equation (10) can be used for calculating tensile strength of composite.

Table 5.15 Predicted tensile strength of M30-MGFRC from equation (9) and (10)

L_f (1)	Vf, % (2)	RI_{MF} (3)	η_d (4)	η_θ (5)	η_l (6)	$\sigma^{MFt}{}_u$ (7)	$\sigma^{MF1}{}_{ct}$ (8)	$\sigma^{MF2}{}_{ct}$ (9)	Ratio1 (10)	Ratio2 (11)
3mm	0.1	0.21	0.39	0.62	0.39	3.95	4.09	3.88	1.04	0.98
	0.2	0.43	0.36	0.55		4.07	4.41	3.99	1.08	0.98
	0.3	0.64	0.34	0.52		4.37	4.71	4.09	1.08	0.94
	0.4	0.86	0.33	0.50		4.02	5.00	4.17	1.24	1.04
	0.5	1.07	0.33	0.48		3.93	5.27	4.24	1.34	1.08
6mm	0.1	0.43	0.36	0.55	0.43	3.86	4.08	3.85	1.06	1.00
	0.2	0.86	0.33	0.50		3.99	4.41	3.95	1.11	0.99
	0.3	1.29	0.32	0.47		4.21	4.71	4.03	1.12	0.96
	0.4	1.71	0.31	0.45		3.90	4.99	4.10	1.28	1.05
	0.5	2.14	0.30	0.43		3.85	5.26	4.16	1.36	1.08
12mm	0.1	0.86	0.33	0.50	0.51	3.78	3.99	3.84	1.05	1.02
	0.2	1.71	0.31	0.45		3.87	4.24	3.93	1.10	1.02
	0.3	2.57	0.30	0.42		4.08	4.46	4.00	1.09	0.98
	0.4	3.43	0.29	0.40		3.78	4.68	4.07	1.24	1.08
	0.5	4.29	0.28	0.39		3.76	4.89	4.12	1.30	1.10
20mm	0.1	1.43	0.32	0.46	0.58	3.71	4.13	3.83	1.12	1.03
	0.2	2.86	0.29	0.42		3.77	4.49	3.91	1.19	1.04
	0.3	4.29	0.28	0.39		3.93	4.83	3.98	1.23	1.01
	0.4	5.71	0.27	0.37		3.75	5.14	4.04	1.37	1.08
	0.5	7.14	0.27	0.36		3.69	5.45	4.10	1.47	1.11

$\sigma^{MFt}{}_{u,}$ = Experimental ultimate tensile Strength ($\sigma^{Q}{}_{t}$) of M30-MGFRC is given in column 5 of Table 5.1, $\sigma^{MF1}{}_{ct}$ = Calculated ultimate tensile Strength of MGFRC from equation (9), $\sigma^{MF2}{}_{ct}$ = Calculated ultimate tensile Strength of MGFRC from equation (10), σ_{mt} = 3.68 MPa, ε_{mt} = 1.18 X 10^{-4}, σ_{fu} = 1700 MPa, Ratio1= $\sigma^{MF1}{}_{ct}$ / $\sigma^{MFt}{}_{u}$, Ratio2= $\sigma^{MF2}{}_{ct}$ / $\sigma^{MFt}{}_{u}$

Table 5.16 Predicted tensile strength of M50-MGFRC from equation (9) and (10)

L_f (1)	Vf, % (2)	RI_{MF} (3)	η_d (4)	η_θ (5)	η_l (6)	$\sigma^{MFt}{}_u$ (7)	$\sigma^{MF1}{}_{ct}$ (8)	$\sigma^{MF2}{}_{ct}$ (9)	Ratio1 (10)	Ratio2 (11)
3mm	0.1	0.21	0.39	0.62	0.45	6.22	6.10	5.86	0.98	0.94
	0.2	0.43	0.36	0.55		6.51	6.47	5.99	0.99	0.92
	0.3	0.64	0.34	0.52		6.95	6.82	6.10	0.98	0.88
	0.4	0.86	0.33	0.50		6.35	7.14	6.19	1.12	0.97
	0.5	1.07	0.33	0.48		6.05	7.46	6.27	1.23	1.04
6mm	0.1	0.43	0.36	0.55	0.50	6.10	6.10	5.83	1.00	0.96
	0.2	0.86	0.33	0.50		6.30	6.47	5.94	1.03	0.94
	0.3	1.29	0.32	0.47		6.68	6.81	6.03	1.02	0.90
	0.4	1.71	0.31	0.45		6.22	7.13	6.11	1.15	0.98
	0.5	2.14	0.30	0.43		5.92	7.44	6.18	1.26	1.04
12mm	0.1	0.86	0.33	0.50	0.58	5.90	5.94	5.81	1.01	0.99
	0.2	1.71	0.31	0.45		6.16	6.18	5.91	1.00	0.96
	0.3	2.57	0.30	0.42		6.50	6.41	5.99	0.99	0.92
	0.4	3.43	0.29	0.40		6.14	6.63	6.06	1.08	0.99
	0.5	4.29	0.28	0.39		5.79	6.83	6.12	1.18	1.06
20mm	0.1	1.43	0.32	0.46	0.64	5.74	6.13	5.80	1.07	1.01
	0.2	2.86	0.29	0.42		6.01	6.52	5.89	1.08	0.98
	0.3	4.29	0.28	0.39		6.33	6.88	5.96	1.09	0.94
	0.4	5.71	0.27	0.37		6.06	7.23	6.02	1.19	0.99
	0.5	7.14	0.27	0.36		5.66	7.56	6.08	1.34	1.07

$\sigma^{MFt}{}_{u,}$ = Experimental ultimate tensile strength ($\sigma^{Q}{}_{t}$) of M50-MGFRC is given in column 5 of Table 5.2, $\sigma^{MF1}{}_{u}$ = Calculated ultimate tensile strength of MGFRC from equation (9), $\sigma^{MF2}{}_{u}$ = Calculated ultimate tensile Strength of MGFRC from equation (10), σ_{mt} = 5.63 MPa, ε_{mt} = 1.18 X 10^{-4}, σ_{fu} = 1700 MPa, Ratio1= $\sigma^{MF1}{}_{u}$ / $\sigma^{MFt}{}_{u}$, Ratio2= $\sigma^{MF2}{}_{u}$ / $\sigma^{MFt}{}_{u}$

5.10.3 Tensile strain (ε_{ct}) at Tensile strength of composite (σ_{ct})

Tensile strain (ε_{ct}) mainly depends on the composite tensile strength (σ_{ct}) and energy absorption capacity of the composite. The tensile strain (ε_{ct}) of the composite is calculated by using equation (11). This equation is derived from experimental energy absorption (EA_{MF}^{SHR}) in strain hardening region, area of area of the trapezium (GPQH) shown in Fig 5.34.

EA_{MF}^{SHR} = area of the trapezium (GPQH)

$$EA_{MF}^{SHR} = \frac{\sigma_{ct} + \sigma_{mt}}{2} (\varepsilon_{ct} - \varepsilon_{mt})$$

$$\text{Tensile strain of the composite } (\boldsymbol{\varepsilon_{ct}}) = \frac{2EA_{MF}^{SHR}}{(\sigma_{ct} + \sigma_{mt})} + \boldsymbol{\varepsilon_{mt}} \text{ ---------- (11)}$$

EA_{MF}^{SHR} is computed from the stress strain diagram (M30-MGFRC and M50-MGFRC) given in Fig. 5.6 to 5.15 and is given in column 11 Table 5.1 and 5.2. The reinforcing index (RI_{MF}) of each mix was calculated and is given in column 3 of Table 5.17 and 5.18. In order to understand the variation of EA_{MF}^{SHR} with RI_{MF}, points are plotted as shown in Fig.5.35 (a). An examination of the plot and various trails to arrive at the best fit, led to understand that EA_{MF}^{SHR} varies as power function of RI_{MF} in the form of $EA_{MF}^{SHR} = k / (RI_{MF})^n$. The power function is modified by multiplying both sides by RI_{MF}. The modified relation is $(RI_{MF})\ EA_{MF}^{SHR} = k\ (RI_{MF})^{(1-n)}$. Now points are plotted with RI_M as abscissa and $RI_{MF}.\ EA_{MF}^{SHR}$ as ordinate is shown in Fig.5.35 (b). The regression expression obtained is $(RI_{MF})\ EA_{MF}^{SHR} = 2.799\ (RI_{MF})^{1.9235}$ with regression coefficient $R^2 = 0.9675$. Then the relation between RI_{MF} and EA_{MF}^{SHR} can be expressed as.

$$EA_{MF}^{SHR} = (2.80\ .\ (RI_{MF})^{0.9235}) \text{ ---------- (12)}$$

Energy absorption of the strain hardening region (EA_{MF}^{SHR}) for M30-MGFRC and M50-MGFRC is calculated from equation (12) and reported in column 4 of Table 5.17 and 5.18.The strain (ε_{ct}) at ultimate tensile strength (σ_{ct}) of each M30-MGFRC and M50-MGFRC is calculated based on equation (11) and the values are reported in column 6 of Table.5.17 and 5.18 and these values are compared with the experimental tensile strain (ε_{ct}) values in column 7 of Table.5.17 and 5.18. The ratio of the calculated tensile strain of fiber composite to that of experimental tensile strain are also shown in column 8 of Table 5.17 and 5.18. It can be noted that the strain at composite strength (ε_{ct}) values obtained from equation (11) are close to the experimental tensile strain (ε_{ct}) values in both M30-MGFRC and M50-MGFRC.

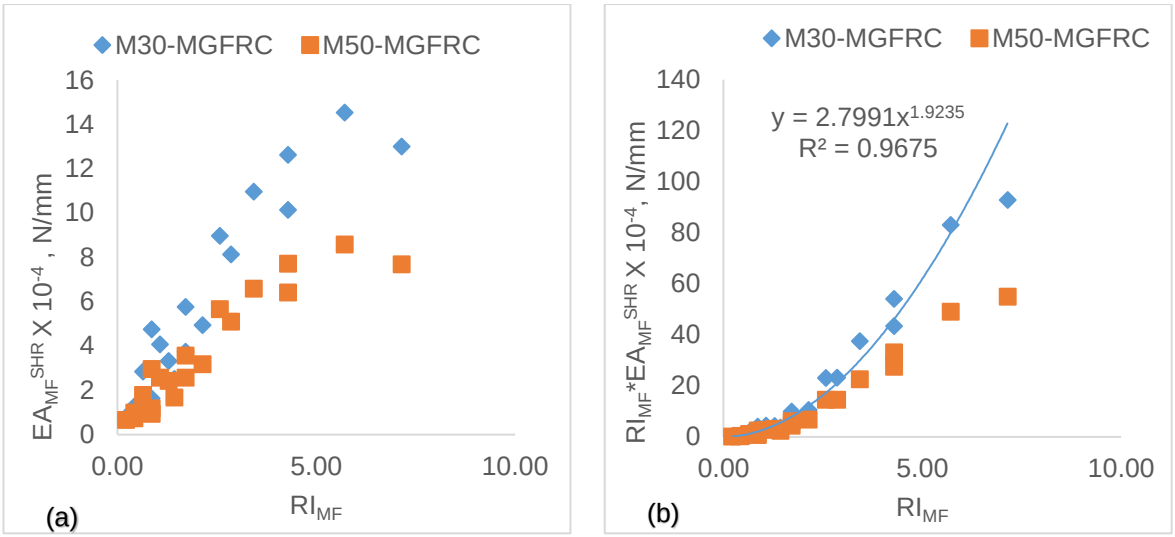

Fig. 5.35 Energy Absorption (EA_{MF}^{SHR}) Vs RI_{MF} for MGFRC

Table 5.17 Predicted tensile strain of M30-MGFRC

L_f (1)	V_f, % (2)	RI_{MF} (3)	EA_{MF}^{SHR} ($X10^{-4}$) N/mm (4)	$\sigma^{MF2}u$ ($X10^{-4}$) (5)	ε_{ct}		Ratio = (6)/(7) (8)
					Theoretical ($X10^{-4}$) (6)	Experimental ($X10^{-4}$) (7)	
3mm	0.1	0.21	0.84	3.88	1.22	1.15	1.07
	0.2	0.43	1.49	3.99	1.39	1.26	1.10
	0.3	0.64	2.08	4.09	1.54	1.50	1.03
	0.4	0.86	2.64	4.17	1.68	1.72	0.98
	0.5	1.07	3.18	4.24	1.81	2.07	0.87
6mm	0.1	0.43	1.49	3.85	1.40	1.20	1.16
	0.2	0.86	2.64	3.95	1.69	1.37	1.23
	0.3	1.29	3.70	4.03	1.96	1.75	1.12
	0.4	1.71	4.69	4.10	2.21	2.00	1.10
	0.5	2.14	5.65	4.16	2.44	2.42	1.01
12mm	0.1	0.86	2.64	3.84	1.70	1.33	1.28
	0.2	1.71	4.69	3.93	2.24	2.05	1.09
	0.3	2.57	6.57	4.00	2.71	2.49	1.09
	0.4	3.43	8.34	4.07	3.15	3.11	1.01
	0.5	4.29	10.04	4.12	3.57	3.75	0.95
20mm	0.1	1.43	4.03	3.83	2.08	1.71	1.21
	0.2	2.86	7.17	3.91	2.89	2.49	1.16
	0.3	4.29	10.04	3.98	3.61	3.18	1.14
	0.4	5.71	12.74	4.04	4.29	3.86	1.11
	0.5	7.14	15.34	4.10	4.92	4.53	1.09

ε_{ct} = Experimental tensile strain (ε^{Q}_{t}) of M30-MGFRC is given in column 6 of Table 5.1, σ_{mt} = 3.68, ε_{mt} = 1.18 X 10^{-4}, Ratio = Theoretical (ε_{ct}) / Experimental (ε_{ct}).

Table 5.18 Predicted tensile strain of M50-MGFRC

L_f (1)	V_f, % (2)	RI_{MF} (3)	EA_{MF}^{SHR} ($X10^{-4}$) N/mm (4)	$\sigma^{MF2}u$ ($X10^{-4}$) (5)	ε_{ct}		Ratio = (6)/(7) (8)
					Theoretical ($X10^{-4}$) (6)	Theoretical ($X10^{-4}$) (6)	
3mm	0.1	0.21	0.72	5.86	1.31	1.15	1.14
	0.2	0.43	1.37	5.99	1.42	1.26	1.13
	0.3	0.64	1.99	6.10	1.52	1.50	1.02
	0.4	0.86	2.60	6.19	1.62	1.72	0.95
	0.5	1.07	3.20	6.27	1.72	2.07	0.83
6mm	0.1	0.43	1.37	5.83	1.42	1.20	1.18
	0.2	0.86	2.60	5.94	1.63	1.37	1.19
	0.3	1.29	3.78	6.03	1.83	1.75	1.04
	0.4	1.71	4.94	6.11	2.02	2.00	1.01
	0.5	2.14	6.06	6.18	2.21	2.42	0.91
12mm	0.1	0.86	2.60	5.81	1.64	1.33	1.23
	0.2	1.71	4.94	5.91	2.04	2.05	0.99
	0.3	2.57	7.18	5.99	2.42	2.49	0.97
	0.4	3.43	9.36	6.06	2.78	3.11	0.89
	0.5	4.29	11.50	6.12	3.13	3.75	0.84
20mm	0.1	1.43	4.17	5.80	1.91	1.71	1.12
	0.2	2.86	7.91	5.89	2.55	2.49	1.03
	0.3	4.29	11.50	5.96	3.16	3.18	0.99
	0.4	5.71	15.00	6.02	3.75	3.86	0.97
	0.5	7.14	18.44	6.08	4.32	4.53	0.95

ε_{ct} = Experimental tensile strain (ε^{Q}_{t}) of M50-MGFRC is given in column 6 of Table 5.2, σ_{mt} = 5.63, ε_{mt} = 1.18 X 10^{-4}, Ratio = Theoretical (ε_{ct}) / Experimental (ε_{ct}).

5.10.4 Experimental Vs idealized Stress Strain diagram for MGFRC

The experimental tensile stress–strain curves of two concrete mixes, namely, M30-0.3%-3mm and M50-0.3%-20mm are plotted in Fig.5.36 (a) and (b). The predicted tensile stress–strain values are obtained from equation (10) and (11) for M30-0.3%-3mm and M50-0.3%-20mm and shown in Fig.5.36 (a) and (b). In the pre-crack region and post-crack region, the predicted curves shows a lower stiffness in both M30 and M50 grade of concrete. In the post-crack region, the strain at ultimate strength showed slightly higher values in case of M30 grade of concrete whereas in case of M50 grade of concrete strain at ultimate strength showed lower value. Proposed equations have

shown close correlation with experimental results of both M30 and M50 grade of concrete.

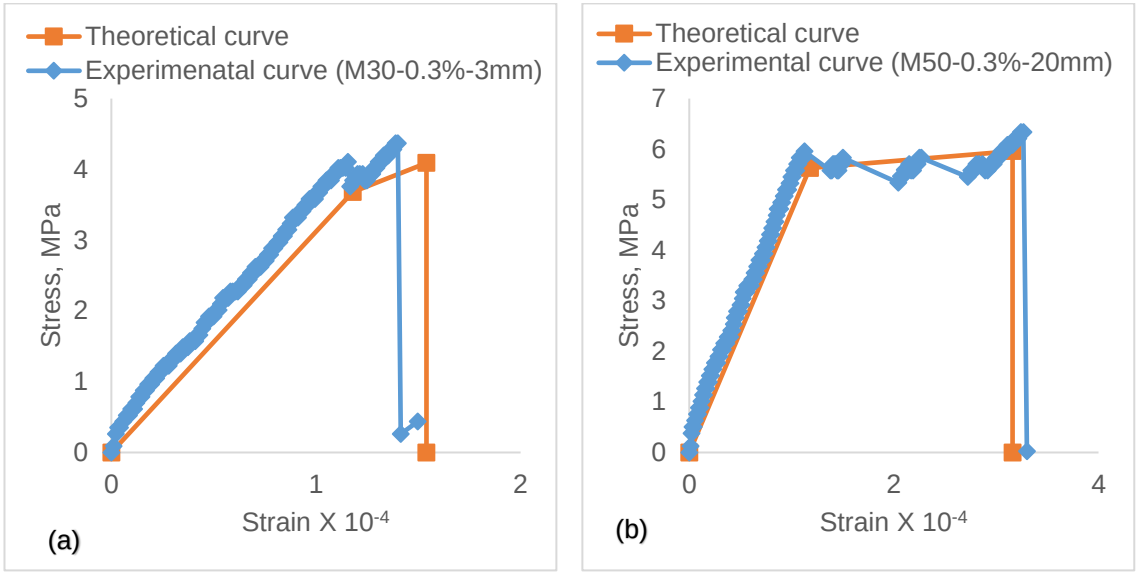

Fig.5.36. Experimental Vs idealized Stress Strain diagram for MGFRC

5.11 Compressive stress strain behaviour of MGFRC

Compressive Stress-Strain curves are drawn for each prism specimen and average curve of three specimens for each parameter is shown in Fig.5.37 to 5.46 for M30 and M50 grade of MGFRC. An observation of each stress-strain diagrams for compression shows that the stress-strain behaviour of plane concrete and GFRC specimens is similar and linear nearly up to 85% of peak stress, which means that stress-strain relation is not influenced by the presence of fiber in the elastic region and up to formation cracks under compression. Stress strain behaviour is nonlinear from cracking to ultimate and also beyond till failure. Irrespective of length of fiber peak stress increased for specimens with 0.3% volume fraction compared to specimens with all other volume fractions. Strain at peak stress and strain at failure increased with the increase in fiber content. It may be understood that the fiber action come in to play when dilation in concrete initiates, that is to say that fiber participate in delaying the crack formation and bridging of cracks, thus facilitating the concrete to undergo higher deformation than plain concrete in compression. For any given percentage volume of fibers, short length fibers of 3mm and 6mm contributed to increase in load carrying capacity compared to long length fibers of 12mm and 20mm. Similarly long length

fibers contributed to increase in deformation capacity compared to short length fibers. There is definite gradual and progressive improvement in deformation capacity with increase in length of fiber and volume of fibers.

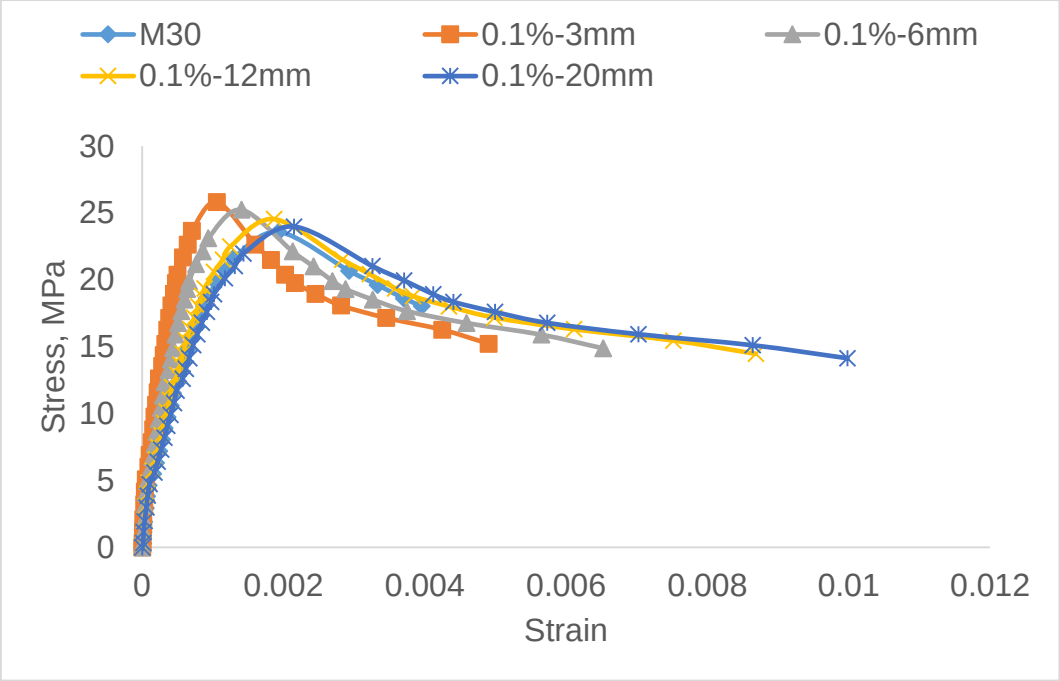

Fig.5.37 Compressive Stress-Strain behaviour of M30-MGFRC with V_f = 0.1%

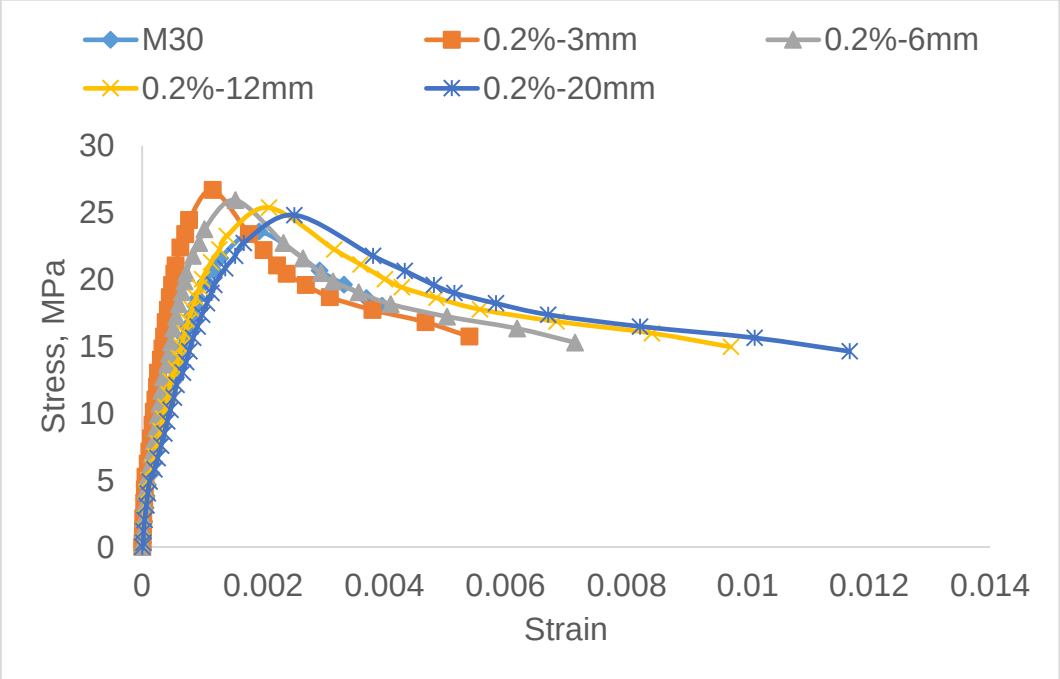

Fig.5.38 Compressive Stress-Strain behaviour of M30-MGFRC with V_f = 0.2%

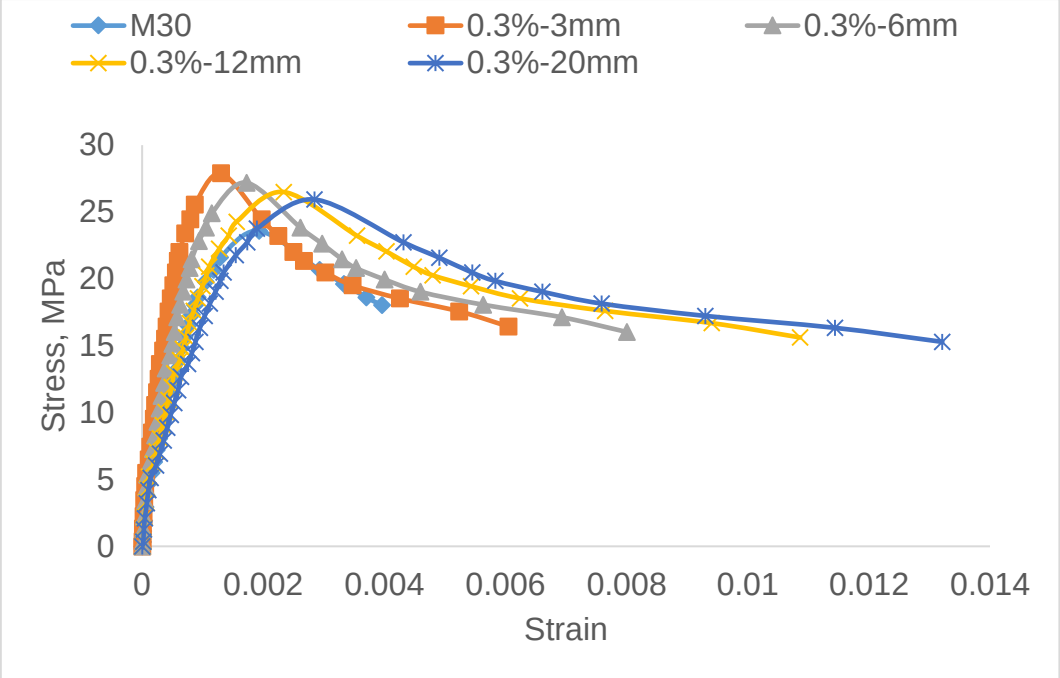

Fig.5.39 Compressive Stress-Strain behaviour of M30-MGFRC with V_f = 0.3%

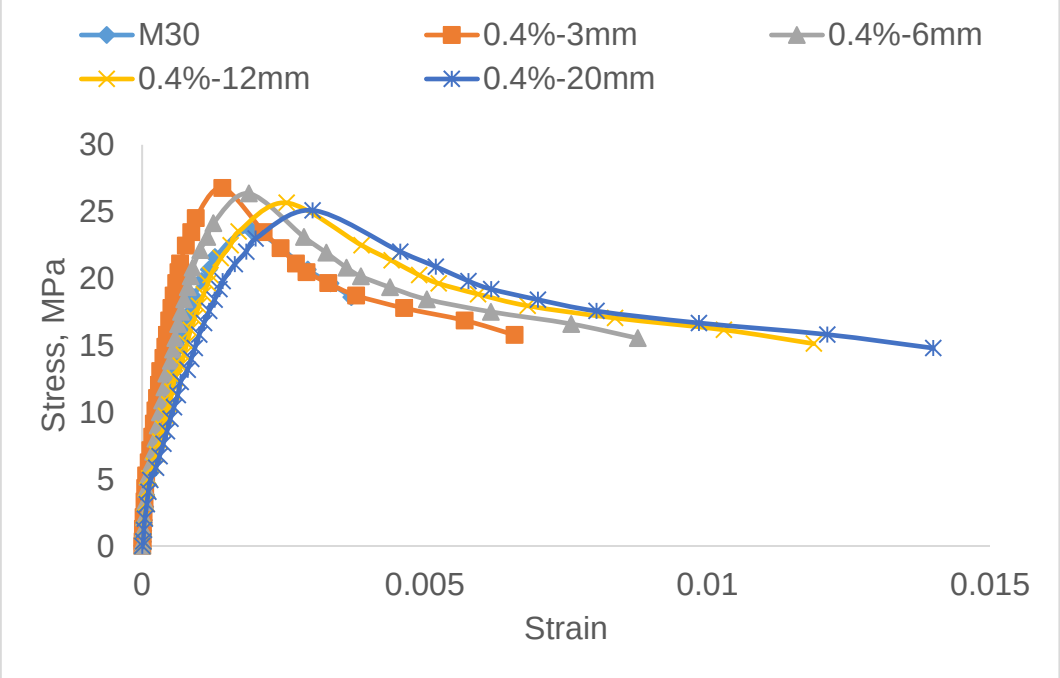

Fig.5.40 Compressive Stress-Strain behaviour of M30-MGFRC with V_f = 0.4%

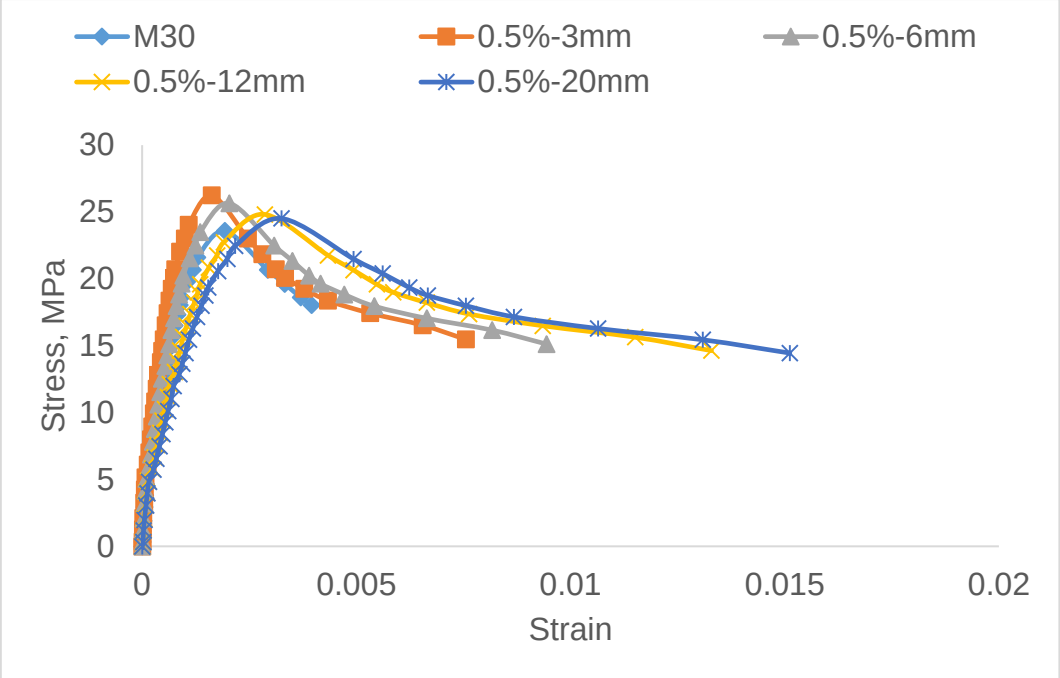

Fig.5.41 Compressive Stress-Strain behaviour of M30-MGFRC with V_f = 0.5%

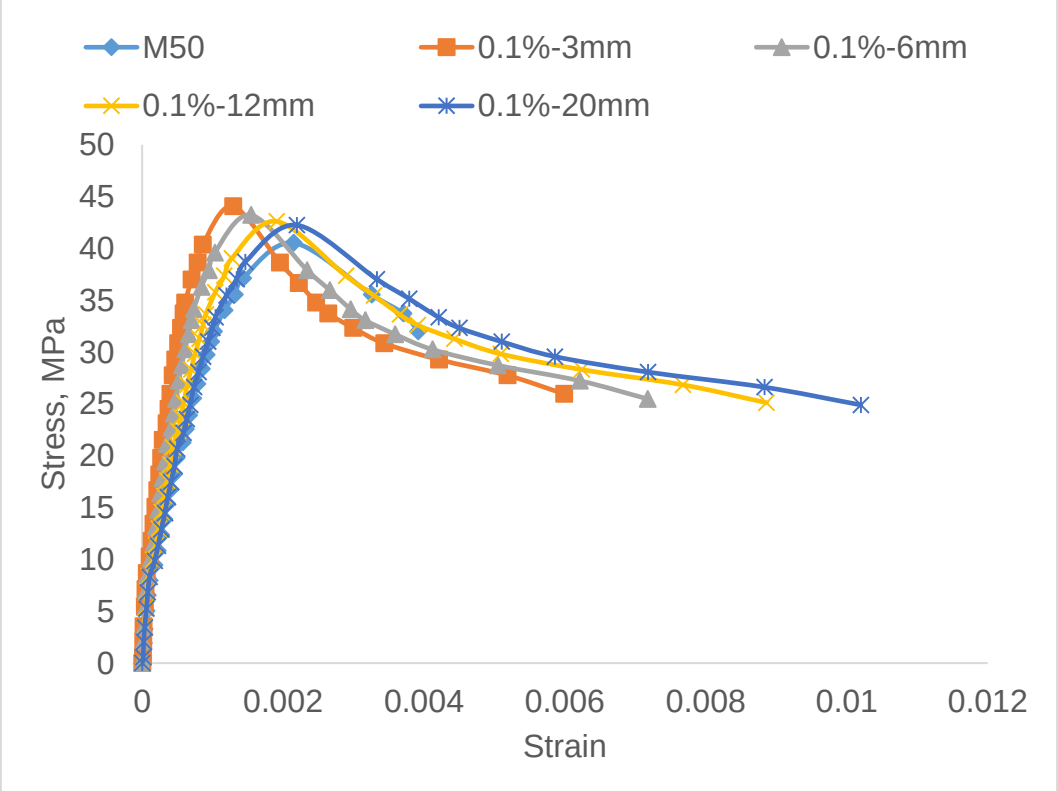

Fig.5.42 Compressive Stress-Strain behaviour of M50-MGFRC with V_f = 0.1%

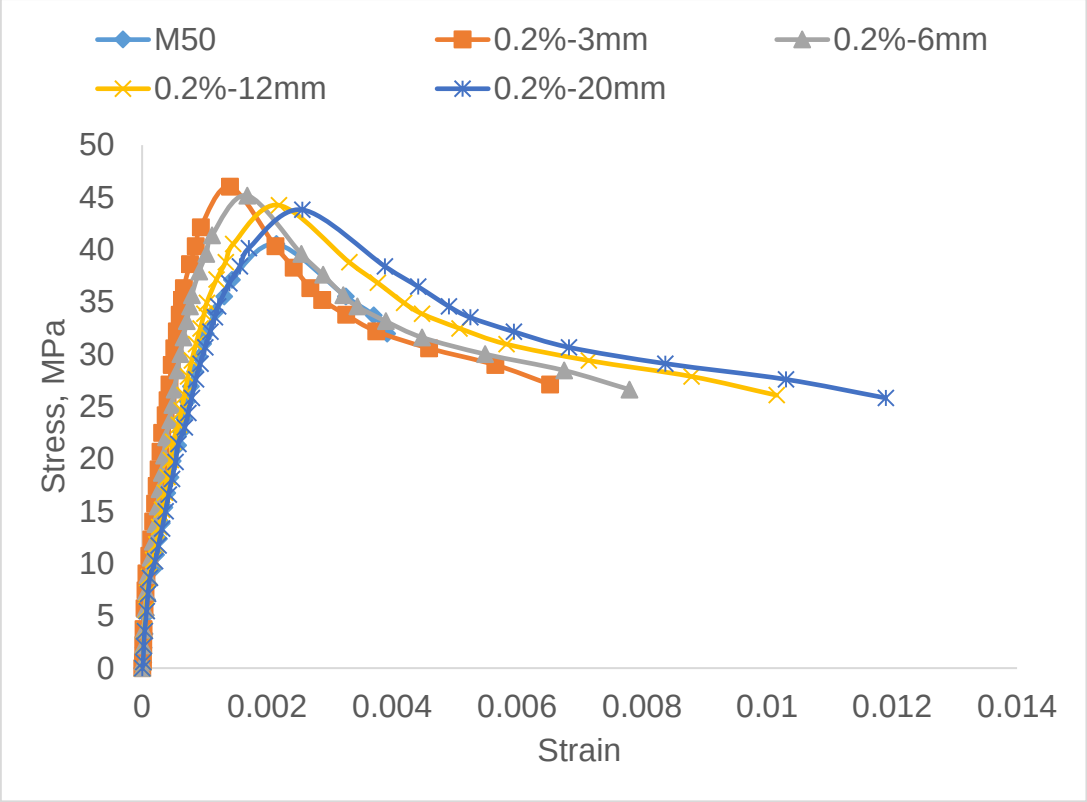

Fig.5.43 Compressive Stress-Strain behaviour of M50-MGFRC with V_f = 0.2%

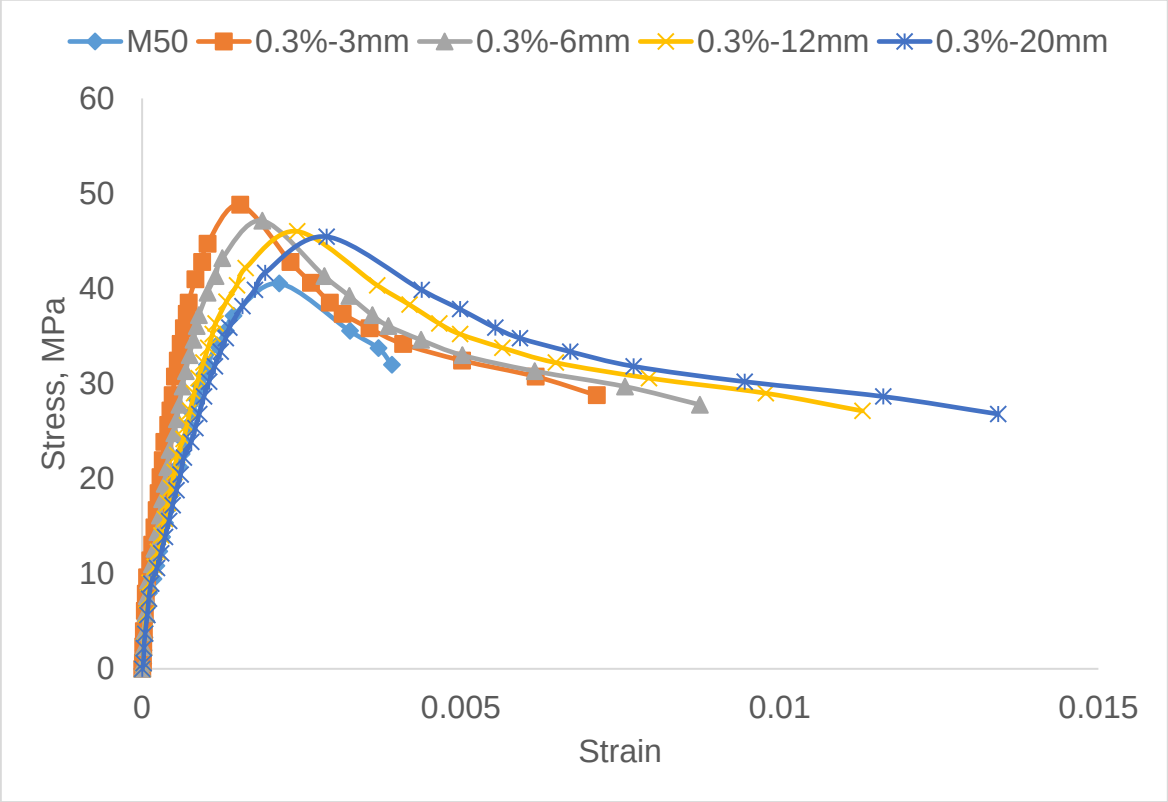

Fig.5.44 Compressive Stress-Strain behaviour of M50-MGFRC with V_f = 0.3%

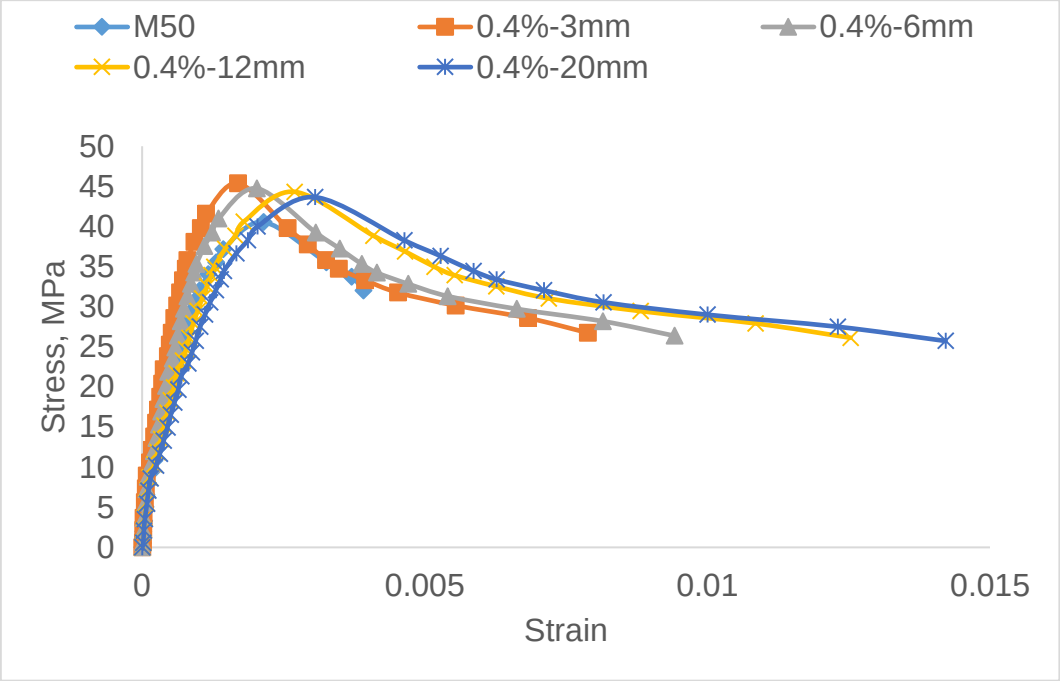

Fig.5.45 Compressive Stress-Strain behaviour of M50-MGFRC with V_f = 0.4%

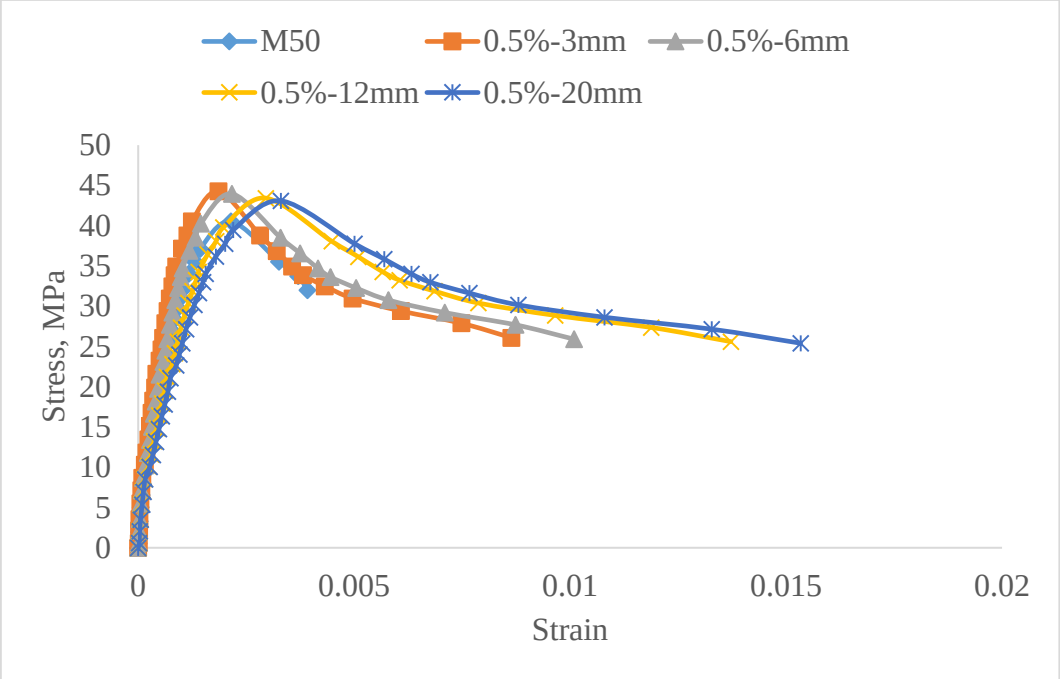

Fig.5.46 Compressive Stress-Strain behaviour of M50-MGFRC with V_f = 0.5%

5.12 Mechanical properties of MGFRC in Compression

The properties that characterize the stress strain behaviour of M30-MGRC and M50-MGFRC in uni-axial compression are peak stress, strain at peak stress, initial slope, strengthening factor, ductility factor, strain softening slope and energy absorption,. Values are taken from the stress strain diagram and are given in Table 5.19 and 5.20.

Typical stress-strain pattern for GFRC in compression is presented in Fig.5.47. Point A is the stress at the onset of cracking, Point B is peak stress, Point C is stress at inflection in strain softening, and Point D is breaking stress. It may be noticed that there is a gradual drop in stress after reaching peak stress to the point C and then the specimens have undergone deformation beyond the point C and up to point D. This shows GFRC specimens exhibit improvement in post peak deformation up to point C by stabilization during transition from A to B and B to C in the region of ABC of stress strain regime of GFRC concrete. Specimen with 0.4% and 0.5% have under gone considerable deformation from point C up to D. Post peak stress strain behaviour of GFRC is concave.

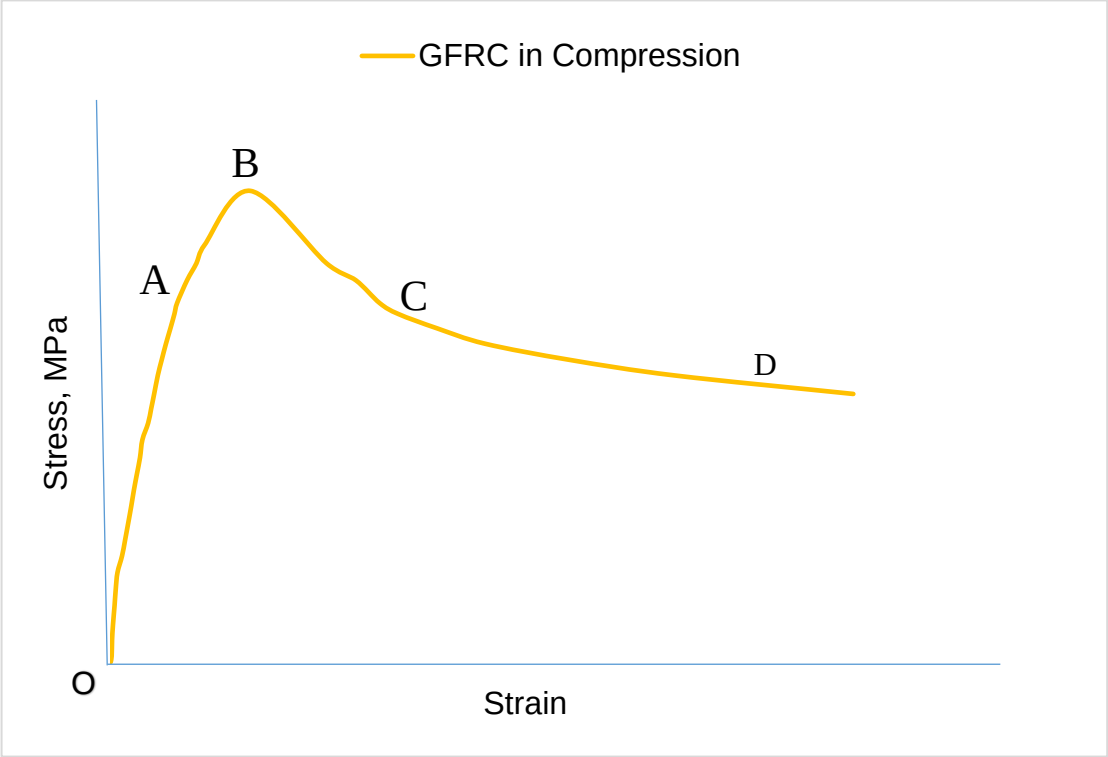

Fig.5.47 Salient features of GFRC Specimen in Compression

Based on the above observation, the stress strain curves are analysed to obtain the initial slope (ratio of stress and strain at point A), strengthening factor (ratio of peak stress (f^{B}_{u}) to the plain concrete peak stress (f_0)), ductility factor (ratio of strain at inflection (ε^{C}_{ip}) to the strain at peak stress (ε^{B}_{u})), strain softening slope (ratio of change in stress (f^{B}_{u}- f^{C}_{IP}) to the change in strain (ε^{C}_{IP} - ε^{B}_{u}) in the strain softening region) and energy absorption capacity (area under stress strain curve) in strain softening region of the composite. The corresponding stress strain values are reported in Table 5.19 and 5.20.

Initial slope ($E^{c}i$), Strengthening factor (STF^{c}), ductility factor (DF^{c}), strain softening slope (E_{ss}) and energy absorption capacity (EA_{SSR}) for different volume fractions i.e., 0.1%, 0.2%, 0.3%, 0.4% and 0.5% with various fiber lengths 3mm, 6mm, 12mm and 20mm are computed for M30-MGFRC and M50-MGFRC and values are reported in column 7, 8, 9, 10 and 11 of Table 5.19 and 5.20 respectively. The variation of these properties with different fiber lengths and fiber volume fractions are shown in Fig.5.48 to 5.52.

The initial slope ($E^{c}i$) for each specimen is plotted as a function of volume fraction shown in Fig.5.48. As the volume of fiber and length of fiber increased the initial slope decreased, similar behaviour was reported by the some of the researchers (Rossi P et al. 1990 and R. D. Neves et, al. 2005). The slump of concrete also decreases with increase in volume of fibers and length of fibers effecting flowability of MGFRC. Hence, the phenomena of decrease in initial slope in MGFRC with the addition of fibers may be viewed as insertion of a flaw or disturbance in the uniform matrix (R. D. Neves et al. 2000). At this point the dilation of the concrete initiates even before the desired strength and it led to decrease in stiffness of the composite gradually. Hence, as the length of fiber and volume of the fiber increased the initial stiffness decreased.

The variation of strengthening factor with respect to volume fraction and length of fiber is shown in Fig.5.49. For any given volume fraction, as the length of the fiber increased from 3mm to 20mm the strengthening factor decreased. Short length fibers (3mm and 6mm) fibers showed higher strengthening factor compared to long length fibers (12mm and 20mm). The fibers provided in the concrete can work at both micro and macro level. The primary purpose of the different fiber lengths in the composite is to resist the propagation of cracks at different levels. In a given volume, shorter the length of fiber, number of fiber will be more and closer will be the spacing of fibers and also

possibly will be near to the micro cracks. Short length fibers may initially contribute to delay the formation of cracks but may be pulled out after micro cracks transformed into macro cracks (N. Banthia 1995 and L.R Betterman 1995). Short length fibers (3mm and 6mm) in concrete helped to resist the opening of marco cracks by arresting the micro cracks and enhancing the peak stress compared to long length fibers (12mm and 20mm) and it led to a higher strengthening factor. Irrespective of length of the fiber, 0.3% volume fraction showed the maximum improvement in strengthening factor compared to all other volume fractions. Fiber dispersion influence the strength of the composites by its role in transferring the load to the other parts of the composite. An effective crack bridging and increase in the strength of the composite can be achieved if the fiber dispersion is better at the first crack location. Fiber dispersion and orientation are found to be higher for the specimens with 0.3% volume of fiber compared to specimens with other volume fractions. Further the balling of fibers is noticed the specimens with higher volume fractions. Thus the specimens with lower volume fractions i,e., 0.1% and 0.2% have not enough fibers to improve peak stress and though there is high volume of fibers for specimens with 0.4% and 0.5%, balling effect and reduction of slump have not contributed to improve peak stress.

The variation of ductility factor for each specimen is plotted as a function of volume fraction as shown in Fig.5.50. For any given volume fraction, as the length of fiber increased from 3mm to 20mm length of fiber ductility factor increased. Ductility factor increased with increase in volume fraction. Long length fibers (12mm and 20mm) fibers showed higher ductility factor compared to short length fibers (3mm and 6mm). Once the micro cracks turns into macro cracks, long length fibers comes in to action to bridge the macro cracks and it restrains the lateral deformation developed in the composite. The resistance against lateral deformation increases with increase in volume fractions. Thus long length fibers provided more ductility compared to the short length fibers. Further examination of Fig.5.50 shows that short length fibers namely, 3mm and 6mm have almost the same ductility. Ductility factor for all volume fraction and long length fibers namely 12mm and 20mm have higher ductility factor and increased with increase in length of fiber and volume of fiber. Thus, it clearly shows that the long length fibers and higher volume fraction contributed to improvement in deformation.

The variation of strain softening slope with reference to volume fraction and length of fiber is shown in Fig.5.51. Strain softening slope is ratio of change of stress to change of strain in the strain softening region. It is noticed that change of stress is more for short length fibers (3mm and 6mm) and change of strain is more for long length fibers (12mm and 20mm). This means that the strain softening is more for higher fiber content and length of fiber. For any given volume fraction, as the length of fiber increased from 3mm to 20mm strain softening increased. Strain softening slope becomes flat with increase in volume fraction and lengh of fiber. Hence, lower strain softening slope shows the higher post peak deformations whereas higher strain softening slope shows the lower post peak deformations.

Energy absorption is computed by tacking area under stress-strain diagram within strain softening region i.e., B to C and variation is shown in Fig.5.52. As the volume of fiber and length of fiber increased energy absorption capacity increased. At a micro level short length fibres (3mm and 6mm) arrest the formation of micro cracks, leading to higher peak strength rather than energy absorption capacity, whereas at a macro level long length fibres (12mm and 20mm) controls the propagation of macro cracks thus it leads to increasing the energy absorption capacity of the composite rather than strength of the composite. The availability of the fibers increased with increase in volume fraction, lead to form the dense mix and it helped to transfer the loads to the other locations of the composite. Thus the energy absorption of the composite increases.

Finally, It can be noted that the strength enhancement for short length fibers (3mm and 6mm) varied from 1·09 to 1.20 and for long length fibers (12mm and 20mm) 1.04 to 1.12. This shows that there is a significant improvement in strength for specimens with short length fibers when compared to the specimens with long length fibers. Significant enhancement in ductility occurred in the case of the long length fibers (12mm and 20mm) i.e., 1.82 to 3.27 compared to short length fibers (3mm and 6mm) i.e., 1.73 to 2.36. Hence the short fibers are more effective in improving the peak strength by arresting the formation of micro cracks and long fibers are more effective in increasing the deformations by bridging the macro cracks.

In all, long length fibers (12mm and 20mm) exhibited higher ductility factor, energy absorption capacity than that of short length fibers (3mm and 6mm). Short length fibers showed higher strengthening and initial slope compared to the long length fibers. Hence, the short length fibers contributed to improve the peak stress of the composite

where as long length fibers contributed to improve the post peak deformations of the composite.

Table 5.19 Summary of test results for M30-MGFRC in compression

SD (1)	V_f (%) (2)	Strain Softening Region				E^{c}_{i} ($X10^4$) MPa (7)	STF^c (8)	DF^c (9)	E_{ss} ($X10^4$) MPa (10)	EA_{SSR} ($X10^{-2}$) N/mm (11)
		f^{B}_{u} (MPa) (3)	ε^{B}_{u} ($X10^{-4}$) (4)	f^{C}_{IP} (MPa) (5)	ε^{C}_{IP} ($X10^{-4}$) (6)					
MF0	0.00	23.58	19.31	21.22	23.18	1.05	1.00	1.20	0.59	0.030
Peak Stress of plain concrete f_0 = 23.58 MPa										
MF3-a	0.1 (a)	25.83	10.56	20.51	19.31	2.00	1.10	1.73	0.76	0.031
MF6-a		25.24	14.05	19.81	26.85	1.53	1.07	1.77	0.49	0.033
MF12-a		24.54	18.70	19.57	33.99	1.10	1.04	1.82	0.33	0.042
MF20-a		23.99	21.49	19.34	39.21	0.97	1.02	1.87	0.24	0.047
MF3-b	0.2 (b)	26.69	11.63	20.04	23.49	1.89	1.13	2.02	0.60	0.035
MF6-b		25.94	15.39	19.81	31.48	1.47	1.10	2.05	0.38	0.045
MF12-b		25.38	20.93	19.34	46.88	1.03	1.08	2.19	0.24	0.060
MF20-b		24.82	25.15	19.10	58.57	0.84	1.05	2.29	0.17	0.070
MF3-c	0.3 (c)	27.89	13.02	20.23	28.03	1.82	1.18	2.15	0.51	0.050
MF6-c		27.19	17.23	19.85	38.98	1.36	1.15	2.19	0.35	0.064
MF12-c		26.50	23.39	19.08	58.33	0.98	1.12	2.49	0.21	0.085
MF20-c		25.94	28.44	18.06	79.90	0.79	1.10	2.80	0.15	0.101
MF3-d	0.4 (d)	26.77	14.18	20.10	31.03	1.63	1.14	2.19	0.39	0.043
MF6-d		26.36	18.88	19.59	42.30	1.18	1.12	2.24	0.29	0.068
MF12-d		25.66	25.59	18.57	65.74	0.84	1.09	2.56	0.18	0.090
MF20-d		25.10	30.13	17.21	90.00	0.71	1.06	3.00	0.13	0.135
MF3-e	0.5 (e)	26.24	16.28	19.98	36.41	1.39	1.11	2.24	0.31	0.048
MF6-e		25.66	20.32	19.34	47.84	1.09	1.09	2.33	0.23	0.072
MF12-e		24.82	28.61	18.06	76.44	0.73	1.05	2.66	0.14	0.097
MF20-e		24.52	32.55	17.18	10.17	0.63	1.04	3.10	0.11	0.142

Note: f^{B}_{u} = Peak Stress at B, ε^{B}_{u} = Peak Strain at B, f^{C}_{IP} = Stress at inflection C, ε^{C}_{IP} = Strain at inflection C, Initial slope (E^{c}_{i}) = f^{A} / ε^{A}, Strengthening Factor (STF^c) = f^{B}_{u} / f_0 Ductility factor (DF) = $\varepsilon^{C}_{IP} / \varepsilon^{B}_{u}$, strain softening slope (E_{ss}) = $(f^{B}_{u} - f^{C}_{IP}) / (\varepsilon^{C}_{IP} - \varepsilon^{B}_{u})$, Energy Absorption capacity (EA_{SSR}) = Area under the stress strain curve in Strain Softening Region, SD = Specimen Designation

Table 5.20 Summary of test results for M50-MGFRC in compression

SD (1)	V_f (%) (2)	Strain Softening Region				E^c_i ($X10^4$) MPa (7)	STF^c (8)	DF^c (9)	E_{ss} ($X10^4$) MPa (10)	EA_{SSR} ($X10^{-2}$) N/mm (11)
		f^B_u (MPa) (3)	ε^B_u ($X10^{-4}$) (3)	f^C_{IP} (MPa) (4)	ε^C_{IP} ($X10^{-4}$) (5)					
MF0	0.00	40.53	21.48	37.41	32.57	1.64	1.00	1.52	0.26	0.058
Peak stress of plain concrete f_0 = 40.53 MPa										
MF3-a	0.1 (a)	44.07	12.89	35.26	23.71	2.88	1.09	1.84	0.80	0.059
MF6-a		43.23	15.44	34.05	28.96	2.45	1.07	1.88	0.66	0.062
MF12-a		42.62	19.07	33.64	37.17	1.91	1.05	1.95	0.50	0.075
MF20-a		42.25	21.96	33.23	44.11	1.63	1.04	2.01	0.41	0.085
MF3-b	0.2 (b)	46.02	14.05	34.45	28.79	2.79	1.14	2.05	0.77	0.073
MF6-b		45.18	16.79	34.05	37.26	2.26	1.11	2.22	0.56	0.085
MF12-b		44.26	21.86	33.23	47.69	1.71	1.09	2.18	0.42	0.109
MF20-b		43.82	25.61	32.83	58.71	1.43	1.08	2.29	0.33	0.126
MF3-c	0.3 (c)	48.81	15.35	34.78	33.82	2.77	1.20	2.20	0.74	0.103
MF6-c		47.13	18.83	34.12	43.58	2.11	1.16	2.31	0.52	0.122
MF12-c		46.02	24.32	32.80	61.02	1.63	1.14	2.51	0.36	0.154
MF20-c		45.46	28.91	31.04	77.12	1.33	1.12	2.67	0.30	0.180
MF3-d	0.4 (d)	45.38	16.97	34.56	39.72	2.27	1.12	2.34	0.47	0.087
MF6-d		44.74	20.27	33.68	49.19	1.90	1.10	2.43	0.38	0.125
MF12-d		44.32	26.98	31.92	73.05	1.40	1.09	2.71	0.27	0.164
MF20-d		43.65	30.60	29.58	92.50	1.20	1.08	3.02	0.23	0.238
MF3-e	0.5 (e)	44.26	18.60	34.34	43.97	1.98	1.09	2.36	0.40	0.093
MF6-e		43.95	21.72	33.24	54.61	1.70	1.08	2.51	0.32	0.131
MF12-e		43.42	29.54	31.04	85.97	1.23	1.07	2.91	0.22	0.176
MF20-e		43.09	33.02	30.28	107.84	1.11	1.06	3.27	0.17	0.254

Note: f^B_u = Peak Stress at B, ε^B_u = Peak Strain at B, f^C_{IP} = Stress at inflection C, ε^C_{IP} = Strain at inflection C, Initial slope (E^c_i) = f^A / ε^A, Strengthening Factor (STF^c) = f^B_u / f_0, Ductility factor (DF) = $\varepsilon^C_{IP} / \varepsilon^B_u$, strain softening slope (E_{ss}) = $(f^B_u - f^C_{IP}) / (\varepsilon^C_{IP} - \varepsilon^B_u)$, Energy Absorption capacity (EA_{SSR}) = Area under the stress strain curve in Strain Softening Region, SD = Specimen Designation.

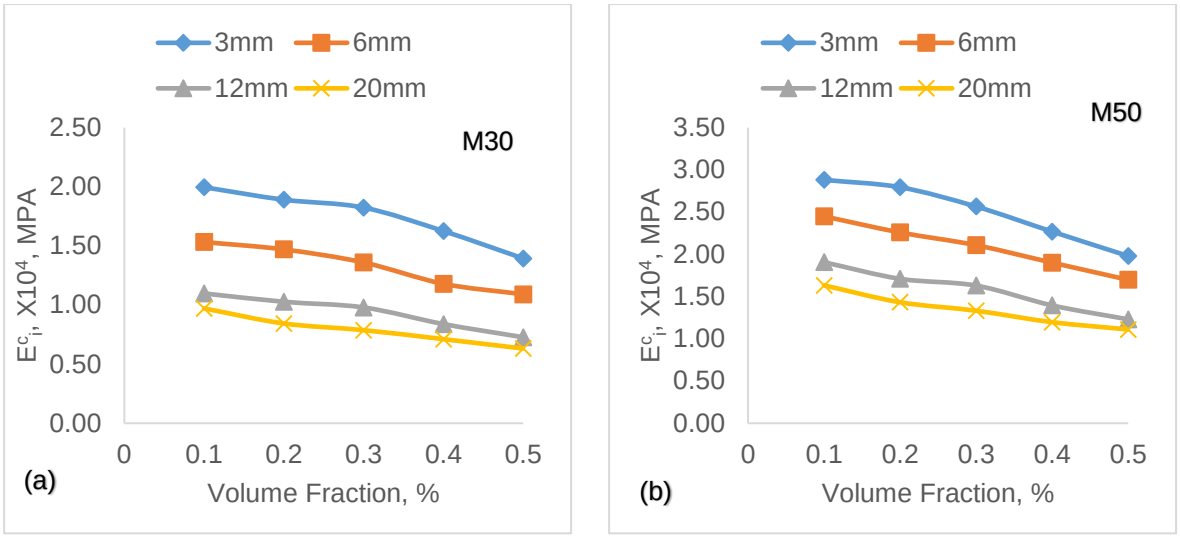

Fig.5.48 Initial slope (E^c_i) as a function of volume fraction in compression

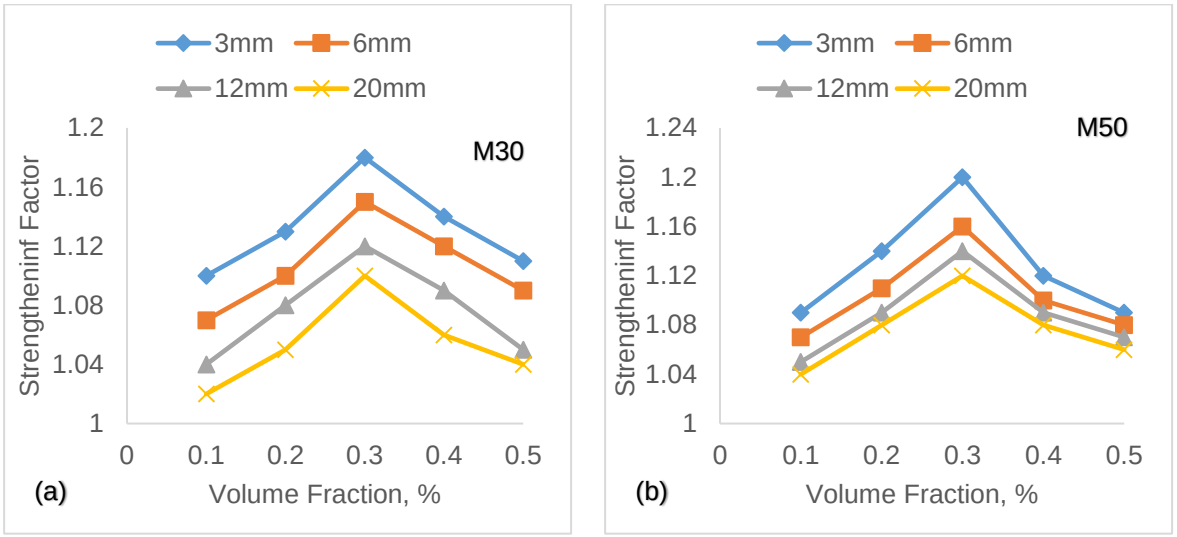

Fig.5.49 Strengthening Factor as a function of volume fraction in compression

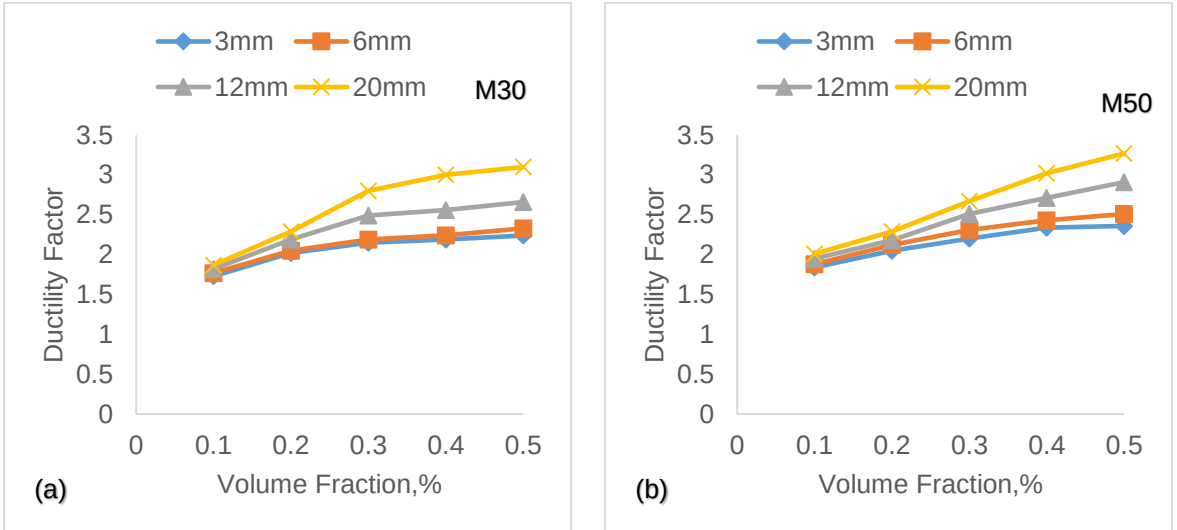

Fig.5.50 Ductility Factor as a function of volume fraction in compression

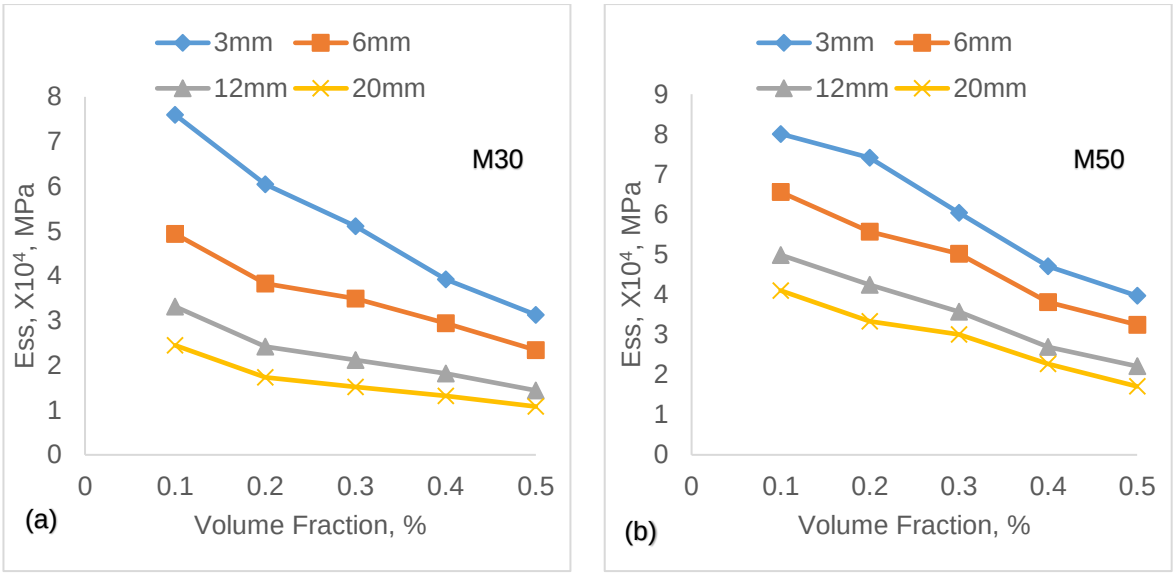

Fig.5.51 Strain softening slope (E_{ss}) as a function of volume fraction in compression

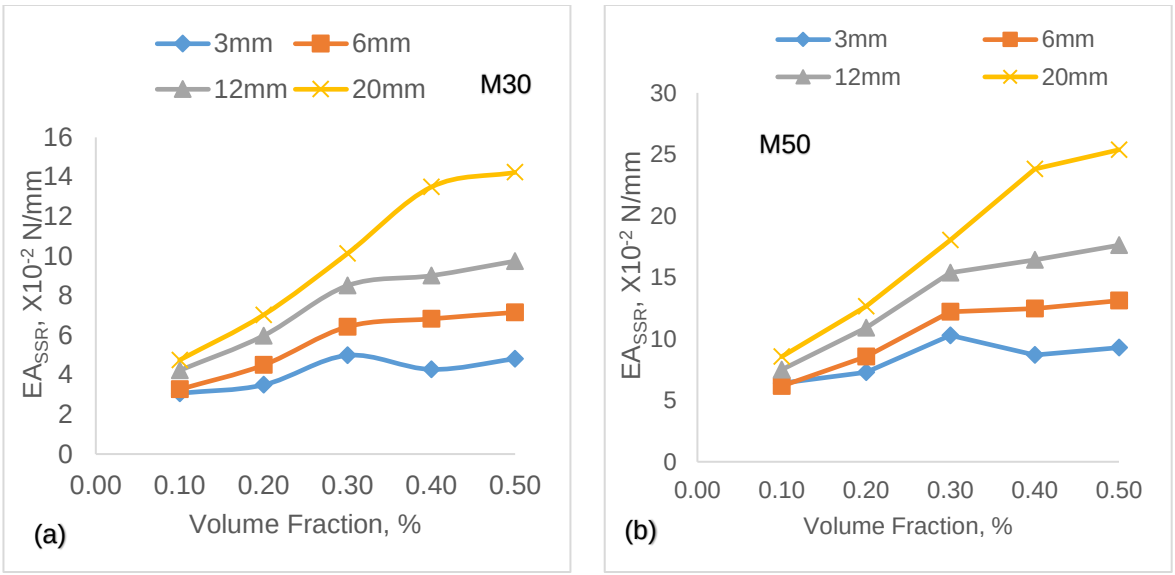

Fig.5.52 Energy absorption in strain softening region (E_{SSR}) as a function of volume fraction in compression.

5.13 Analytical Behaviour for MGFRC in Compression

A typical stress–strain curve of GFRC in compression (Fig.5.47) is redrawn and shown in Figure 5.53 marking salient points. Generally, cracking of concrete begins at around 85% of peak stress and at this point, dilation of concrete initiates. The rate of lateral deformation is very low before the stress reaches the peak point. After reaching the peak point the rate of lateral deformations increase rapidly. Post peak stress strain

behaviour of GFRC is concave. The point at which the curvature changes in the post peak region is the inflection point C. Beyond inflection point, the specimen continue to undergo deformation without much increase in stress till failure. Addition of fibers effect the stress and strain both at peak and inflection points. In this diagram, important points which influence the stress strain behaviour are B and C. In order to predict the stress strain behaviour of MGFRC, the points B (f_u, ε_u) and C (f_{IP}, ε_{IP}) are needed to be determined. The equations have been developed in this investigation for normalised stress strain curves.

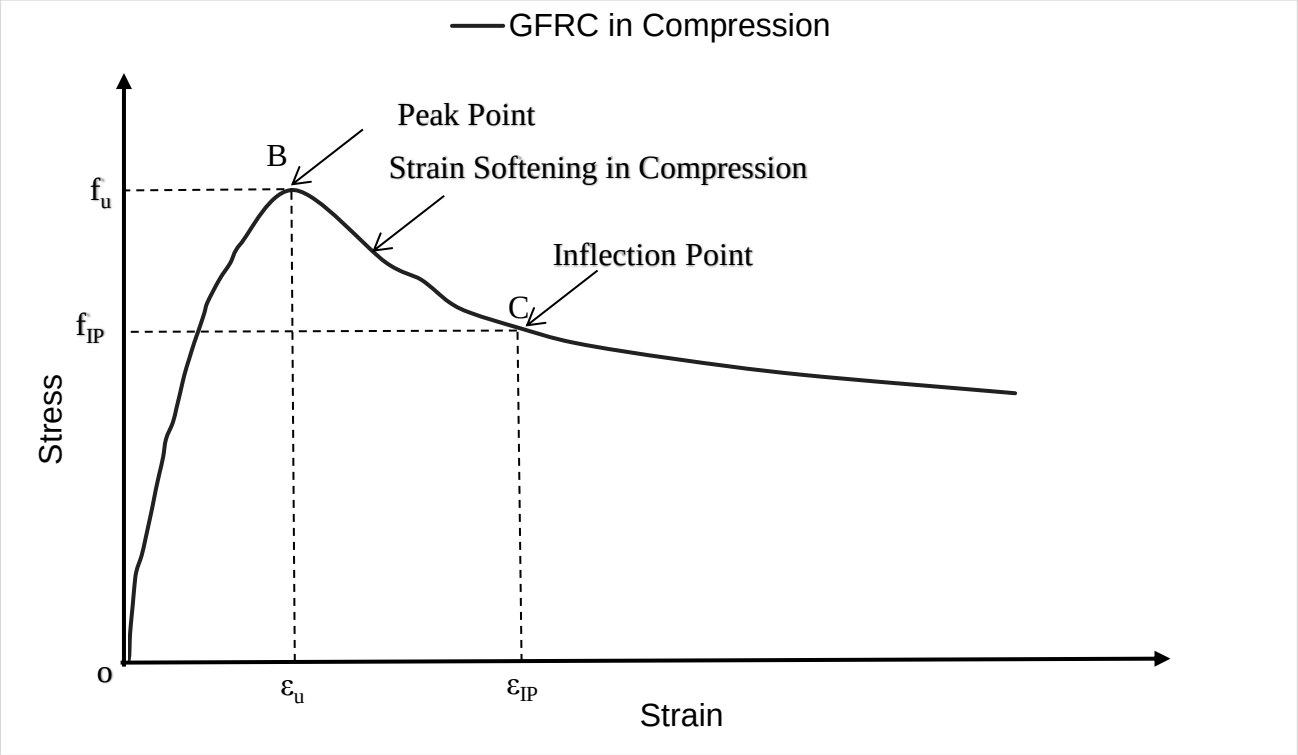

Fig.5.53 Analytical Stress Strain curve of GFRC

All empirical equations available in the literature have been reviewed and the expression (equation (13)) proposed by Carreira and Chu (1985) for uniaxial compression of plain concrete was used by most of the researchers (Ezeldin et al 1992; M.C Natraja et al, 1999; Ou et al. 2012; Aref Abadel et al, 2016) as a basis to obtain an equation for normal strength fiber reinforced concrete. The equation (13) is adopted in the present investigation to propose analytical stress strain diagram.

$$\frac{f_c}{f_u} = \frac{\beta(\varepsilon_c/\varepsilon_u)}{\beta - 1 + (\varepsilon_c/\varepsilon_u)^{\beta}} \quad \text{---------- (13)}$$

Where f_u is the peak strength of fiber reinforced concrete and ε_u is the corresponding peak strain. f_c and ε_c are the stress and strain values on the curve and β is the material parameter that depends on the shape of the stress strain diagram.

In Table 5.19 and 5.20 the strengthening factor and ductility factor for MGFRC specimens are given. An examination of this results showed improvement in strength and also strain with increase in length and volume of fibers. Thus the amount of fiber has direct influence on strength and strain of MGFRC specimens. It is known that length of fiber, diameter of fiber and volume of fiber can be combined into a single non dimensional parameter called as reinforcing index (RI_{MF}), where $RI_{MF} = V_f(L_f/D_f)$. RI_{MF} takes into account the fiber participation in the composite. It is also known that the properties of matrix has direct influence on strength and strain of composite. Thus the peak strength of the composite (f_u) and peak strain of the composite are directly proportional to that of plain concrete and also directly proportional to RI_{MF}. However, the influence of RI_{MF} is linear or nonlinear has to be established from the experimental results. Hence, it can be written that

- $f_u \propto f_0$

  $\propto (RI_{MF})^n$

  Then $f_u = k\, f_0\, (RI_{MF})^n$

  The above expression is rewritten as

- $(f_u / f_0) = k\, (RI_{MF})^n$

Similarly, it can be written for strain as

- $(\varepsilon_u/\varepsilon_0) = k\, (RI_{MF})^n$

The above expression can be used to predict f_u, ε_u for a given value of RI_{MF} i.e., for a set of fiber properties and grade of concrete. In order to construct stress strain diagram as indicated Fig.5.53 the material property defined by β (equation (13)) is the only one now required to be determined. In order to arrive at β for a composite having matrix strength of f_0 and fiber properties (RI_{MF}) the equation (13) is considered in the form

$$\frac{f_u}{f_0} = \frac{\beta(\varepsilon_u/\varepsilon_0)}{\beta-1+(\varepsilon_u/\varepsilon_0)^{\beta}} \text{ ---------- (14)}$$

In the above expression $f_u, f_0, \varepsilon_u, \varepsilon_0$ for each specimen is known and if these values are substituted β can be arrived at for a set of fiber properties indicated by RI_{MF}. Thus for each RI_{MF} the material property β can be evaluated. The variation of β with RI_{MF} can be modelled. Thus in the equation (14) f_u, ε_u and β can be estimated for a grade of concrete and for a set of fiber properties. Hence, the stress strain diagram of the MGFRC can be generated. The limitation for the above equation is that the drooping portion (post peak behaviour) is continuous right up to the stress level becomes zero, which is unrealistic. Hence the post peak behaviour is limited to the point of inflection i.e., point C in the Fig.5.53. In order to identify the point C, the variation of f_{IP} from the experimental data can be noted proposed which intern will be helpful to find the ε_{IP} values for a given f_{IP} from the equation (14). Thus the salient points of stress strain diagram of GFRC given in Fig.5.53 can be estimated theoretically. In the subsequent articles the method of arriving at models for f_u, f_0, ε_u f_{IP} and β are explained.

Table 5.21 Stress ratios, strain ratios and energy absorption of M30-MGFRC

Specimen Designation (1)	RI_{MF} (2)	Strain Softening Region					β (8)
		f_u/f_0 (3)	$\varepsilon_u/\varepsilon_0$ (4)	f_{IP}/f_o (5)	$\varepsilon_{IP}/\varepsilon_o$ (6)	EA_{SSR} / EA^o_{SSR} (7)	
MF0-0	0	1.00	1.00	0.86	1.20	1	-
MF3-a	0.21	1.10	0.55	0.79	1.73	1.02	2.04
MF3-b	0.43	1.13	0.60	0.75	2.02	1.16	2.01
MF3-c	0.64	1.18	0.67	0.73	2.15	1.65	1.98
MF3-d	0.86	1.14	0.73	0.75	2.19	1.42	1.96
MF3-e	1.07	1.11	0.84	0.76	2.24	1.59	1.91
MF6-a	0.43	1.07	0.73	0.78	1.77	1.08	1.99
MF6-b	0.86	1.10	0.80	0.76	2.05	1.49	1.97
MF6-c	1.29	1.15	0.89	0.73	2.19	2.13	1.95
MF6-d	1.71	1.12	0.98	0.74	2.24	2.26	1.92
MF6-e	2.14	1.09	1.05	0.75	2.33	2.37	1.87
MF12-a	0.86	1.04	0.97	0.80	1.82	1.40	1.94
MF12-b	1.71	1.08	1.08	0.76	2.19	1.98	1.92
MF12-c	2.57	1.12	1.21	0.72	2.49	2.82	1.90

MF12-d	3.43	1.09	1.32	0.72	2.56	2.99	1.87
MF12-e	4.29	1.05	1.48	0.73	2.66	3.23	1.82
MF20-a	1.43	1.02	1.11	0.81	1.87	1.57	1.89
MF20-b	2.86	1.05	1.30	0.77	2.29	2.33	1.87
MF20-c	4.29	1.10	1.47	0.70	2.80	3.36	1.85
MF20-d	5.71	1.06	1.56	0.69	3.00	4.47	1.80
MF20-e	7.14	1.04	1.69	0.70	3.10	4.72	1.77

Table 5.22 Stress ratios, strain ratios and energy absorption of M50-MGFRC

Specimen Designation (1)	RI_{MF} (2)	Strain Softening Region					β (8)
		f_u/f_0 (3)	$\varepsilon_u/\varepsilon_0$ (4)	f_{IP}/f_o (5)	$\varepsilon_{IP}/\varepsilon_o$ (6)	EA_{SSR}/EA^o_{SSR} (7)	
MF0-0	0	1.00	1.00	0.84	1.09	1.00	-
MF3-a	0.21	1.09	0.60	0.87	1.10	1.03	2.06
MF3-b	0.43	1.14	0.65	0.85	1.34	1.26	2.01
MF3-c	0.64	1.20	0.71	0.86	1.57	1.78	1.97
MF3-d	0.86	1.12	0.79	0.85	1.85	1.50	1.95
MF3-e	1.07	1.09	0.87	0.85	2.05	1.61	1.94
MF6-a	0.43	1.07	0.72	0.84	1.35	1.12	2.01
MF6-b	0.86	1.11	0.78	0.84	1.73	1.48	1.95
MF6-c	1.29	1.16	0.88	0.84	2.03	2.11	1.92
MF6-d	1.71	1.10	0.94	0.83	2.29	2.16	1.90
MF6-e	2.14	1.08	1.01	0.82	2.54	2.27	1.88
MF12-a	0.86	1.05	0.89	0.83	1.73	1.30	1.95
MF12-b	1.71	1.09	1.02	0.82	2.22	1.89	1.90
MF12-c	2.57	1.14	1.13	0.81	2.84	2.66	1.87
MF12-d	3.43	1.09	1.26	0.79	3.40	2.84	1.85
MF12-e	4.29	1.07	1.38	0.77	4.00	3.05	1.83
MF20-a	1.43	1.04	1.02	0.82	2.05	1.48	1.91
MF20-b	2.86	1.08	1.19	0.81	2.73	2.19	1.86
MF20-c	4.29	1.12	1.35	0.77	3.59	3.13	1.83
MF20-d	5.71	1.08	1.42	0.73	4.31	4.13	1.81
MF20-e	7.14	1.06	1.54	0.75	5.02	4.40	1.80

Peak Stress (f_u):

The reinforcing index of each mix was calculated and is given in column 2 of Table 5.21 and 5.22. The ratio between peak stress of MGFRC (M30 and M50 grade) and plain concrete peak stress (f_u/f_0) is given in column 3 of Table 5.21 and 5.22. In order to understand the variation of f_u/f_0 with RI_{MF}, points are plotted as shown in Fig.5.54 (a). An examination of the plot and various trails to arrive at the best fit, it led to understand that f_u/f_0 varies as power function of RI_{MF} in the form of $f_u/f_0 = k\ (RI_{MF})^{-n}$ instead of + n as envisaged earlier. The power function is modified by multiplying both sides by RI_{MF}. The modified relation is $(RI_{MF})\ f_u/f_0 = k\ (RI_{MF})^{(1-n)}$. Now points are plotted with RI_{MF} as abscissa and $RI_{MF}.\ f_u/f_0$ as ordinate is shown in Fig.5.54 (b). The regression expression obtained is $(RI_{MF})\ f_u/f_0 = 1.0984\ (RI_{MF})^{0.9846}$ with regression coefficient $R^2 = 0.9985$. Then the relation between RI_{MF} and f_u/f_0 can be expressed as.

$$f_u = f_0\ (1.0984\ .\ RI_{MF}^{-0.0154}) \quad \text{----------(15)}$$

Where f_0 and f_u are the peak stress of plain concrete and peak stress of MGFRC respectively.

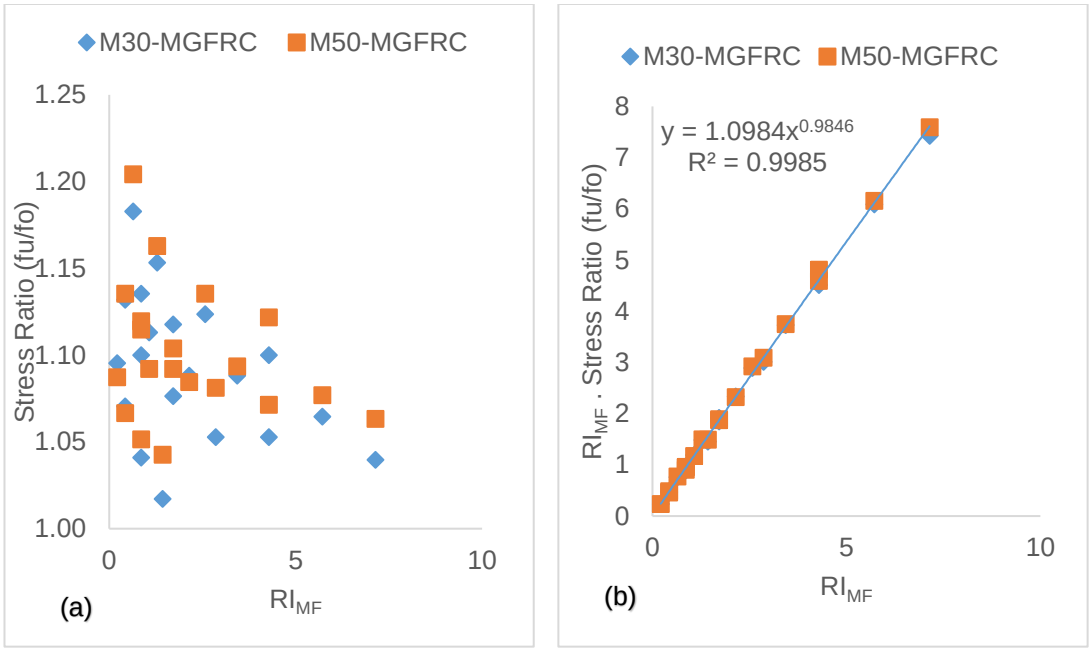

Fig.5.54 Stress ratio at ultimate point as a function of RI_{MF} for MGFRC in compression

Strain at Peat Stress (ε_u):

The reinforcing index of each mix was calculated and is given in column 2 of Table 5.21 and 5.22. The ratio between strain at peak stress of MGFRC (M30 and M50 grade) and strain at peak stress of plain concrete ($\varepsilon_u / \varepsilon_0$) is given in column 4 of Table 5.21 and 5.22. In order to understand the variation of $\varepsilon_u / \varepsilon_0$ with RI_{MF}, points are plotted as shown in Fig.5.55 (a). An examination of the plot and various trails to arrive at the best fit, led to understand that $\varepsilon_u / \varepsilon_0$ varies as power function of RI_{MF} in the form of $\varepsilon_u / \varepsilon_0 = k\,(RI_{MF})^n$ instead of +n as envisaged earlier. The power function is modified by multiplying both sides by RI_{MF}. The modified relation is $(RI_{MF})\ \varepsilon_u / \varepsilon_0 = k\,(RI_{MF})^{(1-n)}$. Now points are plotted with RI_{MF} as abscissa and $RI_{MF}.\ \varepsilon_u / \varepsilon_0$ as ordinate is shown in Fig.5.55 (b). The regression expression obtained is $(RI_{MF})\ \varepsilon_u / \varepsilon_0 = 0.8072\,(RI_{MF})^{1.3407}$ with regression coefficient $R^2 = 0.9963$. Then the relation between RI_{MF} and $\varepsilon_u / \varepsilon_0$ can be expressed as.

$$\varepsilon_u = \varepsilon_0\,(0.8702\ .\ RI_{MF}^{0.3407}) \text{ ----------(16)}$$

Where ε_o and ε_u are the peak strain at peak stress of plain concrete and peak strain at peak stress of MGFRC respectively.

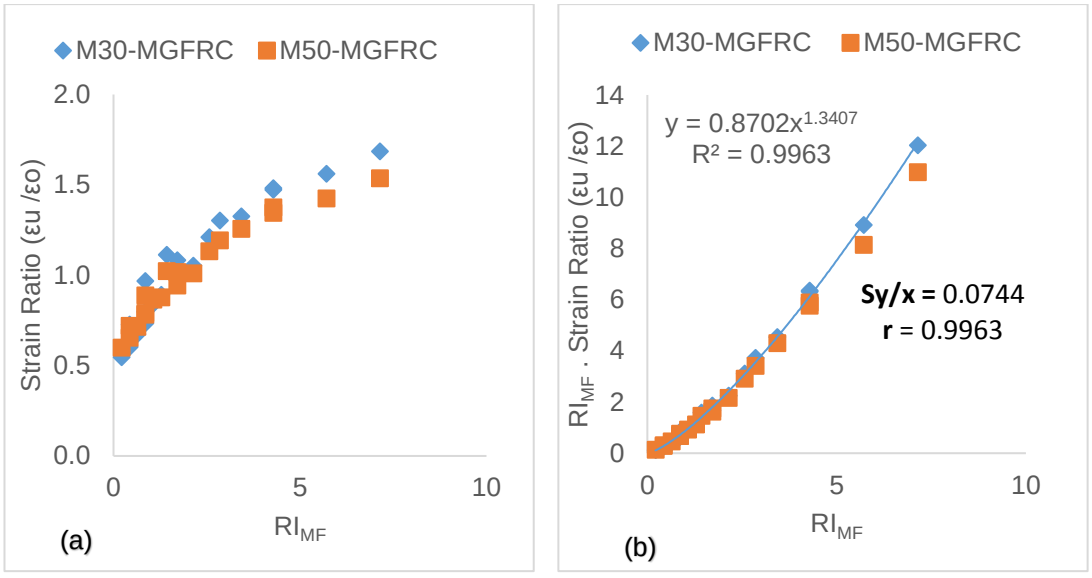

Fig.5.55 strain ratio at ultimate point as a function of RI_{MF} for MGFRC in compression

Stress at inflection (f_{IP}):

The reinforcing index of each mix was calculated and is given in column 2 of Table 5.21 and 5.22. The ratio between stress at inflection of MGFRC (M30 and M50 grade) and plain concrete peak stress (f_{IP}/f_0) is given in column 5 of Table 5.21 and 5.22. In order to understand the variation of f_{IP}/f_0 with RI_{MF}, points are plotted as shown in Fig.5.56. An examination of the plot and various trails to arrive at the best fit, led to understand that f_{IP}/f_0 varies as linear function of RI_{MF} in the form of $f_{IP}/f_0 = m\ (RI_{MF}) + k$. The regression expression obtained is $f_{IP}/f_0 = 0.0214\ RI_{MF} + 0.8625$ with regression coefficient $R^2 = 0.9584$. Then the relation between RI_{MF} and f_{IP}/f_0 can be expressed as.

$$f_{IP} = f_0\ (0.0214\ RI_{MF} + 0.8625) \qquad \text{----------(17)}$$

Where f_0 and f_{IP} are the peak stress of plain concrete and stress at inflection point of MGFRC respectively.

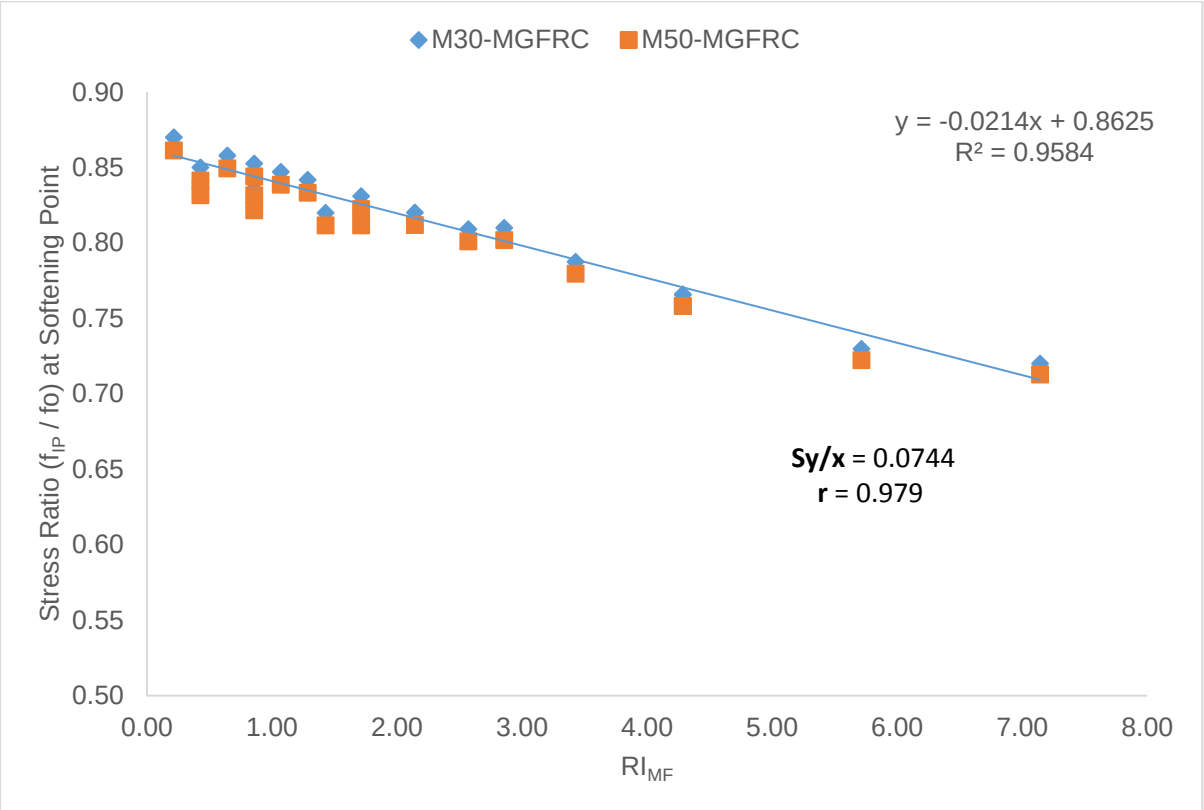

Fig.5.56 stress ratio at inflection point as a function of RI_{MF} for MGFRC in compression

Strain at inflection (ε_{IP}):

The reinforcing index of each mix was calculated and is given in column 2 of Table 5.21 and 5.22. The ratio between stress at inflection of MGFRC (M30 and M50 grade) and plain concrete peak stress ($\varepsilon_{IP}/\varepsilon_0$) is given in column 6 of Table 5.21 and 5.22. In order to understand the variation of $\varepsilon_{IP}/\varepsilon_0$ with RI_{MF}, points are plotted as shown in Fig.5.57. An examination of the plot and various trails to arrive at the best fit, led to understand that $\varepsilon_{IP}/\varepsilon_0$ varies as linear function of RI_{MF} in the form of $\varepsilon_{IP}/\varepsilon_0 = m\,(RI_{MF}) + C$. The regression expression obtained is $\varepsilon_{IP}/\varepsilon_0 = 0.5801\,RI_{MF} + 1.1725$ with regression coefficient $R^2 = 0.9758$. Then the relation between RI_{MF} and $\varepsilon_{IP}/\varepsilon_0$ can be expressed as.

$$\varepsilon_{IP} = \varepsilon_o\,(0.5801\,RI_{MF} + 1.1725) \quad \text{----------(17)}$$

Where ε_o and ε_{IP} are the peak strain at peak stress of plain concrete and strain at inflection of MGFRC respectively.

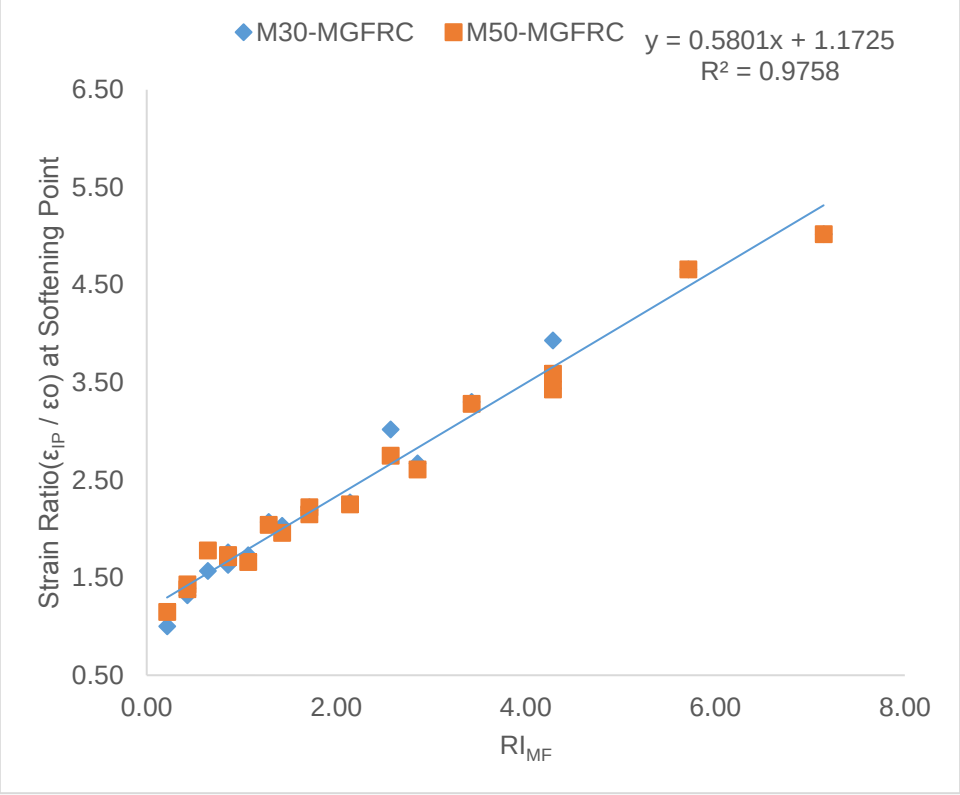

Fig.5.57 strain ratio at inflection point as a function of RI_{MF} for MGFRC in compression

Energy Absorption in strain softening region (EA_{SSR}):

EA_{SSR} is computed from the stress strain diagram (M30-MGFRC and M50-MGFRC) shown in Fig. 5.37 to 5.46 and vales are given in column 11 Table 5.19 and 5.20. The reinforcing index of each mix was calculated and is given in column 2 of Table 5.21 and 5.22. The ratio between energy absorption of MGFRC (M30 and M50 grade) and plain concrete energy absorption (EA_{SSR} / EA^0_{SSR}) is given in column 7 of Table 5.21 and 5.22. In order to understand the variation of EA_{SSR} / EA^0_{SSR} with RI_{MF}, points are plotted as shown in Fig.5.58. An examination of the plot and various trails to arrive at the best fit, led to understand that EA_{SSR} / EA^0_{SSR} varies as power function of RI_{MF} in the form of EA_{SSR} / EA^0_{SSR} = k $(RI_{MF})^n$. The regression expression obtained is EA_{SSR} = 1.6886 $(RI_{MF})^{0.4619}$ with regression coefficient R^2 = 0.93. Then the relation between RI_{MF} and EA_{SSR} / EA^0_{SSR} can be expressed as.

$$EA_{SSR} = EA^o_{SSR} (1.6886\ RI_{MF}^{0.4619}) \text{ ---------- (18)}$$

Where EA^o_{SSR} and EA_{SSR} are the energy absorption in strain softening region of plain concrete and energy absorption in strain softening region of MGFRC respectively.

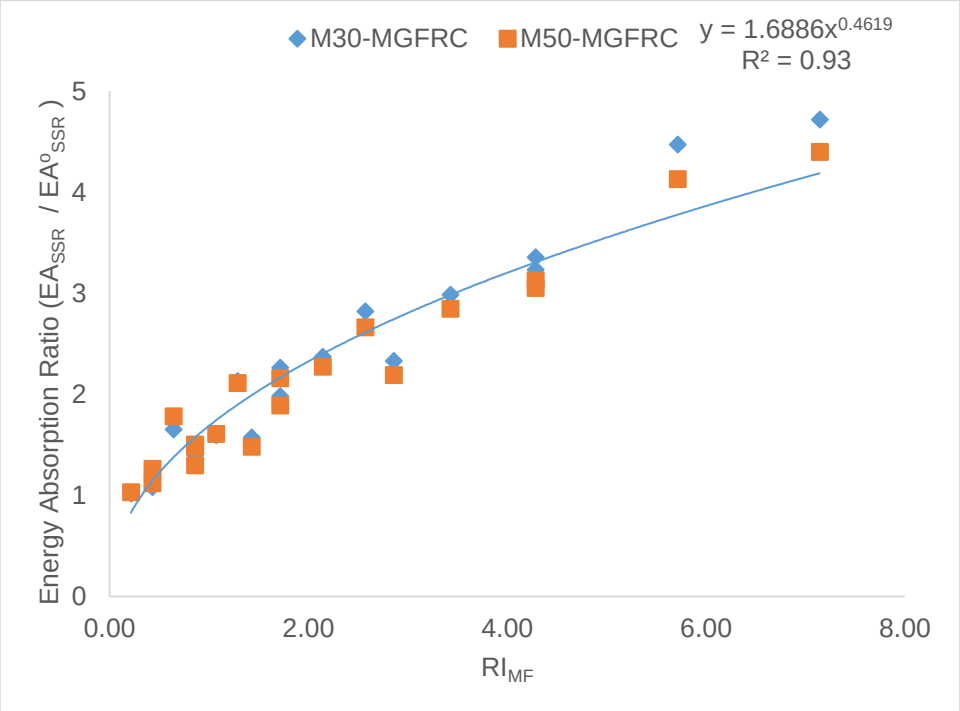

Fig.5.58 Energy absorption in strain softening region as a function of RI_{MF} for MGFRC in compression.

5.13.1 Proposed Material Parameter (β)

f_u/f_0 and $\varepsilon_u/\varepsilon_0$ of experimental stress strain results and equation (14) are used to produce the material parameter (β) for each mix of M30-MGFRC and M50-MGFRC and is given in column 8 of Table 5.21 and 5.22. The reinforcing index (RI_{MF}) of each mix was calculated and is given in column 2 of Table 5.21 and 5.22. In order to understand the variation of β with RI_{MF}, points are plotted as shown in Fig.5.59. An examination of the plot and various trails to arrive at the best fit, led to understand that β varies as power function of RI_{MF} in the form of $\beta = k\,(RI_{MF})^{-n}$. The regression expression obtained is $\beta = 1.9407\,(RI_{MF})^{-0.039}$ with regression coefficient $R^2 = 0.9261$. Then the relation between RI_M and β can be expressed as.

$$\beta = 1.9407\,(RI_{MF})^{-0.039} \text{ ---------- (19)}$$

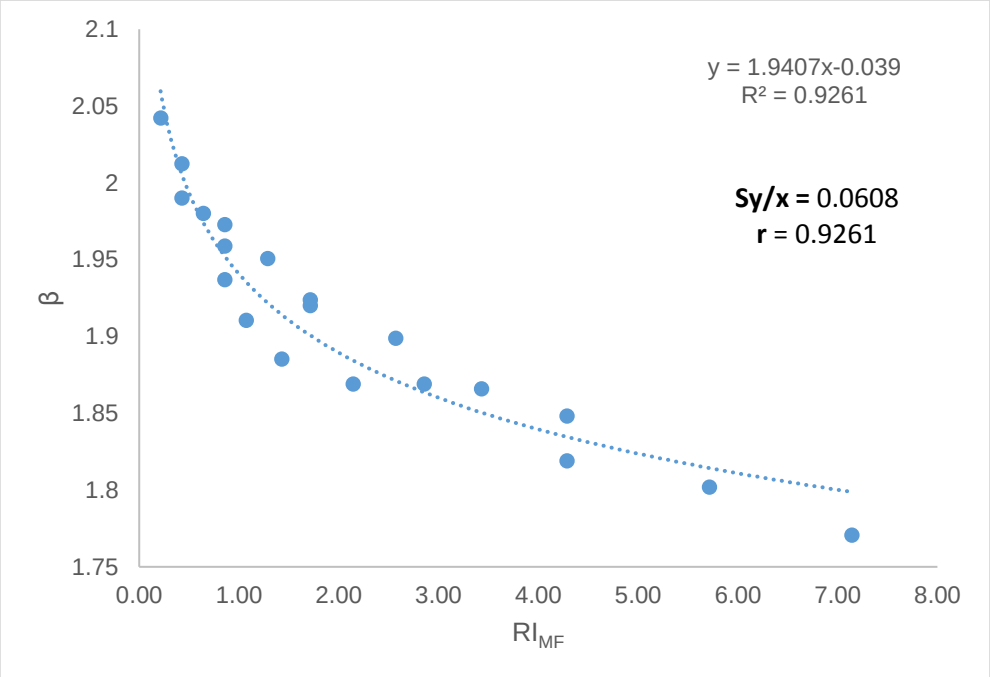

Fig.5.59 Value of parameter β as a function of RI_{MF}

5.13.2 Comparison of stress strain models

The experimental and analytical stress–strain curves of six concrete mixes, namely, M30-MF0-0, M30-MF3-c, M30-MF20-c, M50-MF0-0, M50-MF3-c and M50-MF20-c, are plotted in Fig.5.60 to 5.65 along with the curves predicted using the existing models

of M.C Nataraja et al. (1999), Ou et al. (2012), Aref Abadel et al. (2016). The shape of the softening branch of the curve, which is steep in plain concrete (Fig.5.60 and 5.61), becomes flatter with the addition of fibres (Fig.5.62 to 5.65). For plain concrete, the analytical stress–strain curves by the existing models is close to the experimental stress strain curves. The analytical stress–strain curves for M30-MGFRC and M50-MGFRC drawn using the existing models have deviation from the experimental curves (Fig.5.62 to 5.65). Analytical model Proposed by the equation (13) has shown close correlation with experimental results of both M30 and M50 grade of concrete.

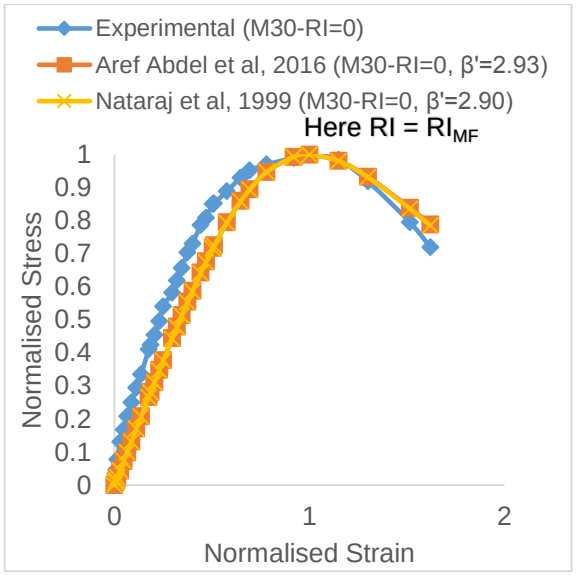

Fig.5.60 Analytical and experimental normalised stress–strain relationship (M30-RI_{MF} = 0)

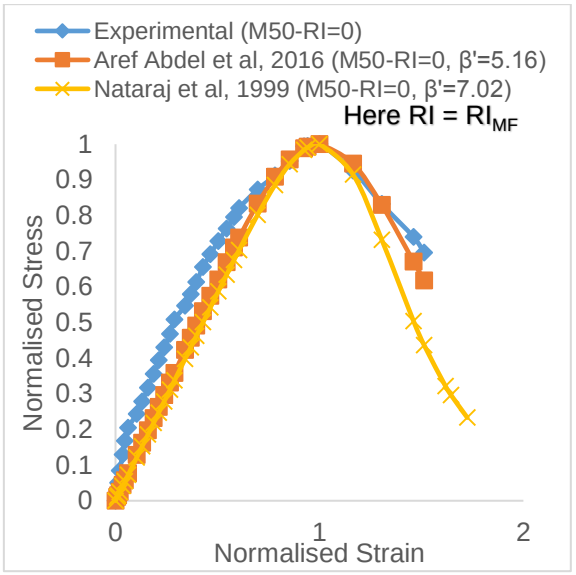

Fig.5.61 Analytical and experimental normalised stress–strain relationship (M50-RI_{MF} = 0)

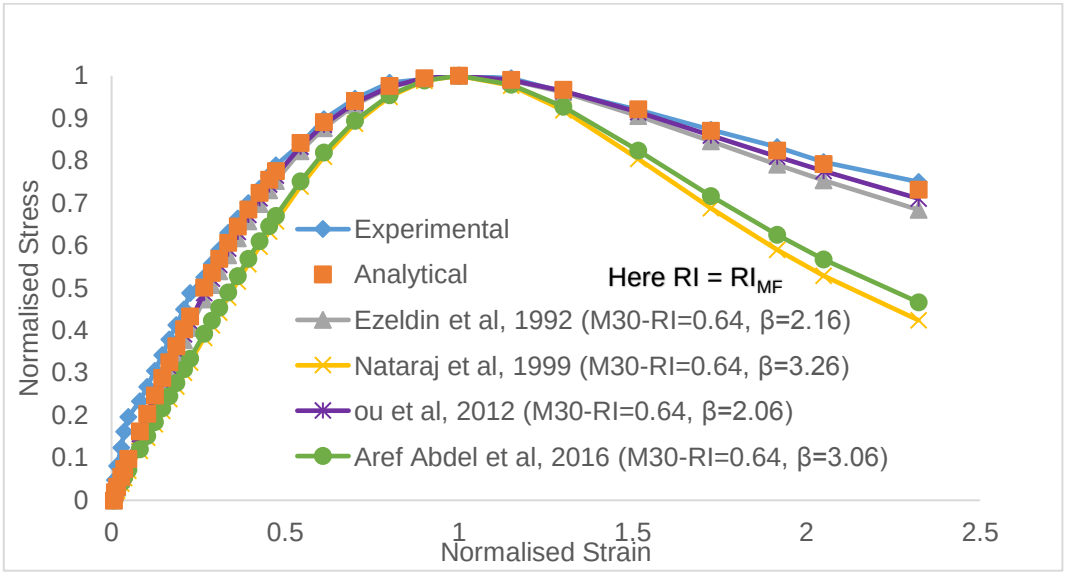

Fig.5.62 Analytical and experimental normalised stress–strain relationship for M30-0.3%-3mm (RI_{MF} = 0.64, β =1.98).

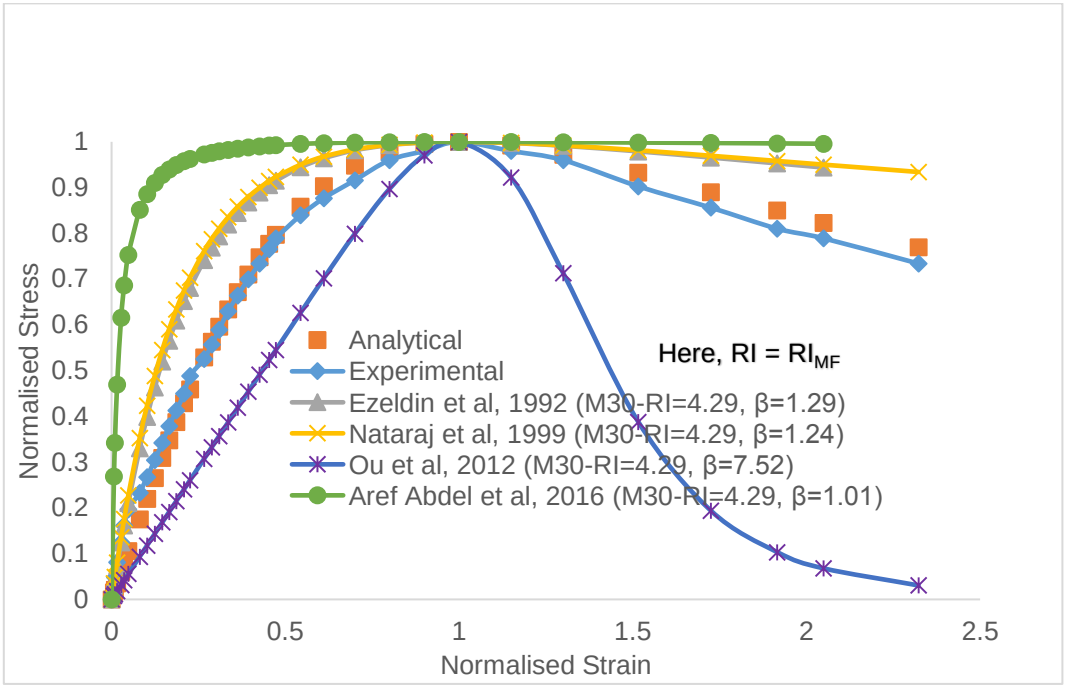

Fig.5.63 Analytical and experimental normalised stress–strain relationship for M30-0.3%-20mm (RI_{MF} = 4.29, β =1.85)

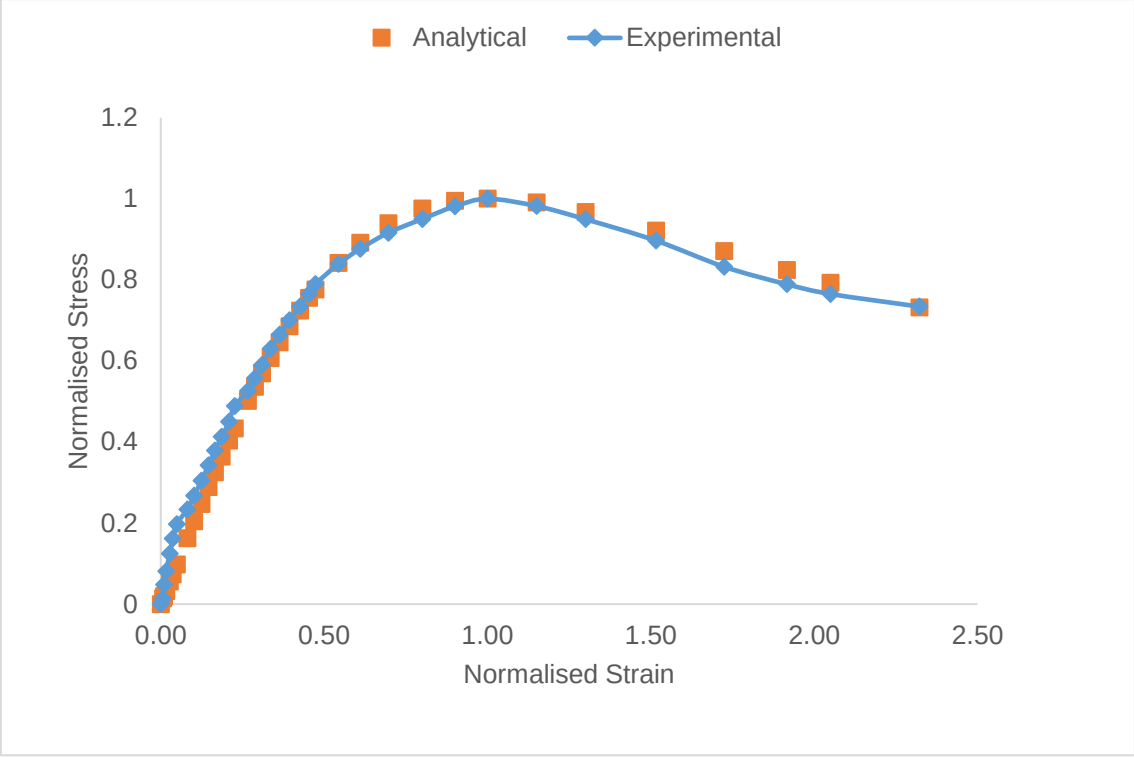

Fig.5.64 Analytical and experimental normalised stress–strain relationship for M50-0.3%-3mm (RI_{MF} = 0.64, β = 1.97).

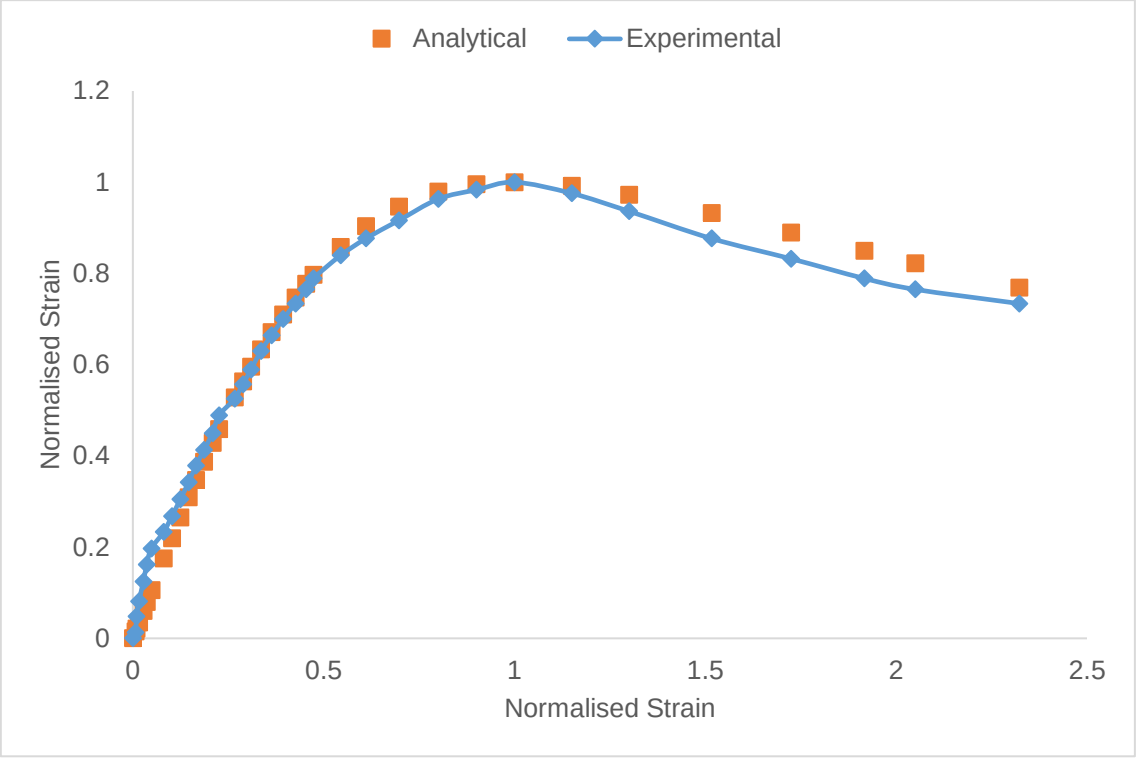

Fig.5.65 Analytical and experimental normalised stress–strain relationship for M50-0.3%-20mm (RI_{MF} = 4.29, β =1.83).

5.14. Strain Hardening in Tension and Strain Softening in Compression of MGFRC

Normal compressive stress generates transverse tensile strain. As the compressive stress reaches peak stress, dilation of concrete initiates and lateral deformation increases. Presence of fibers restrain the lateral deformation and some researchers (Antroula et al, 2017) viewed the lateral restraint provided by fibers as similar to lateral confinement. Degree of resistance offered to lateral deformation is proportional to volume of fibers and the fibers come into action after cracking in concrete in compression which is similar to the action of fibers in concrete after the onset of cracking in tension. The fibers present in concrete will participate by resisting dilation of concrete only after sufficient mobilization of dilation of concrete. That is why there is a remarkable improvement in strain softening of concrete in compression with the increase in fiber content. Hence, the strain hardening of FRC in tension is influencing the strain softening of FRC in compression. The exact relation is however complex. The above phenomena can be noticed in the stress strain behaviour of GFRC.

Irrespective of length of fiber, specimens with 0.3%, 0.4% and 0.5% have exhibited strain hardening in tension and corresponding strain softening is noticed in compression. It is noted that strain hardening in tension is not observed for specimens with 0.1% and 0.2% and corresponding strain softening in compression is not significantly present.

In the present investigation the parameters such as grade of concrete and Reinforcing Index ($RI_{MF} = V_f (L_f/D_f)$) are same for the specimens in tension and compression. Values of stress and strain corresponding to strain hardening region and strain softening region of each specimen are given in Tables 5.1, 5.2, 5.19 and 5.20. Strain hardening behaviour in tension and strain softening behaviour in compression for MGFRC specimens are normalised with corresponding peak stress and peak strain and reported in Table 5.23.

In order to understand the complementary behaviour of strain hardening behaviour in tension and strain softening behaviour in compression, the normalised stress and normalised strain at the onset of strain hardening and at the inflection point of strain softening for M30-MGFRC and M50-MGFRC with RI_{MF} of 0.64, 1.29, 2.57 and 4.59 are shown in Fig.5.64 and 5.65. Similar plot can be drawn for all values of $RI_{MF.}$ The gradient of strain hardening in tension is similar to the gradient of strain softening in compression. Specimens with Short fibers i.e. $RI_{MF} = 0.64$ and $RI_{MF} = 1.29$ producing low strain hardening in tension has similar low strain softening behaviour in compression, where as in specimens with long fibers i.e., $RI_{MF} = 2.57$ and $RI_{MF} = 4.29$ exhibited significant strain hardening in tension has similar significant strain softening behaviour in compression respectively. It can be concluded, for any given reinforcing index (RI_{MF}) of mono fibers as the strain hardening in tension increased the corresponding strain softening increased.

Table.5.23 stress and strain ratio of Stain hardening and strain softening region

Specimen Designation (1)	RI_{MF} (2)	M30-MGFRC				M50-MGFRC			
		Strain Hardening Region		Strain Softening Region		Strain Hardening Region		Strain Softening Region	
		$\sigma^{P}_{t} / \sigma^{Q}_{t}$ (3)	$\varepsilon^{P}_{t} / \varepsilon^{Q}_{t}$ (4)	f^{C}_{IP} / f^{B}_{u} (5)	$\varepsilon^{C}_{IP} / \varepsilon^{B}_{u}$ (6)	$\sigma^{P}_{t} / \sigma^{Q}_{t}$ (7)	$\varepsilon^{P}_{t} / \varepsilon^{Q}_{t}$ (8)	f^{C}_{IP} / f^{B}_{u} (9)	$\varepsilon^{C}_{IP} / \varepsilon^{B}_{u}$ (10)
MF3-a	0.21	1.00	1.00	0.86	1.73	1.00	1.00	0.87	1.84
MF3-b	0.43	1.00	1.00	0.84	2.02	1.00	1.00	0.85	2.05
MF3-c	0.64	0.92	0.79	0.85	2.15	0.90	0.85	0.86	2.20
MF3-d	0.86	0.96	0.62	0.84	2.19	0.91	0.40	0.85	2.34
MF3-e	1.07	0.80	0.36	0.84	2.24	0.80	0.37	0.85	2.36
MF6-a	0.43	1.00	1.00	0.83	1.77	1.00	1.00	0.84	1.88
MF6-b	0.86	1.00	1.00	0.83	2.05	1.00	1.00	0.84	2.22
MF6-c	1.29	0.94	0.76	0.83	2.19	0.94	0.82	0.84	2.31
MF6-d	1.71	0.96	0.63	0.82	2.24	0.92	0.40	0.83	2.43
MF6-e	2.14	0.80	0.36	0.81	2.33	0.77	0.29	0.82	2.51
MF12-a	0.86	1.00	1.00	0.82	1.82	1.00	1.00	0.83	1.95
MF12-b	1.71	0.94	0.83	0.81	2.19	0.94	0.82	0.82	2.18
MF12-c	2.57	0.94	0.50	0.80	2.49	0.92	0.42	0.81	2.51
MF12-d	3.43	0.77	0.27	0.78	2.56	0.77	0.16	0.79	2.71
MF12-e	4.29	0.73	0.20	0.76	2.66	0.74	0.14	0.77	2.91
MF20-a	1.43	0.94	0.83	0.81	1.87	0.94	0.83	0.82	2.01
MF20-b	2.86	0.94	0.52	0.80	2.29	0.92	0.41	0.81	2.29
MF20-c	4.29	0.94	0.37	0.76	2.80	0.94	0.34	0.77	2.67
MF20-d	5.71	0.77	0.21	0.72	3.00	0.76	0.12	0.73	3.02
MF20-e	7.14	0.74	0.15	0.71	3.10	0.73	0.11	0.72	3.27

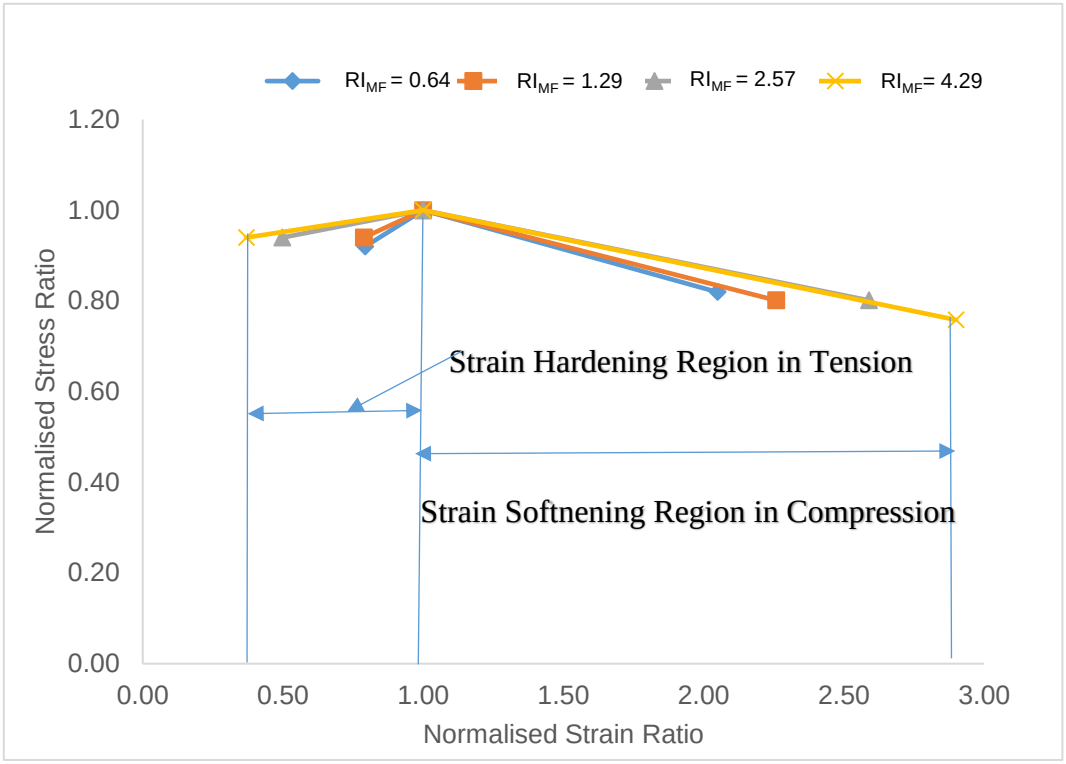

Fig.5.66 Strain hardening vs strain softening (M30-MGFRC)

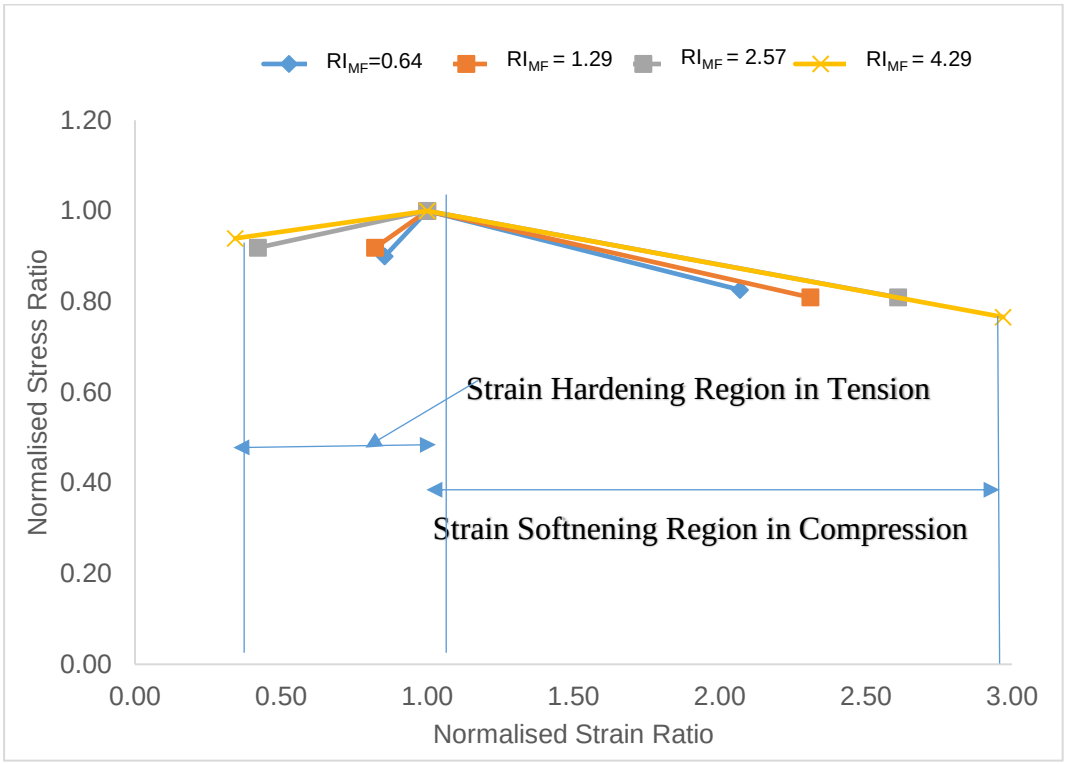

Fig.5.67 Strain hardening vs strain softening (M50-MGFRC)

5.14.1. Relationship between Stress and strain of SSR in compression and SHR in tension for MGFRC:

In order to correlate tensile and compression data, relationship between Reinforcing Index (RI_{MF}) and ($\sigma^{P}_{t} / \sigma^{Q}_{t}$) / ($f^{C}_{IP} / f^{B}_{u}$), ($\varepsilon^{P}_{t} / \varepsilon^{Q}_{t}$) / ($\varepsilon^{C}_{IP} / \varepsilon^{B}_{u}$) is shown in Fig.5.68. Equations (20) and (21) were obtained using the regression analysis performed using all data points of M30-MGFRC and M50-MGFRC.

The reinforcing index of each mix was calculated and is given in column 2 of Table 5.23. The ratios between stress and strains in strain hardening region and strain softening region is considered for MGFRC (M30 and M50 grade) and given in Table 5.23. In order to understand the variation of these ratios with RI_{MF}, points are plotted as shown in Fig.5.68 (a). An examination of the plot and various trails to arrive at the best fit, led to understand that stress and strain ratios varies as power function of RI_{M} in the form of stress ratio or strain ratio = $k / (RI_{MF})^{n}$. The power function is modified by multiplying both sides by RI_{MF}. The modified relation is (RI_{MF}) stress ratio or strain ratio = $k\ (RI_{MF})^{(1-n)}$. Now points are plotted with RI_{MF} as abscissa and $RI_{MF.}$ Stress ratio or strain ratio as ordinate is shown in Fig.5.68 (b). The regression expression obtained is (RI_{MF}) $\sigma^{P}_{t} / \sigma^{Q}_{t} = (f^{C}_{IP} / f^{B}_{u})\ 1.131\ (RI_{MF})^{\ 0.9661}$ with regression coefficient $R^2 = 0.9985$ and (RI_{MF}) $\varepsilon^{P}_{t} / \varepsilon^{Q}_{t} = (\varepsilon^{C}_{IP} / \varepsilon^{B}_{u})\ 0.7985\ (RI_{MF})^{\ 1.1005}$ with regression coefficient $R^2 = 0.9143$. Then the relation between RI_{M} and stress and strains can be expressed as

$$\sigma^{P}_{t} / \sigma^{Q}_{t} = (f^{C}_{IP} / f^{B}_{u})\ (1.131\ RI_{MF}^{-0.0339}) \quad \text{----------(20)}$$

$$\varepsilon^{P}_{t} / \varepsilon^{Q}_{t} = (\varepsilon^{C}_{IP} / \varepsilon^{B}_{u})\ (0.7985\ RI_{MF}^{0.1005}) \quad \text{---------- (21)}$$

Where, $f^{B}_{u,}\ f^{C}_{IP}$ in compression is used to calculate from equation (15) and (17). ε^{B}_{u} ε^{C}_{IP} in tension is used to calculate from equation (16) and (18).

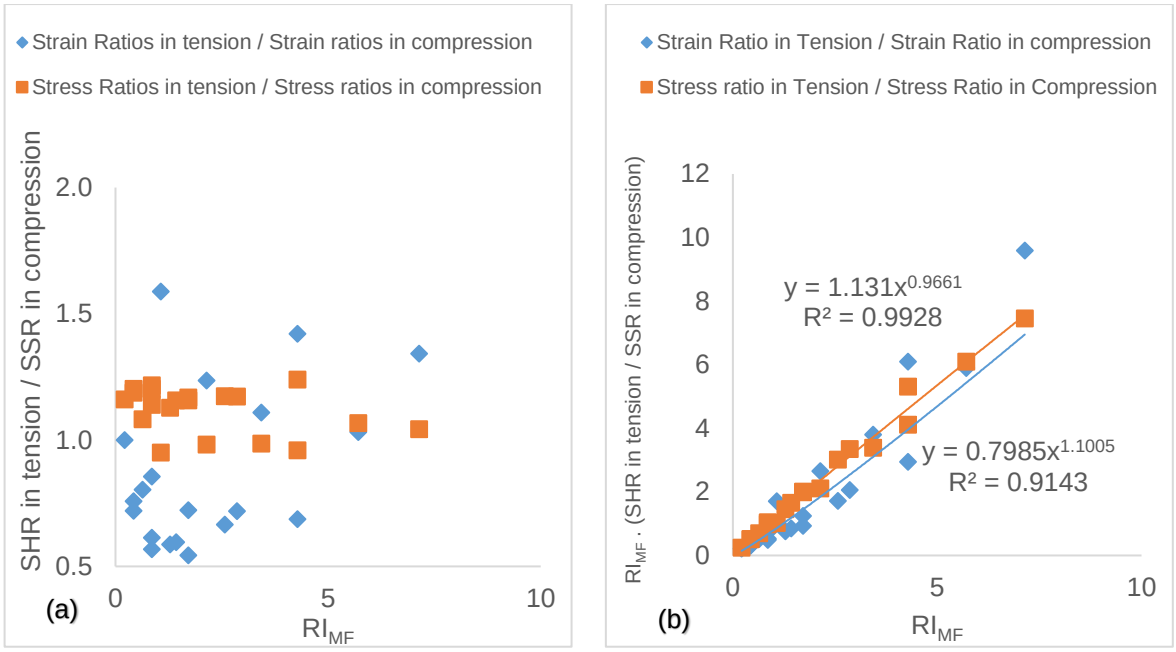

Fig. 5.68 SHR in tension / SSR in compression vs RI_{MF} for MGFRC

5.14.2. Relationship between Energy absorption capacity in tension and compression for MGFRC:

Relationship between energy absorption in strain hardening region and energy absorption in strain softening region is also developed and shown in Fig.5.69. The equation (22) were obtained using the regression analysis performed using all data points of M30-MGFRC and M50-MGFRC. The advantage of the equation (22) is that it can be used to calculate the either energy absorption in strain hardening region in tension or energy absorption in strain softening region, if one of them is known.

Energy absorption capacity in strain hardening region (EA_{SHR}) and energy absorption capacity in strain softening region (EA_{SSR}) is computed from the stress strain diagram (M30-MGFRC and M50-MGFRC). EA_{SHR} is given in column 11 of Table 5.1 and 5.2, and EA_{SSR} is Table 5.19 and 5.20. The reinforcing index of each mix was calculated and is given in column 2 of Table 5.23. In order to understand the variation of EA_{SHR} / EA_{SSR} with RI_{MF}, points are plotted as shown in Fig.5.69. An examination of the plot and various trails to arrive at the best fit, lead to understand that EA_{SHR} / EA_{SSR} varies as power function of RI_{MF} in the form of EA_{SHR} / EA_{SSR} = k $(RI_{MF})^n$. The regression expression obtained is EA_{SHR} / EA_{SSR} = 182.07 $(RI_{MF})^{-0.4619}$ with regression coefficient R^2 = 0.93. Then the relation between RI_M and EA_{SHR} / EA_{SSR} can be expressed as.

$$EA_{SHR} = EA_{SSR} (182.07\ RI_{MF}^{-0.462}) \text{ ---------- (22)}$$

Where EA_{SHR} is the energy absorption capacity in tension and EA_{SSR} is the energy absorption capacity in compression.

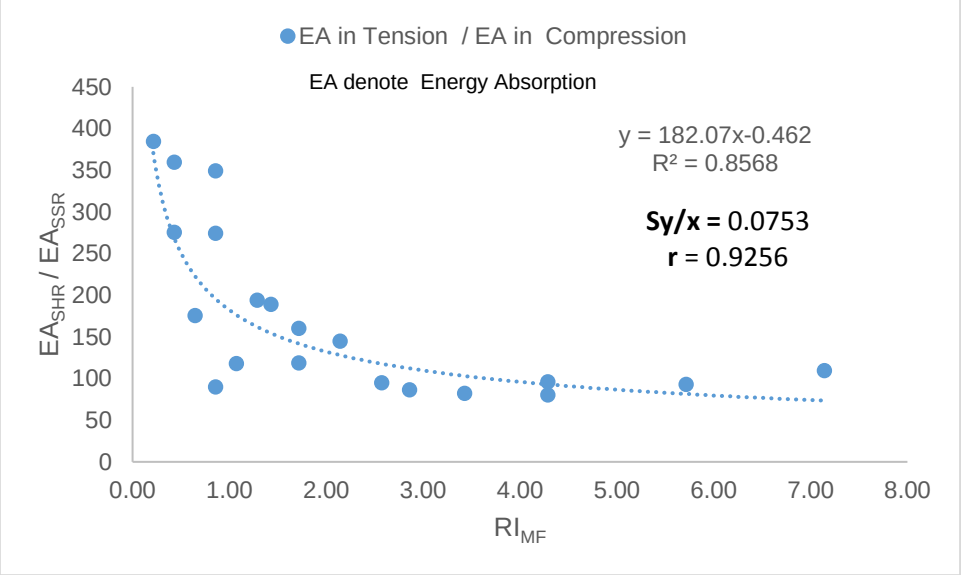

Fig.5.69 Ratio between the Energy absorption in tension and Energy absorption in compression is a function of RI_{MF}.

This page is intentionally left blank

Chapter-6

Study on Graded Glass Fiber Reinforced Concrete

6.1. Introduction

In the precious chapter, influence of fiber length and volume fraction on MGFRC were discussed. In overall, the results have shown short length fibers (3mm and 6mm) contributed to improve the strength of the composite whereas long length fibers (12mm and 20mm) provided the significant deformation. Moreover, short length fibers dispersed and oriented effectively compared to the long length fibers. Equations were proposed to compute the tensile strength and corresponding strain capacity of composite. Equations were given to predict the compressive stress strain curves and tensile stress strain curves for MGFRC.

Based on the MGFRC results, to improve the properties of the composite (strength and deformation) simultaneously different lengths of fibers are mixed together and named as Graded Fibers. The experimental program is designed to study the effect of graded fibers on concrete of grade M30 and M50. In this investigation, two or more length of fibers are mixed to form Graded Fibers. When the mixture consists of 3mm and 6mm is named as Short Graded Fiber (SGF), mixture consisting of 12mm and 20mm is named as Long Graded Fiber (LGF) and mixture of all the four lengths 3mm, 6mm, 12mm and 20mm is named as Combined Graded Fiber (CGF). In the present study uniaxial tension and compression tests were performed on dog-bone specimens and prismatic specimens respectively. The present study was aimed at understanding the effect of Graded fibers on the composite.

6.2 Slump and cube compressive strength of Graded Glass Fiber Reinforced Concrete (GGFRC)

6.2.1 Slump of M30-GGFRC

6.2.1(a) Comparison of M30-GGFRC-0.3% with M30-MGFRC-0.3%

The value of slump for M30-GGFRC with volume of the fiber 0.3% is shown in Fig.6.1. The total volume of fiber is 0.3% for all the specimens. Proportion of different lengths of fibers considered in the mix is given in Table 4.2 of Chapter-4. The slump of M30-GGFRC is compared with M30-MGFRC. Considering short graded fibers SGF-I#c, SGF-II#c, SGF-III#c, SGF-IV#c and SGF-V#c mixes, the slump values are 92 mm, 126 mm, 116 mm, 109 mm and 90 mm respectively. SGF-I#c and SGF-V#c showed

less slump values than that of M30-MGFRC with 3mm and 6mm fibers. There is a progressive slump increase in SGF-IV#c, SGF-III#c and SGF-II#c. Among all the short graded fibers, SGF-II#c showed the highest slump value and also than that of mono fibers (3mm, 6mm). Considering long graded fibers LGF-I#c, LGF-II#c, LGF-III#c, LGF-IV#c and LGF-V#c the slump values are 81 mm, 112 mm, 103 mm, 79 mm and 90 mm respectively. LGF-I and LGF-V showed less slump values than that of MGFRC with mono fibers of 12mm and 20mm length. There is a progressive slump increase in LGF-IV#c, LGF-III#c and LGF-II#c. Among all the long graded fibers, LGF-II#c showed the highest slump value and also than that of mono fibers (12mm, 20mm). It can be seen that short graded fiber mixes showed higher slump values than that of long graded fiber mixes. Considering CGF-I#c, CGF-II#c, CGF-III#c, CGF-IV#c and CGF-V#c the slump values are 108 mm, 140 mm, 129 mm, 121 mm and 106 mm respectively. CGF-I#c and CGF-V#c showed the slump values almost near to the slump of M30-MGFRC with 3mm fibers. There is a progressive slump increase in CGF-IV#c, CGF-III#c and CGF-II#c.

An examination of the above mixes shows that CGF have performed better than MGF (mono glass fibers), SGF, and LGF in any mixture from the type-I (20%+80%) to type-V (80%+20%). In 0.3% volume of fibers and among all the mixes CGF-II#c has given the highest slump value. It was noted earlier while testing MGF specimen that the slump decreased with increase in length of fiber. Now, it can be noticed, in general, there is improvement in slump for graded fiber specimens compared to mono glass fiber specimens. In particular, combined graded fiber specimens have given the best performance in terms of slump. Hence, graded fibers improves workability.

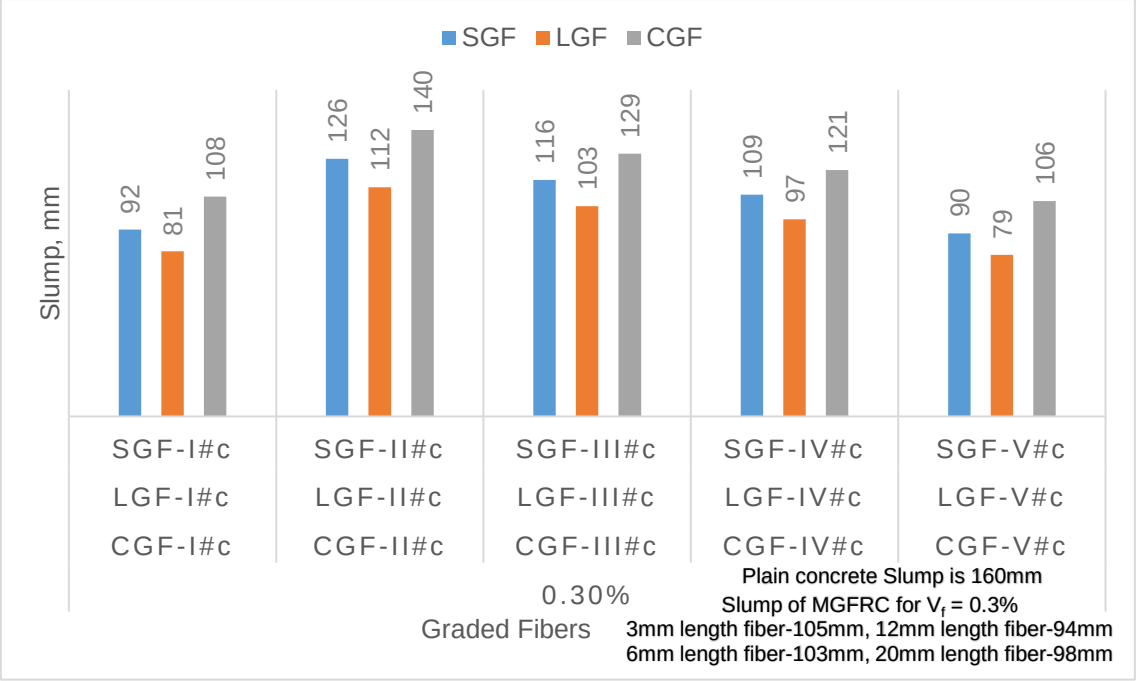

Fig.6.1 Slump of M30-GGFRC with V_f = 0.3%

6.2.1(b) Comparison of M30-GGFRC-0.4% and 0.5% with M30-MGFRC-0.4% and 0.5%

Similar slump test was conducted for M30-GGFRC with 0.4% and 0.5% volume fraction and results shown in Fig.6.2 and 6.3. The mix with 0.4% and 0.5% of MGFRC gave the remarkable reduction in slump and it showed balling of fibers in the composite. Similar to 0.3% volume fraction of M30-GGFRC, in the short graded fibers, SGF-II#d and SGF-II#e showed the highest slump value and also than that of mono glass fibers (3mm, 6mm). Among all the long graded fibers, LGF-II#d and LGF-II#e showed the highest slump value and also than that of mono glass fibers (12mm, 20mm). It can be seen that short graded fiber mixes showed higher slump values than that of long graded fiber mixes. Among all the mixes CGF-II#d and CGF-II#e has given the highest slump value.

An overall observation is that, there is significant difference existed in the loss of the slump for mono glass fibers. The slump loss was small in the concrete with graded fibers. Hence, graded fibers improves workability.

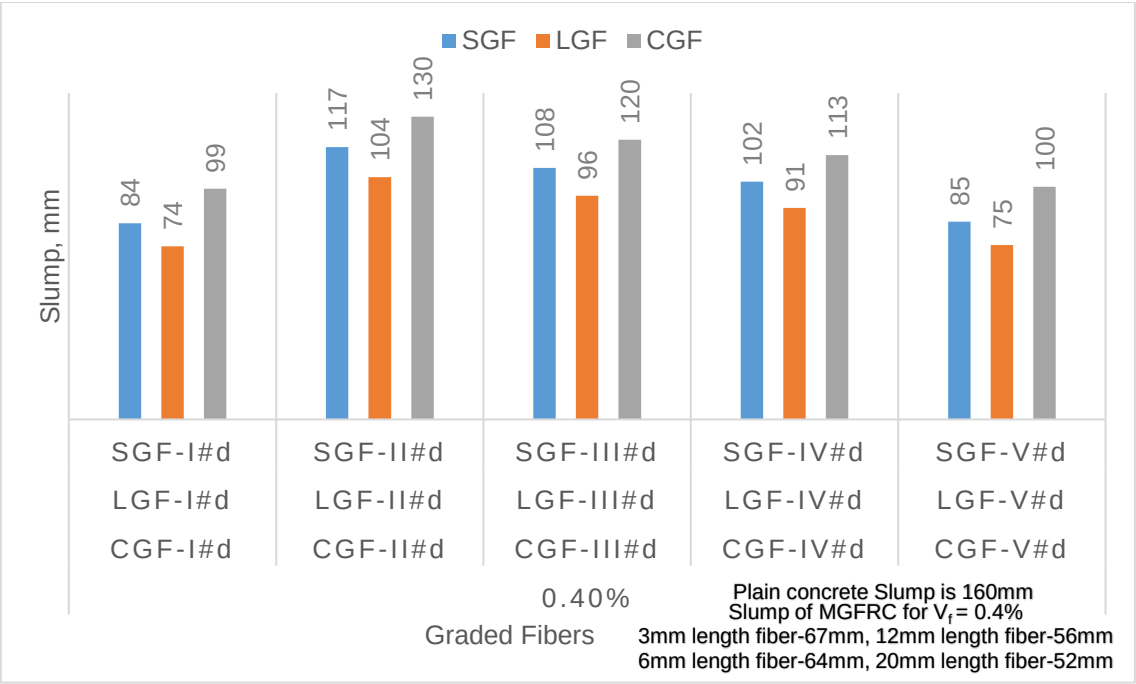

Fig.6.2 Slump of M30-GGFRC with V_f = 0.4%

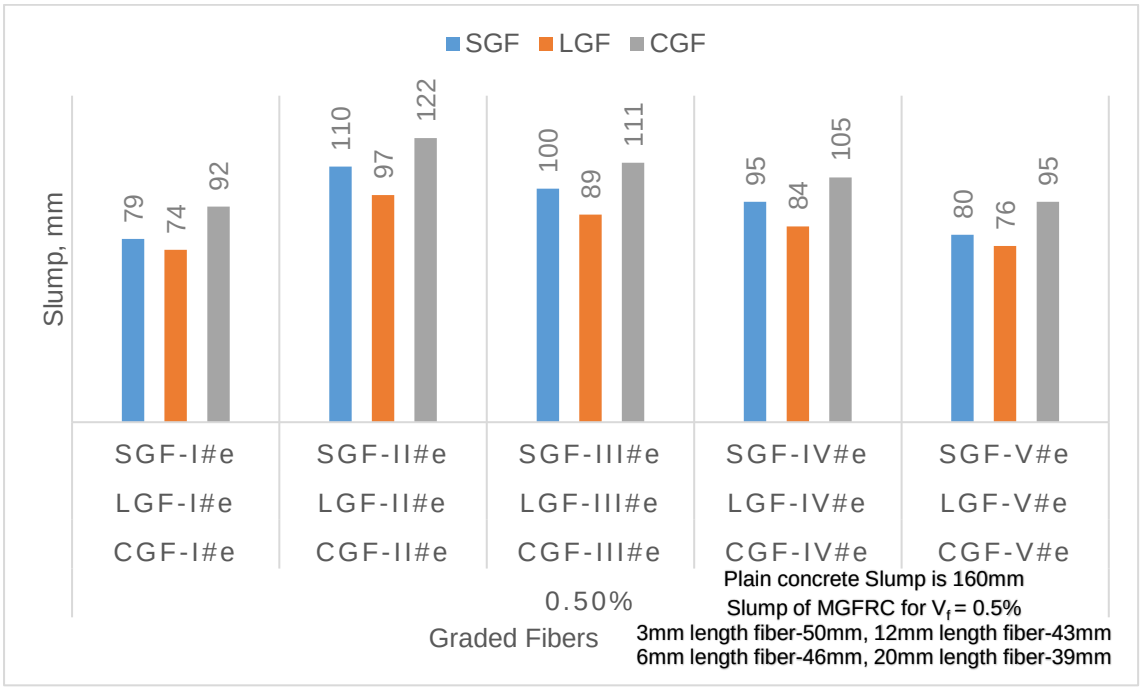

Fig.6.3 Slump of M30-GGFRC with V_f = 0.5%

6.2.2 Slump of M50-GGFRC

In order to understand the graded fiber behaviour in M50 grade of concrete, slump test was conducted for M50-GGFRC with 0.3%, 0.4% and 0.5% volume fraction similar to the M30-GGFRC 0.3%, 0.4% and 0.5% and shown in Fig.6.4 to 6.6. It is noticed that the M50-GGFRC slump behaviour is similar to the M30-GGFRC. An examination with different fiber volume combinations of SGF mixes showed that slump of SGF-II#c > SGF-II#e > SGF-II#d, that in LGF mixes showed LGF-II#c > LGF-II#e > LGF-II#d and that in case of CGF mixes showed CGF-II#c > CGF-II#e > CGF-II#d respectively. In any given volume fraction (0.3%, 0.4% and 0.5%) of M50-GGFRC, among all the mixes shows that CGF have given the best performance in terms of slump compared to MGF, SGF and LGF. It can be concluded that the graded fibers improves the workability of any normal strength concrete.

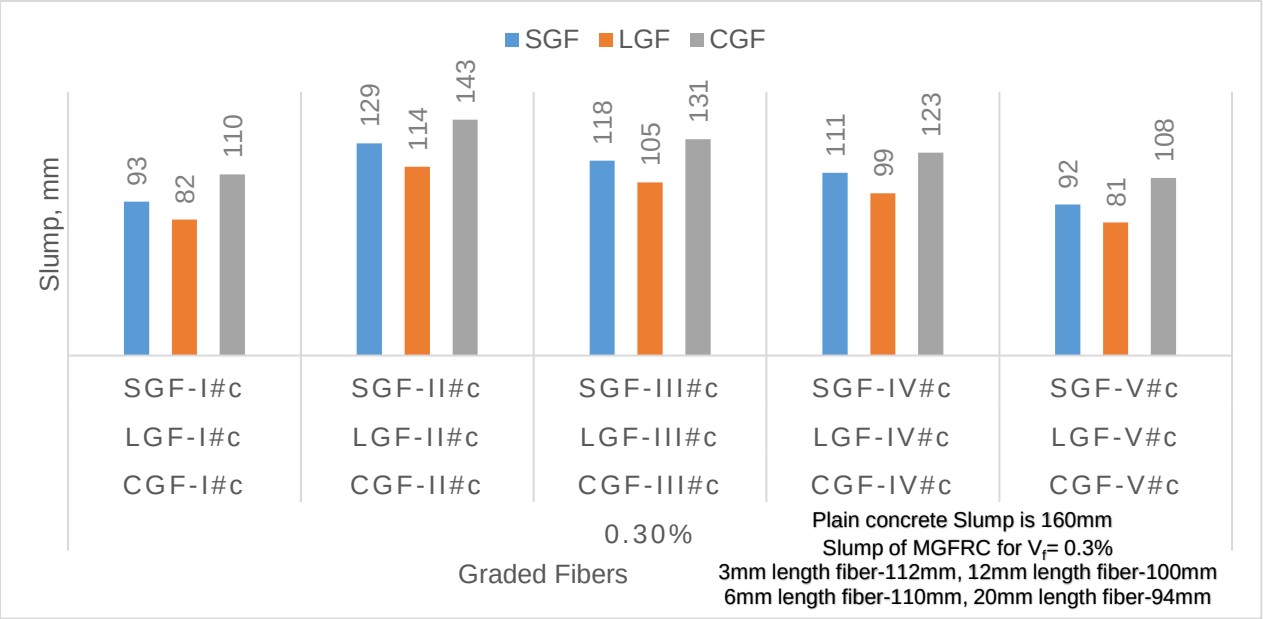

Fig.6.4 Slump of M50-GGFRC with V_f = 0.3%

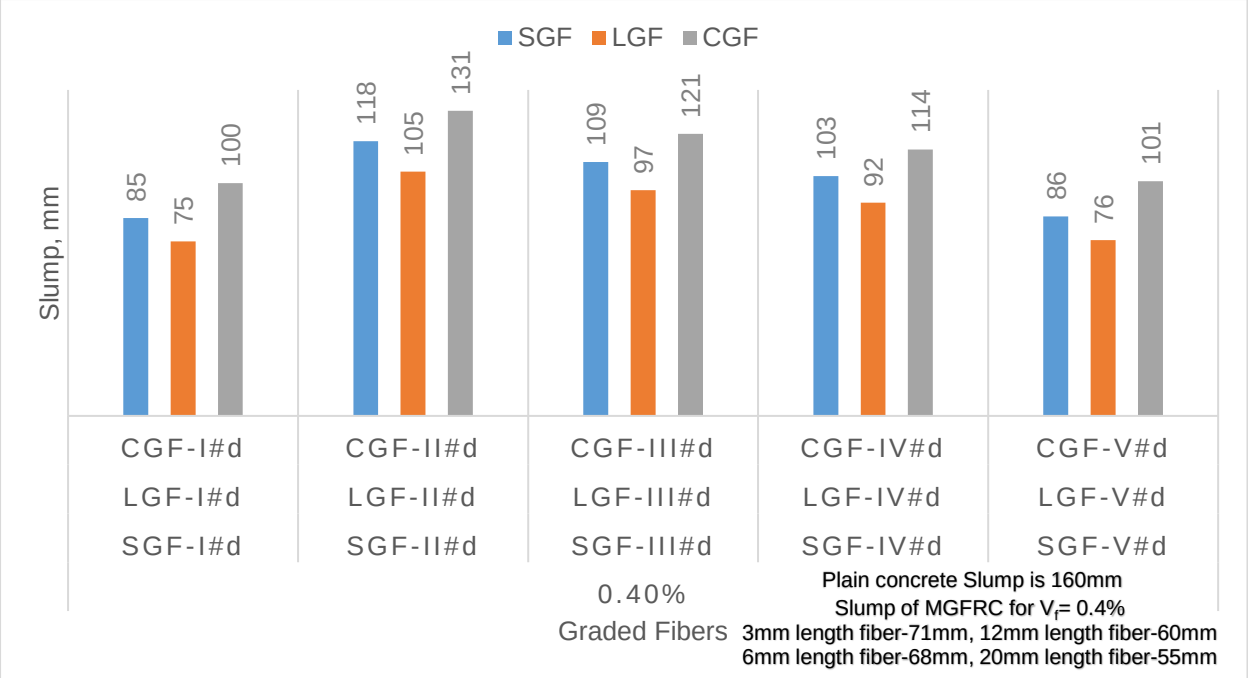

Fig.6.5 Slump of M50-GGFRC with V_f = 0.4%

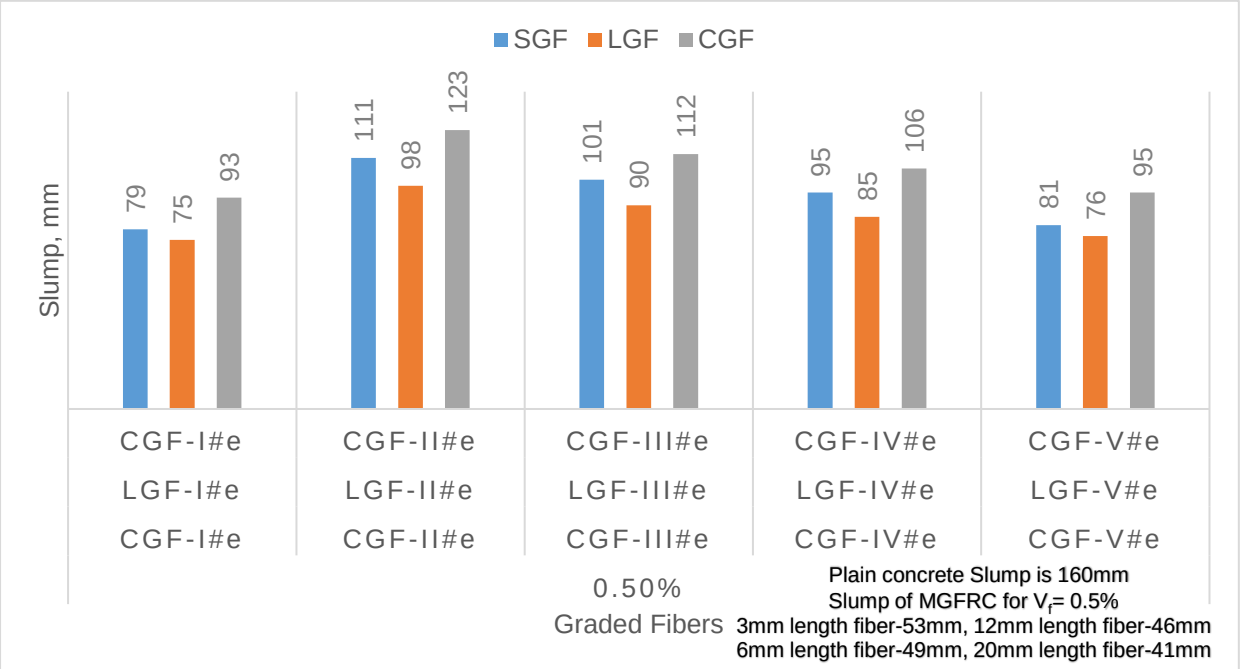

Fig.6.6 Slump of M50-GGFRC with V_f = 0.5%

6.2.3 Cube compressive strength of M30-GGFRC

6.2.3 (a). Comparison of cube compressive strength of M30-GGFRC-0.3% with M30-MGFRC-0.3%

The compressive strength results of M30-GGFRC is shown in Fig.6.7. The compressive strength results of M30-GGFRC is compared with M30-MGFRC.

Considering SGF-I#c, SGF-II#c, SGF-III#c, SGF-IV#c and SGF-V#c mixes, the compressive strength values are 39.08 MPa, 40.80 MPa, 39.75 MPa, 38.76 MPa and 38.04 MPa respectively. SGF-I#c, SGF-III#c, SGF-IV#c and SGF-V#c are showed less improvement in compressive strength than that of mono glass fibers (3 mm and 6 mm). Among all the short graded fibers, SGF-II showed improvement in compressive strength and also than that of mono glass fiber specimen.

Considering LGF-I#c, LGF-II#c, LGF-III#c, LGF-IV#c and LGF-V#c mixes, the compressive strength values are 37.89 MPa, 41.21 MPa, 38.54 MPa, 37.59 MPa and 36.88 MPa respectively. LGF-I#c, LGF-III#c, LGF-IV#c and LGF-V#c showed less improvement in compressive strength than that of mono glass fibers (12mm and 20mm). There is progressive increase of compressive strength in LGF-IV#c, LGF-III#c and LGF-II#c. Among all the short graded fibers, LGF-II#c showed the maximum improvement in compressive strength and also than that of mono glass fiber specimens.

Considering CGF-I#c, CGF-II#c, CGF-III#c, CGF-IV#c and CGF-V#c mixes, the compressive strength values are 39.48 MPa, 42.05 MPa, 40.15 MPa, 39.17 MPa and 38.42 MPa respectively. There is a significant improvement of compressive strength in combined graded fibers than mono glass fibers. However, for the same volume in 0.3% of fibers, among all the mixes CGF-II#c has given the best improvement in compressive strength.

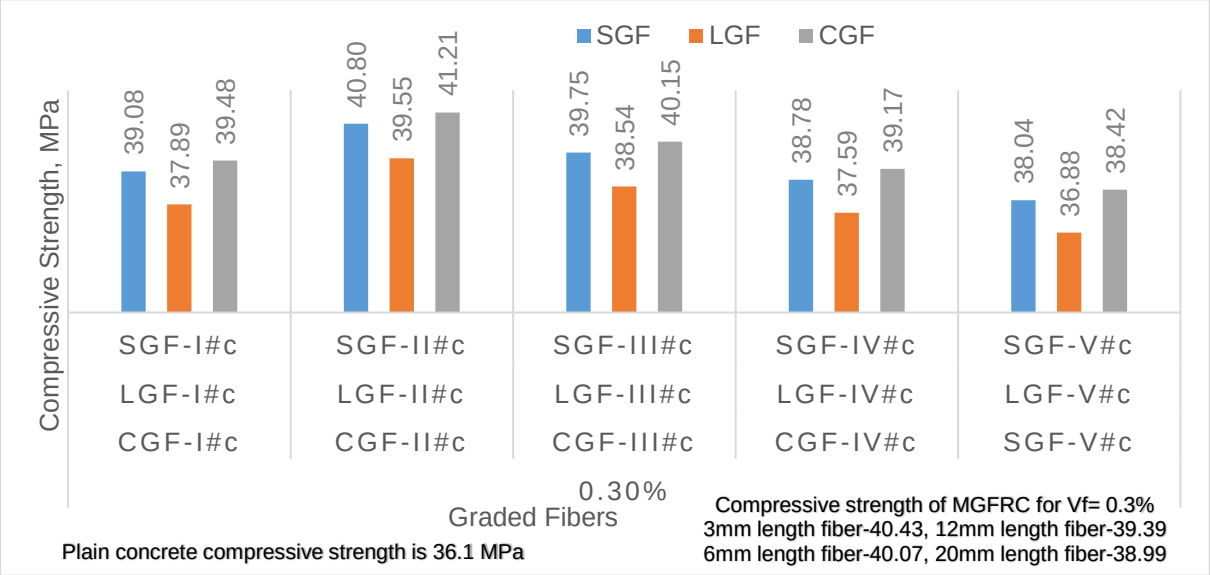

Fig.6.7 Cube Compressive strength of M30-GGFRC with V_f = 0.3%

6.2.3 (b). Comparison of cube compressive strength of M30-GGFRC-0.4% and 0.5% with M30-MGFRC-0.4% and 0.5%

Similar compression test was conducted for M30-GGFRC with 0.4% and 0.5% volume fraction and results shown in Fig.6.8 and 6.9. The mix with 0.4% and 0.5% of MGFRC have given the considerable decrease in compressive strength. That is due to the non-uniform distribution of fiber in the fresh mixes and also may be due to voids and flaws in the hardened composite. similar to 0.3% volume fraction of M30-GGFRC, in the short graded fibers, SGF-II#d and SGF-II#e showed the highest compressive strength and also than that of mono glass fibers (3mm, 6mm). Among all the long graded fibers, LGF-II#d and LGF-II#e showed the highest compressive strength and also than that of mono glass fibers (12mm, 20mm). It can be seen that short graded fiber mixes showed higher compressive strength than that of long graded fiber mixes. Among all the mixes CGF-II#d and CGF-II#e have given the highest compressive strength. An overall observation is that, there is significant increase in the compressive strength of M30-GGFRC than M30-MGFRC.

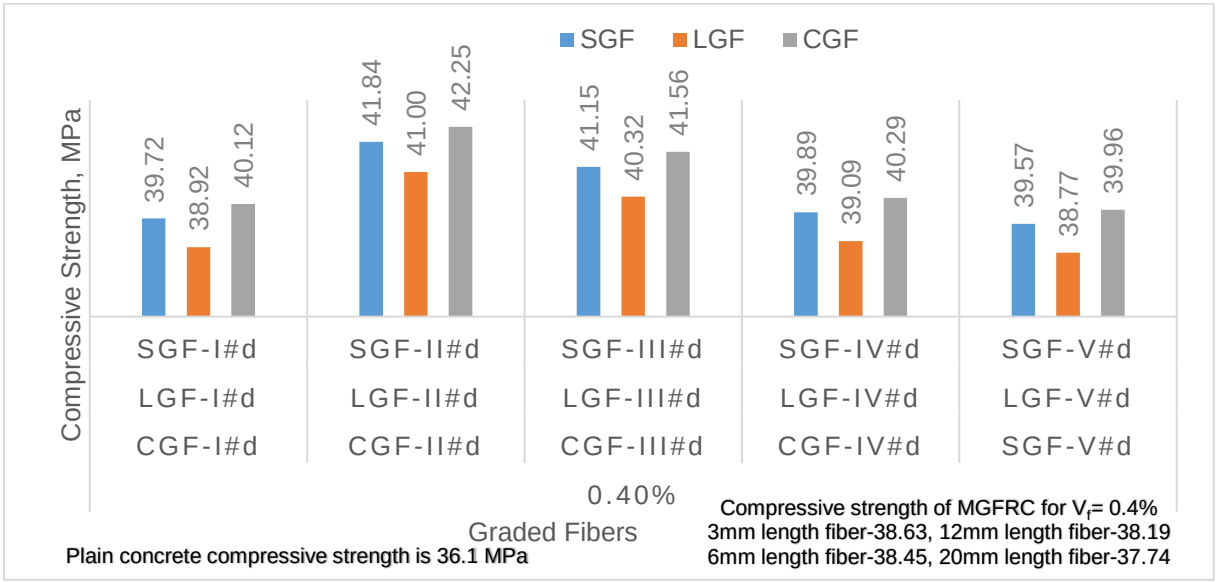

Fig.6.8 Cube Compressive strength of M30-GGFRC with V_f = 0.4%

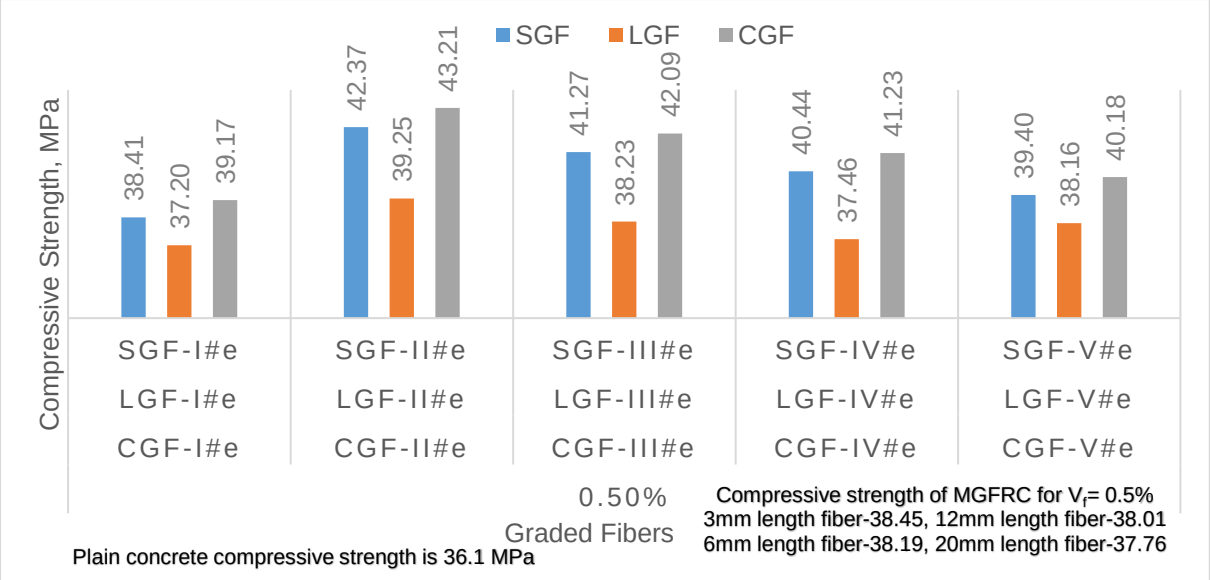

Fig.6.9 Cube Compressive strength of M30-GGFRC with V_f = 0.5%

6.2.4 Cube compressive strength of M50-GGFRC

Compression test was conducted on cube specimens of M50-GGFRC with 0.3%, 0.4% and 0.5% volume fraction as similar to the M30-GGFRC with 0.3%, 0.4% and 0.5% and shown in Fig.6.10 to 6.12. It is noticed that the M50-GGFRC cube compressive strength behaviour is similar to the M30-GGFRC of cube compressive strength behaviour. An examination with different fiber volume combinations of SGF mixes showed that cube compressive strength of SGF-II (40%3mm+60%6mm) is greater than the all other short graded fibers whereas in LGF mixes showed LGF-II (40%12mm+60%20mm) is greater than the all other long graded fibers and in case of CGF mixes showed that cube compressive strength of CGF-II (40%SGF+60%LGF) is also greater than all other combined graded fibers. In any given volume fraction (0.3%, 0.4% and 0.5%) of M50-GGFRC, among all the mixes, CGF have given the best improvement in terms of cube compressive strength compared to MGF, SGF and LGF. It can be concluded that the combined graded fibers (CGF) improves the cube compressive strength of concrete.

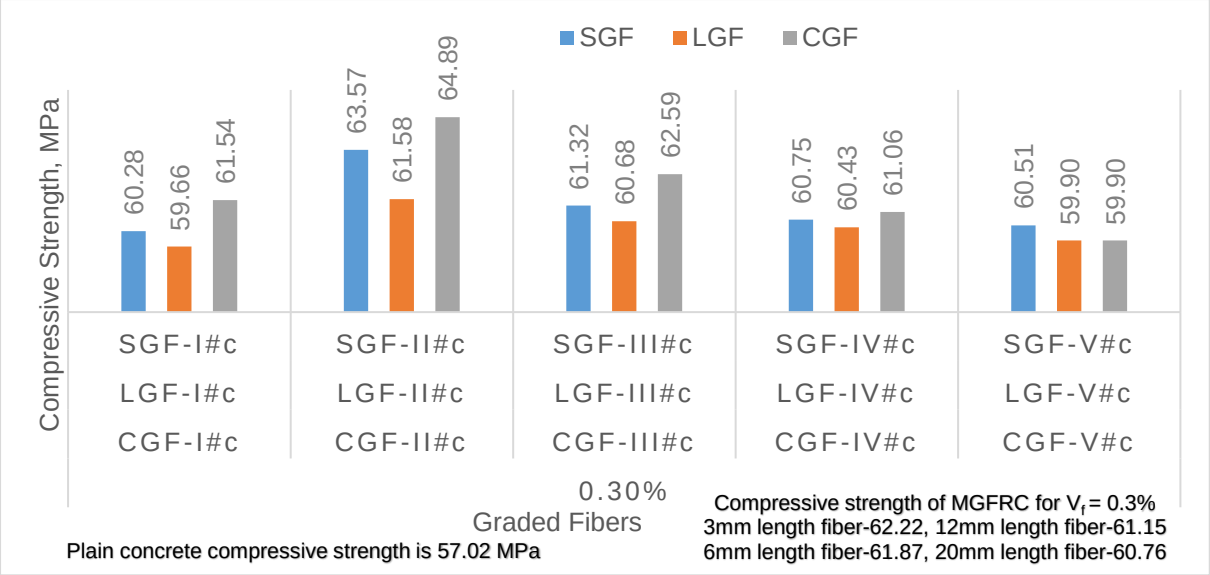

Fig.6.10 Cube Compressive strength of M50-GGFRC with V_f = 0.3%

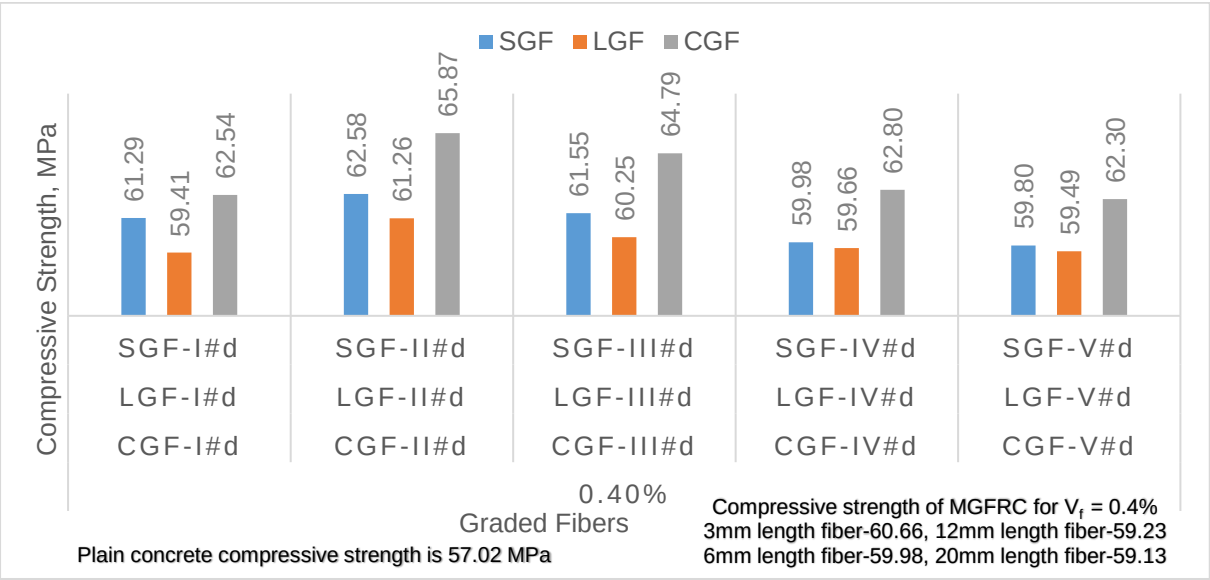

Fig.6.11 Cube Compressive strength of M50-GGFRC with V_f = 0.4%

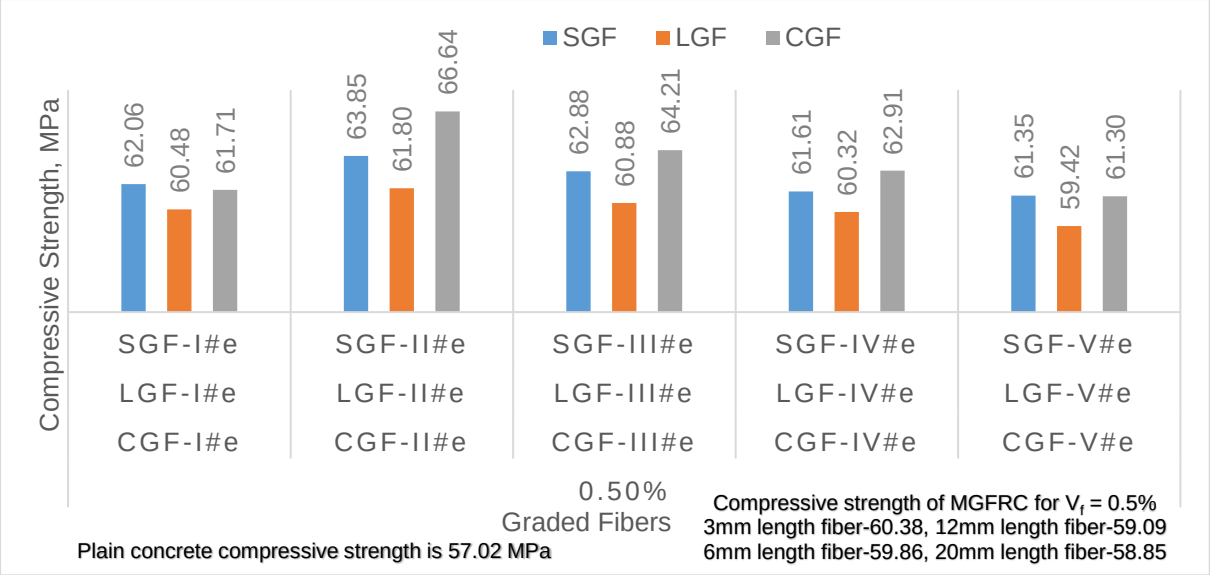

Fig.6.12 Cube Compressive strength of M50-GGFRC with V_f = 0.5%

6.3 Tensile stress strain behaviour of M30-GGFRC

6.3.1 Short Graded Fibers

3mm and 6mm length fibers are combined with five different fiber volume combinations as given in Table 4.2 of Chapter-4. Stress Strain diagram of short graded fibers (3mm+6mm) is given in Fig.6.13. Considering SGF-I#c, there is 80% of 6mm fibers. Hence the behaviour is compared with 100% 6mm fibers and it can be seen that there is not much improvement by replacing 100% 6mm fibers with 80% 6mm + 20% 3mm (SGF-I#c). A similar examination for the 3mm fibers can be observed where there is not much improvement in behaviour by replacing the 100% 3mm with 80% 3mm + 20% 6mm (SGF-V#c). The natural characteristics of mono glass fibers i.e., 3mm is reflected in SGF-V#c and 6mm in SGF-I#c. Further grading of 3mm and 6mm have exhibited completely different behaviour from mono fibers. An equal percentage of volume of fibers 3mm and 6mm i.e., 50% 3mm + 50% 6mm (SGF-III#c) have shown an intermediate behaviour between the SGF-IV#c and SGF-II#c. The specimens containing the 40% of 3mm + 60% 6mm (SGF-II#c) has given the best benefit of improvement in both strength and deformation compared to all other short graded fibers. An overall observation form the behaviour stress strain diagram of short graded fiber specimens shows that a dosage of more than 20% of 3mm or 6mm in the total volume will give an improved performance compared to mono glass fibers.

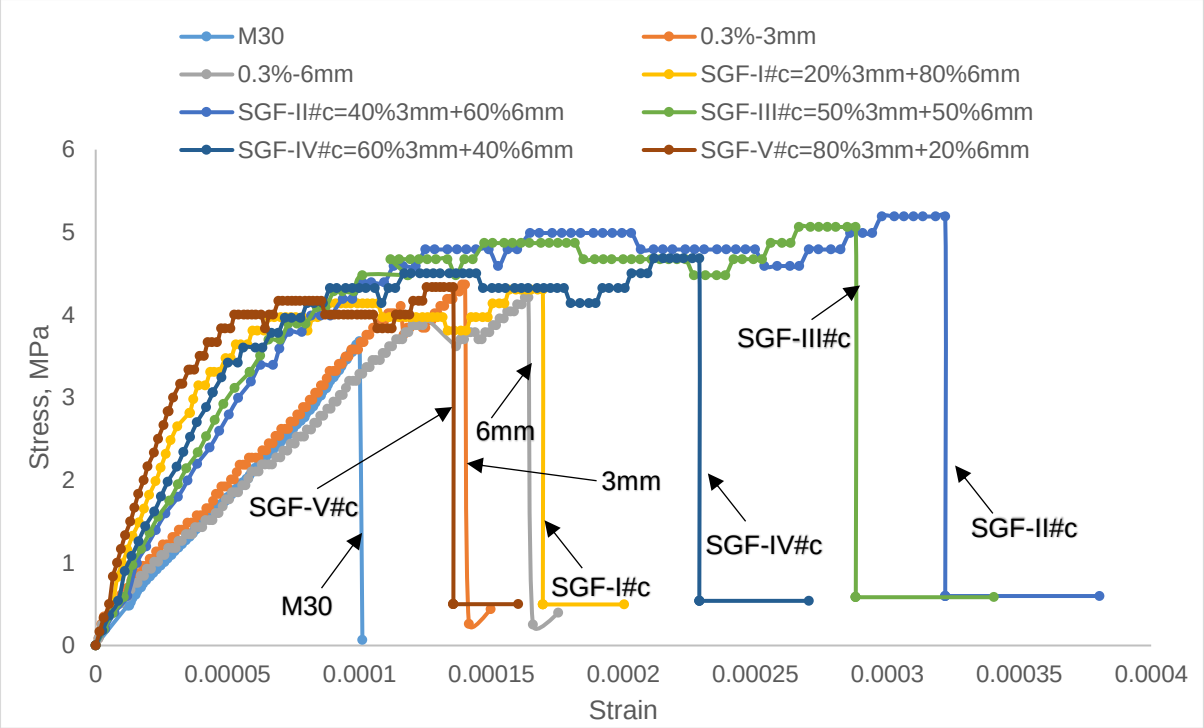

Fig.6.13 Tensile Stress-Strain behaviour of M30-SGF with V_f = 0.3%

6.3.2 Long Graded Fibers

12mm and 20mm length fibers are combined with five different fiber volume combinations are given in Table 4.2 of Chapter-4. Stress strain diagrams for long graded fiber (12mm + 20mm) is given in Fig.6.14. The natural characteristics of mono fibers i.e., 12mm is reflected in LGF-V#c and 20mm in LGF1#c. Further grading of 12mm and 20mm have exhibited completely different behaviour from mono fibers. An equal percentage of volume of fibers 12mm and 20mm i.e., 50% 12mm + 50% 20mm (LGF-III#c) have shown an intermediate behaviour between the combinations of 12mm and 20mm viz. LGF-IV#c and LGF-II#c. The specimens containing the 40% 12mm + 60% 20mm (LGF-II#c) has given the best benefit of improvement in both strength and deformation compared to all other long graded fibers. An overall observation form the behaviour stress strain diagram of long graded fiber specimens shows that a dosage of more than 20% of 12mm or 20mm in the total volume will give an improved performance compared to monofibers.

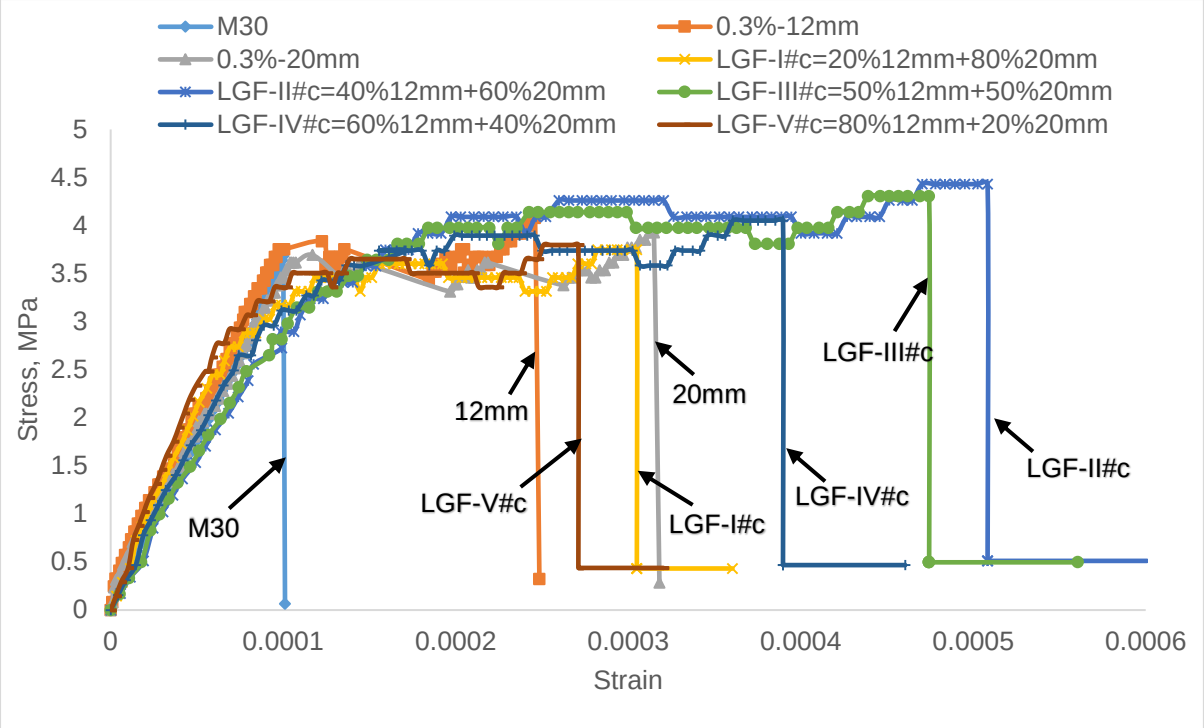

Fig.6.14 Tensile Stress-Strain behaviour of M30-LGF with V_f = 0.3%

6.3.3 Combined Graded Fibers (CGF)

Mixture of Short Fibers namely (3mm, 6mm) and Long Fibers (12mm, 20mm) is combined graded fibers. Total volume fraction in all the specimens of CGF, SGF and LGF is 0.3%. Stress Strain behaviour of CGF is compared with Mono Fibers (MF), SGF and LGF. A very interesting behaviour of stress strain diagram can be noticed with CGF. Actual volume of fibers of each length in percentage in CGF is given in Table 4.2 of Chapter-4.

6.3.3 (a) Comparison with mono fibers

Stress strain diagrams of mono fibers and CGF are shown in Fig.6.15. It can be seen that the deformation of specimens with eighty percent of short graded (3mm+6mm) in CGF-V#c, eighty percent of long graded (12mm + 20mm) in CGF-I#c is nearer to mono fibers 20mm but there is increase in strength of combined graded fiber specimens compared to mono fibers. As the volume of long length fibers increases from 40% to 60% i.e., CGF-IV#c, CGF-III#c and CGF-II#c in combined graded fiber specimen, there is progressive increase in strength and deformation.

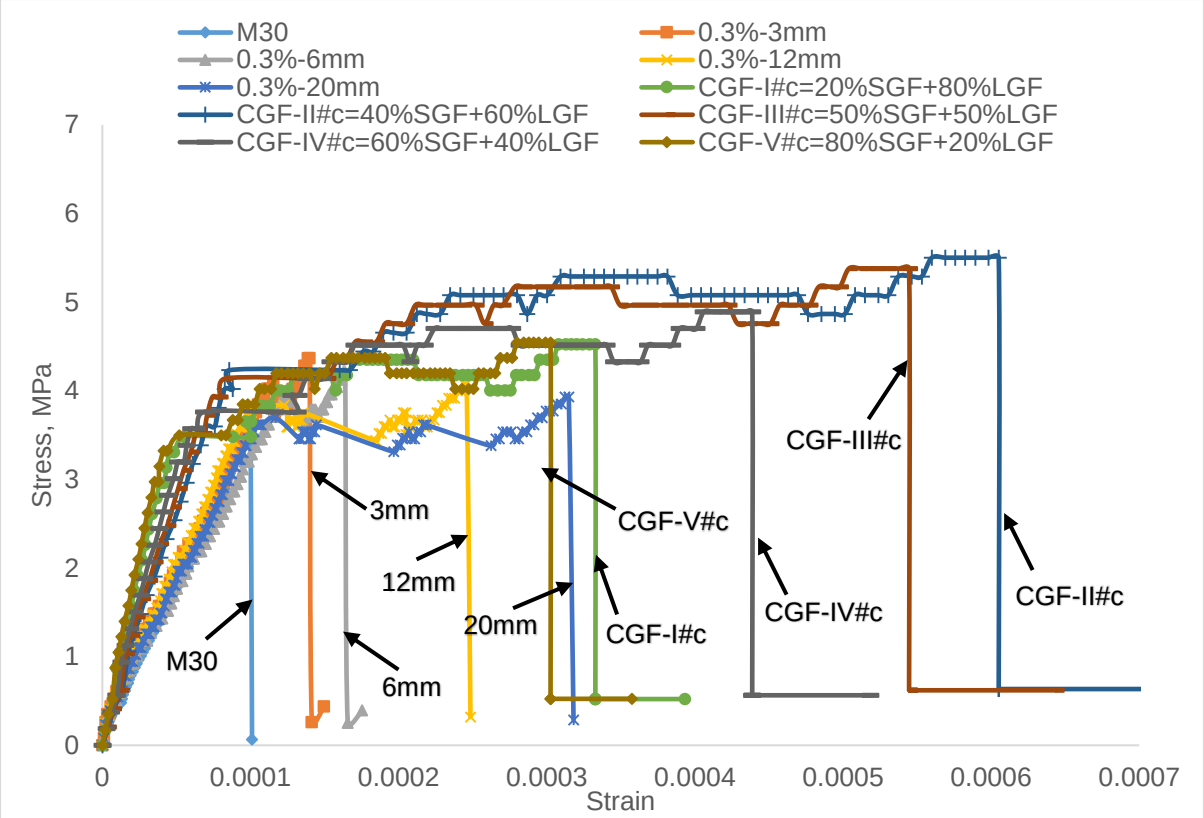

Fig.6.15 Tensile Stress-Strain behaviour of M30-CGF with V_f = 0.3%

6.3.3 (b) Comparison with short graded fibers

Stress strain diagrams of short graded fibers and combined graded fibers are shown in Fig 6.16. Eighty percent of long length fibers in CGF-I#c, eighty percent of short length fibres in CGF-V#c of combined graded fiber specimens have undergone the same amount of deformation as that of short graded fiber specimens (SGF-III#c and SGF-II#c). It is noticed in earlier section in CGF-I#c and CGF-V#c have almost same amount of deformation as mono glass fiber of 20mm length. Thus SGF-II#c, SGF-III#c, CGF-I#c, CGF-V#c and mono glass fibers of 20mm have almost nearly the same amount of of deformation but improvement in strength is highest for SGF-II#c followed by SGF-III#c, CGF-V#c, CGF-I#c compared to mono glass fibers of 20mm. As the volume of long length fibers in combined graded fiber specimen i.e., CGF-IV#c, CGF-III#c and CGF-II#c increases from 40% to 60%, strength and deformation capacity increased.

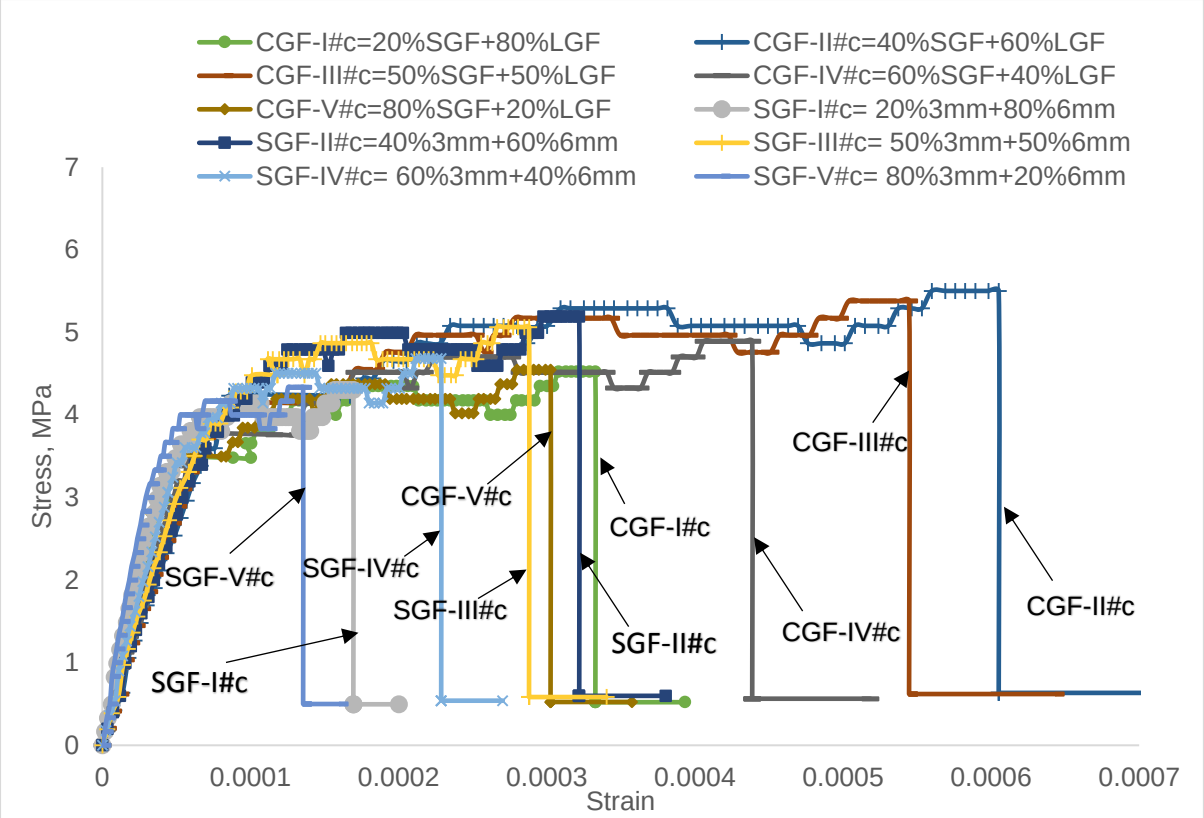

Fig.6.16 Tensile Stress-Strain behaviour of M30-CGF-0.3% compared with M30-SGF-0.3%

6.3.3 (c) Comparison with Long graded fibers

Stress strain diagram for LGF and CGF are shown in Fig.6.17. It is known that LGF means grading with 12mm and 20mm and in the combined graded specimens means the grading with SGF (3mm and 6mm) and LGF (12mm and 20mm). An examination of the above curves shows that CGF have performed better than LGF in any mixture from the type-I (20%+80%) to type-V (80%+20%). That is to say that CGF-I is better than LGF-I and so on. Among all the specimens CGF-II has given the best performance.

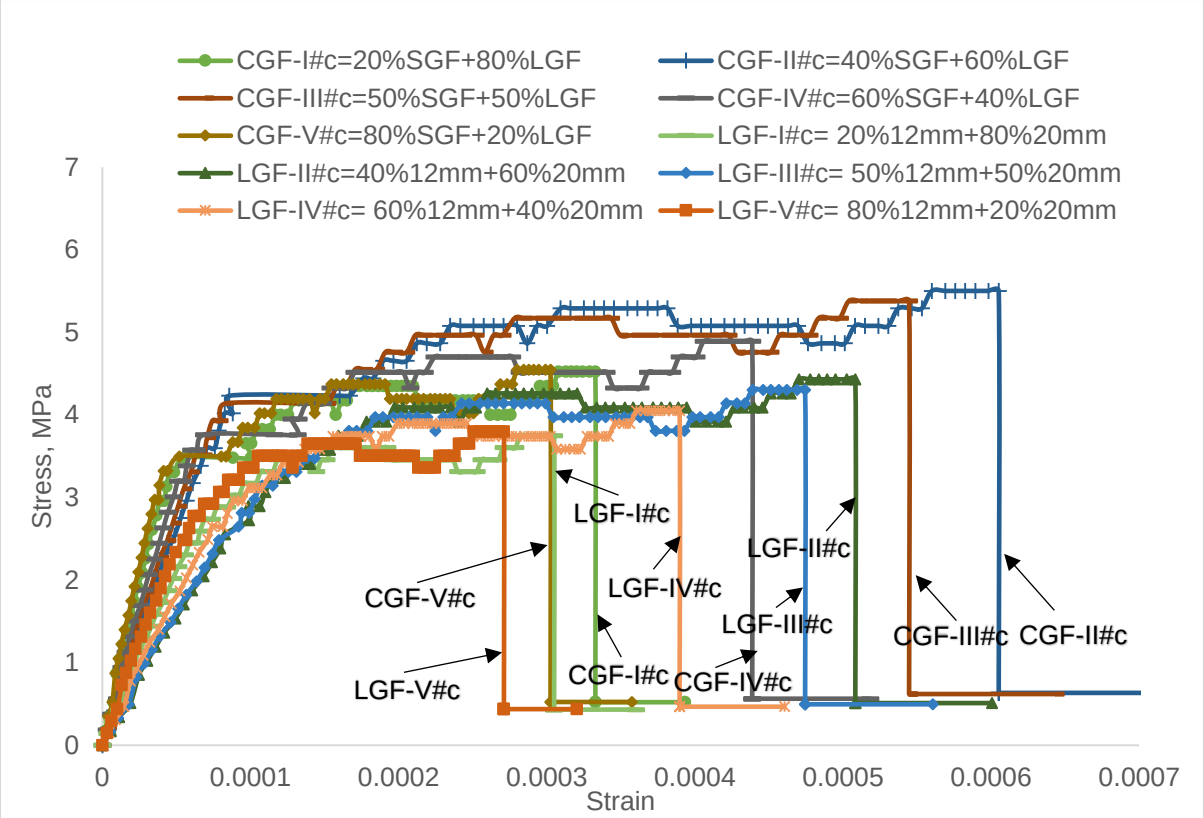

Fig.6.17 Tensile Stress-Strain behaviour of M30-CGF-0.3% compared with M30-LGF-0.3%

6.3.3 (d) Best of the best fiber combination

Stress strain diagram for mono fiber and the best performing specimen in SGF, LGF and CGF are shown in Fig.6.18. It can be seen that short graded fiber specimen results in higher strength and long graded fiber specimen results in higher deformation. Thus for the same volume in 0.3% of fibers CGF-II combined graded has the best performance. Combined graded specimens (CGF-II) have 16% of 3mm, 24% of 6mm, 24% of 12mm and 36% of 20mm length fibers. Different lengths of fibers have controlled the different levels of cracking thus contributing to increase in strength and deformation of Graded Glass Fiber Reinforced Concrete.

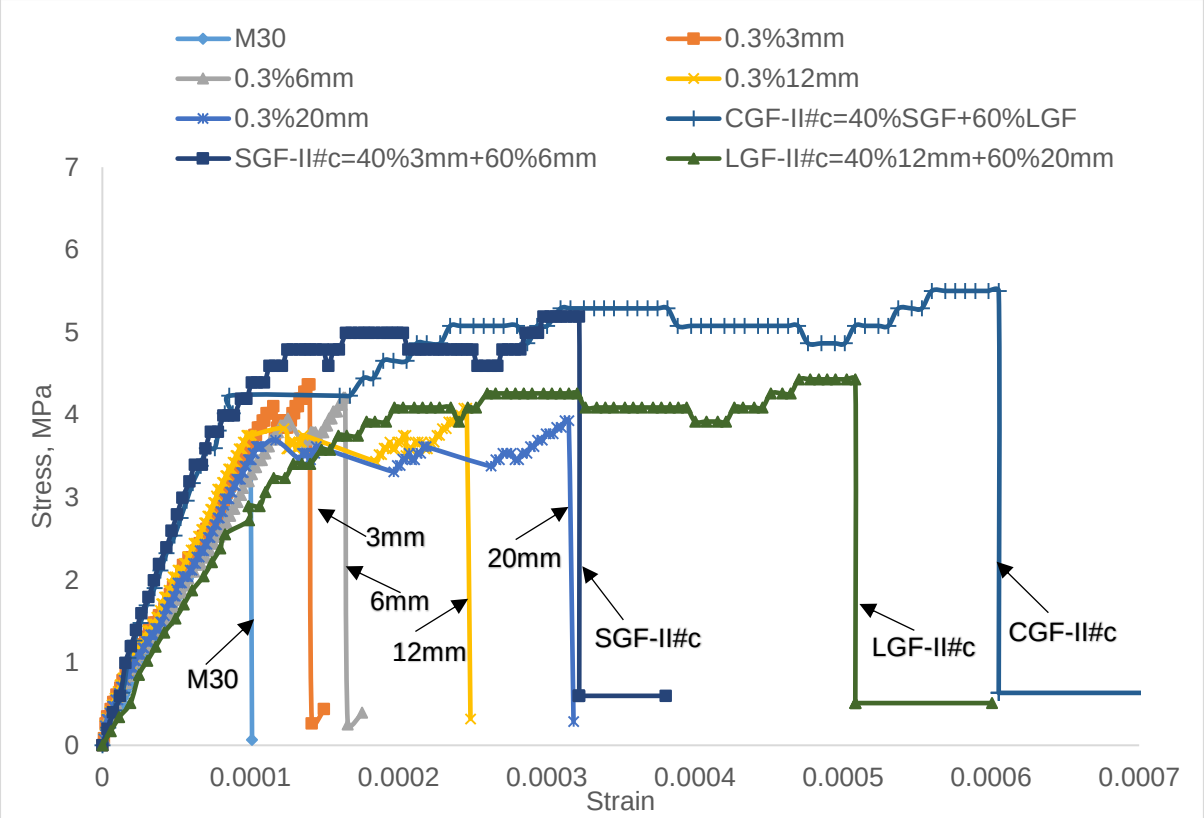

Fig.6.18 Tensile Stress-Strain behaviour of M30-CGF-0.3% compared with corresponding MF, SGF and LGF

6.3.4 Discussion about Short Graded fibers (SGF), Long Graded Fibers (LGF) Combined Graded Fibers (CGF) with volume fraction of 0.4% and 0.5%.

Stress strain diagram for SGF, LGF and CGF with the volume fraction of 0.4% and 0.5% shown in Fig.6.19 to 6.26. The specimens containing the 40% 3mm + 60% 6mm (SGF-II) has given the best benefit of improvement in both strength and deformation compared to all other short graded fibers as shown in Fig.6.19 and 6.23 irrespective of amount of volume fraction of fibers i.e., 0.4% or 0.5%. The specimens containing the 40%3mm + 60%6mm (LGF-II) has given the best benefit of improvement in both strength and deformation compared to all other long graded fibers is shown in Fig. 6.20 and 6.24 irrespective of amount of volume fraction of fibers i.e., 0.4% or 0.5%. An examination of the above curves shows that CGF have performed better than LGF in any specimen from the type-I (20%+80%) to type-V (80%+20%). That is to say that CGF-I is better than LGF-I and so on. Among all the specimens CGF-II has given the best performance is shown in Fig.6.21 and 6.25.

Stress strain diagram for mono fiber and the best performing specimen in SGF, LGF and CGF are shown in Fig.6.22 and 6.26. It can be seen that short graded fiber specimen results in higher strength and long graded fiber results in higher deformation. Thus for the same volume fraction in 0.4% and 0.5% of mixes containing CGF-II (40%SGF+60%LGF) combined graded has the best performance. Irrespective of volume of fibers i.e., 0.3%, 0.4% or 0.5%, different lengths of fibers have controlled the different levels of cracking thus contributing to increase in strength and deformation of Graded Glass Fiber Reinforced Concrete.

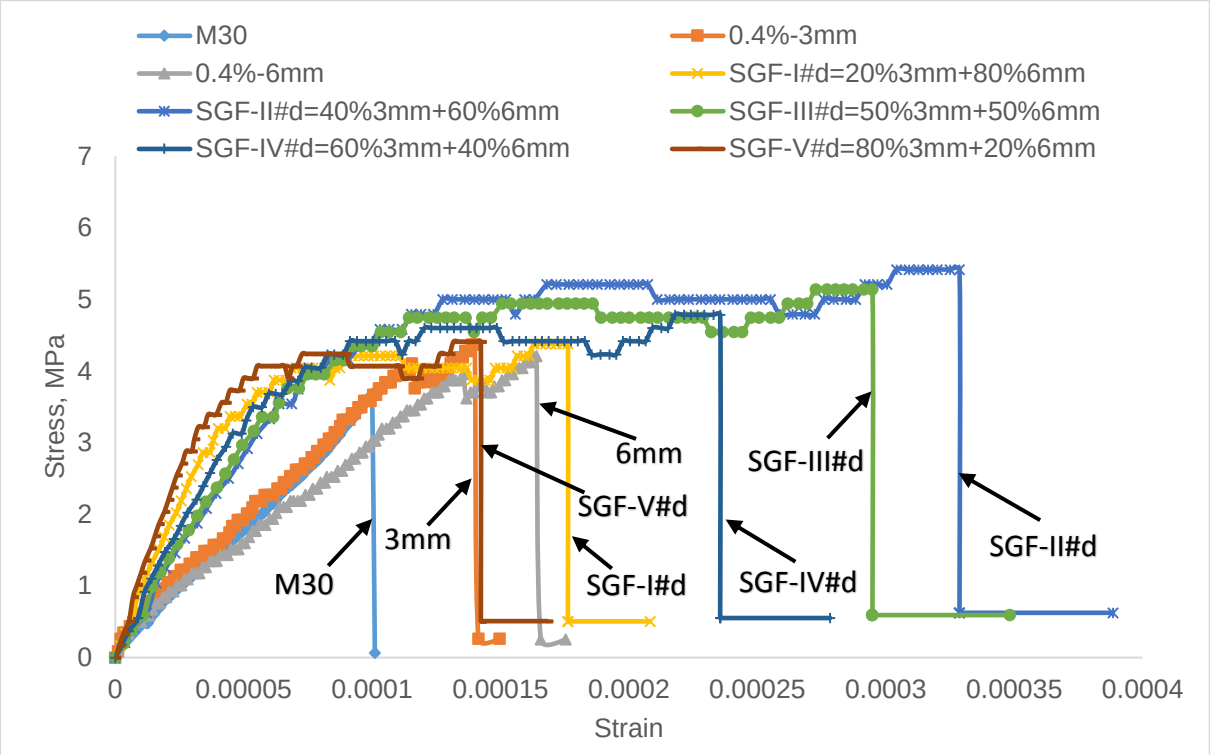

Fig.6.19 Tensile Stress-Strain behaviour of M30-SGF with V_f = 0.4%

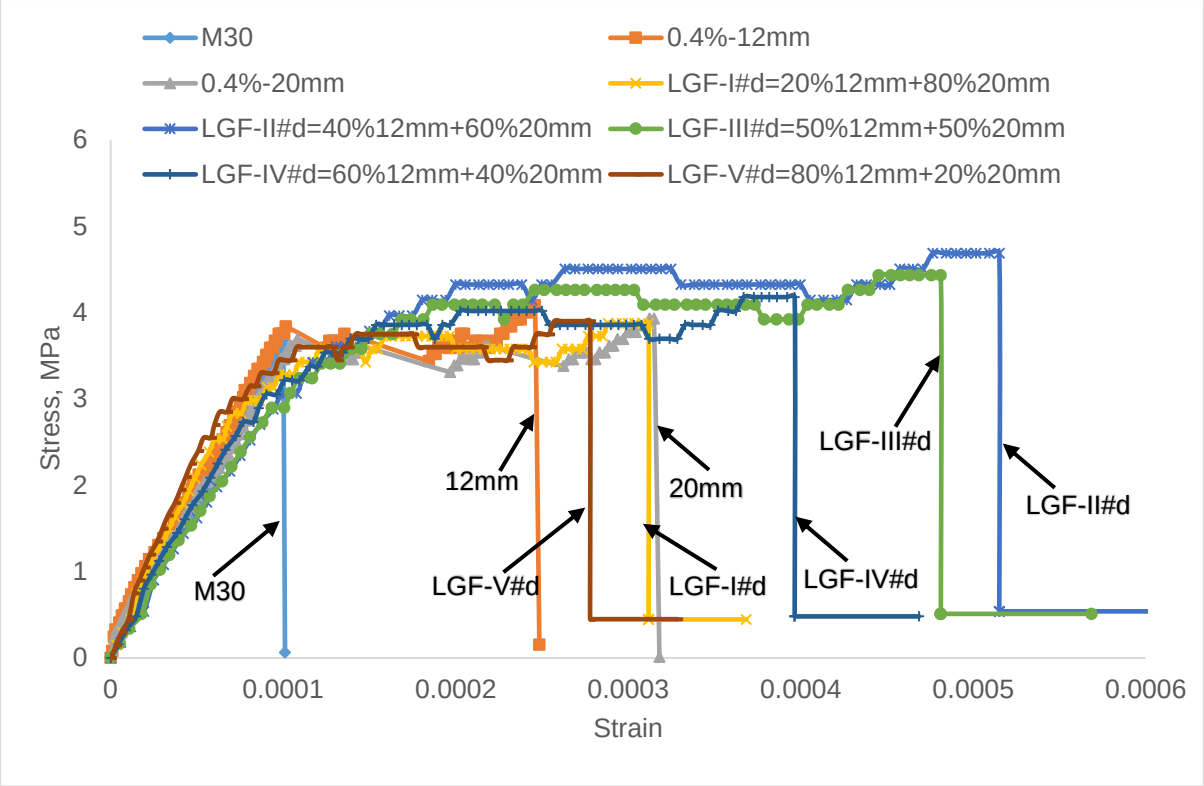

Fig.6.20 Tensile Stress-Strain behaviour of M30-LGF with V_f = 0.4%

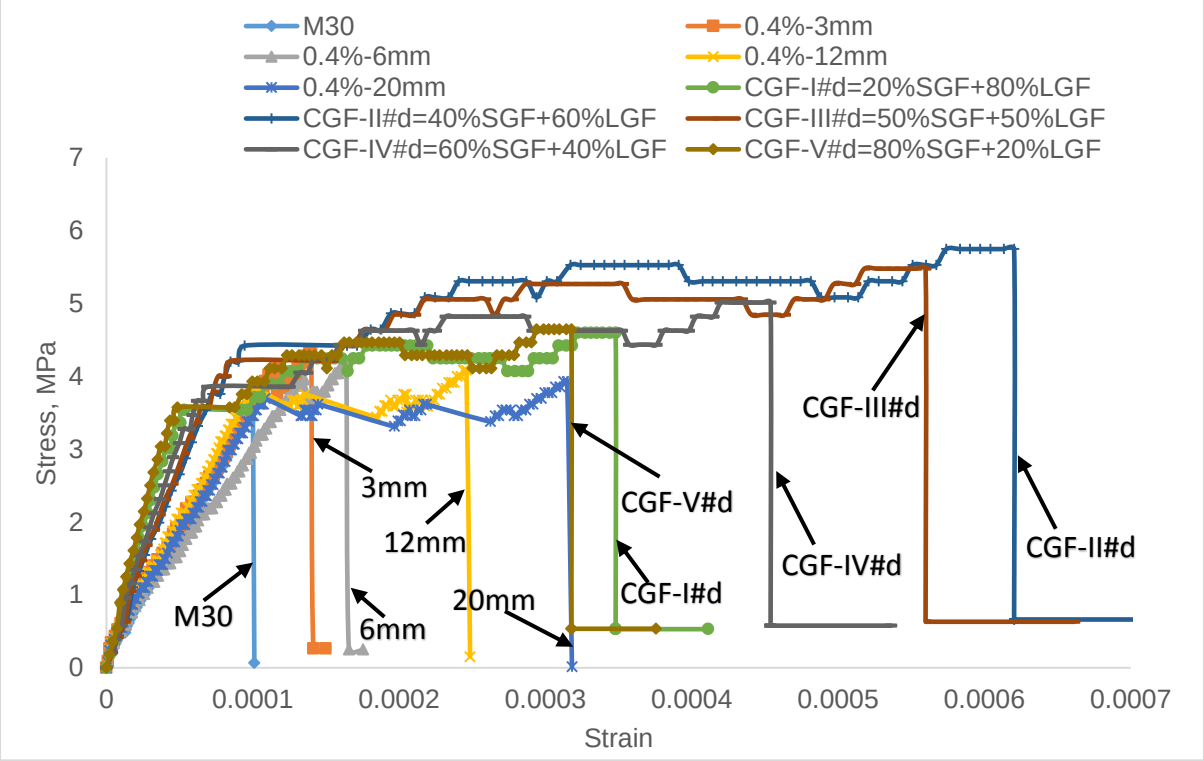

Fig.6.21 Tensile Stress-Strain behaviour of M30-CGF with V_f = 0.4%

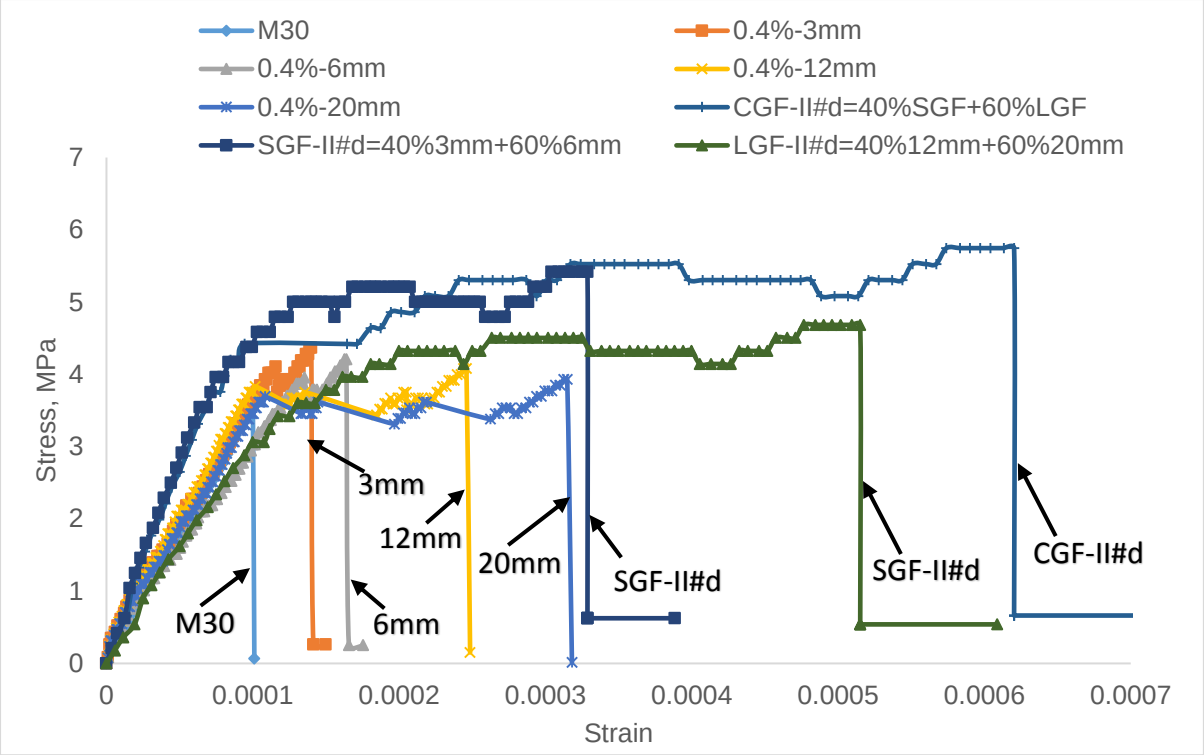

Fig.6.22 Tensile Stress-Strain behaviour of M30-CGF-0.4% compared with corresponding MF, SGF and LGF.

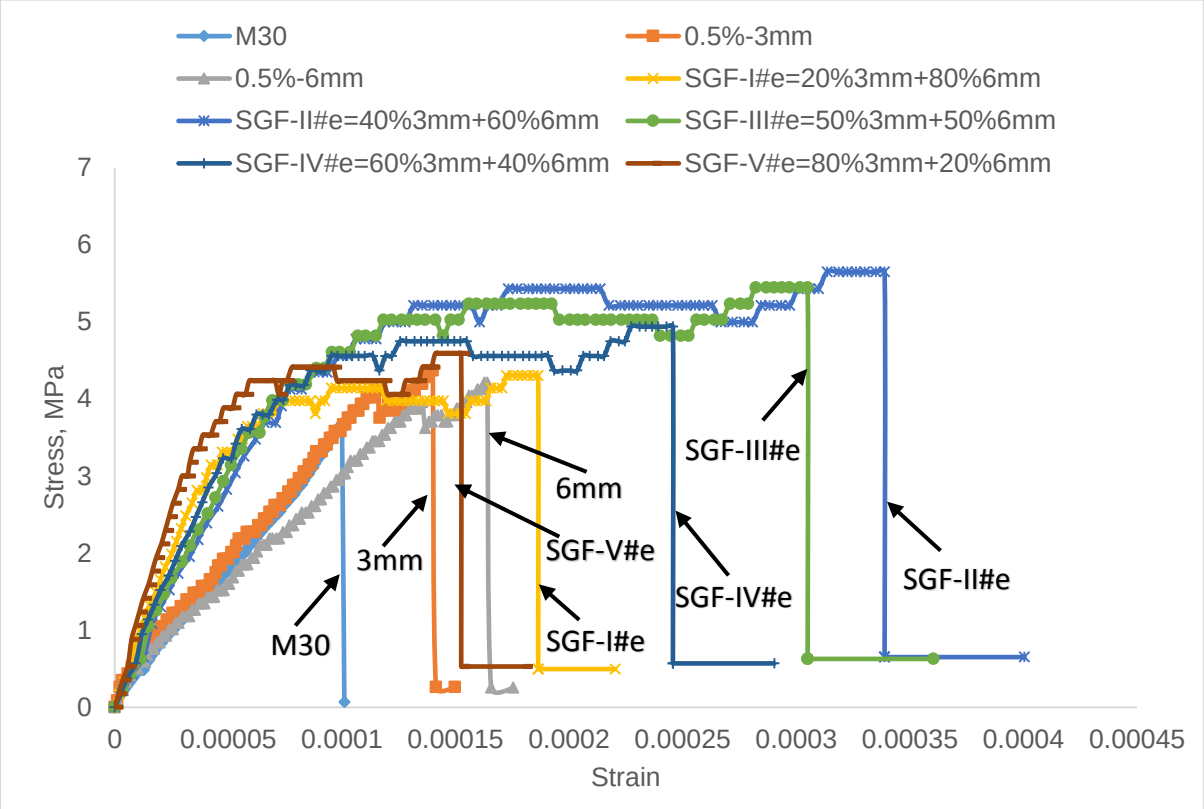

Fig.6.23 Tensile Stress-Strain behaviour of M30-SGF with V_f= 0.5%

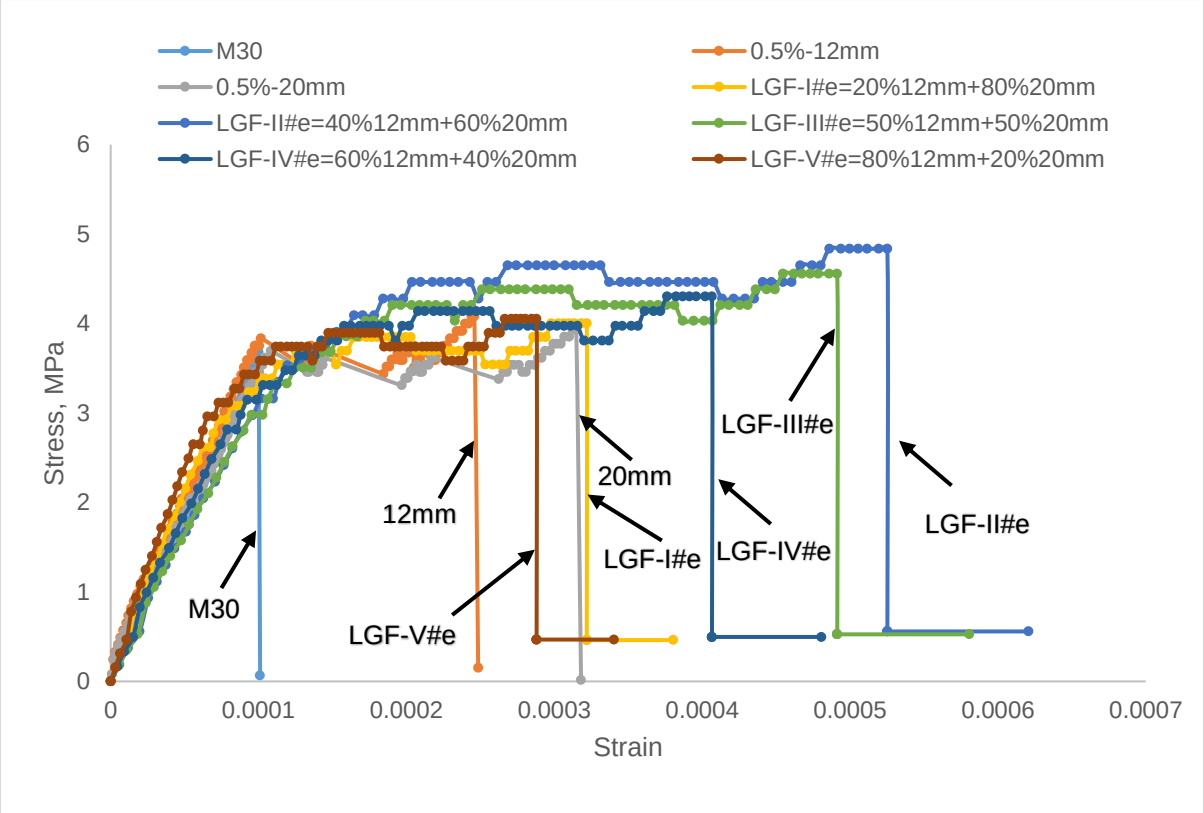

Fig.6.24 Tensile Stress-Strain behaviour of M30-LGF with V_f= 0.5%

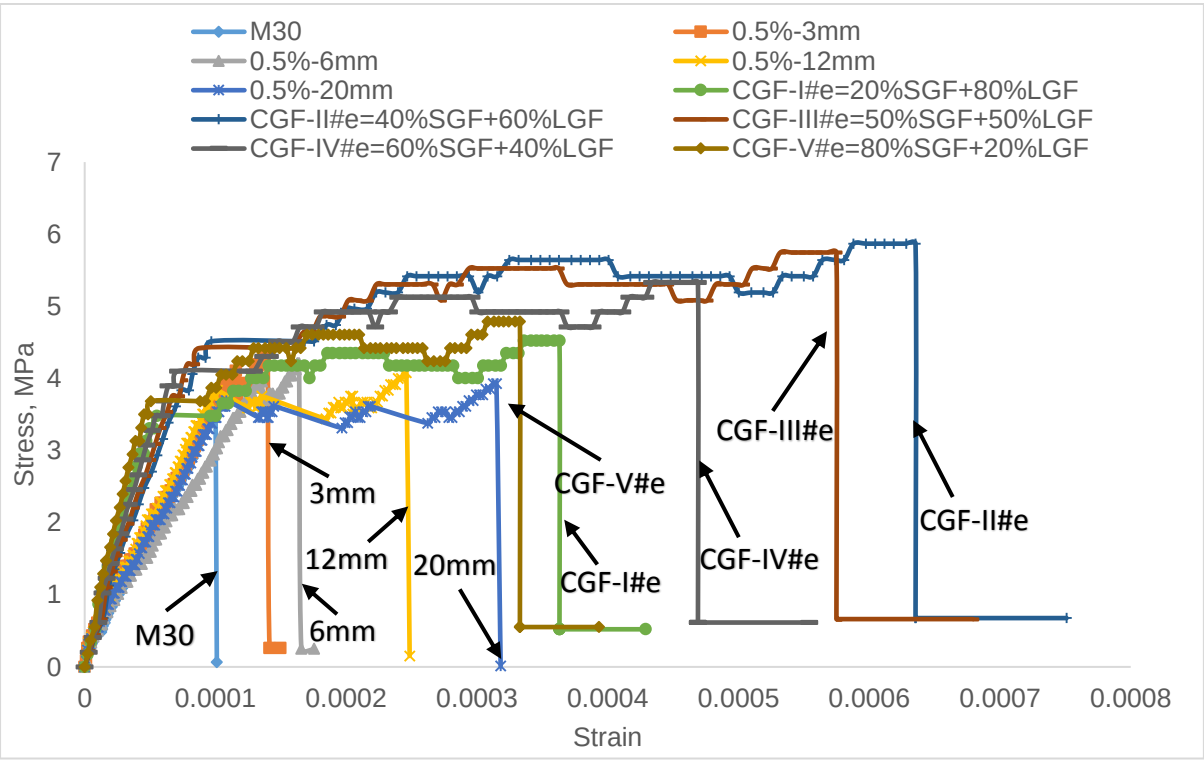

Fig.6.25 Tensile Stress-Strain behaviour of M30-CGF with V_f= 0.5%

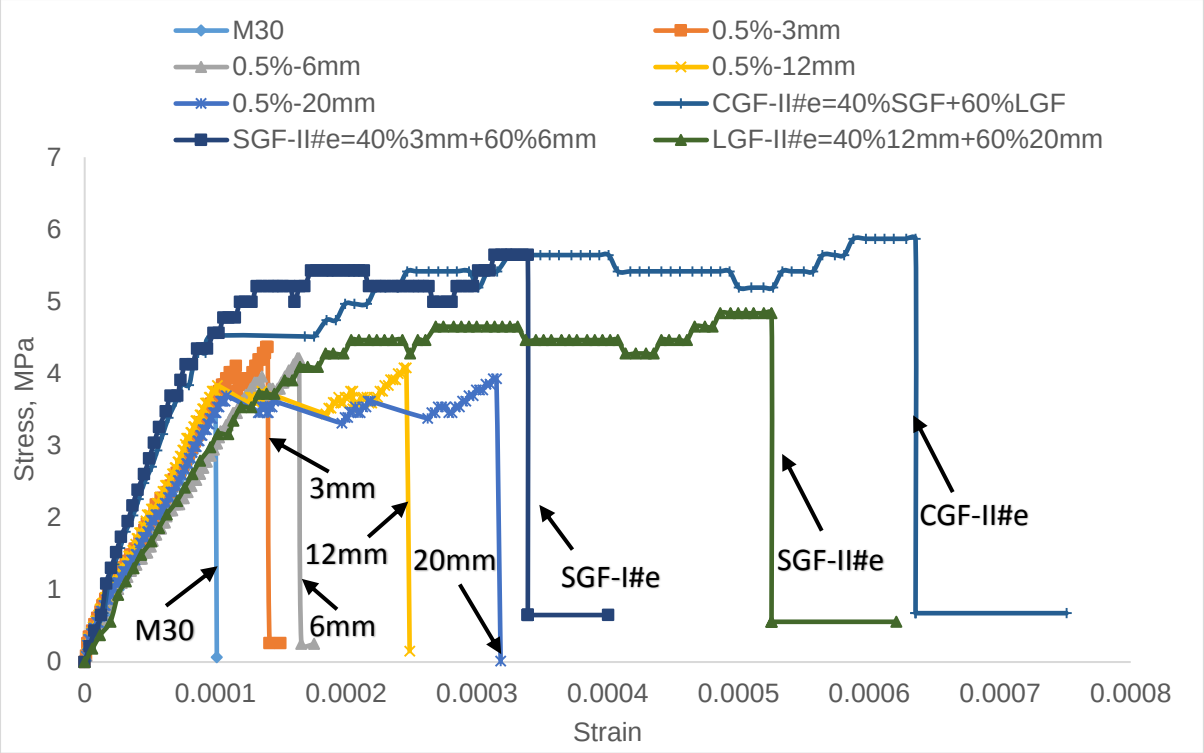

Fig.6.26 Tensile Stress-Strain behaviour of M30-CGF-0.5% compared with corresponding MF, SGF and LGF

6.4 Tensile stress strain behaviour of M50-GGFRC

Stress strain diagrams are drawn for SGF, LGF and CGF of M50 grade of concrete with volume fractions of 0.3%, 0.4% and 0.5% as shown in Fig.6.27 to 6.38. An observation of the stress strain behaviour of M50-GGFRC shows that it is similar to the stress strain behaviour of the M30-GGFRC.

Irrespective of volume of fibers i.e., 0.3%, 0.4% or 0.5%, the natural characteristics of mono glass fibers i.e., 3mm is reflected in SGF-V and 6mm in SGF-I as shown in Fig.6.27 to 6.29. Further grading of 3mm and 6mm have exhibited completely different behaviour from mono fibers. An equal percentage of volume of fibers 3mm and 6mm i.e., 50% 3mm + 50% 6mm (SGF-III) have shown an intermediate behaviour between SGF-IV and SGF-II. The specimens containing the 40% of 3mm + 60% 6mm (SGF-II) has given the best benefit of improvement in both strength and deformation compared to all other short graded fibers and can be seen in Fig.6.27 to 6.29 in all volume of fibers i.e., 0.3%, 0.4% or 0.5%.

Irrespective of volume of fibers i.e., 0.3%, 0.4% or 0.5%, the natural characteristics of mono glass fibers i.e., 12mm is reflected in LGF-V and 20mm in LGF1 as shown in Fig.6.30 to 6.32. Further grading of 12mm and 20mm have exhibited completely different behaviour from mono fibers. An equal percentage of volume of fibers 12mm and 20mm i.e., 50% 12mm + 50% 20mm (LGF-III) have shown an intermediate behaviour between LGF-IV and LGF-II. The specimens containing the 40% 12mm + 60% 20mm (LGF-II) has given the best benefit of improvement in both strength and deformation compared to all other long graded fibers can be seen in Fig.6.30 to 6.32 in all volume of fibers i.e., 0.3%, 0.4% or 0.5%.

Stress strain diagrams of mono fibers and CGF are shown in Fig.6.33 to 35 for 0.3%, 0.4% and 0.5% fiber volume fraction. It can be seen that the deformation of specimens with eighty percent of short graded (3mm+6mm) in CGF-V, eighty percent of long graded (12mm + 20mm) in CGF-I is nearer to mono fibers 20mm but there is increase in strength of combined graded fiber specimens compared to mono fibers. As the volume of long length fibers increases from 40% to 60% i.e., CGF-IV, CGF-III and CGF-II in combined graded fiber specimen, there is progressive increase in strength and deformation.

Stress strain diagram for mono fiber and the best performing specimen in SGF, LGF and CGF are shown in Fig.6.36 to 38 for 0.3%, 0.4% and 0.5% volume fraction. It can be seen that short graded fiber specimen results in higher strength and long graded fiber results in higher deformation. Thus for any given volume of fibers (0.3%, 0.4% and 0.5%) combined graded fibers (CGF-II) specimens has given the best performance when compared to the SGF-II, LGF-II and also MGF specimens.

An overall observation, irrespective of volume of the fiber i.e., 0.3%, 0.4% or 0.5%, Graded Fibers have controlled the different scales of cracking thus contributing to increase in strength and deformation of both M30 and M50 grade of concrete. Hence, it can be concluded that the graded fibers improves the strength and deformation of any normal strength concrete.

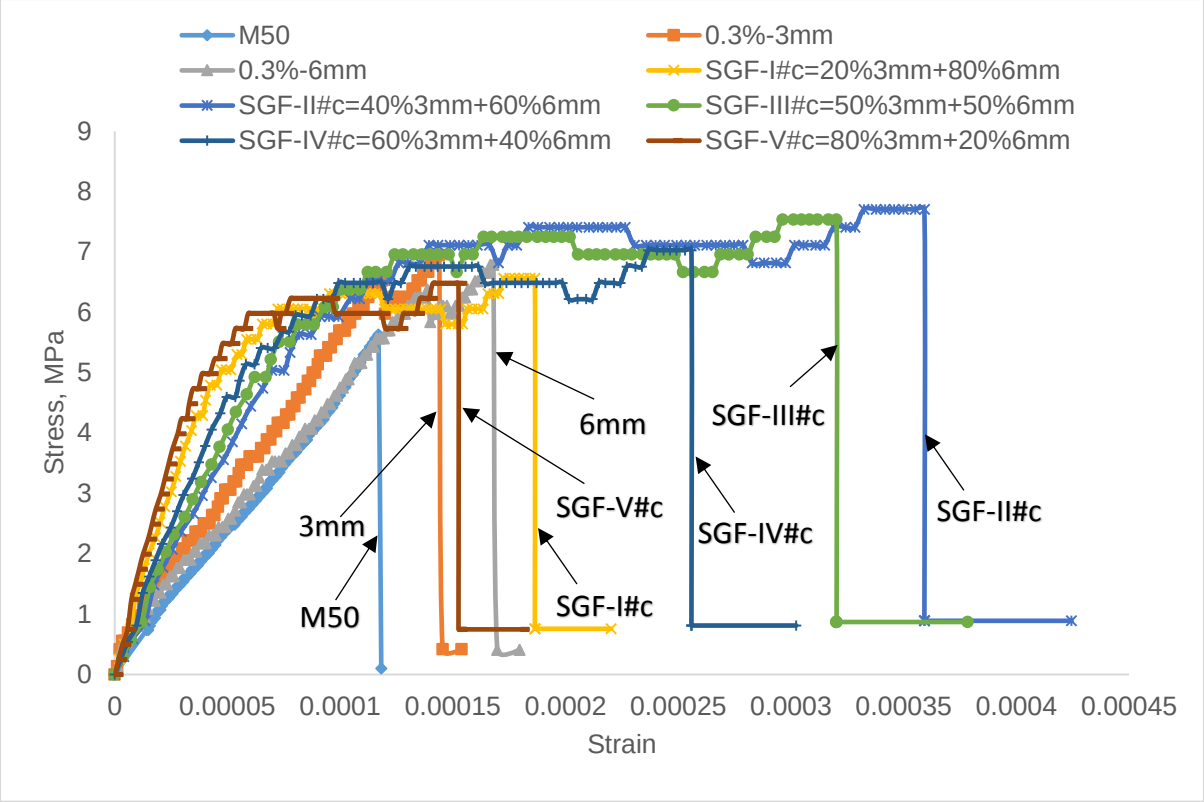

Fig.6.27 Tensile Stress Strain behaviour of M50-SGF with V_f = 0.3%

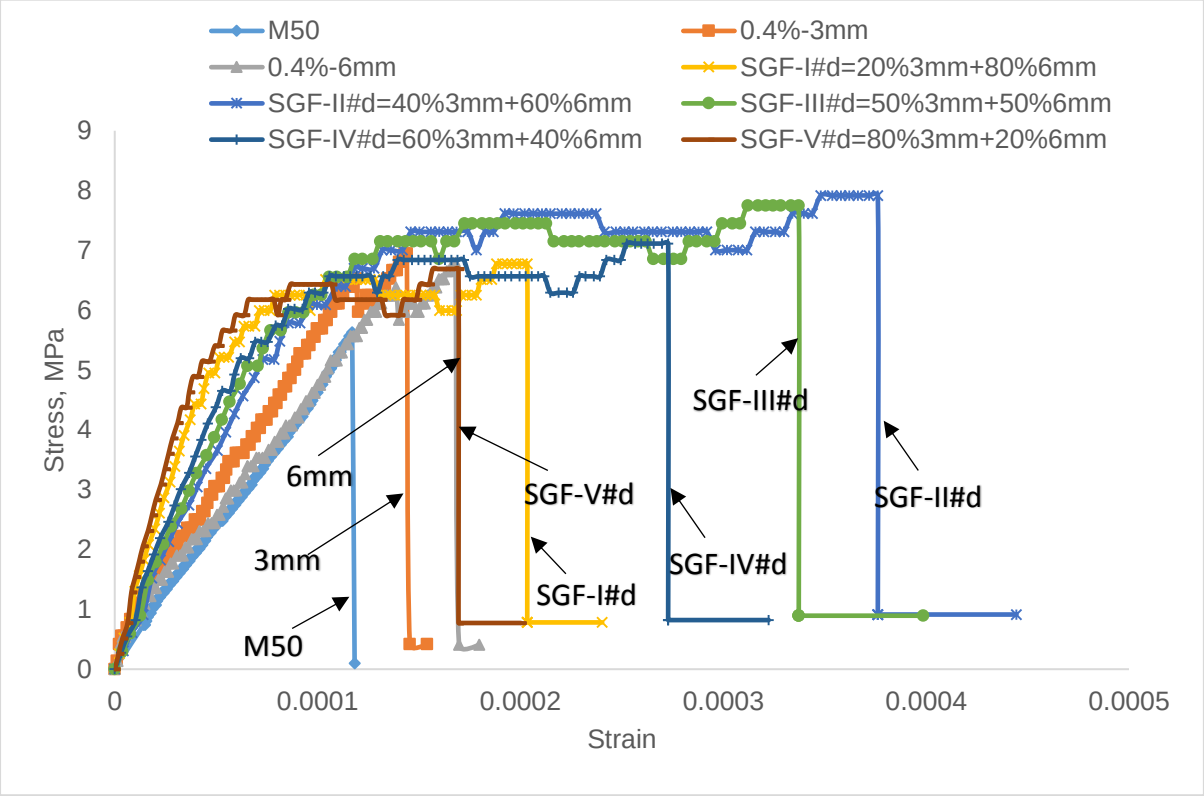

Fig.6.28 Tensile Stress Strain behaviour of M50-SGF with V_f = 0.4%

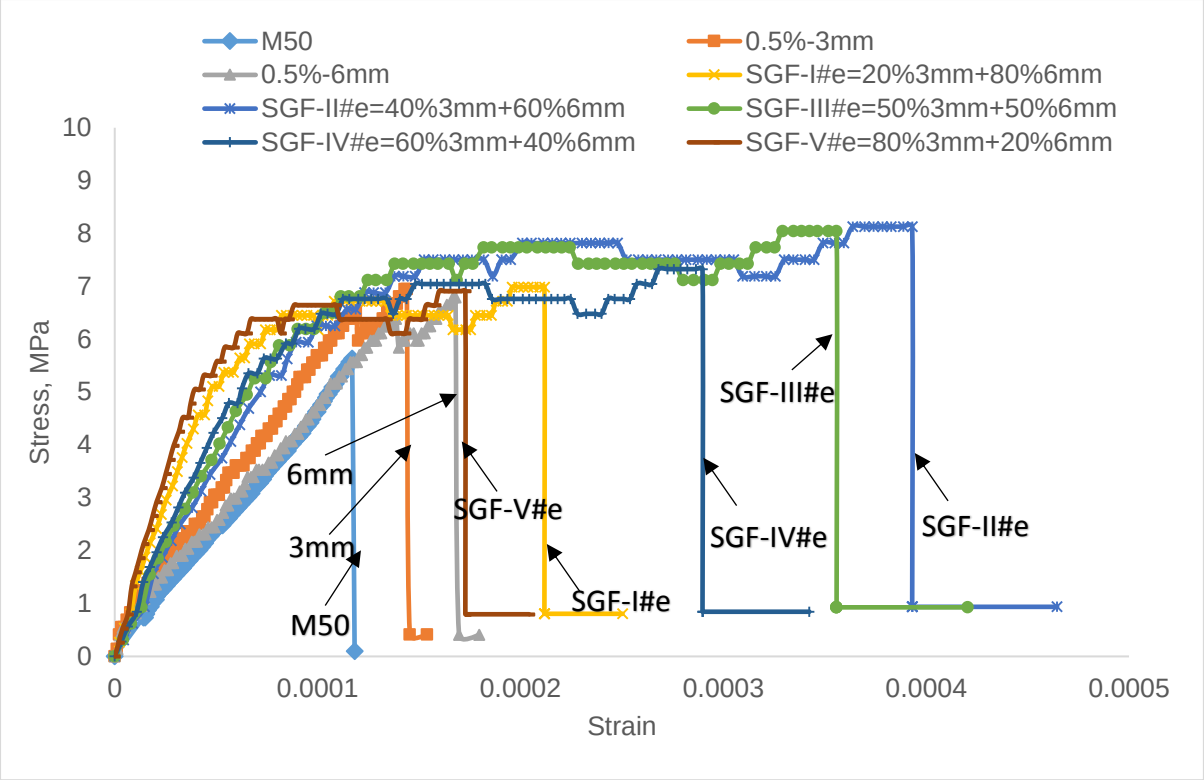

Fig.6.29 Tensile Stress Strain behaviour of M50-SGF with V_f = 0.5%

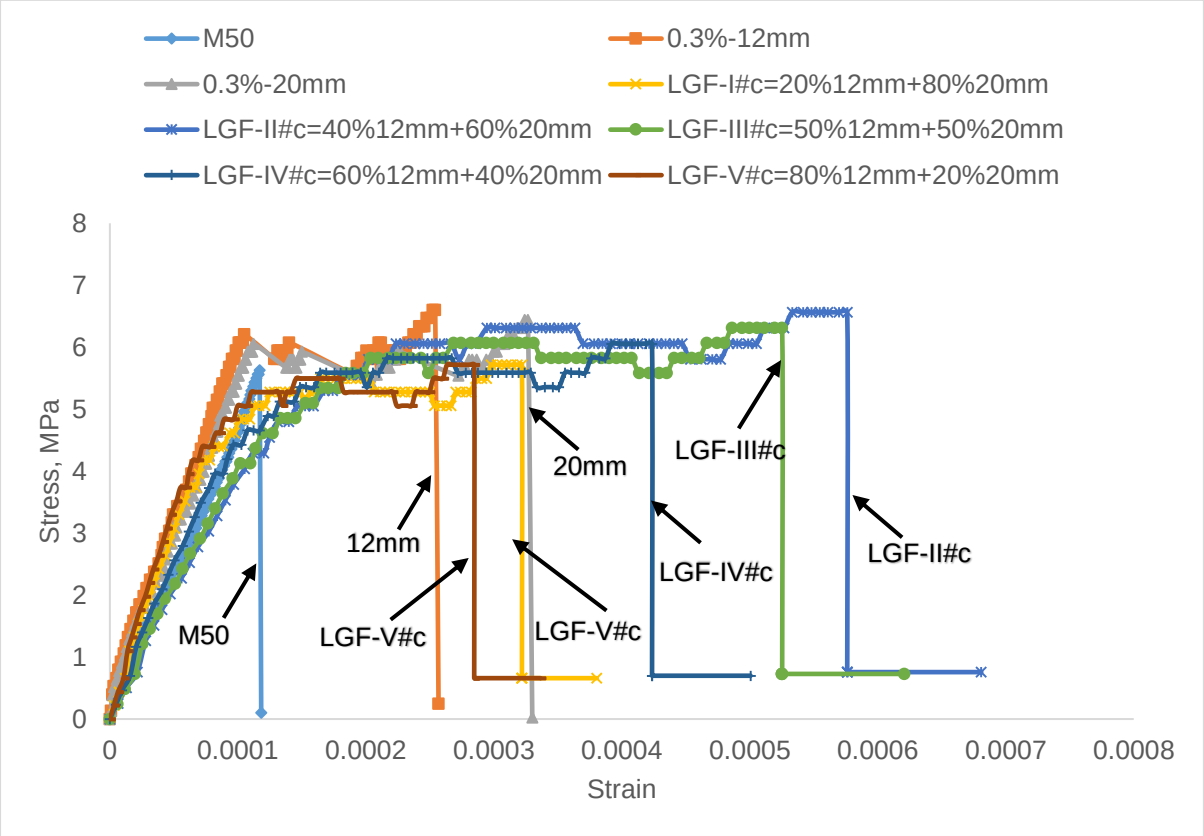

Fig.6.30 Tensile Stress Strain behaviour of M50-LGF with V_f = 0.3%

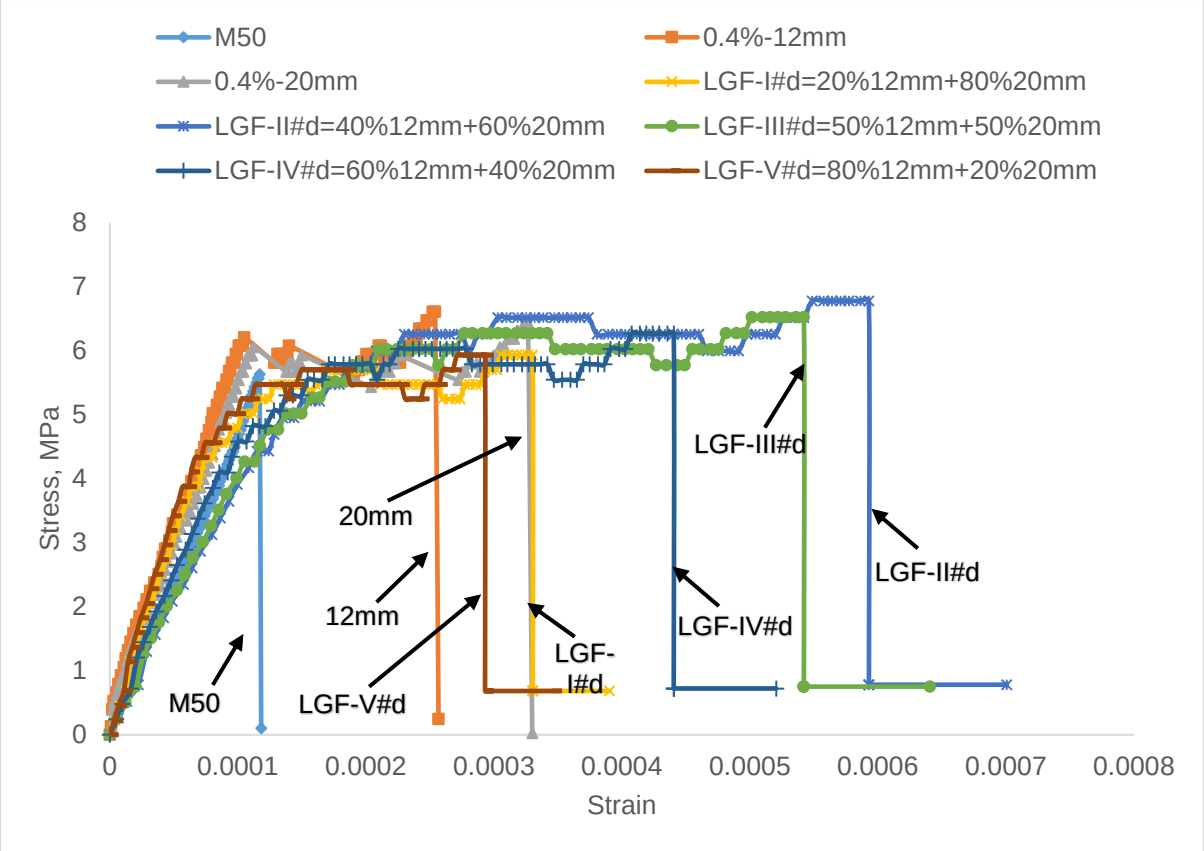

Fig.6.31 Tensile Stress Strain behaviour of M50-LGF with V_f = 0.4%

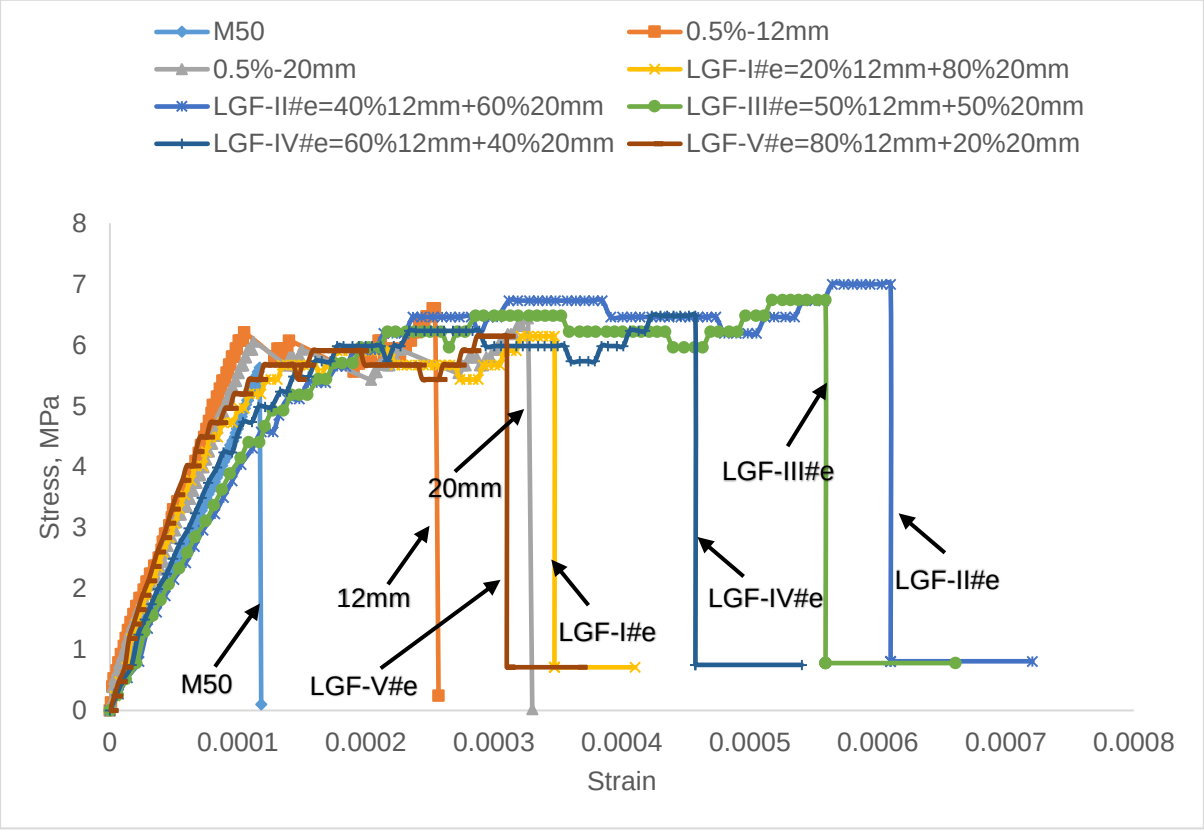

Fig.6.32 Tensile Stress Strain behaviour of M50-LGF with Vf = 0.5%

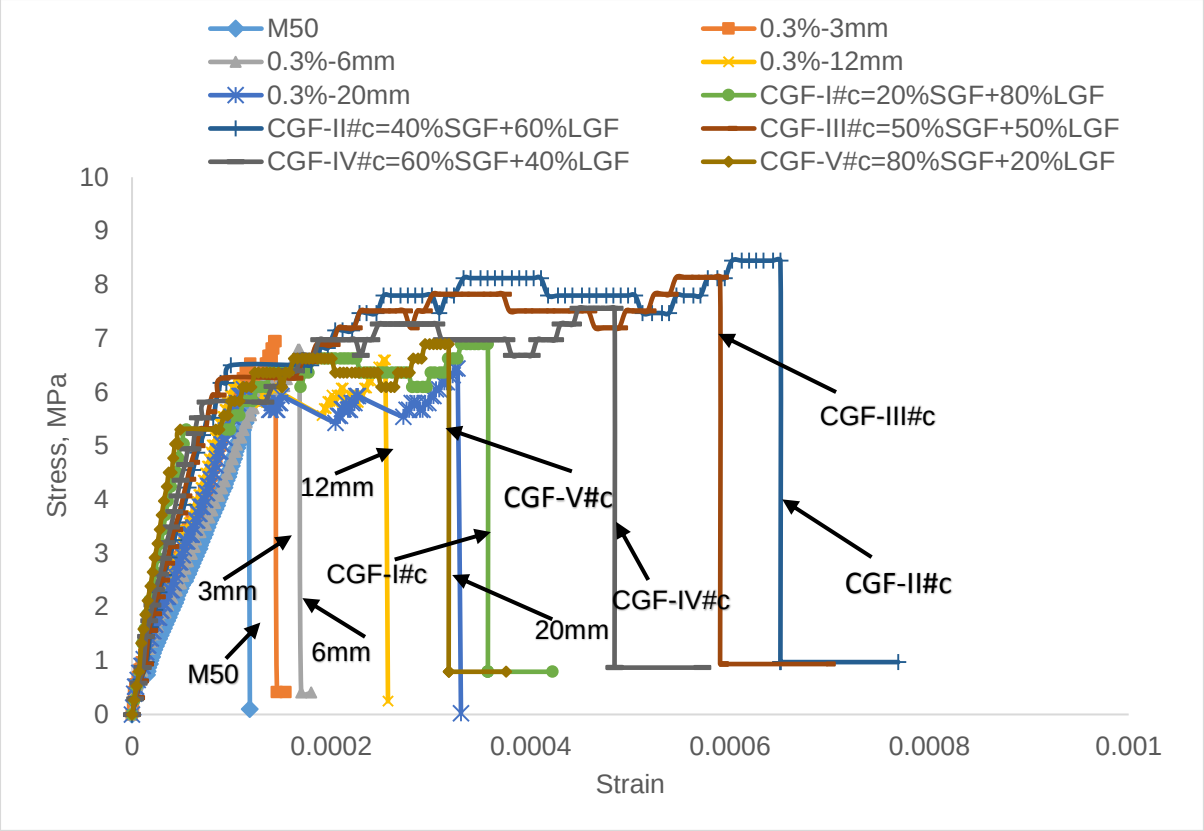

Fig.6.33 Tensile Stress Strain behaviour of M50-CGF with Vf = 0.3%

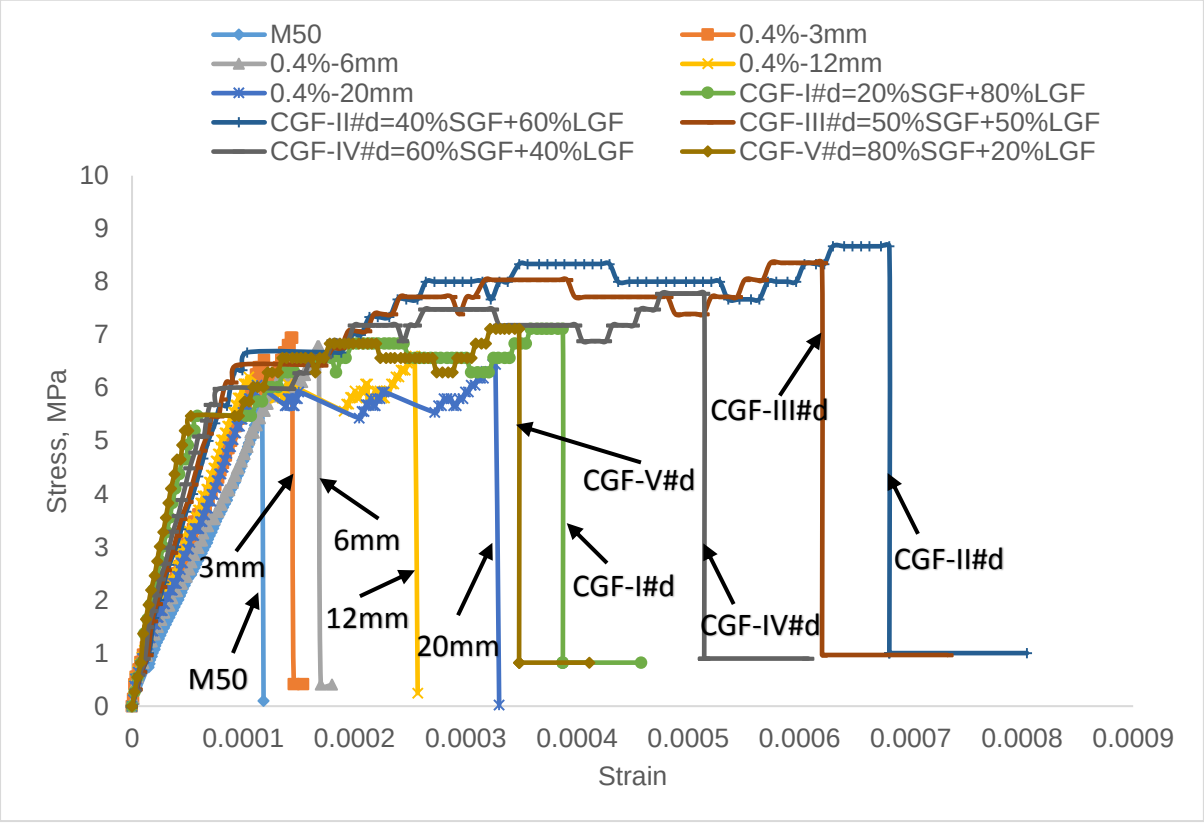

Fig.6.34 Tensile Stress Strain behaviour of M50-CGF with V_f = 0.4%

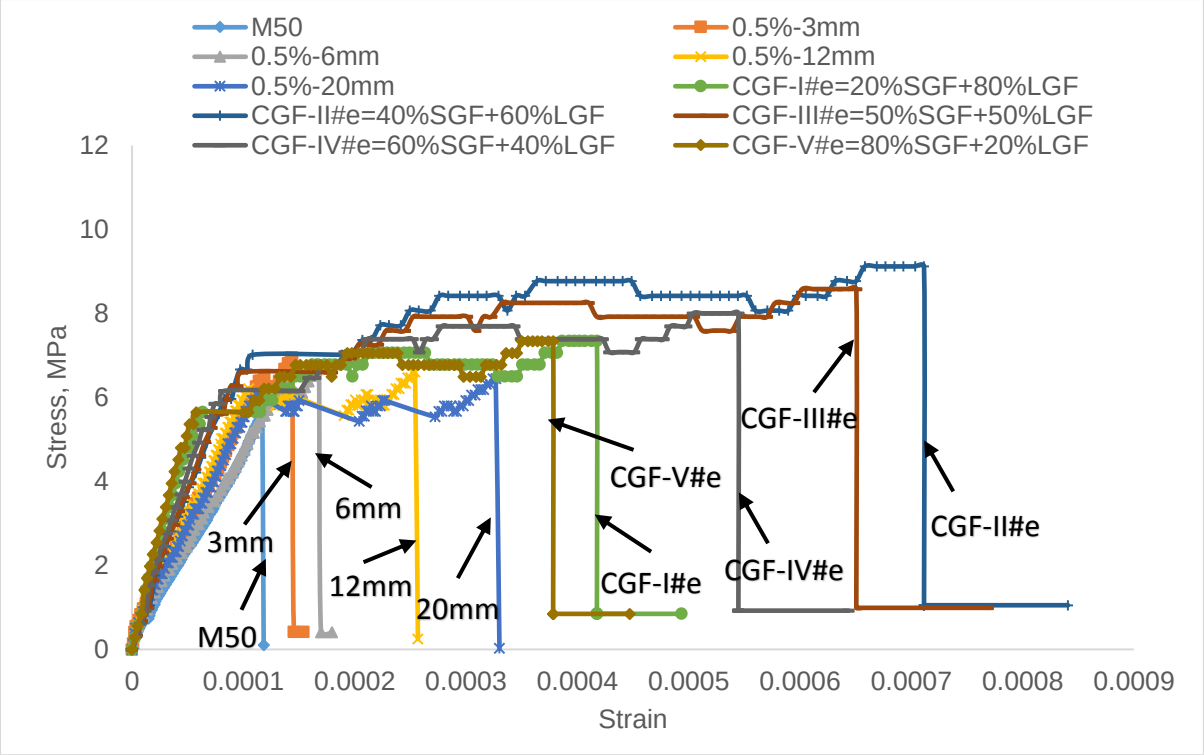

Fig.6.35 Tensile Stress Strain behaviour of M50-CGF with V_f = 0.5%

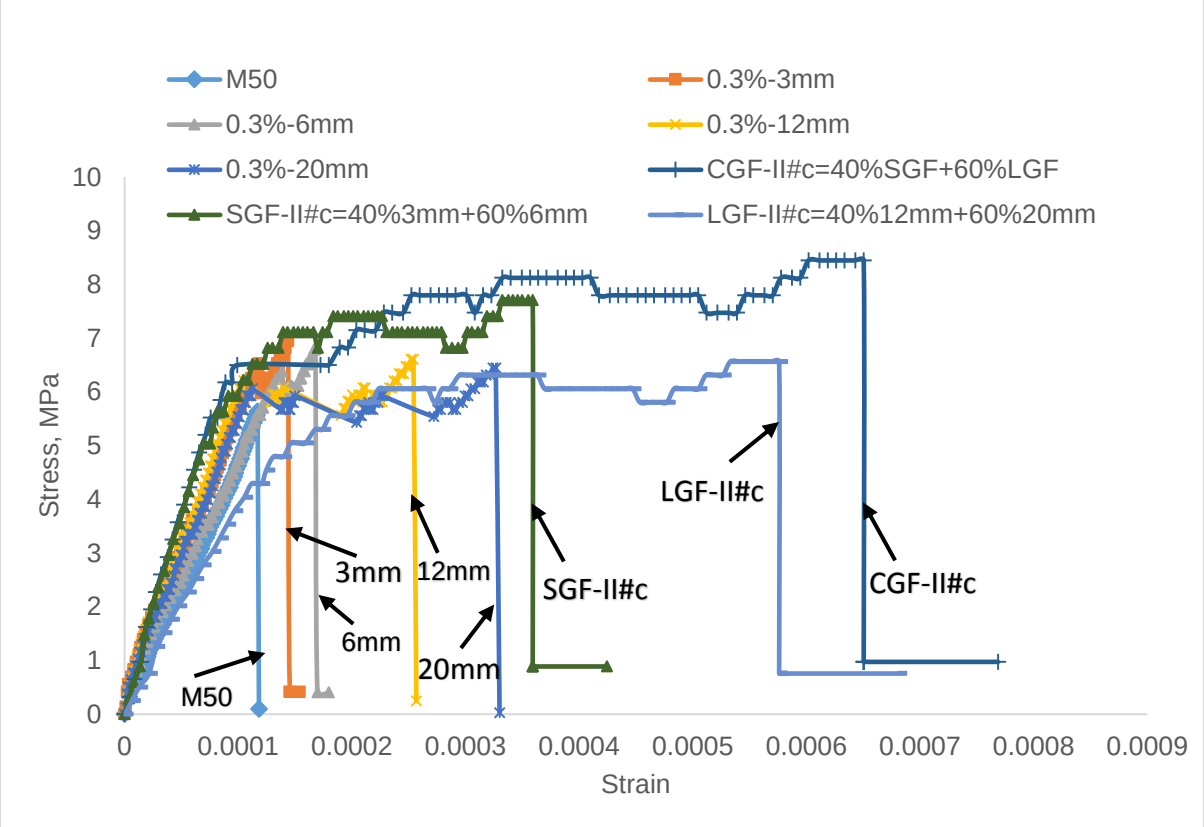

Fig.6.36 Tensile Stress Strain Behaviour of best of the best of M50-CGF-0.3% with corresponding MF, SGF and LGF

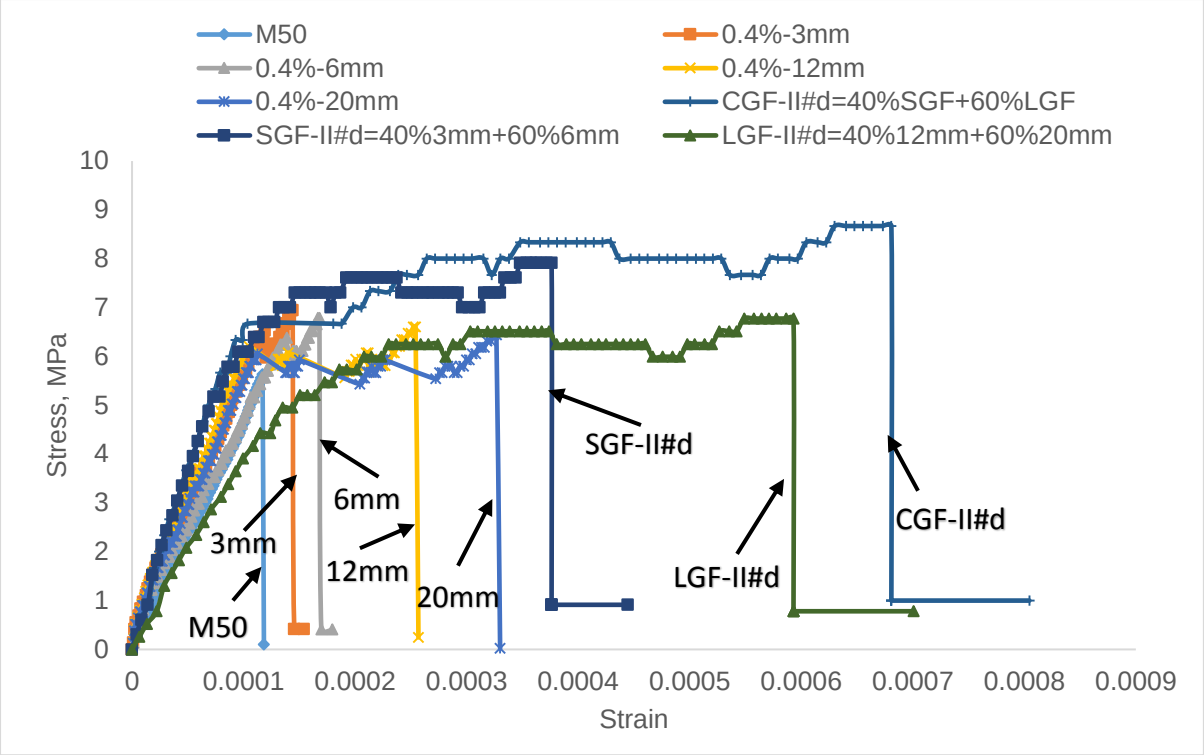

Fig.6.37 Tensile Stress Strain Behaviour of best of the best of M50-CGF-0.4% with corresponding MF, SGF and LGF

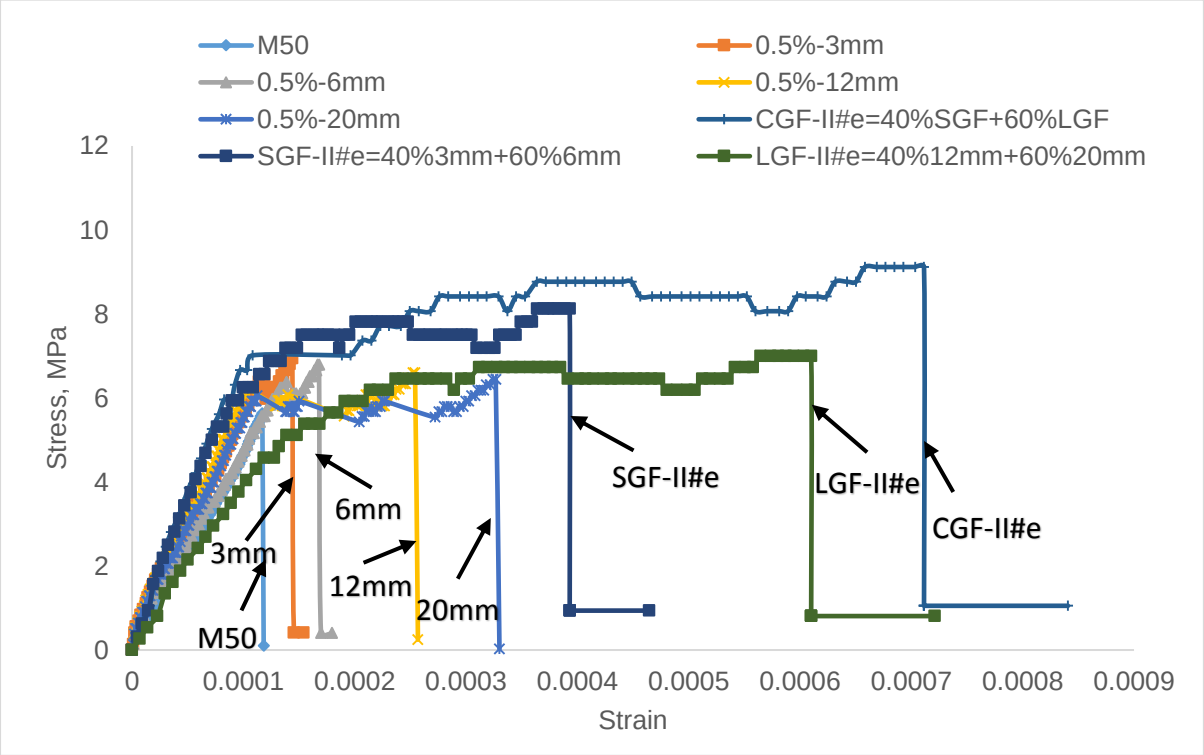

Fig.6.38 Tensile Stress Strain Behaviour of best of the best of M50-CGF-0.5% with corresponding MF, SGF and LGF

6.5 Mechanical properties of GGFRC

The salient points of GGFRC stress strain diagram shows that it is similar to the MGFRC as shown in Fig.5.16 of Chapter-5. Point P is the onset of cracking, point Q is ultimate stress and strain, point R is sudden drop in stress after peak stress and point S is breaking stress. It may be noticed that there is a slow increase in stress after reaching a stress corresponding to point P and then the specimens have undergone large deformation beyond the point P and up to point Q. Hence, the P to Q region can be called as strain hardening region.

Stress strain curves of M30-GGFRC and M50-GGFRC with 0.3%, 0.4% and 0.5% volume fraction are analysed to obtain Initial slope (E^t_i), strengthening factor (STF^t), ductility factor (DF^t), strain hardening slope (E_{SH}) and energy absorption capacity (EA_{SHR}) as similar to the stress strain curves of M30-MGFRC. Stress and strain at ultimate point Q and strain at onset of strain hardening point P are noted from the stress strain diagram for SGF, LGF and CGF and given in column 2, 3, 4 and 5 of Table 6.1, 6.2, 6.3, 6.4, 6.5 and 6.6. Initial slope (E^t_i), strengthening factor (STF^t), ductility factor (DF^t), strain hardening slope (E_{SH}) and energy absorption capacity (EA_{SHR}) are computed and given in column 6, 7, 8, 9 and 10 of Table 6.1, 6.2, 6.3, 6.4, 6.5 and 6.6. The variation of these properties as a function of five different fiber volume combinations i.e., type-I=20%+80% (20:80), II=40%+60% (40:60), III=50%+50% (50:50), IV=60%+40% (60:40) and V=80%+20% (80:20) for SGF, LGF and CGF are shown in Fig.6.39 to 6.44. The detailed explanation of above properties of stress strain curves is given in fallowing articles

6.5. (a) Initial slope (E^t_i)

The variation of initial slope (E^t_i) values for SGF, LGF and CGF with five different fiber volume combinations of 0.3%, 0.4% and 0.5% are shown in Fig.6.39 (a), 6.40 (a) and 6.41 (a). Among all the fiber volume combinations, it can be observed that the specimens with 40% 3mm+60%6mm (SGF-II) has given the lower value compared to the all other short graded fiber specimens. Similarly, in case of long graded fibers and combined graded fibers, specimens with 40% 12mm+60%20mm (LGF-II) and 40%SGF+60%LGF (CGF-II) has given the lower values compared to other long graded and combined graded fiber volume combinations. For a particular fiber volume combination i.e., 40:60, SGF-II given the higher slope than that of CGF-II and LGF-II.

An overall observation shows that, Initial slope values of SGF are more than CGF and LGF in any specimen from the type-I (20:80) to type-V (80:20) as can be seen in Fig.6.39 (a), 6.40 (a) and 6.41 (a) for 0.3%, 0.4% and 0.5% volume fraction. Moreover, it can be concluded that initial slope of SGF is lower than MGF for any given volume fraction (0.3%, 0.4% and 0.5%). Hence, lower the initial slope higher the stiffness of the composite.

The initial slope (E^t_i) behaviour of SGF, LGF and CGF for M50 grade of concrete with 0.3%, 0.4% and 0.5% volume fractions is similar to the M30-GGFRC and can be seen in Fig.6.42 (a), 6.43 (a) and 6.44 (a).

6.5. (b) Strengthening Factor (STF^t)

The variation of strengthening factor (STF) for SGF, LGF and CGF with five different fiber volume combinations of 0.3%, 0.4% and 0.5% are shown in Fig.6.39 (b), 6.40 (b) and 6.41 (b). Among all the fiber volume combinations, it can be noticed that the specimens with 40% 3mm+60%6mm (SGF-II) has given the higher strengthening factor compared to the all other short graded fiber specimens whereas in case of long graded fiber, specimens with 40% 12mm+60%20mm (LGF-II) has given the higher strengthening factor compared to other long graded specimens. An examination of the combined graded fiber, specimens with 40%SGF+60%LGF (CGF-II) showed the higher strengthening factor compared to the other combined graded specimens. For a particular fiber volume combination i.e., 40:60, CGF-II has given the higher strengthening factor than that of SGF-II and LGF-II. An overall observation is that, strengthening factor of CGF are more than SGF and LGF in any specimen from the type-I (20:80) to type-V (80:20) as can be seen in Fig.6.39 (b), 6.40 (b) and 6.41 (b) for 0.3%, 0.4% and 0.5% volume fraction.

Strengthening factor (STF^t) variations of SGF, LGF, CGF for M50 grade of concrete with 0.3%, 0.4% and 0.5% volume fractions is similar to the M30-GGFRC and can be seen in Fig.6.42 (b), 6.43 (b) and 6.44 (b).

6.5. (c) Ductility Factor (DF^t)

The variation of ductility factor (DF^t) for SGF, LGF and CGF with five different fiber volume combinations of 0.3%, 0.4% and 0.5% are shown in Fig.6.39 (c), 6.40 (c) and 6.41 (c). Among all the fiber volume combinations, it can be noticed that the specimens

with 40% 3mm+60%6mm (SGF-II) has given the higher ductility factor compared to the all other short graded fiber specimens whereas in case of long graded fiber, specimens with 40% 12mm+60%20mm (LGF-II) has given the higher ductility compared to other long graded specimens. An examination of the combined graded fiber specimens with 40%SGF+60%LGF (CGF-II) showed the higher ductility compared to the other combined graded specimens. For a particular fiber volume combination i.e., 40:60, CGF-II has given the higher ductility factor than that of SGF-II and LGF-II. An overall observation shows that, ductility factor of CGF are more than SGF and LGF in any specimen from the type-I (20:80) to type-V (80:20) as can be seen in Fig.6.39 (c), 6.40 (c) and 6.41 (c) for 0.3%, 0.4% and 0.5% volume fraction.

Ductility factor (DF^t) variations of SGF, LGF, CGF for M50 grade of concrete with 0.3%, 0.4% and 0.5% volume fractions is similar to the M30-GGFRC and can be seen in Fig.6.42 (c), 6.43 (c) and 6.44 (c).

6.5. (d) Strain Hardening Slope (E_{SH})

The variation of strain hardening slope (E_{SH}) values for SGF, LGF and CGF with five different fiber volume combinations of 0.3%, 0.4% and 0.5% are shown in Fig.6.39 (d), 6.40 (d) and 6.41 (d). Among all the fiber volume combinations, it can be observed that the specimens with 40%3mm+60%6mm (SGF-II) has given the lower strain hardening slope compared to the all other short graded fiber specimens. Similarly, in case of long graded fibers and combined graded fibers, specimens with 40% 12mm+60%20mm (LGF-II) and 40%SGF+60%LGF (CGF-II) has given the lower values of strain hardening slope compared to other long graded and combined graded fiber volume combinations. For a particular fiber volume combination i.e., 40:60, SGF-II given the higher strain hardening slope than that of CGF-II and LGF-II. An overall observation shows that, strain hardening slope values of SGF are more than CGF and LGF in any specimen from the type-I (20:80) to type-V (80:20) as can be seen in Fig.6.39 (d), 6.40 (d) and 6.41 (d) for 0.3%, 0.4% and 0.5% volume fraction. Moreover, it can be concluded that strain hardening slope of CGF is less than that of SGF, LGF and also MGF for any given volume fraction (0.3%, 0.4% and 0.5%). For any given fiber volume fraction, as the grading of fibers changes from SGF (3mm + 20mm) to LGF (12mm+20mm) and to CGF (3mm+6mm+12mm+20mm), strain hardening region increased. Hence, strain hardening region increases with improved fiber grading.

Hence, lower strain hardening slope means higher post crack deformations whereas higher strain hardening slope means lower post crack deformations.

The strain hardening slope (E_{SH}) behaviour of SGF, LGF and CGF for M50 grade of concrete with 0.3%, 0.4% and 0.5% volume fractions is similar to the M30-GGFRC and can be seen in Fig.6.42 (d), 6.43 (d) and 6.44 (d).

6.5. (e) Energy Absorption Capacity (EA_{SHR})

The variation of energy absorption capacity (EA_{SHR}) for SGF, LGF and CGF with five different fiber volume combinations of 0.3%, 0.4% and 0.5% are shown in Fig.6.39 (e), 6.40 (e) and 6.41 (e). Among all the fiber volume combinations, it can be noticed that the specimens with 40% 3mm+60%6mm (SGF-II) has given the higher energy absorption capacity compared to the all other short graded fiber specimens whereas in case of long graded fiber, specimens with 40% 12mm+60%20mm (LGF-II) has given the higher energy absorption capacity compared to other long graded specimens. An examination of the combined graded fiber, specimens with 40%SGF+60%LGF (CGF-II) showed the higher energy absorption capacity compared to the other combined graded specimens. For a particular fiber volume combination i.e., 40:60, CGF-II given the higher energy absorption capacity than that of SGF-II and LGF-II. An overall observation shows that, energy absorption capacity of CGF are more than SGF and LGF in any mixture from the type-I (20:80) to type-V (80:20) as can be seen in Fig.6.39 (e), 6.40 (e) and 6.41 (e) for 0.3%, 0.4% and 0.5% volume fraction

Energy absorption capacity (EA_{SHR}) variations of SGF, LGF, CGF for M50 grade of concrete with 0.3%, 0.4% and 0.5% volume fractions is similar to the M30-GGFRC and can be seen in Fig.6.42 (e), 6.43 (e) and 6.44 (e).

6.5. (f) Comparisons

Finally, It can be noted that the strength enhancement for short graded fibers varied from 1·17 to 1.53 and for long graded fibers 1.02 to 1.31 which shows that there was a significant improvement in strength for specimens with short graded fibers when compared to the specimens with long graded fibers. A significant enhancement in ductility occurred in case of the long graded fibers i.e., between 4.69 and 6.64, compared to short graded fibers i.e., between 3.87 and 5.63. Hence, short graded

fibers are more effective in improving the ultimate strength by delaying the formation of micro cracks and long graded fibers are more effective in increasing the deformations by bridging the macro cracks. The combination of short graded and long graded fibers to form combined graded fibers enhanced the strengthening factor form 1.23 to 1.59 and ductility factor from 5.94 to 7.88. The comparison with best of the best combinations i.e., 40%3mm+60%6mm (SGF-II), 40%12mm+60%20mm (LGF-II) and 40%SGF+60%LGF (CGF-II) showed the clear variation. Specimens with SGF-II gave 1.53 times improvement in strength whereas Specimens with LGF-II gave 6.64 times improvement in ductility. The combination of short graded and long graded i.e., combined graded fibers (CGF-II) gave 1.59 times in strength and 7.88 times in ductility. That is to say that the combined graded fibers have given the best performance compared to short graded fibers and long graded fibers in both strength and deformation. From the above observation, it can be concluded that the combined graded fibers (CGF) are better than mono glass fibers (MGF) or SGF or LGF in terms of strength and deformation.

In all, irrespective of volume of the fiber (0.3%, 0.4% and 0.5%) and grade of concrete (M30 and M50), long graded fibers (LGF) exhibited higher ductility factor, energy absorption capacity than that of short graded fibers (SGF). Short graded fibers showed higher strengthening and initial slope compared to the long graded fibers. Hence, the combination of SGF and LGF i.e., CGF have exhibited the higher strengthening factor, ductility factor and energy absorption capacity than that of SGF, LGF and MGF.

Table 6.1 Summary of test results for M30-GGFRC with V_f = 0.3% in Tension

SD (1)	Strain Hardening Region				E^t_i ($X10^4$) MPa (6)	STF^t (7)	DF^t (8)	E_{SH} ($X10^4$) MPa (9)	EA_{SHR} ($X10^{-2}$) N/mm (10)
	σ^P_t, Mpa (2)	ε^P_t, ($X10^{-4}$) (3)	σ^Q_t, MPa (4)	ε^Q_t, ($X10^{-4}$) (5)					
Short Graded Fibers (SGF), V_f = 0.3%,									
SGF-I#c	2.81	0.40	4.30	1.69	7.10	1.17	4.28	1.15	0.060
SGF-II#c	3.39	0.62	5.19	3.22	5.43	1.41	5.15	0.69	0.136
SGF-III#c	3.70	0.60	5.06	2.88	6.21	1.38	4.84	0.60	0.119
SGF-IV#c	3.42	0.54	4.68	2.29	6.29	1.27	4.21	0.73	0.087
SGF-V#c	3.33	0.35	4.30	1.36	9.51	1.17	3.87	0.97	0.048
Long Graded Fibers (LGF), V_f = 0.3%									
LGF-I#c	2.45	0.59	3.75	3.05	4.18	1.02	5.21	0.53	0.093

LGF-II#c	2.55	0.82	4.43	5.08	3.12	1.20	6.23	0.44	0.184
LGF-III#c	2.48	0.79	4.30	4.74	3.13	1.17	5.99	0.46	0.167
LGF-IV#c	2.65	0.74	4.05	3.90	3.56	1.10	5.24	0.44	0.129
LGF-V#c	2.48	0.55	3.80	2.71	4.51	1.03	4.93	0.61	0.084
Combined Graded Fibers (SGF), V_f = 0.3%									
CGF-I#c	3.48	0.56	4.52	3.33	6.21	1.23	5.94	0.38	0.128
CGF-II#c	4.23	0.86	5.50	6.05	4.92	1.50	7.03	0.24	0.283
CGF-III#c	4.14	0.80	5.38	5.45	5.17	1.46	6.81	0.27	0.249
CGF-IV#c	3.76	0.69	4.89	4.39	5.45	1.33	6.36	0.31	0.183
CGF-V#c	3.50	0.49	4.55	3.03	7.14	1.24	6.18	0.41	0.117
Note:Initial Slope (E^t_i) = σ^P_t, / ε^P_t , Strengthening Factor (STF^t)= σ^Q_t / σ_{mt} , Ductility Factor (DF^t) = ε^Q_t / ε^P_t , Strain Hardening slope (E_{SH}) = (σ^Q_t - σ^P_t) / (ε^Q_t -ε^P_t), Energy Absorption (EA_{SHR}) = Area under the stress strain curve in Strain Hardening Region, SD = Specimen Designation.									

Table 6.2 Summary of test results for M30-GGFRC with V_f = 0.4% in Tension

SD (1)	Strain Hardening Region				E^t_i ($X10^4$) MPa (6)	STF^t (7)	DF^t (8)	E_{SH} ($X10^4$) MPa (9)	EA_{SHR} ($X10^{-2}$) N/mm (10)
	σ^P_t, Mpa (2)	ε^P_t, ($X10^{-4}$) (3)	σ^Q_t, MPa (4)	ε^Q_t, ($X10^{-4}$) (5)					
Short Graded Fibers (SGF), V_f = 0.4%									
SGF-I#d	2.86	0.38	4.38	1.76	7.62	1.19	4.69	1.10	0.063
SGF-II#d	3.54	0.61	5.42	3.29	5.78	1.47	5.37	0.70	0.145
SGF-III#d	3.76	0.60	5.14	2.95	6.31	1.40	4.95	0.59	0.124
SGF-IV#d	3.49	0.54	4.79	2.36	6.49	1.30	4.38	0.71	0.092
SGF-V#d	3.39	0.37	4.41	1.42	9.29	1.20	3.90	0.96	0.051
Long Graded Fibers (LGF), V_f = 0.4%									
LGF-I#d	2.53	0.59	3.87	3.12	4.32	1.05	5.32	0.53	0.099
LGF-II#d	2.70	0.80	4.68	5.15	3.36	1.27	6.42	0.46	0.197
LGF-III#d	2.55	0.79	4.43	4.81	3.23	1.20	6.10	0.47	0.174
LGF-IV#d	2.73	0.73	4.18	3.97	3.75	1.14	5.44	0.45	0.135
LGF-V#d	2.54	0.55	3.90	2.78	4.66	1.06	5.10	0.61	0.088
Combined Graded Fibers (CGF), V_f = 0.4%									
CGF-I#d	3.53	0.55	4.60	3.48	6.42	1.25	6.33	0.36	0.136
CGF-II#d	4.42	0.84	5.75	6.20	5.26	1.56	7.38	0.25	0.303
CGF-III#d	4.21	0.79	5.48	5.60	5.33	1.49	7.09	0.26	0.261
CGF-IV#d	3.85	0.68	5.01	4.54	5.67	1.36	6.68	0.30	0.194
CGF-V#d	3.57	0.50	4.64	3.18	7.15	1.26	6.35	0.40	0.126
Note:Initial Slope (E^t_i) = σ^P_t, / ε^P_t , Strengthening Factor (STF^t)= σ^Q_t / σ_{mt} , Ductility Factor (DF^t) = ε^Q_t / ε^P_t , Strain Hardening slope (E_{SH}) = (σ^Q_t - σ^P_t) / (ε^Q_t -ε^P_t), Energy Absorption (EA_{SHR}) = Area under the stress strain curve in Strain Hardening Region, SD = Specimen Designation.									

Table 6.3 Summary of test results for M30-GGFRC with V_f = 0.5% in Tension

SD (1)	Strain Hardening Region				E^t_i ($X10^4$) MPa (6)	STF^t (7)	DF^t (8)	E_{SH} ($X10^4$) MPa (9)	EA_{SHR} ($X10^{-2}$) N/mm (10)
	σ^P_t, Mpa (2)	ε^P_t, ($X10^{-4}$) (3)	σ^Q_t, MPa (4)	ε^Q_t, ($X10^{-4}$) (5)					
Short Graded Fibers (SGF), V_f = 0.5%									
SGF-I#e	3.61	0.39	4.40	1.86	9.27	1.17	4.78	0.82	0.066
SGF-II#e	3.69	0.60	5.65	3.39	6.12	1.53	5.63	0.66	0.156
SGF-III#e	3.97	0.59	5.44	3.05	6.73	1.48	5.17	0.60	0.136
SGF-IV#e	3.60	0.53	4.94	2.46	6.74	1.34	4.60	0.70	0.099
SGF-V#e	3.52	0.35	4.59	1.53	10.20	1.25	4.42	0.91	0.057
Long Graded Fibers (LGF), V_f = 0.5%									
LGF-I#e	2.61	0.59	4.00	3.22	4.46	1.09	5.50	0.53	0.105
LGF-II#e	2.79	0.79	4.84	5.25	3.52	1.31	6.64	0.46	0.207
LGF-III#e	2.62	0.78	4.56	4.91	3.36	1.24	6.31	0.47	0.183
LGF-IV#e	2.81	0.72	4.30	4.07	3.88	1.17	5.62	0.45	0.143
LGF-V#e	2.64	0.55	4.05	2.88	4.80	1.10	5.24	0.61	0.095
Combined Graded Fibers (CGF=SGF+LGF), V_f = 0.5%									
CGF-I#d	3.48	0.56	4.52	3.63	6.21	1.23	6.48	0.34	0.140
CGF-II#d	4.51	0.81	5.87	6.35	5.60	1.59	7.88	0.24	0.317
CGF-III#d	4.42	0.76	5.75	5.75	5.82	1.56	7.56	0.27	0.281
CGF-IV#d	4.10	0.67	5.33	4.69	6.13	1.45	7.01	0.31	0.213
CGF-V#d	3.68	0.49	4.79	3.33	7.51	1.30	6.79	0.39	0.136

Note:Initial Slope (E^t_i) = σ^P_t, / ε^P_t , Strengthening Factor (STF^t)= σ^Q_t / σ_{mt} ,
Ductility Factor (DF^t) = ε^Q_t / ε^P_t , Strain Hardening slope (E_{SH}) = (σ^Q_t - σ^P_t) / (ε^Q_t -ε^P_t),
Energy Absorption (EA_{SHR}) = Area under the stress strain curve in Strain Hardening Region,
SD = Specimen Designation.

Table 6.4 Summary of test results for M50-GGFRC with V_f = 0.3% in Tension

SD (1)	Strain Hardening Region				E^t_i ($X10^4$) MPa (6)	STF^t (7)	DF^t (8)	E_{SH} ($X10^4$) MPa (9)	EA_{SHR} ($X10^{-2}$) N/mm (10)
	σ^P_t, MPa (2)	ε^P_t, ($X10^{-4}$) (3)	σ^Q_t, MPa (4)	ε^Q_t, ($X10^{-4}$) (5)					
Short Graded Fibers (SGF), V_f = 0.3%									
SGF-I#c	4.53	0.40	6.56	1.86	11.33	1.17	4.66	1.39	0.100
SGF-II#c	5.03	0.69	7.71	3.59	7.29	1.37	5.21	0.92	0.226
SGF-III#c	4.92	0.64	7.54	3.20	7.69	1.34	5.00	1.02	0.197
SGF-IV#c	4.59	0.54	7.03	2.56	8.44	1.25	4.70	1.21	0.147
SGF-V#c	4.48	0.34	6.48	1.53	13.18	1.15	4.49	1.69	0.081
Long Graded Fibers (LGF), V_f = 0.3%									
LGF-I#c	3.73	0.61	5.72	3.22	6.11	1.02	5.28	0.76	0.150
LGF-II#c	3.78	0.91	6.56	5.76	4.14	1.17	6.32	0.57	0.309
LGF-III#c	3.63	0.87	6.31	5.25	4.17	1.12	6.04	0.61	0.271
LGF-IV#c	3.55	0.74	6.06	4.24	4.77	1.08	5.69	0.72	0.209
LGF-V#c	3.48	0.55	5.72	2.85	6.33	1.02	5.18	0.97	0.133
Combined Graded Fibers (CGF), V_f = 0.3%									
CGF-I#c	5.31	0.58	6.89	3.57	9.16	1.22	6.16	0.53	0.209
CGF-II#c	6.17	0.90	8.45	6.51	6.86	1.50	7.23	0.41	0.468
CGF-III#c	5.94	0.85	8.14	5.90	6.99	1.45	6.94	0.43	0.409
CGF-IV#c	5.81	0.73	7.56	4.84	7.96	1.34	6.63	0.43	0.311
CGF-V#c	5.31	0.51	6.89	3.18	10.41	1.22	6.23	0.59	0.186

Table 6.5 Summary of test results for M50-GGFRC with V_f = 0.4% in Tension

SD (1)	Strain Hardening Region				E^t_i ($X10^4$) MPa (6)	STF^t (7)	DF^t (8)	E_{SH} ($X10^4$) MPa (9)	EA_{SHR} ($X10^{-2}$) N/mm (10)
	σ^P_t, Mpa (2)	ε^P_t, ($X10^{-4}$) (3)	σ^Q_t, MPa (4)	ε^Q_t, ($X10^{-4}$) (5)					
Short Graded Fibers (SGF), V_f = 0.4%									
SGF-I#d	4.69	0.43	6.77	2.03	10.91	1.20	4.73	1.30	0.112
SGF-II#d	5.17	0.70	7.92	3.76	7.39	1.41	5.37	0.90	0.243
SGF-III#d	5.06	0.66	7.75	3.37	7.67	1.38	5.11	0.99	0.213
SGF-IV#d	4.65	0.57	7.11	2.73	8.10	1.26	4.75	1.14	0.158
SGF-V#d	4.50	0.38	6.69	1.69	11.84	1.19	4.46	1.67	0.093
Long Graded Fibers (LGF), V_f = 0.4%									
LGF-I#d	3.75	0.62	5.93	3.30	6.05	1.05	5.33	0.81	0.160
LGF-II#d	3.85	0.91	6.77	5.93	4.22	1.20	6.50	0.58	0.328
LGF-III#d	3.76	0.87	6.52	5.42	4.32	1.16	6.23	0.61	0.289
LGF-IV#d	3.61	0.76	6.27	4.41	4.73	1.11	5.77	0.73	0.225
LGF-V#d	3.57	0.56	5.93	2.93	6.38	1.05	5.23	0.99	0.142
Combined Graded Fibers (CGF), V_f = 0.4%									
CGF-I#d	5.47	0.59	7.11	3.87	9.27	1.26	6.56	0.50	0.235
CGF-II#d	6.33	0.92	8.67	6.81	6.88	1.54	7.40	0.40	0.502
CGF-III#d	6.10	0.87	8.36	6.20	7.01	1.48	7.13	0.42	0.441
CGF-IV#d	5.85	0.76	7.78	5.14	7.70	1.38	6.77	0.44	0.341
CGF-V#d	5.31	0.54	7.11	3.48	9.83	1.26	6.44	0.61	0.211

Table 6.6 Summary of test results for M50-GGFRC with V_f = 0.5% in Tension

SD (1)	Strain Hardening Region				E^t_i ($X10^4$) MPa (6)	STF^t (7)	DF^t (8)	E_{SH} ($X10^4$) MPa (9)	EA_{SHR} ($X10^{-2}$) N/mm (10)
	σ^P_t, Mpa (2)	ε^P_t, ($X10^{-4}$) (3)	σ^Q_t, MPa (4)	ε^Q_t, ($X10^{-4}$) (5)					
Short Graded Fibers (SGF), V_f = 0.5%									
SGF-I#e	4.83	0.44	6.99	2.12	10.98	1.24	4.81	1.29	0.121
SGF-II#e	5.31	0.72	8.13	3.93	7.38	1.44	5.46	0.88	0.261
SGF-III#e	5.26	0.68	8.05	3.56	7.74	1.43	5.23	0.97	0.234
SGF-IV#e	4.78	0.58	7.33	2.90	8.19	1.30	4.96	1.10	0.173
SGF-V#e	4.55	0.38	6.91	1.73	11.97	1.23	4.55	1.75	0.098
Long Graded Fibers (LGF), V_f = 0.5%									
LGF-I#e	3.78	0.63	6.14	3.47	6.00	1.09	5.51	0.83	0.174
LGF-II#e	3.97	0.92	7.00	6.10	4.31	1.24	6.62	0.59	0.349
LGF-III#e	3.88	0.88	6.74	5.59	4.41	1.20	6.35	0.61	0.308
LGF-IV#e	3.74	0.77	6.48	4.58	4.83	1.15	5.91	0.72	0.242
LGF-V#e	3.59	0.57	6.15	3.10	6.30	1.09	5.44	1.01	0.156
Combined Graded Fibers (CGF=SGF+LGF), V_f = 0.5%									
CGF-I#d	5.64	0.62	7.34	4.18	9.10	1.30	6.73	0.48	0.261
CGF-II#d	6.66	0.89	9.12	7.11	7.48	1.62	7.99	0.40	0.552
CGF-III#d	6.27	0.83	8.58	6.51	7.55	1.52	7.84	0.41	0.475
CGF-IV#d	5.85	0.76	8.00	5.45	7.70	1.42	7.17	0.46	0.371
CGF-V#d	5.64	0.57	7.34	3.78	9.89	1.30	6.64	0.53	0.236

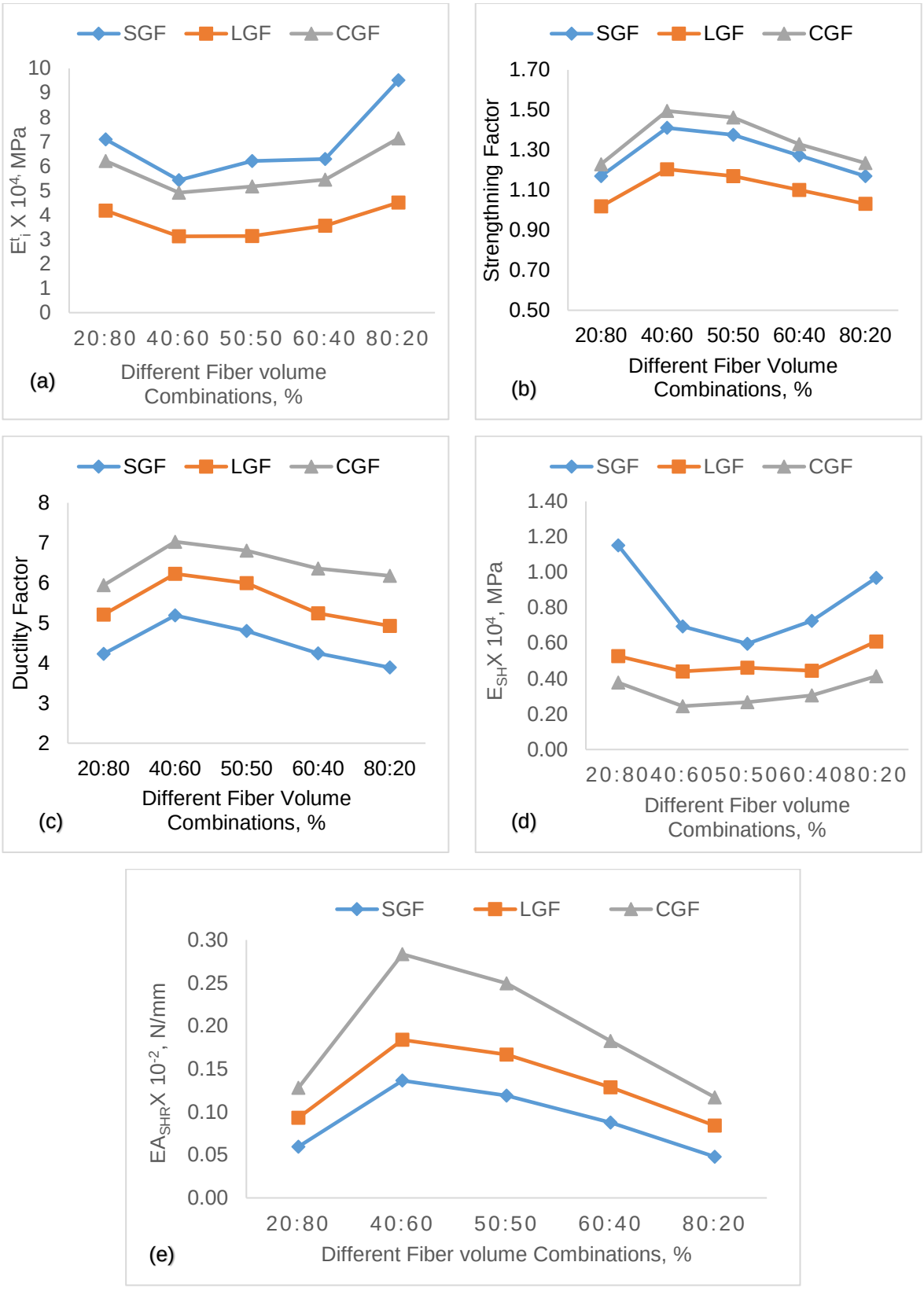

Fig.6.39 Mechanical properties variation of M30-GGFRC-0.3% in Tension

(a) Initial slope (E_i^t), (b) strengthening factor (STF^t), (c) ductility factor (DF^t), (d) strain hardening slope (E_{SH}) and (e) energy absorption capacity in strain hardening region (EA_{SHR}).

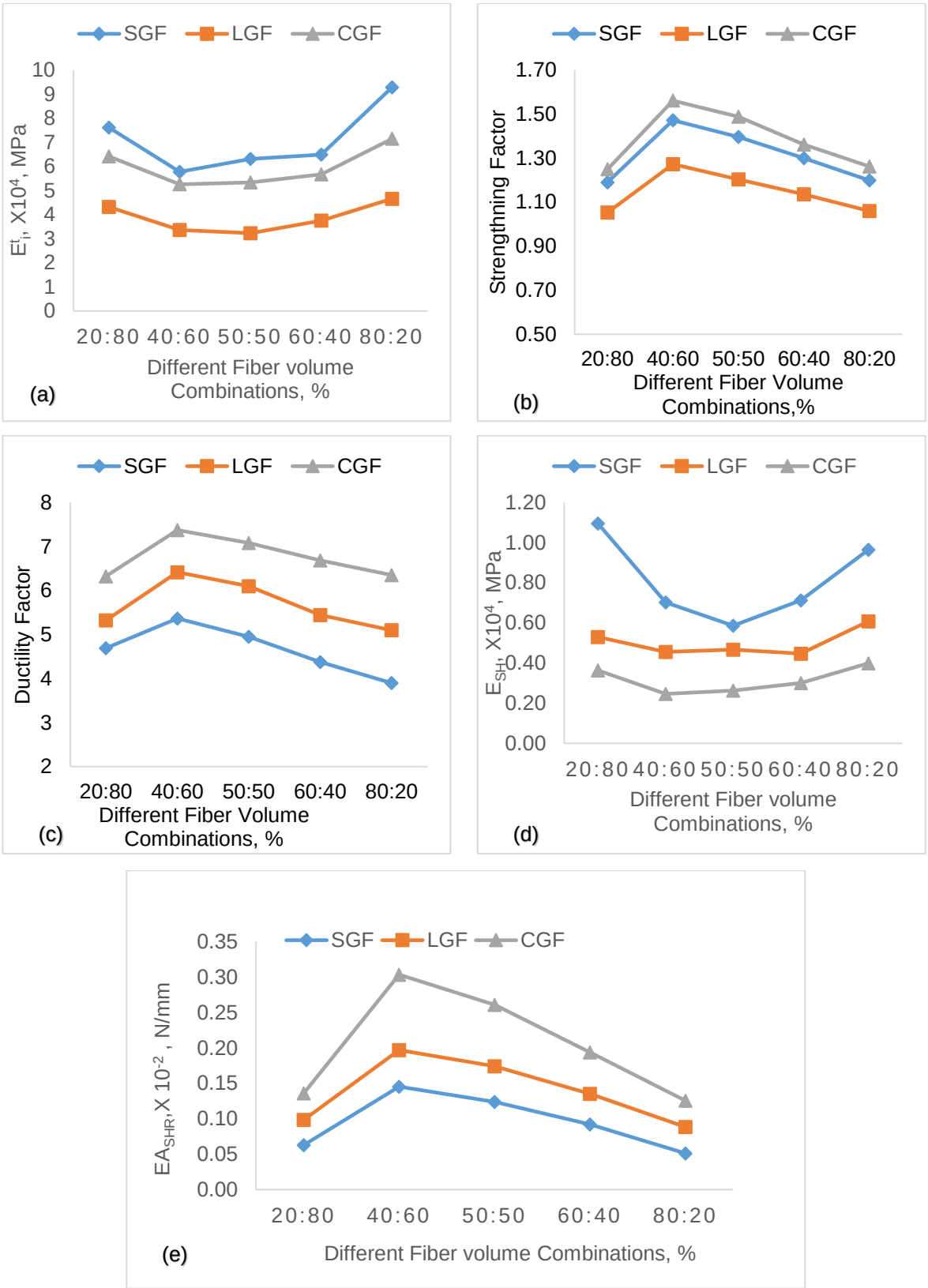

Fig.6.40 Mechanical properties variation of M30-GGFRC-0.4% in Tension

(a) Initial slope (E_i^t), (b) strengthening factor (STF^t), (c) ductility factor (DF^t), (d) strain hardening slope (E_{SH}) and (e) energy absorption capacity in strain hardening region (EA_{SHR}).

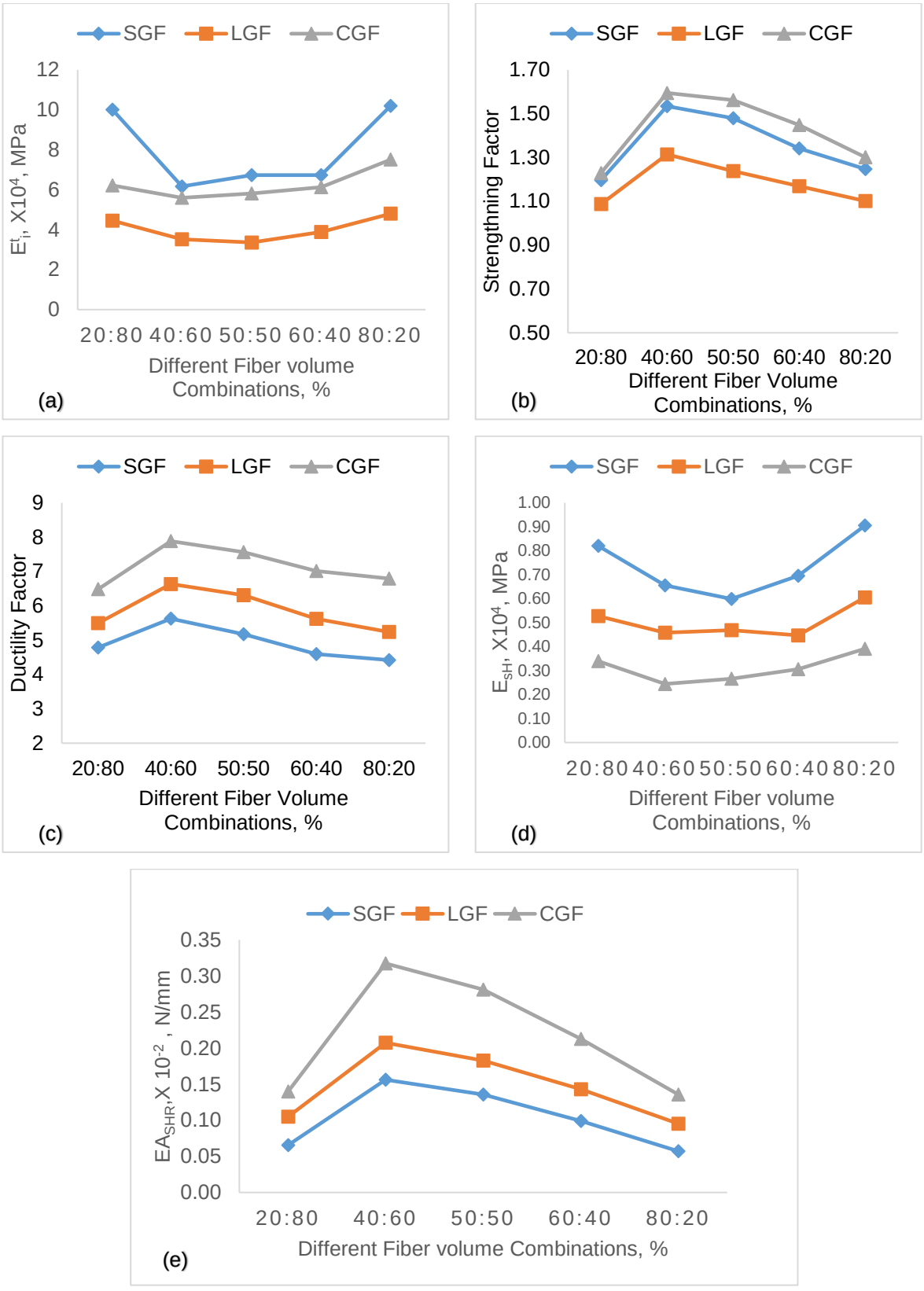

Fig.6.41 Mechanical properties variation of M30-GGFRC-0.5% in Tension

(a) Initial slope (E_i^t), (b) strengthening factor (STF^t), (c) ductility factor (DF^t), (d) strain hardening slope (E_{SH}) and (e) energy absorption capacity in strain hardening region (EA_{SHR}).

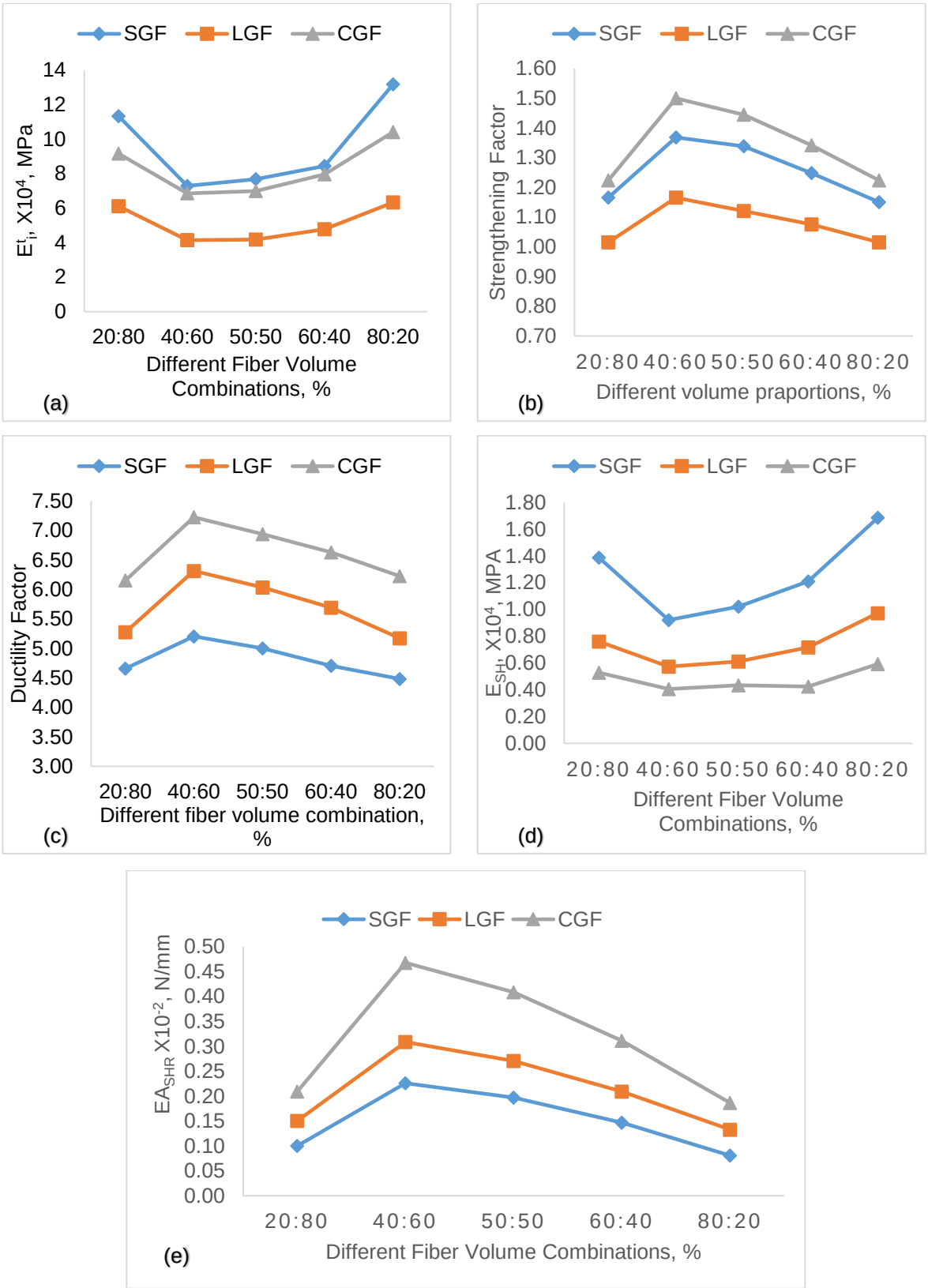

Fig.6.42 Mechanical properties variation of M50-GGFRC-0.3% in Tension

(a) Initial slope (E_i^t), (b) strengthening factor (STF^t), (c) ductility factor (DF^t), (d) strain hardening slope (E_{SH}) and (e) energy absorption capacity in strain hardening region (EA_{SHR}).

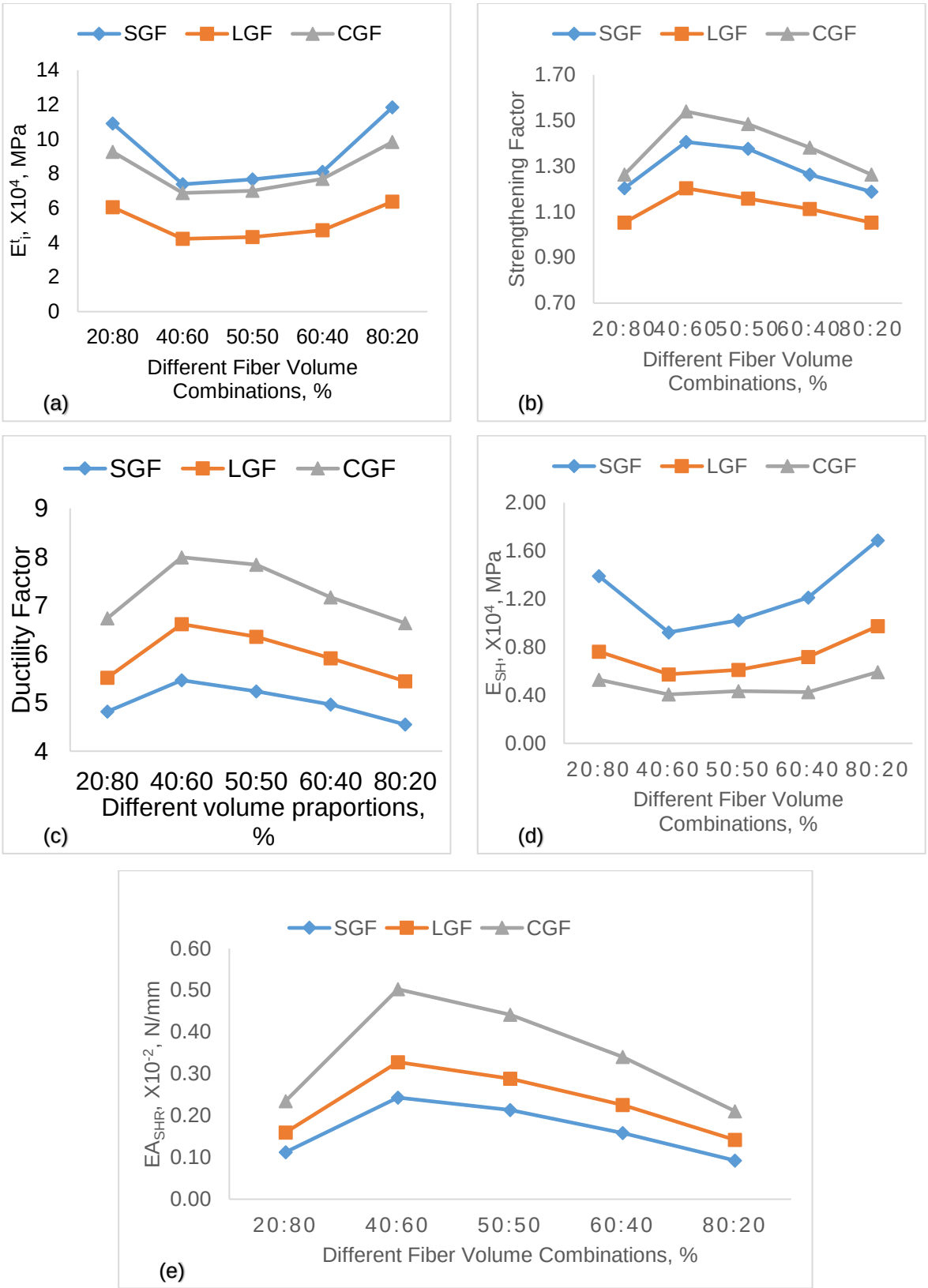

Fig.6.43 Mechanical properties variation of M50-GGFRC-0.4% in Tension

(a) Initial slope (E_i^t), (b) strengthening factor (STF^t), (c) ductility factor (DF^t), (d) strain hardening slope (E_{SH}) and (e) energy absorption capacity in strain hardening region (EA_{SHR}).

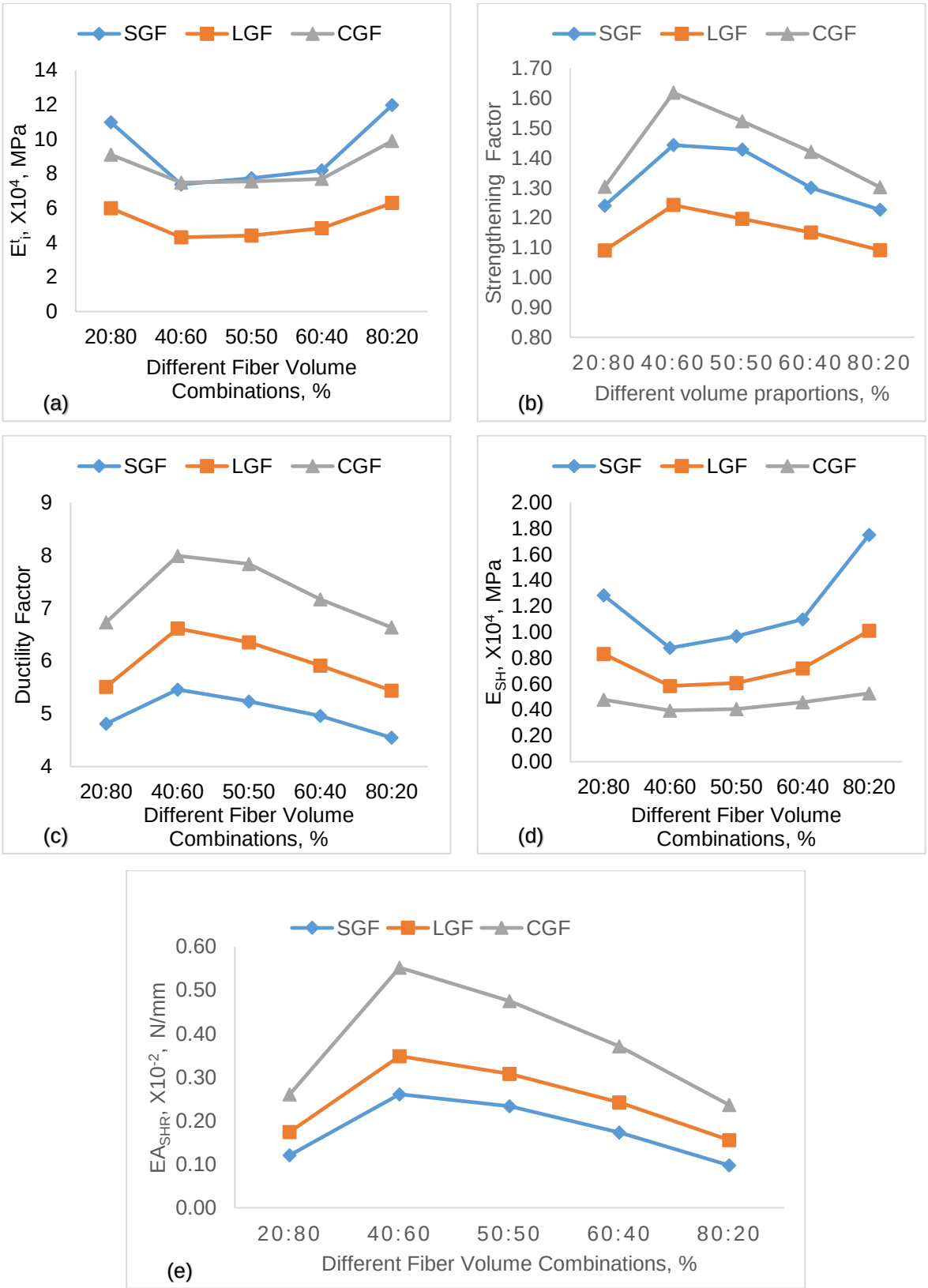

Fig.6.44 Mechanical properties variation of M50-GGFRC-0.5% in Tension

(a) Initial slope (E_i^t), (b) strengthening factor (STF^t), (c) ductility factor (DF^t), (d) strain hardening slope (E_{SH}) and (e) energy absorption capacity in strain hardening region (EA_{SHR}).

6.6 Summary of the Image analysis for GGFRC

Fiber dispersion and orientation are the two important parameters to understand the tensile behaviour of the composite. These parameters are examined on fracture plane of GFRC specimens and detailed procedure was given in the section 5.6 of Chapter-5. In order to determine the fiber dispersion and orientation on fracture plane of GGFRC specimens, the same procedure is followed for the M30-GGFRC and M50-GGFRC failed specimens with 0.3%, 0.4% and 0.5% volume fractions. Fiber density variations was plotted along the thickness and width direction on fracture plane of failed specimens with M30-GGFRC and M50-GGFRC with 0.3%, 0.4% and 0.5% volume fractions and were shown in Fig.6.46 to 6.51. It shows that the composite with SGF, the fiber density is more at the center and less at the edges and corners. Where as in long graded fibers, the fiber density is more at the edges and corners and less at the center. Composite with CGF (containing SGF + LGF) showed the almost uniform distribution. The results of image analyses shows that graded fibers with different fibre volume combinations disperse homogeneously avoiding clumping or balling. Graded fibers showed the higher fiber dispersion coefficient and higher fiber orientation coefficient when compared to the mono fibers. Number of fibers, fiber dispersion coefficient (η_d), fiber orientation coefficient (η_θ) at a cross section on a fracture plane is given in column 4, 5 and 6 of Table 6.9 to 6.14 for M30-GGFRC and M50-GGFRC with 0.3%, 0.4% and 0.5% volume fractions.

6.6 (a) Number of fibers (n_e)

Number of fibers at a cross section on a fracture plane is estimated by image analysis and given in column 4 of Table 6.9 to 6.14 for M30-GGFRC and M50-GGFRC with 0.3%, 0.4% and 0.5% volume fractions. Among all the short graded fibers, the specimens with 40%3mm+60%6mm (SGF-II) showed more number of fibers at a cross section on fracture plane whereas in case of long graded fibers, the specimens with 40%12mm+60%20mm (LGF-II) showed more number of fibers at a cross section on fracture plane compared to other long graded fibers. It can be observed that the number of fibers are more for short graded fibers when compared to the long graded fibers. More number of fibers are available at the cracked composite and it provides the load transfer mechanism across the crack. That is the reason, why the specimens with short graded fiber have given the higher composite strength when compared to specimens with long graded fibers. Among all the combined graded fibers, the

specimens with 40%SGF+60%LGF (CGF-II) has given the higher number of fibers compared to other CGF specimens.

comparison with best of the best combinations i.e., 40%3mm+60%6mm (SGF-II), 40%12mm+60%20mm (LGF-II) and 40%SGF+60%LGF (CGF-II) showed the clear variation in terms of number of fibers. It can be noted that the number of fibers are more for combined graded fibers than that of short graded and long graded fibers. Higher number of fibers can prevent a sudden loss in load-carrying capacity of the cracked composite by providing effective load transfer mechanism across the crack and enhance the bridging efficiency of the fibers at every scale of cracking. That is the reason that the combined graded fibers have given the best performance compared to short graded fibers and long graded fibers in both strength and deformation.

6.6 (b) Fiber dispersion (η_d) and fiber orientation (η_θ)

Fiber dispersion coefficient (η_d), fiber orientation coefficient (η_θ) at a cross section on a fracture plane is estimated through image analysis and given in column 5 and 6 of Table 6.9 to 6.14 for M30-GGFRC and M50-GGFRC with 0.3%, 0.4% and 0.5% volume fractions. It can be noted that the fiber dispersion and fiber orientation for short graded fibers varied from 0.53 to 0.66 and 0.69 to 0.87 respectively and similarly for long graded fibers varied from 0.40 to 0.48 and 0.53 to 0.61 respectively. Among all the short graded fibers, the specimens with 40%3mm+60%6mm (SGF-II) has given the higher fiber dispersion (0.66) and fiber orientation (0.87) whereas in case of long graded fibers, the specimens with 40%12mm+60%20mm (LGF-II) has given the higher dispersion (0.48) and fiber orientation (0.61) compared to other long graded fibers. It can be observed that the fiber dispersion and orientation is higher for short graded fibers when compared to the long graded fibers.

Short randomly dispersed fibers in concrete help to resist the opening of marco cracks by arresting the micro cracks and enhancing the pre crack strength. Moreover, the small fibers uniformly oriented in concrete help to bridge the internal micro cracks thus improve concrete properties in all directions. That is the reason, why the specimens with short graded fiber have given the higher composite strength when compared to specimens with long graded fibers.

The combination of short graded (SGF) and long graded fibers (LGF) forms the combined graded fibers (CGF). Fiber dispersion and fiber orientation for CGF varied

from 0.53 to 0.81 and 0.74 to 0.90 respectively. Among all the combined graded fibers, the specimens with 40%SGF+60%LGF (CGF-II) has given the higher fiber dispersion (0.81) and higher fiber orientation (0.90). Comparison with best of the best combinations i.e., 40%3mm+60%6mm (SGF-II), 40%12mm+60%20mm (LGF-II) and 40%SGF+60%LGF (CGF-II) showed the clear variation in terms of fiber dispersion and fiber orientation . It can be noted that the fiber dispersion and orientation is higher for combined graded fibers than that of short graded and long graded fibers.

The degree of fiber dispersion affects the strength of the composites by its role in transfer the load to the other parts of the composite. An effective crack bridging and increase in the strength of the composite can be achieved if the degree of fiber orientation is better at the first crack location. The degree of fiber dispersion and orientation depends on the fiber grading i.e., SGF (3mm +6mm), LGF (12mm +20mm) and CGF (3mm+6mm+12mm+20mm) with different fiber volume combinations. As the grading of fiber increases the degree of fiber dispersion and orientation increases. Hence, that is the reason that the combined graded fibers have given the best performance compared to short graded fibers and long graded fibers in both strength and deformation.

In all, irrespective of volume of the fiber (0.3%, 0.4% and 0.5%) and grade of concrete (M30 and M50), from the above observation, it can be concluded that the combined graded fibers (CGF) showed higher number of fibers, higher fiber dispersion and higher fiber orientation and better than mono glass fibers (MGF) or SGF or LGF and it leads to a higher strength and deformation.

6.6 (c) Effect of Fiber efficiency ($\eta = \eta_d . \eta_\theta . \eta_l$) on composite tensile strength

Tensile strength of composite is mainly depends on the fiber dispersion coefficient, fiber orientation coefficient and fiber length coefficient. The fiber efficiency is defined as the product of fiber dispersion coefficient, fiber orientation coefficient and fiber length coefficient. Fiber dispersion coefficient (η_d), fiber orientation coefficient (η_θ) and fiber length coefficient (η_l) for mono fibers are already given in column 4, 5 and 6 of Table 5.15 and 5.16. Fiber dispersion coefficient (η_d), fiber orientation coefficient (η_θ) and fiber length coefficient (η_l) for graded fibers is given in column 2, 3 and 4 of Table 6.7. The composite strength of M30-MGFRC and M50-MGFRC are given in column 7 of Table 5.15 and 5.16. The composite strength of M30-GGFRC and M50-MGFRC are given in column 6 of Table 6.7. Fiber efficiency is calculated for mono fibers and

graded fibers, and the variation of composite strength with respect to fiber efficiency for mono fibers and grades as shown in Fig.6.45 (a) and (b). As the fiber efficiency increases the strength of the composite increased. It can be concluded that the fiber efficiency is higher in graded fibers than mono fibers.

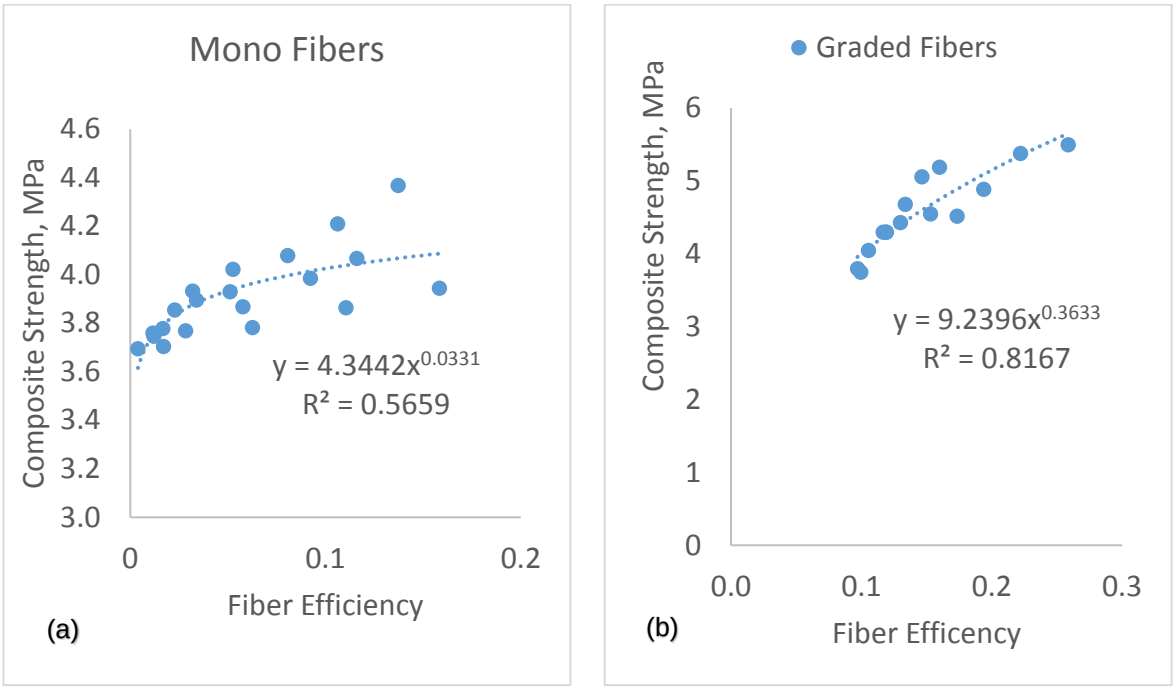

Fig. 6.45 Effect of Fiber efficiency (η) on composite tensile strength

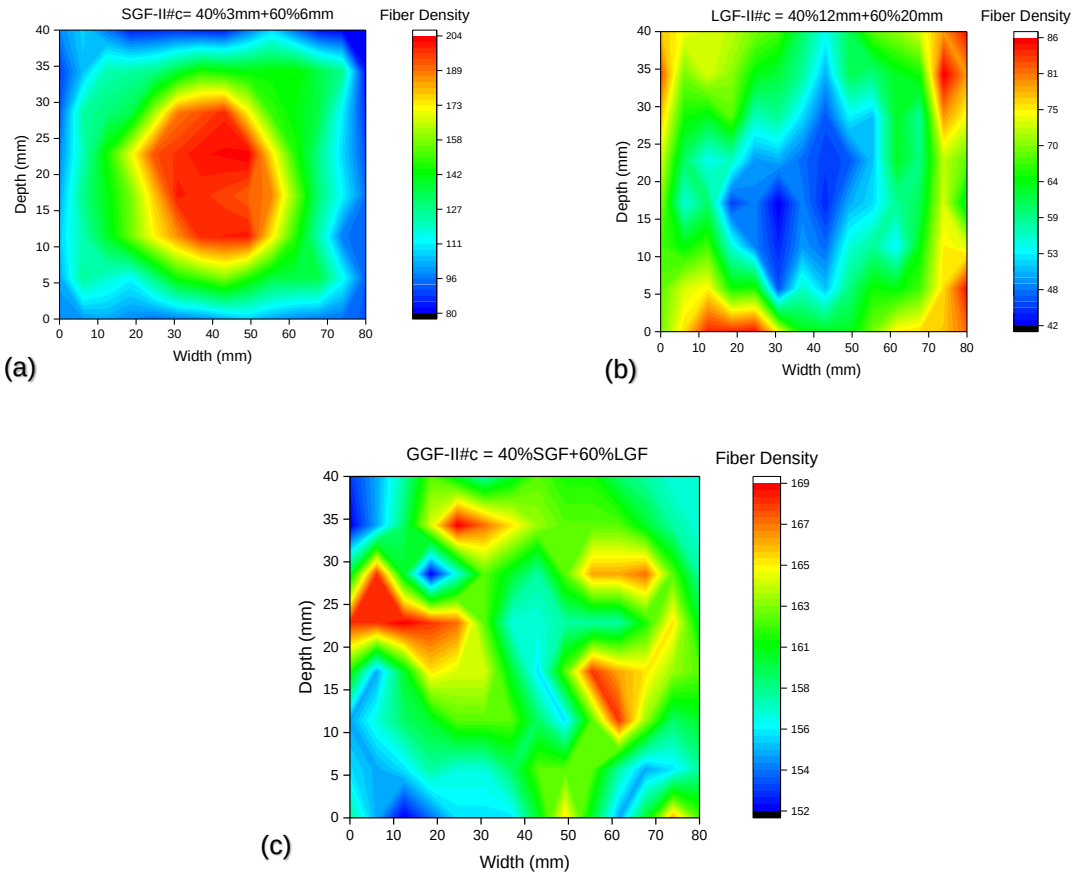

Fig.6.46 Variation of fibers along the thickness and width direction for M30-GGFRC-0.3%.(a) SGF-II#c, (b) LGF-II#c and (c) CGF-II#c

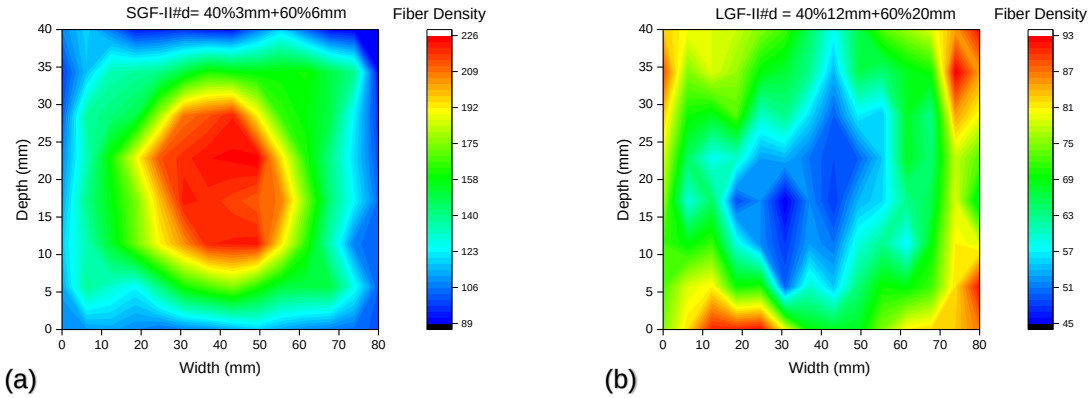

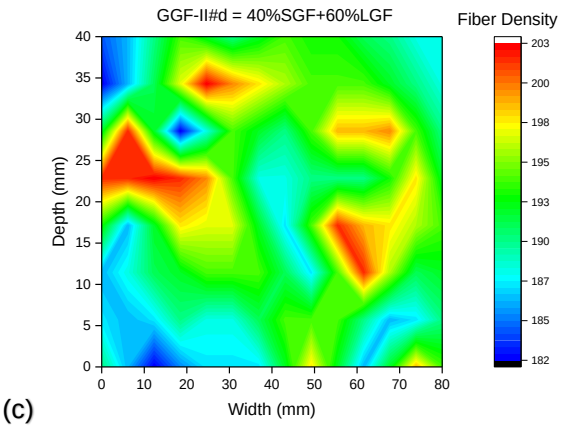

Fig.6.47 Variation of fibers along the thickness and width direction for M30-GGFRC-0.4%. (a) SGF-II#d, (b) LGF-II#d and (c) CGF-II#d

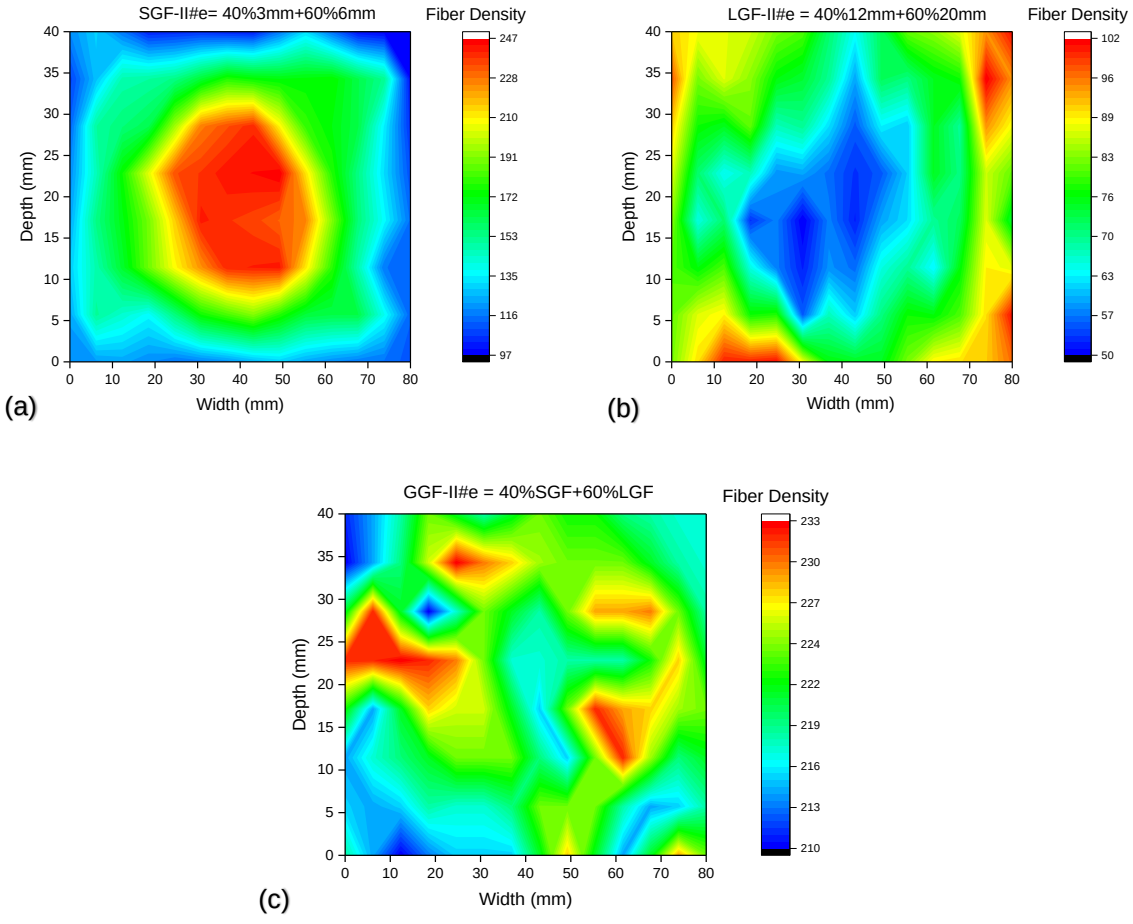

Fig.6.48 Variation of fibers along the thickness and width direction for M30-GGFRC-0.5%. (a) SGF-II#e, (b) LGF-II#e and (c) CGF-II#e

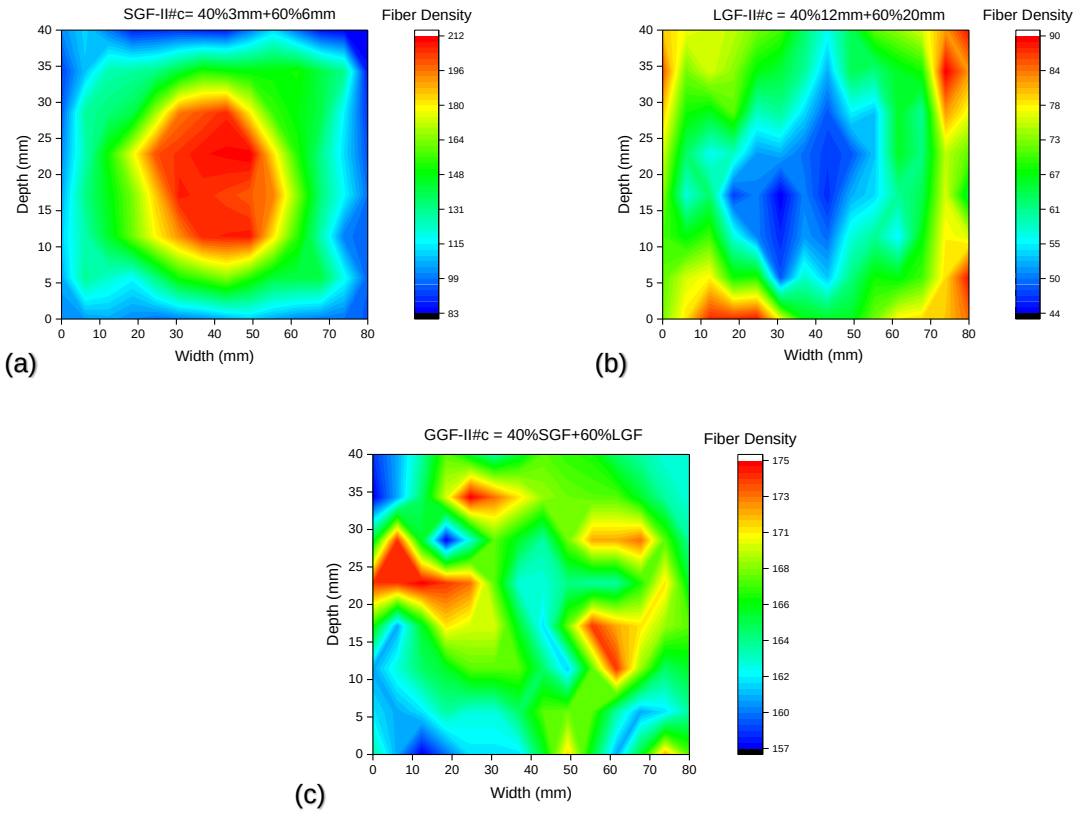

Fig.6.49 Variation of fibers along the thickness and width direction for M50-GGFRC-0.3%. (a) SGF-II#c, (b) LGF-II#c and (c) CGF-II#c

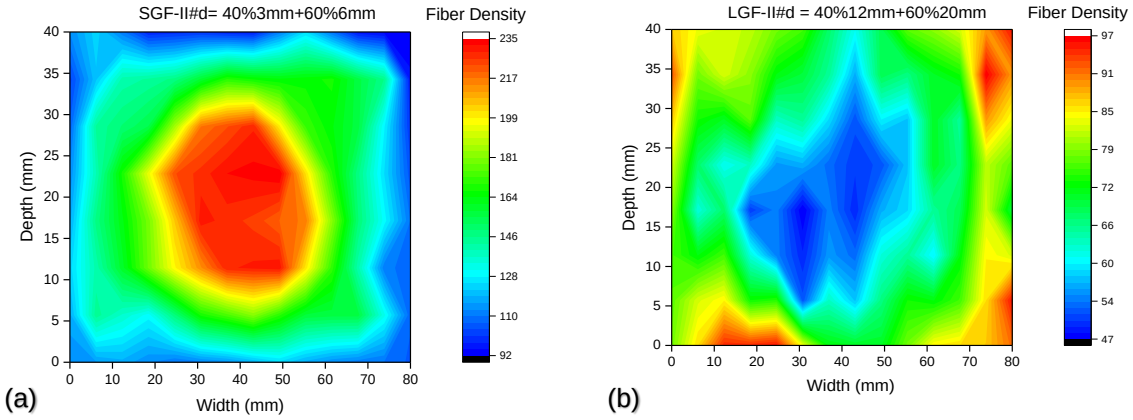

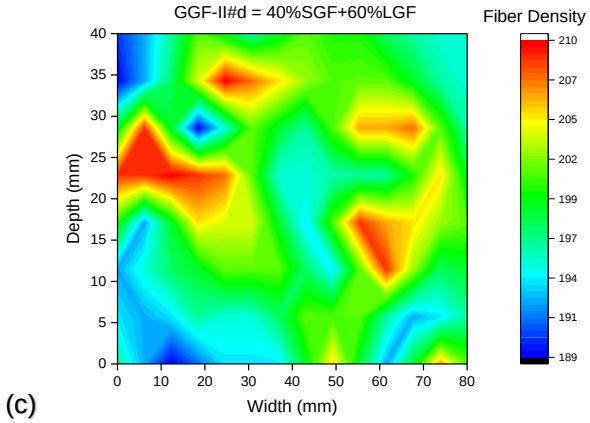

Fig.6.50 Variation of fibers along the thickness and width direction for M50-GGFRC-0.4%.(a) SGF-II#d, (b) LGF-II#d and (c) CGF-II#d

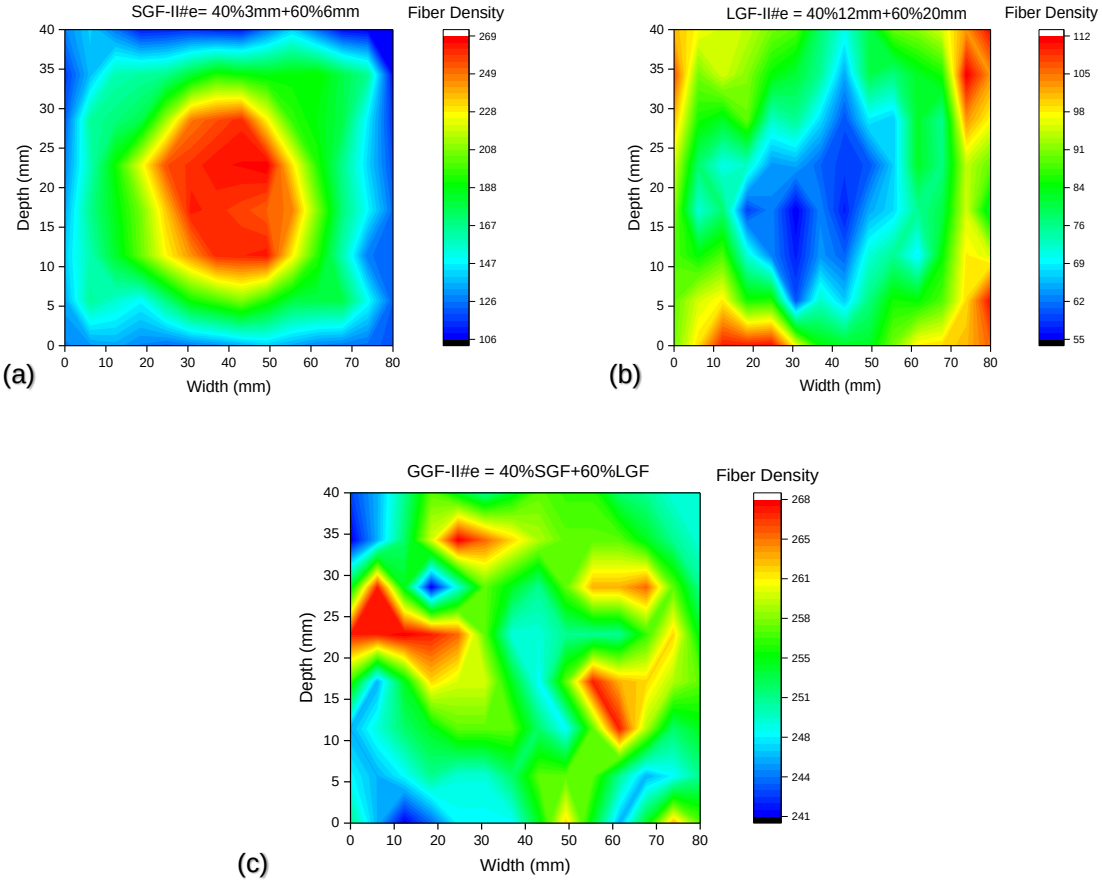

Fig.6.51 Variation of fibers along the thickness and width direction for M50-GGFRC-0.5%. (a) SGF-II#e, (b) LGF-II#e and (c) CGF-II#e

6.6.1 Reinforcing Index for Graded Fibers (RI_{GF})

The composite strength of the GGFRC is influenced by the fiber dispersion coefficient, fiber orientation coefficient and fiber length coefficient, as similar to the MGFRC. Fiber dispersion coefficient (η_d) and fiber orientation coefficient (η_θ) is estimated for 0.3% volume fraction of M30-GGFRC specimens at a cross section on a fracture plane through image analysis as stated in above article 6.6 and they are already given in Table.6.9 η_d and η_θ are extracted from Table 6.9 and noted in column 2, 3 of Table 6.7.

Fiber length coefficient (η_l) of mono glass fibers are given in column 6 of Table 5.15 of Chapter-5. It can be noted from Table 5.15 that η_l for 3mm is 0.39 and η_l for 6mm is 0.43. η_l for graded fibers can be calculated as per the percentage of fiber volume combination. As an example for SGF-I#c (i.e., 20%3mm+80%6mm), η_l = (0.2*0.39) + (0.8*0.43) = 0.42. Similarly, Fiber length coefficient (η_l) for other graded fibers (SGF, LGF and CGF) are calculated and given in 4 of Table 6.7 for M30-GGFRC with 0.3% volume fraction.

The composite tensile strength (σ^{GF}_{ct}) of GGFRC is calculated using equation (10) given in Chapter-5. The tensile strength of the composite (σ^{GF}_{ct}) is calculated for M30-GGFRC (0.3% volume fraction) with experimental η_d, η_θ, η_l values based on the equation (10) and is given column 5 of Table 6.7. These values are compared with the corresponding experimental values given in column 6 of Table 6.7. The ratio of the calculated composite strength values to that of experimental strength values are shown in column 7 of Table 6.7. It can be noted that the calculated composite tensile strength (σ^{GF}_{ct}) values are close to the experimental composite tensile strength (σ^{GF}_{ct}) values.

It can be concluded that knowing η_d,, η_θ and η_l the composite tensile strength of the GGFRC can be calculated . However, the η_d, and η_θ values are difficult to measure on fracture plain of each GGFRC specimen using image analysis or methods.A procedure is required to predict η_d, and η_θ. Efforts are made to use the existing models.

A relation is obtained between η_d and RI_{MF} for mono glass fibers (MGFRC) in chapter-5, equation (7). Similar relation for η_θ is given in equation (8). Reinforcing index (RI_{MF}) for mono fibers is defined as product of volume fraction (V_f) and aspect ratio of fiber (L_f/D_f). It is stated in the article 6.5, that the η_d, and η_θ are influenced by fiber grading.

If reinforcing index for graded fibers (RI_{GF}) can be obtained, the equation (7) and (8) may be used to predict $\eta_{d,}$ and η_{θ} without conducting image analysis.

A simple linear combination method and equation given by M A Rasheed et al (2018) are used to arrive at RI_{GF} for graded fibers and $\eta_{d,}$ η_{θ} are computed and compared with experimental ηd, η_{θ} as illustrated in article 6.6.1(a) and 6.6.1(b). As the two methods have not yielded a satisfactory values of η_{d}, η_{θ}, a new equation is proposed for arriving at RI_{GF} for graded fiber as presented in article 6.7. The proposed method yielded reasonable results.

Table.6.7 Composite strength with Experimental values of $\eta_{d,}$ $\eta_{\theta,}$ η_{l} for M30-GGFRC

Specimen Designation (1)	η_d (2)	η_θ (3)	η_l (4)	σ^{GF}_{ct} (5)	Exp.σ^{GF}_{tu} (6)	Ratio (7) (5/6)
Short Graded Fibers (SGF), V_f = 0.3%						
SGF-I#c	0.44	0.63	0.42	4.28	4.30	0.99
SGF-II#c	0.51	0.75	0.42	4.48	5.19	0.86
SGF-III#c	0.48	0.74	0.41	4.42	5.06	0.87
SGF-IV#c	0.46	0.70	0.41	4.35	4.68	0.93
SGF-V#c	0.45	0.66	0.40	4.28	4.30	0.99
Long Graded Fibers (LGF), V_f = 0.3%						
LGF-I#c	0.35	0.50	0.43	4.18	3.75	1.11
LGF-II#c	0.42	0.56	0.42	4.33	4.43	0.98
LGF-III#c	0.39	0.54	0.41	4.26	4.30	0.99
LGF-IV#c	0.37	0.52	0.41	4.21	4.05	1.04
LGF-V#c	0.36	0.51	0.40	4.16	3.80	1.10
Combined Graded Fibers (CGF), V_f = 0.3%						
CGF-I#c	0.47	0.70	0.43	4.55	4.52	1.01
CGF-II#c	0.65	0.79	0.42	4.99	5.50	0.91
CGF-III#c	0.59	0.78	0.41	4.80	5.38	0.89
CGF-IV#c	0.53	0.77	0.41	4.66	4.89	0.95
CGF-V#c	0.48	0.71	0.40	4.45	4.55	0.98

6.6.1(a) Reinforcing index of graded fibers from Linear combination method (RI''_{GF})

Reinforcing index of mono glass fiber length (MGFRC) i.e., 3mm, 6mm, 12mm and 20mm with 0.3% volume fraction are already calculated and given in column 4 of Table 5.14 of Chapter-5. By considering the reinforcing index of mono fibers, the reinforcing

index of SGF-I#c (20%3mm+40%6mm) is computed by linear combination. It can be noted from Table 5.14 that RI_{MF} for 3mm is 0.64 and RI_{MF} for 6mm is 1.29. Then the RI''_{GF} for graded fibers of SGF-I#c is equal to 1.16 {ì.e.,(0.2 . 0.64) + (0.8 . 1.29)}. Similarly, the reinforcing index of graded fibers (RI''_{GF}) is calculated for various fiber volume combinations and are given in column 4 of Table 6.8. The fiber dispersion coefficient (η_d) and fiber orientation coefficient (η_θ) are calculated from the equation (7) and (8) given in Chapter-5 by substituting RI''_{GF} in place of RI_{MF}. For each RI''_{GF} the corresponding fiber dispersion coefficient (η_d) and fiber orientation coefficient (η_θ) are calculated and given in column 5 and 6 of Table 6.8. These values are compared with the experimental values given in column 2 and 3 of Table 6.8. The ratio of experimental values to the predicted values are given in column 10 and 12 of Table 6.8.

6.6.1(b) M A Rasheed et, al 2018 Method for Reinforcing index of graded fibers (RI'_{GF})

M A Rasheed (2018) considered the synergistic effects of using micro and macro fibers and proposed an expression to estimate RI'_{GF} for graded fibers and given in equation (23) below. Generally 3mm and 6mm can be treated as micro fibers and 12mm and 20mm can be treated as macro fibers. But in this case, the least one is taken as micro for the calculation of $RI'_{\mathbf{GF}}$**.** In case of RI'_{GF} for SGF, 3mm is considered as micro and 6mm as considered as macro whereas RI'_{GF} for LGF, 12mm is taken as micro and 20mm is taken as macro.

Reinforcing index of each fiber length i.e., 3mm, 6mm, 12mm and 20mm with 0.3% volume fraction are already calculated and given in column 4 of Table 5.14 of Chapter-5. It can be noted from Table 5.14 that RI_{MF} for 3mm is 0.64, RI_{MF} for 6mm is 1.29, RI_{MF} for 12mm is 2.57 and RI_{MF} for 20mm is 4.29. Then the $RI'_{\mathbf{GF}}$ for SGF-II#c (40%3mm+60%6mm) is obtained from equation (23) by taking the RI_{Micro} as product of (0.4).(0.64) and RI_{Macro} as product of (0.6).(1.29). $RI'_{\mathbf{GF}}$ for LGF-II#c (40%12mm+60%20mm) is obtained from equation (28) by taking the RI_{Micro} as product of (0.4).(2.57) and RI_{Macro} is product of (0.6).(4.29).

In case of $RI'_{\mathbf{GF}}$ for CGF, RI_{Micro} means $RI'_{\mathbf{GF}}$ of SGF-II and RI_{Macro} means $RI'_{\mathbf{GF}}$ of LGF-II. $RI'_{\mathbf{GF}}$ for CGF-II#c (40%SGF+60%LGF) is obtained from equation (23) by taking the RI_{Micro} as equal to 0.4.$RI'_{\mathbf{GF}}$ of SGF-II#c and RI_{Macro} as equal to 0.6 $RI'_{\mathbf{GF}}$ of LGF-II#c.

Similarly, the reinforcing index of other graded fibers (RI'_{GF}) is calculated for various fiber volume combinations and are given in column 7 of Table 6.8. The fiber dispersion coefficient (η_d) and fiber orientation coefficient (η_θ) are calculated from the equation (7) and (8) given in Chapter-5 by substituting RI'_{GF} in place of RI_{MF}. For each RI'_{GF} the corresponding fiber dispersion coefficient (η_d) and fiber orientation coefficient (η_θ) are calculated and given in column 8 and 9 of Table 6.8. These values are compared with the experimental values given in column 2 and 3 of Table 6.8. The ratio of experimental values to the predicted values are given in column 11 and 13 of Table 6.8.

$$RI'_{GF} = RI_{Macro}^{\frac{1}{(1-2(RI_{Mirco})}} \qquad \text{---------- (23)}$$

It can be observed that η_d and η_θ predicted from linear combination method has variation from18% to 42% and 24% to 38% respectively. Further it can be observed that that η_d and η_θ predicted from M A Rasheed (2018) unrealistic or weird.

Table.6.8 Predicted composite strength Experimental values of $\eta_d, \eta_\theta, \eta_l$ M30-GGFRC-0.3%.

Specimen Designation (1)	Experimental		Linear combination Method			Mohammad et al 2018			Ratio for ηd		Ratio for ηθ	
	η_d (2)	η_θ (3)	RI''_{GF} (4)	η_d (5)	η_θ (6)	RI'_{GF} (7)	η_d (8)	η_θ (9)	(10) 4/2	(11) 7/2	(12) 5/3	(13) 9/3
Short Graded Fibers (SGF), V_f = 0.3%												
SGF-I#c	0.44	0.63	1.16	0.36	0.46	6.96	0.30	0.35	0.82	0.68	0.73	0.55
SGF-II#c	0.51	0.75	1.03	0.36	0.47	12.20	0.28	0.32	0.71	0.55	0.62	0.43
SGF-III#c	0.48	0.74	0.96	0.37	0.47	53.11	0.24	0.26	0.76	0.50	0.64	0.35
SGF-IV#c	0.46	0.70	0.90	0.37	0.48	3×10^{14}	0.01	0.00	0.80	0.02	0.68	0.00
SGF-V#c	0.45	0.66	0.77	0.38	0.49	0.25	0.42	0.58	0.83	0.94	0.74	0.87
Long Graded Fibers (LGF), V_f = 0.3%												
LGF-I#c	0.35	0.50	3.94	0.32	0.38	1.12	0.36	0.46	0.91	1.03	0.76	0.92
LGF-II#c	0.42	0.56	3.60	0.32	0.39	0.99	0.37	0.47	0.76	0.87	0.69	0.84
LGF-III#c	0.39	0.54	3.43	0.32	0.39	0.93	0.37	0.47	0.82	0.94	0.72	0.88
LGF-IV#c	0.37	0.52	3.26	0.32	0.39	0.84	0.37	0.48	0.87	1.01	0.75	0.93
LGF-V#c	0.36	0.51	2.91	0.33	0.40	0.36	0.41	0.55	0.91	1.13	0.78	1.07
Combined Graded Fibers (CGF), V_f = 0.3%												
CGF-I#c	0.47	0.70	0.87	0.37	0.48	99.07	0.23	0.23	0.79	0.48	0.68	0.33
CGF-II#c	0.65	0.79	0.72	0.38	0.49	16446.46	0.13	0.11	0.58	0.20	0.62	0.14
CGF-III#c	0.59	0.78	0.64	0.38	0.50	1.5×10^{31}	0.00	0.00	0.65	0.00	0.64	0.00
CGF-IV#c	0.53	0.77	0.57	0.39	0.51	2.6×10^{-05}	1.10	2.33	0.73	2.07	0.66	3.02
CGF-V#c	0.48	0.71	0.41	0.40	0.54	0.07	0.48	0.70	0.84	1.01	0.76	0.99

6.7 Proposed Reinforcing Index of Graded Fibers (RI_{GF})

A new equation is proposed to arrive at RI_{GF} for graded fibers. This is developed on the basis of stress strain behaviour and fiber density variations of GGFRC with different fiber volume combinations and is explained below.

Fiber density variation on fracture plane of the specimens with different lengths and different fiber volume fraction of the composite are shown in Fig.5.27 to 5.30 of Chapter-5. it can be observed that the less fibers are present at the corners and edges compared to the center of cross-section in case of 3mm and 6mm length of fibers (Fig 5.27 and 5.28). Where as in case of 12mm and 20mm length fibers, less fibers are present at the center of cross-section compared to corners and edges (Fig.5.29 and 5.30). In case of graded fibers. It can be seen that the composite with short graded fibers (SGF), the fiber density is more at the center and less at the edges and corners (Fig.6.47 to 6.57). Where as in long graded fibers (LGF), the fiber density is more at the edges and corners and less at the center (Fig.6.46 to 6.51). In short graded specimen (SGF) the characteristics of short fiber lengths are reflected and in long graded specimen (LGF) the long fiber lengths are reflected.

Composite with CGF (SGF + LGF) showed the almost uniform distribution as can be seen in Fig.6.46 to 6.51. The combinations of the fiber densities of individual fibers are influencing the improvement in dispersion and orientation of the graded fibers. Short fibers are shown higher dispersion and orientation compared to the long fibers. Addition of Short fibers in to the long fibers shows that the dosage of more than 20% in a total volume given an improved dispersion and orientation of the graded fibers compared to monofibers. Thus the long length fibers must be present in the composite to enhance their properties.

Hence, based on the above observation the fiber density factor is an important property to form the synergy in the Graded fiber composites. In order to reflect the synergistic effect of graded fibers. Average fiber density of short and long length fibers in composite is considered as one of the influencing parameter and taken for obtaining RI_{GF} for graded fibers. An observation of the relation η_d,η_θ vs RI_{MF} for mono fibers shows that smaller RI_{MF} values will have better dispersion and orientation coefficients. Hence, in the graded fibers in order to reflect synergy effect, RI_{GF} values must be smaller to satisfy this and to reflect the synergy effect due to short and long fiber

combination. A parameter reflecting short and long fiber reinforcing index {(RI_S/RI_L).r} is considered for obtaining RI_{GF} for graded fibers.

RI_{GF} for graded fibers defined as product of fiber density factor and effective reinforcement index of shot and long fibers. Thus RI_{GF} is written as

$$\text{Reinforcing Index } (RI_{GF}) = (1+0.5(f_{ds} + f_{dL})).\ (RI_s / RI_L).r \text{ ---------- (24)}$$

Where f_d (f_{ds} or f_{dL}) = Fiber density factor of mono fibers, $RI_s = (V_f.\ L_f/D_f)_S$,

$RI_L = (V_f.\ L_f/D_f)_L$,

r = ratio of percentage of small fiber to large fiber

Now it is required to obtain a method to find f_d (f_{ds} or f_{dL}) for mono fibers. The fiber density of mono fibers are computed and these values are given in Table.5.9 of Chapter-5. Reinforcing index of each fiber length i.e., 3mm, 6mm, 12mm and 20mm with 0.3% volume fraction are already calculated and given in column 4 of Table 5.14 of Chapter-5. In order to understand the variation of f_d with RI_{MF}, points are plotted as shown in Fig.6.52. An examination of the plot and various trails to arrive at the best fit, led to understand that $f_d/2$ varies as power function of RI_{MF} in the form of $f_d/2 = k / (RI_{MF})^n$. The regression expression obtained is $f_d/2 = 0.066\ (RI_{MF})^{-0.907}$ with regression coefficient $R^2 = 0.8804$. Then the relation between RI_{MF} and f_d can be expressed as

$$0.5\ f_d = 0.066\ (RI_{MF})^{-0.907} \text{ ---------- (25)}$$

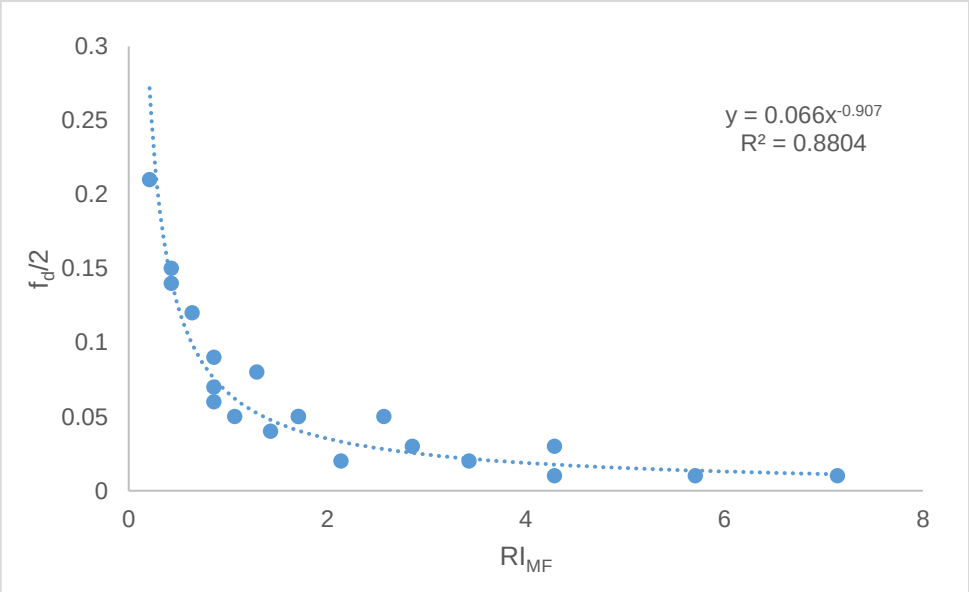

Fig.6.52 Fiber density factor as a function of RI_{MF}

In case of graded fiber $f_d = f_{dS} = f_{dL}$. Here equation (25) is substituted in equation (24) and expression of RI_{GF} is obtained as

$$RI_{GF} = (1+0.06(RI_s^{-0.907} + RI_L^{-0.907})).\ r.\ (RI_s / RI_L) \text{ -------- } (26)$$

The derived equation (26) is used to calculate the reinforcing index (RI_{GF}) of graded fibers. 3mm and 6mm are short fibers and 12mm and 20mm are long fibers. But in this case, the least one is taken as short for the calculation of RI_{GF}**.** In case of RI_{GF} for SGF, 3mm is taken as short and 6mm as taken as long whereas RI_{GF} for LGF, 12mm is taken as short and 20mm is taken as long.

Reinforcing index of each fiber length i.e., 3mm, 6mm, 12mm and 20mm with 0.3% volume fraction are already calculated and given in column 4 of Table 5.14 of Chapter-5. It can be noted from Table 5.14 that RI_{MF} for 3mm is 0.64, RI_{MF} for 6mm is 1.29, RI_{MF} for 12mm is 2.57 and RI_{MF} for 20mm is 4.29. Then the RI_{GF} for SGF-II#c (40%3mm+60%6mm) is obtained from equation (26) by taking the RI_S is 0.64, RI_L is 1.29, and r is ratio of percentage of small fiber to large fiber (0.4/0.6). Thus RI_{GF} for SGF-II#c is 0.39. RI_{GF} for LGF-II#c (40%12mm+60%20mm) is obtained from equation (26) by taking the RI_S is 2.57, RI_L is 4.29, and r is ratio of percentage of small fiber to large fiber (0.4/0.6). Thus RI_{GF} for SGF-II#c is 0.43.

In case of RI_{GF} for CGF, RI_S means RI_{GF} of SGF-II and RI_L means RI_{GF} of LGF-II. RI_{GF} for CGF-II#c (40%SGF+60%LGF) is obtained from equation (26) by taking the RI_S as equal to RI'_{GF} of SGF-II#c and RI_L as equal to RI'_{GF} of LGF-II#c and r is ratio of percentage of small fiber to large fiber (0.4/0.6). Thus RI_{GF} for CGF-II#c is 0.24.

(a) SGF-II#c

$RI_{GF} = (1+0.06(0.64^{-0.907}+1.29^{-0.907})).\ (0.4/0.6).\ (0.64/1.29) = 0.39$

(b) LGF-II#c

$RI_{GF} = (1+0.06(2.57^{-0.907}+4.29^{-0.907})).\ (0.4/0.6).\ (2.57/4.29) = 0.43$

(c) CGF-II#c

$RI_{GF} = (1+0.06(0.39^{-0.907}+0.43^{-0.907})).\ (0.4/0.6).\ (0.39/0.43) = 0.24$

Similarly, reinforcing index (RI_{GF}) is calculated for M30-GGFRC and M50-GGFRC with 0.3%, 0.4% and 0.5% volume fractions using equation (26) and given in column 3 of Table 6.9 to 6.14. The corresponding fiber dispersion and orientation is calculated for

M30-GGFRC and M50-GGFRC by using equation (7) and (8) given in Chapter-5 and these values are reported in column 7 and 8 of Table 6.9 to 6.14. These values are compared with the experimental values given in column 5 and 6 of Table 6.9 to 6.14. The ratio of experimental values to the predicted values are given in column 9 and 10 of Table 6.9 to 6.14. The predicted values of fiber dispersion and orientation are closer to the experimental values and the proposed RI_{GF} is exhibiting the synergistic effect in graded fiber combinations Hence, RI_{GF} can be adopted as an effective reinforcing index for graded fibers.

Table 6.9 η_d', η_θ' calculations for M30-GGFRC with 0.3% volume fraction

Specimen Designation (1)	Combination (2)	RI_{GF} (3)	n_e (4)	Experimental		Predicted		Ratios	
				η_d (5)	η_θ (6)	η_d' (7)	η_θ' (8)	η_d'/η_d (9)	η_θ'/η_θ (10)
Short Graded Fibers (SGF), V_f = 0.3%									
SGF-I#c	20%F3+80%F6	0.15	11018	0.44	0.63	0.54	0.65	1.23	1.03
SGF-II#c	40%F3+60%F6	0.39	16552	0.51	0.75	0.44	0.56	0.87	0.75
SGF-III#c	50%F3+50%F6	0.59	15366	0.48	0.74	0.41	0.53	0.85	0.72
SGF-IV#c	60%F3+40%F6	0.88	13666	0.46	0.70	0.38	0.50	0.81	0.71
SGF-V#c	80%F3+20%F6	2.36	11934	0.45	0.66	0.31	0.43	0.68	0.65
Long Graded Fibers (LGF), V_f = 0.3%									
LGF-I#c	20%F12+80%F20	0.16	5408	0.35	0.50	0.53	0.64	1.51	1.30
LGF-II#c	40%F12+60%F20	0.43	8248	0.42	0.56	0.44	0.55	1.05	0.98
LGF-III#c	50%F12+50%F20	0.64	7524	0.39	0.54	0.40	0.52	1.02	0.96
LGF-IV#c	60%F12+40%F20	0.96	6644	0.37	0.52	0.37	0.49	0.99	0.93
LGF-V#c	80%F12+20%F20	2.54	5924	0.36	0.51	0.30	0.42	0.85	0.82
Combined Graded Fibers (CGF), V_f = 0.3%									
CGF-I#c	20%SGF+80%LGF	0.09	13750	0.47	0.70	0.60	0.70	1.28	1.00
CGF-II#c	40%SGF+60%LGF	0.24	20504	0.65	0.79	0.49	0.61	0.75	0.76
CGF-III#c	50%SGF+50%LGF	0.35	19116	0.59	0.78	0.45	0.57	0.77	0.73
CGF-IV#c	60%SGF+40%LGF	0.53	16772	0.53	0.77	0.42	0.54	0.78	0.70
CGF-V#c	80%SGF+20%LGF	1.42	15072	0.48	0.71	0.34	0.46	0.71	0.65
Note: Number of fibers for MGFRC-0.3% n_e for 3mm is 13718, n_e for 6mm is 9800, n_e for 12mm is 6278, n_e for 20mm is 3696									

Table 6.10 η_d', η_θ' calculations for M30-GGFRC with 0.4% volume fraction

Specimen Designation (1)	Combination (2)	RI_{GF} (3)	n_e (4)	Experimental		Predicted		Ratios	
				η_d (5)	η_θ (6)	η_d' (7)	η_θ' (8)	η_d' / η_d (9)	$\eta_\theta' / \eta_\theta$ (10)
Short Graded Fibers (SGF), V_f = 0.4%									
SGF-I#d	20%F3+80%F6	0.14	11568	0.53	0.69	0.55	0.66	1.04	0.95
SGF-II#d	40%F3+60%F6	0.37	17378	0.61	0.80	0.45	0.57	0.73	0.71
SGF-III#d	50%F3+50%F6	0.56	16134	0.58	0.79	0.41	0.53	0.71	0.68
SGF-IV#d	60%F3+40%F6	0.83	14350	0.56	0.75	0.38	0.50	0.68	0.67
SGF-V#d	80%F3+20%F6	1.67	12530	0.54	0.72	0.33	0.45	0.61	0.63
Long Graded Fibers (LGF), V_f = 0.4%									
LGF-I#d	20%F12+80%F20	0.16	5652	0.40	0.53	0.53	0.65	1.35	1.22
LGF-II#d	40%F12+60%F20	0.42	8620	0.47	0.60	0.44	0.56	0.94	0.92
LGF-III#d	50%F12+50%F20	0.62	7864	0.44	0.58	0.40	0.52	0.92	0.90
LGF-IV#d	60%F12+40%F20	0.94	6944	0.42	0.56	0.37	0.49	0.89	0.88
LGF-V#d	80%F12+20%F20	2.50	6192	0.40	0.55	0.30	0.42	0.76	0.77
Combined Graded Fibers (LGF), V_f = 0.4%									
CGF-I#d	20%SGF+80%LGF	0.08	14196	0.53	0.74	0.61	0.71	1.16	0.96
CGF-II#d	40%SGF+60%LGF	0.22	21170	0.74	0.84	0.50	0.61	0.68	0.73
CGF-III#d	50%SGF+50%LGF	0.33	19738	0.66	0.82	0.46	0.58	0.69	0.70
CGF-IV#d	60%SGF+40%LGF	0.49	17318	0.60	0.78	0.42	0.54	0.70	0.69
CGF-V#d	80%SGF+20%LGF	1.30	15562	0.54	0.76	0.35	0.47	0.64	0.62
Note: Number of fibers for MGFRC-0.4% n_e for 3mm is 10308, n_e for 6mm is 5964, n_e for 12mm is 3310, n_e for 20mm is 2294									

Table 6.11 η_d', η_θ' calculations for M30-GGFRC with 0.5% volume fraction

Specimen Designation (1)	Combination (2)	RI_{GF} (3)	n_e (4)	Experimental		Predicted		Ratios	
				η_d (5)	η_θ (6)	η_d' (7)	η_θ' (8)	η_d' / η_d (9)	$\eta_\theta' / \eta_\theta$ (10)
Short Graded Fibers (SGF), V_f = 0.5%									
SGF-I#e	20%F3+80%F6	0.13	12032	0.55	0.74	0.55	0.66	1.00	0.90
SGF-II#e	40%F3+60%F6	0.36	18074	0.64	0.86	0.45	0.57	0.70	0.66
SGF-III#e	50%F3+50%F6	0.54	16778	0.60	0.84	0.42	0.54	0.69	0.64
SGF-IV#e	60%F3+40%F6	0.80	14924	0.58	0.80	0.38	0.50	0.66	0.63
SGF-V#e	80%F3+20%F6	2.14	13030	0.57	0.77	0.31	0.43	0.55	0.57
Long Graded Fibers (LGF), V_f = 0.5%									
LGF-I#e	20%F12+80%F20	0.15	5972	0.44	0.57	0.54	0.65	1.21	1.14
LGF-II#e	40%F12+60%F20	0.41	9110	0.52	0.65	0.44	0.56	0.84	0.86
LGF-III#e	50%F12+50%F20	0.61	8310	0.49	0.62	0.40	0.52	0.82	0.84
LGF-IV#e	60%F12+40%F20	0.92	7338	0.47	0.60	0.37	0.49	0.80	0.82
LGF-V#e	80%F12+20%F20	2.45	6544	0.45	0.59	0.30	0.42	0.68	0.72
Combined Graded Fibers (CGF), V_f = 0.5%									
CGF-I#e	20%SGF+80%LGF	0.08	14556	0.61	0.79	0.62	0.72	1.01	0.91
CGF-II#e	40%SGF+60%LGF	0.21	21708	0.79	0.89	0.50	0.62	0.64	0.69
CGF-III#e	50%SGF+50%LGF	0.31	20238	0.73	0.87	0.46	0.58	0.64	0.66
CGF-IV#e	60%SGF+40%LGF	0.47	17758	0.68	0.83	0.43	0.55	0.63	0.66
CGF-V#e	80%SGF+20%LGF	1.25	15958	0.67	0.80	0.35	0.47	0.53	0.59
Note: Number of fibers for M30-GGFRC-0.5% n_e for 3mm is 9200, n_e for 6mm is 4802, n_e for 12mm is 2718, n_e for 20mm is 2058									

Table 6.12 η_d', η_θ' calculations for M50-GGFRC with 0.3% volume fraction

Specimen Designation (1)	Combination (2)	RI_{GF} (3)	n_e (4)	Experimental		Predicted		Ratios	
				η_d (5)	η_θ (6)	η_d' (7)	η_θ' (8)	η_d'/η_d (9)	η_θ'/η_θ (10)
Short Graded Fibers (SGF), V_f = 0.3%									
SGF-I#c	20%F3+80%F6	0.15	11142	0.45	0.64	0.54	0.65	1.20	1.02
SGF-II#c	40%F3+60%F6	0.39	16740	0.52	0.76	0.44	0.56	0.85	0.74
SGF-III#c	50%F3+50%F6	0.59	15538	0.49	0.74	0.41	0.53	0.83	0.71
SGF-IV#c	60%F3+40%F6	0.88	13822	0.48	0.71	0.38	0.50	0.79	0.70
SGF-V#c	80%F3+20%F6	2.36	12068	0.46	0.66	0.31	0.43	0.66	0.64
Long Graded Fibers (LGF), V_f = 0.3%									
LGF-I#c	20%F12+80%F20	0.16	5474	0.36	0.50	0.53	0.64	1.47	1.29
LGF-II#c	40%F12+60%F20	0.43	8350	0.42	0.57	0.44	0.55	1.02	0.97
LGF-III#c	50%F12+50%F20	0.64	7618	0.40	0.55	0.40	0.52	1.00	0.95
LGF-IV#c	60%F12+40%F20	0.96	6726	0.38	0.53	0.37	0.49	0.97	0.92
LGF-V#c	80%F12+20%F20	2.54	5998	0.37	0.52	0.30	0.42	0.83	0.81
Combined Graded Fibers (CGF), V_f = 0.3%									
CGF-I#c	20%SGF+80%LGF	0.09	13958	0.48	0.71	0.60	0.70	1.25	0.99
CGF-II#c	40%SGF+60%LGF	0.24	20816	0.67	0.80	0.49	0.61	0.74	0.76
CGF-III#c	50%SGF+50%LGF	0.35	19408	0.60	0.79	0.45	0.57	0.75	0.73
CGF-IV#c	60%SGF+40%LGF	0.53	17028	0.54	0.78	0.42	0.54	0.76	0.69
CGF-V#c	80%SGF+20%LGF	1.42	15302	0.49	0.72	0.34	0.46	0.69	0.64
Note: Number of fibers for MGFRC-0.3% n_e for 3mm is 14808, n_e for 6mm is 10174, n_e for 12mm is 6700, n_e for 20mm is 3886									

Table 6.13 η_d', η_θ' calculations for M50-GGFRC with 0.4% volume fraction

Specimen Designation (1)	Combination (2)	RI_{GF} (3)	n_e (4)	Experimental		Predicted		Ratios	
				η_d (5)	η_θ (6)	η_d' (7)	η_θ' (8)	η_d' / η_d (9)	$\eta_\theta' / \eta_\theta$ (10)
Short Graded Fibers (SGF), V_f = 0.4%									
SGF-I#d	20%F3+80%F6	0.14	11600	0.54	0.70	0.55	0.66	1.01	0.94
SGF-II#d	40%F3+60%F6	0.37	17426	0.63	0.81	0.45	0.57	0.71	0.70
SGF-III#d	50%F3+50%F6	0.56	16176	0.59	0.79	0.41	0.53	0.70	0.67
SGF-IV#d	60%F3+40%F6	0.83	14388	0.57	0.76	0.38	0.50	0.67	0.66
SGF-V#d	80%F3+20%F6	1.67	12564	0.55	0.72	0.33	0.45	0.59	0.62
Long Graded Fibers (LGF), V_f = 0.4%									
LGF-I#d	20%F12+80%F20	0.16	5722	0.41	0.54	0.53	0.65	1.32	1.21
LGF-II#d	40%F12+60%F20	0.42	8726	0.48	0.61	0.44	0.56	0.92	0.91
LGF-III#d	50%F12+50%F20	0.62	7962	0.45	0.59	0.40	0.52	0.90	0.89
LGF-IV#d	60%F12+40%F20	0.94	7030	0.43	0.57	0.37	0.49	0.87	0.87
LGF-V#d	80%F12+20%F20	2.50	6268	0.41	0.56	0.30	0.42	0.74	0.76
Combined Graded Fibers (CGF), V_f = 0.4%									
CGF-I#d	20%SGF+80%LGF	0.08	14412	0.54	0.75	0.61	0.71	1.13	0.95
CGF-II#d	40%SGF+60%LGF	0.22	21492	0.75	0.85	0.50	0.61	0.66	0.72
CGF-III#d	50%SGF+50%LGF	0.33	20038	0.68	0.83	0.46	0.58	0.68	0.69
CGF-IV#d	60%SGF+40%LGF	0.49	17582	0.61	0.79	0.42	0.54	0.69	0.69
CGF-V#d	80%SGF+20%LGF	1.30	15800	0.56	0.76	0.35	0.47	0.62	0.61
Note: Number of fibers for MGFRC-0.4% n_e for 3mm is 10838, n_e for 6mm is 8832, n_e for 12mm is 3450, n_e for 20mm is 2374									

Table 6.14 η_d', η_θ' calculations for M50-GGFRC with 0.5% volume fraction

Specimen Designation (1)	Combination (2)	RI_{GF} (3)	n_e (4)	Experimental		Predicted		Ratios	
				η_d (5)	η_θ (6)	η_d' (7)	η_θ' (8)	η_d'/η_d (9)	η_θ'/η_θ (10)
Short Graded Fibers (SGF), V_f = 0.5%									
SGF-I#e	20%F3+80%F6	0.13	12064	0.57	0.74	0.55	0.66	0.98	0.89
SGF-II#e	40%F3+60%F6	0.36	18122	0.66	0.87	0.45	0.57	0.69	0.66
SGF-III#e	50%F3+50%F6	0.54	16822	0.62	0.85	0.42	0.54	0.67	0.63
SGF-IV#e	60%F3+40%F6	0.80	14964	0.60	0.81	0.38	0.50	0.64	0.62
SGF-V#e	80%F3+20%F6	2.14	13066	0.58	0.78	0.31	0.43	0.54	0.56
Long Graded Fibers (LGF), V_f = 0.5%									
LGF-I#d	20%F12+80%F20	0.15	5722	0.41	0.54	0.53	0.65	1.32	1.21
LGF-II#d	40%F12+60%F20	0.41	8726	0.48	0.61	0.44	0.56	0.92	0.91
LGF-III#d	50%F12+50%F20	0.61	7962	0.45	0.59	0.40	0.52	0.90	0.89
LGF-IV#d	60%F12+40%F20	0.92	7030	0.43	0.57	0.37	0.49	0.87	0.87
LGF-V#d	80%F12+20%F20	2.45	6268	0.41	0.56	0.30	0.42	0.74	0.76
Combined Graded Fibers (CGF), V_f = 0.5%									
CGF-I#e	20%SGF+80%LGF	0.08	14778	0.63	0.80	0.62	0.72	0.98	0.90
CGF-II#e	40%SGF+60%LGF	0.21	22038	0.81	0.90	0.50	0.62	0.62	0.69
CGF-III#e	50%SGF+50%LGF	0.31	20546	0.75	0.88	0.46	0.58	0.62	0.66
CGF-IV#e	60%SGF+40%LGF	0.47	18028	0.69	0.84	0.43	0.55	0.62	0.65
CGF-V#e	80%SGF+20%LGF	1.25	16200	0.68	0.81	0.35	0.47	0.51	0.58
Note: Number of fibers for M30-GGFRC-0.5% n_e for 3mm is 9580, n_e for 6mm is 5080, n_e for 12mm is 2814, n_e for 20mm is 2134									

6.8 Theoretical analysis for predicting the tensile stress strain behaviour of GGFRC

6.9 Tensile strength of composite (σ^{GF}_{ct}) for GGFRC

The composite tensile strength (σ^{GF}_{ct}) of GGFRC is calculated similar to the MGFRC by using equation (10) given in Chapter-5 and rewritten below. Fiber dispersion coefficients (η_d') and fiber orientation coefficients (η_θ') from equation (7) and (8) with RI_{GF} of short graded fibers, long graded fibers and combined graded fibers are reported in column 3, 4 of Table 6.15 to 6.20 for M30-GGFRC and M50-GGFRC with 0.3%, 0.4% and 0.5% volume fraction. Fiber length coefficient (η_l') is calculated as explained in article 6.1 for all specimens and given in column 5 of Table 6.15 to 6.20. Then the composite tensile strength (σ^{GF}_{ct}) of M30-GGFRC and M50-GGFRC with 0.3%, 0.4% and 0.5% volume fraction is calculated and the values are reported in

column 6 of Table 6.15 to 6.20 and these values are compared with the corresponding experimental values given in column 7 of Table 6.15 to 6.20. The ratio of the calculated composite strength values to that of experimental strength values are shown in column 8 of Table 6.15 to 6.20. It can be noted that the composite strength values obtained from equation 10 are close to the experimental composite strength values of both M30 and M50 grade of concrete with 0.3%,0.4% and 0.5% volume fraction.

$$\sigma^{GF}_{ct} = \eta_d' \eta_\theta' \eta_l' V_f \sigma_{fu} + V_m \sigma_{mt}$$

Table 6.15 Predicted composite tensile strength (σ^{GF}_{ct}) of M30-GGFRC-0.3%

Specimen Designation (1)	RI_{GF} (2)	η_d' (3)	η_θ' (4)	η_l' (5)	σ^{GF}_{ct} (6)	σ^{GF}_{tu} (7)	Ratio = (6)/(7) (8)
Short Graded Fibers (SGF), V_f = 0.3%							
SGF-I#c	0.15	0.54	0.65	0.42	4.43	4.30	1.03
SGF-II#c	0.39	0.44	0.56	0.42	4.20	5.19	0.81
SGF-III#c	0.59	0.41	0.53	0.41	4.12	5.06	0.81
SGF-IV#c	0.88	0.38	0.50	0.41	4.06	4.68	0.87
SGF-V#c	2.36	0.31	0.43	0.40	3.94	4.30	0.92
Long Graded Fibers (LGF), V_f = 0.3%							
LGF-I#c	0.16	0.53	0.64	0.43	4.66	3.75	1.24
LGF-II#c	0.43	0.44	0.55	0.42	4.35	4.43	0.98
LGF-III#c	0.64	0.40	0.52	0.41	4.25	4.30	0.99
LGF-IV#c	0.96	0.37	0.49	0.41	4.17	4.05	1.03
LGF-V#c	2.54	0.30	0.42	0.40	4.01	3.80	1.06
Combined Graded Fibers (CGF), V_f = 0.3%							
CGF-I#c	0.09	0.60	0.70	0.43	4.81	4.52	1.06
CGF-II#c	0.24	0.49	0.61	0.42	4.43	5.50	0.81
CGF-III#c	0.35	0.45	0.57	0.41	4.31	5.38	0.80
CGF-IV#c	0.53	0.42	0.54	0.41	4.21	4.89	0.86
CGF-V#c	1.42	0.34	0.46	0.40	4.03	4.55	0.88
σ_{mt} = 3.68, ε_{mt} = 1.18 x 10^{-4}							

Table 6.16 Predicted composite tensile strength (σ^{GF}_{ct}) of M30-GGFRC-0.4%

Specimen Designation (1)	RI_{GF} (2)	η_d (3)	η_θ (4)	η_l (5)	σ^{GF}_{ct} (6)	σ^{GF}_{tu} (7)	Ratio = (6)/(7) (8)
ShortGraded Fibers (SGF), V_f = 0.4%							
SGF-I#d	0.14	0.55	0.66	0.42	4.45	4.38	1.02
SGF-II#d	0.37	0.45	0.57	0.42	4.21	5.42	0.78
SGF-III#d	0.56	0.41	0.53	0.41	4.13	5.14	0.80
SGF-IV#d	0.83	0.38	0.50	0.41	4.07	4.79	0.85
SGF-V#d	1.67	0.33	0.45	0.40	3.97	4.41	0.90
Long Graded Fibers (LGF), V_f = 0.4%							
LGF-I#d	0.16	0.53	0.65	0.43	4.67	3.87	1.21
LGF-II#d	0.43	0.44	0.56	0.42	4.36	4.68	0.93
LGF-III#d	0.64	0.40	0.52	0.41	4.26	4.43	0.96
LGF-IV#d	0.96	0.37	0.49	0.41	4.17	4.18	1.00
LGF-V#d	2.54	0.30	0.42	0.40	4.01	3.90	1.03
Combined Graded Fibers (CGF), V_f = 0.4%							
CGF-I#d	0.08	0.61	0.71	0.43	4.84	4.60	1.05
CGF-II#d	0.22	0.50	0.61	0.42	4.45	5.75	0.77
CGF-III#d	0.33	0.46	0.58	0.41	4.33	5.48	0.79
CGF-IV#d	0.49	0.42	0.54	0.41	4.22	5.01	0.84
CGF-V#d	1.30	0.35	0.47	0.40	4.04	4.64	0.87

Table 6.17 Predicted composite tensile strength (σ^{GF}_{ct}) of M30-GGFRC-0.5%

Specimen Designation (1)	RI_{GF} (2)	η_d (3)	η_θ (4)	η_l (5)	σ^{GF}_{ct} (6)	σ^{GF}_{tu} (7)	Ratio = (6)/(7) (8)
ShortGraded Fibers (SGF), V_f = 0.5%							
SGF-I#e	0.13	0.55	0.66	0.42	4.46	4.30	1.04
SGF-II#e	0.36	0.45	0.57	0.42	4.22	5.65	0.75
SGF-III#e	0.54	0.42	0.54	0.41	4.14	5.44	0.76
SGF-IV#e	0.80	0.38	0.50	0.41	4.07	4.94	0.82
SGF-V#e	2.14	0.31	0.43	0.40	3.95	4.59	0.86
Long Graded Fibers (LGF), V_f = 0.5%							
LGF-I#e	0.15	0.54	0.65	0.43	4.68	4.00	1.17
LGF-II#e	0.41	0.44	0.56	0.42	4.36	4.84	0.90
LGF-III#e	0.61	0.40	0.52	0.41	4.26	4.56	0.94
LGF-IV#e	0.92	0.37	0.49	0.41	4.18	4.30	0.97
LGF-V#e	2.45	0.30	0.42	0.40	4.02	4.05	0.99

Combined Graded Fibers (CGF), V_f = 0.5%							
CGF-I#e	0.08	0.62	0.72	0.43	4.86	4.52	1.07
CGF-II#e	0.21	0.50	0.62	0.42	4.46	5.87	0.76
CGF-III#e	0.31	0.46	0.58	0.41	4.34	5.75	0.75
CGF-IV#e	0.47	0.43	0.55	0.41	4.23	5.33	0.79
CGF-V#e	1.25	0.35	0.47	0.40	4.04	4.79	0.84

Table 6.18 Predicted composite tensile strength (σ^{GF}_{ct}) of M50-GGFRC-0.3%

Specimen Designation (1)	RI_{GF} (2)	η_d (3)	η_θ (4)	η_l (5)	σ^{GF}_{ct} (6)	σ^{GF}_{tu} (7)	Ratio = (6)/(7) (8)
Short Graded Fibers (SGF), V_f = 0.3%							
SGF-I#c	0.15	0.54	0.65	0.49	6.49	6.56	0.99
SGF-II#c	0.39	0.44	0.56	0.48	6.22	7.71	0.81
SGF-III#c	0.59	0.41	0.53	0.48	6.14	7.54	0.81
SGF-IV#c	0.88	0.38	0.50	0.47	6.06	7.03	0.86
SGF-V#c	2.36	0.31	0.43	0.46	5.92	6.48	0.91
Long Graded Fibers (LGF), V_f = 0.3%							
LGF-I#c	0.16	0.53	0.64	0.63	6.71	5.72	1.17
LGF-II#c	0.43	0.44	0.55	0.62	6.37	6.56	0.97
LGF-III#c	0.64	0.40	0.52	0.61	6.26	6.31	0.99
LGF-IV#c	0.96	0.37	0.49	0.60	6.17	6.06	1.02
LGF-V#c	2.54	0.30	0.42	0.59	6.00	5.72	1.05
Combined Graded Fibers (CGF), V_f = 0.3%							
CGF-I#c	0.09	0.60	0.70	0.59	6.88	6.89	1.00
CGF-II#c	0.24	0.49	0.61	0.56	6.47	8.45	0.77
CGF-III#c	0.35	0.45	0.57	0.55	6.33	8.14	0.78
CGF-IV#c	0.53	0.42	0.54	0.53	6.22	7.56	0.82
CGF-V#c	1.42	0.34	0.46	0.51	6.02	6.89	0.87
σ_{mt} = 5.63, ε_{mt} = 1.18 X 10^{-4}							

Table 6.19 Predicted composite tensile strength (σ^{GF}_{ct}) of M50-GGFRC-0.4%

Specimen Designation (1)	RI_{GF} (2)	η_d (3)	η_θ (4)	η_l (5)	σ^{GF}_{ct} (6)	σ^{GF}_{tu} (7)	Ratio = (6)/(7) (8)
Short Graded Fibers (SGF), V_f = 0.4%							
SGF-I#d	0.14	0.55	0.66	0.49	6.51	6.77	0.96
SGF-II#d	0.37	0.45	0.57	0.48	6.23	7.92	0.79
SGF-III#d	0.56	0.41	0.53	0.48	6.15	7.75	0.79
SGF-IV#d	0.83	0.38	0.50	0.47	6.07	7.11	0.85
SGF-V#d	1.67	0.33	0.45	0.46	5.96	6.69	0.89
Long Graded Fibers (LGF), V_f = 0.4%							
LGF-I#d	0.16	0.53	0.65	0.63	6.72	5.93	1.13
LGF-II#d	0.43	0.44	0.56	0.62	6.38	6.77	0.94
LGF-III#d	0.64	0.40	0.52	0.61	6.27	6.52	0.96
LGF-IV#d	0.96	0.37	0.49	0.60	6.17	6.27	0.99
LGF-V#d	2.54	0.30	0.42	0.59	6.00	5.93	1.01
Combined Graded Fibers (CGF), V_f = 0.4%							
CGF-I#d	0.08	0.61	0.71	0.59	6.92	7.11	0.97
CGF-II#d	0.22	0.50	0.61	0.56	6.49	8.67	0.75
CGF-III#d	0.33	0.46	0.58	0.55	6.36	8.36	0.76
CGF-IV#d	0.49	0.42	0.54	0.53	6.24	7.78	0.80
CGF-V#d	1.30	0.35	0.47	0.51	6.03	7.11	0.85

Table 6.20 Predicted composite tensile strength (σ^{GF}_{ct}) of M50-GGFRC-0.5%

Specimen Designation (1)	RI_{GF} (2)	η_d (3)	η_θ (4)	η_l (5)	σ^{GF2}_{ct} (6)	σ^{GF}_{tu} (7)	Ratio = (6)/(7) (8)
Short Graded Fibers (SGF), V_f = 0.5%							
SGF-I#e	0.13	0.55	0.66	0.49	6.52	6.99	0.93
SGF-II#e	0.36	0.45	0.57	0.48	6.24	8.13	0.77
SGF-III#e	0.54	0.42	0.54	0.48	6.15	8.05	0.76
SGF-IV#e	0.80	0.38	0.50	0.47	6.07	7.33	0.83
SGF-V#e	2.14	0.31	0.43	0.46	5.93	6.91	0.86
Long Graded Fibers (LGF), V_f = 0.5%							
LGF-I#e	0.15	0.54	0.65	0.63	6.73	6.14	1.09
LGF-II#e	0.41	0.44	0.56	0.62	6.38	7.00	0.91
LGF-III#e	0.61	0.40	0.52	0.61	6.27	6.74	0.93
LGF-IV#e	0.92	0.37	0.49	0.60	6.18	6.48	0.95
LGF-V#e	2.45	0.30	0.42	0.59	6.00	6.15	0.98

Combined Graded Fibers (CGF), V_f = 0.5%							
CGF-I#e	0.08	0.62	0.72	0.59	6.94	7.34	0.95
CGF-II#e	0.21	0.50	0.62	0.56	6.51	9.12	0.71
CGF-III#e	0.31	0.46	0.58	0.55	6.37	8.58	0.74
CGF-IV#e	0.47	0.43	0.55	0.53	6.25	8.00	0.78
CGF-V#e	1.25	0.35	0.47	0.51	6.04	7.34	0.82

6.10 Tensile strain at peak tensile strength of composite (ε^{GF}_{ct}) for GGFRC

The composite tensile strain (ε^{GF}_{ct}) of GGFRC is calculated similar to the MGFRC by using equation (11) given in Chapter-5. Equation (11) is rewritten below.

$$\text{Tensile strain of the composite } (\varepsilon_{ct}^{MF}) = \frac{2EA_{MF}^{SHR}}{(\sigma_{ct}^{MF} + \sigma_{mt})} + \boldsymbol{\varepsilon_{mt}}$$

In case of graded fibers,the MF (mono fibers) is to be replaced with GF (garded fibers), ε_{ct}^{GF} = composite tensile strain, σ_{ct}^{GF} = composite tensile strength, EA_{GF}^{SHR} = energy absorption in strain hardening region.

Tensile strain (ε^{GF}_{ct}) mainly depends on the composite tensile strength (σ^{GF}_{ct}) and energy absorption capacity of the composite. The above calculated composite tensile strength (σ^{GF}_{ct}) of M30-GGFRC and M50-GGFRC are extracted from column 6 of Table 6.15 to 6.20 and given in column of 4 of Table 6.21 to 6.26. EA_{GF}^{SHR} is computed already and is given in column 10 Table 6.1 to 6.6. The reinforcing index of each mix was calculated and is given in column 2 of Table 6.21 to 6.26. In order to understand the variation of EA_{GF}^{SHR} with RI_G, points are plotted as shown in Fig.6.53 (a). An examination of the plot it is understood that EA_{GF}^{SHR} varies as power function of RI_{GF} in the form of $EA_{GF}^{SHR} = k / (RI_{GF})^n$. The power function is modified by multiplying both sides by RI_{GF}. The modified relation is $(RI_G)\ EA_{GF}^{SHR} = k\ (RI_{GF})^{(1-n)}$. Now points are plotted with RI_G as abscissa and $RI_{GF}.\ EA_{GF}^{SHR}$ as ordinate is shown in Fig.6.53 (b). The regression expression obtained is $(RI_{GF})\ EA_{GF}^{SHR} = 9.75 \times 10^{-4}\ (RI_{GF})^{0.816}$ with regression coefficient $R^2 = 0.86$. Then the relation between RI_G and EA_{GF}^{SHR} can be expressed as.

$$EA_{GF}^{SHR} = 9.75X10^{-4}\ RI_{GF}^{-0.184} \text{ ---------- (27)}$$

Energy absorption of the strain hardening region (EA_{GF}^{SHR}) for M30-MGFRC and M50-MGFRC with 0.3%, 0.4%, 0.5% volume fractions are calculated from equation (27)

and reported in column 3 of Table 6.21 to 6.26.The experimental strain (ε^{GF}_{ct}) at ultimate tensile strength of each M30-GGFRC and M50-GGFRC is computed from equation (11) and reported in column 5 of Table 6.21 to 6.26 and these values are compared with the experimental tensile strain (ε_{ct}) values in column 6 of Table 6.21 to 6.26. The ratio of the calculated tensile strain of fiber composite to that of experimental tensile strain are also shown in column 7 of Table 6.21 to 6.26. It can be noted that the strain at composite strength (ε^{GF}_{ct}) values obtained from equation (11) are close to the experimental tensile strain (ε^{GF}_{ct}) values in both M30-GGFRC and M50-GGFRC.

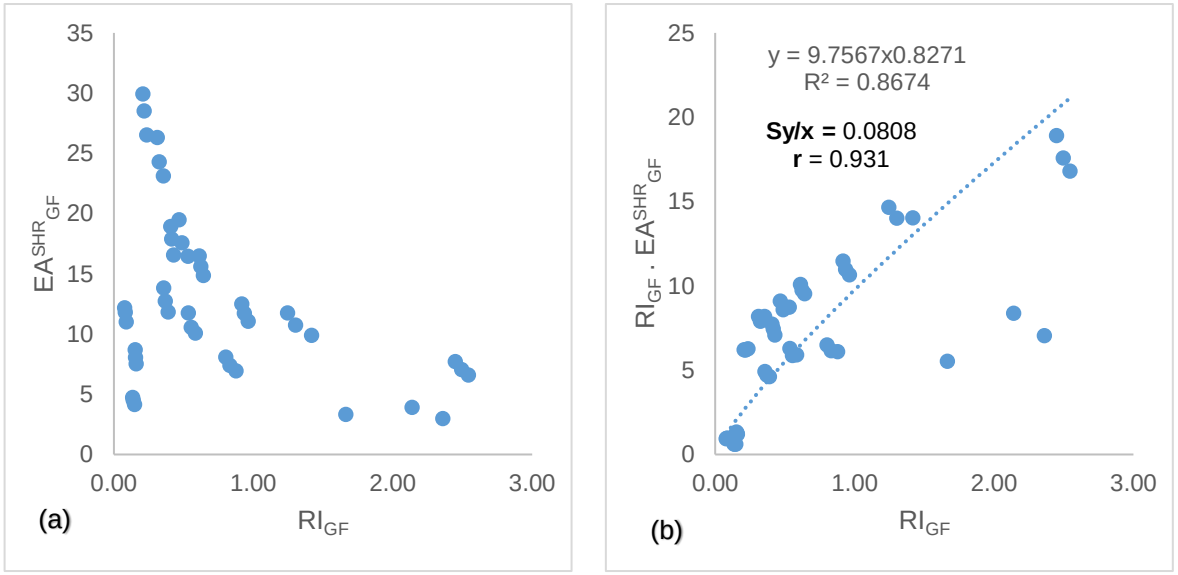

Fig.6.53 Energy absorption of Graded fibers is a function of RI_{GF}

Table 6.21 Predicted tensile strain of M30-GGFRC-0.3%

Specimen Designation (1)	RI_{GF} (2)	EA^{SHR}_{GF} (3)	σ^{GF}_{ct} (4)	ε^{GF}_{ct}		Ratio = (5)/(6) (7)
				Theoretical (5)	Experimental (6)	
Short Graded Fibers (SGF), V_f = 0.3%						
SGF-I#c	0.15	14.21	4.43	4.50	1.69	2.66
SGF-II#c	0.39	11.88	4.20	4.02	3.22	1.25
SGF-III#c	0.59	11.03	4.12	3.83	2.88	1.33
SGF-IV#c	0.88	10.24	4.06	3.65	2.29	1.59
SGF-V#c	2.36	8.54	3.94	3.24	1.36	2.39
Long Graded Fibers (LGF), V_f = 0.3%						
LGF-I#c	0.16	14.01	4.66	4.36	3.05	1.43
LGF-II#c	0.43	11.68	4.35	3.91	5.08	0.77

LGF-III#c	0.64	10.85	4.25	3.73	4.74	0.79
LGF-IV#c	0.96	10.07	4.17	3.57	3.90	0.92
LGF-V#c	2.54	8.43	4.01	3.19	2.71	1.18
Combined Graded Fibers (CGF), V_f = 0.3%						
CGF-I#c	0.09	15.60	4.81	4.68	3.33	1.40
CGF-II#c	0.24	13.03	4.43	4.21	6.05	0.70
CGF-III#c	0.35	12.10	4.31	4.03	5.45	0.74
CGF-IV#c	0.53	11.23	4.21	3.85	4.39	0.88
CGF-V#c	1.42	9.38	4.03	3.43	3.03	1.14
σ_{mt} = 3.68 MPa, ε_{mt} = 1.18 X 10^{-4}						

Table 6.22 Predicted tensile strain of M30-GGFRC-0.4%

Specimen Designation (1)	RI_{GF} (2)	EA_{GF}^{SHR} (3)	σ^{GF}_{ct} (4)	ε^{GF}_{ct}		Ratio = (5)/(6) (7)
				Theoretical (5)	Experimental (6)	
Short Graded Fibers (SGF), V_f = 0.4%						
SGF-I#d	0.14	15.13	4.45	4.53	1.69	2.68
SGF-II#d	0.37	16.28	4.21	4.04	3.22	1.26
SGF-III#d	0.56	13.77	4.13	3.85	2.88	1.34
SGF-IV#d	0.83	11.13	4.07	3.67	2.29	1.60
SGF-V#d	1.67	7.23	3.97	3.38	1.36	2.49
Long Graded Fibers (LGF), V_f = 0.4%						
LGF-I#d	0.16	16.46	4.67	4.37	3.05	1.43
LGF-II#d	0.42	15.61	4.36	3.92	5.08	0.77
LGF-III#d	0.62	13.00	4.26	3.75	4.74	0.79
LGF-IV#d	0.94	10.40	4.17	3.58	3.90	0.92
LGF-V#d	2.50	5.47	4.01	3.20	2.71	1.18
Combined Graded Fibers (CGF), V_f = 0.4%						
CGF-I#d	0.08	-0.39	4.84	4.72	3.33	1.42
CGF-II#d	0.22	17.92	4.45	4.25	6.05	0.70
CGF-III#d	0.33	16.93	4.33	4.07	5.45	0.75
CGF-IV#d	0.49	14.60	4.22	3.89	4.39	0.89
CGF-V#d	1.30	8.49	4.04	3.47	3.03	1.15

Table 6.23 Predicted tensile strain of M30-GGFRC-0.5%

Specimen Designation (1)	RI_{GF} (2)	EA_{GF}^{SHR} (3)	σ^{GF}_{ct} (4)	ε^{GF}_{ct}		Ratio = (5)/(6) (7)
				Theoretical (5)	Experimental (6)	
Short Graded Fibers (SGF), V_f = 0.4%						
SGF-I#e	0.13	14.60	4.46	4.55	1.69	2.69
SGF-II#e	0.36	16.48	4.22	4.06	3.22	1.26
SGF-III#e	0.54	14.02	4.14	3.87	2.88	1.34
SGF-IV#e	0.80	11.36	4.07	3.69	2.29	1.61
SGF-V#e	2.14	6.09	3.95	3.28	1.36	2.42
Long Graded Fibers (LGF), Vf = 0.4%						
LGF-I#e	0.15	16.28	4.68	4.38	3.05	1.43
LGF-II#e	0.41	15.72	4.36	3.93	5.08	0.77
LGF-III#e	0.61	13.13	4.26	3.76	4.74	0.79
LGF-IV#e	0.92	10.52	4.18	3.59	3.90	0.92
LGF-V#e	2.45	5.55	4.02	3.20	2.71	1.18
Combined Graded Fibers (CGF), V_f = 0.5%						
CGF-I#e	0.08	-2.72	4.86	4.74	3.33	1.42
CGF-II#e	0.21	17.88	4.46	4.28	6.05	0.71
CGF-III#e	0.31	17.13	4.34	4.09	5.45	0.75
CGF-IV#e	0.47	14.89	4.23	3.91	4.39	0.89
CGF-V#e	1.25	8.73	4.04	3.49	3.03	1.15

Table 6.24 Predicted tensile strain of M50-GGFRC-0.3%

Specimen Designation (1)	RI_{GF} (2)	EA_{GF}^{SHR} (3)	σ^{GF}_{ct} (4)	ε^{GF}_{ct}		Ratio = (5)/(6) (7)
				Theoretical (5)	Experimental (6)	
Short Graded Fibers (SGF), V_f = 0.3%						
SGF-I#c	0.15	14.21	6.49	4.69	1.86	2.52
SGF-II#c	0.39	11.88	6.22	4.19	3.59	1.17
SGF-III#c	0.59	11.03	6.14	3.99	3.20	1.25
SGF-IV#c	0.88	10.24	6.06	3.81	2.56	1.49
SGF-V#c	2.36	8.54	5.92	3.40	1.53	2.23
Long Graded Fibers (LGF), V_f = 0.3%						
LGF-I#c	0.16	14.01	6.71	4.59	3.22	1.42
LGF-II#c	0.43	11.68	6.37	4.10	5.76	0.71
LGF-III#c	0.64	10.85	6.26	3.92	5.25	0.75
LGF-IV#c	0.96	10.07	6.17	3.74	4.24	0.88
LGF-V#c	2.54	8.43	6.00	3.35	2.85	1.18

Combined Graded Fibers (CGF), V_f = 0.3%						
CGF-I#c	0.09	15.60	6.88	4.92	3.57	1.38
CGF-II#c	0.24	13.03	6.47	4.41	6.51	0.68
CGF-III#c	0.35	12.10	6.33	4.21	5.90	0.71
CGF-IV#c	0.53	11.23	6.22	4.02	4.84	0.83
CGF-V#c	1.42	9.38	6.02	3.60	3.18	1.13
σ_{mt} = 5.63 MPa, ε_{mt} = 1.18 X 10^{-4}						

Table 6.25 Predicted tensile strain of M50-GGFRC-0.4%

Specimen Designation (1)	RI_{GF} (2)	EA_{GF}^{SHR} (3)	σ^{GF}_{ct} (4)	ε^{GF}_{ct}		Ratio = (5)/(6) (7)
				Theoretical (5)	Experimental (6)	
Short Graded Fibers (SGF), V_f = 0.4%						
SGF-I#d	0.14	15.13	6.51	4.73	2.03	2.33
SGF-II#d	0.37	16.28	6.23	4.21	3.76	1.12
SGF-III#d	0.56	13.77	6.15	4.02	3.37	1.19
SGF-IV#d	0.83	11.13	6.07	3.83	2.73	1.40
SGF-V#d	1.67	7.23	5.96	3.54	1.69	2.09
Long Graded Fibers (LGF), V_f = 0.4%						
LGF-I#d	0.16	16.46	6.72	4.60	3.30	1.39
LGF-II#d	0.42	15.61	6.38	4.11	5.93	0.69
LGF-III#d	0.62	13.00	6.27	3.93	5.42	0.72
LGF-IV#d	0.94	10.40	6.17	3.75	4.41	0.85
LGF-V#d	2.50	5.47	6.00	3.36	2.93	1.15
Combined Graded Fibers (CGF), V_f = 0.4%						
CGF-I#d	0.08	0.39	6.92	4.97	3.87	1.28
CGF-II#d	0.22	17.92	6.49	4.45	6.81	0.65
CGF-III#d	0.33	16.93	6.36	4.25	6.20	0.69
CGF-IV#d	0.49	14.60	6.24	4.06	5.14	0.79
CGF-V#d	1.30	8.49	6.03	3.63	3.48	1.04

Table 6.26 Predicted tensile strain of M50-GGFRC-0.5%

Specimen Designation (1)	RI_{GF} (2)	EA_{GF}^{SHR} (3)	σ^{GF}_{ct} (4)	ε^{GF}_{ct}		Ratio = (5)/(6) (7)
				Theoretical (5)	Experimental (6)	
Short Graded Fibers (SGF), V_f = 0.5%						
SGF-I#e	0.13	14.60	6.52	4.75	2.12	2.24
SGF-II#e	0.36	16.48	6.24	4.23	3.93	1.08
SGF-III#e	0.54	14.02	6.15	4.04	3.56	1.13
SGF-IV#e	0.80	11.36	6.07	3.85	2.90	1.33

SGF-V#e	2.14	6.09	5.93	3.44	1.73	1.99
Long Graded Fibers (LGF), V_f = 0.5%						
LGF-I#e	0.15	16.28	6.73	4.61	3.47	1.33
LGF-II#e	0.41	15.72	6.38	4.12	6.10	0.68
LGF-III#e	0.61	13.13	6.27	3.94	5.59	0.70
LGF-IV#e	0.92	10.52	6.18	3.76	4.58	0.82
LGF-V#e	2.45	5.55	6.00	3.37	3.10	1.09
Combined Graded Fibers (CGF), V_f = 0.5%						
CGF-I#e	0.08	2.72	6.94	4.99	4.18	1.20
CGF-II#e	0.21	17.88	6.51	4.48	7.11	0.63
CGF-III#e	0.31	17.13	6.37	4.28	6.51	0.66
CGF-IV#e	0.47	14.89	6.25	4.08	5.45	0.75
CGF-V#e	1.25	8.73	6.04	3.65	3.78	0.96

6.11. Experimental Vs idealized Stress Strain diagram for GGFRC

The experimental tensile stress–strain curves of two concrete mixes, namely, M30-LGF-II#c and M50-LGF-II#c are plotted in Fig.6.54 (a) and (b). The predicted tensile stress–strain values are obtained from equation (10) and (11) for M30-LGF-II#c and M50-LGF-II#c and shown in Fig.6.54 (a) and (b). In the pre-crack region and post-crack region, the predicted curves shows a higher stiffness in both M30 and M50 grade of concrete. In the strain hardening region, the proposed method under estimated strain at ultimate strength.

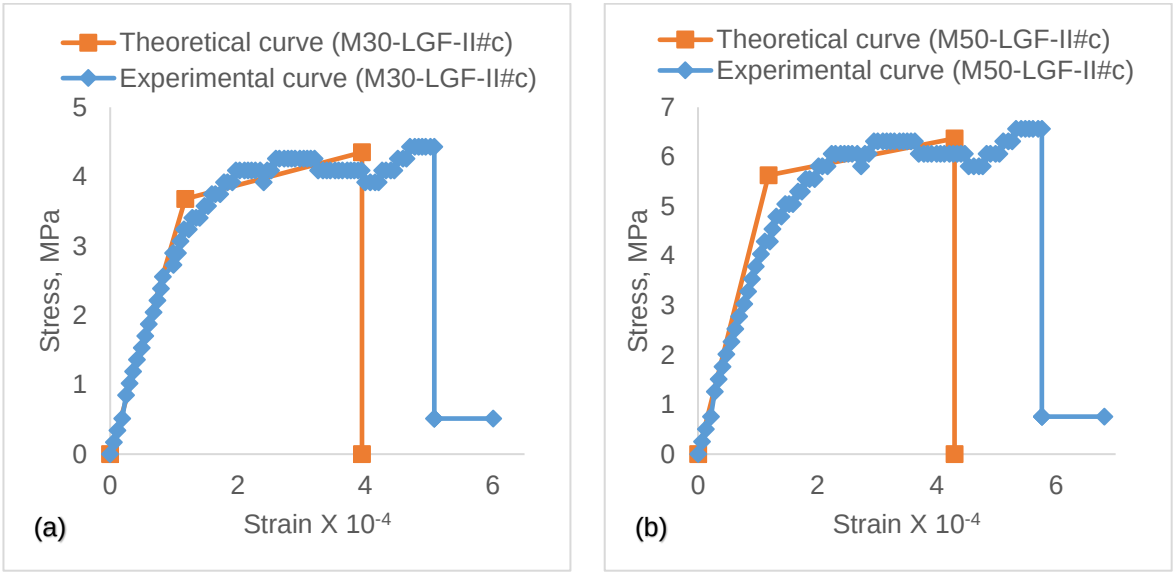

Fig. 6.54. Experimental Vs idealized Stress Strain diagram for GGFRC

6.12. Compressive stress strain behaviour of M30-GGFRC

6.12.1. Short Graded Fibers

3mm and 6mm length fibers are combined as given in Table 4.2 of chapter-4. Compressive stress Strain diagram of short graded fibers (3mm+6mm) is given in Fig.6.55. Considering SGF-I#c, there is 80% of 6mm fibers. Hence the behaviour is compared with 100% 6mm fibers and it can be seen that there is not much improvement in post peak deformation by replacing 100% 6mm fibers with 80% 6mm + 20% 3mm (SGF-I#c). A similar examination for the 3mm fibers can be observed where there is not much improvement in peak strength by replacing the 100% 3mm with 80% 3mm + 20% 6mm (SGF-V#c). The natural characteristics of mono fibers i.e., 3mm is reflected in SGF-V#c and 6mm in SGF-I#c. Further grading of 3mm and 6mm have exhibited completely different behaviour from mono fibers. An equal percentage of volume of fibers 3mm and 6mm i.e., 50% 3mm + 50% 6mm (SGF-III#c) have shown an intermediate behaviour between the SGF-IV#c and SGF-II#c. The specimens containing the 40% of 3mm + 60% 6mm (SGF-II#c) has given the best benefit of improvement in both peak strength and post peak deformation compared to all other short graded fibers. An overall observation form the behaviour stress strain diagram of short graded fiber specimens shows that a dosage of more than 20% of 3mm or 6mm in the total volume will give significant improved performance compared to mono fibers.

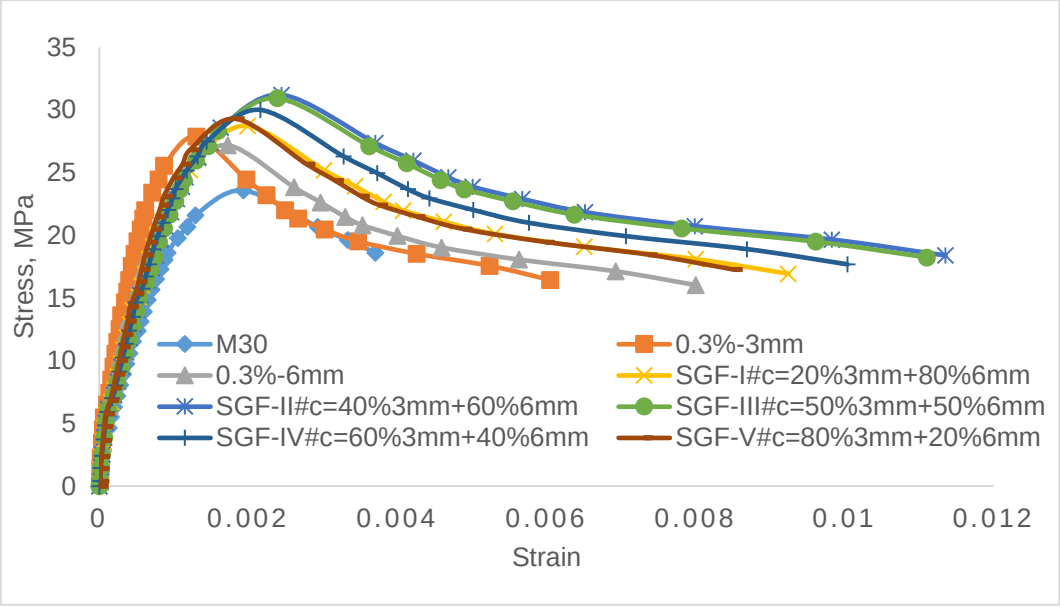

Fig.6.55 Compressive Stress-Strain behaviour of M30-SGF with Vf=0.3%

6.12.2 Long Graded Fibers

12mm and 20mm length fibers are combined as given in Table 4.2 of chapter-4. Compressive stress strain diagrams for long graded fiber (12mm + 20mm) is given in Fig.6.56. The natural characteristics of mono fibers i.e., 12mm is reflected in LGF-V#c and 20mm in LGF1#c. Further grading of 12mm and 20mm have exhibited completely different behaviour from mono fibers. An equal percentage of volume of fibers 12mm and 20mm i.e., 50% 12mm + 50% 20mm (LGF-III#c) have shown an intermediate behaviour between the LGF-IV#c and LGF-II#c. The specimens containing the 40%12mm + 60%20mm (LGF-II#c) has given the best benefit of improvement in both peak strength and post peak deformation compared to all other long graded fibers. An overall observation from the behaviour stress strain diagram of long graded fiber specimens shows that a dosage of more than 20% of 12mm or 20mm in the total volume will give an improved performance compared to monofibers.

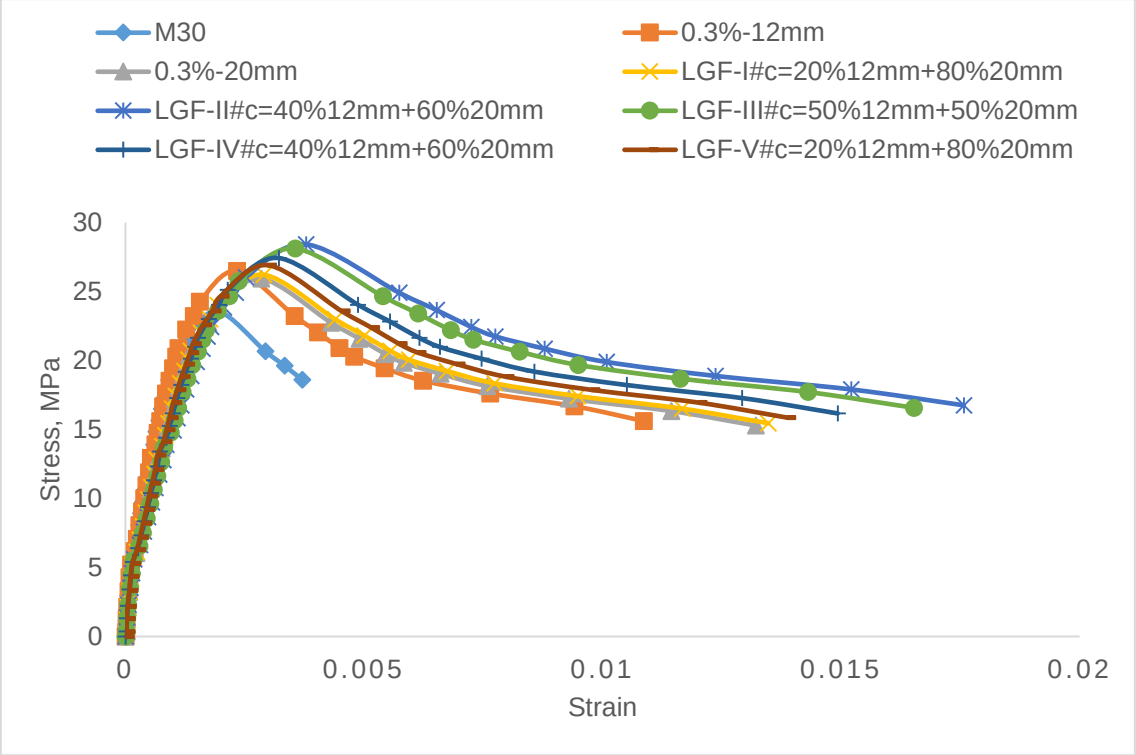

Fig.6.56 Compressive Stress-Strain behaviour of M30-LGF with V_f = 0.3%

6.12.3 Combined Graded Fibers

Mixture of Short Fibers namely (3mm, 6mm) and Long Fibers (12mm, 20mm) is combined graded fibers. Total volume fraction in all the specimens of CGF, SGF and LGF is 0.3%. Stress Strain behaviour of CGF is compared with Mono Fibers (MF), SGF and LGF. A very interesting behaviour of stress strain diagram can be noticed with CGF. Actual volume of fibers of each length in percentage in CGF is given in Table 4.2 of Chapter-4.

6.12.3 (a) Comparison with mono fibers

Compressive stress strain diagrams of mono fibers and CGF are shown in Fig.6.57. It can be seen that the deformation of specimens with eighty percent of short graded (3mm+6mm) in CGF-V#c, eighty percent of long graded (12mm + 20mm) in CGF-I#c is nearer to mono fibers 20mm but there is significant increase in strength of combined graded fiber specimens compared to mono fibers. As the volume of long length fibers increases from 40% to 60% i.e., CGF-IV#c, CGF-III#c and CGF-II#c in combined graded fiber specimen, there is progressive increase in peak strength and post peak deformation.

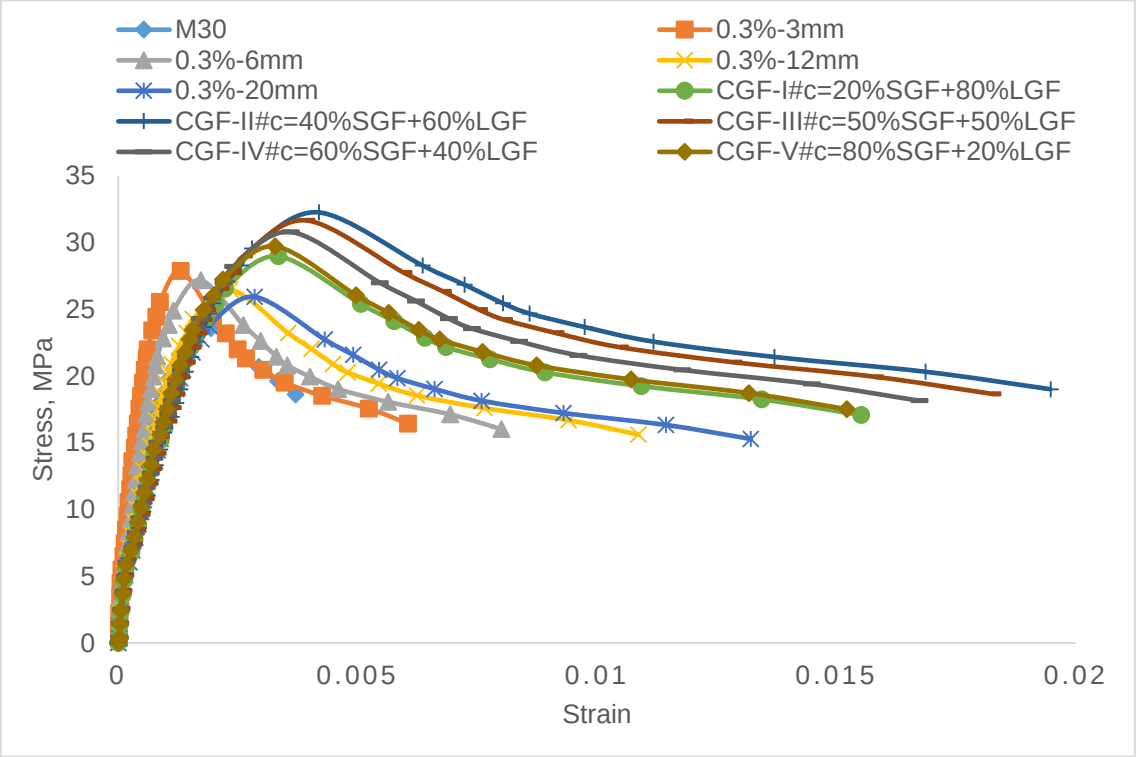

Fig.6.57 Compressive Stress-Strain behaviour of M30-CGF with V_f = 0.3%

6.12.3 (b) Comparison with short graded fibers

Compressive stress strain diagrams of short graded fibers and combined graded fibers are shown in Fig.6.58. Eighty percent of long length fibers in CGF-I#c, eighty percent of short length fibres in CGF-V#c of combined graded fiber specimens have undergone the same amount of deformation as that of short graded fiber specimens (SGF-III#c and SGF-II#c). It is noticed in earlier section in CGF-I#c and CGF-V#c have almost same amount of deformation as mono fiber of 20mm. Thus SGF-II#c, SGF-III#c, CGF-I#c, CGF-V#c and 20mm have almost nearly the same amount of deformation but improvement in peak strength is highest for SGF-II#c fallowed by SGF-III#c, CGF-V#c, CGF-I#c and mono fibers of 20mm. As the volume of long length fibers in combined graded fiber specimen i.e., CGF-IV#c, CGF-III#c and CGF-II#c increases from 40% to 60%, peak strength and post peak deformation capacity increases. Hence, CGF specimens performed better than SGF specimens. Among all the specimens CGF-II has given the best performance.

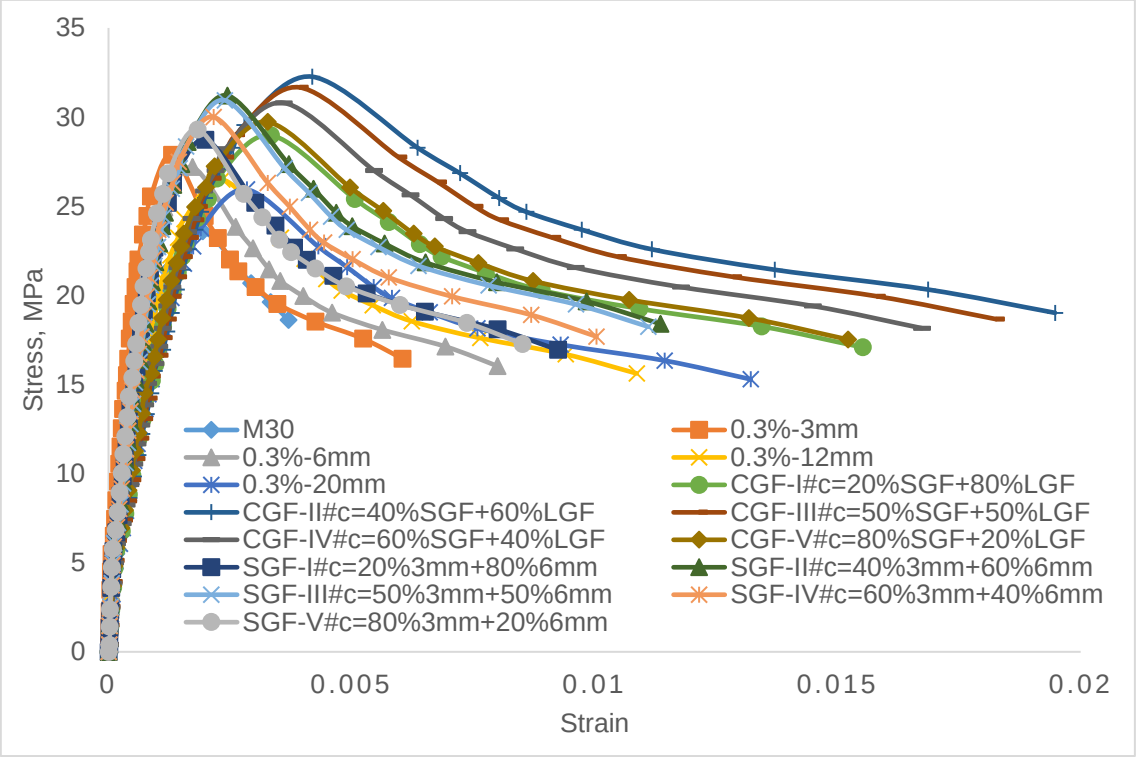

Fig.6.58 Compressive Stress-Strain behaviour of M30-CGF-0.3% compared with M30- SGF-0.3%

6.12.3 (c) Comparison with long graded fibers

Compressive stress strain diagram for LGF and CGF are shown in Fig.6.59. It is known that LGF grading with 12mm and 20mm and in the combined graded specimens the grading with SGF (3mm and 6mm) and LGF (12mm and 20mm). An examination of the above curves shows that CGF have performed better than LGF in any specimen from the type-I (20%+80%) to type-V (80%+20%). That is to say that CGF-I is better than LGF-I and so on. Among all the specimens CGF-II has given the best performance.

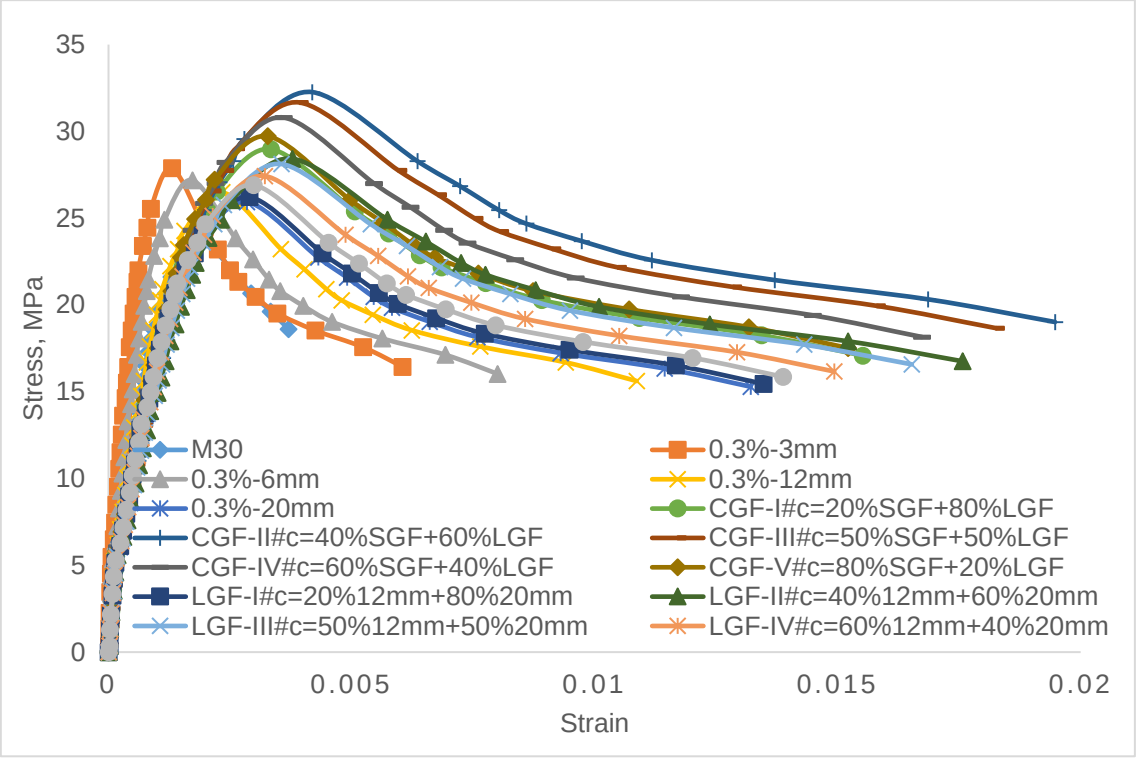

Fig.6.59 Compressive Stress-Strain behaviour of M30-CGF-0.3% compared with M30-LGF-0.3%

6.12.3 (d) Best of the best fiber combination

Compressive stress strain diagram for mono fiber and the best performing specimen in SGF, LGF and CGF are shown in Fig.6.60. It can be seen that short graded fiber specimen results in higher peak strength and long graded fiber specimen results in higher post peak deformation. Thus for the same volume in 0.3% of fibers CGF-II combined graded has the best performance. Combined graded specimens have 16% of 3mm, 24% of 6mm, 24% of 12mm and 36% of 20mm length fibers. Hence, different grading of fiber lengths have controlled the different scales of cracking contributing to increases in pre peak strength and post peak deformation of Graded Glass Fiber Reinforced Concrete. An overall observation of all the stress strain diagram, viz, mono fibers, short graded, long graded and combined graded fiber specimens are that grading delayed on set of non-linearity in the pre cracking region, improved peak strength, delayed on set of inflection in the post peak region, and improved deformation.

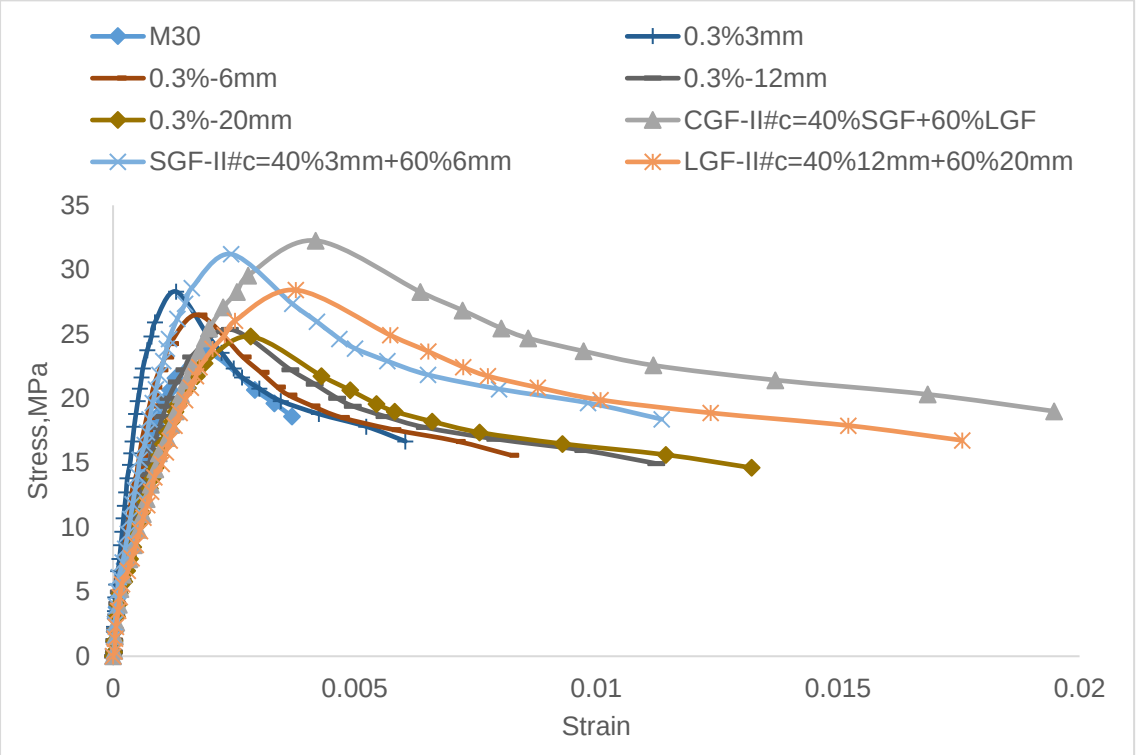

Fig.6.60 Compressive Stress-Strain behaviour of M30-CGF-0.3% compared with corresponding MF, SGF and LGF

6.12.4 Discussion about Short Graded fibers (SGF), Long Graded Fibers (LGF) Combined Graded Fibers (CGF) with volume fraction of 0.4% and 0.5%.

Compressive stress strain diagram for SGF, LGF and CGF with the volume fraction of 0.4% and 0.5% shown in Fig.6.61 to 6.68. The specimens containing 40% 3mm + 60% 6mm (SGF-II) has given the best benefit of improvement in both peak strength and post peak deformation compared to all other short graded fibers as shown in Fig.6.61 and 6.65 irrespective of amount of volume fraction of fibers i.e., 0.4% or 0.5%. The specimens containing the 40%3mm + 60%6mm (LGF-II) has given the best benefit of improvement in both peak strength and post peak deformation compared to all other long graded fibers is shown in Fig. 6.62 and 6.66 irrespective of amount of volume fraction of fibers i.e., 0.4% or 0.5%. An examination of the SGF and LGF stress strain curves shows that CGF have performed better than SGF and LGF in any specimen from the type-I (20%+80%) to type-V (80%+20%). That is to say that CGF-I is better than that of SGF-I and LGF-I and so on. Among all the specimens, CGF-II has given the best performance (Fig.6.63 and 6.67).

Stress strain diagram for mono fiber and the best performing specimen in SGF, LGF and CGF are shown in Fig 6.64 and 6.68. It can be seen that short graded fiber specimen results in higher peak strength and long graded fiber results in higher post deformation. Thus for the same volume fraction in 0.4% and 0.5% of mixes containing CGF-II (40%SGF+60%LGF) has the best performance. Irrespective of volume of fibers i.e., 0.3%, 0.4% or 0.5%, different lengths of fibers have controlled the different levels of cracking thus contributing to increases in peak strength and post peak deformation of Graded Glass Fiber Reinforced Concrete.

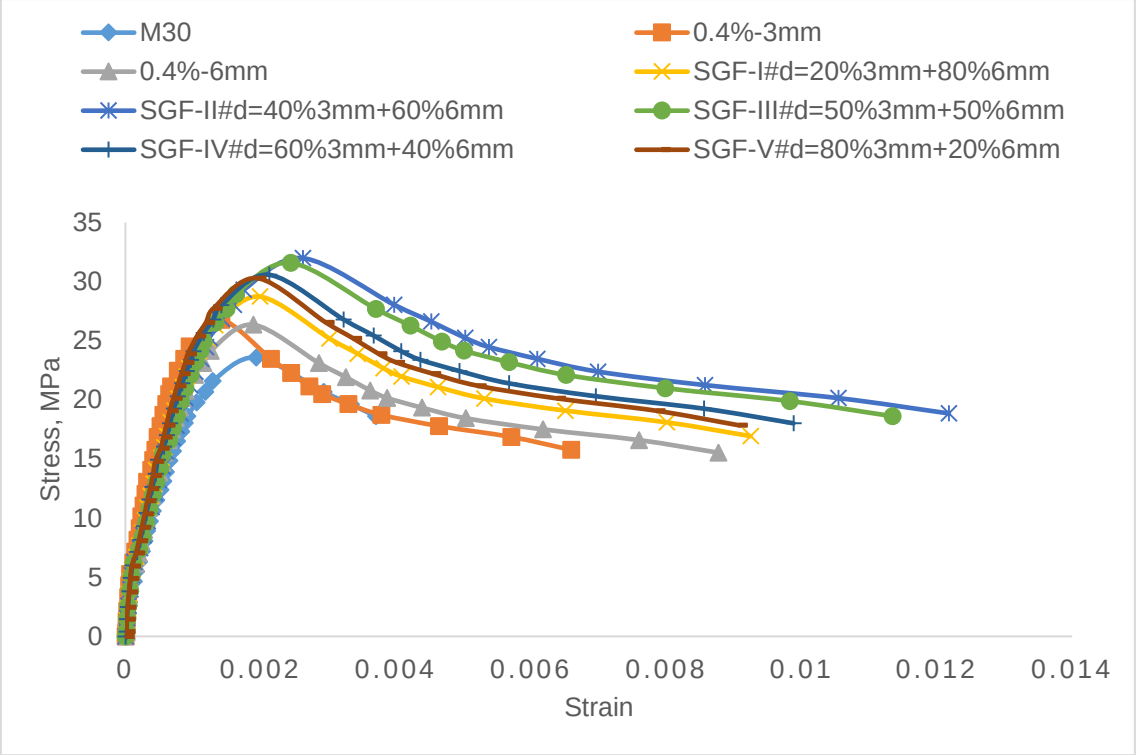

Fig.6.61 Compressive Stress-Strain behaviour of M30-SGF with V_f = 0.4%

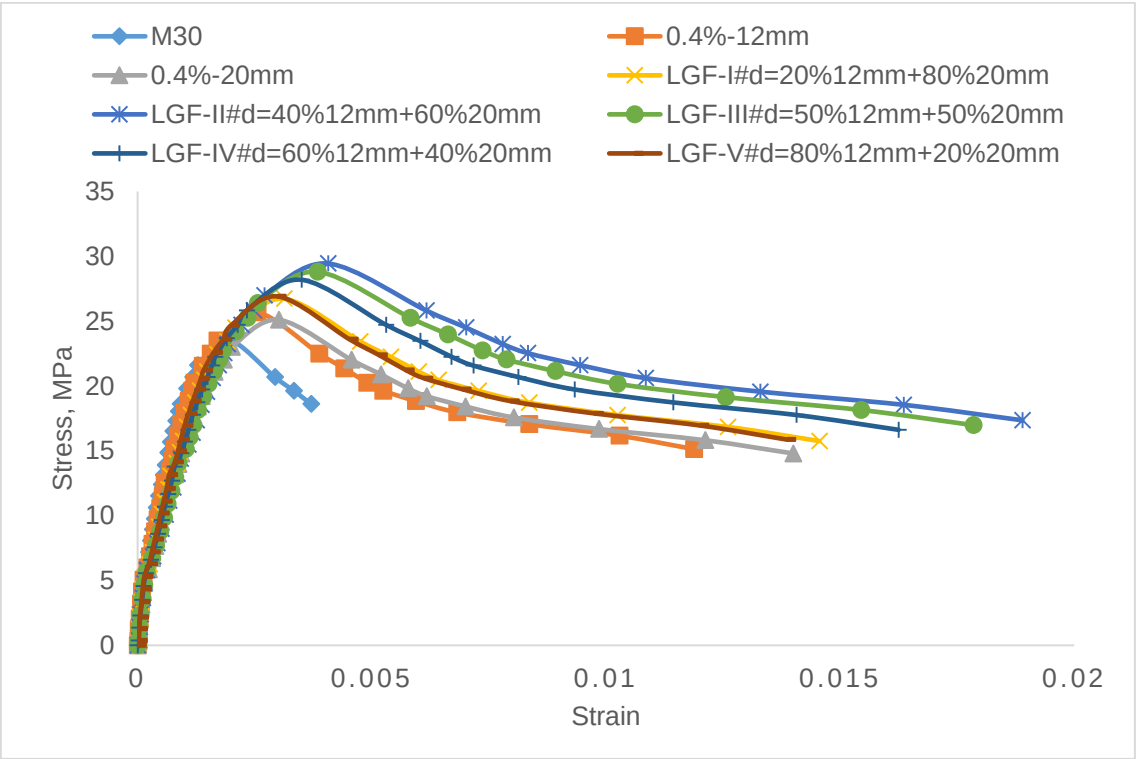

Fig.6.62 Compressive Stress-Strain behaviour of M30-LGF with V_f = 0.4%

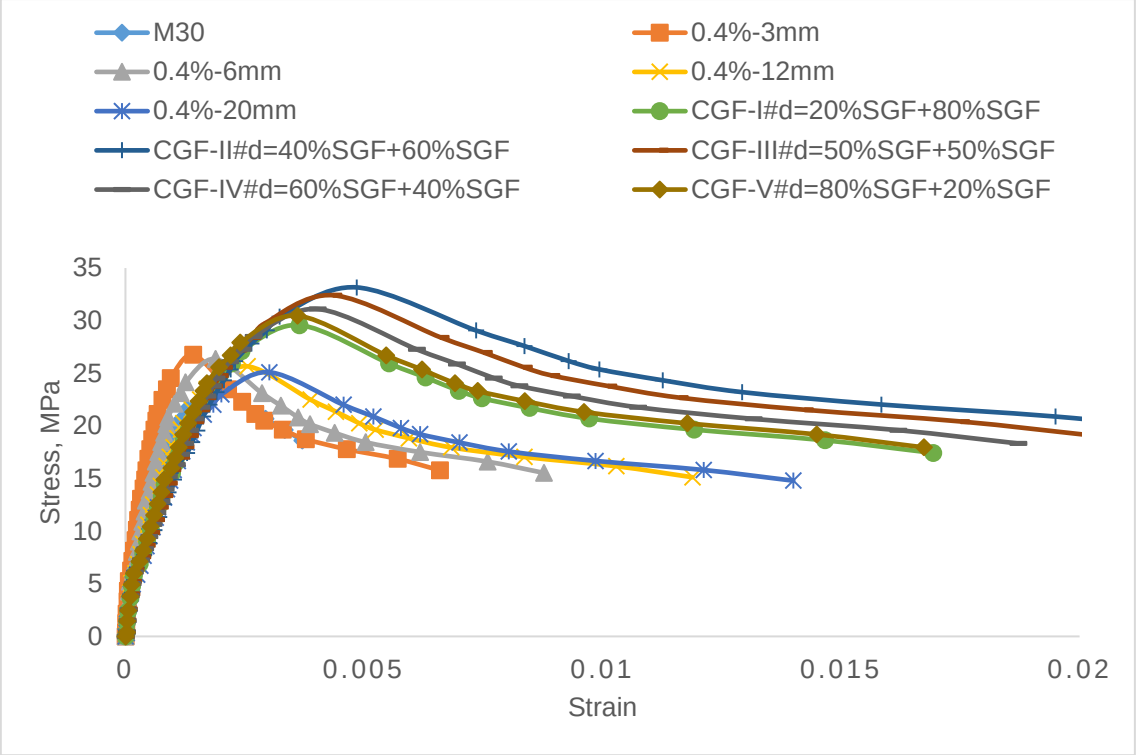

Fig.6.63 Compressive Stress-Strain behaviour of M30-CGF with V_f = 0.4%

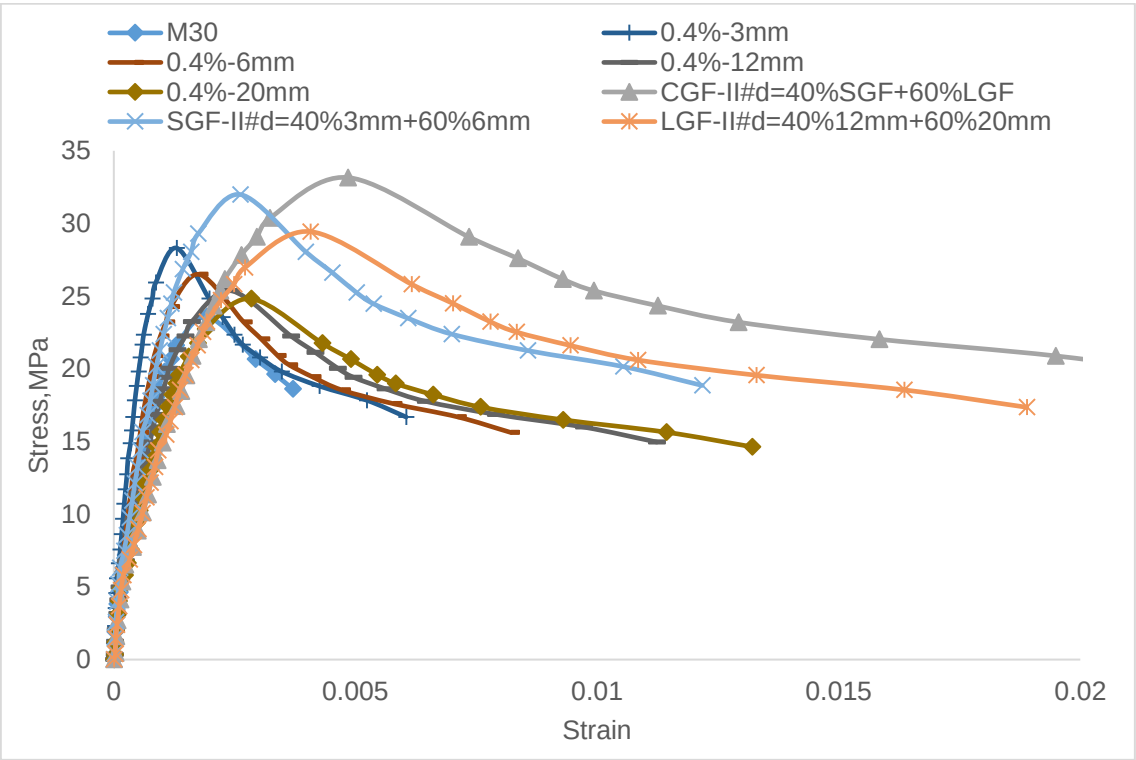

Fig.6.64 Compressive Stress-Strain behaviour of M30-CGF-0.4% compared with corresponding MF, SGF and LGF

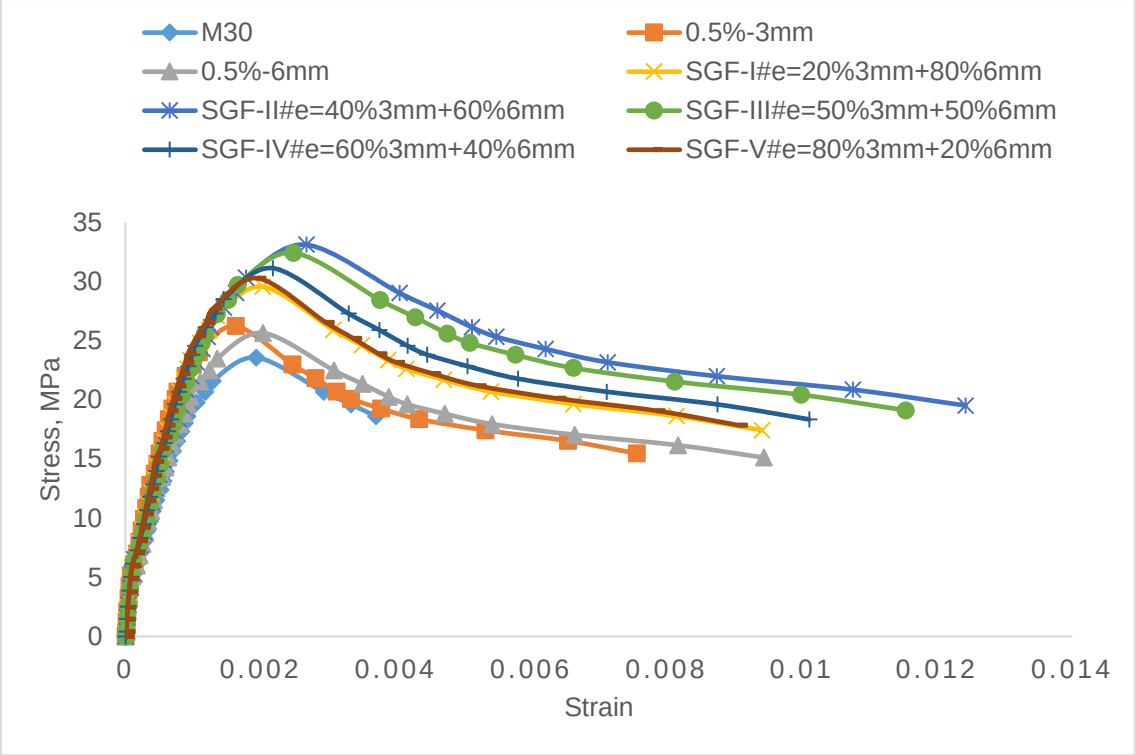

Fig.6.65 Compressive Stress-Strain behaviour of M30-SGF with V_f = 0.5%

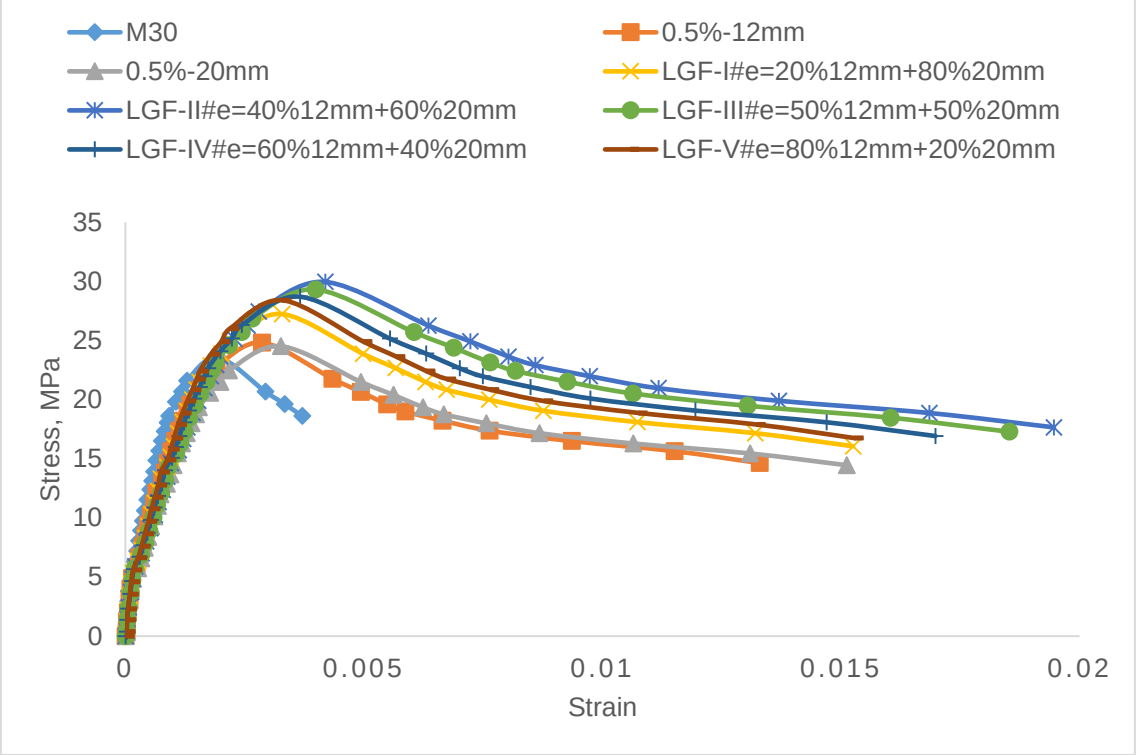

Fig.6.66 Compressive Stress-Strain behaviour of M30-LGF with V_f = 0.5%

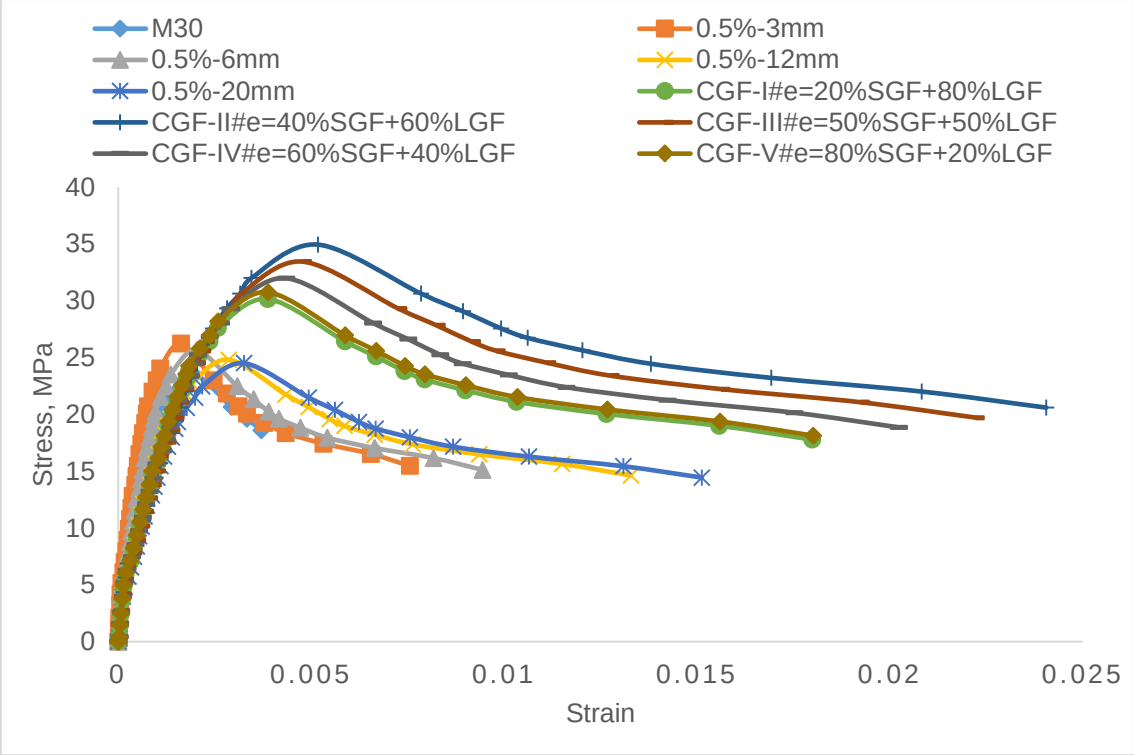

Fig.6.67 Compressive Stress-Strain behaviour of M30-CGF with V_f = 0.5%

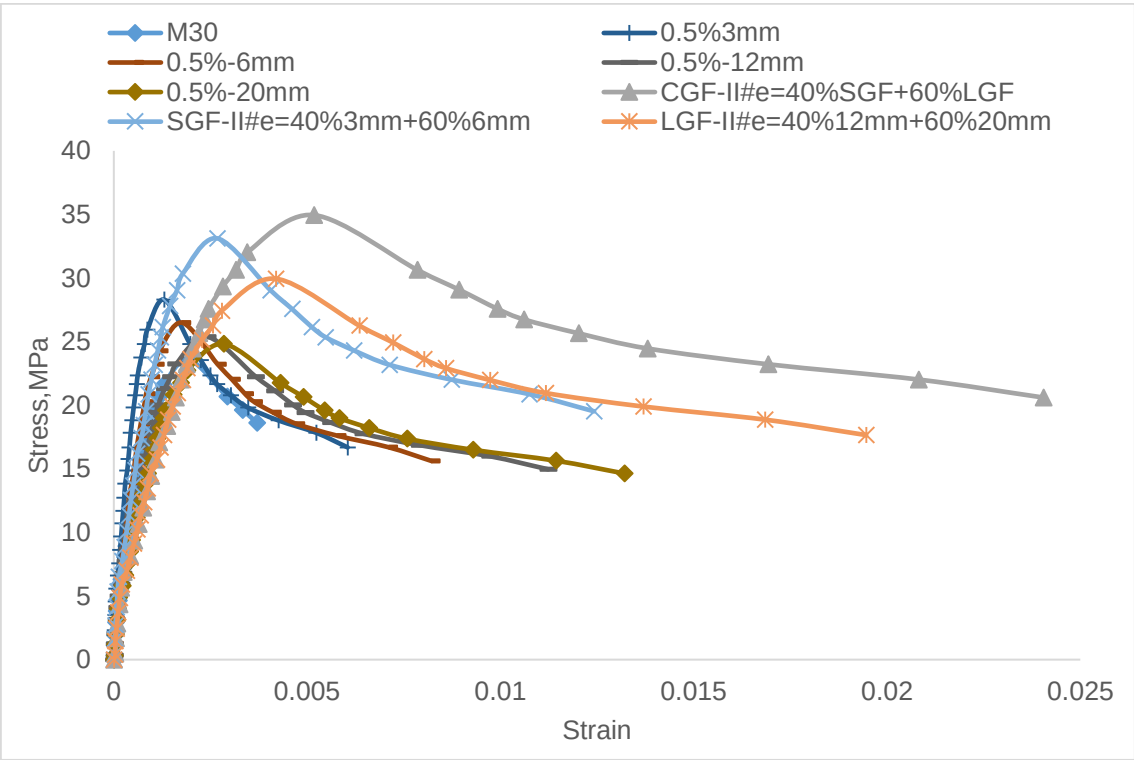

Fig.6.68 Compressive Stress-Strain behaviour of M30-CGF-0.5% compared with corresponding MF, SGF and LGF.

6.13 Compressive stress strain behaviour of M50-GGFRC

Compressive stress strain diagrams are drawn for SGF, LGF and CGF of M50 grade of concrete with volume fractions of 0.3%, 0.4% and 0.5% as shown in Fig.6.69 to 6.80. An observation of the compressive stress strain behaviour of M50-GGFRC shows that it is similar to the compressive stress strain behaviour of the M30-GGFRC.

Irrespective of volume of fibers i.e., 0.3%, 0.4% or 0.5%, the natural characteristics of mono glass fibers, 3mm is reflected in SGF-V and 6mm in SGF-I as shown in Fig.6.69 to 6.71. Further grading of 3mm and 6mm have exhibited completely different behaviour from mono fibers. An equal percentage of volume of fibers 3mm and 6mm i.e., 50% 3mm + 50% 6mm (SGF-III) have shown an intermediate behaviour between SGF-IV and SGF-II. The specimens containing the 40% of 3mm + 60% 6mm (SGF-II) has given the best benefit of improvement in both peak strength and post peak deformation compared to all other short graded fibers and can be seen in Fig.6.69 to 6.71 in all volume of fibers i.e., 0.3%, 0.4% or 0.5%.

Irrespective of volume of fibers i.e., 0.3%, 0.4% or 0.5%, the natural characteristics of mono glass fibers i.e., 12mm is reflected in LGF-V and 20mm in LGF1 as shown in Fig.6.72 to 6.74. Further grading of 12mm and 20mm have exhibited completely different behaviour from mono fibers. An equal percentage of volume of fibers 12mm and 20mm i.e., 50% 12mm + 50% 20mm (LGF-III) have shown an intermediate behaviour between LGF-IV and LGF-II. The specimens containing the 40% 12mm + 60% 20mm (LGF-II) has given the best benefit of improvement in both peak strength and post peak deformation compared to all other long graded fibers and can be seen in Fig.6.72 to 6.74 in all volume of fibers i.e., 0.3%, 0.4% or 0.5%.

Compressive stress strain diagrams of mono fibers and CGF are shown in Fig.6.75 to 77 for 0.3%, 0.4% and 0.5% fiber volume fraction. It can be seen that the post deformation of specimens with eighty percent of short graded (3mm+6mm) in CGF-V, eighty percent of long graded (12mm + 20mm) in CGF-I is nearer to mono fibers 20mm but there is increase in peak strength of combined graded fiber specimens compared to mono fibers. As the volume of long length fibers increases from 40% to 60% i.e., CGF-IV, CGF-III and CGF-II in combined graded fiber specimen, there is progressive increase in peak strength and post peak deformation.

Compressive stress strain diagram for mono fiber and the best performing specimen in SGF, LGF and CGF are shown in Fig.6.78 to 80 for 0.3%, 0.4% and 0.5% volume fraction. It can be seen that short graded fiber specimen results in higher peak strength and long graded fiber results in higher post peak deformation. Thus for any given volume of fibers (0.3%, 0.4% and 0.5%) combined graded fibers (CGF-II) specimens has given the best performance interms of peak strength and post peak deformation when compared to the SGF-II, LGF-II and also MGF specimens.

An overall observation, irrespective of volume of the fiber i.e., 0.3%, 0.4% or 0.5%, Graded Fibers have controlled the different scales of cracking thus contributing to increase in peak strength and post peak deformation of both M30 and M50 grade of concrete. Hence, it can be concluded that the graded fibers improves the pre peak and post peak behaviour of any normal strength concrete under uniaxial compression.

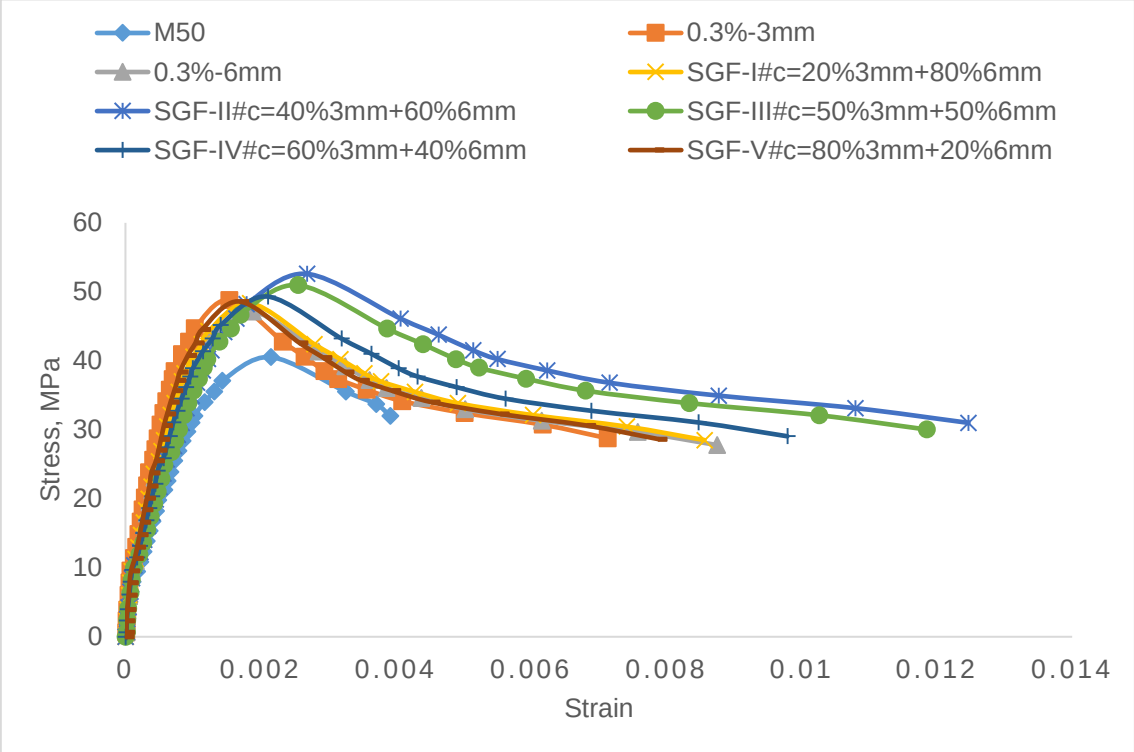

Fig.6.69 Compressive Stress-Strain behaviour of M50-SGF with V_f = 0.3%

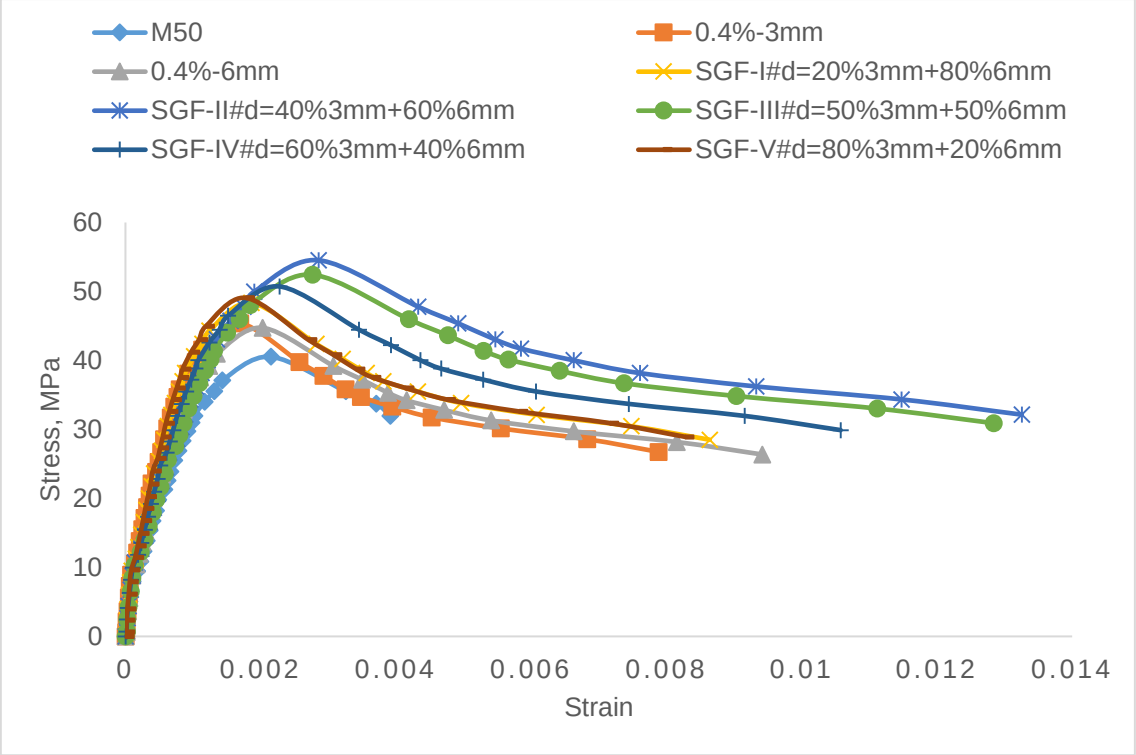

Fig.6.70 Compressive Stress-Strain behaviour of M50-SGF with V_f = 0.4%

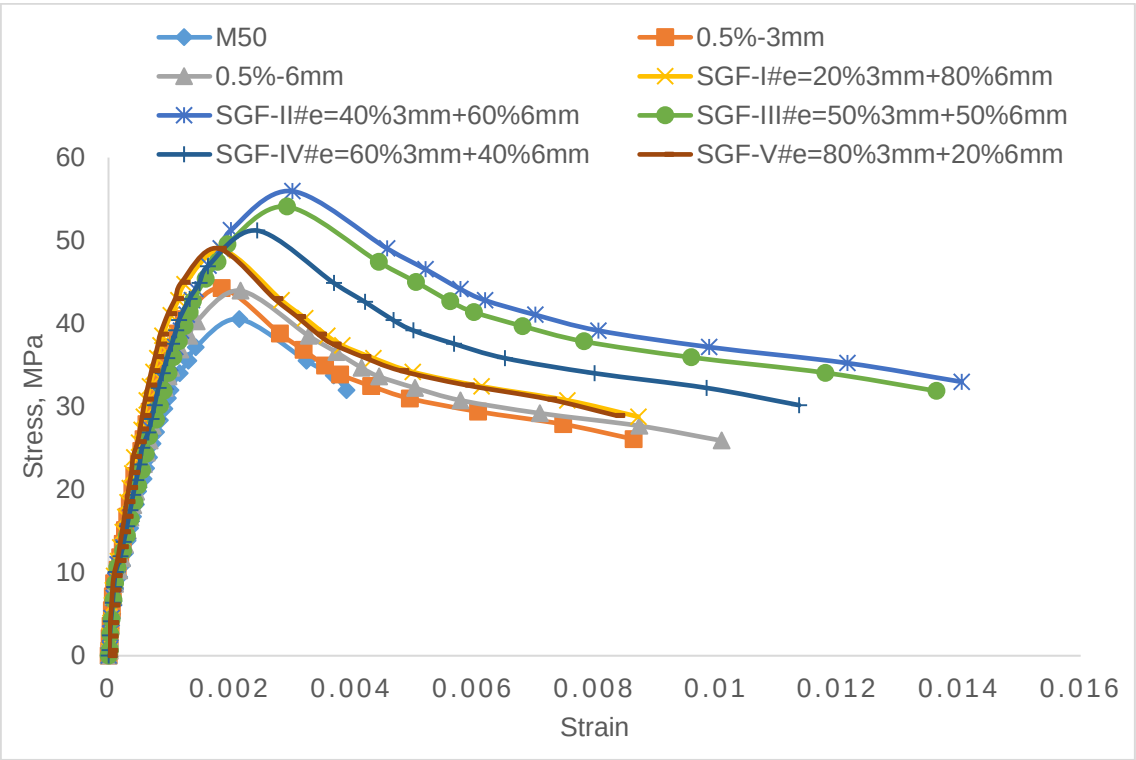

Fig.6.71 Compressive Stress-Strain behaviour of M50-SGF with V_f = 0.5%

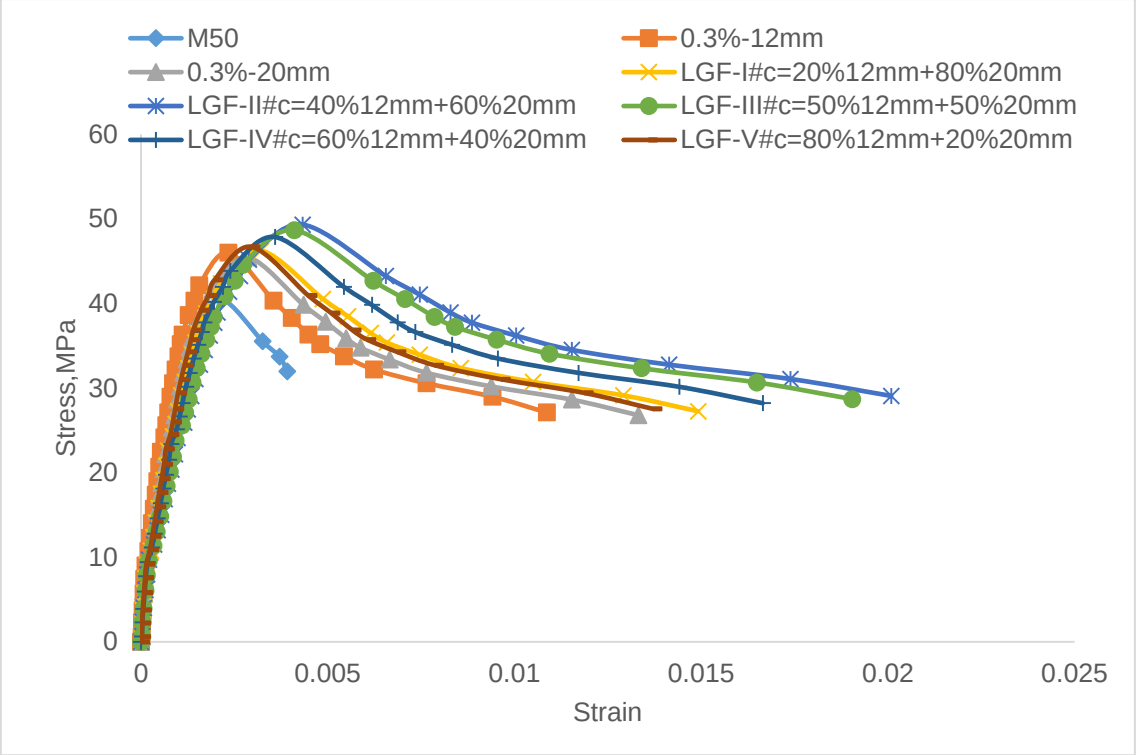

Fig.6.72 Compressive Stress-Strain behaviour of M50-LGF with V_f = 0.3%

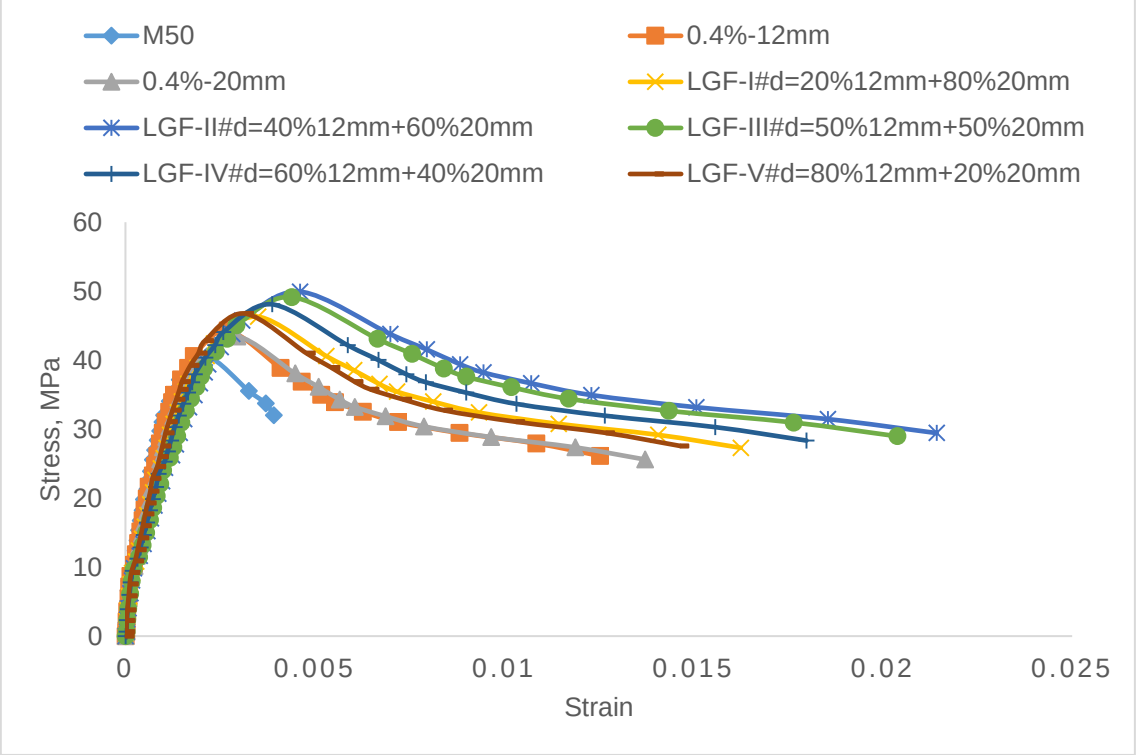

Fig.6.73 Compressive Stress-Strain behaviour of M50-LGF with V_f = 0.4%

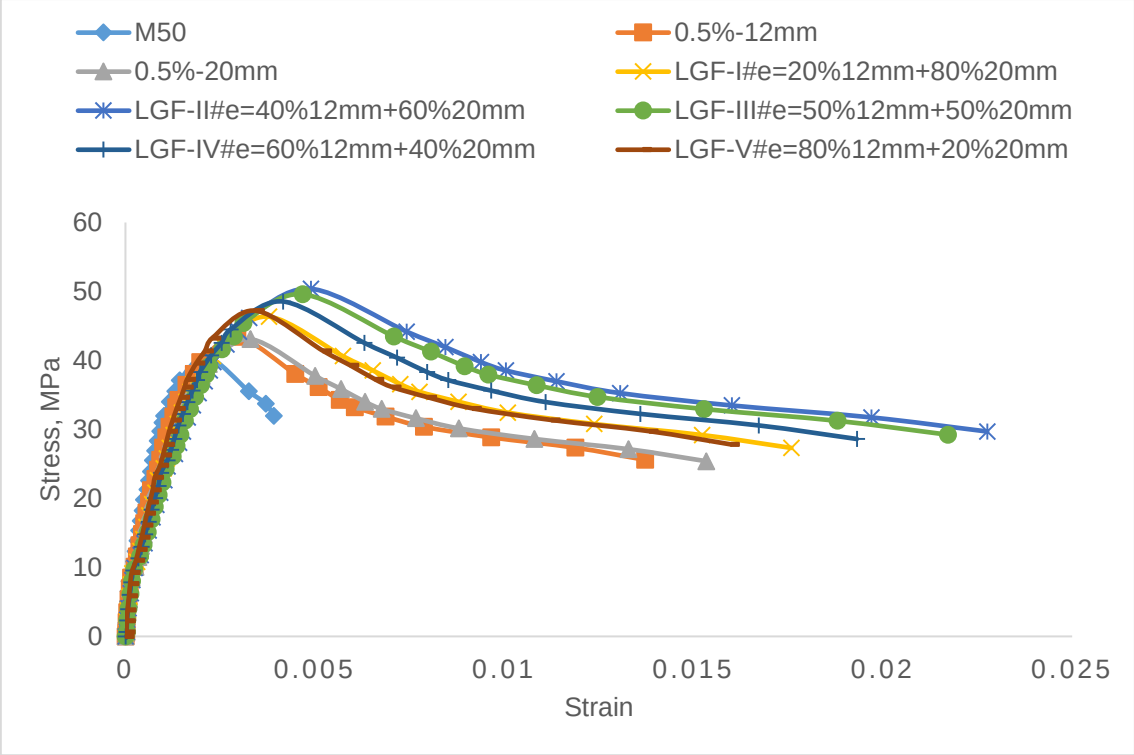

Fig.6.74 Compressive Stress-Strain behaviour of M50-LGF with V_f = 0.5%

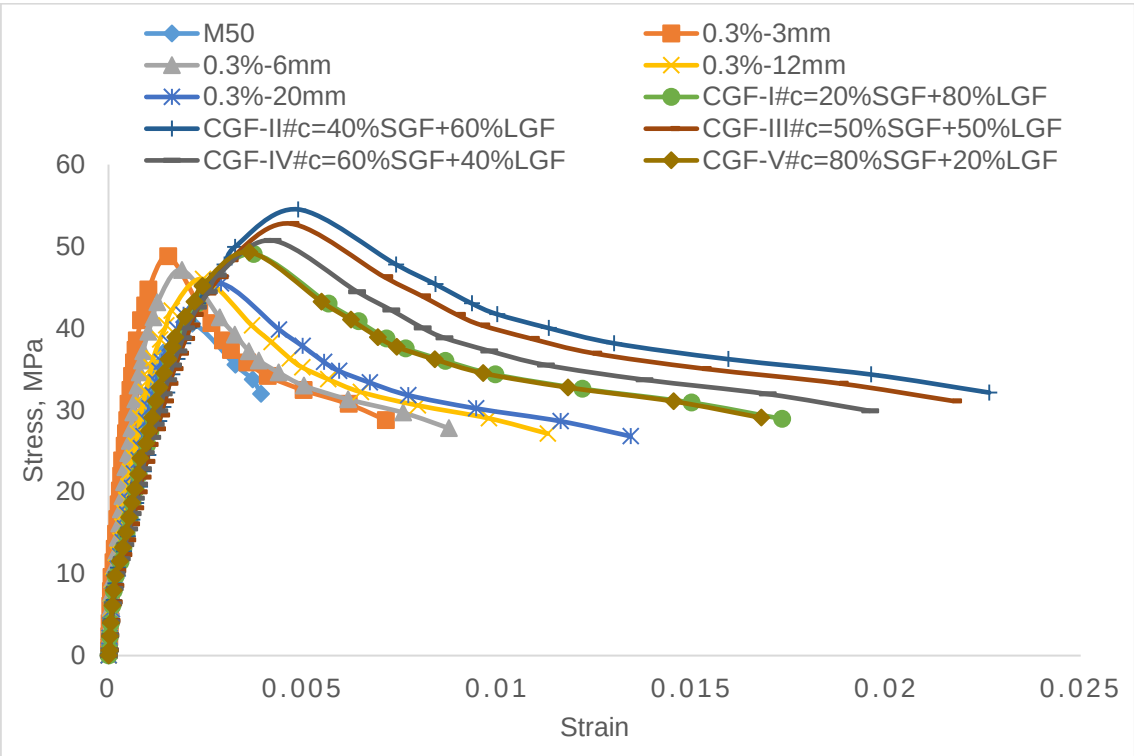

Fig.6.75 Compressive Stress-Strain behaviour of M50-CGF with V_f = 0.3%

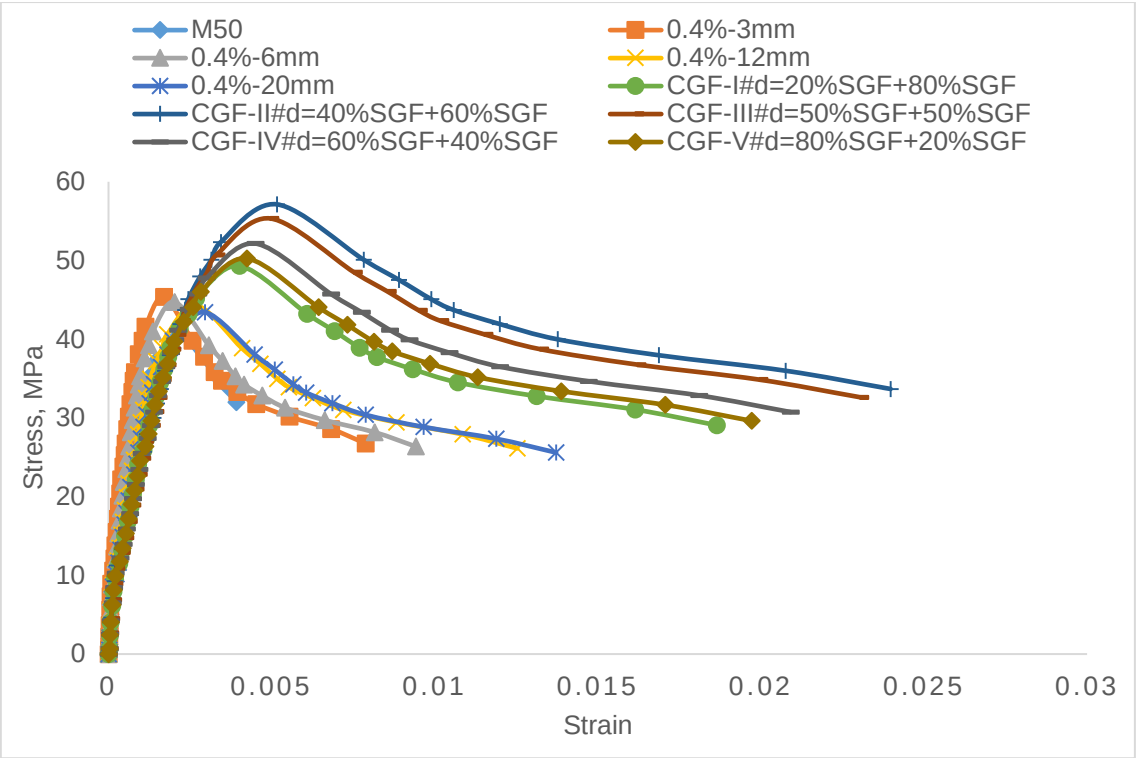

Fig.6.76 Compressive Stress-Strain behaviour of M50-CGF with V_f = 0.4%

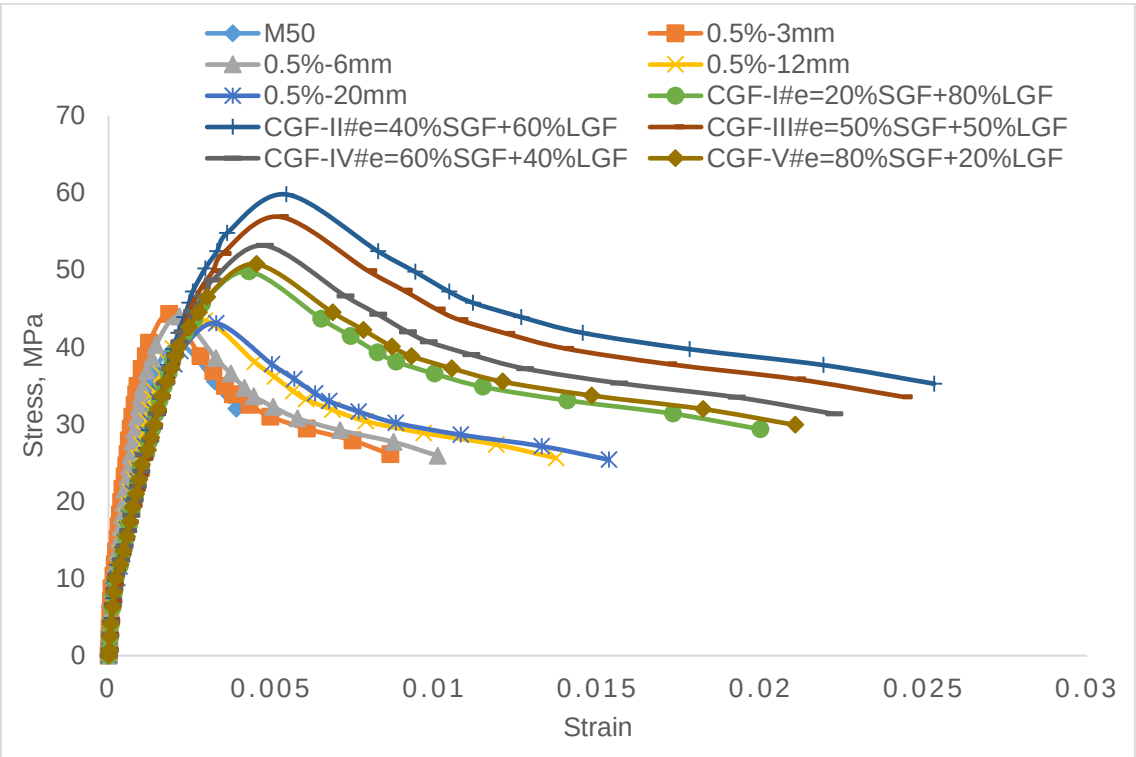

Fig.6.77 Compressive Stress-Strain behaviour of M50-CGF with V_f = 0.5%

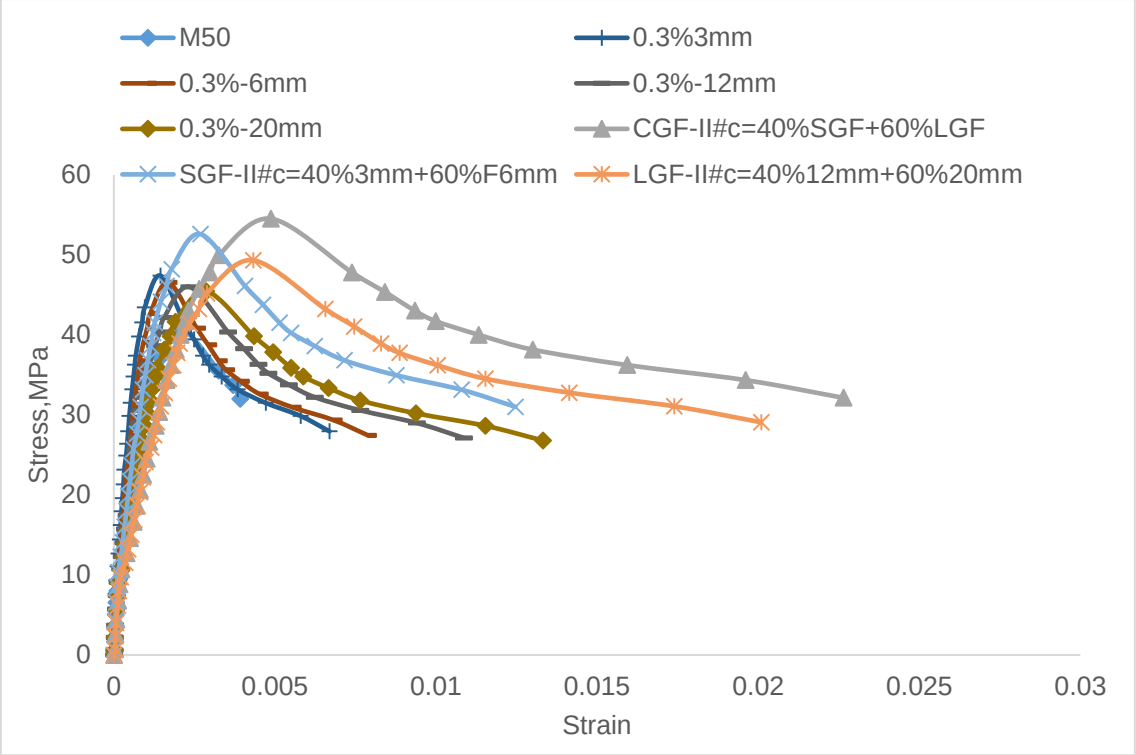

Fig.6.78 Compressive Stress-Strain behaviour of M50-CGF-0.3% compared with corresponding MF, SGF and LGF

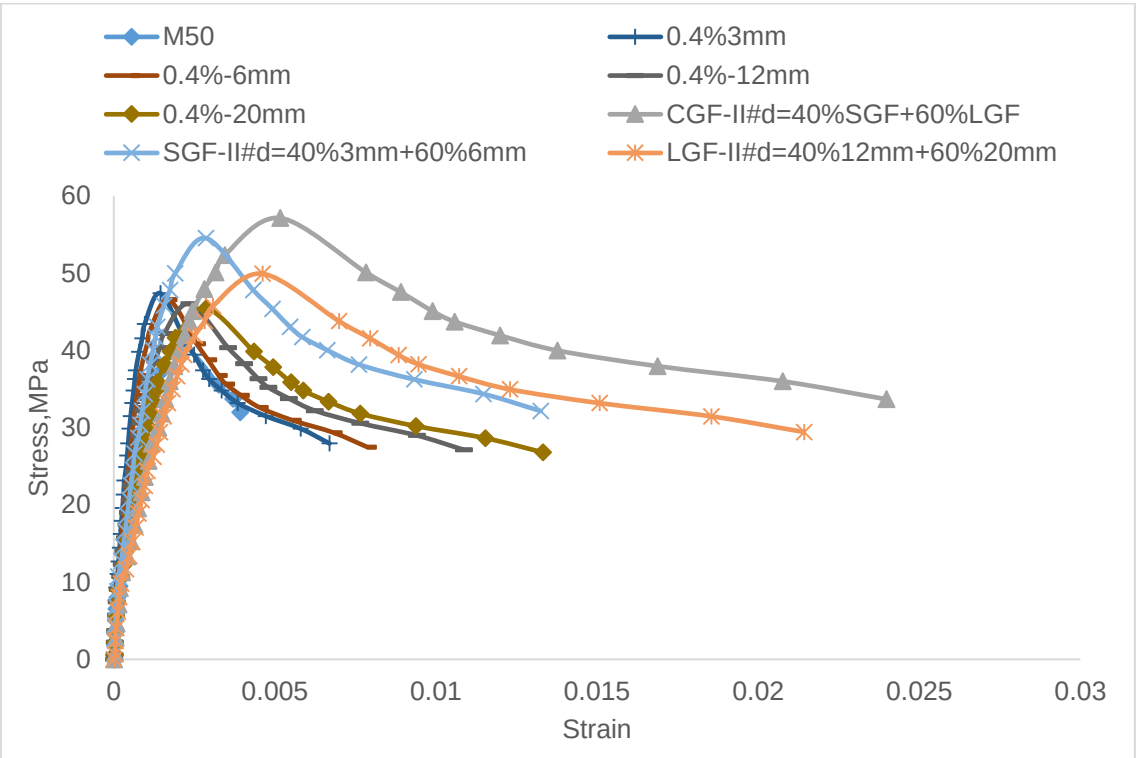

Fig.6.79 Compressive Stress-Strain behaviour of M50-CGF-0.4% compared with corresponding MF, SGF and LGF

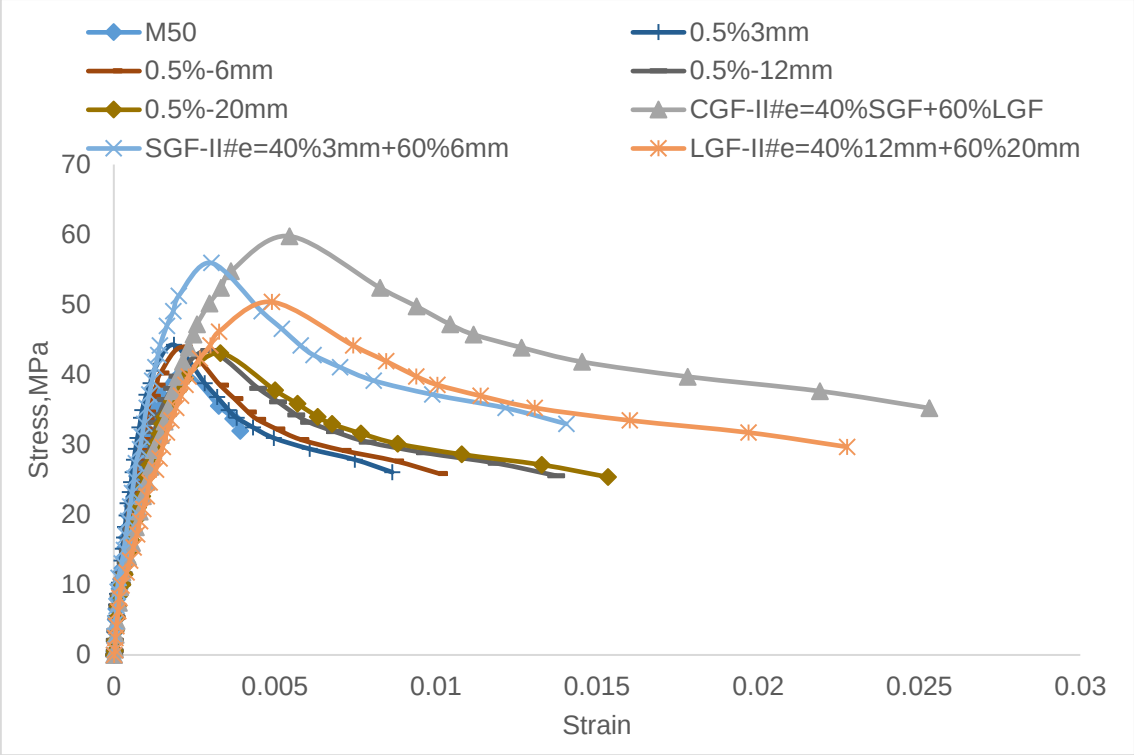

Fig.6.80 Compressive Stress-Strain behaviour of M50-CGF-0.5% compared with corresponding MF, SGF and LGF.

6.14 Mechanical properties of GGFRC

The salient points of GGFRC stress strain diagram in compression shows that it is similar to the MGFRC in compression as shown in Fig.5.47 of Chapter-5. Point A is the stress at the onset of cracking, Point B is peak stress, Point C is stress at inflection in strain softening, and Point D is breaking stress. It may be noticed that there is a gradual drop in stress after reaching peak point B to the point C and then the specimens have undergone large deformation beyond the point B and up to point C. Hence, the B to C region can be called as strain softening region.

Compressive stress strain curves of M30-GGFRC and M50-GGFRC with 0.3%, 0.4% and 0.5% volume fraction is analysed to obtain Initial slope (E^c_i), strengthening factor (STF^c), ductility factor (DF^c), strain softening slope (E_{SS}) and energy absorption capacity (EA_{SSR}) as similar to the stress strain curves of M30-MGFRC in compression. Stress and strain at peak point B and strain at inflection point C are noted from the stress strain diagram for SGF, LGF and CGF and given in column 2, 3, 4 and 5 of Table 6.27 to 6.32. Initial slope (E^c_i), strengthening factor (STF^c), ductility factor (DF^c), strain softening slope (E_{SS}) and energy absorption capacity (EA_{SSR}) are computed and

given in column 6, 7, 8, 9 and 10 of Table 6.27 to 6.32. The variation of these properties as a function of five different fiber volume combinations i.e., type-I=20%+80% (20:80), II=40%+60% (40:60), III=50%+50% (50:50), IV=60%+40% (60:40) and V=80%+20% (80:20) for SGF, LGF and CGF are shown in Fig.6.81 to 6.86. The detailed explanation of above properties of stress strain curves in compression is given in fallowing articles.

6.14. (a) Initial slope (E^c_i)

The variation of initial slope (E^c_i) values for SGF, LGF and CGF with five different fiber volume combinations of 0.3%, 0.4% and 0.5% are shown in Fig.6.81 (a), 6.82 (a) and 6.83 (a). Among all the fiber volume combinations, it can be observed that the specimens with 40% 3mm+60%6mm (SGF-II) has given the lower value compared to the all other short graded fiber specimens. Similarly, in case of long graded fibers and combined graded fibers, specimens with 40% 12mm+60%20mm (LGF-II) and 40%SGF+60%LGF (CGF-II) has given the lower values compared to other long graded and combined graded fiber volume combinations. For a particular fiber volume combination i.e., 40:60, SGF-II given the higher slope than that of CGF-II and LGF-II. An overall observation shows that, Initial slope values of SGF are more than CGF and LGF in any mixture from the type-I (20:80) to type-V (80:20) as can be seen in Fig.6.81 (a), 6.82 (a) and 6.83 (a) for 0.3%, 0.4% and 0.5% volume fraction. Moreover, it can be concluded that initial slope of SGF is lower than MGF for any given volume fraction (0.3%, 0.4% and 0.5%). Hence, lower the initial slope higher the stiffness of the composite.

The initial slope (E^c_i) behaviour of SGF, LGF and CGF for M50 grade of concrete with 0.3%, 0.4% and 0.5% volume fractions is similar to the M30-GGFRC and can be seen in Fig.6.84 (a), 6.85 (a) and 6.86 (a).

6.14. (b) Strengthening Factor (STF^c)

The variation of strengthening factor (STF^c) for SGF, LGF and CGF with five different fiber volume combinations of 0.3%, 0.4% and 0.5% are shown in Fig.6.81 (b), 6.82 (b) and 6.83 (b). Among all the fiber volume combinations, it can be noticed that the specimens with 40% 3mm+60%6mm (SGF-II) has given the higher strengthening factor compared to the all other short graded fiber specimens whereas in case of long graded fiber, specimens with 40% 12mm+60%20mm (LGF-II) has given the higher strengthening factor compared to other long graded specimens. An examination of the

combined graded fiber, specimens with 40%SGF+60%LGF (CGF-II) showed the higher strengthening factor compared to the other combined graded specimens. For a particular fiber volume combination i.e., 40:60, CGF-II has given the higher strengthening factor than that of SGF-II and LGF-II. An overall observation is that, strengthening factor of CGF are more than SGF and LGF in any mixture from the type-I (20:80) to type-V (80:20) as can be seen in Fig.6.81 (b), 6.82 (b) and 6.83 (b) for 0.3%, 0.4% and 0.5% volume fraction.

Strengthening factor (STF^c) variations of SGF, LGF, CGF for M50 grade of concrete with 0.3%, 0.4% and 0.5% volume fractions is similar to the M30-GGFRC and can be seen in Fig.6.84 (b), 6.85 (b) and 6.86 (b).

6.14. (c) Ductility Factor (DF^c)

The variation of ductility factor (DF^c) for SGF, LGF and CGF with five different fiber volume combinations of 0.3%, 0.4% and 0.5% are shown in Fig.6.81 (c), 6.82 (c) and 6.83 (c). Among all the fiber volume combinations, it can be noticed that the specimens with 40% 3mm+60%6mm (SGF-II) has given the higher ductility factor compared to the all other short graded fiber specimens whereas in case of long graded fiber, specimens with 40%12mm+60%20mm (LGF-II) has given the higher ductility compared to other long graded specimens. An examination of the combined graded fiber specimens with 40%SGF+60%LGF (CGF-II) showed the higher ductility compared to the other combined graded specimens. For a particular fiber volume combination i.e., 40:60, CGF-II has given the higher ductility factor than that of SGF-II and LGF-II. An overall observation shows that, ductility factor of CGF are more than SGF and LGF in any mixture from the type-I (20:80) to type-V (80:20) as can be seen in Fig.6.81 (c), 6.82 (c) and 6.83 (c) for 0.3%, 0.4% and 0.5% volume fraction.

Ductility factor (DF^c) variations of SGF, LGF, CGF for M50 grade of concrete with 0.3%, 0.4% and 0.5% volume fractions is similar to the M30-GGFRC and it can be seen in Fig.6.84 (c), 6.85 (c) and 6.86 (c).

6.14. (d) Strain softening Slope (E_{SS})

The variation of strain softening slope (E_{SS}) values for SGF, LGF and CGF with five different fiber volume combinations of 0.3%, 0.4% and 0.5% are shown in Fig.6.81 (d), 6.82 (d) and 6.83 (d). Among all the fiber volume combinations, it can be observed

that the specimens with 40%3mm+60%6mm (SGF-II) has given the lower strain softening slope compared to the all other short graded fiber specimens. Similarly, in case of long graded fibers and combined graded fibers, specimens with 40% 12mm+60%20mm (LGF-II) and 40%SGF+60%LGF (CGF-II) has given the lower values of strain softening slope compared to all other long graded and combined graded fiber volume combinations. For a particular fiber volume combination i.e., 40:60, SGF-II given the higher strain softening slope than that of CGF-II and LGF-II. An overall observation is that, strain softening slope values of SGF are more than CGF and LGF in any mixture from the type-I (20:80) to type-V (80:20) as can be seen in Fig.6.81 (d), 6.82 (d) and 6.83 (d) for 0.3%, 0.4% and 0.5% volume fraction. Moreover, it can be concluded that strain softening slope of CGF is less than that of SGF, LGF and also MGF for any given volume fraction (0.3%, 0.4% and 0.5%). For any given fiber volume fraction, as the grading of fibers changes from SGF (3mm + 20mm) to LGF (12mm+20mm) and to CGF (3mm+6mm+12mm+20mm), strain softening region increased. Hence, strain softening region increases with improved fiber grading. Lower strain softening slope means higher post peak deformations whereas higher strain softening slope means lower post peak deformations.

The above strain softening slope (E_{SS}) behaviour of SGF, LGF and CGF for M50 grade of concrete with 0.3%, 0.4% and 0.5% volume fractions is similar to the M30-GGFRC and it can be seen in Fig.6.84 (d), 6.85 (d) and 6.86 (d).

6.14. (e) Energy Absorption Capacity (EA_{SSR})

The variation of energy absorption capacity in strain softening region (EA_{SSR}) for SGF, LGF and CGF with five different fiber volume combinations of 0.3%, 0.4% and 0.5% are shown in Fig.6.81 (e), 6.82 (e) and 6.83 (e). Among all the fiber volume combinations, it can be noticed that the specimens with 40% 3mm+60%6mm (SGF-II) has given the higher energy absorption capacity compared to the all other short graded fiber specimens whereas in case of long graded fiber, specimens with 40% 12mm+60%20mm (LGF-II) has given the higher energy absorption capacity compared to other long graded specimens. An examination of the combined graded fiber, specimens with 40%SGF+60%LGF (CGF-II) showed the higher energy absorption capacity compared to the other combined graded specimens. For a particular fiber volume combination i.e., 40:60, CGF-II given the higher energy absorption capacity

than that of SGF-II and LGF-II. An overall observation shows that, energy absorption capacity of CGF are more than SGF and LGF in any specimen from the type-I (20:80) to type-V (80:20) as can be seen in Fig.6.81 (e), 6.82 (e) and 6.83 (e) for 0.3%, 0.4% and 0.5% volume fraction

Energy absorption capacity (EA_{SSR}) variations of SGF, LGF, CGF for M50 grade of concrete with 0.3%, 0.4% and 0.5% volume fractions is similar to the M30-GGFRC and it can be seen in Fig.6.84 (e), 6.85 (e) and 6.86 (e).

6.14. (f) Comparisons

Finally, It can be noted that the strength enhancement for short graded fibers varied from 1·19 to 1.38 and for long graded fibers 1.11 to 1.24 which shows that there was a significant improvement in peak strength for specimens with short graded fibers when compared to the specimens with long graded fibers. A significant enhancement in ductility occurred in case of the long graded fibers i.e., between 2.71 and 4.15, compared to short graded fibers i.e., between 2.62 and 3.81. Hence, short graded fibers are more effective in improving the ultimate strength by delaying the formation of micro cracks and long graded fibers are more effective in increasing the deformations by bridging the macro cracks. The combination of short graded and long graded fibers to form combined graded fibers enhanced the strengthening factor from 1.21 to 1.47 and ductility factor from 2.92 to 4.39. The comparison with best of the best combinations i.e., 40%3mm+60%6mm (SGF-II), 40%12mm+60%20mm (LGF-II) and 40%SGF+60%LGF (CGF-II) showed the clear variation. Specimens with SGF-II gave 1.38 times improvement in peak strength whereas Specimens with LGF-II gave 4.15 times improvement in ductility. The combination of short graded and long graded i.e., combined graded fibers (CGF-II) gave 1.47 times in peak strength and 4.39 times in ductility. That is to say that the combined graded fibers have given the best performance compared to short graded fibers and long graded fibers in both peak strength and post peak deformation. From the above observation, it can be concluded that the combined graded fibers (CGF) are better than mono glass fibers (MGF) or SGF or LGF in terms of peak strength and post peak deformation.

In all, irrespective of volume of the fiber (0.3%, 0.4% and 0.5%) and grade of concrete (M30 and M50), long graded fibers (LGF) exhibited higher ductility factor, energy absorption capacity than that of short graded fibers (SGF). Short graded fibers showed

higher strengthening and initial slope compared to the long length fibers. Hence, the combination of SGF and LGF i.e., CGF have exhibited the higher strengthening factor, ductility factor and energy absorption capacity than that of SGF, LGF and MGF.

Table 6.27 Summary of test results for M30-GGFRC with V_f = 0.3% in Compression

Specimen Designation (1)	Strain Softening Region				E^c_i ($X10^4$) MPa (6)	STF^c (7)	DF^c (8)	E_{SS} ($X10^4$) MPa (9)	EA_{SSR} ($X10^{-2}$) N/mm (10)
	f^B_u (MPa) (2)	ε^B_u ($X10^{-4}$) (3)	f^C_{IP} (MPa) (4)	ε^C_{IP} ($X10^{-4}$) (5)					
Short Graded Fibers (SGF), V_f = 0.3%									
SGF-I#c	28.73	19.90	20.04	52.25	1.23	1.22	2.62	0.27	0.0468
SGF-II#c	31.21	24.44	20.38	87.59	1.09	1.32	3.58	0.17	0.0624
SGF-III#c	30.94	23.91	20.27	78.57	1.10	1.31	3.29	0.20	0.0605
SGF-IV#c	30.01	21.61	20.09	62.94	1.18	1.27	2.91	0.24	0.0530
SGF-V#c	29.30	18.33	20.51	48.07	1.36	1.24	2.62	0.30	0.0439
Long Graded Fibers (LGF), V_f = 0.3%									
LGF-I#c	26.22	29.01	20.04	78.52	0.77	1.11	2.71	0.12	0.0622
LGF-II#c	28.43	37.83	20.36	140.93	0.64	1.21	3.73	0.08	0.0879
LGF-III#c	28.12	35.58	20.23	125.09	0.67	1.19	3.52	0.09	0.0818
LGF-IV#c	27.43	32.14	20.04	98.63	0.73	1.16	3.07	0.11	0.0721
LGF-V#c	26.91	29.86	19.81	82.10	0.77	1.14	2.75	0.14	0.0657
Combined Graded Fibers (SGF), V_f = 0.3%									
CGF-I#c	28.98	33.40	20.28	97.59	0.74	1.23	2.92	0.14	0.0792
CGF-II#c	32.26	41.92	20.48	165.68	0.65	1.37	3.95	0.10	0.1106
CGF-III#c	31.67	39.30	20.40	146.16	0.68	1.34	3.72	0.11	0.1018
CGF-IV#c	30.80	36.02	20.30	115.71	0.73	1.31	3.21	0.13	0.0907
CGF-V#c	29.72	32.75	20.75	93.59	0.77	1.26	2.86	0.15	0.0796

Note: f^B_u = Peak Stress at B, ε^B_u = Peak Strain at B, f^C_{IP} = Stress at inflection C, ε^C_{IP} = Strain at inflection C, Intial Slope (E^c_i) = f^A / ε^A, Strengthening Factor (STF^c) = f^B_u / f_0, Ductility factor (DF^c) = $\varepsilon^C_{IP} / \varepsilon^B_u$, Strain Softening Slope (E_{SS}) = $(f^B_u - f^C_{IP}) / (\varepsilon^C_{IP} - \varepsilon^B_u)$, Energy Absorption capacity (EA_{SSR}) = Area under the stress strain curve in Strain Softening Region.

Table 6.28 Summary of test results for M30-GGFRC with V_f = 0.4% in Compression

Specimen Designation (1)	Strain Softening Region				E^c_i ($X10^4$) MPa (6)	STF^c (7)	DF^c (8)	E_{SS} ($X10^4$) MPa (9)	EA_{SSR} ($X10^{-2}$) N/mm (10)
	f^B_u (MPa) (2)	ε^B_u ($X10^{-4}$) (3)	f^C_{IP} (MPa) (4)	ε^C_{IP} ($X10^{-4}$) (5)					
Short Graded Fibers (SGF), V_f = 0.4%									
SGF-I#d	28.76	19.90	20.04	54.15	1.23	1.22	2.72	0.25	0.0477
SGF-II#d	31.99	26.21	20.40	98.05	1.04	1.36	3.74	0.16	0.0686
SGF-III#d	31.59	24.42	20.29	85.40	1.10	1.34	3.50	0.19	0.0631
SGF-IV#d	30.57	21.27	20.13	64.84	1.22	1.30	3.05	0.24	0.0532
SGF-V#d	30.29	19.53	20.04	52.70	1.32	1.28	2.70	0.31	0.0484
Long Graded Fibers (LGF), V_f = 0.4%									
LGF-I#d	26.73	31.3438	20.28	89.17	0.72	1.13	2.84	0.11	0.0685
LGF-II#d	29.44	40.6730	20.37	158.19	0.62	1.25	3.89	0.08	0.0979
LGF-III#d	28.81	38.4212	20.25	141.63	0.64	1.22	3.69	0.08	0.0905
LGF-IV#d	28.19	34.9845	20.06	113.99	0.68	1.20	3.26	0.10	0.0806
LGF-V#d	27.67	31.3154	20.28	91.21	0.75	1.17	2.91	0.12	0.0709
Combined Graded Fibers (SGF), V_f = 0.4%									
CGF-I#d	29.57	36.4506	20.75	110.99	0.69	1.25	3.04	0.12	0.0881
CGF-II#d	33.16	48.4699	20.49	199.87	0.58	1.41	4.12	0.08	0.1314
CGF-III#d	32.41	43.5574	20.43	170.21	0.63	1.37	3.91	0.09	0.1154
CGF-IV#d	31.10	40.2824	20.33	140.42	0.66	1.32	3.49	0.11	0.1024
CGF-V#d	30.47	36.0249	20.28	110.57	0.72	1.29	3.07	0.14	0.0898

Table 6.29 Summary of test results for M30-GGFRC with V_f = 0.5% in Compression

Specimen Designation (1)	Strain Softening Region				E^c_i ($X10^4$) MPa (6)	STF^c (7)	DF^c (8)	E_{SS} ($X10^4$) MPa (9)	EA_{SSR} ($X10^{-2}$) N/mm (10)
	f^B_u (MPa) (2)	ε^B_u ($X10^{-4}$) (3)	f^C_{IP} (MPa) (4)	ε^C_{IP} ($X10^{-4}$) (5)					
Short Graded Fibers (SGF), V_f = 0.5%									
SGF-I#e	29.58	20.26	20.04	55.87	1.24	1.25	2.76	0.27	0.0490
SGF-II#e	33.12	26.74	20.41	101.93	1.05	1.40	3.81	0.17	0.0724
SGF-III#e	32.44	24.83	20.30	90.30	1.11	1.38	3.64	0.19	0.0659
SGF-IV#e	31.14	21.77	20.14	70.91	1.22	1.32	3.26	0.22	0.0554
SGF-V#e	30.29	19.53	20.04	55.50	1.32	1.28	2.84	0.28	0.0484
Long Graded Fibers (LGF), V_f = 0.5%									
LGF-I#e	27.23	32.83	20.04	94.48	0.71	1.15	2.88	0.12	0.0731
LGF-II#e	29.95	41.90	20.37	165.29	0.61	1.27	3.95	0.08	0.1026
LGF-III#e	29.31	39.88	20.25	150.96	0.62	1.24	3.79	0.08	0.0956
LGF-IV#e	28.70	36.55	20.07	125.02	0.67	1.22	3.42	0.10	0.0858
LGF-V#e	28.40	32.91	20.04	97.08	0.73	1.20	2.95	0.13	0.0764
Combined Graded Fibers (SGF), V_f = 0.5%									
CGF-I#e	30.17	38.71	20.04	124.26	0.66	1.28	3.21	0.12	0.0955
CGF-II#e	34.95	51.78	20.49	220.46	0.57	1.48	4.26	0.09	0.1480
CGF-III#e	33.46	47.85	20.43	193.79	0.59	1.42	4.05	0.09	0.1309
CGF-IV#e	32.00	43.56	20.34	157.21	0.62	1.36	3.61	0.10	0.1140
CGF-V#e	30.77	38.78	20.51	126.05	0.67	1.30	3.25	0.12	0.0976

Table 6.30 Summary of test results for M50-GGFRC with V_f = 0.3% in Compression

Specimen Designation (1)	Strain Softening Region				E^c_i ($X10^4$) MPa (6)	STF^c (7)	DF^c (8)	E_{SS} ($X10^4$) MPa (9)	EA_{SSR} ($X10^{-2}$) N/mm (10)
	f^B_u (MPa) (2)	ε^B_u ($X10^{-4}$) (3)	f^C_{IP} (MPa) (4)	ε^C_{IP} ($X10^{-4}$) (5)					
Short Graded Fibers (SGF), V_f = 0.3%									
SGF-I#c	48.36	18.43	35.67	50.49	2.23	1.19	2.74	0.40	0.1224
SGF-II#c	52.61	26.84	35.55	96.27	1.67	1.30	3.59	0.25	0.1938
SGF-III#c	50.97	25.51	35.34	85.81	1.70	1.26	3.36	0.26	0.1785
SGF-IV#c	49.31	21.07	35.01	62.63	1.99	1.22	2.97	0.34	0.1426
SGF-V#c	48.60	16.97	35.67	45.93	2.43	1.20	2.71	0.45	0.1132
Long Graded Fibers (LGF), V_f = 0.3%									
LGF-I#c	46.26	32.12	35.26	89.74	1.22	1.14	2.79	0.19	0.1673
LGF-II#c	49.33	43.25	35.51	162.45	0.97	1.22	3.76	0.12	0.2403
LGF-III#c	48.69	41.01	35.27	144.95	1.01	1.20	3.53	0.13	0.2248
LGF-IV#c	47.87	35.85	34.91	110.15	1.14	1.18	3.07	0.17	0.1932
LGF-V#c	46.71	29.54	35.67	81.38	1.34	1.15	2.76	0.21	0.1554
Combined Graded Fibers (SGF), V_f = 0.3%									
CGF-I#c	49.07	37.28	36.07	111.00	1.12	1.21	2.98	0.18	0.2511
CGF-II#c	54.52	48.75	35.73	193.40	0.95	1.35	3.97	0.13	0.2993
CGF-III#c	52.79	46.74	35.59	173.74	0.96	1.30	3.72	0.14	0.2779
CGF-IV#c	50.73	42.15	35.40	137.02	1.02	1.25	3.25	0.16	0.2408
CGF-V#c	49.31	36.13	35.67	103.94	1.16	1.22	2.88	0.20	0.2446

Note: f^B_u = Peak Stress at B, ε^B_u = Peak Strain at B, f^C_{IP} = Stress at inflection C, ε^C_{IP} = Strain at inflection C, Intial Slope (E^c_i) = f^A / ε^A, Strengthening Factor (STF^c) = f^B_u / f_0, Ductility factor (DF^c) = $\varepsilon^C_{IP} / \varepsilon^B_u$, Strain Softening Slope (E_{SS}) = $(f^B_u - f^C_{IP}) / (\varepsilon^C_{IP} - \varepsilon^B_u)$, Energy Absorption capacity (EA_{SSR}) = Area under the stress strain curve in Strain Softening Region.

Table 6.31 Summary of test results for M50-GGFRC with V_f = 0.4% in Compression

Specimen Designation (1)	Strain Softening Region				E^c_i ($X10^4$) MPa (6)	STF^c (7)	DF^c (8)	E_{SS} ($X10^4$) MPa (9)	EA_{SSR} ($X10^{-2}$) N/mm (10)
	f^B_u (MPa) (2)	ε^B_u ($X10^{-4}$) (3)	f^C_{IP} (MPa) (4)	ε^C_{IP} ($X10^{-4}$) (5)					
Short Graded Fibers (SGF), V_f = 0.4%									
SGF-I#d	48.36	18.60	35.67	53.07	2.21	1.19	2.85	0.37	0.1235
SGF-II#d	54.53	28.53	35.58	108.50	1.62	1.35	3.80	0.24	0.2136
SGF-III#d	52.44	27.63	35.38	98.50	1.61	1.29	3.56	0.24	0.1989
SGF-IV#d	50.73	22.77	35.08	70.80	1.89	1.25	3.11	0.33	0.1586
SGF-V#d	49.07	17.82	35.67	50.19	2.34	1.21	2.82	0.41	0.1200
Long Graded Fibers (LGF), V_f = 0.4%									
LGF-I#d	46.30	34.99	35.67	102.99	1.12	1.14	2.94	0.16	0.1824
LGF-II#d	49.93	46.12	34.88	184.80	0.92	1.23	4.01	0.11	0.2593
LGF-III#d	49.15	43.88	35.30	163.93	0.95	1.21	3.74	0.12	0.2428
LGF-IV#d	48.09	38.71	34.95	130.31	1.06	1.19	3.37	0.14	0.2096
LGF-V#d	46.76	31.54	35.67	94.51	1.26	1.15	3.00	0.18	0.1661
Combined Graded Fibers (SGF), V_f = 0.4%									
CGF-I#d	49.31	40.15	35.67	123.09	1.04	1.22	3.07	0.16	0.2717
CGF-II#d	57.13	51.62	35.75	218.10	0.94	1.41	4.23	0.13	0.3321
CGF-III#d	55.34	49.61	35.63	199.09	0.95	1.37	4.01	0.13	0.3091
CGF-IV#d	52.15	45.02	35.45	159.04	0.98	1.29	3.53	0.15	0.3223
CGF-V#d	50.26	42.44	35.67	131.91	1.01	1.24	3.11	0.16	0.2928

Table 6.32 Summary of test results for M50-GGFRC with V_f = 0.5% in Compression

Specimen Designation (1)	Strain Softening Region				E^c_i ($X10^4$) MPa (6)	STF^c (7)	DF^c (8)	E_{SS} ($X10^4$) MPa (9)	EA_{SSR} ($X10^{-2}$) N/mm (10)
	f^B_u (MPa) (2)	ε^B_u ($X10^{-4}$) (3)	f^C_{IP} (MPa) (4)	ε^C_{IP} ($X10^{-4}$) (5)					
Short Graded Fibers (SGF), V_f = 0.5%									
SGF-I#e	48.84	18.77	35.67	55.91	2.21	1.20	2.98	0.35	0.1258
SGF-II#e	55.96	30.23	35.60	115.22	1.57	1.38	3.81	0.24	0.2322
SGF-III#e	54.10	29.33	35.40	108.90	1.57	1.33	3.71	0.23	0.2178
SGF-IV#e	51.21	24.47	35.10	82.53	1.78	1.26	3.37	0.28	0.1720
SGF-V#e	49.07	17.99	35.26	52.85	2.32	1.21	2.94	0.40	0.1212
Long Graded Fibers (LGF), V_f = 0.5%									
LGF-I#e	46.35	37.85	35.26	115.21	1.04	1.14	3.04	0.14	0.2408
LGF-II#e	50.39	48.99	35.53	203.06	0.87	1.24	4.15	0.10	0.3389
LGF-III#e	49.61	46.74	35.31	181.46	0.90	1.22	3.88	0.11	0.2611
LGF-IV#e	48.55	41.58	34.96	143.76	0.99	1.20	3.46	0.13	0.2273
LGF-V#e	47.22	34.41	35.26	109.52	1.17	1.17	3.18	0.16	0.1830
Combined Graded Fibers (SGF), V_f = 0.5%									
CGF-I#e	49.78	43.01	35.67	135.72	0.98	1.23	3.16	0.15	0.2940
CGF-II#e	59.78	54.49	35.76	239.10	0.93	1.47	4.39	0.13	0.4471
CGF-III#e	56.88	52.48	35.65	220.06	0.92	1.40	4.19	0.13	0.4098
CGF-IV#e	53.15	47.89	35.47	175.28	0.94	1.31	3.66	0.14	0.3494
CGF-V#e	50.73	45.31	35.67	149.22	0.95	1.25	3.29	0.14	0.3155

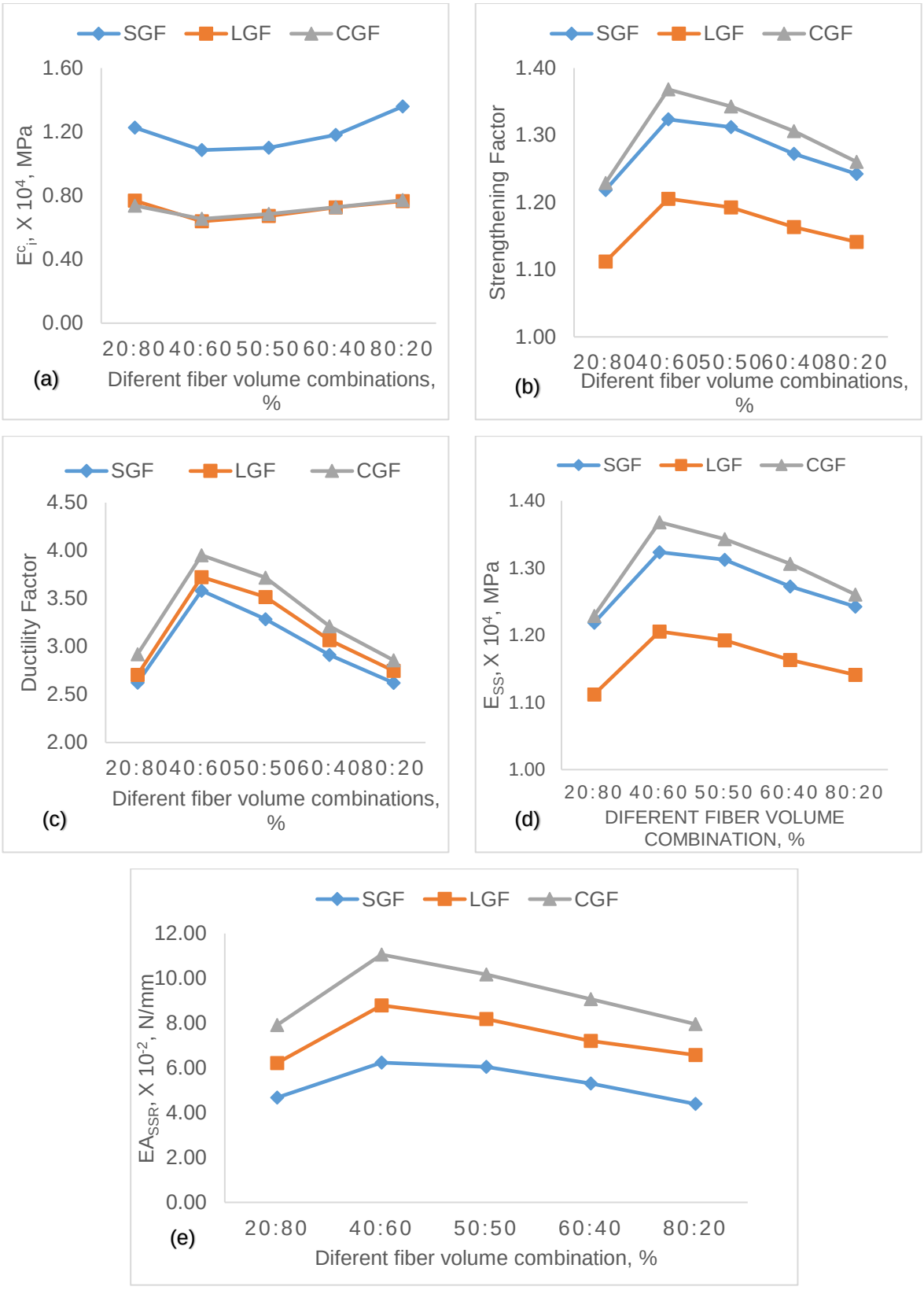

Fig.6.81 Mechanical properties variation of M30-GGFRC-0.3% in Compression (a) Initial slope (E^c_i), (b) strengthening factor (STF^c), (c) ductility factor (DF^c), (d) strain softening slope (E_{SS}) and (e) energy absorption capacity in strain softening region (EA_{SSR}).

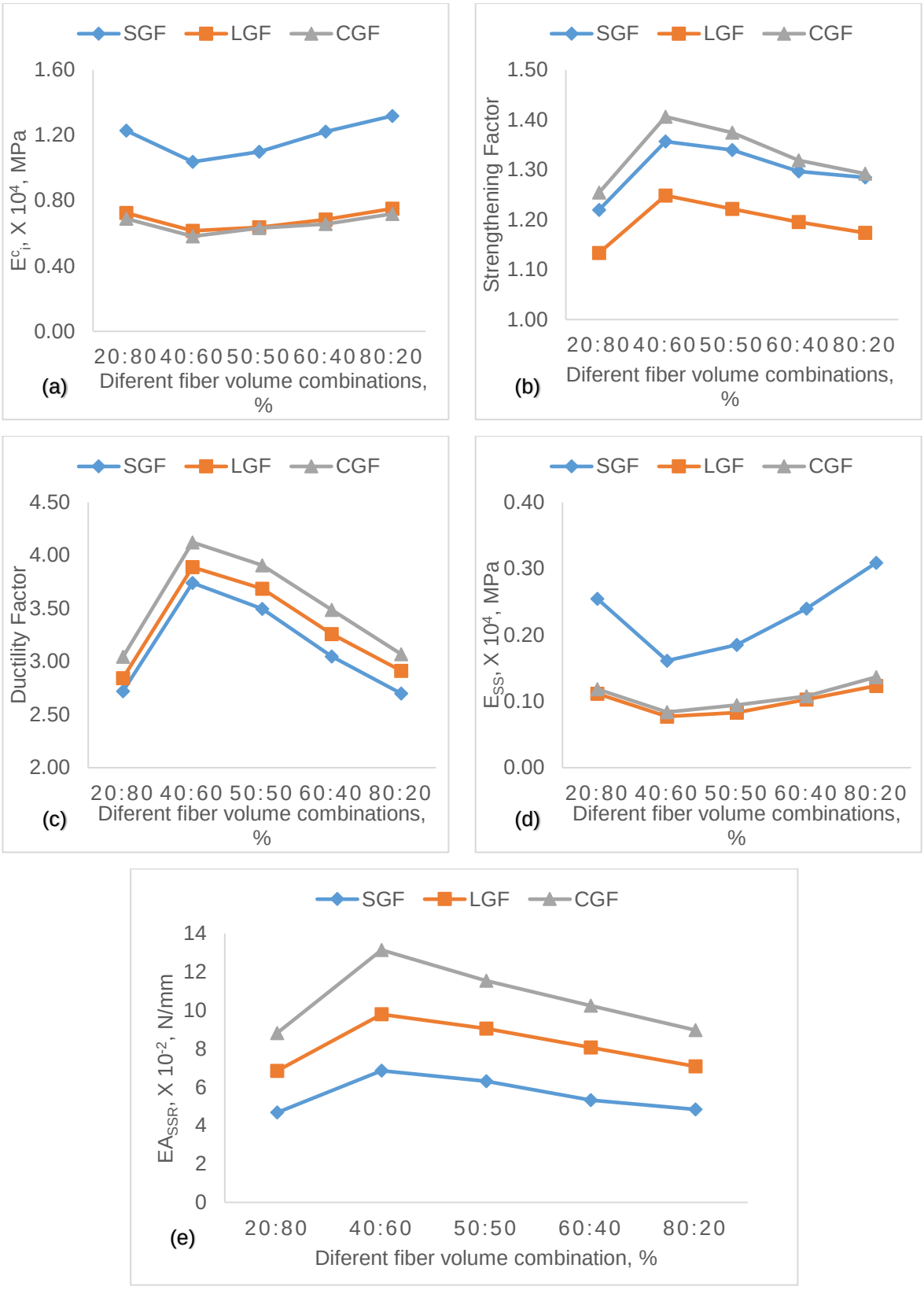

Fig.6.82 Mechanical properties variation of M30-GGFRC-0.4% in Compression (a) Initial slope (E^c_i), (b) strengthening factor (STF^c), (c) ductility factor (DF^c), (d) strain softening slope (E_{SS}) and (e) energy absorption capacity in strain softening region (EA_{SSR}).

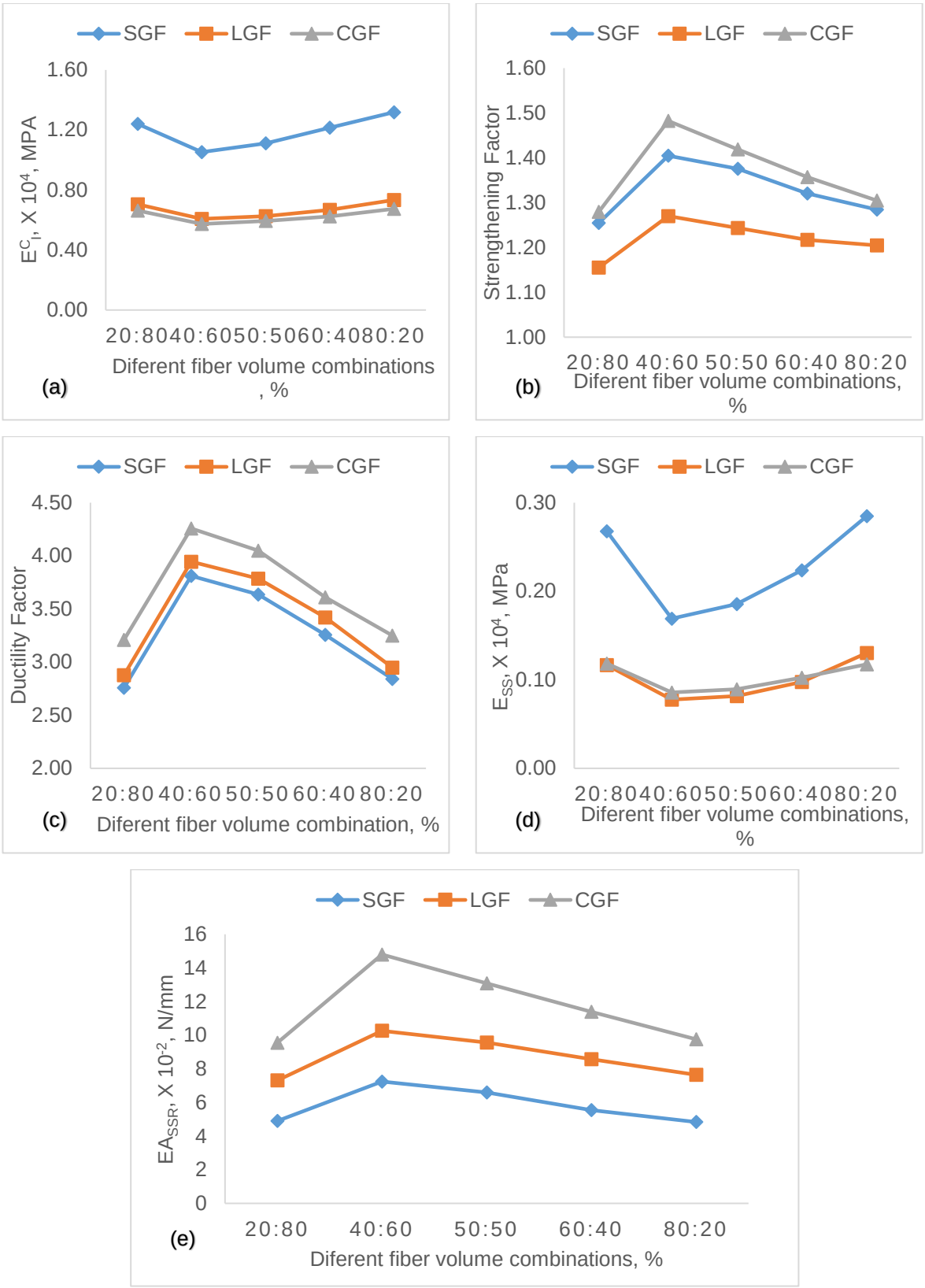

Fig.6.83 Mechanical properties variation of M30-GGFRC-0.5% in Compression (a) Initial slope (E^c_i), (b) strengthening factor (STF^c), (c) ductility factor (DF^c), (d) strain softening slope (E_{SS}) and (e) energy absorption capacity in strain softening region (EA_{SSR}).

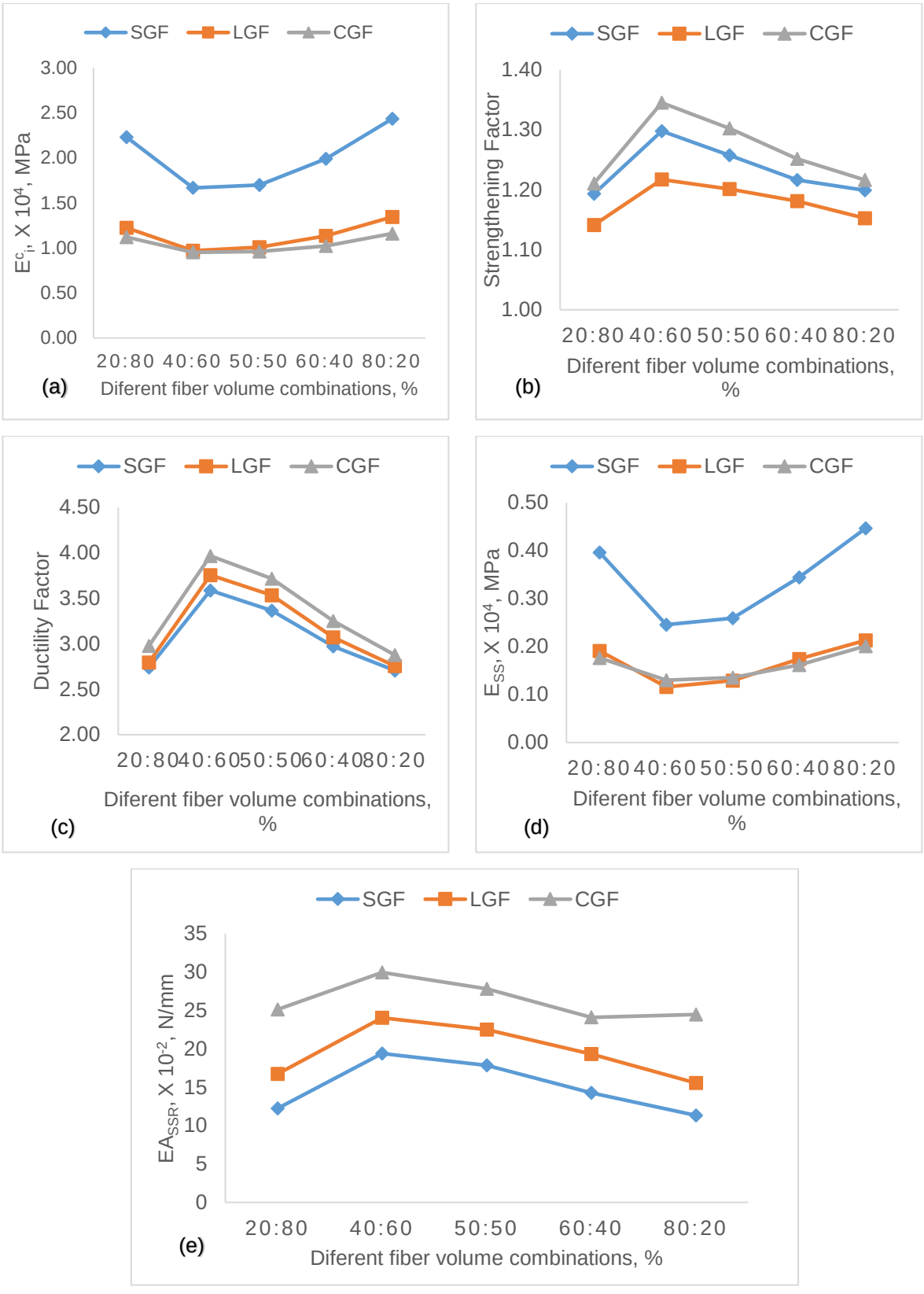

Fig.6.84 Mechanical properties variation of M50-GGFRC-0.3% in Compression (a) Initial slope (E^c_i), (b) strengthening factor (STF^c), (c) ductility factor (DF^c), (d) strain softening slope (E_{SS}) and (e) energy absorption capacity in strain softening region (EA_{SSR}).

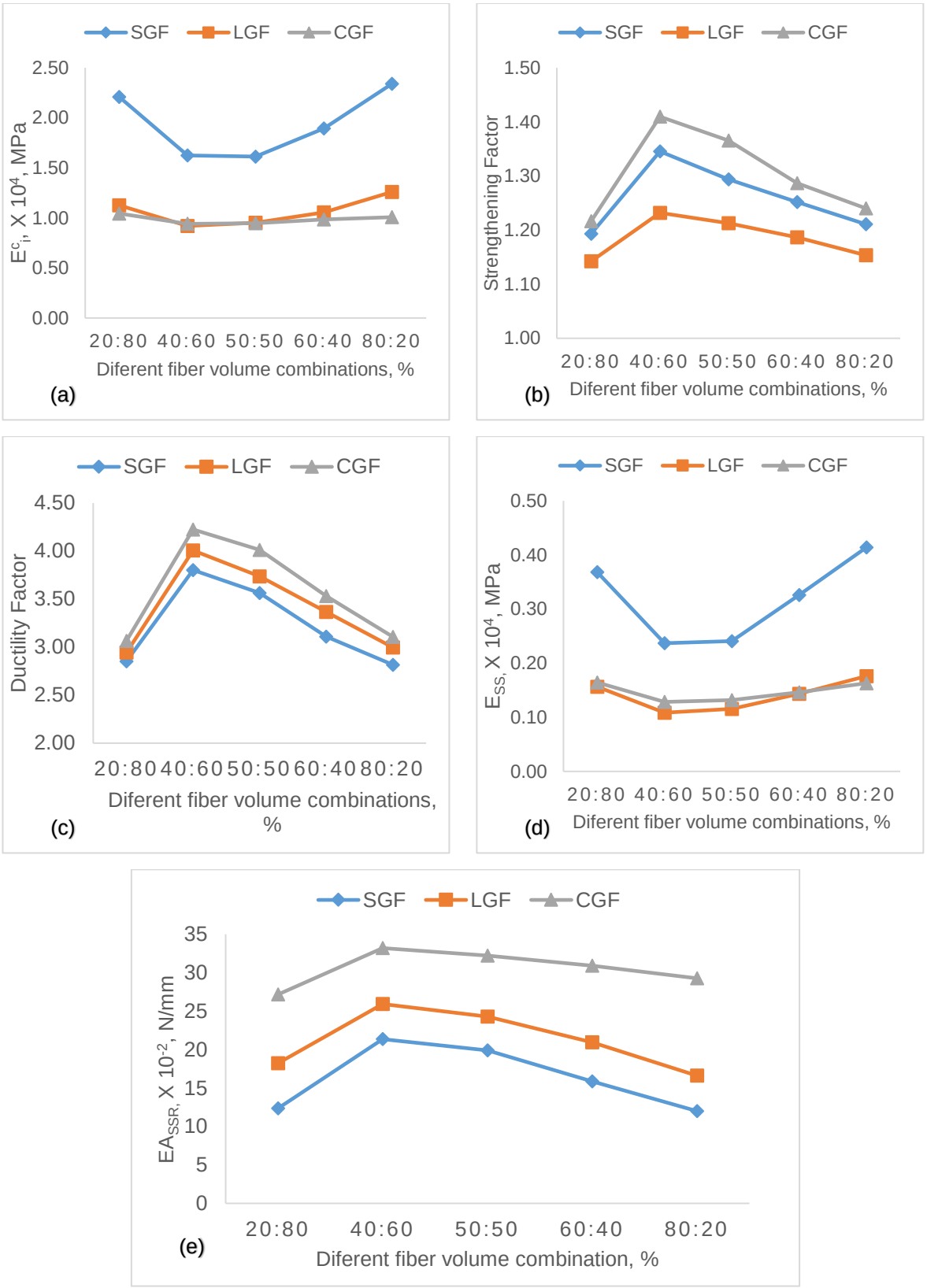

Fig.6.85 Mechanical properties variation of M50-GGFRC-0.4% in Compression (a) Initial slope (E^c_i), (b) strengthening factor (STF^c), (c) ductility factor (DF^c), (d) strain softening slope (E_{SS}) and (e) energy absorption capacity in strain softening region (EA_{SSR}).

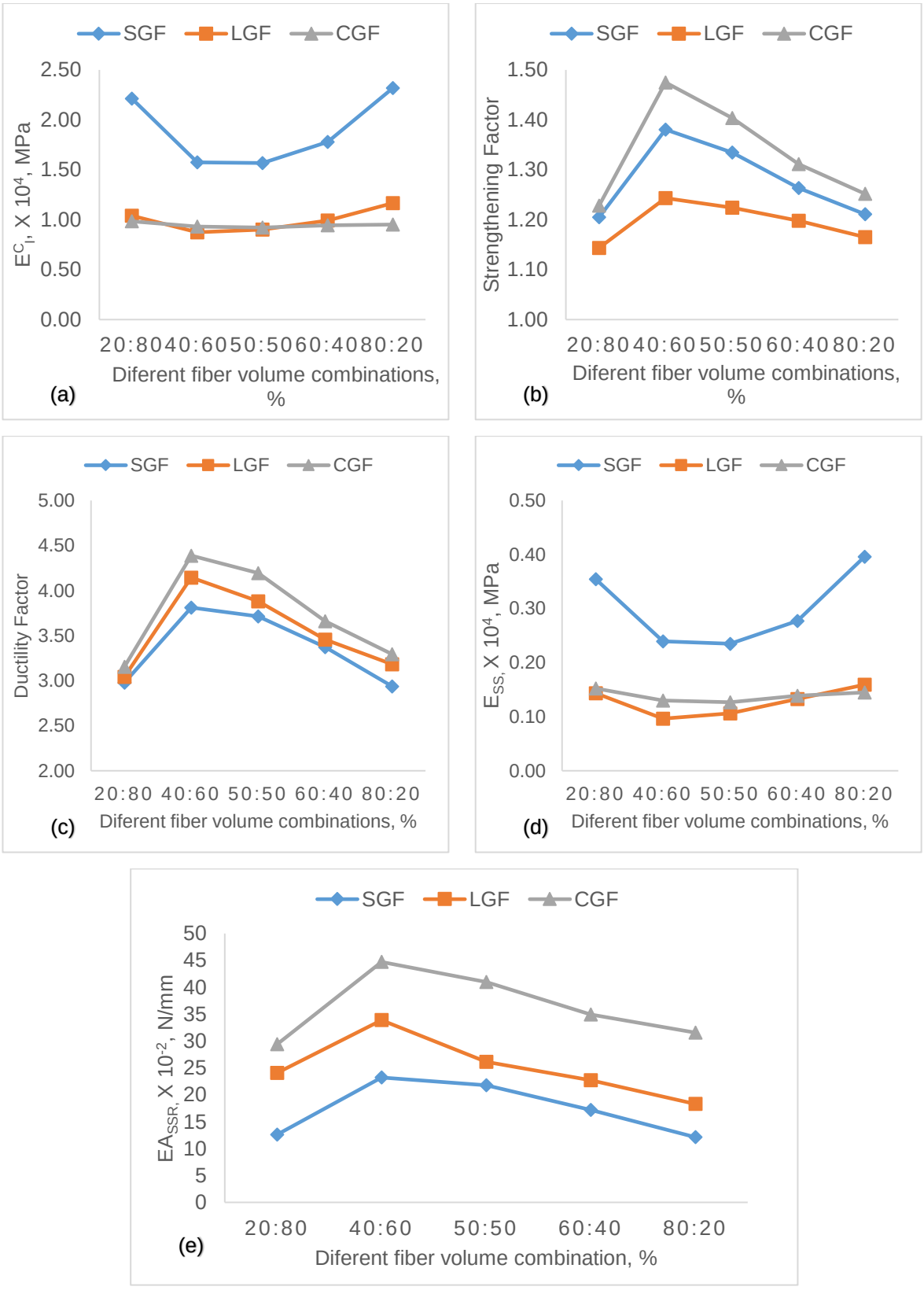

Fig.6.86 Mechanical properties variation of M50-GGFRC-0.5% in Compression (a) Initial slope (E^{c}_{i}), (b) strengthening factor (STF^{c}), (c) ductility factor (DF^{c}), (d) strain softening slope (E_{SS}) and (e) energy absorption capacity in strain softening region (EA_{SSR}).

6.15 Analytical model for Behaviour of GGFRC in compression

Analytical stress strain curves are predicted for GGFRC in compression similar to the MGFRC in compression. A typical stress-strain curve of GFRC in compression is shown in Fig.5.53 marking salient points and already given in Chapter-5. Grading of fibers (SGF, LGF and CGF) in the composite effect the stress and strain both at peak and inflection points. In this diagram, important points which influence the stress strain behaviour are B and C. In order to predict the stress strain behaviour of GGFRC, the points B (f_u, ε_u) and C (f_{IP}, ε_{IP}) are needed to be determined. The equations have been developed in this investigation for normalised stress strain curves.

In the present study to predict analytical stress strain diagram for GGFRC an equation (13) given in Chapter-5 is used and re written below.

$$\frac{f_c}{f_u} = \frac{\beta(\varepsilon_c/\varepsilon_u)}{\beta-1+(\varepsilon_c/\varepsilon_u)^{\beta}}$$

Where $f_u$the peak strength of fiber reinforced concrete and ε_u is the corresponding peak strain. f_c and ε_c are the stress and strain values on the curve and β is the material parameter that depends on the shape of the stress strain diagram.

In Table 6.27 to 6.32 the strengthening factor and ductility factor for GGFRC specimens are given. An examination of this results showed improvement in strength and also strain with increase in grading of fibers (SGF, LGF and CGF) and fiber volume combination. Thus the amount of fiber grading with percentage of volume combination has direct influence on strength and strain of GGFRC specimens. In the graded fibers in order to reflect synergy effect, a parameter RI_{GF} is considered as given in article 6.7. RI_{GF} takes into account the fiber participation in the composite. It is also known that the properties of matrix has direct influence on strength and strain of composite. Thus the peak strength of the composite (f_u) and peak strain of the composite are directly proportional to that of plain concrete and also directly proportional to RI_{GF}. However, the influence of RI_{GF} is linear or nonlinear has to be established from the experimental results. Hence, it can be written that

- $f_u \propto f_0$

  $\propto (RI_{GF})^n$

Then $f_u = k\, f_0\, (RI_{GF})^n$

The above expression is rewritten as

- $(f_u / f_0) = k\, (RI_{GF})^n$

Similarly, it can be written for strain as

- $(\varepsilon_u/\varepsilon_0) = k\, (RI_{GF})^n$

The above expression can be used to predict f_u, ε_u for a given value of RI_{GF} i.e., for a set of fiber properties. In order to construct compressive stress strain diagram as indicated Fig 5.53 given in Chapter-5, the material property defined by β given in the equation (13) is the only one now required to be determined for graded fiber specimen. In order to arrive at β for fiber properties (RI_{GF}) of GGFRC, the equation (19) is taken from the chapter-5 and re written below.

$$\beta = 1.9407\, (RI_{GF})^{-0.039}$$

Here RI_{MF} is replaced with RI_{GF} for GGFRC. The RI_{GF} (using equation (26)) is calculated for M30-GGFRC and M50-GGFRC with 0.3%, 0.4% and 0.5% fiber volume fraction and given in column 2 of Table 6.33 to 6.38. For each RI_{GF} the corresponding β values are calculated and given in column 8 of Table 6.33 to 6.38.

In the above expression f_u, ε_u, and β for each specimen is known and if these values are substituted in equation (13) and it generates the stress strain diagram of GGFRC for a set of fiber properties indicated by RI_{GF}.

The limitation for the above equation is that the drooping portion (post peak behaviour) is continuous right up to the stress level becomes zero, which is unrealistic. Hence the post peak behaviour is limited to the point of inflection i.e., point C in the Fig.5.53. In order to identify the point C, the variation of f_{IP} from the experimental data can be noted and an equation is proposed which will be helpful to find the ε_{IP} values for a given f_{IP} from the equation (14) given in chapter-5. Thus the salient points of stress strain diagram of GFRC given in Fig.5.53 can be estimated theoretically. In the subsequent articles the method of arriving at models for f_u, f_0, ε_u and f_{IP} are explained.

Table 6.33 Stress ratios, strain ratios and energy absorption of M30-GGFRC-0.3% in Compression

Specimen Designation (1)	RI_{GF} (2)	Strain Softening Region					β (8)
		f_u/f_0 (3)	$\varepsilon_u/\varepsilon_0$ (4)	f_{IP}/f_o (5)	$\varepsilon_{IP}/\varepsilon_o$ (6)	EA_{SSR}/EA^o_{SSR} (7)	
Short Graded Fibers (SGF), V_f = 0.3%							
SGF-I#c	0.15	1.22	1.02	0.85	2.69	1.55	2.09
SGF-II#c	0.39	1.32	1.26	0.86	4.50	2.07	2.013
SGF-III#c	0.59	1.31	1.23	0.86	4.41	2.00	1.980
SGF-IV#c	0.88	1.27	1.11	0.85	3.57	1.76	1.951
SGF-V#c	2.36	1.24	0.94	0.87	2.47	1.46	1.880
Long Graded Fibers (LGF), V_f = 0.3%							
LGF-I#c	0.16	1.11	1.49	0.85	3.01	2.06	2.080
LGF-II#c	0.43	1.21	1.94	0.86	4.77	2.91	2.006
LGF-III#c	0.64	1.19	1.83	0.86	4.48	2.71	1.971
LGF-IV#c	0.96	1.16	1.65	0.85	3.77	2.39	1.940
LGF-V#c	2.54	1.14	1.54	0.84	3.51	2.18	1.871
Combined Graded Fibers (CGF), V_f = 0.3%							
CGF-I#c	0.09	1.23	1.72	0.86	4.50	2.62	2.130
CGF-II#c	0.24	1.37	2.15	0.87	8.52	3.66	2.053
CGF-III#c	0.35	1.34	2.02	0.87	6.49	3.37	2.020
CGF-IV#c	0.53	1.31	1.85	0.86	5.95	3.01	1.991
CGF-V#c	1.42	1.26	1.68	0.88	4.41	2.64	1.910

Table 6.34 Stress ratios, strain ratios and energy absorption of M30-GGFRC-0.4% in Compression

Specimen Designation (1)	RI_{GF} (2)	Strain Softening Region					β (8)
		f_u/f_0 (3)	$\varepsilon_u/\varepsilon_0$ (4)	f_{IP}/f_o (5)	$\varepsilon_{IP}/\varepsilon_o$ (6)	EA_{SSR}/EA^o_{SSR} (7)	
Short Graded Fibers (SGF), V_f = 0.4%							
SGF-I#d	0.14	1.22	1.02	0.85	2.78	1.58	2.10
SGF-II#d	0.37	1.36	1.35	0.87	4.83	2.27	2.02
SGF-III#d	0.56	1.34	1.26	0.86	4.49	2.09	1.990
SGF-IV#d	0.83	1.30	1.09	0.85	3.52	1.76	1.950
SGF-V#d	1.67	1.28	1.00	0.85	3.22	1.60	1.900
Long Graded Fibers (SGF), V_f = 0.4%							
LGF-I#d	0.16	1.13	1.61	0.86	3.46	2.27	2.091
LGF-II#d	0.42	1.25	2.09	0.86	6.09	3.24	2.008
LGF-III#d	0.62	1.22	1.98	0.86	5.18	3.00	1.982

LGF-IV#d	0.94	1.20	1.80	0.85	4.72	2.67	1.951
LGF-V#d	2.50	1.17	1.61	0.86	4.22	2.35	1.870
Combined Graded Fibers (CGF), V_f = 0.4%							
CGF-I#d	0.08	1.25	1.87	0.88	4.91	2.92	2.141
CGF-II#d	0.22	1.41	2.49	0.87	8.93	4.35	2.065
CGF-III#d	0.33	1.37	2.24	0.87	8.85	3.83	2.030
CGF-IV#d	0.49	1.32	2.07	0.86	7.41	3.39	2.001
CGF-V#d	1.30	1.29	1.85	0.86	5.95	2.97	1.920

Table 6.35 Stress ratios, strain ratios and energy absorption of M30-GGFRC-0.5% in Compression

Specimen Designation (1)	RI_{GF} (2)	Strain Softening Region					β (8)
		f_u/f_0 (3)	$\varepsilon_u/\varepsilon_0$ (4)	f_{IP}/f_o (5)	$\varepsilon_{IP}/\varepsilon_o$ (6)	EA_{SSR} / EA^o_{SSR} (7)	
Short Graded Fibers (SGF), V_f = 0.5%							
SGF-I#e	0.13	1.25	1.67	0.85	3.04	1.62	2.100
SGF-II#e	0.36	1.40	2.21	0.87	5.48	2.40	2.020
SGF-III#e	0.54	1.38	2.05	0.86	5.34	2.18	1.991
SGF-IV#e	0.80	1.32	1.80	0.85	4.00	1.84	1.960
SGF-V#e	2.14	1.28	1.61	0.85	3.42	1.60	1.881
Long Graded Fibers (LGF), V_f = 0.5%							
LGF-I#e	0.15	1.15	1.69	0.85	3.83	2.42	2.090
LGF-II#e	0.41	1.27	2.15	0.86	5.99	3.40	2.010
LGF-III#e	0.61	1.24	2.05	0.86	5.70	3.17	1.980
LGF-IV#e	0.92	1.22	1.88	0.85	5.23	2.84	1.951
LGF-V#e	2.45	1.20	1.69	0.85	4.15	2.53	1.870
Combined Graded Fibers (LGF), V_f = 0.5%							
CGF-I#e	0.08	1.28	1.99	0.85	6.39	3.16	2.140
CGF-II#e	0.21	1.48	2.66	0.87	10.52	4.90	2.063
CGF-III#e	0.31	1.42	2.46	0.87	9.72	4.34	2.031
CGF-IV#e	0.47	1.36	2.24	0.86	8.85	3.78	2.001
CGF-V#e	1.25	1.30	1.99	0.87	6.41	3.23	1.922

Table 6.36 Stress ratios, strain ratios and energy absorption of M50-GGFRC-0.3% in Compression

Specimen Designation (1)	RI_{GF} (2)	Strain Softening Region					β (8)
		f_u/f_0 (3)	$\varepsilon_u/\varepsilon_0$ (4)	f_{IP}/f_o (5)	$\varepsilon_{IP}/\varepsilon_o$ (6)	EA_{SSR}/EA^o_{SSR} (7)	
Short Graded Fibers (SGF), V_f = 0.3%							
SGF-I#c	0.15	1.13	0.87	0.84	2.38	2.09	2.091
SGF-II#c	0.39	1.23	1.27	0.83	3.76	3.30	2.013
SGF-III#c	0.59	1.19	1.20	0.83	3.21	3.04	1.982
SGF-IV#c	0.88	1.16	0.99	0.82	2.66	2.43	1.951
SGF-V#c	2.36	1.14	0.80	0.84	1.86	1.93	1.877
Long Graded Fibers (LGF), V_f = 0.3%							
LGF-I#c	0.16	1.08	1.52	0.83	3.10	2.85	2.085
LGF-II#c	0.43	1.16	2.04	0.83	5.09	4.10	2.006
LGF-III#c	0.64	1.14	1.94	0.83	4.49	3.83	1.975
LGF-IV#c	0.96	1.12	1.69	0.82	3.93	3.29	1.944
LGF-V#c	2.54	1.09	1.39	0.84	2.86	2.65	1.871
Combined Graded Fibers (CGF), V_f = 0.3%							
CGF-I#c	0.09	1.15	1.76	0.85	4.09	4.28	2.133
CGF-II#c	0.24	1.28	2.30	0.84	7.52	5.10	2.053
CGF-III#c	0.35	1.24	2.21	0.83	7.21	4.74	2.021
CGF-IV#c	0.53	1.19	1.99	0.83	5.30	4.11	1.989
CGF-V#c	1.42	1.16	1.71	0.84	3.96	4.17	1.914

Table 6.37 Stress ratios, strain ratios and energy absorption of M50-GGFRC-0.4% in Compression

Specimen Designation (1)	RI_{GF} (2)	Strain Softening Region					β (8)
		f_u/f_0 (3)	$\varepsilon_u/\varepsilon_0$ (4)	f_{IP}/f_o (5)	$\varepsilon_{IP}/\varepsilon_o$ (6)	EA_{SSR}/EA^o_{SSR} (7)	
Short Graded Fibers (SGF), V_f = 0.4%							
SGF-I#d	0.14	1.13	0.88	0.84	2.69	2.11	2.096
SGF-II#d	0.37	1.28	1.35	0.83	4.40	3.64	2.017
SGF-III#d	0.56	1.23	1.30	0.83	4.26	3.39	1.986
SGF-IV#d	0.83	1.19	1.07	0.82	2.87	2.70	1.955
SGF-V#d	1.67	1.15	0.84	0.84	2.10	2.05	1.902
Long Graded Fibers (LGF), V_f = 0.4%							
LGF-I#d	0.16	1.09	1.65	0.84	3.28	3.11	2.087
LGF-II#d	0.42	1.17	2.18	0.82	5.80	4.42	2.008
LGF-III#d	0.62	1.15	2.07	0.83	5.16	4.14	1.977

LGF-IV#d	0.94	1.13	1.83	0.82	4.25	3.58	1.946
LGF-V#d	2.50	1.10	1.49	0.84	3.05	2.83	1.873
Combined Graded Fibers (CGF), V_f = 0.4%							
CGF-I#d	0.08	1.16	1.89	0.84	4.15	4.63	2.140
CGF-II#d	0.22	1.34	2.44	0.84	8.88	5.66	2.060
CGF-III#d	0.33	1.30	2.34	0.84	8.54	5.27	2.027
CGF-IV#d	0.49	1.22	2.13	0.83	6.31	5.50	1.996
CGF-V#d	1.30	1.18	2.00	0.84	5.00	4.99	1.921

Table 6.38 Stress ratios, strain ratios and energy absorption of M50-GGFRC-0.5% in Compression

Specimen Designation (1)	RI_{GF} (2)	Strain Softening Region					β (8)
		f_u/f_0 (3)	$\varepsilon_u/\varepsilon_0$ (4)	f_{IP}/f_o (5)	$\varepsilon_{IP}/\varepsilon_o$ (6)	EA_{SSR} / EA^o_{SSR} (7)	
Short Graded Fibers (SGF), V_f = 0.5%							
SGF-I#e	0.13	1.14	0.89	0.84	2.79	2.15	2.099
SGF-II#e	0.36	1.31	1.43	0.83	5.74	3.96	2.020
SGF-III#e	0.54	1.27	1.38	0.83	4.11	3.71	1.989
SGF-IV#e	0.80	1.20	1.15	0.82	3.08	2.93	1.957
SGF-V#e	2.14	1.15	0.85	0.83	2.12	2.07	1.884
Long Graded Fibers (LGF), V_f = 0.5%							
LGF-I#e	0.15	1.09	1.79	0.83	3.66	4.11	2.088
LGF-II#e	0.41	1.18	2.31	0.83	6.17	5.78	2.010
LGF-III#e	0.61	1.16	2.21	0.83	5.88	4.45	1.978
LGF-IV#e	0.92	1.14	1.96	0.82	4.90	3.88	1.947
LGF-V#e	2.45	1.11	1.62	0.83	3.55	3.12	1.874
Combined Graded Fibers (CGF), V_f = 0.5%							
CGF-I#e	0.08	1.17	2.03	0.84	5.06	5.01	2.144
CGF-II#e	0.21	1.40	2.57	0.84	11.14	7.62	2.063
CGF-III#e	0.31	1.33	2.48	0.84	9.96	6.99	2.031
CGF-IV#e	0.47	1.25	2.26	0.83	5.25	5.96	1.999
CGF-V#e	1.25	1.19	2.14	0.84	6.71	5.38	1.924

Peak Stress (f_u):

The reinforcing index of each mix was calculated and is given in column 2 of Table 6.33 to 6.38. The ratio between peak stress of GGFRC (M30 and M50 grade) and plain concrete peak stress (f_u/f_0) is given in column 3 of Table 6.33 to 6.38. In order to understand the variation of f_u/f_0 with RI_{GF}, points are plotted as shown in Fig.6.87 (a). An examination of the plot and various trails to arrive at the best fit, led to understand that f_u/f_0 varies as power function of RI_{GF} in the form of $f_u/f_0 = k\ (RI_{GF})^{-n}$ instead of +n as envisaged earlier. The power function is modified by multiplying both sides by RI_{GF}. The modified relation is $(RI_{GF})\ f_u/f_0 = k\ (RI_{GF})^{(1-n)}$. Now points are plotted with RI_M as abscissa and $RI_{GF}.\ f_u/f_0$ as ordinate is shown in Fig.6.87 (b). The regression expression obtained is $(RI_{GF})\ f_u/f_0 = 1.172\ (RI_{GF})^{0.9868}$ with regression coefficient $R^2 = 0.954$. Then the relation between RI_{GF} and f_u/f_0 can be expressed as.

$$f_u = f_0\ (1.172\ .\ RI_{GF}^{-0.013}) \quad \text{----------(28)}$$

Where f_0 and f_u are the peak stress of plain concrete and peak stress of GGFRC respectively.

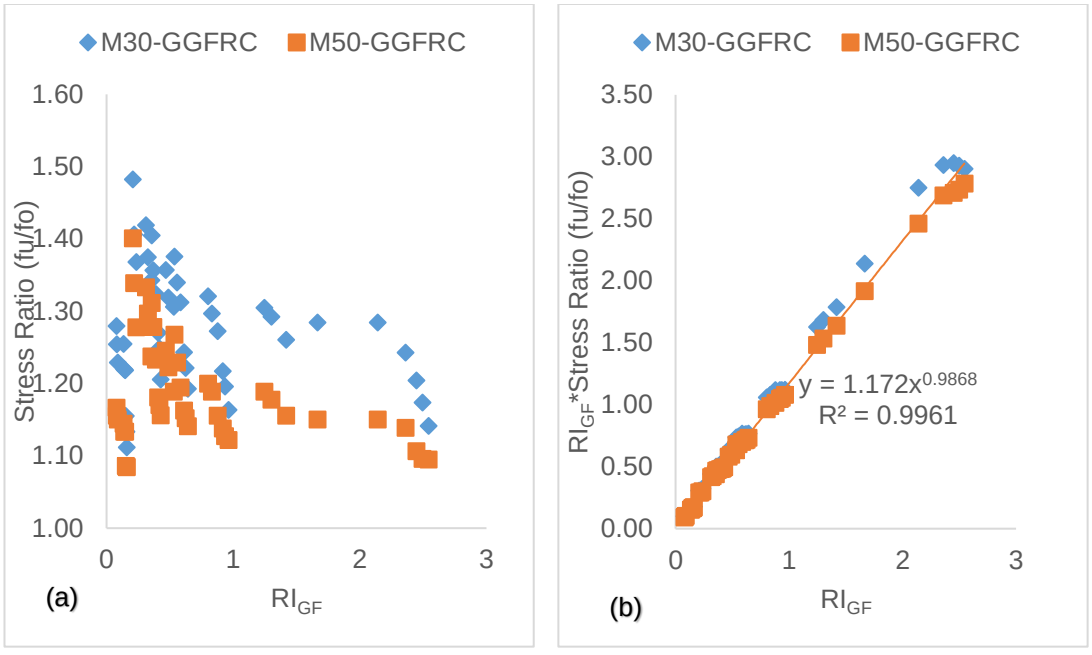

Fig.6.87 stress ratio at ultimate point as a function of RI_{GF} for GGFRC in Compression

Strain at Peat Stress (ε_u):

The reinforcing index of each mix was calculated and is given in column 2 of Table 6.33 to 6.38. The ratio between strain at peak stress of GGFRC (M30 and M50 grade) and strain at peak stress of plain concrete (ε_u / ε_0) is given in column 4 of Table 6.33 to 6.38. In order to understand the variation of ε_u / ε_0 with RI_{GF}, points are plotted as shown in Fig.6.88 (a). An examination of the plot and various trails to arrive at the best fit, led to understand that f_u/f_0 varies as power function of RI_{GF} in the form of ε_u / $\varepsilon_0 = k (RI_{GF})^{-n}$. The power function is modified by multiplying both sides by RI_{GF}. The modified relation is $(RI_{GF})\ \varepsilon_u$ / $\varepsilon_0 = k (RI_{GF})^{(1-n)}$. Now points are plotted with RI_{GF} as abscissa and $RI_{GF}.\ \varepsilon_u$ / ε_0 as ordinate is shown in Fig.6.88 (b). The regression expression obtained is $(RI_{GF})\ \varepsilon_u$ / $\varepsilon_0 = 1.6305\ (RI_{GF})^{0.943}$ with regression coefficient $R^2 = 0.9251$. Then the relation between RI_{GF} and ε_u / ε_0 can be expressed as.

$$\varepsilon_u = \varepsilon_0\ (1.6305\ \ RI_{GF}^{-0.057}) \text{ ----------(29)}$$

Where ε_o and ε_u are the peak strain at peak stress of plain concrete and peak strain at peak stress of GGFRC respectively.

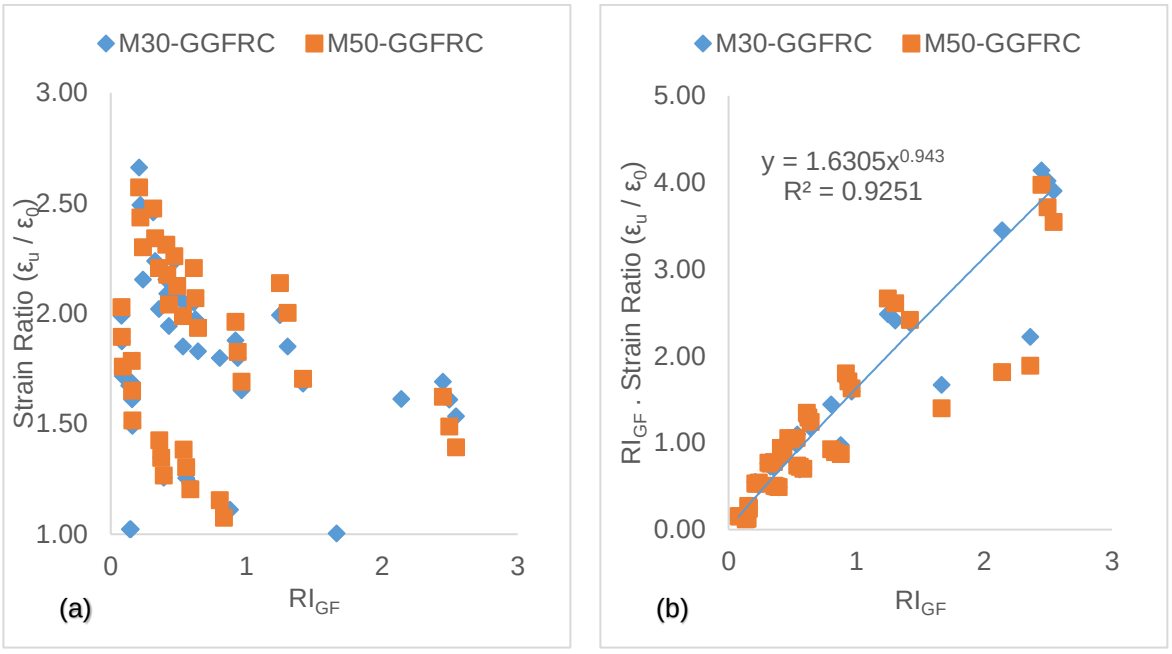

Fig.6.88 strain ratio at ultimate point as a function of RI_{GF} for GGFRC in Compression

Stress at inflection (f_{IP}):

The reinforcing index of each mix was calculated and is given in column 2 of Table 6.33 to 6.38. The ratio between stress at inflection of MGFRC (M30 and M50 grade) and plain concrete peak stress (f_{IP}/f_0) is given in column 5 of Table 6.33 to 6.38. In order to understand the variation of f_{IP}/f_0 with RI_{GF}, points are plotted as shown in Fig.6.89. An examination of the plot and various trails to arrive at the best fit, led to understood that f_{IP}/f_0 varies as linear function of RI_{GF} in the form of $f_{IP}/f_0 = m\ (RI_{GF}) + k$. The regression expression obtained is $f_{IP}/f_0 = -0.079\ RI_{GF} + 0.901$ with regression coefficient $R^2 = 0.8564$. Then the relation between RI_{GF} and f_{IP}/f_0 can be expressed as.

$$f_{IP} = f_0\ (-0.079\ RI_{GF} + 0.901) \qquad \text{----------(30)}$$

Where f_0 and f_{IP} are the peak stress of plain concrete and stress at inflection point of GGFRC respectively.

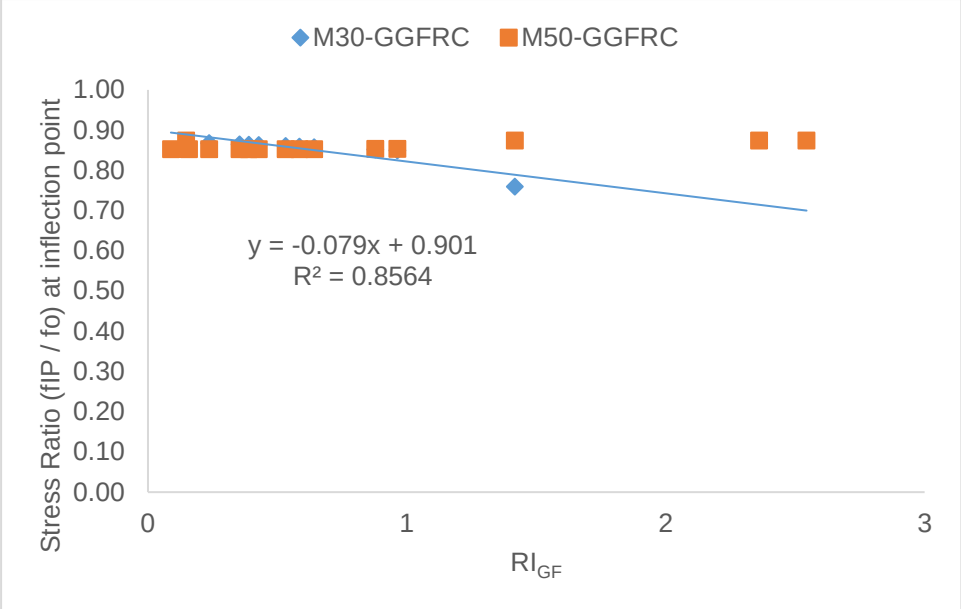

Fig.6.89 stress ratio at inflection point as a function of RI_{GF} for GGFRC in Compression

Strain at inflection (ε_{IP}):

The reinforcing index of each mix was calculated and is given in column 2 of Table 6.33 to 6.38. The ratio between strain at peak stress of GGFRC (M30 and M50 grade) and strain at peak stress of plain concrete ($\varepsilon_{IP} / \varepsilon_0$) is given in column 6 of Table 6.33 to 6.38. In order to understand the variation of $\varepsilon_{IP} / \varepsilon_0$ with RI_{GF}, points are plotted as shown in Fig.6.90 (a). An examination of the plot and various trails to arrive at the best fit, led to understand that $\varepsilon_{IP} / \varepsilon_0$ varies as power function of RI_{GF} in the form of $\varepsilon_{IP} / \varepsilon_0 =$

k $(RI_{GF})^{-n}$ instead of +n as envisaged earlier. The power function is modified by multiplying both sides by RI_{GF}. The modified relation is $(RI_{GF})\ \varepsilon_{IP} / \varepsilon_0 = k\ (RI_{GF})^{(1-n)}$. Now points are plotted with RI_{GF} as abscissa and $RI_{GF.}\ \varepsilon_{IP} / \varepsilon_0$ as ordinate is shown in Fig.6.90 (b). The regression expression obtained is $(RI_{GF})\ \varepsilon_{IP} / \varepsilon_0 = 0.856\ (RI_{GF})^{\ 0.9985}$ with regression coefficient $R^2 = 0.99$. Then the relation between RI_{GF} and $\varepsilon_{IP} / \varepsilon_0$ can be expressed as.

$$\varepsilon_{IP} = \varepsilon_o\ (0.856.RI_{GF}^{-0.07}) \quad \text{----------(31)}$$

Where ε_o and ε_{IP} are the peak strain at peak stress of plain concrete and strain at inflection of GGFRC respectively.

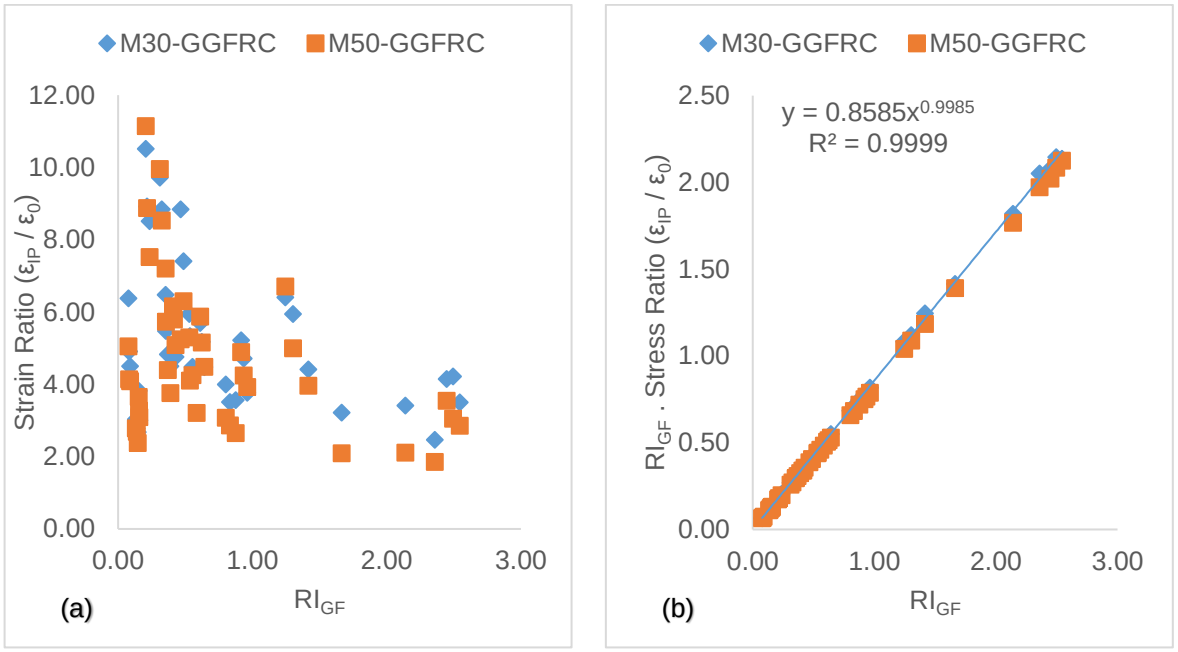

Fig.6.90 strain ratio at inflection point as a function of RI_{GF} for GGFRC in Compression.

Energy Absorption in strain softening region (EA_{SSR}):

EA_{SSR} is computed from the stress strain diagram (M30-GGFRC and M50-GGFRC) shown in Fig.6.55 to 6.80 and vales are given in column 11 Table 6.27 to 6.32. The reinforcing index of each mix was calculated and is given in column 2 of Table 6.33 to 6.38. The ratio between energy absorption of GGFRC (M30 and M50 grade) and plain concrete energy absorption (EA_{SSR} / EA^0_{SSR}) is given in column 7 of Table 6.33 to 6.38. In order to understand the variation of EA_{SSR} / EA^0_{SSR} with RI_{GF}, points are plotted as shown in Fig.6.91 (a). An examination of the plot and various trails to arrive at the best

fit, led to understand that EA_{SSR} / EA^0_{SSR} varies as power function of RI_{GF} in the form of EA_{SSR} / EA^0_{SSR} = k $(RI_{GF})^{-n}$ instead of +n as envisaged earlier. The power function is modified by multiplying both sides by RI_{GF}. The modified relation is (RI_{GF}) EA_{SSR} / EA^0_{SSR} = k $(RI_{GF})^{(1-n)}$. Now points are plotted with RI_{GF} as abscissa and $RI_{GF.}$ EA_{SSR} / EA^0_{SSR} as ordinate is shown in Fig.6.91 (b). The regression expression obtained is (RI_{GF}) EA_{SSR} / EA^0_{SSR} = 3.5018 $(RI_{GF})^{0.9287}$ with regression coefficient R^2 = 0.898. Then the relation between RI_{GF} and EA_{SSR} / EA^0_{SSR} can be expressed as.

$$EA_{SSR} = EA^o_{SSR} (3.5018\ RI_{GF}^{-0.071}) \text{ ---------- (32)}$$

Where EA^o_{SSR} and EA_{SSR} are the energy absorption in strain softening region of plain concrete and energy absorption in strain softening region of GGFRC respectively.

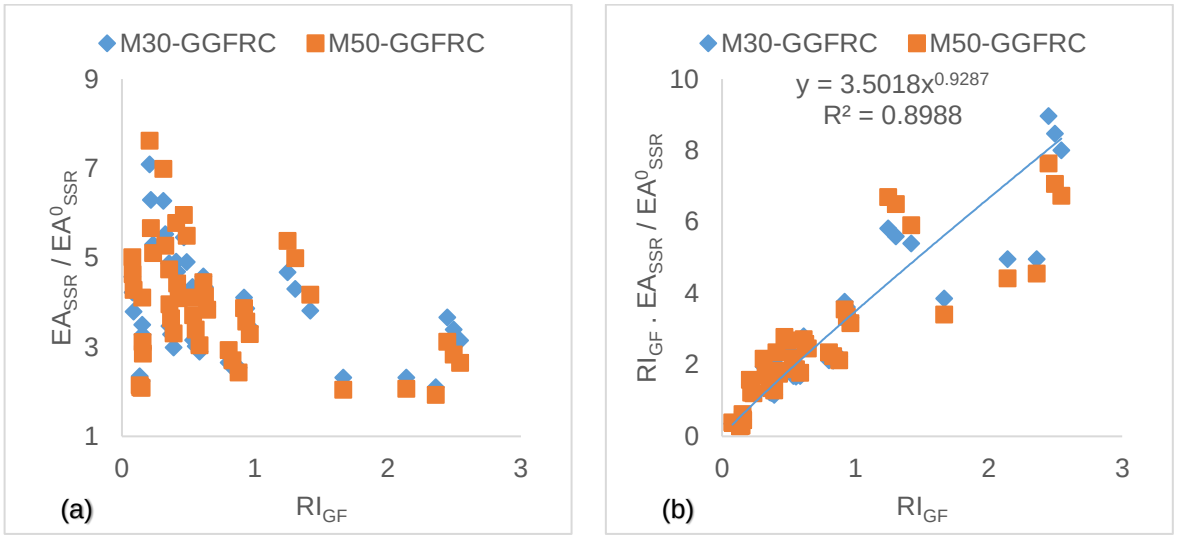

Fig.6.91 Energy absorption as a function of RI_{GF} for GGFRC in Compression

6.16. Comparison of compressive stress strain models for GGFRC

The experimental stress–strain curves of six composite mixes, namely, M30-SGF-II#c, M30-LGF-II#c, M30-CGF-II#c, M50-SGF-II#e, M50-LGF-II#e and M50-CGF-II#e are plotted in Fig.6.92 (a) to (f) along with the curves predicted using the adopted model (equation (13)) and equation (19) given in Chapter-5. The shape of the strain softening branch of the curve, which is steep in plain concrete becomes flatter with the addition of fibres. The prediction of stress–strain curves for GGFRC using the proposed model is closer to the experimental curves is shown in Fig.6.92 (a) to (f). Analytical model Proposed by the equation has shown close correlation with experimental results of both M30 and M50 grade of concrete.

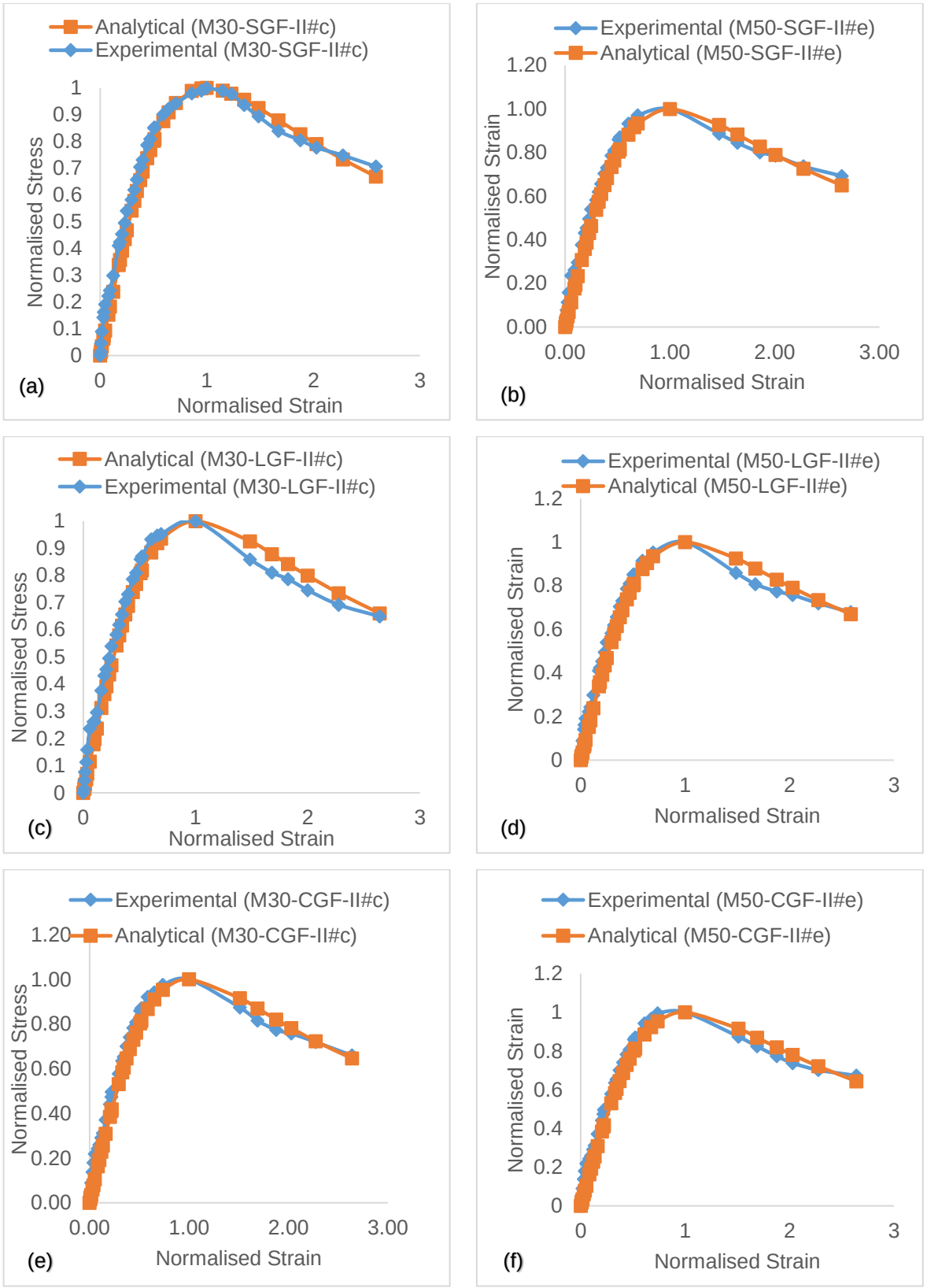

Fig.6.92 Analytical and experimental normalised stress–strain relationship for (a) M30-SGF-II#c (RI_{GF} =0.39, β = 2.013), (b) M50-SGF-II#e (RI_{GF} =0.24, β = 2.063), (c) M30-LGF-II#c (RI_{GF} =0.43, β = 2.006), (d) M50-LGF-II#e (RI_{GF} =0.41, β = 2.010), (e) M30-CGF-II#c (RI_{GF} =0.24, β = 2.053) and (f) for M50-CGF-II#e (RI_{GF} =0.24, β = 2.063).

6.17. Strain Hardening in Tension and Strain Softening in Compression of GGFRC

The phenomena of strain hardening in tension and strain softening in compression for GFRC is explained in article 5.14 of chapter-5. The strain hardening in tension and strain softening in compression phenomena is noticed in the stress strain behaviour of GGFRC similar to the MGFRC. Degree of resistance offered to lateral deformation is proportional to grading of fibers (SGF, LGF and CGF) and volume of fibers (0.3%, 0.4% and 0.5%). The fibers come into action after cracking in concrete in compression which is similar to the action of fibers in concrete after the onset of cracking in tension. With the grading of fibers, the strain hardening in tension increased and thereby there is increase of strain softening in compression for the same volume fraction.

In the present investigation the parameters such as grade of concrete and grading of fibers (SGF, LGF and CGF) with volume of fibers (0.3%, 0.4% and 0.5%) are same for the specimens in tension and compression. Values of stress and strain corresponding to strain hardening region and strain softening region of each specimen are given in column 2,3,4,5 and 6 of Tables 6.1 to 6.6 and 6.27 to 6.32 respectively. Strain hardening behaviour in tension and strain softening behaviour in compression for GGFRC specimens is normalised with corresponding peak stress and peak strain are reported in Table 6.39 to 6.41.

In order to understand the complementry behaviour of strain hardening in tension and strain softening in compression, the normalised stress and normalised strain at the onset of strain hardening and at the inflection point of strain softening for M30-GGFRC and M50-GGFRC for 0.3% volume fraction with RI_{GF} of 0.39, 0.43 and 0.24 are shown in Fig.6.93 and 6.94. Similar plot can be drawn for all values of $RI_{GF.}$ The gradient of increase of strain hardening in tension is similar to the gradient of strain softening in compression for the specimen with the same and it is influenced by RI_{GF}. The gradient of strain hardening in tension is similar to the gradient of strain softening in compression. Specimen with Short graded fibers i.e. RI_{GF} = 0.39 producing low strain hardening in tension as similar low strain softening behaviour in compression, where as in specimen with long graded fibers i.e., RI_{GF} = 0.43 exhibited significant strain hardening in tension as similar significant strain softening behaviour in compression respectively. Specimens with combined graded fibers i.e., RI_{GF} = 0.24 exhibited both significant strain hardening in tension and corresponding strain softening in

compression. It can be concluded, for any given reinforcing index as the strain hardening in tension increased the corresponding strain softening increased.

Table.6.39 Stress and Strain Ratio of SHR and SSR-GGFRC-0.3%

Specimen Designation (1)	RI_{GF} (2)	M30-GGFRC				M50-GGFRC			
		Strain Hardening Region		Strain softening Region		Strain Hardening Region		Strain softening Region	
		$\sigma^{P}{}_{t} / \sigma^{Q}{}_{t}$ (3)	$\varepsilon^{P}{}_{t} / \varepsilon^{Q}{}_{t}$ (4)	$f^{C}{}_{IP} / f^{B}{}_{u}$ (5)	$\varepsilon^{C}{}_{IP} / \varepsilon^{B}{}_{u}$ (6)	$\sigma^{P}{}_{t} / \sigma^{Q}{}_{t}$ (7)	$\varepsilon^{P}{}_{t} / \varepsilon^{Q}{}_{t}$ (8)	$f^{C}{}_{IP} / f^{B}{}_{u}$ (9)	$\varepsilon^{C}{}_{IP} / \varepsilon^{B}{}_{u}$ (10)
Short Graded Fibers (SGF), V_f = 0.3%									
SGF-I#c	0.15	0.65	0.23	0.85	2.69	0.69	0.21	0.84	2.38
SGF-II#c	0.39	0.65	0.19	0.86	4.50	0.65	0.19	0.83	3.76
SGF-III#c	0.59	0.73	0.21	0.86	4.41	0.65	0.20	0.83	3.21
SGF-IV#c	0.88	0.73	0.24	0.85	3.57	0.65	0.21	0.82	2.66
SGF-V#c	2.36	0.77	0.26	0.87	2.47	0.69	0.22	0.84	1.86
Long Graded Fibers (LGF), V_f = 0.3%									
LGF-I#c	0.16	0.65	0.19	0.85	3.01	0.65	0.19	0.83	3.10
LGF-II#c	0.43	0.58	0.16	0.86	4.77	0.58	0.16	0.83	5.09
LGF-III#c	0.64	0.58	0.17	0.86	4.48	0.58	0.17	0.83	4.49
LGF-IV#c	0.96	0.65	0.19	0.85	3.77	0.59	0.18	0.82	3.93
LGF-V#c	2.54	0.65	0.20	0.84	3.51	0.61	0.19	0.84	2.86
Combined Graded Fibers (SGF), V_f = 0.3%									
CGF-I#c	0.09	0.77	0.17	0.86	4.50	0.77	0.16	0.85	4.09
CGF-II#c	0.24	0.77	0.14	0.87	8.52	0.73	0.14	0.84	7.52
CGF-III#c	0.35	0.77	0.15	0.87	6.49	0.73	0.14	0.83	7.21
CGF-IV#c	0.53	0.77	0.16	0.86	5.95	0.77	0.15	0.83	5.30
CGF-V#c	1.42	0.77	0.16	0.88	4.41	0.77	0.16	0.84	3.96

Table.6.40 Stress and Strain Ratio of SHR and SSR-GGFRC-0.4%

Specimen Designation (1)	RI_{GF} (2)	M30-GGFRC				M50-GGFRC			
		Strain Hardening Region		Strain softening Region		Strain Hardening Region		Strain softening Region	
		$\sigma^{P}{}_{t} / \sigma^{Q}{}_{t}$ (3)	$\varepsilon^{P}{}_{t} / \varepsilon^{Q}{}_{t}$ (4)	$f^{C}{}_{IP} / f^{B}{}_{u}$ (5)	$\varepsilon^{C}{}_{IP} / \varepsilon^{B}{}_{u}$ (6)	$\sigma^{P}{}_{t} / \sigma^{Q}{}_{t}$ (7)	$\varepsilon^{P}{}_{t} / \varepsilon^{Q}{}_{t}$ (8)	$f^{C}{}_{IP} / f^{B}{}_{u}$ (9)	$\varepsilon^{C}{}_{IP} / \varepsilon^{B}{}_{u}$ (10)
Short Graded Fibers (SGF), V_f = 0.4%									
SGF-I#d	0.14	0.65	0.21	0.85	2.78	0.69	0.21	0.84	2.69
SGF-II#d	0.37	0.65	0.19	0.87	4.83	0.65	0.19	0.83	4.40
SGF-III#d	0.56	0.73	0.20	0.86	4.49	0.65	0.20	0.83	4.26
SGF-IV#d	0.83	0.73	0.23	0.85	3.52	0.65	0.21	0.82	2.87
SGF-V#d	1.67	0.77	0.26	0.85	3.22	0.67	0.22	0.84	2.10

Long Graded Fibers (LGF), V_f = 0.4%									
LGF-I#d	0.16	0.65	0.19	0.86	3.46	0.63	0.19	0.84	3.28
LGF-II#d	0.42	0.58	0.16	0.86	6.09	0.57	0.15	0.82	5.80
LGF-III#d	0.62	0.58	0.16	0.86	5.18	0.58	0.16	0.83	5.16
LGF-IV#d	0.94	0.65	0.18	0.85	4.72	0.58	0.17	0.82	4.25
LGF-V#d	2.50	0.65	0.20	0.86	4.22	0.60	0.19	0.84	3.05
Combined Graded Fibers (SGF), V_f = 0.4%									
CGF-I#d	0.08	0.77	0.16	0.88	4.91	0.77	0.15	0.84	4.15
CGF-II#d	0.22	0.77	0.14	0.87	8.93	0.73	0.14	0.84	8.88
CGF-III#d	0.33	0.77	0.14	0.87	8.85	0.73	0.14	0.84	8.54
CGF-IV#d	0.49	0.77	0.15	0.86	7.41	0.75	0.15	0.83	6.31
CGF-V#d	1.30	0.77	0.16	0.86	5.95	0.75	0.16	0.84	5.00

Table.6.41 Stress and Strain Ratio of SHR and SSR-GGFRC-0.5%

Specimen Designation (1)	RI_{GF} (2)	M30-GGFRC				M50-GGFRC			
		Strain Hardening Region		Strain softening Region		Strain Hardening Region		Strain softening Region	
		$\sigma^{P}_{t} / \sigma^{Q}_{t}$ (3)	$\varepsilon^{P}_{t} / \varepsilon^{Q}_{t}$ (4)	f^{C}_{IP} / f^{B}_{u} (5)	$\varepsilon^{C}_{IP} / \varepsilon^{B}_{u}$ (6)	$\sigma^{P}_{t} / \sigma^{Q}_{t}$ (7)	$\varepsilon^{P}_{t} / \varepsilon^{Q}_{t}$ (8)	f^{C}_{IP} / f^{B}_{u} (9)	$\varepsilon^{C}_{IP} / \varepsilon^{B}_{u}$ (10)
Short Graded Fibers (SGF), V_f = 0.5%									
SGF-I#e	0.13	0.82	0.21	0.85	3.04	0.69	0.21	0.84	2.79
SGF-II#e	0.36	0.65	0.18	0.87	5.48	0.65	0.18	0.83	5.74
SGF-III#e	0.54	0.73	0.19	0.86	5.34	0.65	0.19	0.83	4.11
SGF-IV#e	0.80	0.73	0.22	0.85	4.00	0.65	0.20	0.82	3.08
SGF-V#e	2.14	0.77	0.23	0.85	3.42	0.66	0.22	0.83	2.12
Long Graded Fibers (LGF), V_f = 0.5%									
LGF-I#e	0.15	0.65	0.18	0.85	3.83	0.62	0.18	0.83	3.66
LGF-II#e	0.41	0.58	0.15	0.86	5.99	0.57	0.15	0.83	6.17
LGF-III#e	0.61	0.57	0.16	0.86	5.70	0.58	0.16	0.83	5.88
LGF-IV#e	0.92	0.65	0.18	0.85	5.23	0.58	0.17	0.82	4.90
LGF-V#e	2.45	0.65	0.19	0.85	4.15	0.58	0.18	0.83	3.55
Combined Graded Fibers (SGF), V_f = 0.5%									
CGF-I#e	0.08	0.77	0.15	0.85	6.39	0.77	0.15	0.84	5.06
CGF-II#e	0.21	0.77	0.13	0.87	10.52	0.73	0.13	0.84	11.14
CGF-III#e	0.31	0.77	0.13	0.87	9.72	0.73	0.13	0.84	9.96
CGF-IV#e	0.47	0.77	0.14	0.86	8.85	0.73	0.14	0.83	5.25
CGF-V#e	1.25	0.77	0.15	0.87	6.41	0.77	0.15	0.84	6.71

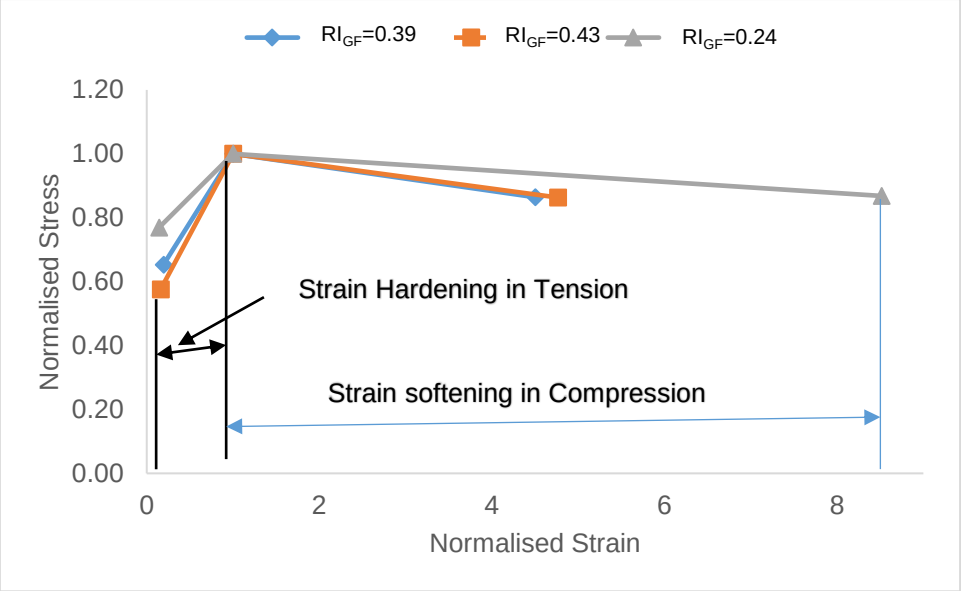

Fig.6.93 Strain hardening vs strain softening (M30-GGFRC)

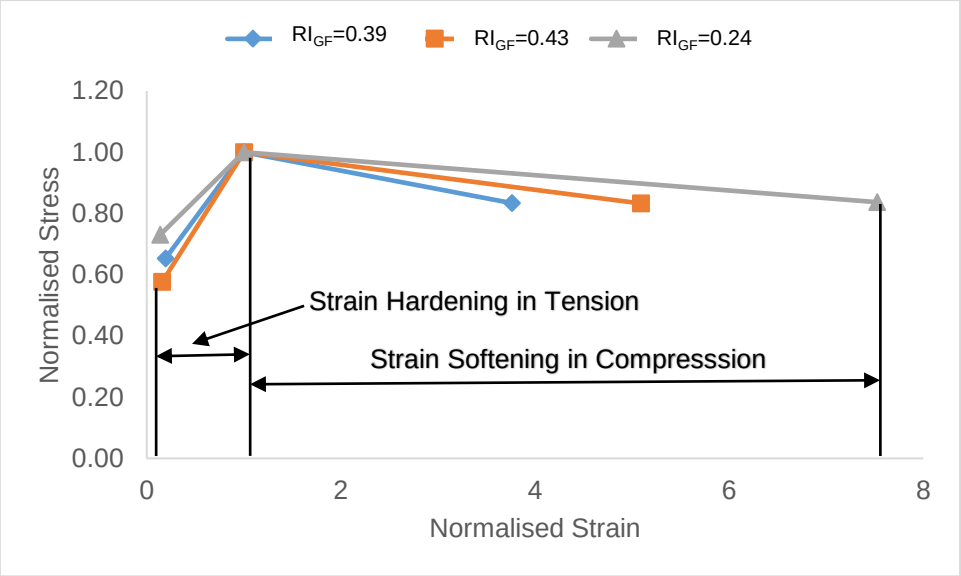

Fig.6.94 Strain hardening vs strain softening (M50-GGFRC)

6.16.1. Relationship between Stress and strain of SSR in compression and SHR in tension for GGFRC:

In order to correlate tensile and compression data, relationship between Reinforcing Index (RI_{GF}) and (σ^{P}_{t} / σ^{Q}_{t}) / (f^{C}_{IP} / f^{B}_{u}), (ε^{P}_{t} /ε^{Q}_{t}) / (ε^{C}_{IP} / ε^{B}_{u}) is shown in Fig.6.95. Equations (33) and (34) are obtained using the regression analysis performed using all data points of M30-GGFRC and M50-GGFRC.

The reinforcing index of each mix was calculated and is given in column 2 of Table 6.39 to 6.41. The ratios between stress and strains in strain hardening region and strain softening region is considered for GGFRC (M30 and M50 grade) and given in Table 6.39 to 6.41. In order to understand the variation of these ratios with RI_M, points are plotted as shown in Fig.6.95 (a). An examination of the plot and various trails to aims at the best fit, led to understand that stress and strain ratios varies as power function of RI_{GF} in the form of stress ratio or strain ratio = $k / (RI_{GF})^n$. The power function is modified by multiplying both sides by RI_{GF}. The modified relation is (RI_{GF}) stress ratio or strain ratio = $k (RI_{GF})^{(1-n)}$. Now points are plotted with RI_{GF} as abscissa and RI_{GF}. Stress ratio or strain ratio as ordinate is shown in Fig.6.95 (b). The regression expression obtained is $(RI_{GF})\ \sigma^{P}_{t} / \sigma^{Q}_{t} = (f^{C}_{IP} / f^{B}_{u})\ 1.162\ (RI_{GF})^{1.0062}$ with regression coefficient $R^2 = 0.9985$ and $(RI_{GF})\ \varepsilon^{P}_{t} / \varepsilon^{Q}_{t} = (\varepsilon^{C}_{IP} / \varepsilon^{B}_{u})\ 0.8098\ (RI_{GF})^{0.9932}$ with regression coefficient $R^2 = 0.9143$. Then the relation between RI_{GF} and stress and strains can be expressed as.

$$\sigma^{P}_{t} / \sigma^{Q}_{t} = (f^{C}_{IP} / f^{B}_{u})\ (1.162\ RI_{GF}^{0.0062}) \quad \text{----------(33)}$$

$$\varepsilon^{P}_{t} / \varepsilon^{Q}_{t} = (\varepsilon^{C}_{IP} / \varepsilon^{B}_{u})\ (0.8098\ RI_{GF}^{-0.007}) \quad \text{---------- (34)}$$

Where, f^{B}_{u}, f^{C}_{IP} in compression is used to calculate from equation (28) and (30). ε^{B}_{u} ε^{C}_{IP} in tension is used to calculate from equation (29) and (31).

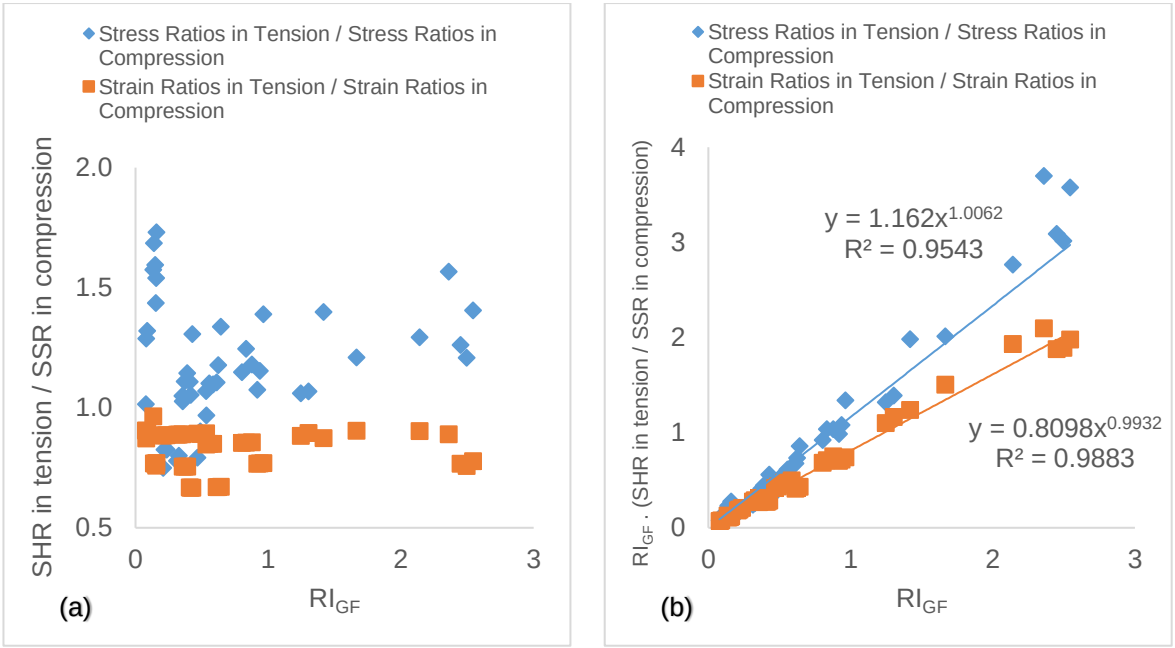

Fig.6.95 SHR in tension / SSR in compression vs RI_{GF}

6.16.2. Relationship between Energy absorption capacity in tension and compression for GGFRC:

Relationship between energy absorption in strain hardening region and energy absorption in strain softening region is also developed and shown in Fig.6.96. The equation (35) is obtained using the regression analysis performed using all data points of M30-GGFRC and M50-GGFRC. The advantage of the equation (35) is that it can be used to calculate the either energy absorption in strain hardening region in tension or energy absorption in strain softening region, if one of them is known.

Energy absorption in strain hardening region (EA_{SHR}) is already given in column 11 of Table 6.1 to 6.6, and energy absorption capacity in strain softening region (EA_{SSR}) is already given column 11 of Table 6.27 to 6.33. The reinforcing index of each mix was calculated and is given in column 2 of Table 6.39 to 6.41. In order to understand the variation of EA_{SHR} / EA_{SSR} with RI_{GF}, points are plotted as shown in Fig.6.96. An examination of the plot and various trails to arrive at the best fit, led to understand that EA_{SHR} / EA_{SSR} varies as power function of RI_{GF} in the form of $EA_{SHR} / EA_{SSR} = k (RI_{GF})^n$. The regression expression obtained is $EA_{SHR} / EA_{SSR} = 70.071 (RI_{GF})^{0.3038}$ with regression coefficient $R^2 = 0.8197$. Then the relation between RI_{GF} and EA_{SHR} / EA_{SSR} can be expressed as.

$$EA_{SHR} = EA_{SSR} (70.071\ RI_{GF}^{0.3036}) \text{ ---------- (35)}$$

Where EA_{SHR} is the energy absorption capacity in tension and EA_{SSR} is the energy absorption capacity in compression

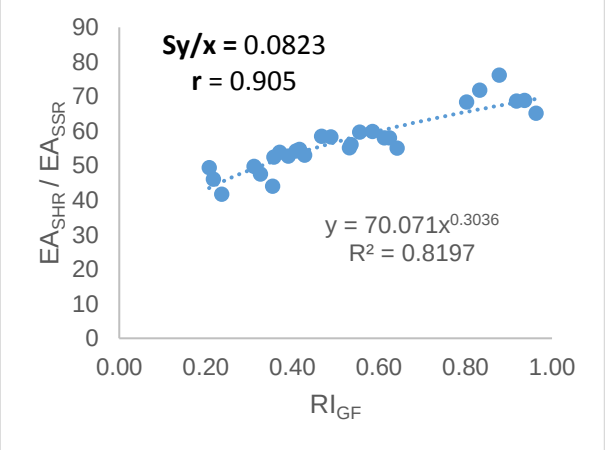

Fig.6.96 Ratio of Energy absorption in Tension / Energy absorption in Compression is a function of RI_{GF}.

This page is intentionally left blank

Chapter-7
Conclusions

7.1 Conclusions

A detailed study consisting of different lengths of glass fiber (3mm, 6mm, 12mm and 20mm) named as Mono Glass Fibers, and combination of different lengths of mono fibers named as Graded Glass Fiber. Five different volume fractions 0.1%, 0.2%, 0.3%, 0.4% and 0.5% and two normal strength concrete mix M30, M50 and the parameters were presented in the earlier chapters. Stress strain behaviour in tension and compression of 1188 specimens each was reported and discussed. Image analysis technique was used to quantitatively evaluate the fiber efficiency characteristics i.e., fiber dispersion coefficient, fiber orientation coefficient and fiber length coefficient with respect to loading direction.

Broad outcome of the research area is divided into two phases namely, Phase-I is Study on Mono Glass Fiber Reinforced Concrete and Phase-II is Study on Graed Glass Fiber Reinforced Concrete is presented below.

Phase-I: Study on Mono Glass Fiber Reinforced Concrete (MGFRC)

Influence of the Mono Glass Fibers (3mm, 6mm, 12mm and 20mm) on the compressive and tensile stress-strain behaviour for normal grade concrete (M30 and M50) was studied with 0.1%, 0.2%, 0.3%, 0.4%, and 0.5% fiber volume fractions. In order to understand the behaviour of Mono Glass Fiber Reinforced Concrete (MGFRC) at fresh and hardened state, slump test, uniaxial compression and uniaxial tension test was conducted and the following conclusions are drawn.

1. Workability decreased with increase in fiber content and fiber length. MGFRC with 0.3% volume fraction shown maximum improvement in compressive strength.
2. Specimens with Short length fibers (3mm and 6mm) have given higher tensile strength than the specimens with Long length fibers (12mm and 20mm). Specimens with long length fibers (12mm and 20mm) have contributed more post crack deformation capacity than the specimens with short length fibers (3mm and 6 mm) in tension.

3. Specimens with Short length fibers (3mm and 6mm) have given higher peak strength than the specimens with Long length fibers (12mm and 20mm). Specimens with long length fibers (12mm and 20mm) have contributed more post peak deformation capacity than the specimens with short length fibers (3mm and 6 mm) in compression.

4. Irrespective of volume of the fiber (0.3% to 0.5%) and grade of concrete (M30 and M50), long length fibers (12mm and 20mm) exhibited higher ductility factor, energy absorption capacity than that of short length fibers (3mm and 6mm). Short length fibers showed higher strengthening and initial slope compared to the long length fibers. Hence, the short length fibers contributed to improve the strength of the composite where as long length fibers contributed to improve the deformations of the composite in both tension and compression.

5. Optical Microscope study and Image analysis was used to examine fiber dispersion and fiber orientation on a fracture plain. Fiber dispersion, fiber orientation and fiber embedded length influences strength and deformation of GFRC specimens.

6. An equation with fiber dispersion coefficient (η_d), along with fiber orientation coefficient (η_θ) and fiber length coefficient (η_l) estimates composite tensile strength almost equal to experimental strength.

7. A relation is obtained between strain at ultimate strength of composite in tension and RI_{MF}. Predicted results are good correlation with the experimental results.

8. Fibers are not distributed uniformly across the section. In case of Short fibers, less fibers are present at the corners and edges compared to the centre of cross-section when compared to the long length fibers. Fiber density at fracture plane decreased with the increase in volume of fiber.

9. Short fibers dispersed and oriented effectively in the composite better than the longer fibers

10. Higher the fiber dispersion coefficient (η_d) and fiber orientation coefficient (η_θ) higher the strength of composite and these parameters are estimated using the reinforcing index (RI_M).

11. A model is developed for predicting stress–strain curves of MFRC in tension and compression. All properties required for the generation of compressive stress strain curves are estimated using the reinforcing index (RI_M). A material parameter β is developed for predicting stress–strain curves of MGFRC. The analytical curves show good correlation with experimental test results of MGFRC.

12. Increase in fiber content and fiber length improved post peak behaviour in compression which is strain softening and pre peak behaviour in tension which is strain hardening. It is noticed that strain softening behaviour in compression is influenced by strain hardening behaviour in tension of MGFRC.

Phase-II: Study on Graded Glass Fiber Reinforced Concrete (GGFRC)

Effect of Graded Glass Fibers (SGF, LGF and CGF) on the compressive and tensile stress-strain behaviour for normal grade concrete (M30 and M50) was studied with 0.3%, 0.4%, and 0.5% fiber volume fractions. In order to understand the behaviour of Graded Glass Fiber Reinforced Concrete (GGFRC) at fresh and hardened state, slump test, uniaxial compression and uniaxial tension test was conducted and the following conclusions are drawn.

1. Graded fibers improved workability of GFRC
2. Specimens containing the 40% of 3mm + 60% 6mm (SGF-II) has given the best benefit of improvement in both strength and deformation compared to all other short graded fibers whereas specimens containing the 40% 12mm + 60% 20mm (LGF-II) has given the best benefit of improvement in both strength and deformation compared to all other long graded fibers. Specimens containing the 40% SGF + 60% LGF (CGF-II) has given the best benefit of improvement in both strength and deformation compared to all other combined graded fibers
3. Short length fibers (3mm+6mm) can be mixed in a proportion (namely Short Graded Fibers) to improve strength, similarly Long length fibers (12mm+20mm) can be mixed in a proportion (namely Long Graded Fibers) to improve deformation. Both strength and deformation can be improved by properly proportionating short and long length fibers in a given volume fraction.

4. Irrespective of volume of the fiber (0.3%, 0.4% and 0.5%) and grade of concrete (M30 and M50), long graded fibers (LGF) exhibited higher ductility factor, energy absorption capacity than that of short graded fibers (SGF). Short graded fibers showed higher strengthening and initial slope compared to the long length fibers. Hence, the combination of SGF and LGF i.e., CGF have exhibited the higher strengthening factor, ductility factor and energy absorption capacity than that of SGF, LGF and MGF in both tension and compression.
5. Optical Microscope study and Image analysis was used to examine fiber dispersion and fiber orientation on a fracture plain. Fiber dispersion, fiber orientation and fiber embedded length influences strength and deformation of GGFRC specimens. Proposed method incorporates fiber dispersion coefficient (η_d), fiber orientation coefficient (η_θ) and fiber length coefficient (η_l) estimates composite strength almost equal to experimental strength.
6. The composite with SGF, the fiber density is more at the center and less at the edges and corners. Where as in long graded fibers, the fiber density is more at the edges and corners and less at the center. Composite with CGF (containing SGF + LGF) showed the almost uniform distribution. The results of image analyses shows that graded fibers with different fibre volume combinations disperse homogeneously avoiding clumping or balling. Graded fibers showed the higher fiber dispersion coefficient and higher fiber orientation coefficient when compared to the mono fibers.
7. Fiber dispersion coefficient (η_d) and fiber orientation coefficient (η_θ) is higher for the Graded fibers than Mono fibers for the same volume fraction.
8. The strength, deformation capacity and energy absorption capacity is higher for Graded Glass Fiber Reinforced concrete than Mono Glass Fiber Reinforced Concrete.
9. An expression is proposed to account for synergy of graded fibers to calculate RI_{GF}.
10. Models are developed as a function of a more comprehensive reinforcing index (RI_{GF}) for the prediction of the mechanical properties of GGFRC, such as peak stress, strain at peak stress, tensile strength, strain at tensile strength and energy absorption index. All these properties increase with decreased reinforcing index (RI_{GF}).

11. A model is developed for predicting stress–strain curves of GGFRC in tension and compression. All parameters required for the generation of stress strain curves are estimated using the proposed reinforcing index (RI_{GF}). The analytical curves show good correlation with experimental test results of GGRC.
12. Increase in grading of fibers and fiber content improved post peak behaviour in compression which is strain softening and pre crack behaviour in tension which is strain hardening. It is noticed that strain softening behaviour in compression is influenced by strain hardening behaviour in tension of GGFRC.

Final Conclusions

1. Graded fibers improved workability and compressive strength compared to Mono fibers
2. Short length fibers (3mm and 6mm) have given higher ultimate strength than the long length fibers (12mm and 20 mm) whereas long length fibers have contributed more improvement in deformations than the short length fibers in both tension and compression.
3. Short Graded Glass Fibers shown the better peak strength and the Long Graded fibers have shown more post peak deformation capacity. Combined Graded fibers (SGF +LGF) have shown overall better performance among all other combinations and it improved the strength and deformation of the composite both in compression and tension.
4. The strength, deformation and energy absorption capacity is higher for GGFRC than MGFRC in both tension and compression.
5. The results of image analyses shown the combined graded fibers (Short length fibers + long length fibers) dispersed homogeneously without clumping and orientated effectively across the failure cross section compared to short graded fibers , long graded fibers and mono fibers.
6. Higher the fiber dispersion coefficient (η_d) and fiber orientation coefficient (η_θ) higher the strength of composite. Fiber dispersion coefficient (η_d) and fiber orientation coefficient (η_θ) is higher for the Graded fibers than Mono fibers.
7. Graded fiber resulted an effective mixing comparing to the mono fiber mixing in concrete. Fiber efficiency is higher for Graded Fibers than that of Mono Fibers.

8. Tensile strength and corresponding tensile strain of MGFRC and GGFRC are predicted using the reinforcing index and it showed good correlation with experimental test results.
9. All properties required for the generation of stress–strain curves are estimated using the reinforcing index (RI_{GF}). A model is developed for predicting compressive stress–strain curves of MGFRC and GGFRC. The analytical curves showed good correlation with experimental test results**.**

7.2 Specific contribution from this work

1. Studied the influence of grading of glass fibers of different lengths for various fiber volume combinations at length.
2. Development of reinforcing index for graded fibers (RI_{GF}).
3. Relationship between strain hardening in tension and strain softening in compression is quantified.

7.3 Scope for further study

1. The method of grading can be applied to concrete reinforced with different types of fibers (steel, polypropylene, PVA etc.)
2. There is need to study the effect of graded fibers on behaviour of special concretes (high strength concrete, high performance concrete and self compacting concrete).
3. To study the structural behaviour of Graded Hybrid Fiber Reinforced Concrete.

References

A.E. Naaman., Namur, G.G., Alwan, J.M. and Najm, H.S., 1991. Fiber pullout and bond slip. I: Analytical study. Journal of Structural Engineering, 117(9), pp.2769-2790.

A.Sivakumar and Santhanam, M., 2007. Mechanical properties of high strength concrete reinforced with metallic and non-metallic fibres. *Cement and Concrete Composites*, *29*(8), pp.603-608.

ACI Committee 544, "Report on Fiber Reinforced Concrete (ACI 544.1R-96)", American Concrete Institute, Farmington Hills, MI, USA, 2009

ACI Committee 549, "Report on Glass Fiber Reinforced Concrete Premix (ACI 549.3R-09)", American Concrete Institute, Farmington Hills, MI, USA 2009.

Amin Noushini, Vessalas, K. and Samali, B., 2014. Static mechanical properties of polyvinyl alcohol fibre reinforced concrete (PVA-FRC). *Magazine of Concrete Research*, *66*(9), pp.465-483.

Amon Bentur, and Mindess, S., 2014. *Fibre reinforced cementitious composites*. CRC Press.

Antroula V G. and Pantazopoulou, S.J., 2017. Experimental investigation on the confining effect of fibers in SHFRCC. Composite Structures.

Aref Abadel, Abbas, H., Almusallam, T., Al-Salloum, Y. and Siddiqui, N., 2015. Mechanical properties of hybrid fibre-reinforced concrete–analytical modelling and experimental behaviour. Magazine of Concrete Research, 68(16), pp.823-843.

B. P. Hughes and Fattuhi, N.I., 1976. The workability of steel-fibre-reinforced concrete. *Magazine of concrete research*, *28*(96), pp.157-161.

Bang Yeon Lee, Kim, J.K., Kim, J.S. and Kim, Y.Y., 2009. Quantitative evaluation technique of Polyvinyl Alcohol (PVA) fiber dispersion in engineered cementitious composites. *Cement and Concrete Composites*, *31*(6), pp.408-417.

Banthia, N., 1990. A study of some factors affecting the fiber–matrix bond in steel fiber reinforced concrete. *Canadian Journal of Civil Engineering*, *17*(4), pp.610-620.

Barros J.A. and Figueiras J.A., 1999. Flexural behavior of SFRC: testing and modeling. Journal of materials in civil engineering, 11(4), pp.331-339.

Benjamin A. Graybeal, 2007. Compressive behavior of ultra-high-performance fiber-reinforced concrete. *ACI materials journal*, *104*(2), p.146.

Bing Chen and Liu, J., 2005. Contribution of hybrid fibers on the properties of the high-strength lightweight concrete having good workability. *Cement and Concrete Research*, *35*(5), pp.913-917.

Burcu Akcay and Tasdemir, M.A., 2012. Mechanical behaviour and fibre dispersion of hybrid steel fibre reinforced self-compacting concrete. *Construction and Building Materials*, *28*(1), pp.287-293.

C.R Chiang, 1994. A statistical theory of the tensile strength of short-fiber-reinforced composites. Composites science and technology, 50(4), pp.479-482.

Carreira D.J. and Chu, K.H., 1985, November. Stress-strain relationship for plain concrete in compression. In Journal Proceedings, 82(6), pp. 797-804.

Chaohua Jiang, Fan, K., Wu, F. and Chen, D., 2014. Experimental study on the mechanical properties and microstructure of chopped basalt fibre reinforced concrete. *Materials & Design*, *58*, pp.187-193.

CK. YI and Ostertag, C.P., 2001. Strengthening and toughening mechanisms in microfiber reinforced cementitious composites. *Journal of materials science*, *36*(6), pp.1513-1522.

Doo-Yeol Yoo, Park, J.J. and Kim, S.W., 2017. Fiber pullout behavior of HPFRCC: Effects of matrix strength and fiber type. Composite Structures, 174, pp.263-276.

Ezeldin A.S. and Balaguru P.N., 1992. Normal-and high-strength fiber-reinforced concrete under compression. Journal of materials in civil engineering, 4(4), pp.415-429.

Fanella D.A. and Naaman A.E., 1985. Stress-strain properties of fiber reinforced mortar in compression, Journal of the American Concrete Institute, 82(4).pp. 475-483.

Fantilli A.P, Mihashi, H. and Vallini, P., 2009. Multiple cracking and strain hardening in fiber-reinforced concrete under uniaxial tension. Cement and Concrete Research, 39(12), pp.1217-1229.

G B Kim, Pilakoutas, K. and Waldron, P., 2010. Development of GFRP-reinforced GFRC for thin permanent formwork applications. *Magazine of Concrete Research*, *62*(4), pp.283-290.

G. Barluenga and Hernández-Olivares, F., 2007. Cracking control of concretes modified with short AR-glass fibers at early age. Experimental results on standard concrete and SCC. *Cement and Concrete Research*, *37*(12), pp.1624-1638.

Gopalaratnam, V.S. and Cheng J, 1988. On the modelling of inelastic interfaces in fibrous composites. Cement based composites: Bonding in cementitious composites. In Symposia Proceedings, 114, pp. 225-231.

Guild F.J. and Summerscales, J., 1993. Microstructural image analysis applied to fibre composite materials: a review. Composites, 24(5), pp.383-393.

Irem S¸ anal, Özyurt, N. and Hosseini, A., 2016. Characterization of hardened state behaviour of self-compacting fiber-reinforced cementitious composites (SC-FRCC's) with different beam sizes and fiber types. *Composites Part B: Engineering*, *105*, pp.30-45.

Irem Sanal and Zihnioğlu, N.Ö., 2013. To what extent does the fiber orientation affect Mechanical performance? Construction and Building Materials, 44, pp.671-681.

IS 10262: 2009. “Concrete mix proportioning – guidelines”, Bureau of Indian Standards, New Delhi 2009.

IS: 12269 - 2013, “Indian Standard Ordinary Portland Cement, 53 Grade – Specification”, Bureau of Indian Standards”, New Delhi 2013

IS: 383 – 1970 (Reaffirmed 2016), “Indian Standard Specification for Coarse and Fine Aggregates from Natural Sources for Concrete”, Bureau of Indian Standards, New Delhi 2016.

IS: 516–1959, Methods of Tests for Strength of Concrete, Bureau of Indian Standards, New Delhi 1959.

IS: 7320–1974 (Reaffirmed 2008), Specification for concrete slump test apparatus, Bureau of Indian Standards, New Delhi 1959.

IS-456. 2000. “Plain and Reinforced Concrete-Code of Practice”, Bureau of Indian Standards, New Delhi, Manak Bhawan, 2000, 9.

Ivan Markovic, 2006. High-performance hybrid-fibre concrete: development and utilisation. IOS Press.

John E Morgan and Rewland G Morgan, 1998, The Armature that made History: The boats of Joseph Loui‟s Lambot, Proc sixth International Symposium on Ferrocement, 11-33.

Kamile Tosun-Felekoglu, Felekoğlu, B., Ranade, R., Lee, B.Y. and Li, V.C., 2014. The role of flaw size and fiber distribution on tensile ductility of PVA-ECC. *Composites Part B: Engineering*, *56*, pp.536-545.

L.R Betterman, Ouyang, C. and Shah, S.P., 1995. Fiber-matrix interaction in microfiber-reinforced mortar. *Advanced Cement Based Materials*, *2*(2), pp.53-61.

L.Vandewalle, 2007, June. Postcracking behaviour of hybrid steel fiber reinforced concrete. In *Fracture Mechanics of Concrete and Concrete Structures–FraMCoS, in: Proceedings of the 6th International Conference, Catania, Italy* (pp. 17-22).

M. Jamal Shannag, Brincker, R. and Hansen, W., 1997. Pullout behavior of steel fibers from cement-based composites. Cement and Concrete Research, 27(6), pp.925-936.

M.A Rasheed and Prakash, S.S., 2018. Behaviour of hybrid-synthetic fiber reinforced cellular lightweight concrete under uniaxial tension–Experimental and analytical studies. Construction and Building Materials, 162, pp.857-870.

M.C. Nataraja, Dhang N. and Gupta A.P, 1999. Stress–strain curves for steel-fiber reinforced concrete under compression. Cement and concrete composites, 21(5-6), pp.383-390.

Machine Hsie, Tu, C. and Song, P.S., 2008. Mechanical properties of polypropylene hybrid fiber-reinforced concrete. *Materials Science and Engineering: A*, *494*(1-2), pp.153-157.

Marsh H.N. and Clarke, L.L., 1985. Glass fiber reinforced cement base materials. Special Publication, Detroit, MI: American Concrete Institute 44, pp.247-264.

Mustafa Sahmaran., Yurtseven, A. and Yaman, I.O., 2005. Workability of hybrid fiber reinforced self-compacting concrete. *Building and Environment*, *40*(12), pp.1672-1677.

N. Banthia and Bindiganavile, V., 2013. Performance synergy in hybrid fiber reinforced concrete under impact. *J. of Frontiers in Construction Engineering*, *2*(4), pp.75-82.

N. Banthia and Nandakumar, N., 2003. Crack growth resistance of hybrid fiber reinforced cement composites. *Cement and Concrete Composites*, *25*(1), pp.3-9.

N. Banthia and R. Gupta, 2004. Hybrid fiber reinforced concrete (HyFRC): fiber synergy in high strength matrices. *Materials and Structures*, *37*(10), pp.707-716.

N. Banthia and Sappakittipakorn, M., 2007. Toughness enhancement in steel fiber reinforced concrete through fiber hybridization. *Cement and Concrete Research, 37(9), pp.1366-1372.*

N. Banthia, N.B.A.U.O.B.C., Moncef, A.B.A.U.L., Chokri, K.B.A.U.L. and Sheng, J.B.A.U.L., 1995. Uniaxial tensile response of microfibre reinforced cement composites. *Materials and Structures*, *28*(9), pp.507-517.

Ou, Y.C., Tsai, M.S., Liu, K.Y. and Chang, K.C., 2012. Compressive behaviour of steel-fiber-reinforced concrete with a high reinforcing index. Journal of Materials in Civil Engineering, 24(2), pp.207-215.

P. Di Maida, Radi, E., Sciancalepore, C. and Bondioli, F., 2015. Pullout behavior of polypropylene macro-synthetic fibers treated with nano-silica. Construction and Building Materials, 82, pp.39-44.

R. D. Neves and De Almeida, J.F., 2005. Compressive behaviour of steel fibre reinforced concrete. *Structural concrete*, *6*(1), pp.1-8.

Romualdi, J.P. and Mandel, J.A., 1964, June. Tensile strength of concrete affected by uniformly distributed and closely spaced short lengths of wire reinforcement. In *Journal Proceedings,* 61(6), pp. 657-672).

Rossi P. and Harrouche, N., 1990. Mix design and mechanical behaviour of some steel-fibre-reinforced concretes used in reinforced concrete structures. Materials and Structures, 23(4), pp.256.

S.F.U Ahmed and Maalej, M., 2009. Tensile strain hardening behaviour of hybrid steel-polyethylene fibre reinforced cementitious composites. Construction and Building Materials, 23(1), pp.96-106.

S.T. Tassew and Lubell, A.S., 2014. Mechanical properties of glass fiber reinforced ceramic concrete. *Construction and Building Materials*, *51*, pp.215-224.

Sehaj Singh, Shukla, A. and Brown, R., 2004. Pullout behavior of polypropylene fibers from cementitious matrix. Cement and Concrete Research, 34(10), pp.1919-1925.

Shah S.P. and Jenq Y.S., 1987. Fracture mechanics of interfaces. MRS Online Proceedings Library Achieve, 114.

Shaikh Faiz Uddin Ahmed and Mihashi, H., 2011. Strain hardening behaviour of lightweight hybrid polyvinyl alcohol (PVA) fiber reinforced cement composites. Materials and structures, 44(6), pp.1179-1191.

Shao-Yun Fu and Lauke, B., 1996. Effects of fiber length and fiber orientation distributions on the tensile strength of short-fiber-reinforced polymers. *Composites Science and Technology*, *56*(10), pp.1179-1190.

Supat W. Suwannakarn 2009. Post-Cracking Characteristics of High Performance Fiber reinforced cementitious composite.

Su-Tae Kang and Kim, J.K., 2011. The relation between fiber orientation and tensile behavior in an Ultra High Performance Fiber Reinforced Cementitious Composites (UHPFRCC). *Cement and Concrete Research*, *41*(10), pp.1001-1014.

Su-Tae Kang, Lee, B.Y., Kim, J.K. and Kim, Y.Y., 2011. The effect of fibre distribution characteristics on the flexural strength of steel fibre-reinforced ultra-high strength concrete. *Construction and Building Materials*, *25*(5), pp.2450-2457.

T.A Söylev, and Özturan, T., 2014. Durability, physical and mechanical properties of fiber-reinforced concretes at low-volume fraction. *Construction and Building materials*, *73*, pp.67-75.

Tehmina Ayub, Shafiq, N. and Khan, S.U., 2015. Compressive stress-strain behavior of HSFRC reinforced with basalt fibers. *Journal of Materials in Civil Engineering*, *28*(4), p.06015014.

Tejal Desai, Rimpal, S.H.A.H., Peled, A. and Mobasher, B., 2003. Mechanical properties of concrete reinforced with AR-glass fibers. In *Brittle Matrix Composites 7* (pp. 223-232).

Tetsushi Kanda Lin, Z. and Li, V.C., 2000. Tensile stress-strain modelling of pseudo strain hardening cementitious composites. Journal of Materials in Civil Engineering, 12(2), pp.147-156.

Torigoe S.I., Horikoshi, T., Ogawa, A., Saito, T. and Hamada, T., 2003. Study on evaluation method for PVA fiber distribution in engineered cementitious composite. *Journal of Advanced Concrete Technology*, *1*(3), pp.265-268.

Wang, Y., Li, V.C. and Backer, S., 1987. Analysis of synthetic fiber pull-out from a cement matrix. MRS Online Proceedings Library Archive, 114.

Wen-Cheng Liao, Perceka, W. and Liu, E.J., 2015. Compressive stress-strain relationship of high strength steel fiber reinforced concrete. *Journal of Advanced Concrete Technology*, *13*(8), pp.379-392.

Yang, Y, 2002. Methods study on dispersion of fibers in CFRC. Cement and concrete research, 32(5), pp.747-750.

Yilmaz Akkaya, Picka, J. and Shah S.P., 2000. Spatial distribution of aligned short fibers in cement composites. *Journal of materials in civil engineering*, *12*(3), pp.272-279.

Yilmaz Akkaya, Shah, S.P. and Ankenman, B., 2001. Effect of fiber dispersion on multiple cracking of cement composites. *Journal of Engineering Mechanics*, *127*(4), pp.311-316.

Yin Chi, Xu, L. and Zhang, Y., 2012. Experimental study on hybrid fiber–reinforced concrete subjected to uniaxial compression. *Journal of Materials in Civil Engineering*, *26*(2), pp.211-218.

Youjiang Wang, Li, V.C. and Backer, S., 1988. Modelling of fiber pull-out from a cement matrix.

Zollo, R. F. 1982. Fiber reinforced concrete. New York: Construction Press.

Publications related to PhD Work

Journal Papers:

- Kasagani, H. and Rao, C.B.K., 2016. The influence of hybrid glass fibers addition on stress–strain behavior of concrete. Cement-Wapno-Beton, 83, pp.361-372.
- Kasagani, H. and Rao, C.B.K., 2018. Effect of short glass fibre on dilated concrete in compression and tension. *Proceedings of the Institution of Civil Engineers–Structures and Buildings*, pp.1-12.
- Kasagani, H. and Rao, C.B.K., 2018. Effect of graded fibers on stress strain behaviour of Glass Fiber Reinforced Concrete in tension. *Construction and Building Materials*, *183*, pp.592-604.

Conference Papers

- Hanuma Kasagani and C B K Rao“Effect of Graded Fibers on the Strength and Post Peak Deformation Capacity of Glass Fiber Reinforced Concrete”. International Conference – Structural Engineering Convention (SEC – Dec-(17-20)-2016)- -SERC-Chennai